AD NUMBER

ADB020280

LIMITATION CHANGES

TO:

Approved for public release; distribution is unlimited.

FROM:

Distribution authorized to U.S. Gov't. agencies only; Test and Evaluation; OCT 1976. Other requests shall be referred to Air Force Materials Laboratory, Attn: AFML/LC, Wright-Patterson AFB, OH 45433.

AUTHORITY

AFML ltr, 15 Oct 1982

AFML-TR-76-191

R77AEG302

EUTECTIC COMPOSITE TURBINE BLADE DEVELOPMENT

AIRCRAFT ENGINE GROUP, GE
CINCINNATI, OHIO 45215

November 1976

TECHNICAL REPORT AFML-TR-76-191

Final Report for Period 1 April 1973-30 November 1976

AIR FORCE MATERIALS LABORATORY
AIR FORCE WRIGHT AERONAUTICAL LABORATORIES
AIR FORCE SYSTEMS COMMAND
WRIGHT-PATTERSON AIR FORCE BASE, OHIO 45433

NOTICE

When Government drawings, specifications, or other data are used for any purpose other than in connection with a definitely related Government procurement operation, the United States Government thereby incurs no responsibility nor any obligation whatsoever; and the fact that the government may have formulated, furnished, or in any way supplied the said drawings, specifications, or other data, is not to be regarded by implication or otherwise as in any manner licensing the holder or any other person or corporation, or conveying any rights or permission to manufacture, use, or sell any patented invention that may in any way be related thereto.

This final report was submitted by the Material and Process Technology Laboratories of General Electric's Aircraft Engine Group, Cincinnati, Ohio 45215, under contract no. F33615-73-C-5050, project no. 69CW, with the Air Force Materials Laboratory, Wright-Patterson AFB, Ohio 45433. Capt. Brian A. Kosmal, AFML/LC, was the Air Force Materials Laboratory Project Manager.

This technical report has been reviewed and is approved for publication.

BRIAN A. KOSMAL, CAPT., USAF
Project Manager, Advanced Development Division

FOR THE COMMANDER

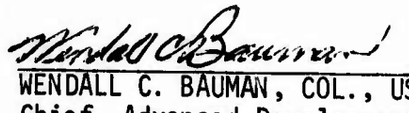

WENDALL C. BAUMAN, COL., USAF
Chief, Advanced Development Division

Copies of this report should not be returned unless return is required by security considerations, contractual obligations, or notice on a specific document.

AIR FORCE - 20 JUN 77 - 100

UNCLASSIFIED

SECURITY CLASSIFICATION OF THIS PAGE *(When Data Entered)*

REPORT DOCUMENTATION PAGE

READ INSTRUCTIONS BEFORE COMPLETING FORM

1. REPORT NUMBER (18) AFML-TR-76-191 (19)	2. GOVT ACCESSION NO.
3. RECIPIENT'S CATALOG NUMBER	
4. TITLE *(and Subtitle)* (6) EUTECTIC COMPOSITE TURBINE BLADE DEVELOPMENT	5. TYPE OF REPORT & PERIOD COVERED (9) Final Technical Report, 1 Apr 1973 to 30 Nov 1976
6. PERFORMING ORG. REPORT NUMBER (14) R77AEG302	
7. AUTHOR(s) (10) CA Bruch, RC Haubert, MFX Gigliotti, and MF Henry	8. CONTRACT OR GRANT NUMBER(s) (15) F33615-73-C-5050
9. PERFORMING ORGANIZATION NAME AND ADDRESS Aircraft Engine Group, General Electric Co. Cincinnati, OH 45215	10. PROGRAM ELEMENT, PROJECT, TASK AREA & WORK UNIT NUMBERS
11. CONTROLLING OFFICE NAME AND ADDRESS (11) Air Force Materials Laboratory (AFML/LC) Air Force Systems Command Wright-Patterson AFB, Ohio 45433	12. REPORT DATE November 1976
	13. NUMBER OF PAGES 353 (12) 355p
14. MONITORING AGENCY NAME & ADDRESS *(if different from Controlling Office)*	15. SECURITY CLASS. *(of this report)* Unclassified
	15a. DECLASSIFICATION/DOWNGRADING SCHEDULE N/A

16. DISTRIBUTION STATEMENT *(of this Report)*

Distribution Limited to U.S. Government Agencies [redacted] only since this Report concerns the Test and Evaluation of Technology Directly Applicable to Military Hardware (October 1976). Requests for Additional Copies or Further Distribution of this Document Must be Referred to Air Force Materials Laboratory (AFML/LC), Wright-Patterson AFB, Ohio 45433.

17. DISTRIBUTION STATEMENT *(of the abstract entered in Block 20, if different from Report)*

18. SUPPLEMENTARY NOTES

19. KEY WORDS *(Continue on reverse side if necessary and identify by block number)*

Eutectics, Directional Solidification, Planar Front Solidification, Investment Casting, Turbine Blades, Blade Design Analysis, Blade Life Analysis, Mechanical Properties, Physical Properties, Oxidation, Hot Corrosion, Coatings, Machinability, Bench Tests, Spin Tests.

20. ABSTRACT *(Continue on reverse side if necessary and identify by block number)*

The overall program objective was the development of materials, design, and fabrication technology required for the application of eutectic composites in turbine blades for aircraft engines. An MC carbide fiber reinforced eutectic alloy, NiTaC-13 and the low pressure turbine (LPT) blade of the J101 engine were selected to demonstrate the high potential of eutectics, by producing an uncooled eutectic blade having a predicted life equal to that predicted for the cooled superalloy blade. A major accomplishment was the scale-up of a

DD FORM 1 JAN 73 1473 EDITION OF 1 NOV 65 IS OBSCLETE

Unclassified

SECURITY CLASSIFICATION OF THIS PAGE *(When Data Entered)*

403 468

laboratory planar front solidification process, required to achieve the aligned fiber composite microstructure, for producing 1-5/8 inch diameter bars and solid J101 LPT blades. Airfoils of the blades were equivalent to bars in microstructure and stress-rupture properties; hence, extensive property data were obtained with aligned fiber material from bars. Nearly all measured longitudinal strength properties of NiTaC are superior to the best conventionally cast superalloys, including: ultimate tensile, creep-rupture, thermal fatigue, LCF and HCF. * Because blade dovetails contained misaligned fiber regions, property data were also obtained for this type of material. Preliminary blade life analysis was performed for two J101 LPT uncooled eutectic blade designs, solid and hollow-tip, and the results indicated both were satisfactory. Therefore, sixty oversize solid blades were cast. In a more detailed analysis of the two blade designs, both bare and coated, results indicated that the bare hollow-tip blade design most closely approached blade life goals and that the dovetail was satisfactory. The analysis also indicated that bare blades of either design would be preferred for engine testing because of substantially higher HCF and rupture life than blades coated with an available coating. Because of difficulties and risk of low yield in machining a tip cavity for the hollow-tip blade design, the solid blade design was selected. Bench tests generally confirmed design analysis predictions and clearly demonstrated the superiority of the bare blade in HCF. These tests also showed that rupture lives of simulated airfoils were about twice those predicted from test bar data, possibly due to a size effect. The adequacy of the blade dovetail in tension and LCF was proven in a 5,000 cycle spin test of 12 blades to 100 percent rotor speed, without failure. A comparison of blade life analysis predictions with bench and spin test results clearly demonstrated the adequacy of the eutectic blade for engine testing. Therefore, in an extension to this program, six uncooled NiTaC-13 blades together with 76 cooled superalloy blades will be tested in a J101 engine early in 1977. This test is expected to demonstrate effectively the high potential of the NiTaC eutectic system for meeting advanced turbine blade requirements of future engines.

* low cycle fatigue and high cycle fatigue.

PREFACE

This Final Technical Report, covering the period from 1 April 1973 to 30 November 1976, was prepared by the Material and Process Technology Laboratories (M&PTL) of General Electric's Aircraft Engine Group (AEG), Cincinnati, Ohio, 45215, under United States Air Force Contract F33615-73-C-5050, Project 61-69-CW.

The work at General Electric was performed under the direction of RW Harrison with CA Bruch as the Principal Investigator. William J. Schulz and Capt. Brian A. Kosmal, AFML/LC/W, were Technical Managers for the Air Force.

During the course of this program, there were many major GE participants, listed by activity, as follows:

Major GE Contributors

Turbine Blade Design Analysis:	AP Sterman, CH Gay, RC Haubert, RL Hall, RH Andersen, WG Jameson and DR Dins
Casting Process Development:	CS Wukusick, RW Smashey, CR Muncy, MF Henry, MFX Gigliotti, L Buchakjian TF Sawyer and FS Halsey
Property Data:	A Coles, RR Morehead, and RG Baur
Coating Evaluation:	DR Chang, JJ Grisik, JP Young and PA Bergman
NDI Evaluation:	JR Zurbrick and FH Bray
Machinability Evaluation:	GR Dearth and CE Glynn

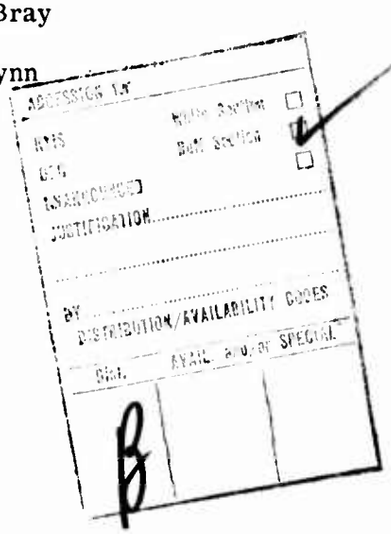

SUMMARY

The overall program objective was the development of materials, design, and fabrication technology required for the application of eutectic composites in turbine blades for aircraft engines. An MC carbide fiber reinforced eutectic alloy, NiTaC-13 and the low pressure turbine blade of the J101 engine were selected to demonstrate the high potential of eutectics, by producing an uncooled eutectic blade having a predicted life equal to that of the cooled superalloy blade. Specific major objectives necessary to meet the overall objective included:

- Application of advanced design and blade life analysis techniques
- Development of a process technique for casting eutectic blades close to final size
- Acquisition of engineering property data for use in design and life analysis of the demonstration component
- Evaluation of eutectic blade performance in bench and spin tests
- System analysis to assess total payoffs of eutectics to the engine selected
- Fabrication and assembly of a partial set of instrumented eutectic blades in a rotor, suitable for engine test.

Of the six objectives above, significant progress was made toward the first two and the last four were fully met.

A laboratory planar front solidification (PFS) process for casting NiTaC-13 was successfully scaled up to produce 1-5/8 inch diameter bars and J101 LPT blade airfoils having equivalent microstructures and stress-rupture properties. The blade dovetails, however, had misaligned fiber regions but analysis indicated that properties were satisfactory for the test program. Sixty blades were cast with a 0.04 inch envelope to provide excess stock for removal of surface defects and to avoid problems with dimensional factors.

During PFS, the alloying elements in NiTaC-13 segregate producing continuous changes in chemistry and decreases in stress-rupture strength and density. Through judicious design of the eutectic blade casting, segregation was held to a low level.

Perturbations to the PFS facility during casting, including power and mechanical disturbances, can produce bands of misaligned carbide fibers extending across the entire cross section of the castings. Because properties of bands were somewhat lower than those of aligned fiber material, the casting equipment was successfully modified by virtually eliminate band formation in the airfoils, and only blades with band-free airfoils were accepted for test evaluation.

The process scale-up efforts of this program have confirmed the high potential of the NiTaC eutectic alloy system for turbine blade applications. Nearly all measured longitudinal strength properties of NiTaC-13 are superior to the best available conventionally cast superalloys, including: ultimate tensile, creep-rupture, thermal fatigue, low cycle fatigue (LCF), and high cycle fatigue (HCF). The yield strength of NiTaC-13 is somewhat below the best superalloys up to about 1600°F, but is superior at higher temperatures. Transverse strength properties are lower than longitudinal due to the anisotropic microstructure of NiTaC-13, and this characteristic must be factored into blade design and life analysis.

Oxidation and hot corrosion tests showed that NiTaC-13 requires a coating. The Ni-20Cr-10Al-1Y coating evaluated in this program did provide excellent oxidation protection, but was deficient in severely corrosive environments. Even more important, however, was the observation that the coating material/process reduced HCF strength substantially. An improved coating for NiTaC alloys is required.

Blade life analysis predicted that a bare, hollow-tip blade design most closely approached the program goal of equal predicted lives for the uncooled NiTaC-13 and the cooled superalloy J101 LPT blades. The analysis also indicated that the dovetail was satisfactory and that the bare blade would be preferred over coated blades for engine testing because of substantially higher HCF and rupture life.

A solid blade design was selected for bench tests because of difficulties and risk of low yield in machining a tip cavity in the solid catings. Bench tests substantiated or exceeded the analysis predictions. First, the HCF superiority of the bare over the coated blade was clearly demonstrated. The adequacy of the blade dovetail in tension and LCF was demonstrated first in pull tests, and then in a 5,000-cycle spin test of 12 bare blades to 100 percent of maximum J101 rotor speed, without failure. Tests of simulated airfoils, however, showed that rupture life was about twice as high as predicted on the basis of test bar rupture data, possibly due to a size effect. Thus, these bench test results indicated that blade rupture lives may actually meet the program goal, but proof of this would require extended engine testing.

Further life analysis showed that the bare solid blade was entirely satisfactory for testing in a J101 engine. Therefore, in an extension to this program, six instrumented uncooled NiTaC-13 blades together with 76 cooled superalloy blades will be tested early in 1977.

As a result of the significant progress toward all specific objectives, it is concluded that the program has made substantial progress toward the overall program objective of developing the materials, design and fabrication technology required for the application of eutectic composites in turbine blade components of gas turbine engine.

Finally, the program has demonstrated the high potential of the NiTaC eutectic system for ultimately meeting turbine blade requirements for advanced engines. Specific advantages of NiTaC-13 over conventional superalloys have been demonstrated, and required improvements of NiTaC alloys have been identified.

TABLE OF CONTENTS

LIST OF ILLUSTRATIONS

LIST OF ILLUSTRATIONS (Cont'd)

LIST OF ILLUSTRATIONS (Cont'd)

LIST OF ILLUSTRATIONS (Cont'd)

LIST OF ILLUSTRATIONS (cont'd)

LIST OF ILLUSTRATIONS (Cont'd)

LIST OF TABLES

LIST OF TABLES (Cont'd)

LIST OF TABLES (Cont'd)

LIST OF TABLES (Cont'd)

LIST OF TABLES (Cont.)

1.0 INTRODUCTION

In the early 1970's several eutectic composite systems were identified that appeared to have potential for application to aircraft engine turbine blade hardware. The potential benefits offered by these materials may be realized in several ways. An increase of 150°F in metal service temperature appeared to be attainable with some of the eutectic materials systems identified. This can in turn be translated to a reduced amount of cooling air required and/or a higher turbine inlet temperature for improved engine performance. Alternatively, the higher stress rupture properties would allow a higher design stress for a given part at the same design temperature. Further, a direct materials substitution could be made, with the design stresses and temperatures remaining the same, and the payoff could be realized in terms of longer part life. In light of the potential offered by eutectic composites, the identification of specific material systems which appeared to fulfill this potential, and the fact that there currently were no conventional superalloy materials in being or in development which could meet the requirements projected for future advanced engines, the advanced development of eutectic composites for turbine engine blade applications was warranted.

Therefore, this program was established by the United States Air Force with the overall objective of developing the materials, design and fabrication technology required for the application of eutectic composites in turbine blade components of gas turbine engines. Prior to initiation of this program by the Air Force, General Electric conducted an experimental evaluation of critical properties of the most promising high temperature eutectic composite systems available in 1972, in order to select the highest potential eutectic system for the program. Eutectic alloys evaluated included MC (metallic carbide) fiber reinforced nickel- and cobalt-base eutectics (NiTaC and CoTaC) and Ni_3Cb lamella reinforced nickel-base eutectics. It was concluded that the NiTaC system offered highest potential for meeting the properties required of turbine blade materials for advanced engines and the eutectic alloy, NiTaC-13 developed by General Electric, was selected for use in the program. This alloy had a potential use temperature advantage of about 150°F over the best conventionally cast turbine blade superalloys then available, in the component selected for evaluation in the program.

The component selected for demonstration of the potential of NiTaC eutectic composites was the low pressure turbine (LPT) rotor blade of the J101 engine. In the existing design this unshrouded blade was air cooled. It was anticipated that the use of NiTaC-13 would allow direct substitution of an uncooled blade design, which would effectively demonstrate the potential for eutectics.

Specific major objectives necessary to meet the overall program objective included:

- Application of advanced design techniques to establish the requirements to be met by the eutectic blade.
- Development of a process technique for casting eutectic blades close to final size. The process technique was to have the potential for high yield and fabrication of eutectic blades on a production basis.
- Acquisition of engineering data for use in the design of the demonstration component, using eutectic material fabricated by the process to be used for final components.
- Evaluation of eutectic blade performance in both a bench test and a spin test program.
- System analysis to identify all applications of the eutectic technology developed to the engine selected and to assess the total payoff.
- Fabrication and assembly of a partial set of instrumented eutectic blades in an LPT rotor, suitable for engine test.

The program was initiated with Howmet Corporation as a major subcontractor having responsibility for the development of a process for casting NiTaC-13 test bars and blades, under the guidance of General Electric. Using proprietary mold materials, Howmet Corporation was to develop a mold system suitable for casting of NiTaC-13, and solidification equipment required for the General Electric casting process.

Early in the program it became apparent that mold materials under development by Howmet Corporation were not meeting expectations. The molds reacted with molten NiTaC-13 and removed substantial quantities of carbon, thereby reducing the amount available for the formation of strengthening MC carbide fibers.

The Corporate Research & Development Center (CRD) of General Electric then performed blade casting process development using a mold system demonstrated by CRD on Company funded programs to have high potential for casting NiTaC-13, and the Materials and Process Technology Laboratories (M&PTL) of General Electric performed test bar casting process development. Upon successful completion of the process development phases of the program, blades were produced for bench testing and engine evaluation.

This report covers all work performed in the program except system analysis and the engine test. The system analysis work has been reported separately in a classified final report. (1) The engine test, which will consist of approximately 30 hours of testing starting in early 1977, and ensuing post-test analysis will be reported after the completion of that work.

2.0 NiTaC-13 CASTING PROCESS DEVELOPMENT

Small bars, 1/2 inch in diameter by 8 inches in length, were cast for pre-program development and preliminary evaluation of NiTaC-13. Major challenges of this program were to scale up the small bar process to achieve a capability for single casting of 1-5/8 inch diameter bars and J101 LPT blades with sufficiently high yields to provide the quantities required for the program.

Primary goals for this phase of the work included:

- Test bars were to have aligned fiber sections about 4-1/2 inches long.
- Blades were to be cast as close to final dimensions as practicable and the finished blades were to have aligned fibers throughout.
- Test bar and blade acceptability criteria and inspection procedures were to be established.

All of the above goals were met except that for blade microstructure. Although a fully aligned fiber airfoil section was produced, portions of the platform/dovetail section contained misaligned carbide fibers; however, evaluation of critical properties of material containing carbide defect structures showed that the blade casting would meet the overall program objective, and 60 blades were cast for evaluation.

Blades were cast oversize, with at least a 0.04 inch envelope, to allow sufficient stock for removing surface defects, to reduct formation of misaligned fibers in the dovetail section, and to avoid problems with dimensional factors.

Details of the process development work are given in the sections that follow.

2.1 PLANAR FRONT SOLIDIFICATION

The achievement of an aligned carbide fiber composite microstructure and the accompanying high strength of NiTaC-13 requires planar front solidification (PFS), which is a very stringent type of directional solidification (DS). During solidification, the liquid/solid interface must be planar on a microscopic scale. Otherwise the reinforcing phase will not be fully aligned in the solidification direction and strength properties will generally be degraded to some extent. PFS requires meeting the following processing conditions:

$$\left[\frac{G_L}{R}\right]_{\text{Actual}} \geq \left[\frac{G_L}{R}\right]_{\text{Critical}} = K^* \qquad (1)$$

where G_L = temperature gradient in the liquid metal at the liquid/solid interface

R = solidification rate

K^* = alloy constant

Equation (1) shows that only two factors, K^* and G_L, govern the casting rate. With the selection of NiTaC-13 for this program, G_L was the sole variable governing the maximum rate for PFS of NiTaC-13.

An objective of this program was to cast test bars and blades at a minimum rate of 1/4 inch/hour. Pre-program measurements by Benz[2] had indicated that K^* for NiTaC-13 was about 1000°F hour/inch^2; hence, a minimum G_L of 250°F/inch would be required. Because of the uncertainty in the value of K^*, a goal for process development was to design a gradient furnace capable of producing a G_L of at least 300°F/inch.

The approach selected for the program was to cast test bars and blades singly. A theoretical analysis by Benz[2] of factors affecting the maximum attainable G_L in eutectic solidification, showed the following for cylindrical geometry:

$$G_L\,(\max) = (T_s - T_e)\ \sqrt{C} \qquad (2)$$

$$\text{where } C = \frac{2K_i}{K_l\ r_m^{\,2}\ \ln\ (1 + t_i/r_m)} \qquad (3)$$

T_s = mold outside surface temperature

T_e = eutectic solidification temperature

K_i = thermal conductivity of the ceramic

K_l = thermal conductivity of the liquid eutectic

r_m = radius of the metal

t_i = mold thickness

In equation (2), the maximum G_L attainable is shown to vary directly with $T_S - T_e$ which approximately equals the metal superheat temperature. One method to increase G_L, then, is to increase T_S to levels approaching the temperature capability of the mold.

Analysis of factors in equation (3) shows that, after an alloy has been selected, methods available to increase G_L (max) include:

- Increase K_i
- Decrease r_m
- Decrease t_i

Some improvement in K_i may be obtained by selection of the basic ceramic material; however, there are other more demanding requirements of molds and cores that may not permit selection of the ceramic on the basis of K_i. The mold thickness, t_i, may be decreased but strength considerations limit the allowable reduction. Finally, the minimum metal thickness, r_m, is dictated by the blade design. Equation (3) implies that the thinner airfoil section can be cast at a higher rate than the platform/dovetail region.

Equations (2) and (3) apply to an isothermal furnace, which is not achieved in practice because heat is lost through the furnace bottom. Consequently, in gradient furnace development, it would be necessary to emphasize methods for improving furnace bottom insulation and increasing the thermal flux to the metal in the region slightly above the furnace bottom in order to approach isothermal furnace conditions more closely.

Thus one challenge of process scale-up for this program was the development of high G_L PFS furnace configurations. The second challenge was the development of a blade mold that had sufficient strength and chemical compatibility to withstand the severe conditions required for PFS of NiTaC-13.

2.2 NiTaC-13 PROCUREMENT

The first 300-pound heat was ordered from Special Metals Corporation. Several problems were encountered with this heat (DS 729), causing it to be scrapped. These included: runout of 92 pounds of metal during the pouring operation and; the composition was out of specification due to addition of Re powder late in the melting process which had not completely melted at the start of the pour. For expediency, a 200-pound heat was ordered from and successfully produced by CRD. It was then decided to purchase the salvageable scrap from SMC and have all subsequent heats produced by CRD.

During the course of the program, 1278 pounds of qualified NiTaC-13 were produced by CRD in eight relatively large heats. In addition, about 45 pounds were produced by CRD in small heats weighing two or ten pounds each.

2.2.1 Melting Procedures

Table 1 shows the chemistry specification for NiTaC-13, which is based on elemental limits acceptable to melting vendors and is not based on detailed knowledge of effects of alloy chemistry on NiTaC-13 properties. The carbon level specified for the first heat was 0.54 wt% but, on the basis of work in the program, this was reduced to 0.48 wt% for subsequent heats. Charge materials are also shown in Table 1.

TABLE 1

NiTaC-13 CHEMISTRY SPECIFICATION AND CHARGE USED FOR LARGE HEATS

Element	Chemistry Specification, Wt. %	Charge Material
Ni	Balance	INCO Grade 270
Co	3.3 ± 0.2	INCO Electrolytic
Cr	4.4 ± 0.3	Shield Alloy Corp.
W	3.1 ± 0.3	High Purity Pressed & Sintered Bar
Re	6.2 ± 0.3	Pressed & Sintered Pieces
Al	5.4 ± 0.2	99.99%
V	5.6 ± 0.3	V-Al Master Alloy
Ta	8.1 ± 0.3	NRC Double Vacuum Arc Melted Chips
C	0.48 ± 0.04	National Carbon ECV Electrode
S&B	0.01 max (each)	-
Zr	0.05 max	-
Fe	0.2 max	-
Cb, Cu, Hf, Mn, Si	0.10 max (each)	-

Trace Elements	*Max., PPM	Element
	1	Bi
	3	Tl, Te
	5	Ag
	10	Pb
	15	Se
	25	Sb, As, Ba, Br, Cd, Ca Cs, Ce, Cl, Er, Ga, Ge Au, Ho, In, I, Ir, La Li, Lu, Hg, Nd, Os, Pd Pt, K, Pr, Rh, Rb, Ru Sr, Th, Tm, Sn, U, Yb Y, Zn

* Sum of all trace elements must be less than 400 ppm

The melting procedure for the large heats depended on whether or not scrap NiTaC-13 from previous heats was part of the charge. For large virgin heats, all charge materials in Table 1, except C, Al, and V were loaded into the melting crucible, which was MgO (low boron) manufactured by Lava Crucible-Refractories Company. After an initial evacuation of the cold charge, power from a 1920 cycle, 200 KW motor-generator set was turned on and flowing hydrogen was admitted at a pressure of two mm. After the charge melted, the hydrogen was shut off and the heat was solidified in the crucible under vacuum to remove hydrogen. The heat was then vacuum remelted, resolidified, and remelted again in vacuum to further remove hydrogen. After the heat was molten and quiet in vacuum, static argon at a pressure of one atmosphere was admitted to the chamber and the carbon was added. When visual observations indicated that the carbon had dissolved, the aluminum and vanadium additions were made. At this point, the heat was brought to a temperature of 2950° ± 25°F in about seven minutes and pouring was started. Each heat was poured into graphite split molds about 36" long and 1.45" or 2" in diameter. The molds rested on copper chill blocks that had been flame sprayed with zirconia. After cooling, ingot samples for heat qualification tests were cut from the bottom of the first ingot, the top of the last ingot, and a section from the appropriate ingot near the middle of the pour.

Large heats containing rejected NiTaC-13 as part of the charge presented the problem of minimizing oxidation of the aluminum and vanadium. Therefore, these heats were melted quickly and only once under static argon at a pressure of one atmosphere. Initially, partial scrap heats of this type were made with late additions of C, Al and V. However, the addition of carbon in the form of graphite rods was found to be unsatisfactory because the rods became coated with dross and did not dissolve completely. The use of the Ni-C eutectic alloy (2.2 wt % C) for the carbon addition in the initial charge overcame this problem.

The melting practice for the ten-pound heats was the same as used for the large virgin heats. For the two-pound heats, the Ni, Co, Cr, W, Re and Ta were first melted together in a magnesia crucible under one atmosphere of argon. After the metal was molten, the C was added and, after it had dissolved, V and Al were added. When the latter had dissolved, the melt was heated to about 2730°F and poured into two 0.8" diameter copper chill molds. Hydrogen degassing was not used in the two-pound heats because the nickel and cobalt had been previously hydrogen degassed.

2.2.2 Heat Qualification Tests

Two tests used to qualify the large NiTaC-13 heats were: complete chemical analysis, and stress rupture tests of aligned fiber material produced by PFS of ingot samples. For the decision on heat acceptability, emphasis was placed on the stress rupture test results, because the effects of small deviations from the chemistry specification on material properties had not been determined. Qualification tests were not performed for the small heats.

2.2.2.1 Chemical Analysis - Chemical analysis for the major elements in NiTaC-13 was performed on samples from the first and last ingots of each heat. Minor and trace element analysis was performed either with samples from the same two ingots, or from only one sample from the middle ingot.

Chemical analysis for all major elements, except nickel and carbon, was performed by X-ray fluorescence. For standards, four carbon-free alloy variations of NiTaC-13 listed in Table 2, were melted and chill cast. These ingots were assumed to meet the target chemistries and were used for calibration purposes throughout the program. In addition, one NiTaC-13 sample from the fourth heat (V-384-C) was used as a reference and analyzed along with samples from subsequent heats. The effect of surface preparation on analysis results was explored, and it was found that most consistent results were obtained with diamond polished samples. This technique was therefore used throughout.

Carbon analysis was performed by a standard gravimetric method employing apparatus manufactured by Laboratory Equipment Corp., Model 5-7-100. Minor and trace element analysis was performed by Accu-Lab Research, Inc., using a spark source mass spectrometer.

2.2.2.2 Stress Rupture Tests and Metallographic Evaluation - For this qualification test, samples from the first and last ingots of each heat were induction melted and chill cast into 1/2 inch diameter split copper molds. The resulting bars were then PFS using procedures to be described in Section 2.3.1. For inspection purposes, a flat was ground the full length of each PFS bar, polished, and examined microscopically. Bars not having at least a 4-1/2 inch length of aligned fibers were PFS again. The sectioning plan for acceptable bars, Figure 1, shows the location of bottom and top material for stress rupture tests, and bottom, middle and top material for evaluation of microstructure. Stress rupture test specimens were machined to have gage sections 0.65 ± 0.01 inches long and 0.1075 ± 0.0025 inches in diameter. These were tested in air at 1800°F/44 ksi. After rupture, the final diameter at the fracture location was measured to determine percent reduction in area and, when possible, the overall length was measured to determine percent elongation. For the latter calculation, it was assumed that the total increase in length occurred in the gage section.

Each metallographic sample was polished on a plane transverse to the growth direction and examined for carbide fiber alignment. Cellular or dendritic-cellular carbide morphologies are most easily detected in transverse sections.

2.2.3 Summary of Heats

All large heats produced by GE/CRD during the program are listed in Table 3, together with the results of qualification tests and some pertinent information about each heat. The two criteria established for heat acceptance were:

1. Stress rupture life of bottom material from each PFS bar must be $\geq$50 hours at 1800°F/44 ksi. This was the average life minus two standard deviations estimated for NiTaC-13 on the basis of data obtained in 1972. This criterion applied only to the bottom section of the PFS bar because it is stronger than the top section due to segregation effects (Section 3.2), and it is most representative of airfoil material.

2. Chemical analysis must be within the chemistry specification. Because the effects of chemistry variations on properties had not been established, some small deviations from the specification were allowed for heats that met the first criterion listed above.

TABLE 2

TARGET COMPOSITIONS OF CHEMISTRY CALIBRATION STANDARDS FOR NiTaC-13

	Composition, Weight Percent				
Element	NiTaC-13	Std. 1	Std. 2	Std. 3	Std. 4
Ni	63.4	66	63	71	57
Co	3.3	3	6	1	8
Cr	4.4	4	6	2	8
W	3.1	3	2	5	1
Re	6.2	6	9	4	5
Al	5.4	5	7	3	9
V	5.6	5	3	8	2
Ta	8.1	8	4	6	10
C	0.48	-	-	-	-

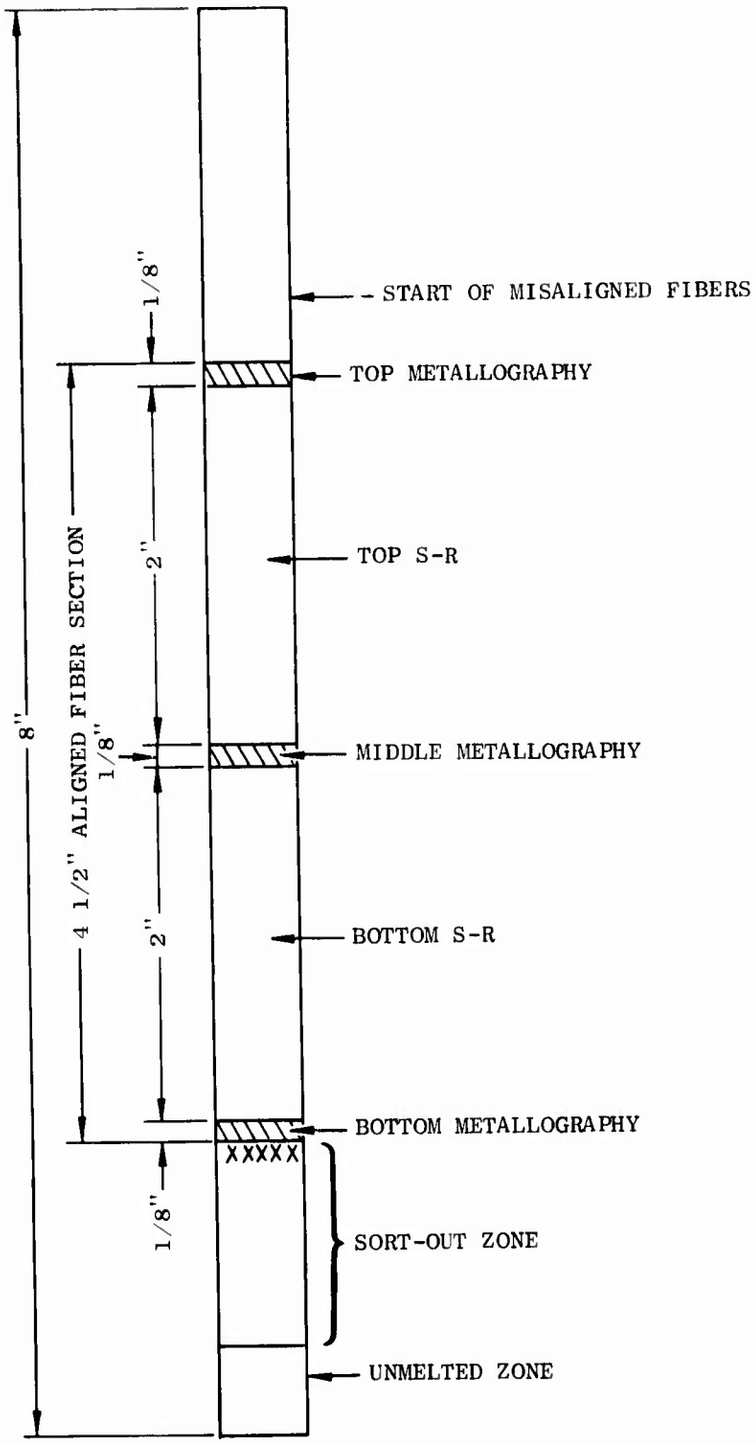

Figure 1. Cut Up Plan for 1/2-Inch Diameter PFS Bars Used for Heat Qualification

TABLE 3

SUMMARY OF LARGE NiTaC-13 HEATS MADE BY GE/CRD

Heat Number	V-319-C	V-363-C	V-371-C	V-384-C	V-385-C	V-390-C	V-391-C	V-400-C	V-401-C	V-416-C	V-423-C	V-435-B
Heat Weight, lbs.	200	180	180	145	145	110	110	115	195	217	208	105
Rejected NiTaC-13 Wt, lbs.	0	90.5	91.5	0	0	0	0	93	113.2	171	188.7	0
Rejected NiTaC-13 Source	-	D5-729	D5-729	-	-	-	--	V-390 & 391-C	V-390 & 391-C	V-401-C	V-416-C	
Heat Disposition	Accepted	Accepted	Accepted	Accepted	Accepted	Rejected	Rejected	Accepted	Rejected	Rejected	Accepted	Accepted
Ingot Number	1B 6T	1B 6T	1B 6T	1B 6T	1B 6T	1B 6T	1B 6T	1B 6T	1B 6T	1B 6T	1B 6T	1B 4T
Element Specification												
Ni Balance	- -	- -	- -	- -	- -	- -	- -	- -	- -	- -	- -	- -
Co 3.3 ± 0.2	3.3 3.3	3.3 3.3	3.3 3.4	3.2 3.2	3.2 3.2	3.2 3.2	3.2 3.2	3.4 3.4	3.4 3.4	3.3 3.3	3.5 3.5	3.1 3.1
Cr 4.4 ± 0.3	4.4 4.4	4.4 4.4	4.4 4.4	4.5 4.5	4.3 4.3	4.3 4.4	4.3 4.4	4.5 4.5	4.5 4.4	4.4 4.4	4.4 4.4	4.4 4.6
W 3.1 ± 0.3	3.1 3.1	3.3 3.3	3.3 3.4	3.0 2.8	3.3 3.2	3.0 3.0	2.9 3.0	2.6 2.6	2.8 2.7	2.9 2.7	3.2 3.1	3.0 2.9
Re 6.2 ± 0.3	6.2 5.9	6.6 6.7	6.3 6.3	6.3 6.4	6.5 6.3	6.0 5.8	5.9 6.0	6.2 6.2	6.4 6.2	6.2 6.3	6.2 6.2	6.0 5.9
Al 5.4 ± 0.2	5.6 5.6	5.8 5.9	5.6 5.6	5.4 5.4	5.4 5.4	5.2 5.3	5.1 5.3	5.4 5.3	5.2 5.2	5.4 5.1	4.9 5.0	5.3 5.3
V 5.6 ± 0.3	5.7 5.6	5.4 5.4	5.4 5.3	5.5 5.5	5.5 5.5	6.5 6.6	6.5 6.6	5.3 5.3	5.3 5.3	5.4 5.4	5.2 5.2	5.4 5.4
Ta 8.1 ± 0.3	8.1 8.0	8.3 8.1	8.3 8.0	8.2 7.8	8.2 8.2	8.0 8.0	8.1 7.7	8.1 7.9	8.2 8.6	7.8 7.7	8.0 8.0	8.2 8.3
C 0.48 ± 0.04	0.49 0.50	0.41 0.42	0.49 0.47	0.52 0.50	0.51 0.50	0.52 0.50	0.50 0.46	0.48 0.49	0.38 0.51	0.35 0.36	0.47 0.41	0.47 0.44
RESULTS OF STRESS-RUPTURE TESTS IN AIR AT 1800°F/44 KSI												
Bottom Section of PFS Bar												
Life, Hrs.	110.6 100.8	100.8 86.1	87.3 96.1	87.7 115.6	85.4 88.7	23.8 21.6	19.9 34.1	25.8 128.9	65.2 85.7	Tests Not	116.4 122.2	111.2 93.1
Elongation, %	- 10.6	14.3 14.3	- -	- -	- -	- -	12.6 12.1	6.6 -	- 6.9	Performed	- -	15.4 13.9
Reduction in Area, %	19.3 16.4	7.8 7.3	28.6 29.1	27.3 29.6	25.2 27.7	30.8 -	38.4 36.3	15.9 23.3	23.2 31.2	Because Heat Did	24.5 12.7	35.3 21.1
TOP SECTION OF PFS BAR										Not Meet		
Life, Hrs.	23.4 23.0	64.1 61.6	52.9 59.2	46.5 44.9	31.7 34.5	- -	11.6 -	21.6 68.8	19.3 20.6	Chemical	48.7 25.7	23.6 34.1
Elongation, %	- 10.1	15.9 12.6	- -	- -	20.2 -	- -	10.0 -	6.3 14.4	3.8 5.1		- -	8.8 13.1
Reduction in Area, %	10.8 21.4	15.5 13.2	17.8 16.4	20.6 20.2	30.1 17.5	- -	29.0 -	15.7 22.6	2.7 15.7	Spec.	17.8 22.8	21.0 22.8
Ingot Number	1B 6T	1B 6T	4B	4B	4B	4B	4B	4B	4B		4B	2T
S 0.010 Max	.005 .010	.001 .004	.002	.002	.004	.004	.008	.001	.001	Analysis	.001	.002
P 0.010 Max	.001 .002	<.001 <.001	<.001	<.001	<.001	<.001	<.001	<.001	<.001		<.001	<.001
Zr 0.05 Max	<.001 <.001	<.001 <.001	<.001	<.001	<.001	<.001	<.001	<.001	<.001		<.001	<.001
Fe 0.2 Max	.140 .160	.150 .110	.027	.043	.054	.096	.096	.029	.029	Not	.062	.029
Cb 0.1 Max	.001 <.001	.001 <.001	<.001	<.001	<.001	<.001	<.001	.001	<.001		<.001	<.001
Cu 0.1 Max	.002 .002	.008 .015	.008	.007	.008	.005	.005	.007	.003		.003	.005
Hf 0.1 Max	<.001 <.001	<.001 <.001	<.001	<.001	<.001	<.001	<.001	<.001	<.001	Performed	<.001	<.001
Mn 0.1 Max	.013 .006	.004 .004	.004	.002	.001	.002	.005	.001	.001		<.001	<.001
Si 0.1 Max	.009 .005	.064 .057	.035	.038	.096	.11	.079	.087	.100		.100	.083
TRACE ELEMENTS (GE Spec. No. P29TF19)	Met Met	Met Met	Met	Met	Met	Met	Met	Met	Met		Met	Met

Of the 12 heats made, Table 3, eight were accepted and four were rejected. Five of the accepted heats (V-319-C, V-371-C, V-384C, V-385-C and V-435-B) met both acceptance criteria. A discussion of decisions concerning the other seven heats now follows.

Heat V-363-C was accepted on the basis of excellent stress rupture test results for both bottoms and tops of PFS bars. Failure to meet the chemistry specifications for Re, Al and C was due to uncertainties in the composition of the rejected NiTaC-13 used as part of the charge. An equal quantity of the same rejected heat of NiTaC-13 was used successfully in the next heat, V-371-C, by correcting the charge on the basis of the chemical analysis of V-363-C.

Heat V-400-C was accepted even though the stress rupture test result for ingot 1B was very low. The only chemistry deviation occurred with tungsten and was small. The low stress rupture test result, however, was a concern and additional testing was done using material from ingot 4B, since no additional material was available from ingot 1B. Test results at 1800°F/44 ksi were as follows:

	PFS Bar Bottom	PFS Bar Top
Life, Hours	80.3	58.5
Reduction in Area, %	75.9	20.8

These excellent results, when combined with those in Table 3 for ingot 6T, indicated that the PFS bar from ingot 1B of heat V-400-C may have been faulty and the decision was made to accept this heat.

Heat V-423-C was also accepted on the basis of excellent stress rupture test results. Three elements, Al, V, and C, were slightly below specification. Presumably the Al and V losses were due to oxidation during melting of the heat because 188.7 pounds of the 215-pound charge was from the rejected heat V-416-C. Because of the possible problem with the carbon level, analysis was performed for all ingots from heat V-423-C with the following results:

Ingot	1B	2B	3B	4B	5B	6B	6T
Wt %C	.47	0.49	0.51	0.47	0.50	.49	.45

These results showed that the heat met the carbon specification and it was accepted.

The first two heats to be rejected, V-390-C and V-391-C, were melted together as one heat. Approximately half of this heat, V-390-C, was poured into six 1.45 inch diameter graphite molds and the remainder was solidified in the crucible. After removal of the first set of ingots, the remaining portion of the heat was remelted and poured into the same six molds and was designated heat V-391-C. The data in Table 3 show that the two heats failed to meet the stress rupture acceptance criterion, presumably due to the high vanadium contents. After searching the heat records and chemically analyzing the V-Al alloy charge material, it was concluded that an untraceable weighing error was responsible for the high vanadium content.

Heat V-401-C was rejected because of carbon variability. All ingots of this heat were analyzed for carbon with the following results:

Ingot	1B	1T	2B	3B	4B	5B	6B	6T
Wt %C	.38	.38	.37	.41	.39	.48	.48	.51

As shown, the first four ingots were below specification. A check of the heat history and crucible residue revealed that the carbon rod additive became entrapped in dross and did not fully dissolve.

Heat V-416-C was also rejected because carbon was below specification, once again due to entrapment of the carbon rod addition. At this point, it was decided to use the Ni-C eutectic alloy for adding carbon whenever the charge contained a large amount of previously melted NiTaC-13. This method was successfully demonstrated with heat V-423-C.

It is significant to note that all rejected heats were corrected through remelting and yielded material with excellent stress rupture properties.

2.3 SMALL BAR SOLIDIFICATION STUDIES

Liquid metal temperature measurements made prior to this program showed that, under standardized conditions established for a PFS facility for producing 1/2 inch diameter bars with well-aligned carbide fibers, the maximum metal superheat temperature (T_{max}) was about 3100°F and the temperature gradient at the liquid/solid interface (G_L) was about 600°F/in. Thereafter, this facility was used with only simple controls. Most notably, power input to the furnace was controlled instead of furnace temperature, and well-aligned NiTaC-13 bars were produced repetitively at a withdrawal rate of 1/4 inch/hour.

When problems were encountered early in this program, studies were undertaken in the small bar facility to provide information important to the most pressing scale-up problems, including:

- The significant decrease in stress rupture strength from bottom to top of 1/2 inch diameter PFS bars made for heat qualification tests, and
- The lack of success by Howmet Corp. in efforts to produce a large bar with well-aligned fibers.

These studies were aimed at obtaining improved understanding of the effects of major PFS parameters on the chemistry, rupture strength, and microstructure of bars.

2.3.1 PFS Facility and Operational Procedures

The furnace, illustrated schematically in Figure 2, had a gradient wound molybdenum wire resistance heater and water cooled side and bottom chills. Power to the furnace was controlled manually by means of a voltmeter and Variac. Cooling water flow rates through the chills were controlled manually by means of valves and flow meters. Withdrawal was accomplished with a screw mechanism driven by a variable speed motor. Two furnaces, having a common withdrawal system were located within one controlled atmosphere tank for PFS of two bars simultaneously.

For all experiments, a premelted and chill cast NiTaC-13 bar was placed in an 8 inch long recrystallized alumina crucible, having a 3/4 inch outer diameter and a nominal 1/8 inch thick wall and bottom. After loading the charge into the cold furnace, the tank was closed, flowing argon was admitted, cooling water circulation was set, and power to the furnace was turned on at a low setting. During heatup, power was gradually increased until it reached the selected level. After making the final power setting, the charge was held for from 30 to 60 minutes after which withdrawal at a selected rate was initiated. When withdrawal was completed, power was turned off and the bar was allowed to cool before removal from the tank.

A typical PFS NiTaC-13 bar, illustrated previously in Figure 1, also shows the usual microstructural features and cutup plan for evaluation samples.

2.3.2 Liquid Metal Superheat Temperature Study

This study was undertaken to evaluate material produced at different levels of T_{max}. The results were qualitative because furnace power was the controlled variable and T_{max} was not measured.

Using procedures described in the preceding section, four runs at 1/4 inch per hour were made at different power settings with NiTaC-13 from the following sources:

1B-2:	Heat V-319-C	Ingot 1B
6T-2:	Heat V-319-C	Ingot 6T
H-179A & B:	600-gram heat made at M&PTL	

Samples from the bottom, middle and top of the 4-1/2 inch long aligned fiber sections were chemically analyzed by methods described in Section 2.2. The results for each element, presented in Figure 3, showed the following variations from bottom to top of the aligned fiber section:

- Cr, V, and Al concentrations increased.
- W, Re, and C concentrations decreased.

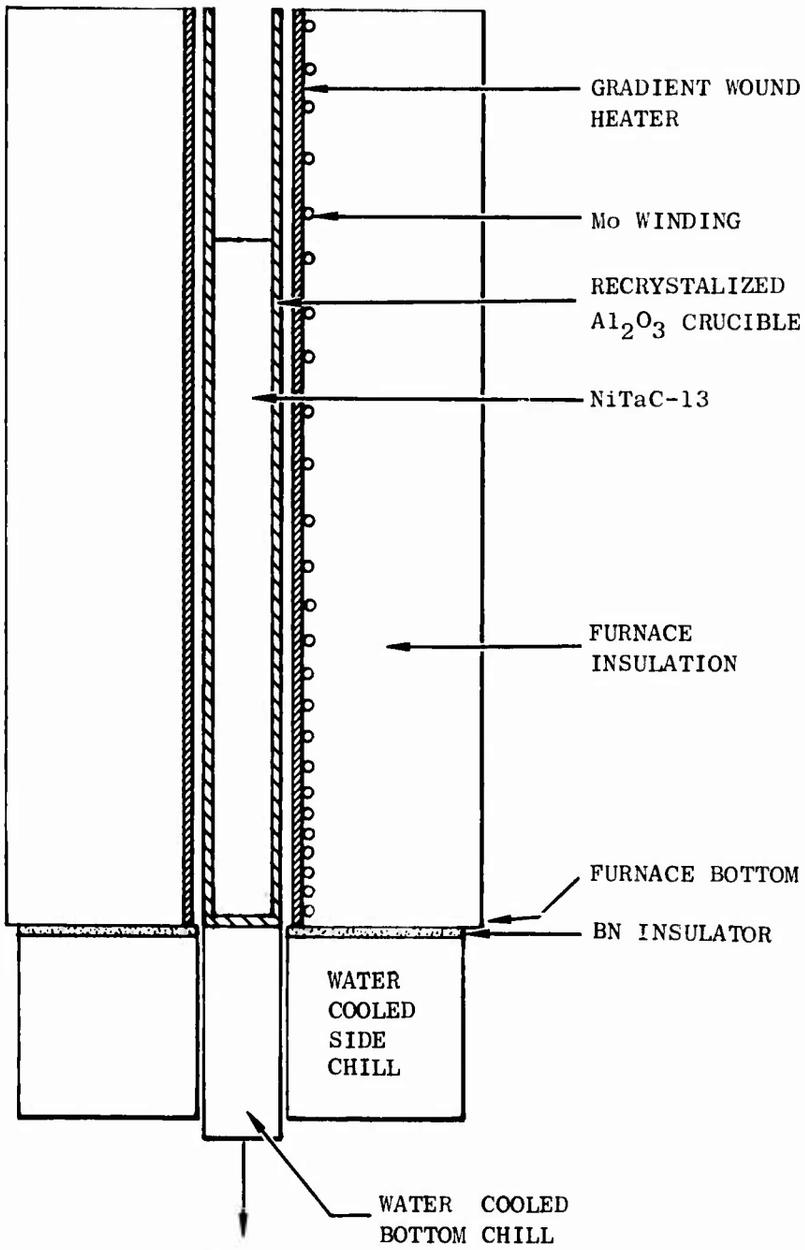

Figure 2. Schematic Drawing of Furnace Used for PFS of 1/2-Inch Diameter Bars

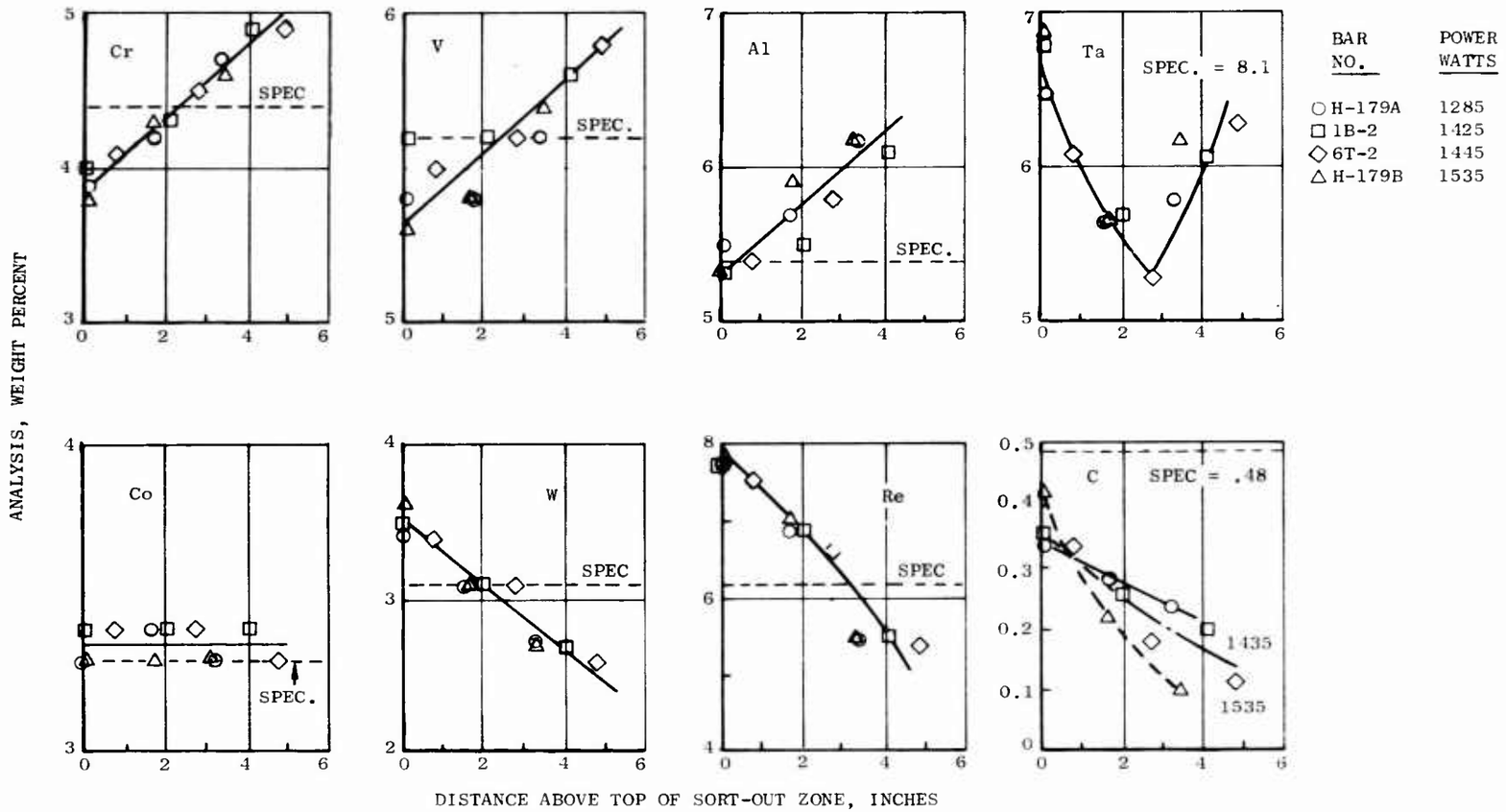

Figure 3. Variations in NiTaC-13 Alloy Element Concentrations With Position in PFS Bars Cast at Several Furnace Power Levels

- Ta concentration decreased to a minimum and then increased.
- Co concentration remained constant.

For all elements except carbon, the scatter in results around the curves drawn was small and there was no apparent effect of furnace power (T_{max}) on compositional gradients. The results for carbon, however, indicate that T_{max} was a prominent factor in that the reduction in carbon during solidification increased with increasing furnace power. The strong possibility existed that carbon was reacting with contaminants in the furnace atmosphere and/or the alumina crucible to form gaseous products, thereby reducing the carbon content of the melt. It was concluded that the lowest power level used, 1285 watts, produced the best results.

Stress rupture test specimens having a 0.10 inch gage diameter were machined from top and bottom halves of the 4-1/2 inch long aligned sections from the four bars. Results of air tests at 1800°F/44 ksi are shown in Figure 4 as a function of carbon content, which was estimated on the basis of the fracture location in each specimen and the data in Figure 3. In Figure 4, the dashed line drawn through the data points indicated a strong effect of carbon concentration on rupture life. Associated variations in concentrations of the other alloying elements, Figure 3, may also have contributed to the observed reduction in rupture strength that occurred in the solidification direction, but experiments to evaluate this possibility were considered beyond the scope of this program.

On the basis of the results obtained in this study, it was concluded that 1285 watts should be the upper limit for power to the furnace configuration being used. Higher power levels produced a less uniform bar with respect to carbon content and rupture life. The possibility existed that power levels below 1285 watts would result in even lower carbon gradients and more uniform rupture properties in PFS bars.

2.3.3 Solidification Rate Study

Early attempts to produce large, well-aligned fiber bars were unsuccessful. Because G_L was lower in the large bar facility (< 300°F/inch) than in the 1/2 inch diameter bar facility (~ 600°F/inch), a lower solidification rate would be expected to improve fiber alignment This study was undertaken to evaluate material produced at a withdrawal rate lower than the 1/4 inch/hour normally used.

For evaluation, two 1/2 inch diameter, 8 inch long bars of NiTaC-13 from ingot 3T of heat V-319-C were PFS using a furnace power level of 1255 watts. Bars 3T-1 and 3T-2 were withdrawn at 1/8 and 1/4 inch/hour, respectively. Carbon concentration profiles are compared in Figure 5 with previous results for bars made from this heat. It can be seen that the carbon profile for 3T-2 was above those for bars 1B-2 and 6T-2 made with a higher average power level of 1435 watts, but at the same withdrawal rate. The data for 3T-1 indicated that the 1/8 inch/hour withdrawal rate resulted in a slightly steeper carbon gradient.

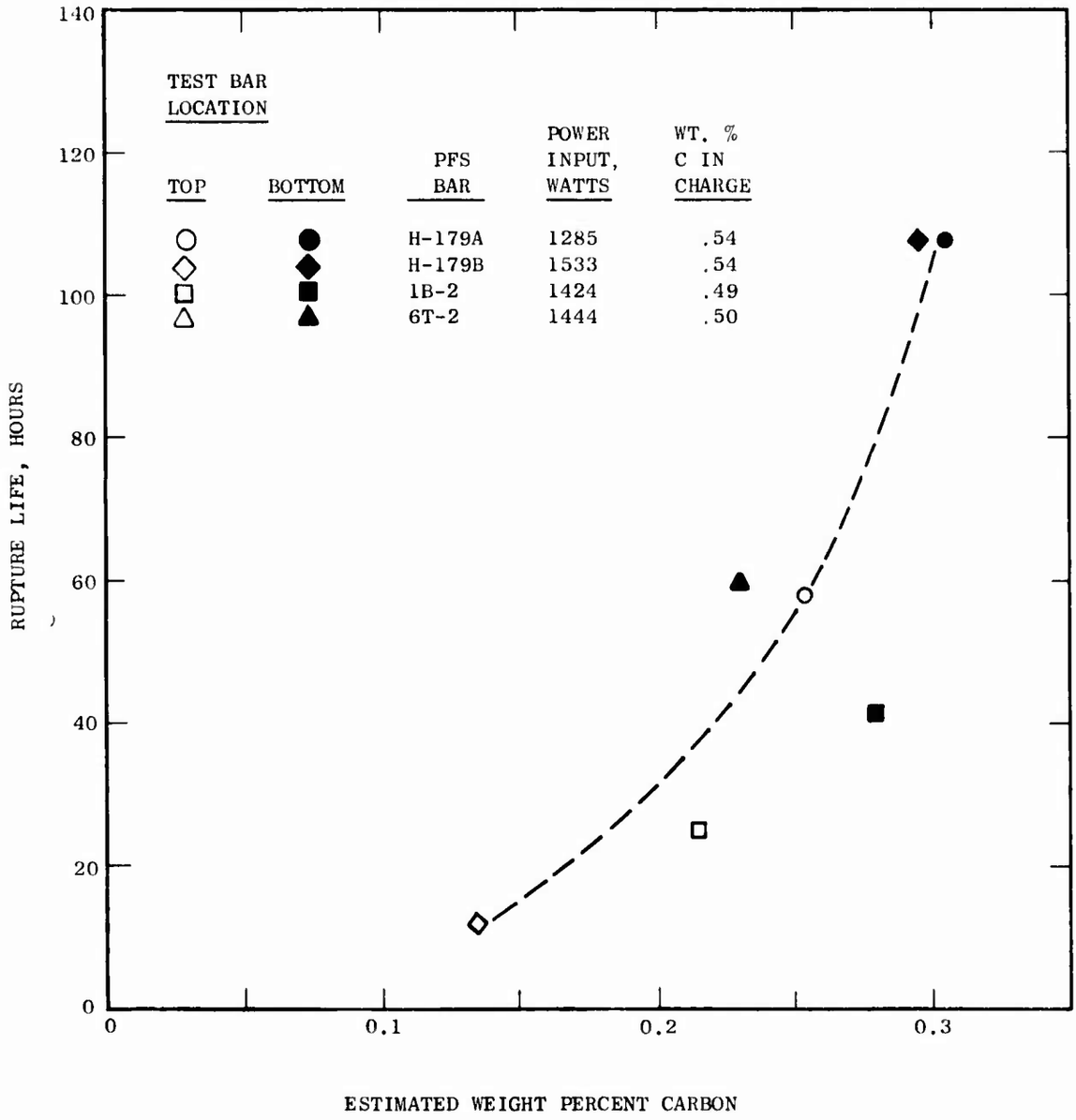

Figure 4. Rupture Life of 1/2-Inch Diameter PFS Bars Tested in Air at 1800°F/44 KSI Versus Estimated Carbon Concentration at Fracture Surface

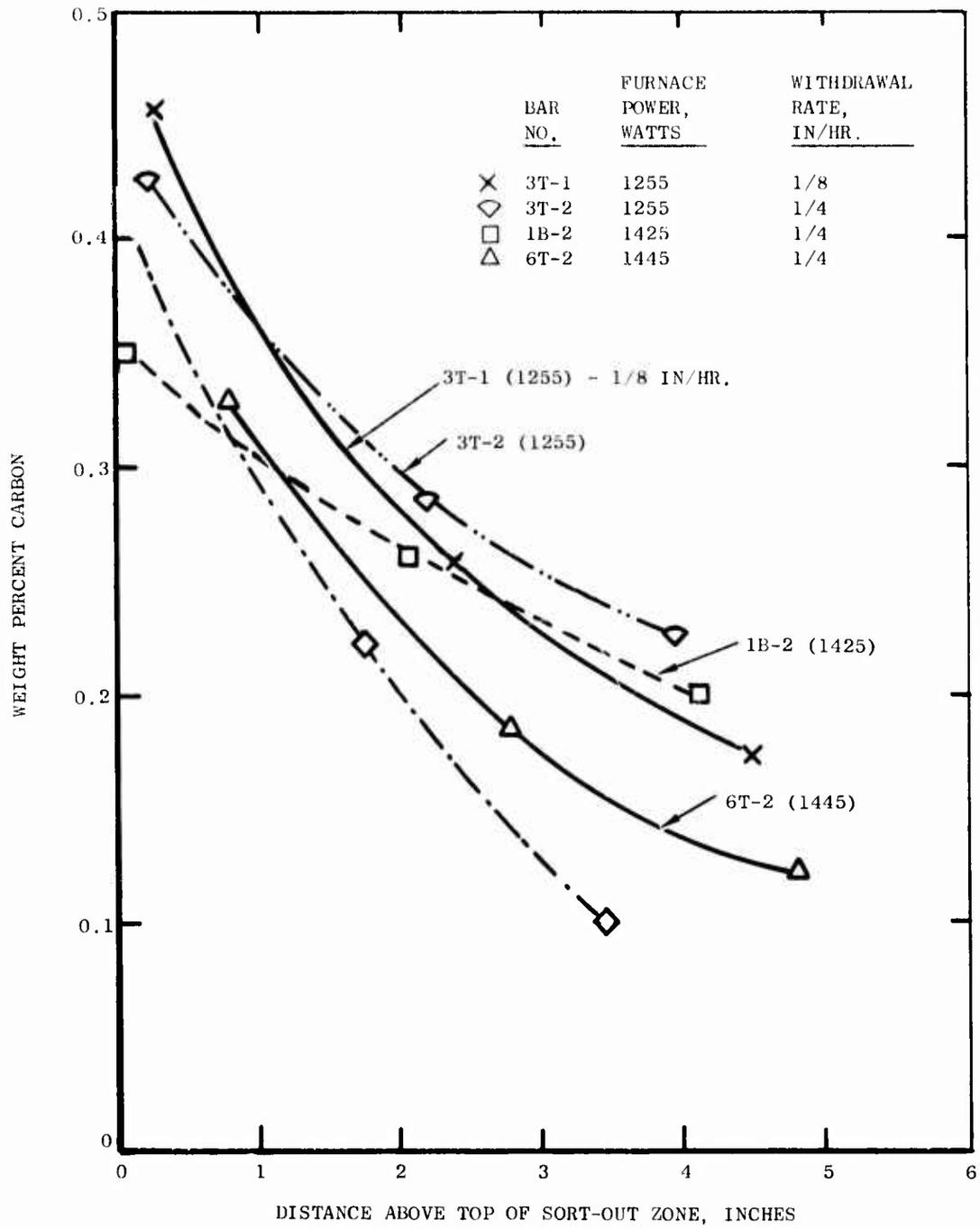

Figure 5. Effects of Furnace Power and Withdrawal Rate on Carbon Concentration Profile in 1/2-Inch Diameter PFS NiTaC-13 Bars

To characterize the two bars further, fiber population densities were determined metallographically with transverse samples from the bottom, middle and top of each. Stress rupture tests were also performed at 1800°F/44 ksi in air. These results are shown graphically in Figure 6 as a function of carbon concentration, which was estimated on the basis of sample location or fracture surface and the appropriate curve in Figure 5.

In Figure 6A, it is shown that the fiber population density was very much higher in material withdrawn at 1/4 inch/hour. Both curves in Figure 6A flatten with decreasing carbon concentration indicating that the fiber population densities reached a limiting value during solidification. Microscopically, it was observed in both bars that bottom material had a mixture of carbide fibers and blades, whereas top material had only carbide fibers, possibly finer than those in bottom material. These observations indicate that average fiber sizes also decreased with decreasing carbon concentration.

The stress rupture test results in Figure 6B indicated a strong effect of withdrawal rate, particularly in bottom material. The metallographic results indicate that the higher rupture life of 1/4 inch/hour material was due to the smaller fiber size and interfiber spacing, both of which are inversely related to fiber population density.

It was concluded that a withdrawal rate of at least 1/4 inch per hour would be required to meet the program strength goals. This in turn, led to the conclusion that furnace configurations resulting in higher G_L had to be developed for the test bar process.

2.3.4 Liquid Metal Temperature Gradient Studies

These experiments were undertaken to verify pre-program measurements of T_{max} and G_L cited previously and to evaluate changes in these parameters during withdrawal.

For the measurements, NiTaC-13 was melted as described in Section 2.3.1 and the furnace heater power level was maintained at 1260 watts. With the crucible held stationary at a measured position, a thermocouple probe was inserted into the melt until it contacted the liquid/solid interface. The probe consisted of an iridium/iridium-40 rhodium thermocouple bead inside an alumina protection tube that was sealed at the end with plasma sprayed alumina. This distance between the end of the probe and the thermocouple bead was about 1/4 inch. After measuring temperature with the probe in contact with the liquid/solid interface, the probe was raised a measured amount, held for about one minute to stabilize, and temperature was measured. This procedure was repeated until the probe tip was near the top of the melt. The crucible was then withdrawn to a new measured position and the temperature profile was measured again.

Figure 7 illustrates a typical temperature profile. In this case, the crucible bottom was 1/16 inch above the furnace bottom. As shown in the figure, G_L was about 580°F per inch at a position about 1/4 inch from the liquid/solid interface. Extrapolation of the curve to the solidus temperature (slightly below 2500°F) would yield a much higher G_L; however, there were too many uncertainties in the measurements to justify this extrapolation procedure. Finally, in Figure 7 it is shown that the liquid/solid interface was about 0.45 inch above the furnace bottom.

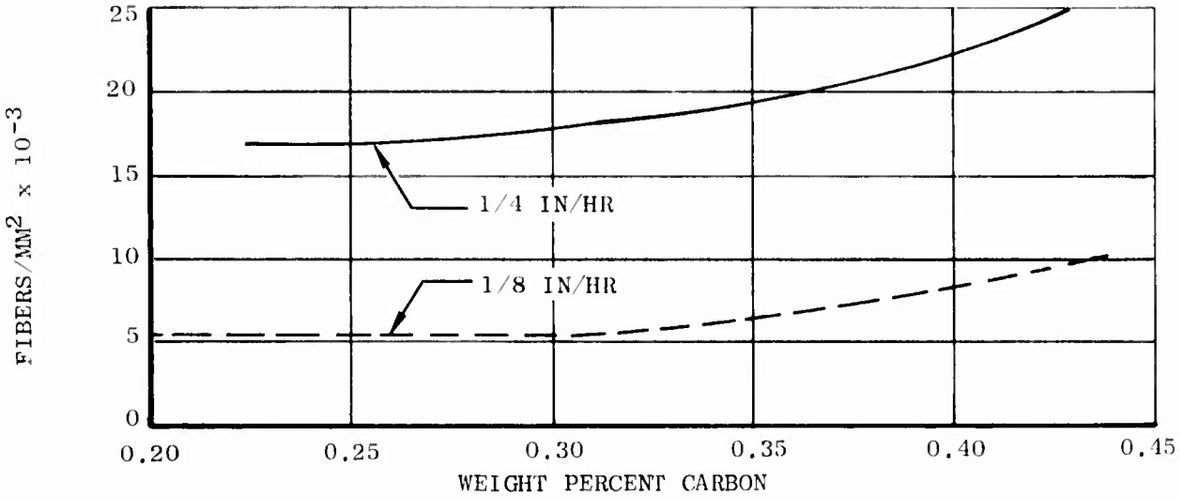

A. FIBER POPULATION DENSITY

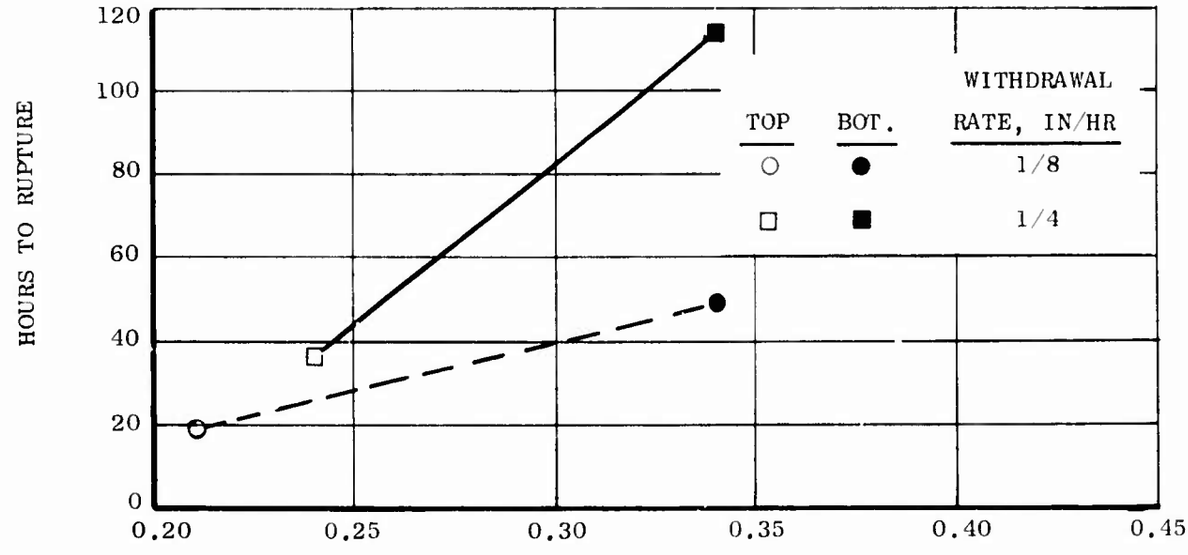

B. STRESS-RUPTURE LIFE AT 1800°F/44 KSI IN AIR

Figure 6. Effects of Withdrawal Rate On Carbide Fiber Population Density and Rupture Life of NiTaC-13 Bars Cast Using Furnace Power of 1255 Watts

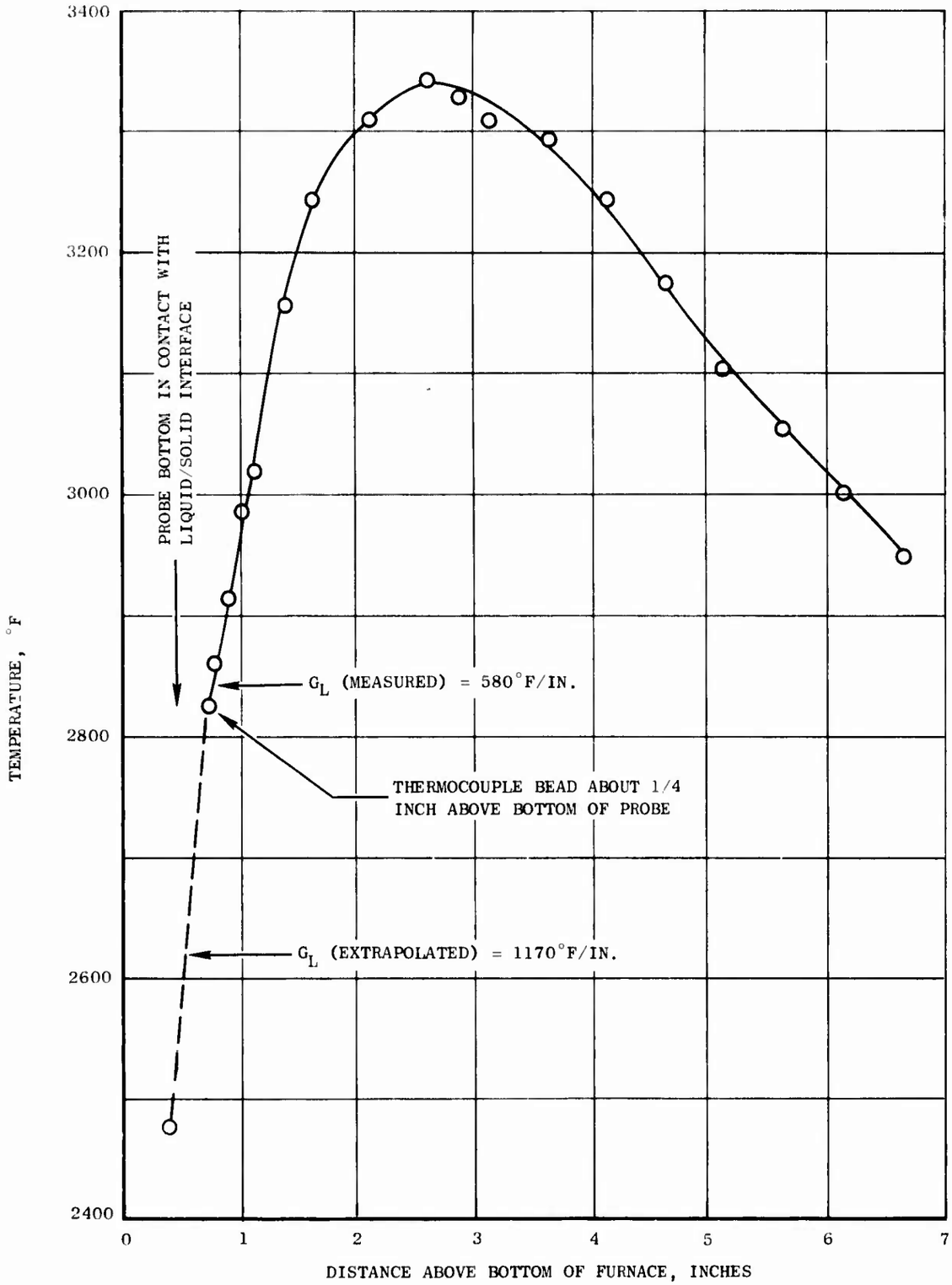

Figure 7. Liquid Metal Temperature Profile in 1/2-Inch Diameter Bar Facility with Crucible Bottom 1/16-Inch Above Furnace Bottom and 1260 Watts Heater Power

The results of all measurements are presented in Figure 8. Average curves have been drawn through the data points which indicate that, during three inches of withdrawal:

- G_L was approximately constant at 600°F/inch.
- T_{max} increased from about 3275° to 3380°F.
- The position of the liquid/solid interface remained stationary at about one inch above the furnace bottom.

These results confirmed pre-contract measured values of G_L, but showed that T_{max} was about 180° to 280°F higher than the earlier value. The newer measurements also indicated that G_L was stable during the first 3 inches of withdrawal.

A very interesting result was the position of the liquid/solid interface. Prior GE/M&PTL experience had shown that better carbide fiber alignment was achieved when a ceramic insulator was placed between the NiTaC-13 bar and the bottom chill. This was accomplished by using a crucible instead of an open-ended tube. The new results showed that the interface remained one inch above the furnace bottom and, therefore, that the ratio of heat input to heat withdrawal was too low. Because of this interface position, heat from the furnace is transferred to the solidified portion of the bar, thereby reducing G_L. As discussed by Benz [2], the rate at which high temperature eutectic alloys can be PFS is directly related to G_L which in turn is limited by the rate of heat input. For a given furnace configuration, G_L can be maximized by balancing the heat input/heat withdrawal ratio so that the liquid/solid interface is at the furnace bottom. Measurement of the interface position is an effective and relatively simple method to determine under what conditions the ratio is optimized.

On the basis of these results, it was concluded that T_{max} in the 1/2 inch diameter bar facility operating at 1260 watts, was probably higher than was practicable for blade casting because of the larger size furnace required and mold temperature capability limitations. However, the accompanying G_L of about 600°F/in. was higher than required for PFS of NiTaC-13 at 1/4 inch/hour, so it was considered likely that satisfactory aligned fiber material could be produced at a significantly lower T_{max}.

2.4 SEGREGATION IN NiTaC-13

Preliminary studies of PFS NiTaC-13 bars, Section 2.3.2, showed that there were compositional gradients and a general trend of decreasing stress rupture strength from bottom to top. These studies also showed an increase in carbon gradient with increasing furnace power level, indicating that chemical reaction may play some role in the phenomena observed. To gain further insight into the segregation phenomenon and its effects, additional studies were conducted by CR&D.[3] Results will be reviewed here.

2.4.1 Theoretical Considerations

A major feature of NiTaC and most other eutectic alloys of practical interest for high temperature structural applications is a large freezing range and a low allowable solidification rate, R, to achieve a fully aligned microstructure.

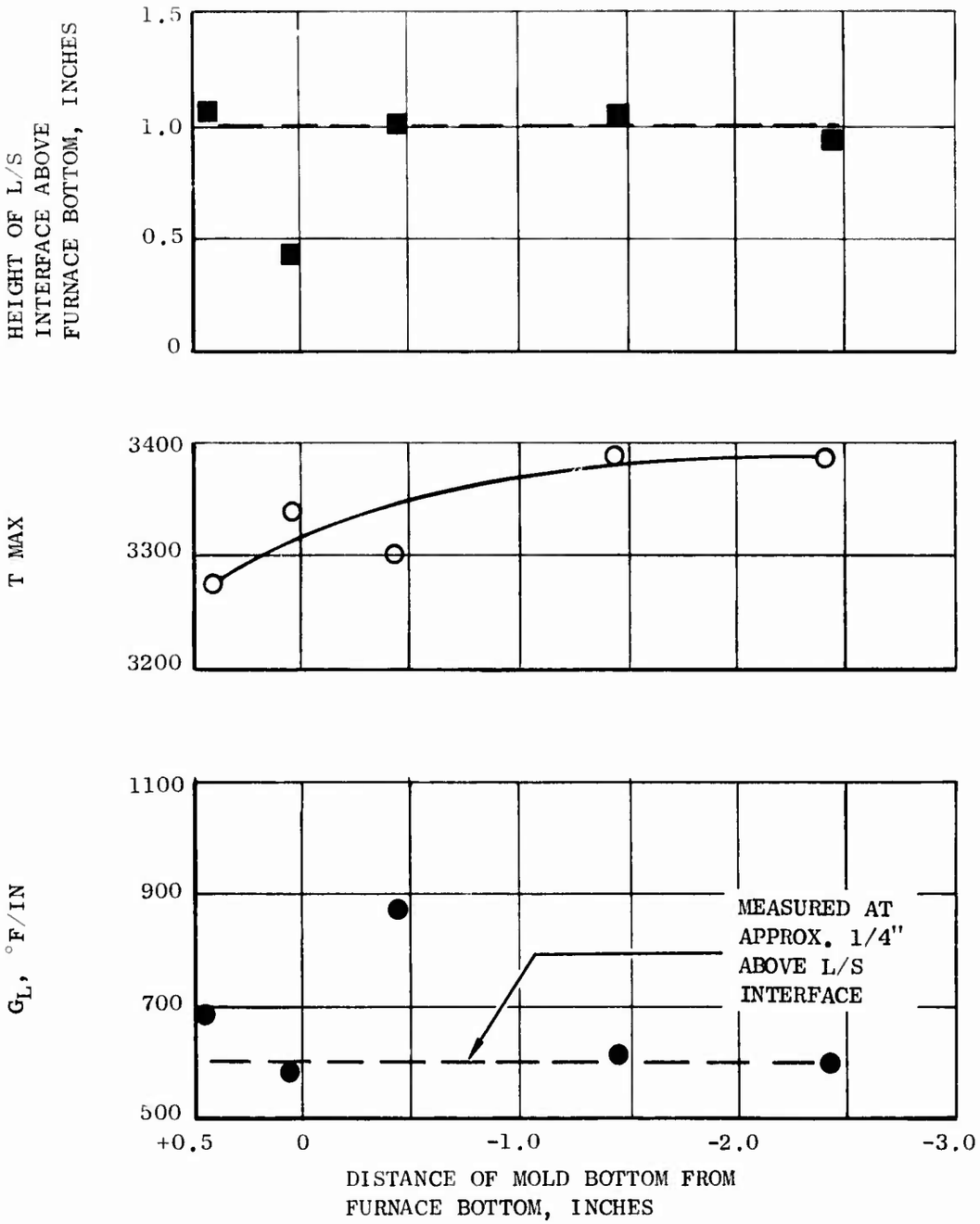

Figure 8. Effect of Mold Position on G_L, Tmax, and Liquid/Solid Interface Position with Furnace Power of 1260 Watts in 1/2-Inch Diameter Bar Facility

The freezing range associated with eutectics affects the composition profile in the liquid ahead of the solid/liquid interface, and for each alloying element there can be a defined distribution coefficient, k, which is the ratio of the solid composition to the composition of the liquid from which it is freezing.

For the case of solidification in which the composition of the solid is the same as the composition of the liquid far from the interface, there must be a region in the liquid adjacent to the solid/liquid interface where the composition varies from the bulk average to accomodate the distribution coefficients. This effect was treated analytically for single phase growth by Tiller et al [4] and their result is equally applicable to eutectic solidification. The composition profile in the liquid ahead of the solid/liquid interface is given by:

$$C_L = C_O \left[1 + \frac{1-k}{k} \exp\left(\frac{-R}{D}\right) X\right] \qquad (4)$$

where C_L is the composition of the liquid; C_O is the composition of the solid and of the liquid far from the interface; D is the diffusion coefficient in the liquid; and X is the distance from the solid/liquid interface. In equation (4) the only extrinsic parameter is R, and it has a strong effect on the length of the zone of liquid in which there are composition gradients. This point is illustrated in Figure 9, which shows composition-distance curves as a function of R, calculated using equation (4) and the following assumed values for constants: C_O = 2 atomic percent, k = 1.3, and D = 5×10^{-3} mm^2/sec. As shown in the figure, the composition profile in the liquid would extend about 10 mm ahead of the interface for a value of R equal to 6.35 mm/hr (1/4 in/hr). However, these composition profiles cannot be maintained due to their large size, convective stirring, density inversions and, in many cases, the electro-magnetic stirring from the furnace heating source. Therefore, equation (4) is not applicable to eutectics that require low values of R for phase alignment.

The reduction or elimination of composition profiles due to liquid motion causes a gradual change in solid composition as a function of the amount of liquid solidified. This phenomenon has been described by Pfann [5] for single phase alloys where the composition variations within a solidified body are given:

$$C = k\, C_o\, (1-g)^{(k-1)} \qquad (5)$$

where: C is the composition of the solid at a selected point; k is a distribution coefficient; C_O is the initial bulk average composition; and g is the volume fraction solidified to the selected point. The amount of stirring in the liquid and thus the amount of segregation determines the value of k which can vary from the equilibrium value in the most extreme case, to a value close to 1 when there is no mixing in the liquid. The moxt extreme case, perfect mixing in the liquid, is what is to be expected for the solidification conditions required for eutectics such as NiTaC-13.

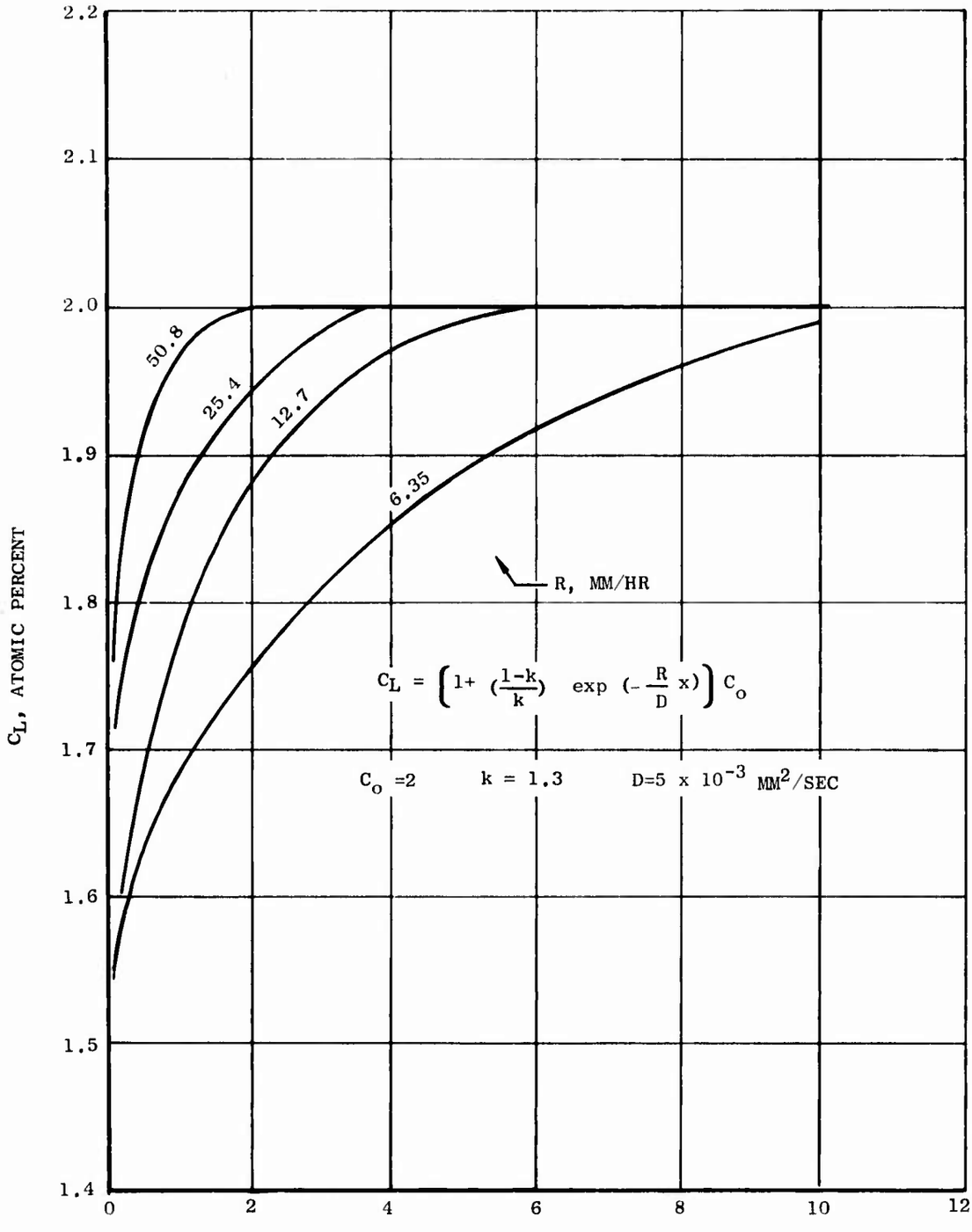

Figure 9. Effect of Solidification Rate, R, on Calculated Composition Profile in Liquid, C_L

2.4.2 Measurements of Segregation

For a more detailed study of segregation, three 8 inch long NiTaC-13 bars were PFS in 7/8 inch diameter recrystallized alumina crucibles at a rate of 1/4 inch/hour. The furnace heater was a graphite susceptor heated by RF induction. To study effects due to metal-mold reaction, bars were solidified at the following three levels of T_{max}: DS 1340 at 2930°F, DS 1354 at 3120°F and DS 1395 at 3300°F. After solidification, the bars were sectioned at several locations for chemical analysis and material was obtained from the bottom and top of each bar for stress-rupture tests to be discussed later in Section 2.4.4. Chemical analysis for carbon was performed by combustion and for all other elements, by X-ray fluorescence. The latter utilized an intensity versus composition correlation developed from eight alloy standards which contained different combinations of all elements in NiTaC-13, except carbon.

Table 4 presents the chemical analysis data in atomic percent and the associated values of g_b (volume fraction solidified), which were calculated on the basis of the total volume of molten alloy present prior to the start of withdrawal.

The carbon profiles for the three bars are presented in Figure 10 where it is shown that the bars solidified with T_{max} of 2930° and 3120°F had equivalent profiles. In contrast, there was a slight decrease in the profile of bar DS 1395 made with a T_{max} of 3300°F. Since metal-mold reactions are thermally activated processes, it was concluded that there was little or no reaction at the two lower temperatures, while there was reaction at 3300°F. Therefore, the observed gradients in carbon for bars DS 1340 and DS 1354 must be attributed to segregation phenomena. The variations in concentrations of all other major alloying elements are presented in Figure 11, using the data of Table 4. Curves had been drawn in Figure 11 to suggest the segregation trends for all elements, except Al where there was a large amount of scatter. A comparison of the results in Figure 11 with preliminary results in Figure 3, shows similar trends in gradients for all elements with the following exceptions:

- Results in Figure 11 indicate V content decreased as solidification proceeded, but previous results showed the opposite.
- Results in Figure 11 indicate Co content decreased as solidification proceeded, but previous results showed no change.

After an evaluation of the analysis techniques, it was concluded that the previous analysis results for Al and V were more reliable.

The major variations in composition with g_b were typified by the data for Re and Cr. As shown in Figure 12, the data for these two elements from Table 4 can be fitted to equation (5) using k equal to 1.3 for Re and 0.78 for Cr.

Chemical segregation in a blade casting, LB86, was also evaluated and found to be equivalent to that found in bars. The resulting curves for Re and Cr, presented in Figure 13, are similar in shape to those illustrated previously for bar data.

TABLE 4

CHEMICAL ANALYSIS OF PFS NiTaC-13 BARS SOLIDIFIED FROM THREE DIFFERENT SUPERHEAT TEMPERATURES

Bar No.	T_{max}, °F	g_b	Atom Percent								
			Ni	Co	Cr	Al	W	Re	V	Ta	C
DS 1340	2930	.18	65.0	4.1	3.8	11.4	1.2	2.5	7.8	2.0	2.15
		.43	66.2	4.1	4.4	12.5	1.1	2.2	6.4	1.8	1.46
		.63	66.5	4.2	4.6	12.2	1.0	2.1	6.0	2.0	1.29
		.87	66.4	3.6	5.9	12.4	1.0	1.7	5.7	2.3	0.95
		.96	65.7	2.3	8.3	12.8	1.0	1.0	5.5	2.9	0.56
DS 1354	3120	.19	65.7	3.5	4.5	12.2	1.1	2.3	6.7	2.0	2.12
		.39	66.8	3.6	4.7	12.2	1.0	2.2	6.0	2.0	1.54
		.63	67.0	2.7	5.6	12.7	1.1	1.8	5.9	1.9	1.23
		.82	67.6	3.5	6.0	11.8	0.9	1.7	5.2	2.3	1.01
		.93	67.2	3.0	6.9	11.8	1.0	1.4	5.3	2.6	.85
		.97	66.5	2.2	8.5	11.7	1.0	1.1	5.5	2.7	.63
DS 1395	3300	.17	64.6	3.4	2.9	13.0	1.3	2.4	7.8	1.0	2.72
		.35	66.5	3.9	3.5	12.2	1.2	2.3	7.3	1.7	1.54
		.48	66.8	3.7	6.1	11.7	0.9	2.0	5.4	2.0	1.29
		.60	67.0	3.4	5.8	12.0	1.0	2.1	5.9	1.8	1.00
		.78	66.8	2.6	4.9	13.0	1.3	1.7	7.0	1.9	0.79
		.89	67.1	3.1	7.4	10.9	1.0	1.5	5.6	2.4	1.10
		.92	67.4	2.9	0.1	10.7	0.8	1.1	4.7	2.8	0.55
		.97	65.8	2.3	8.3	11.8	1.0	1.1	6.2	2.9	0.50

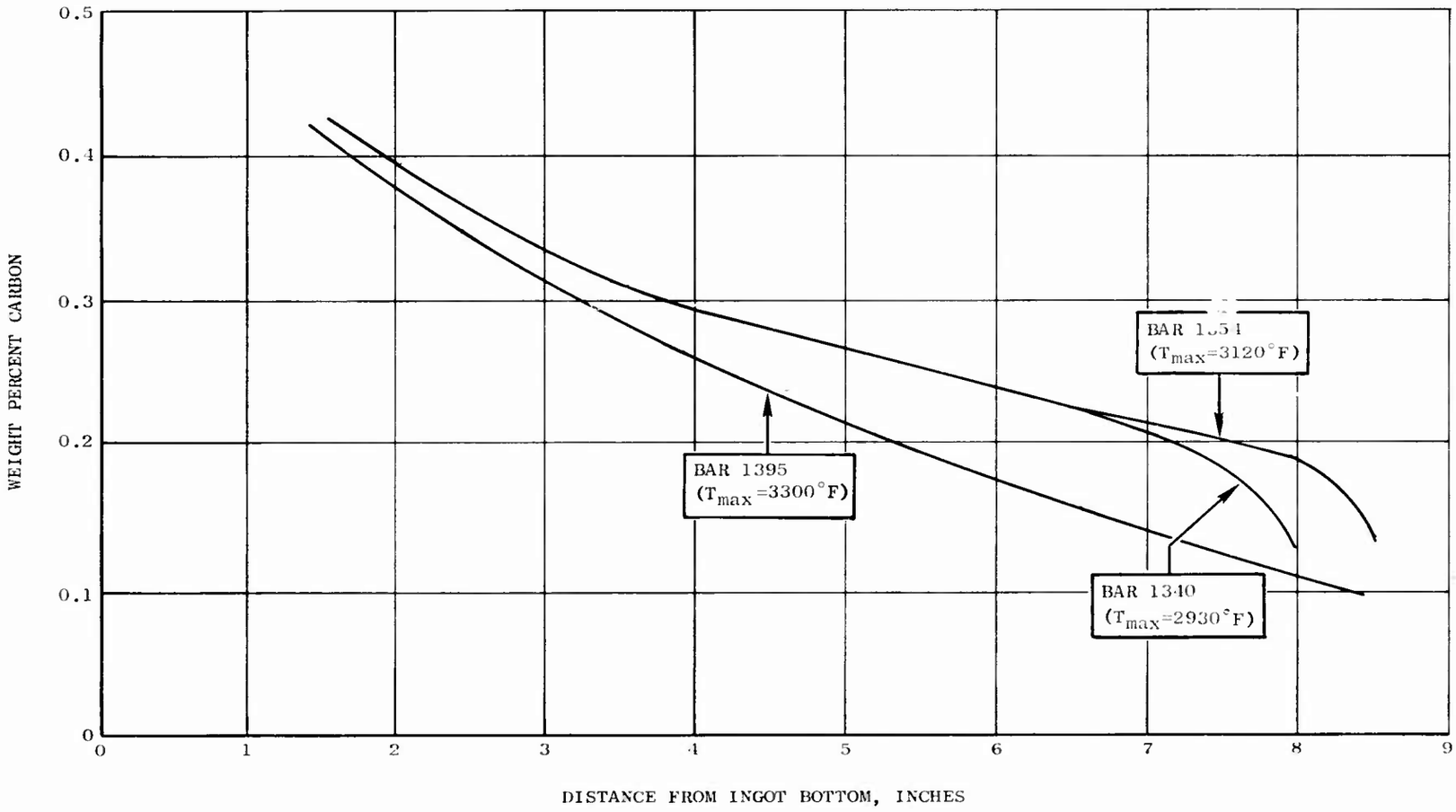

Figure 10. The Effect of Melt Superheat on Carbon Profiles in PFS NiTaC-13 Bars

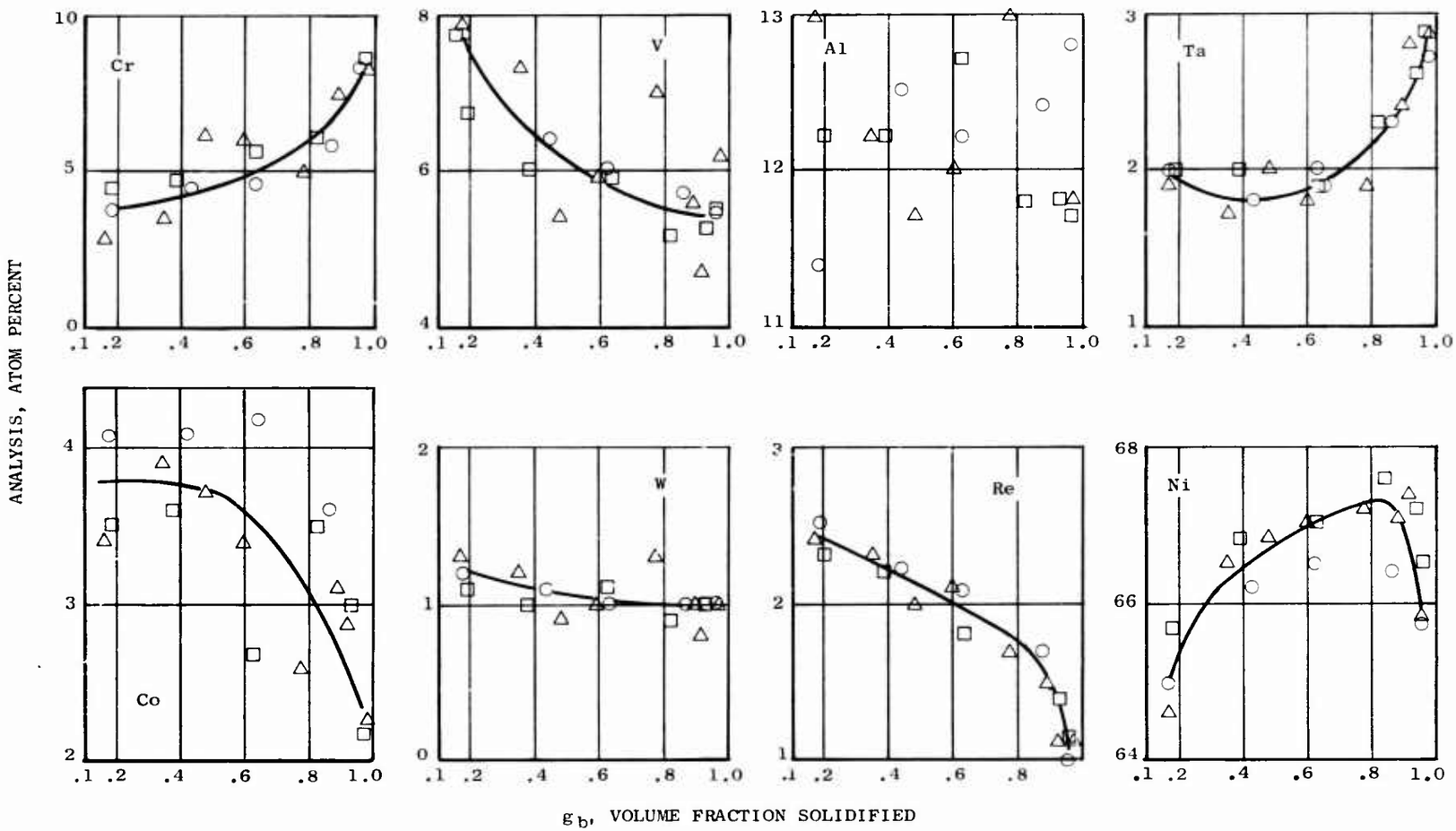

Figure 11. Segregation of Alloy Elements in PFS NiTaC-13 Bars
(○ = DS1340; □ = DS1354; △ = DS1395)

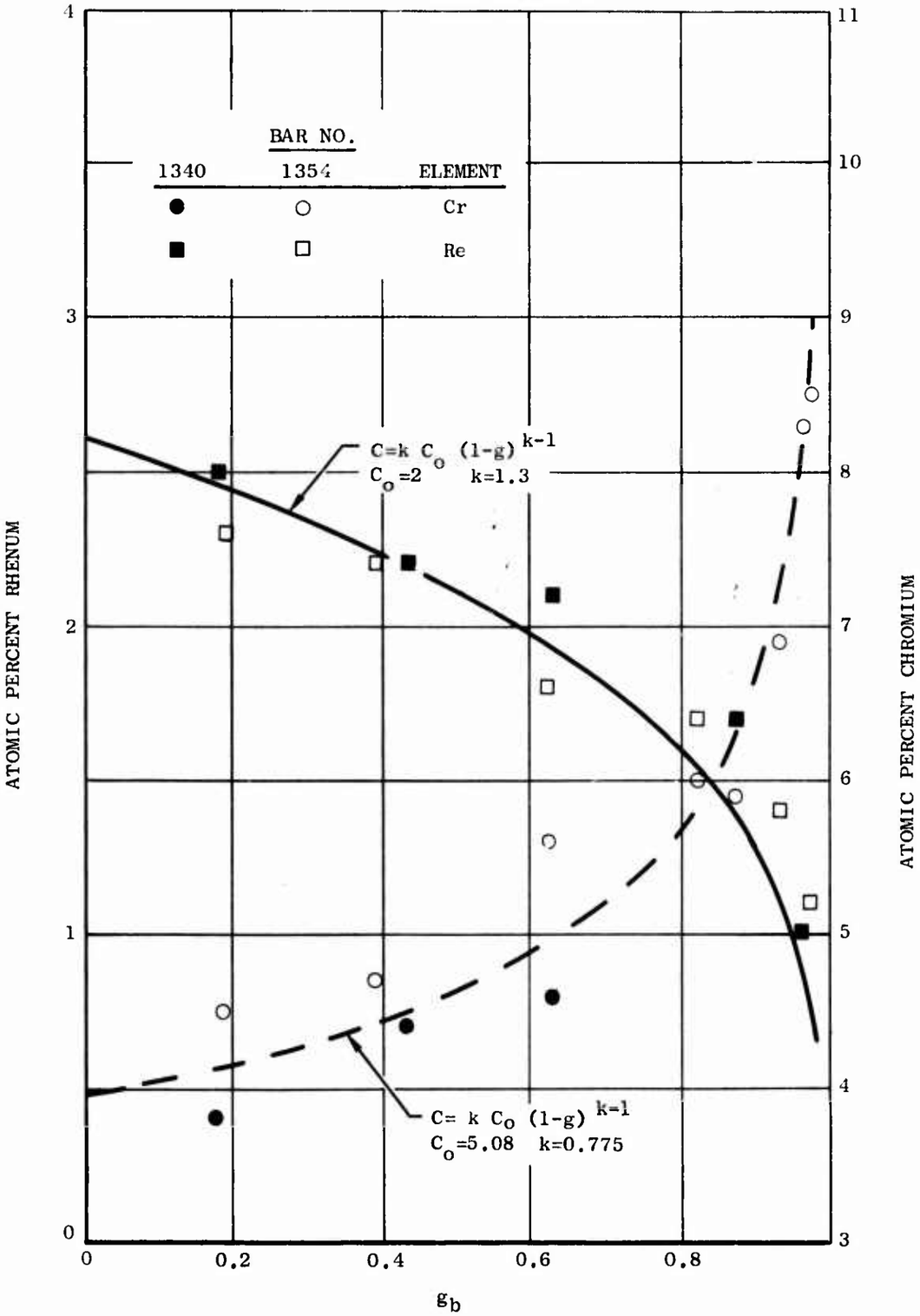

Figure 12. Composition Profiles for Re and Cr in NiTaC-13, Compared with Theoretical Curves for Normal Freezing

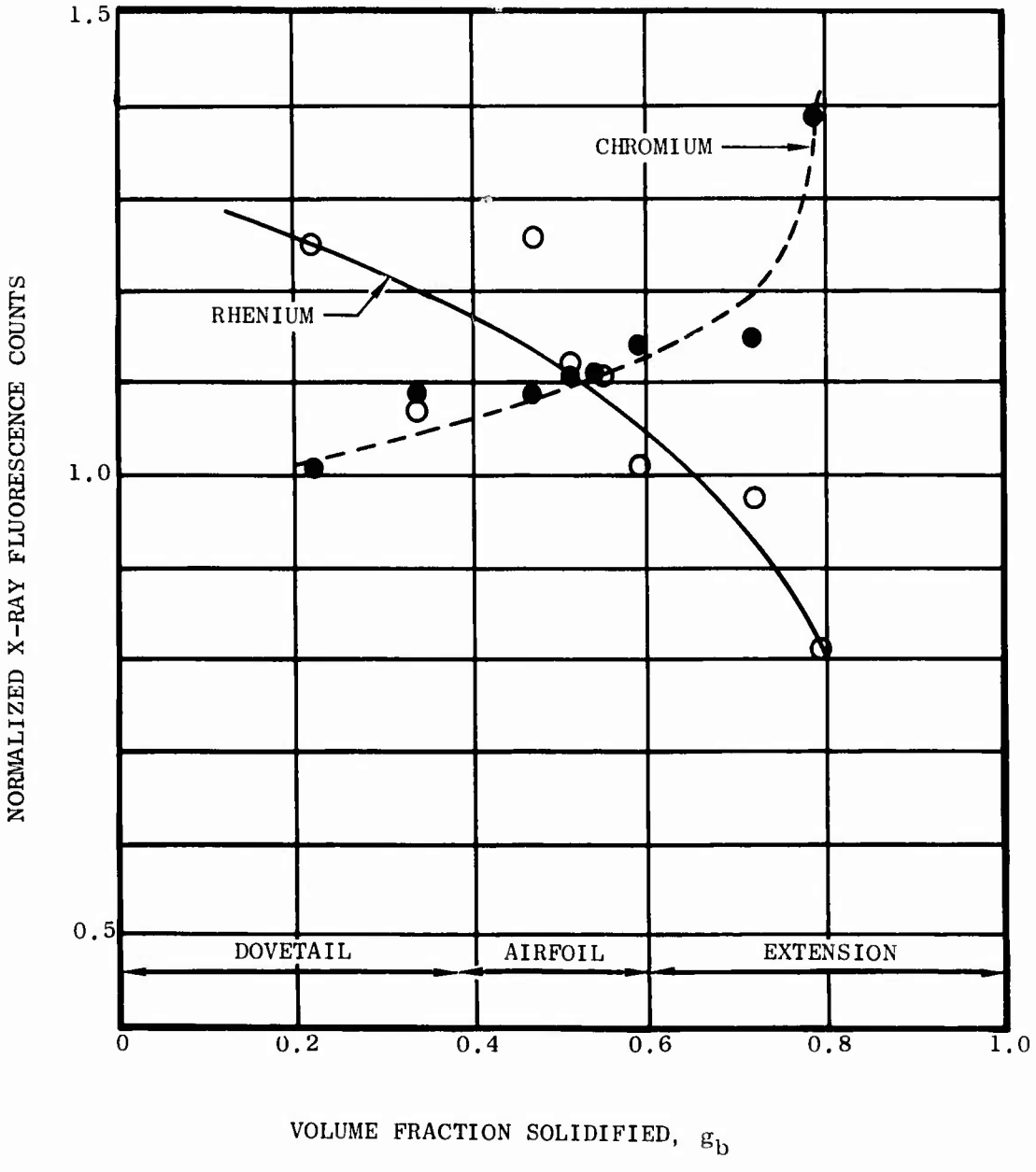

Figure 13. Re and Cr Segregation in PFS NiTaC-13 Blade Casting, LB 86

2.4.3 Segregation in Carbide-Free NiTaC-13 Matrix

The average matrix composition of NiTaC-13 was estimated by subtracting the composition $Ta_{.75}V_{.25}C$ from the NiTaC-13 composition with the following result, in atom percent: Ni-3.53Co-5.34Cr-12.62Al-1.06W-2.10Re-6.30V-0.93Ta. For this evaluation, bar DS 1414 of the matrix composition was solidified at 1/4 inch/hour and sections at various g_b locations were chemically analyzed. From inspection of the data presented in Table 5, it can be seen that the same type of segregation observed in NiTaC-13 occured in the matrix alloy; however, the Ta segregation curve in the matrix alloy changed to a form similar to that shown for Cr in Figure 12.

TABLE 5

CHEMICAL ANALYSIS OF NiTaC-13 MATRIX ALLOY AFTER PFS

	Atom Percent							
g_b	Ni	Co	Cr	Al	W	Re	V	Ta
.11	68.2	4.4	3.6	12.0	1.3	2.8	7.3	0.5
.20	69.1	3.5	4.4	11.7	1.3	2.6	6.9	0.6
.39	68.3	4.6	4.1	11.7	1.1	2.5	6.9	0.6
.58	68.4	4.5	5.5	11.7	1.1	2.2	5.8	0.8
.77	68.7	3.2	5.6	12.2	1.3	1.7	6.3	1.0
.87	68.7	3.6	7.9	11.3	1.0	1.4	4.7	1.4
.91	69.0	3.2	8.0	10.8	1.0	1.1	5.0	1.9
.95	69.2	2.7	9.1	11.0	0.9	0.8	4.1	2.2

A further comparison of NiTaC-13 with the matrix alloy was made by subtracting the composition $Ta_{.75}V_{.25}C$ from the previous chemical analysis data for NiTaC-13 in Table 4. The results for Re and Cr, shown as graphs of composition versus g_b in Figures 14 and 15, respectively, are in good agreement with the corresponding data for the PFS matrix alloy and with the theoretical curves for normal freezing, also shown in the figures. On the basis of these results, it was concluded that segregation in NiTaC-13 was closely related to segregation in the matrix. The conclusion that g_b, the volume fraction solidified, is the parameter governing segregation was further supported by the fact that the matrix bar, DS 1414, was only 4 inches long whereas the NiTaC-13 data used to estimate matrix composition were obtained from an 8-inch long bar.

2.4.4 Effect of Segregation on Stress-Rupture Strength

Previous work described in Section 2.3, showed that segregation from bottom of top of bars was accompanied by a reduction in 1800°F rupture strength. To evaluate this effect in more detail, tests were performed with NiTaC-13 from several 7/8 inch diameter bars, 3.5 inches or 8 inches long. Specimens were machined from bottoms and tops of the bars to have gage section centers at g_f values of 0.15 and 0.67, respectively. In this case

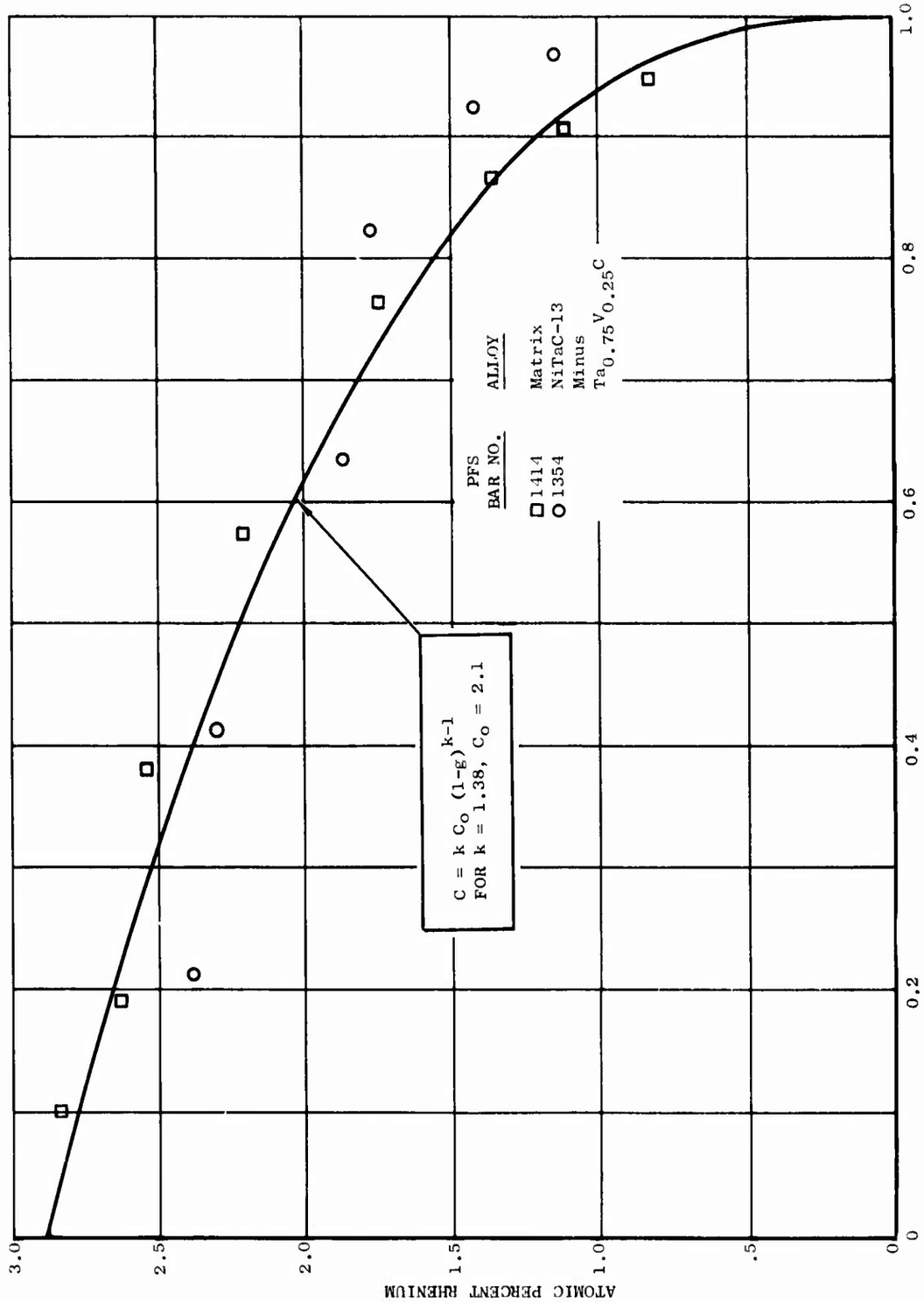

Figure 14. Re Segregation in NiTaC-13 Matrix Compared to Theoretical Curve for Normal Freezing

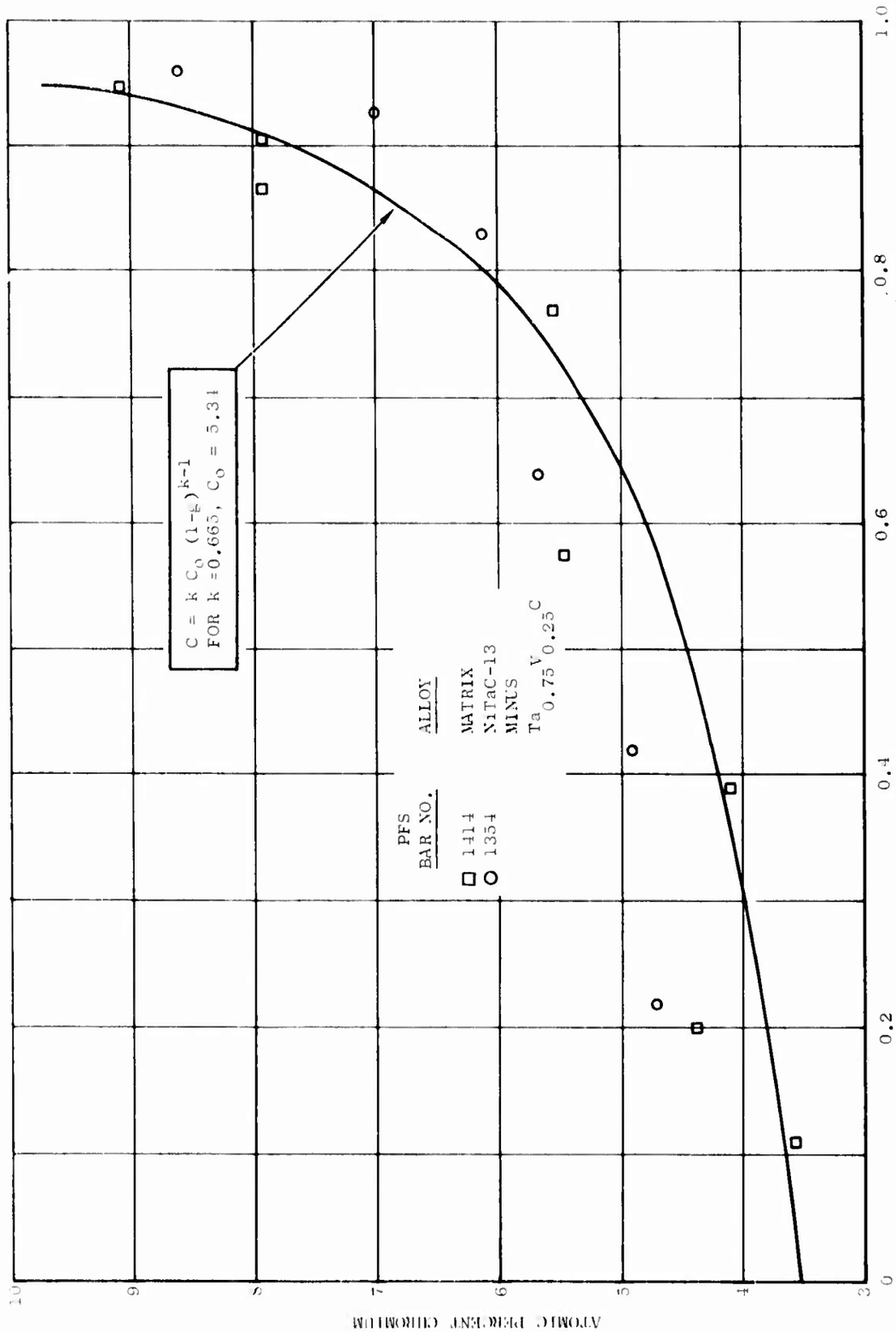

Figure 15. Cr Segregation in NiTaC-13 Matrix (see Text) Compared to Theoretical Curve for Normal Freezing

volume fraction solidified (g_t) was calculated on the basis of the volume of liquid metal present at the start of aligned fiber growth (top of sort-out zone). Stress rupture tests were performed in air at temperatures ranging from 1600° to 2000°F and stresses ranging from 80 to 10 ksi. The specimens had a nominal 0.375 inch gage length and a 0.100 inch gage diameter.

The stress rupture data are given in Table 6. Separate regression analyses were performed with the data for bottom and top specimens, resulting in the following equations:

PFS Bar Location	g_t	No. of Tests	Equation
Bottom	0.15	12	$P_B = 57.25 - 0.213OS + 8.259 \times 10^{-4}S^2$ (6)
Top	0.70	14	$P_T = 57.22 - 0.27225 + 1.423 \times 10^{-3}S^2$ (7)

where P = Larson-Miller Parameter x 10^{-3} with a constant of 20, T in °R, and t in hours

S = stress in ksi

The data from Table 6 are presented in Figure 16 together with curves calculated with equations (6) and (7). The regression analyses gave good fits to a Gaussian distribution and yielded ± 3 σ deviations of ± 0.49 for equation (6) and ± 0.53 for equation (7). A scatter band of ± 3 σ for a Gaussian distribution includes 99.7% of all data points. These equations apply only for short time air tests in the stress range of 10 to 80 ksi.

The segregation effect was evaluated further as part of a separate General Electric program in which rupture specimens were machined from a 1-1/2 inch diameter NiTaC-13 bar, DS 1632, to have g_t values in the center of the gage section ranging from 0.1 to 0.7 in steps of 0.1. Sets of specimens were tested at 1600°F/74 ksi in air and at 2000°F/20 ksi in argon to avoid complications that could be caused by oxidation. The test results, presented in Figure 17, show a strong dependence of rupture life on g_t. The fractional loss in life due to an increase in g_t from 0.1 to 0.7 was greater at 2000° than at 1600°F, possibly due to a larger contribution of fiber strengthening to the total strength at 2000°F.

2.4.5 Minimization of Segregation

On the basis of the various studies just discussed, the reason for segregation (chemistry gradients) in TiTaC-13 is considered well understood: it is due to normal freezing of an alloy that has a freezing range, and segregation cannot be eliminated. However, consideration of equation (5) showed that segregation can be minimized in castings by operating in the regime of low g_b values. This is a practical approach because, as illustrated in Figures 12 and 13, severe segregation occurs only at very high values of g_b, above 0.7 and 0.8. Hence, in order to minimize segregation in a casting such as the J101 LPT blade, it is necessary to maximize the ratio of liquid to solid metal present when the casting is completed. This requires the presence of a molten metal reservoir above the casting. The reservoir, however, need not be PFS: it can be quickly frozen and will not add to the total PFS casting time, but will add to scrap.

TABLE 6

STRESS-RUPTURE DATA FOR BOTTOM AND TOP MATERIAL FROM PFS NiTaC-13 BARS

Bar No.	Spec. No.	Stress, Ksi	Temp., ^{o}F	Life, Hrs.	$10^{-3} xP_{20}$ (^{o}R, hr.)
BOTTOM SPECIMENS, g_t = 0.15					
1284	1007	44	1800	77.4	49.47
1284	1008	44	1800	92.0	49.64
1340	1027	19	1950	137.0	53.35
1340	1028	77	1600	169.3	45.79
1354	1038	13.5	2000	146.0	54.52
1354	1039	40	1800	133.1	50.00
1354	1040	78	1600	178.8	45.84
1284	1052	12.5	2000	184.7	54.78
1284	1053	75	1600	124.8	45.52
1395	1074	13.5	2000	164.3	54.65
1395	1075	78	1600	165.8	45.77
1449	1097	44	1800	78.0	49.48
TOP SPECIMENS, g_t = 0.67					
1284	1009	44	1800	20.6	48.17
1288	1019	17.5	1950	96.5	52.98
1288	1021	52.5	1700	47.6	46.82
1288	1022	75	1600	56.5	44.81
1340	1029	19	1950	68.0	52.62
1340	1030	77	1600	43.0	44.56
1354	1041	10.5	2000	132.2	54.42
1354	1042	34	1800	53.8	49.11
1354	1043	68	1600	115.5	45.45
1284	1054	10.5	2000	168.6	54.68
1395	1076	10.5	2000	136.0	54.45
1395	1077	68	1600	93.9	45.26
1449	1098	44	1800	20.8	48.18
1450	1100	44	1800	17.0	47.98

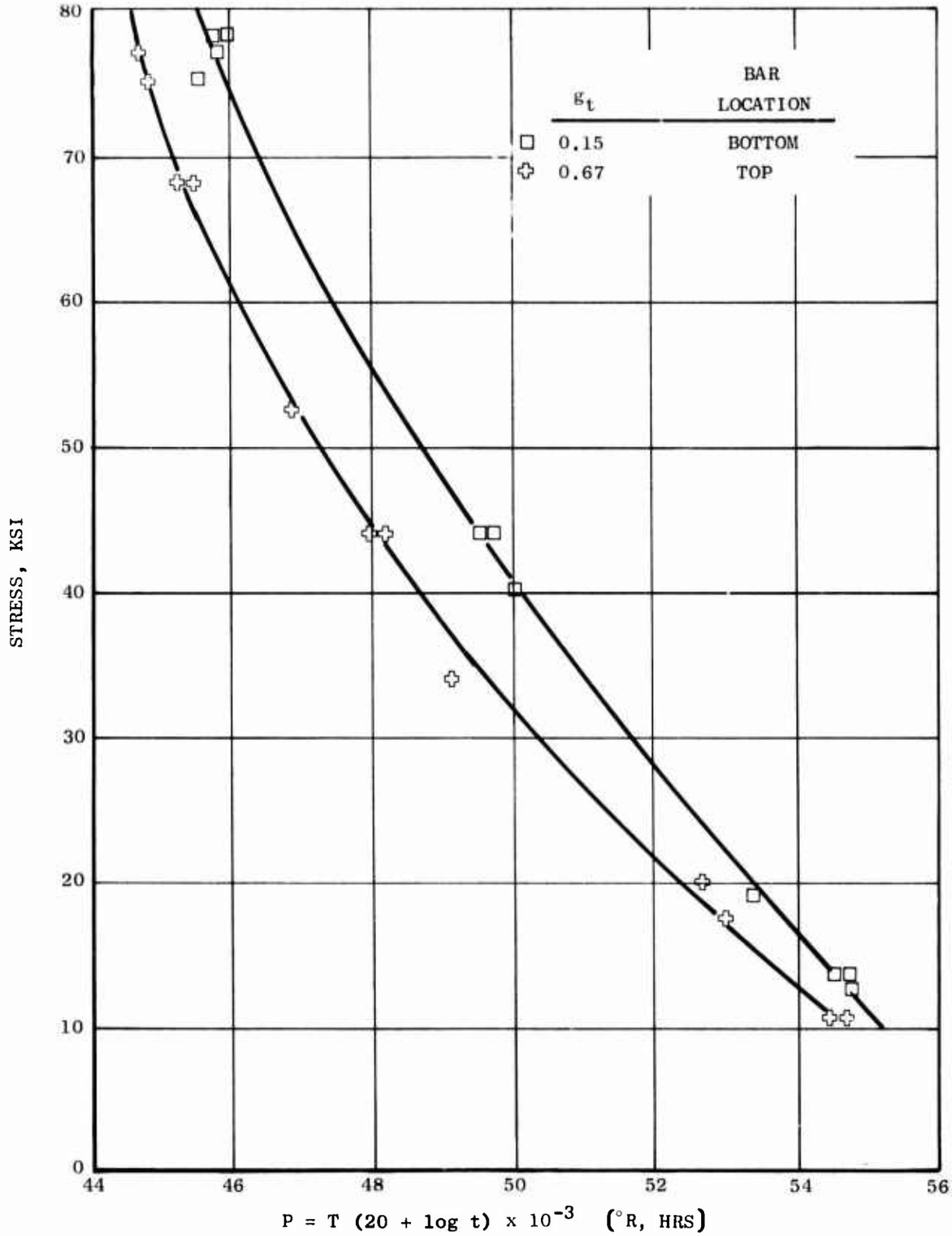

Figure 16. The Effect of Segregation on the Rupture Strength of PFS NiTaC-13

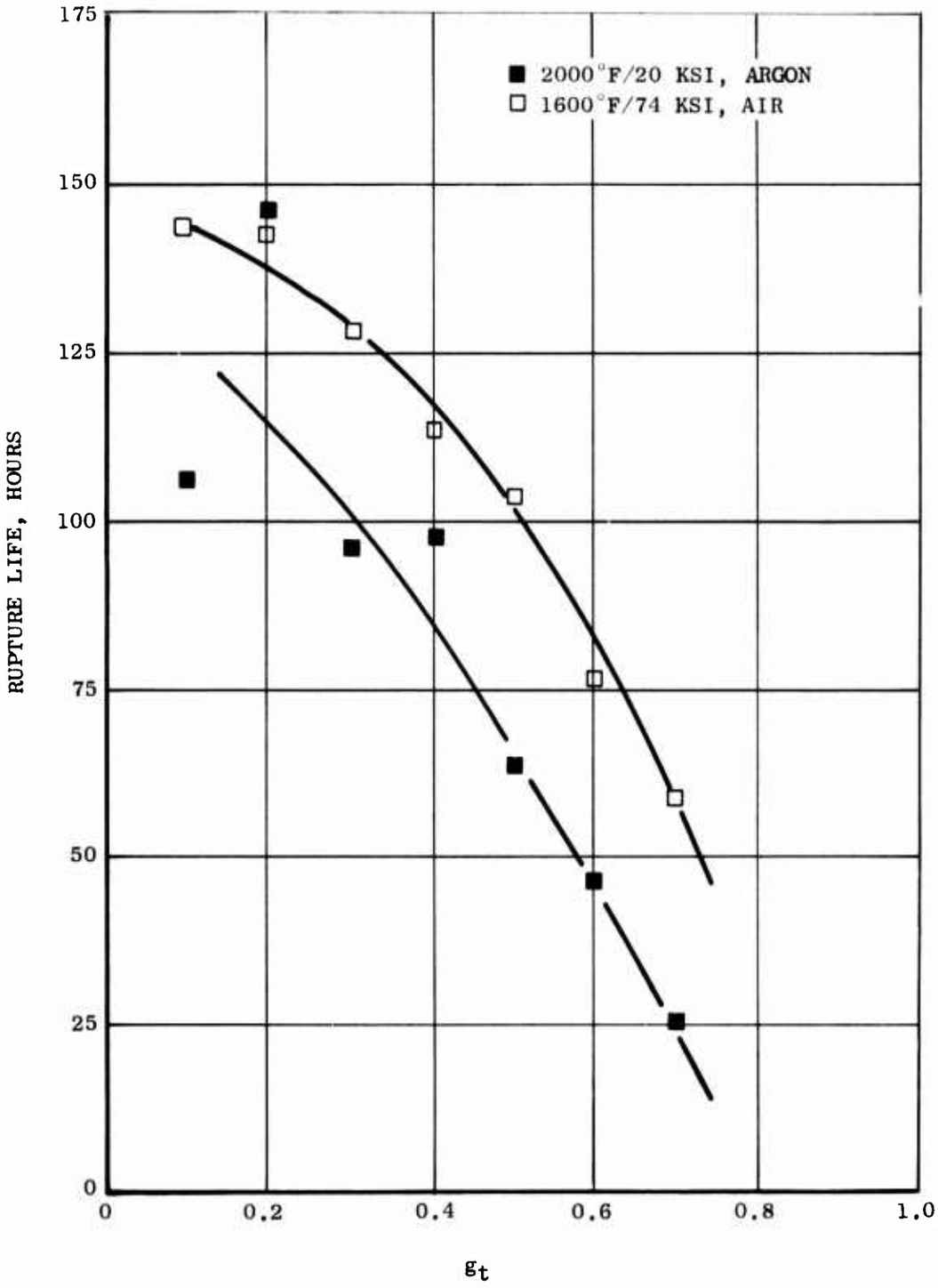

Figure 17. The Effect of Segregation on 1600° and 2000°F Rupture Life of PFS NiTaC-13

To aid in maximizing the size of the liquid metal reservoir in a furnace of fixed height, it is very desirable to reduce the amount of metal at the bottom of the casting that must be discarded because it does not contain aligned fibers for the following reasons:

1) In the case of in situ melting, some alloy at the bottom of the crucible or mold does not melt. In the case of pouring liquid metal into a hot mold, some of the alloy is chill cast. In both cases the solid alloy present before mold withdrawal commences must be discarded.

2) Prior to withdrawal and after withdrawal is initiated, nonfibrous MC carbides are precipitated as the chemistry of NiTaC-13 self adjusts to the proper eutectic composition. This region containing precipitated hypereutectic carbide is the sort-out zone. After this adjustment in composition is completed, aligned fiber growth begins. The sort-out zone must also be discarded.

The basic methods for reducing the amount of unmelted alloy or chill cast metal, include raising the initial position of the mold or crucible bottom with respect to the furnace bottom and increasing the ratio of the heat input rate to the heat withdrawal rate.

The method for reducing the amount of alloy wasted due to sort-out is to modify the alloy composition to the average of that which exists in liquid NiTaC-13 when fiber growth begins. Development of a NiTaC-13 modification was undertaken in a separate internally funded GE program. The modified alloy, NiTaC-13F, did eliminate the sort-out zone and was considered for use in the program. However, this change was not incorporated because there was insufficient time in the schedule to permit an adequate evaluation of the modified alloy properties to make certain that there would be no risk to the program. This general approach to optimization of NiTaC alloy compositions is sound and should be incorporated into future development of improved alloys.

2.5 TEST BAR CASTING DEVELOPMENT

To reduce the total time needed to cast the NiTaC-13 required for data acquisition, it was decided to scale-up the small bar process to one capable of producing 1-5/8 inch diameter bars. This large bar also represented a back up position because J101 LPT blades could be machined from them in the event that blade casting process development was unsuccessful.

The goals established for the test bars included:

- Fully aligned carbide fiber section $\geq$ 4-1/2 inches long
- Life of $\geq$ 50 hours in stress-rupture tests at 1800°F/44 KSI in air of material from the bottom half of aligned fiber sections.

A further requirement of the bar process was that it must be similar to the blade process so that material from the two processes would be equivalent in microstructure and rupture strength. These equivalencies would add confidence to the assumption that property data obtained with bar material was applicable to blade castings.

2.5.1 Test Bar Casting Facilities

During the course of the program, three General Electric PFS facilities, designated B, M and 3B were used. Facilities B and M were similar and consisted of a controlled atmosphere chamber, a molybdenum-wound resistance heated furnace, a water chill system, and a screw drive withdrawal mechanism. The furnace and chill system are illustrated in Figure 18. In both facilities, bars were cast individually.

Facility 3B was larger and capable of casting three bars simultaneously through the use of three furnaces similar to those used in B and M, and a common screw driven withdrawal mechanism.

2.5.2 Preliminary Test Bar Furnace Configuration Development

At the start of the program, Facility B was available for preliminary experiments while modifications to it were in progress and Facility 3B was being designed. The objective of the experiments was to identify approximate PFS parameters required for scale-up to 1-5/8 inch diameter bars. In subsequent work the process parameters were to be refined.

2.5.2.1 Experimental Approach - Different furnace configurations were designed, constructed and evaluated by means of casting trials in Facility B in which the three major PFS parameters, T_{max}, G_L and R, were varied. Features of the furnace in Figure 18 that were varied to comprise a furnace configuration included: heater design, furnace bottom insulation and radiation shield, furnace side insulation, furnace top insulation, and furnace lid. The bottom and side chills were never changed. Casting trials were made using 1-1/2 to 1-5/8 inch diameter recrystallized alumina crucibles (with bottoms) and NiTaC-13 or NiTaC-7. The latter was selected for some of this work because it is similar to NiTaC-13 but substantially lower in cost because it does not contain rhenium. Attempts were made in most runs to measure T_{max} and G_L. After the casting runs, bars were evaluated for microstructure and density and, in the later stages of this preliminary work, for stress-rupture properties.

2.5.2.2 Series 1 Casting Runs - The first of two series of trial casting runs involved 19 runs in five furnace configurations, A through E, inclusive. Details of these configurations are presented in Table 7 and details of the furnace heater designs using 0.04 inch diameter molybdenum wire are shown in Figure 19.

Several types of power supplies and controls to be described briefly later were used for the furnace heaters. During casting runs, water flow rates were held constant at 15 and 5 gals/hr for the side and bottom chills, respectively. These flow rates were sufficient to maintain cooling water temperatures below 90°F.

For each run, the alloy charge was loaded into the crucible and raised into the cold furnace. The tank was then closed and flowing argon was circulated through it. Next, the furnace was brought to temperature and the alloy was melted in situ. After this and prior to withdrawal, the axial temperature profile of the liquid metal was measured by means of an

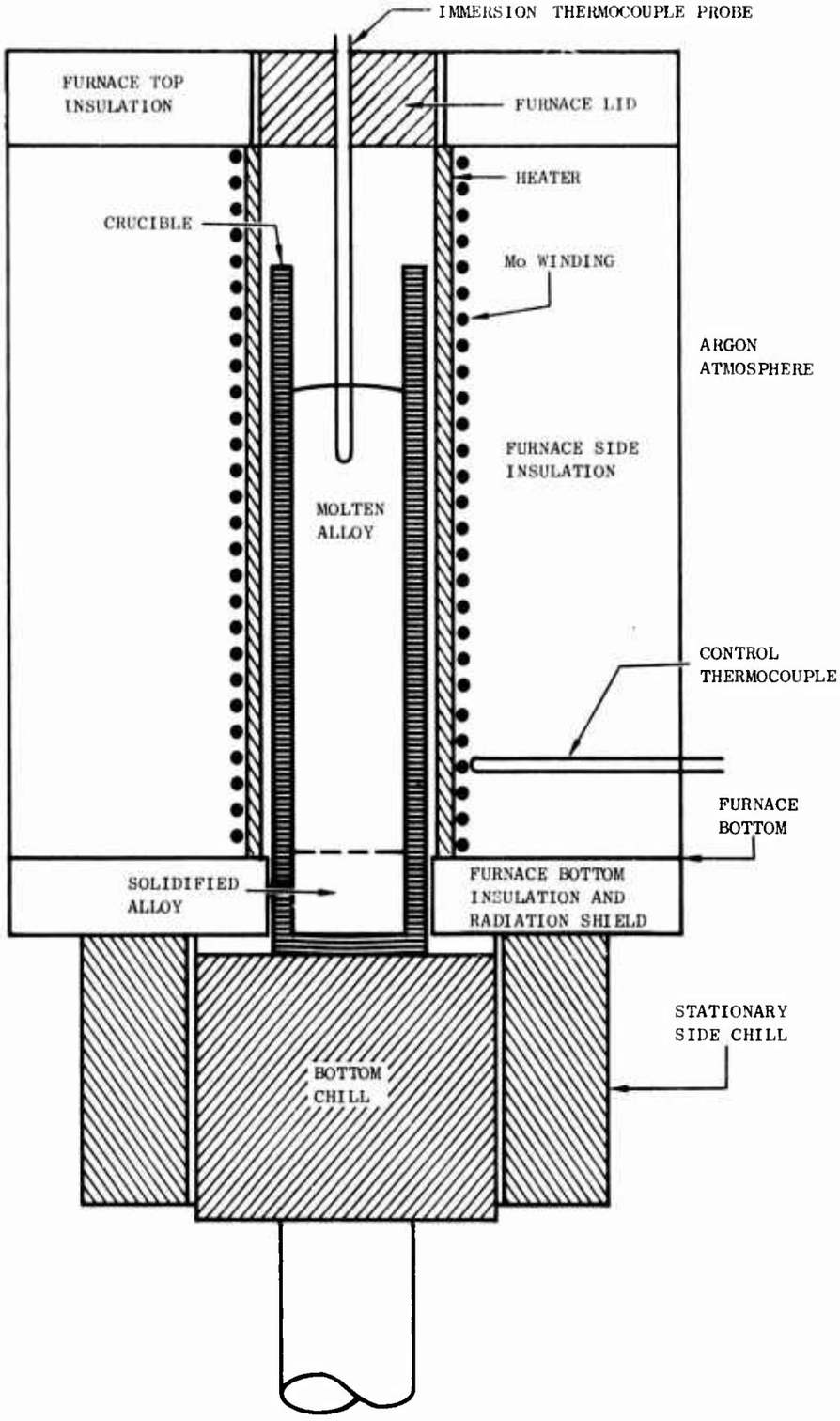

Figure 18. Schematic View of PFS Furnace in Facility B

TABLE 7

DETAILS OF FURNACE CONFIGURATION USED IN TEST BAR PROCESS DEVELOPMENT

Furnace Component	Configuration Designation A	B	C	D	E	F
Heater Type (See Figure 19)	H-1	H-1	H-1	H-2	H-3	H-4
Furnace Lid Insulation						
Material	None	None	Kao-Lite	None	None	None
Thickness, Inches	---	---	1-3/4	---	---	---
Furnace Top Insulation						
Material	None	None	Kao-Lite	Kao-Lite	WRP-H	WRP-H
Thickness, Inches	---	---	1-3/4	1-3/4	1/2	1/2
Furnace Side Insulation						
Material	Kao-Lite	Kao-Lite	Kao-Lite	Kao-Lite	WRP-H	WRP-H
Thickness, Inches	2-3/8	3-1/3	3-1/3	1-3/4	1/3-4	1-3/4
Furnace Bottom Insulation						
Material	Kao-Lite	BN + Kao-Lite	Composite*	BN	BN + Fiberfrax**	BN + Fiberfrax**
Thickness	1/2	1/2	1/4	1/8	3/8	3/8
Mold/Radiation Shield						
Clearance, Inches	1/32	1/32	1/32	1/32	1/16	1/16

* 1/8" thick BN + Kao-Tab on each side + Fiberfrax layer on each side
** 1/8" thick BN insert in 3/8" thick Fiberfrax pad

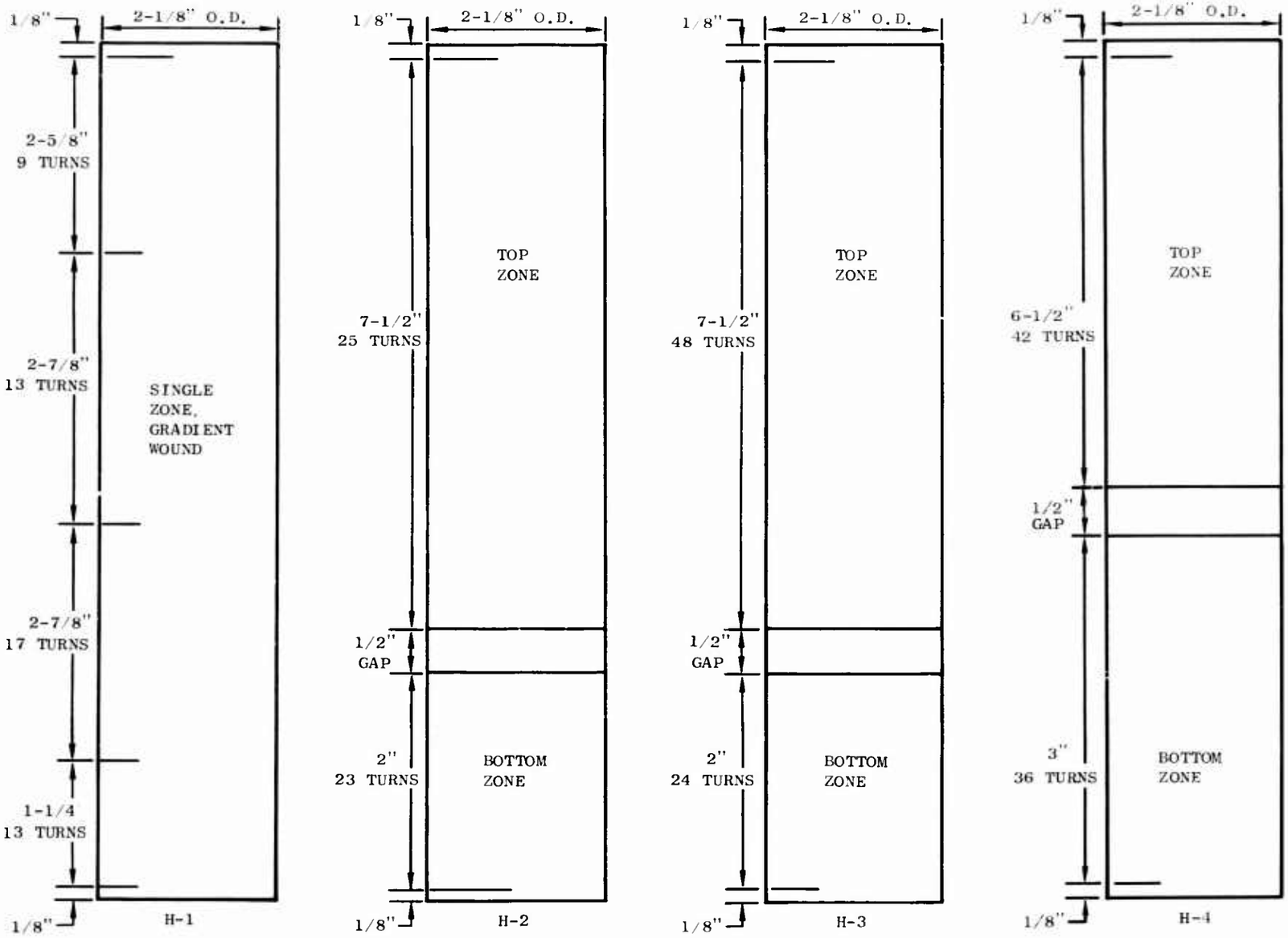

Figure 19. Furnace Heater Designs

immersion thermocouple (Ir/Ir-40Rh) probe. The closest approach of the thermocouple bead to the liquid/solid interface was about 1/16 inch, which was the average thickness of the plasma sprayed alumina layer used to protect the thermocouple tip. Following temperature measurements, the intent in every run was to withdraw the crucible at 1/4 inch/hour, which is the rate normally used to obtain the aligned carbide fiber microstructure in both NiTaC-7 and NiTaC-13. Many runs were not completed, due to problems encountered with various furnace configurations and crucible breakage.

Additional details of the first set of runs, presented in Table 8, show that withdrawal was successfully completed in eight of the 19 runs. Temperature profiles for these eight runs are shown in Figure 20, and are compared with results shown previously, Figure 7, for the 1/2 inch diameter facility at a power level of 1260 watts. For each curve, only the measurement point closest to the liquid/solid interface is shown. The results in Figure 20 and Table 8 showed that, in all large diameter bar runs, T_{max} and G_L were substantially lower than in the 1/2 inch diameter bar facility. The results will be discussed further according to furnace configuration.

(1) Furnace Configuration A - As shown in Table 8 for Run 1, G_L was only slightly above the estimated minimum value of 250°F/in. required for PFS of NiTaC-13 at 1/4 inch/hour, but the microstructure was poor. Other reasons assigned to the poor result included:

- Poor quality of the NiTaC-13 used in the first six runs.
- Inadequate control of power and temperature. These runs were made before installation of control thermocouples; hence, power disturbances or changes would not be corrected.
- Possible mechanical disturbances to equipment or crucible during withdrawal.

(2) Furnace Configuration B - Only Run 2 was completed with this configuration. A much higher G_L was achieved with the same furnace heater used in Run 1, but the result was poor and attributed to the same causes assigned to Run 1, except G_L.

(3) Furnace Configuration C - No runs were successfully completed with this configuration due to problems with the power supplies.

(4) Furnace Configuration D - The main features of this configuration included: first, the use of a fiber cloth insulation, Type WRP-H manufactured by Refractory Products Co., and; second, improvements in the power supply noted in Table 8. The new type of insulation was extremely efficient, permitting the attainment of high temperatures at relatively low power levels.

TABLE 8

SUMMARY OF SERIES 1 PRELIMINARY CASTING RUNS AT 1/4 INCH/HOUR WITHDRAWAL RATE

Run No.	Furnace Config.	Heater Type	Furnace No.	Charge NiTaC No.	Charge Wt., Lbs.	Type Power Supply†	Initial Conditions Total Heater Power, Watts	Initial Conditions T_{max}, °F	Initial Conditions G_L, °F/In.	Bar Microstructure
1	A	H-1	1	13*	2.0	I	2040	2960	265	Cells/Dendrites
2	B	H-1	1	13*	3.4	I	2240	3130	390	Fibers/Cells
3	B	H-1	1	13*	2.3	I	2355	3200	---	----
4	C	H-1	2	13*	3.6	I	2095	3090	305	----
5	C	H-1	2	13*	4.0	I	2250	---	---	----
6	C	H-1	3	13*	3.0	II	1600	---	---	----
7	D	H-2	4	7	3.8	II	1370	2850	225	----
8	D	H-2	5	7	3.9	II	390	---	---	----
9	D	H-2	6	7	3.8	II	335	---	---	----
10	D	H-2	7	7	3.8	III	1230	---	---	----
11	D	H-2	8	7	3.8	III	---	2870	170	----
12	E	H-3	9	7	3.8	IV	920	2920	360	----
13	E	H-3	10	7	3.8	IV	760	2980	295	Excellent Fibers - No Bands
14	E	H-3	11	7	3.9	IV	725	2820	205	Fibers/Cells/Bands
15	E	H-3	11	13	4.0	IV	780	2930	295	Fibers/Cells/Bands
16	E	H-3	11	13	4.0	IV	860	2980	275	Excellent Fibers/Bands
17	E	H-3	11	13	4.0	IV	930	3005	315	Excellent Fibers/Bands
18	E	H-3	11	13	4.0	IV	1020	---	---	----
19	E	H-3	12	13	4.0	IV	1090	3060	330	Excellent Fibers - No Bands

* Scrap NiTac-13

† Type Power Supply
- I Variac with constant setting - no temperature control
- II Industrial Research SCR's running off 220 volt supply from variac
- III West, Type JAD SCR's running off 220 volt supply from variac
- IV West, Type JAD SCR's running directly from 120 volt/20 ampere line

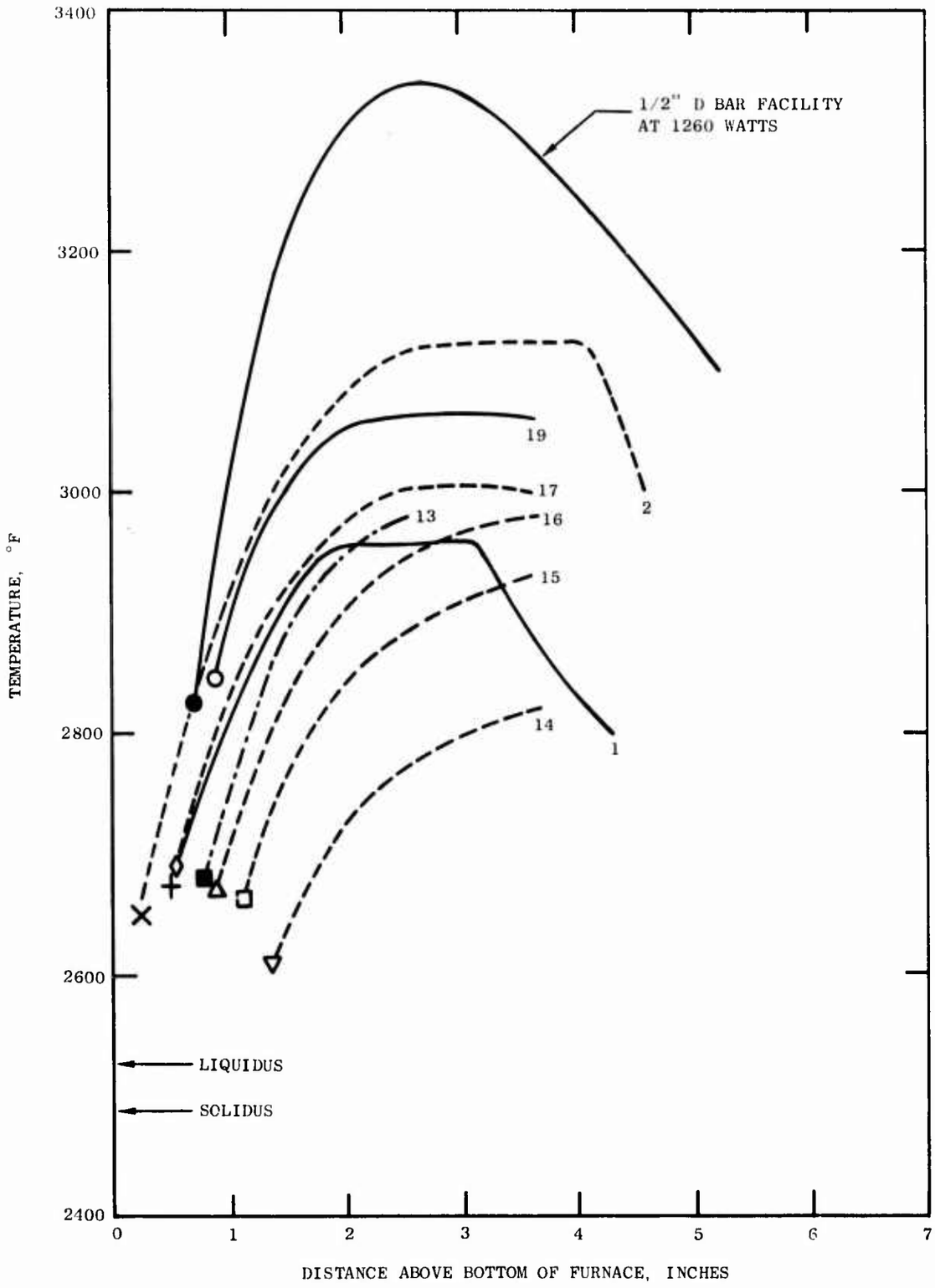

Figure 20. Liquid Metal Temperature Profiles in Series 1 Preliminary Casting Runs

A total of six runs were successfully completed with this furnace configuration. Run 13, made with NiTaC-7 was very successful in that a well aligned microstructure free of misaligned fiber bands was obtained. Bands will be discussed in detail in Section 2.6. Run 14 with NiTaC-7, purposely made at a lower gradient, resulted in a poor microstructure.

Subsequent runs were all made with NiTaC-13 at progressively increasing power input levels with accompaning increases in T_{max} and G_L. Runs 16 and 17 produced acceptable fibers, but there were numerous misaligned fiber bands.

Investigations into the cause of bands indicated that they could have been caused by mechanical disturbances such as movements of the crucible. Therefore, in Run 19 steps were taken to prevent movement of the crucible. Also, the power input was further increased to increase T_{max} and G_L. As shown in Figure 20, the temperature profile was nearly equivalent to Run 2. However, the bar produced in Run 19 contained about a five-inch length of well aligned fibers and was completely free of bands.

As a result of the first series of runs, a furnace configuration and approximate PFS process parameters were identified for producing large diameter bars with aligned fibers. Although G_L was substantially lower than that achieved in the 1/2 inch diameter bar facility, it was adequate for PFS of NiTaC-13 at 1/4 inch/hour and at a substantially lower T_{max}.

2.5.2.3 Series 2 Casting Runs - The objectives of this series of runs in Facility B were to evaluate configuration E and a new F configuration in detail, and to select a final configuration for process refinement work. As shown in Table 7, configuration F differed from E only in the heater design illustrated in Figure 19.

Fourteen runs were made using procedures similar to those used in Series 1, with the following exceptions: First, the withdrawal rate for two runs was 3/8 instead of 1/4 inch/hour, and; second, liquid metal temperature profiles were measured after 4 inches of withdrawal in several runs. The results of the runs are presented in Table 9 where it can be seen that only seven runs were completed. Reasons for incompleted runs included: crucible breakage, heater failure, or crucible sticking to the heater tube or radiation shield.

By referring to Table 8 and 9, it can be seen that one excellent bar (Run 19) was produced with configuration E and two excellent bars (Runs 39 and 49), with configuration F. In all three runs, the length of aligned fibers was at least 4-1/4 inches. It was also noted that banding continued to be a problem and was assumed due to small clearances between the crucible and furnace bottom insulation that caused rubbing, crucible vibration, and band formation.

TABLE 9

SUMMARY OF SERIES 2 PRELIMINARY CASTING RUNS

Run No.	Furnace Config.	Heater Type	NiTaC No.	Wt., Lbs	*Type Power Supply	Initial Conditions: Total Heater Power, Watts	Initial Conditions: T_{max}, °F	Initial Conditions: G_L, °F/In.	Initial Conditions: R, In/Hr	Bar Microstructure
20	E	H-3	13	5.5	IV	1198	>3100	315	-	Crucible Broke
21	E	H-3	13	5.5	IV	1022	-	-	-	Crucible Broke
22	E	H-3	13	4.4	IV	755	3045	250	1/4	Crucible Stuck
26	E	H-3	13	5.0	IV	870	-	-	1/4	Heater Failure
29	E	H-3	13	4.9	IV	870	-	-	1/4	Fibers, Bands, Heater Failure
36	E	H-3	7	4.8	IV	820	-	-	1/4	Fibers, Bands
37	E	H-3	13	5.0	IV	940	-	-	1/4	Fibers, Bands
38	F	H-4	7	-	IV	880	3025	315	1/4	Fibers, Heater Failure
39	F	H-4	13	4.9	IV	815	3050	330	1/4	Excellent Fibers
40	F	H-4	13	5.0	IV	840	-	-	-	Crucible Broke
41	F	H-4	13	4.9	IV	795	3075	325	1/4	Crucible Stuck
43	F	H-4	13	4.9	IV	780	3060	260	3/8	Fibers, Crucible Stuck
46	F	H-4	13	-	IV	870	3020	315	3/8	Cells
49	F	H-4	13	-	IV	820	-	-	1/4	Excellent Fibers

* Refer to Table 8 Footnote

To evaluate the stability of T_{max} and G_L during withdrawal, temperature profiles were measured in Runs 38 and 39 before the start of withdrawal and after crucible had been withdrawn 4 inches. The results were similar in the two runs, and those for Run 38 are presented in Figure 21. As shown, T_{max} decreased by about 100°F during the 4-inch withdrawal, but there was only a small decrease in G_L. Two reasons for the decrease in T_{max} were: first, the silicon controlled rectifiers (SCR) were operating on thermocouple control, but the power band width was set too low to meet the power demands and; second, the heat input/heat withdrawal ratio was decreased by the decreasing volume of liquid metal during withdrawal. As can be determined from data in Figure 21, a 10 percent increase in total power to the furnace heater restored the temperature profile and G_L to the original level.

In subsequent runs, the SCR power band widths were progressively increased. Results of temperature profile measurements at different withdrawal positions in Run 46 are presented in Table 10. These results show that, although T_{max} decreased by about 120°F during 7 inches of withdrawal, both G_L and the position of the liquid/solid interface remained essentially constant. These results were similar to those described for the 1/2 inch diameter bar facility in Section 2.3.4.

As a final consideration in the selection of the furnace configuration, data from Tables 8 and 9 are shown in Figure 22 as a graph of T_{max} versus G_L. The dotted line suggests that there was a strong direct relationship, in agreement with theory discussed in Section 2.1. Most points fall within ± 20 percent of the line drawn. Through study of the data points, it was concluded that the furnace configurations evaluated played a minor role and that the most important parameter was T_{max}. The data in Figure 22 further indicated that the desired minimum G_L of 300°F/inch could be achieved with a T_{max} of about 3000°F.

After reviewing all results, furnace configuration F was selected for process refinement work for the following reasons:

1) Essentially perfect PFS bars were produced with configurations E and F.

2) The heater life with configuration F was about double that with configuration E.

3) The use of two-zone heaters offered more flexibility in shaping temperature profiles than the single-zone gradient wound heater, H-1, that was used in configurations A, B and C. The attainable temperature profile with the H-1 type heater is largely fixed by the design.

4) The WRP-H insulation used in configurations E and F offered two substantial advantages over the Kao-Lite insulation: first, the furnace construction was simpler and; second, the WRP-H was a more efficient insulation and allowed the attainment of high temperatures with greatly reduced power requirements over the Kao-Lite insulation.

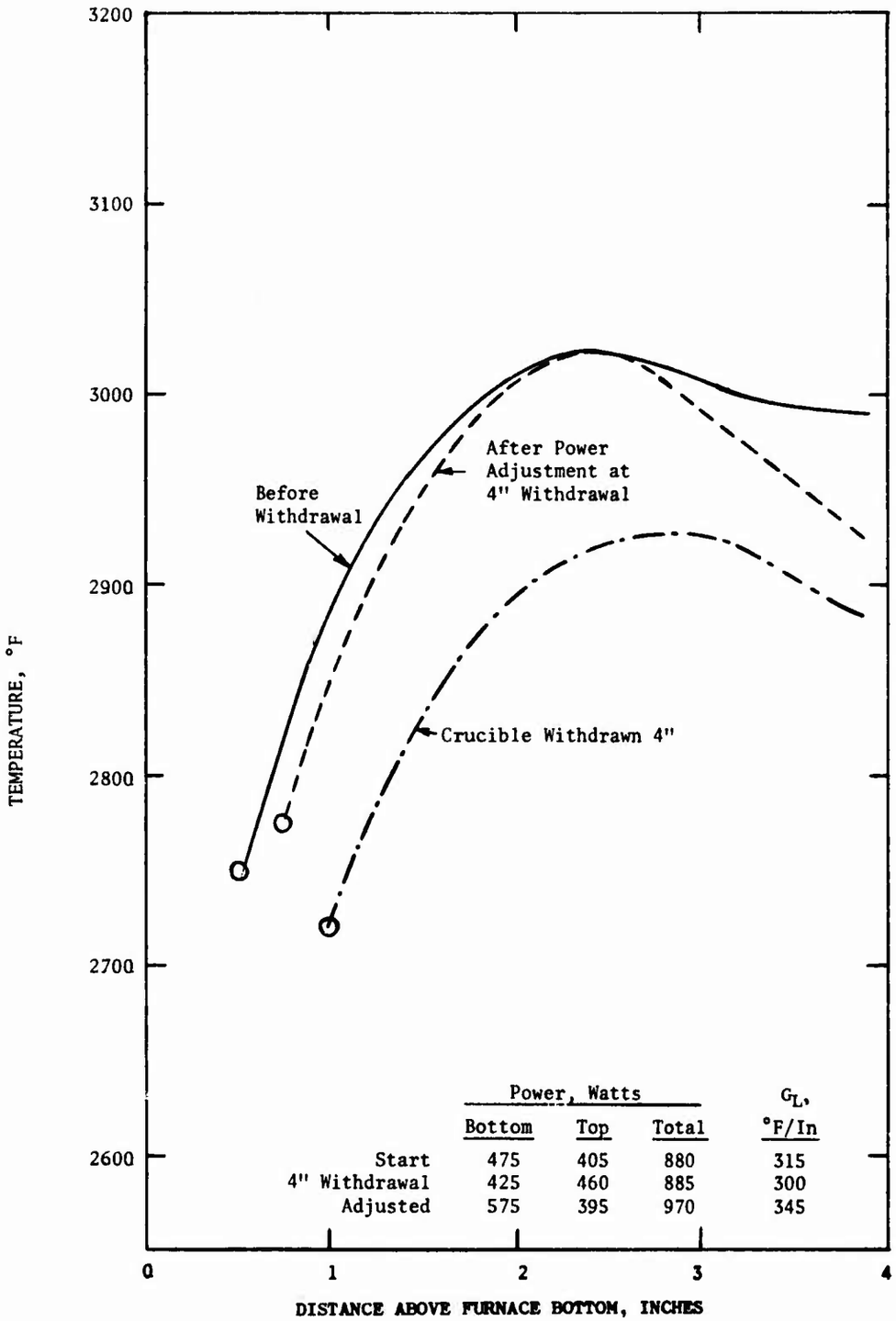

Figure 21. The Decrease in Temperature Profile and G_L in Run 38 After Crucible was Withdrawn 4 Inches, and Power Increase Required to Return Approximately to the Initial Temperature Profile. Furnace Configuration F

TABLE 10

EFFECT OF CRUCIBLE POSITION ON PFS CONDITIONS DURING RUN 46

*Crucible Position, Inches	Power Input, Watts			+Height of Liquid/Solid Interface Above Furnace Bottom, Inc.	Max. Metal Temp., F	G_L, °F/In.
	Bottom Zone	Top Zone	Total			
0.38	485	385	870	0.76	3020	310
3.9	465	485	950	9.75	2955	335
5.8	485	530	1015	9.5	2895	300
7.0	520	485	1005	0.76	2900	360

*Distance crucible bottom was below furnace bottom

+Not corrected for thermal expansion of thermocouple probe. Corrections would decrease the height of interface.

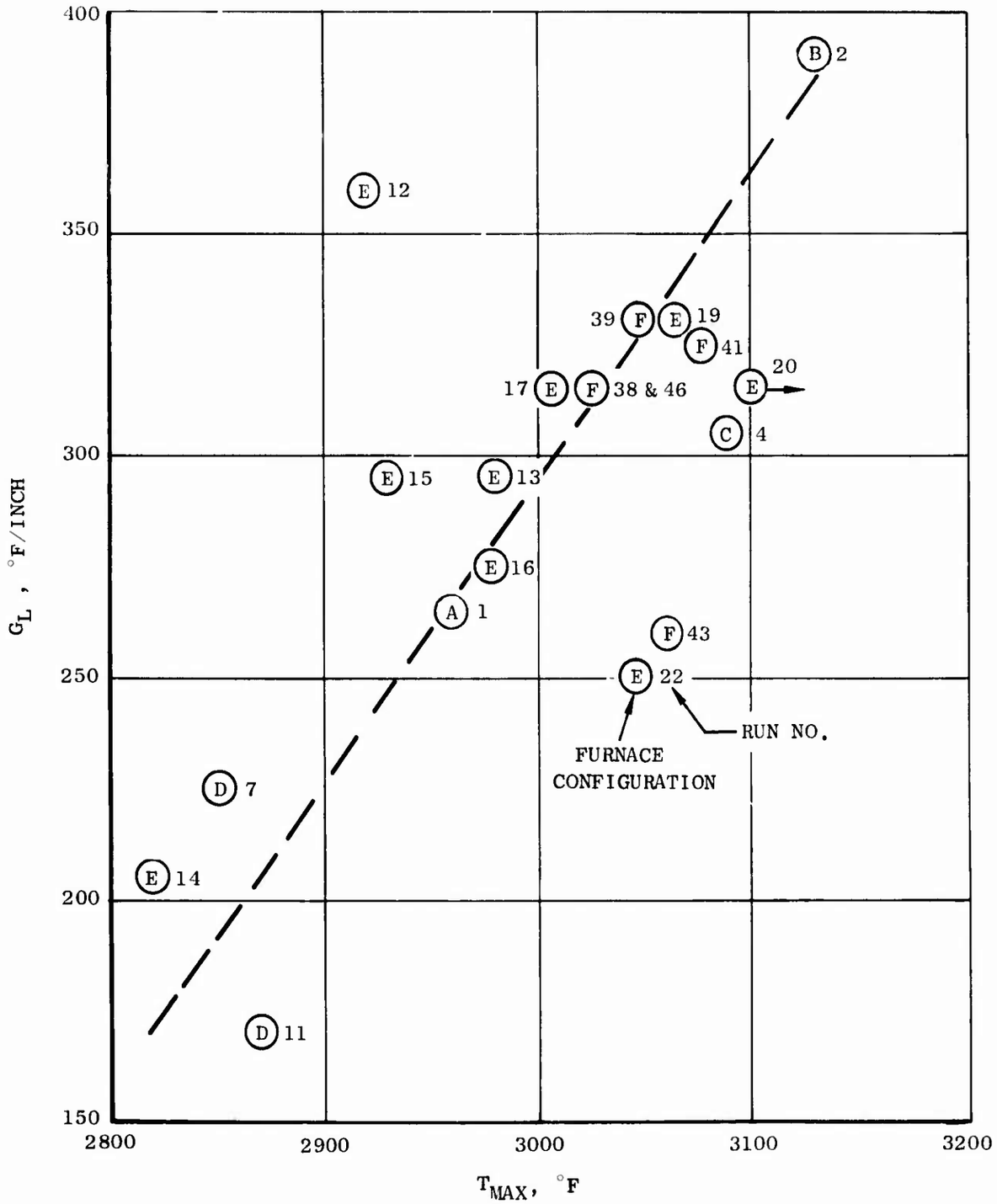

Figure 22. The Relationship Between T_{MAX} and G_L

2.5.3 Test Bar Process Refinement

The objectives of this work were:

- Further develop the PFS process parameters with furnace configuration F to product 1-5/8 inch diameter bars having an aligned fiber section about 4-1/2 inches long.
- Establish the maximum casting rate.

The experimental approach was to cast 18 bars using three different withdrawal rates and six different power levels. T_{max} of the test bar process was to be limited to 3100°F, which was the approximate temperature limitation of the General Electric mold being used for J101 LPT blade casting in the program.

2.5.3.1 Use of Metal Powders to Reduce Crucible Breakage - In all runs, the charge was melted in-situ in recrystallized alumina crucibles. During the first several runs, there was an unusually high incidence of crucible failures that caused metal run out and premature termination of runs. Inspection of cracked crucibles and corresponding bars suggested that liquid metal from the first region of the charge to melt ran down into the approximately 0.1 inch gap between crucible and charge near the bottom, quickly solidified and then, as heating continued, expanded and cracked the crucible near the bottom. A solution to the problem, based on the suggested failure mechanism, involved placing metal powder in the crucible bottom and in the gap between charge and crucible to prevent run down of molten metal. Use of this technique proved to be effective in that only one crucible failure occurred thereafter, but this was due to an inadequate height of metal powder in the gap. Experience indicated that the radial gap should be filled to a height of about 1/8 to 1/4 inch.

Nickel and tungsten powders were used successfully. Nickel was selected first as the element that would cause the minimum change in alloy chemistry, if it melted. About 100 grams of nickel powder were used per run, and measurements of powder remaining after several runs indicated that the maximum amount that could have been dissolved by the molten NiTaC-13 was 30 grams. This small amount would have caused less than a two percent reduction in the amount of each alloying element in NiTaC-13, which was within analytical error and was much less than the chemistry specification range for each element.

Tungsten powder was also used because it has a much higher melting point and density than NiTaC-13. For these reasons the amount dissolved by the melt, if any, should be much lower than for nickel powders; however, dissolution of a small amount would put the molten alloy above the chemistry specification for tungsten.

No evidence of unmelted Ni or W powder particles was observed metallographically in any of the bars. To check for powder dissolution, X-ray emission chemical analysis was performed at the bottom of the aligned fiber section from two bars, B70 and B73. The analysis results are compared in Table 11 with corresponding results for 1/2 inch diameter bars from Figure 3. Analyses of bar B70 (Ni powder) and bar B73 (W powder) were in excellent agreement, indicating no effect of either powder on composition. Small bar

TABLE 11

CHEMICAL ANALYSIS OF NiTaC-13 BARS AT BOTTOM OF ALIGNED FIBER SECTION

PFS Bar No.	Bar Diam., In.	Type Powder	Composition, Weight Percent						
			Co	Cr	W	Re	Al	V	Ta
H-179A	1/2	--	3.3	3.9	3.4	7.7	5.5	5.4	6.5
H-179B	1/2	--	3.3	3.8	3.6	7.9	5.3	5.3	6.9
1B-2	1/2	--	3.4	4.0	3.5	7.7	5.3	5.6	6.8
6T-2	1/2	--	3.4	4.1	3.4	7.5	5.4	5.5	6.2
Average	1/2	--	3.35	3.95	3.48	7.7	5.38	5.45	6.6
70	1-5/8	Ni	3.3	4.0	3.6	8.0	4.8	5.3	6.5
73	1-5/8	W	3.3	4.1	3.6	8.0	4.8	5.4	6.1

results for Re were slightly lower and those for Al were significantly higher than large bar results. These differences may have been due to changes made in analysis techniques subsequent to the time the small bars were analyzed, and did not affect the conclusion that, at most, only insignificant amounts of the Ni or W packing powders were dissolved by molten NiTaC-13.

2.5.3.2 Experimental Results - More details of the 18 runs are presented in Table 12. The cutup plan for obtaining evaluation samples from each bar is illustrated in Figure 23. Evaluation of microstructure and stress-rupture properties of the 18 bars will be discussed in the sections that follow. The results of density measurements are discussed in Section 3.2.9.

Metallography - During examination of the 18 bars, several distinct types of carbide morphology were found: dendrites, fibers, cells, and dentritic cells. Carbide fibers present in the bottom, middle and top sections of Bar B70 are shown in Figure 24. From inspection of this figure, it can be seen that there were both rod and blade fibers in all three sections, and that the fiber population density decreased from bottom to top. Three other types of carbide morphology, present in Bar 72, are illustrated in Figure 25. The bottom section in Figure 25 contained cells and a type of dendrite found only near the sort-out zone. The cells had aligned fibers in the centers, but misaligned fibers at the perimeters. The dendrites had a characteristic cross shape, and were a continuation of coarser dendrites from the sort-out zone that eventually gave way to one of the other types of carbide morphology. In the middle and top sections, illustrated in Figure 25, it is shown that the aligned carbide fiber centers of the cells were progressively smaller and dendritic cellular carbide areas between the cell centers were progressively larger. Longitudinal views of dendrites and cells present in the bottom section of Bar B37 are shown in Figure 26. View A shows a transition region between an aligned fiber section and a band consisting of cells and dendrites. The latter have a characteristic diagonal arm. A scanning electron microscope (SEM) view in Figure 26B of the perimeter of a cell shows that there were carbide blades from which fibers grew perpendicular to the solidification direction. Figure 26C is a SEM view illustrating a carbide dendrite with many closely spaced arms having plate morphology.

Dendritic cells present in the top section of Bar B72, are shown in Figure 27. In this case, there were very few aligned fibers in the cell centers. The dendrites consist of a lattice-like structure of carbide fibers and plates.

The carbide morphology classifications just described were assigned to the 18 bars, and the results have been summarized in Table 12. As shown, five of the bars had aligned fibers over a 4-1/2 inch length, but one of these (B67) had two bands;hence, four of the 18 bars met the microstructural goal completely.

The microstructural results for the 18 bars withdrawn at three different rates are compared in Table 13. At 1/4 inch/hour a substantial length of fully aligned fibers was produced under all PFS conditions used. Fibers were also produced at the 5/16 inch/hour withdrawal rate, but the aligned fiber section length was less than the 4-1/2 inch goal. In contrast,

TABLE 12

SUMMARY OF TEST BAR PROCESS REFINEMENT CASTING RUNS MADE

WITH FURNACE CONFIGURATION F

Run No.	Heat No.	Type Powder	Total Power, Watts	Approx. T_{max}, °F	Approx. G_L, °F/In.	Withdrawal Rate, In/Hr	Approx. Length, In. Bar	Aligned Fiber Section	No. of Bands	*Microstructure Bottom	Middle	Top
B46	V-384	None	870	3020	315	3/8	7.9	0	0	C	C	D-C
B62	V-384	Ni	840	3000	300	5/16	8.1	0	0	C	C	D-C
B63	V-384	Ni	820	3000	300	1/4	8.2	4	0	F	F	D-C
B64	V-384	Ni	855	2950	250	1/4	8.5	4-1/2	0	F	F	F
B65	V-384	Ni	890	2920	250	5/16	8.0	1-1/2	0	C	C	D-C
B66	V-384	Ni	890	2920	250	3/8	8.6	0	8	C	D-C	D-C
B67	V-385	Ni	925	3040	345	1/4	8.1	4-1/2	2	F	F	F
B68	V-385	Ni	940	3030	285	5/16	8.0	4	0	F	F	D-C
B69	V-385	Ni	1025	3020	310	3/8	8.5	0	1	C	C	D-C
B70	V-385	Ni	1070	3100	400	1/4	8.7	5	0	F	F	F
B71	V-385	W	975	3020	300	5/16	8.6	3-3/4	0	F	F	D-C
B72	V-385	W	1065	3100	400	3/8	8.3	0	0	C	D-C	D-C
B73	V-385	W	1090	3100	400	1/4	8.3	5	0	F	F	F
B77	V-384	W	1105	3090	400	5/16	8.3	0	0	F	C	D-C
B78	V-384	W	1120	3100	400	3/8	8.3	0	0	C	C	D-C
B79	V-385	W	990	3120	400	1/4	7.7	4-1/2	0	F	F	F
B83	V-385	W	905	3080	400	1/4	7.8	4	0	F	F	D-C
B84	V-385	W	920	3080	400	5/16	7.7	0	0	F	D-C	D-C

* F = Aligned Fibers
C = Cells
D-C = Dendritic Cells

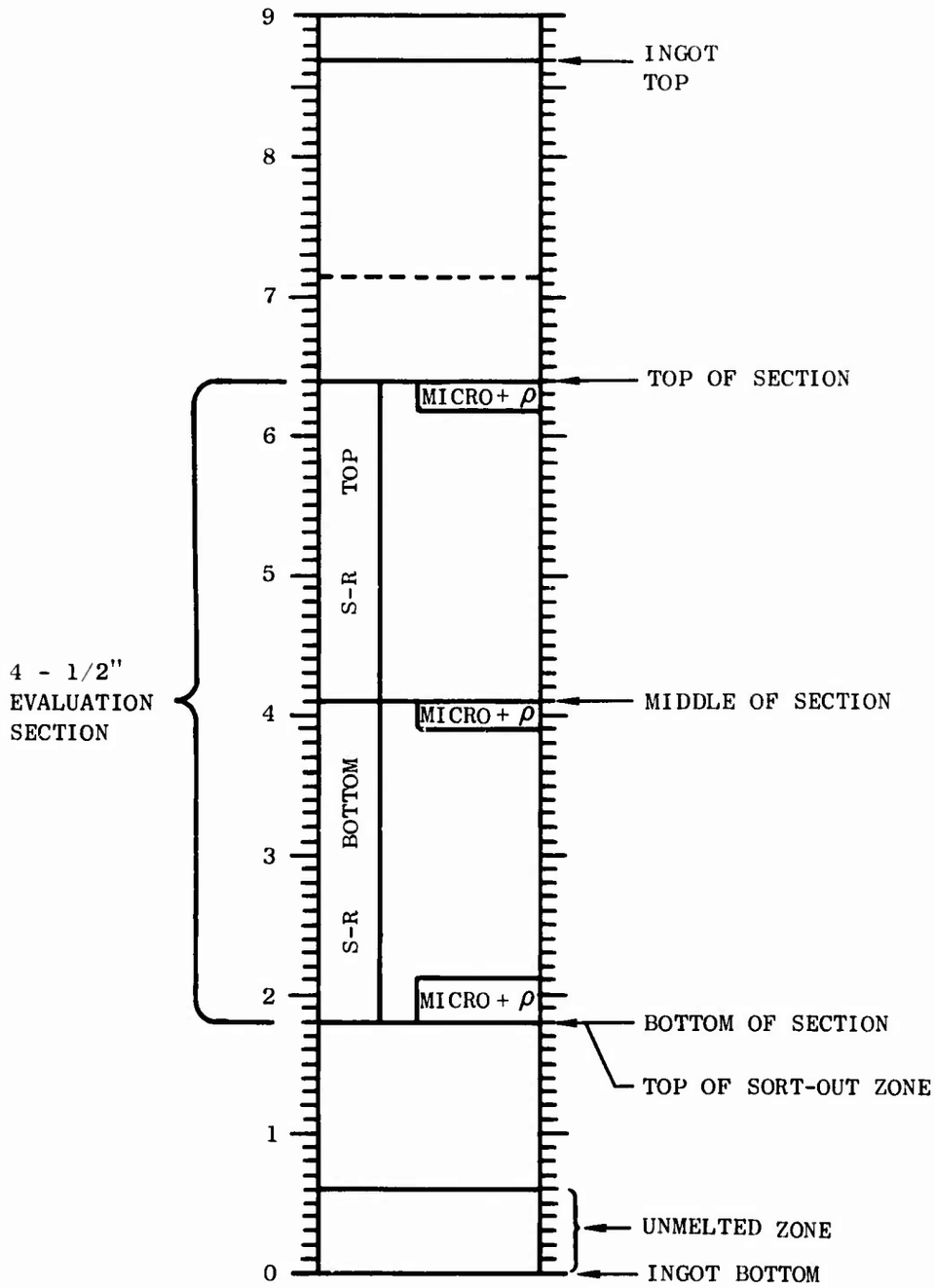

Figure 23. Test Bar Cut Up Plan

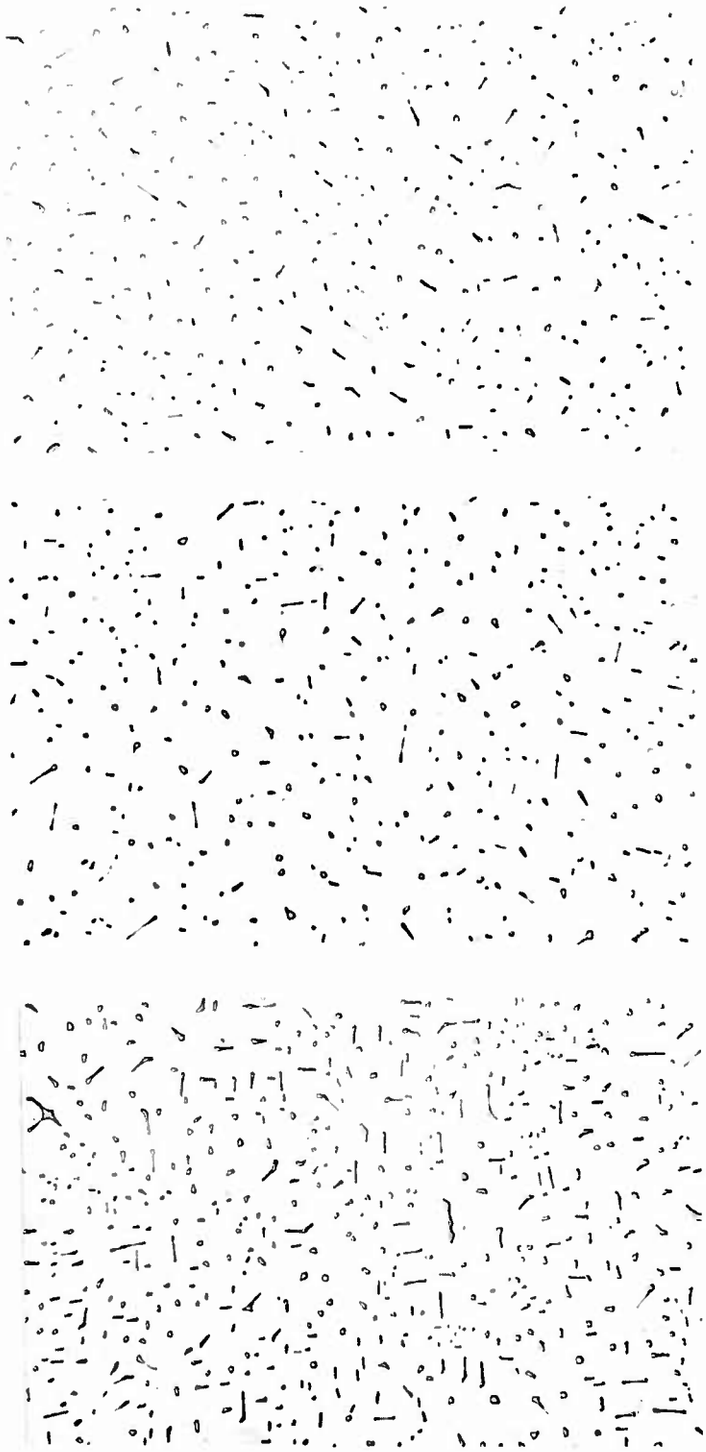

Figure 24. Transverse Microstructure of Bar B70 Illustrating Carbide Fiber Cross Sections at 500X Magnification

A. TOP
(Dendritic Cells)

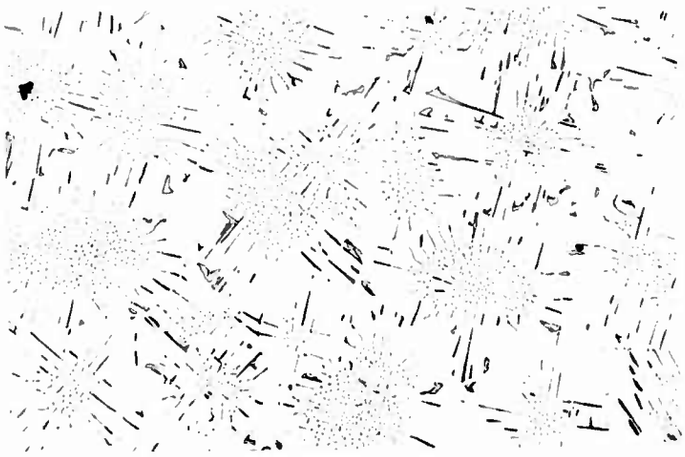

B. MIDDLE
(Dendritic Cells)

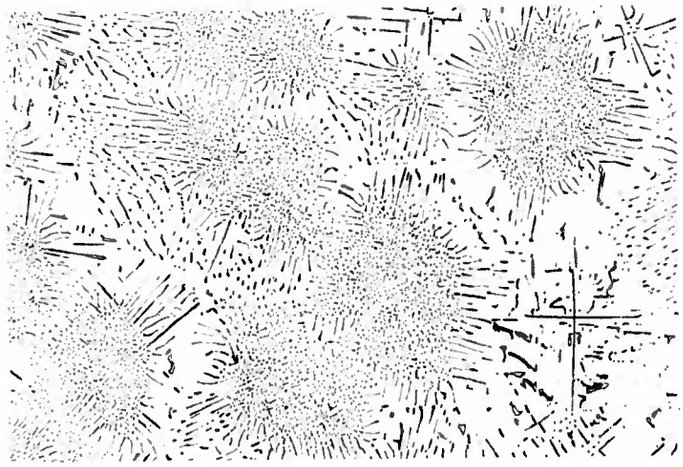

C. BOTTOM
(Dentrites and Cells)

Figure 25. Transverse Microstructures of Bar B72 Illustrating Carbide Dendrites, Cells, and Dendritic Cells at 100X Magnification

A. Transition From Cells and Dendrites to Aligned Fibers. Light Optical - 100X

B. Peripheral Region of Cell. SEM-750X

C. Dendrite. SEM-310X

GROWTH DIRECTION

Figure 26. Longitudinal Microstructures of Banded Region in Bottom of Bar B37 Illustration Aligned Fibers, Cells and Dendrities

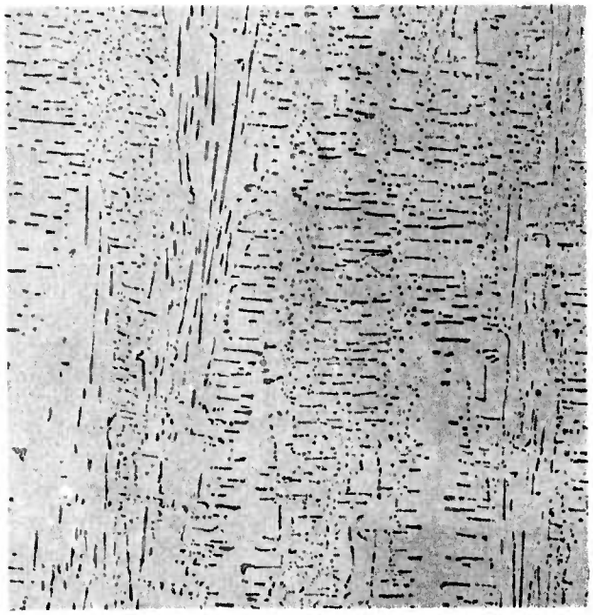

A. LIGHT OPTICAL

100X

GROWTH
DIRECTION

B. SEM

665X

Figure 27. Longitudinal Microstructure of Bar B72 Top Section Illustrating Carbide Dendritic Cells

TABLE 13

LENGTHS OF ALIGNED FIBER SECTIONS IN TEST BARS CAST DURING PROCESS REFINEMENT

Aligned Fiber Length, In.	Bar Numbers Withdrawal Rate, In/Hr		
	1/4	5/16	3/8
> 4-1/2	64, 67, 70, 73, 79	---	---
< 4-1/2 > 2-1/4	63, 83	68, 71	---
< 2-1/4 > 1/4	---	77, 84	---
0	---	62, 65	46, 66, 69, 72, 78
TOTAL	7	6	5

fully aligned fibers were not produced under any PFS conditions used at the 3/8 inch/hour withdrawal rate. Since G_L values up to 400°F/inch were used for all three withdrawal rates, these results indicate that the critical G_L/R ratio for NiTaC-13 exceeds 1060 but is less than 1280°F hr/in^2. This is only slightly higher than the value of 1000°F hr/in^2 estimated in an early stage of process development[2].

Longitudinal Stress-Rupture Properties

Results of stress-rupture tests conducted at 1800°F/44 ksi in air are summarized in Table 14 which shows rupture lives, Larson-Miller parameter numbers, percent elongation and percent reduction in area. Also shown are microstructural classifications based on metallographic examination of longitudinal sections of all specimens at the fracture surface. The rupture life data from Table 14 are presented in Figure 28 according to withdrawal rate, location in bar (bottom or top), and microstructure. For comparison, preliminary average data for 1/2 inch diameter bars are shown as a horizontal line. The -2σ and -3σ lines were estimated on the basis of conventional superalloy behavior.

Important observations from Figure 28 are:

1) Best rupture strengths for both bottom and top sections were obtained with fibrous material grown at 1/4 inch/hour.

2) Rupture strength was significantly reduced with increasing withdrawal rate, presumably due to increasing fiber misalignment. The effect was somewhat greater for top sections.

3) The results indicated the possibility of meeting the 50-hour minimum rupture life requirement in both bottom and top sections by using a withdrawal rate of 1/4 inch/hour.

On the basis of the foregoing results and observations, it was concluded that the 1/4 inch/hour withdrawal rate offered the highest potential for meeting the program goals throughout test bar production.

2.5.4 Selection of Final Test Bar Process

The best balances in rupture strengths of top and bottom sections of material cast at 1/4 inch/hour were obtained with bars B70 and B73. As shown in Table 12, the estimated T_{max} for both was 3100°F, and estimated G_L for both was 400°F/inch. Although the blade process development work had not been completed, there were sufficient results to indicate that the final blade PFS parameters would be close to those just cited for bars B70 and B73. Hence, the final test bar process was established on the basis of the two test bars as follows:

1) Cut and clean, by spot grinding and grit blasting, about 10-1/2 inch lengths (about 5.2 pounds) of 1-1/2 inch diameter remelt ingot.

TABLE 14

STRESS-RUPTURE RESULTS FOR BARS CAST DURING PROCESS REFINEMENT AND TESTED IN AIR AT 1800°F/44 KSI

Bar No.	R, In./Hr.	+Bottom Section **Micro-structure	Life, Hrs.	P x 10^3 (C=20)	% Elong	% RA	+Top Section **Micro-structure	Life, Hrs.	P x 10^3 (C=20)	% Elong	% RA
B46	3/8	C	58.1	49.18	27.4	36.0	D-C	31.7	48.59	22.1	30.9
B62	5/16	C	61.1	49.23	17.4	31.8	D-C	18.2	48.04	16.1	23.8
B63	1/4	F	91.9	49.63	13.7	30.0	F	34.3	48.66	*	22.7
B64	1/4	F	101.8	49.73	12.0	30.9	F	34.9	48.68	12.4	17.9
B65	5/16	C	98.3	49.70	11.7	33.9	C	48.6	49.00	*	22.4
B66	3/8	C	56.8	49.16	22.3	24.4	D-C	25.3	48.36	11.7	15.4
B67	1/4	F	111.9	49.82	14.0	31.2	F	33.2	48.63	14.3	20.2
B68	5/16	F	108.9	49.80	14.0	33.0	F	39.4	48.80	9.4	17.3
B69	3/8	C	79.5	49.49	18.8	23.1	C	23.9	48.31	11.0	23.1
B70	1/4	F	90.8	49.62	20.2	43.1	F	63.1	49.26	24.1	25.2
B71	5/16	F	43.3	48.89	*	38.5	F	42.1	48.86	12.6	24.2
B72	3/8	C	67.7	49.33	24.5	32.6	D-C	18.8	48.08	*	10.7
B73	1/4	F	102.3	49.74	21.3	35.4	F	47.3	48.98	14.4	27.8
B77	5/16	C	63.6	49.27	15.1	36.1	C	22.5	48.25	17.3	29.7
B78	3/8	C	42.4	48.96	*	40.5	D-C	13.6	47.75	12.1	33.1
B79	1/4	F	110.6	49.81	*	34.1	F	30.1	48.53	12.7	19.7
B83	1/4	F	79.6	49.49	*	41.1	F	26.5	48.41	14.4	28.9
B84	5/16	F	92.8	49.64	*	31.9	D-C	18.7	48.07	25.5	31.6

* F = Aligned Fibers, C = Cells, D-C = Dendritic Cells

+ $g_b \simeq 0.27$ for bottom sections and $\simeq 0.66$ for top sections

* Sample could not be removed from grips for measurement

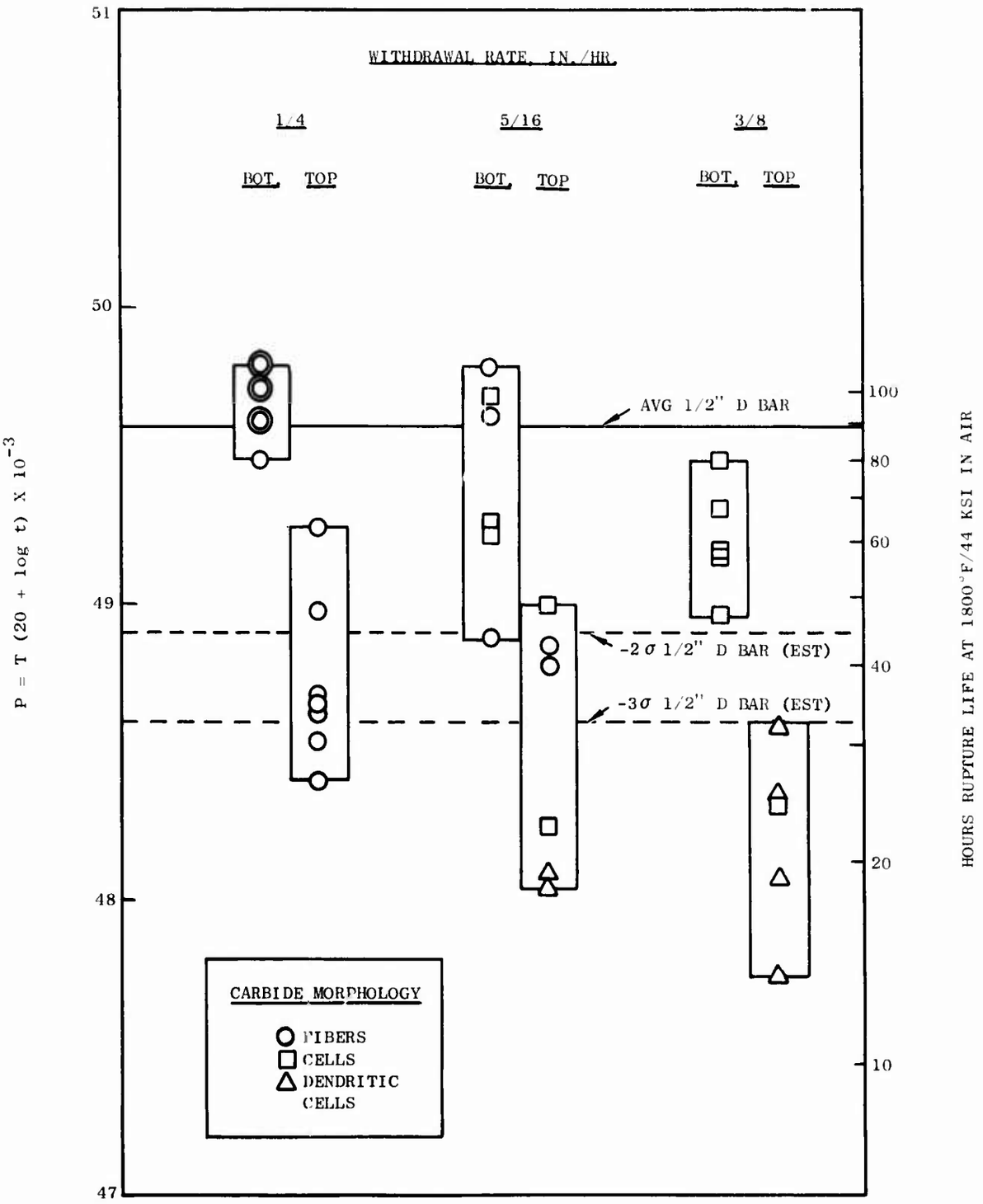

Figure 28. Longitudinal Stress-Rupture Data for NiTaC-13 Test Bars Cast During Process Refinement Compared with Preliminary Data for 1/2-Inch Diameter Bars

2) Place about 30 grams of tungsten powder in the bottom of a recrystallized alumina crucible. Load the charge into the center of the crucible. Pour about 70 grams of tungsten powder around the charge and level with a wire tool.

3) Load the crucible into the furnace, utilizing configuration F, Table 7. Center the crucible and make certain it does not rub the furnace sidewall or radiation shield. Adjust height of bottom chill to starting position.

4) Replace tank cover, purge with argon, and bring to temperature over a period of 3 to 4 hours, using manual power control and flowing argon.

5) Manually adjust the total power level to about 1080 watts supplying about 625 watts to the bottom zone and about 455 watts to the top zone. The objective is to achieve a liquid metal temperature gradient of approximately 375° to 400°F/inch, and a maximum liquid temperature of about 3100°F. After power stabilizes, begin automatic temperature control and withdrawal at 1/4 inch/hour.

6) Periodically, verify PFS conditions by measuring the liquid metal temperature profile prior to the initiation of withdrawal in selected runs.

7) During each run monitor current, voltage, and control thermocouple temperature for both heater zones.

8) Shut furnace off automatically at the completion of withdrawal.

9) Grind flats the length of each bar, polish, and examine metallographically. Submit for NDE those bars indicated to have aligned fibers without bands over a 4-1/2 inch length.

2.6 FIBER DEFECT STRUCTURES

Aligned fiber NiTaC-13 can be grown at a withdrawal rate of 1/4 inch/hour when G_L exceeds about 300°F/in. However, even under these conditions, three types of carbide defect structures have been observed and classified as follows:

Type I - a zone of aligned fibers with size and spacing different from the fibers in adjacent material

Type II - a zone of cells or dendritic-cells within aligned fiber material. Both of these have been termed "bands" and differ only in degree of fiber misalignment

Type III - a zone of fibers much thicker than those in adjacent material. This defect is termed an "arrest line".

All of these defect structures occupy zones of variable length in the solidification direction and extend across the entire cross section of the casting perpendiular to the growth direction.

2.6.1 Mechanisms of Carbide Defect Structure Formation

Proposed mechanisms for formation of Type I and II defects are based on the previously cited criterion for PFS:

$$(G_L/R)_{\text{Actual}} \geq (G_L/R)_{\text{Critical}} = K^* \qquad (1)$$

The value of $(G_L/R)_{\text{Critical}}$ is a material parameter which remains constant for a non-segregating alloy. For segregating alloys such as NiTaC-13, it can be expected that the value of $(G_L/R)_{\text{Critical}}$ will not be a constant, but will change as solidification (and segregation) proceeds. For the discussion that follows, a non-segregating carbide eutectic alloy will first be considered.

Models for the formation of Type I and II defect structures are illustrated schematically in Figure 29, which shows several perturbations that could occur in the actual G_L/R during solidification. Also shown in Figure 29 is $(G_L/R)_{\text{Critical}}$ below which cellular and dendritic-cellular growth of MC carbides occurs. In Case A of Figure 29, the pertubation in G_L/R does not fall below the critical. If the perturbation is due solely to an increase in R, a decrease in fiber size and spacing will occur and result in the Type I band shown. If the perturbation is due solely to a change in G_L, no microstructural change will result[6].

In Case B of Figure 29, the perturbation causes the actual G_L/R to fall below the minimum and produces a Type II band which in NiTaC-13 is generally a mixture of cells and dendritic cells. In Case B the perturbation could be due to changes in G_L, R or both. A change in G_L causes the position of the liquid-solid interface to change and thus produces a change in R.

The perturbations that lead to the two types of bands just discussed could be caused by mechanical or thermal fluctuations. During work on this program, it has been demonstrated experimentally that Type II bands can be caused to form either by electric power disturbances that affect the heat input rate, or by mechanical disturbances such as irregular movement of the mold or crucible during withdrawal, or by mechanical shocks delivered to the equipment.

The models in Figure 29 may be too simple to explain observed Type II bands that are relatively long, 0.1 inch or more. At a solidification rate of 1/4 inch/hour, the interface would be expected to advance about 0.0042 inches/minute. For a 0.1-inch long band, the perturbation would have to exist for about 25 minutes by the models proposed. It is possible that there is a hysteresis effect that causes a delay in restoration of aligned fiber growth after subsidence of a perturbation that initiated band formation. Because of a hysterisis effect, then, a short perturbation could cause a relatively long band.

Another possible reason for band formation is a significant change in $(G_L/R)_{\text{Critical}}$ that may occur during solidification of a segregating alloy, such as NiTaC-13. Changes in composition of the molten alloy could reduce the amount that the actual G_L/R exceeds the critical value. Segregation could also occur discontinuously as solute "dumping" of one or more elements, and could result in Type II bands. For example, chemical analysis of

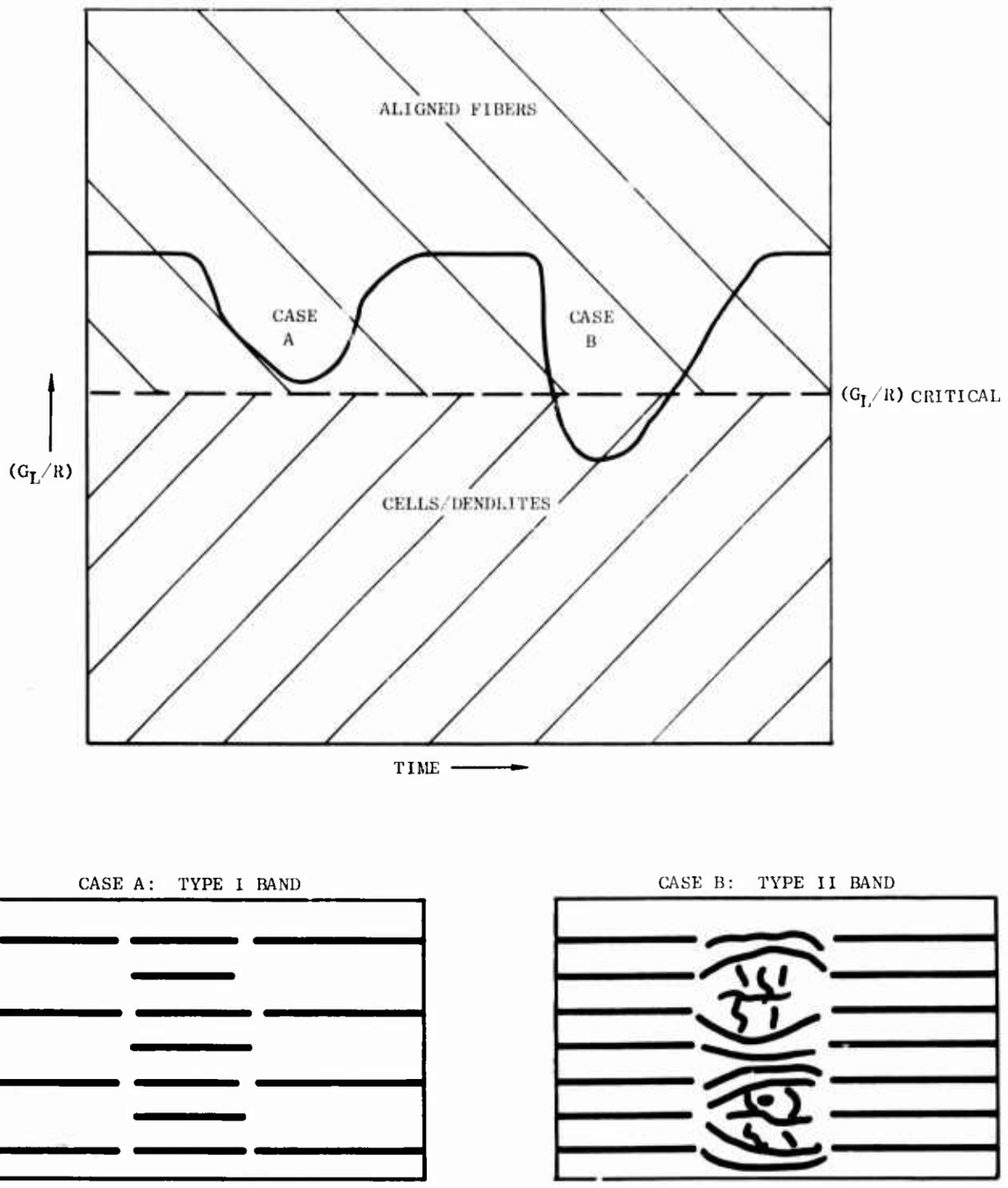

Figure 29. Band Formation Models

one or more lements, and could result in Type II bands. For example, chemical analysis of one dendritic cellular band indicated a significantly higher chromium concentration over that in the adjacent aligned fibrous region, 6.7 versus 5.3 weight percent, respectively. The concentration of other elements were within typical values for the alloy and it is not evident whether the high chromium was the cause or the effect of the band.

In an experiment to assess causes of Type II bands, three 3/8 inch diameter NiTaC-13 bars were ?FS simultaneously at 1/4 inch/hour in a single furnace using a common withdrawal system. After the bars were polished and etched, many bands were observed at positions common to the three bars, as illustrated in Figure 30. The most likely cause of these bands was a perturbation in one or more process parameters. If the bands were due to inherent instabilities in NiTaC-13 eutectic growth, it is expected that they would have occurred more randomly and not in the same positions in all ingots.

Type III defects, arrest lines, have been rarely observed. They were however, successfully produced in a controlled experiment in which the furnace power was abruptly changed by 2 to 12 percent every 2 or 3 hours. For increases in furnace power of 2 to 6 percent, arrest lines were produced such as the one illustrated in Figure 31. In another experiment, instantaneous changes in withdrawal rate were made, including stopping of the drive motor, but these changes failed to produce arrest lines.

A proposed mechanism for arrest line formation during sudden furnace power (and temperature) increases is that the interface velocity slows toward zero, perhaps even melting back some of the solidified bar. During this event, as the velocity approaches or passes through zero, the fibers thicken and merge.

The three models for formation of fiber defect structures discussed here are relatively independent of whether the sources of perturbations to G and/or R are mechanical, electrical/thermal, or chemical. One method to reduce the defects, which is also independent of the cause, is to maximize the amount that the actual G_L/R is above $(G_L/R)_{Critical}$. This should be done through increased G_L rather than decreased R since, as illustrated previously in Figure 6, decreases in R result in material with coarser fibers and lower stress-rupture strength. A second method is to reduce the magnitude of fluctuations in G_L/R by adequate control of mechanical, electrical/thermal, or chemical factors.

2.6.2 Longitudinal Properties

During the course of test bar and blade process development, it appeared likely that carbide defect structures could not be completely eliminated. Therefore, work was undertaken to evaluate effects of some of the defect structures on longitudinal (growth direction) mechanical properties. In this section, results of the following longitudinal property tests of material from NiTaC-13 bars will be discussed: stress-rupture, tensile, low cycle fatigue (LCF) and high cycle fatigue (HCF). The defect structures evaluated included completely cellular or dendritic cellular material, and aligned fiber material containing Type II cellular bands. Arrest line defects were not tested because of their rarity and observed very low ductility. Rejection of any blade casting containing arrest lines was considered mandatory. The test results showed that carbide defect structures cause some reduction in almost all of the measured properties.

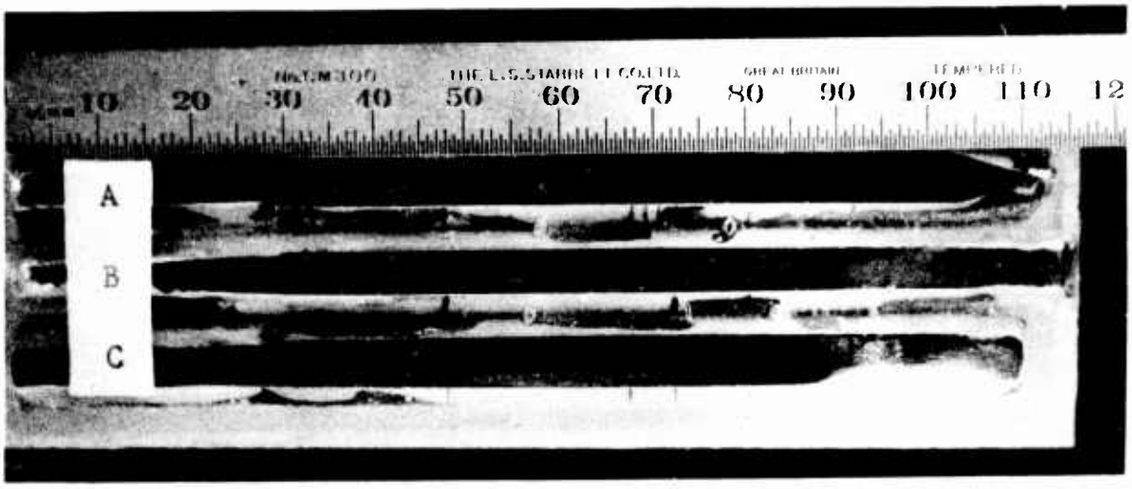

Figure 30. Photographs of Three NiTaC-13 Bars Solidified Simultaneously. All Bars Had Prominent Bands Located at 48, 72.5, and 81 mm

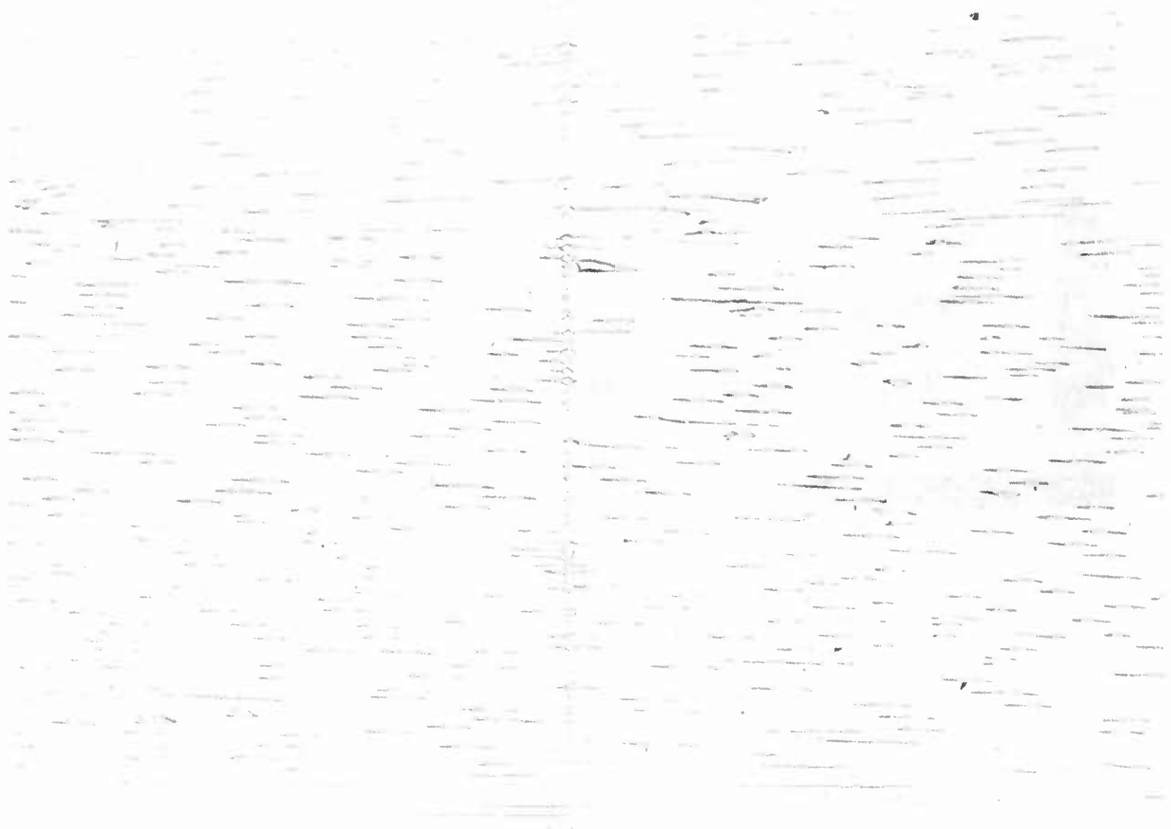

Figure 31. Type III Carbide Defect Structure, Arrest Line, in PFS NiTaC-13

In addition to the results presented here, other property measurements of carbide defect structures were made near the culmination of test bar and blade process development. These results are presented in Sections 2.5.3.2 and 2.7.5.2, repsectively.

2.6.2.1 Stress-Rupture - To evaluate the effect of bands, a 7/8 inch diameter NiTaC-13 bar (DS 1288) that was grown at 1/4 inch/hour and had a 0.03 inch long Type II dendritic cellular band near the bottom, was machined to yield four test specimens with this planar band in the gage section. The specimens were stress rupture tested in air over a range of temperatures from 1600° to 1950°F. The results are presented in Table 15 and, for comparison, are plotted in Figure 32 against the $\pm 3\sigma$ scatter band calculated with equation (6) given previously in Section 2.4.4.

TABLE 15

LONGITUDINAL STRESS RUPTURE DATA FROM BANDED NiTaC-13

(Bar DS 1288 All tests in air)

Test Temp., °F	Stress, ksi	Hrs. to Failure	$Px10^{-3}$ for C=20
1950	17.5	147.38	53.43
1850	30	127.17	51.06
1700	52.5	123.63	47.72
1600	75	136.99	45.60

The data in Figure 32 indicate that the band caused in small reduction in rupture strength, because the data points fall very close to the -3σ curve. The maximum loss due to the band is 0.5 Larson-Miller parameter numbers. However, metallographic observations of the samples after test indicate that the band may not have caused any reduction in rupture strength. Examination of the samples tested at 1950° and 1850°F showed that the fracture occurred within the band, but those tested at 1700° and 1600°F failed outside of the band. Photomicrographs to illustrate this point are presented in Figure 33. Because the band was not a source of weakness for two test conditions and the four points fell on a smooth curve parallel to those in Figure 32, there is the possibility that this particular bar may have had stress-rupture properties at the low end of the $\pm 3\sigma$ scatter band and, therefore, that the dendritic-cellular band had no effect.

A second observation concerning the test results of the same four banded samples is that no failures occurred in the transition regions where fiber morphology changed from fibers to cells or cells to fibers. Transition zones are, therefore, not unusually weak in rupture tests.

To evaluate fully dendritic cellular material, bar DS 1666 (7/8 inch diameter) was grown at 1/2 inch/hour and bar DS 1765 (1-1/2 inch diameter) was grown at 1 inch/hour. During growth of DS 1666, the crucible was rocked several times and this produced sharp bands of exaggerated dendritic cellular material. Otherwise, microstructures of both bars were classified as dendritic cellular. Photomicrographs of DS 1765 are shown in Figure 34. Results of stress rupture tests performed with bottom material from both bars, and top material from DS 1666 are presented in Table 16. The results for bottom and top

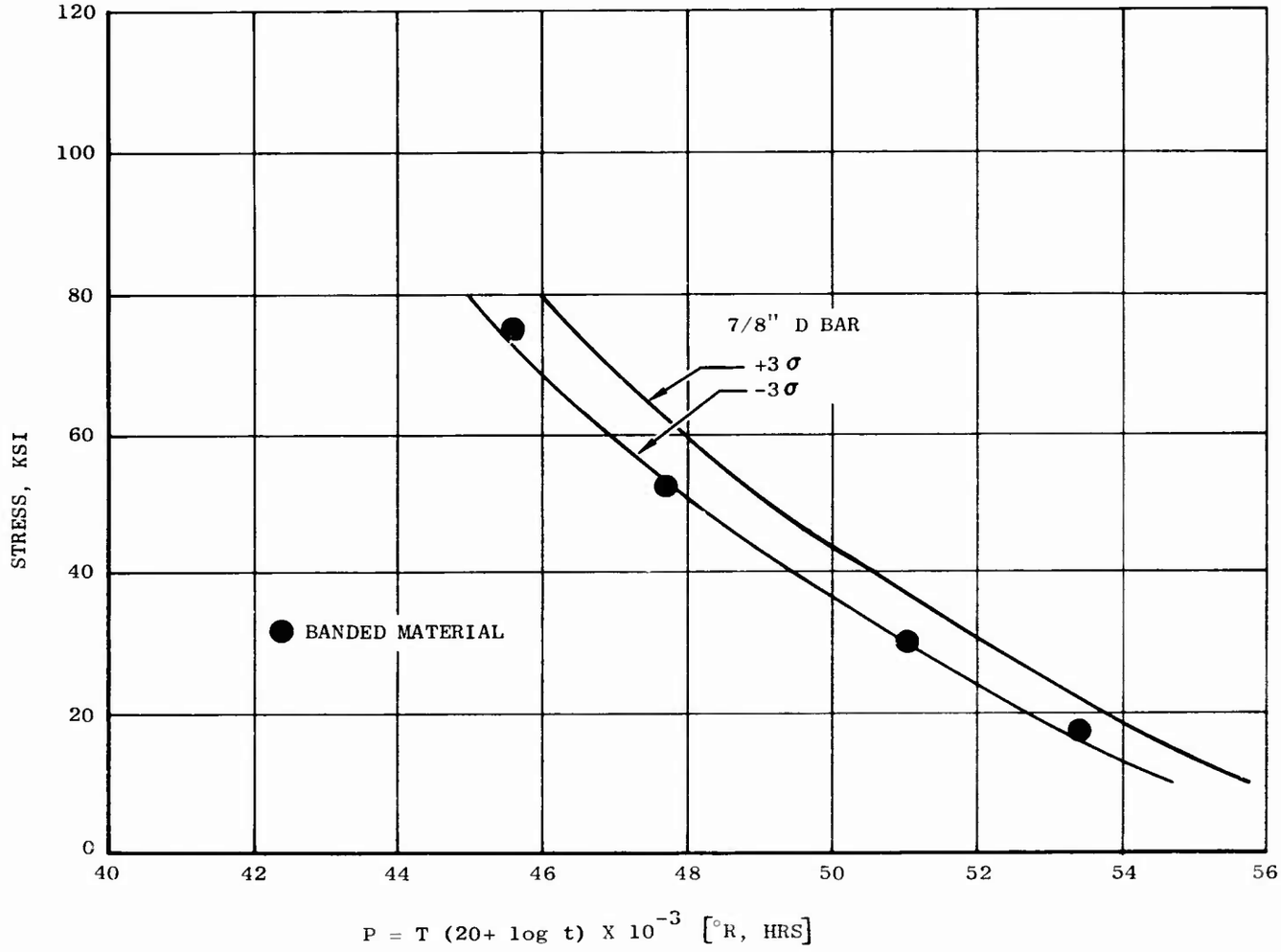

Figure 32. Longitudinal Stress-Rupture Strength of Banded NiTaC-13 Compared with 7/8-Inch Diameter Aligned Fiber Bars. All Data for Bottom Material Solidified at 1/4-Inch per Hour and Tested in Air

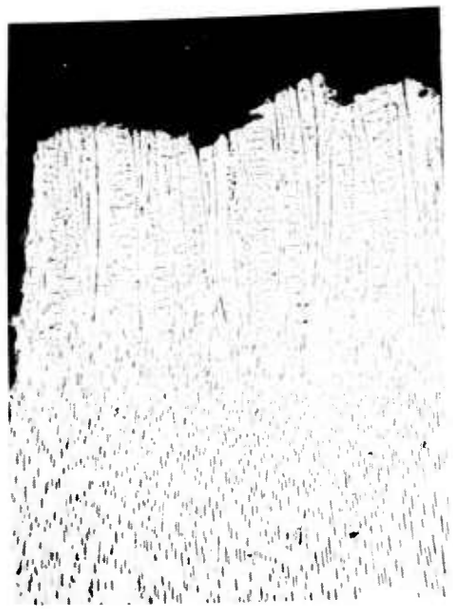

A. 1850°F/30 Ksi 75X
FRACTURE IN BAND

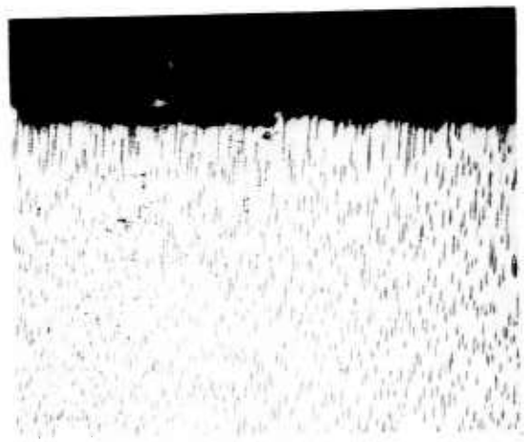

B. 1700°F/52.5 Ksi 75X
FRACTURE IN ALIGNED FIBERS

C. 1600°F/75 Ksi 25X
FRACTURE IN ALIGNED FIBERS

Figure 33. Photomicrographs of Longitudinal Sections Near Fracture Surface of Banded Stress-Rupture Test Specimens from Bar DS 1288

A. LONGITUDINAL SECTION 50X

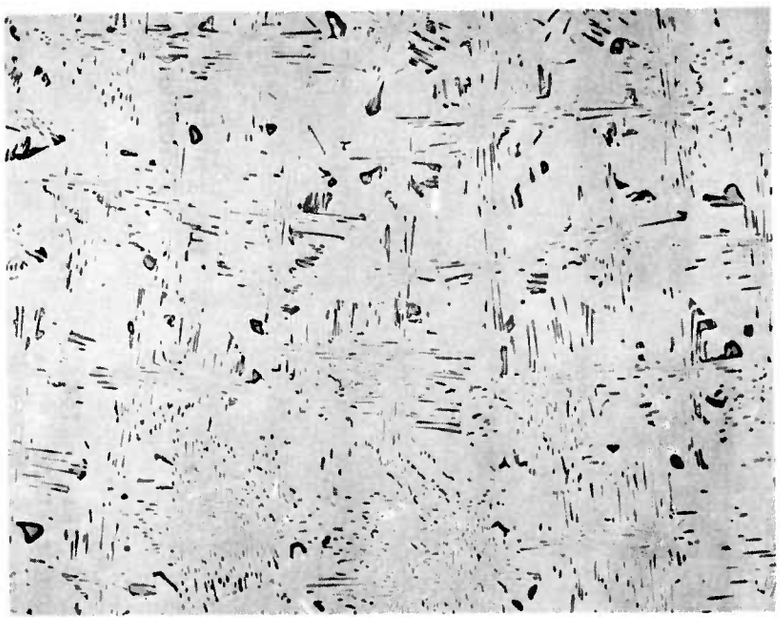

B. TRANSVERSE SECTION 100X

Figure 34. Dendritic Cellular Microstructure of 1-1/2 Inch Diameter NiTaC-13 Bar Grown at 1 Inch per Hour in 320°F/Inch Gradient

TABLE 16

LONGITUDINAL STRESS-RUPTURE TEST RESULTS FOR FULLY DENDRITIC CELLULAR NiTaC-13

*Ingot Position	Test Temp., ^{o}F	Stress, Ksi	Hours to Rupture	$Px10^{3}$ C=20, ^{o}R, Hrs.
BAR DS 1666 CAST AT 1/2 INCH/HOUR				
B	1600	82	124.0	45.5
B	1800	42	73.0	49.4
B	2000	15	96.0	54.1
T	1600	70	74.3	45.0
T	1800	34	49.5	49.0
T	2000	12	116.1	54.3
BAR DS 1725 CAST AT 1 INCH/HOUR				
B	1600	82	73.7	45.0
B	1800	42	37.8	48.8
B	2000	15	73.7	53.8

* B = Bottom, T = Top

specimens from DS 1666 are also compared in Figure 35 to best fit average curves for aligned fiber NiTaC-13 from equations (6) and (7), Section 2.4.4. This comparison indicates little or no degradation due to the dendritic cellular microstructure.

Results for bottom material from all three bars, DS-1288, 1666, and 1765 are compared in Figure 36 with the $\pm 3\sigma$ scatter band (also used in Figure 32) for aligned fiber NiTaC-13. This comparison indicates that the Type II carbide defect structures evaluated, including banded material, caused a small loss in stress-rupture strength, equivalent to not more than 0.5 Larson-Miller parameter numbers. This result is in agreement with results for test bars discussed in Section 2.5.3.2.

Additional stress-rupture tests of aligned fiber and carbide defect structures were performed at 1400°F using material from test bars discussed in Section 2.5.3, Table 12, and from a 7/8 inch diameter bar (DS 1782) that was grown at 1/2 inch/hour. The test results are given in Table 17 and the rupture life data are presented in Figure 37. As shown in the figure, rupture life at 1400°F increased with increasing growth rate, suggesting that fiber misalignment increased rupture strength at 1400°F. However, because other microstructural features possibly changed with increasing withdrawal rate, such as fiber size, fiber spacing, degree of fiber misalignment, grain structure, and gamma-prime structure, the reason for increasing rupture life at 1400°F with increasing withdrawal rate cannot be assigned solely to fiber defect structures at this time. It is possible that the carbides do not play a significant role at 1400°F. In other stress rupture tests at 1800°F, described in Section 2.5.3, Figure 28, the opposite effect was observed: rupture life decreased with increasing growth rate and fiber misalignment.

In both sets of tests, Tables 14 and 17, rupture ductility (% RA) decreased with increasing solidification rate.

2.6.2.2 1200°F Tensile - To determine effects of Type II defect structures, tensile tests were conducted in air at 1200°F, which approximates the maximum J101 LPT blade shank temperature. NiTaC-13 for test included fibrous, cellular and dendritic cellular material from bottom and top sections of 1-5/8 inch diameter bars described in Section 2.5.3, and the dendritic-cellular bar DS 1765 described in the previous section. Also, to evaluate the relative strength of carbide morphology transition zones which occur on both ends of a band, specimens were also machined from two 1-1/2 inch diameter bars, DB22 and DB9. Each contained a band in the bottom section at a g_t value of about 0.24. Bar DB22 was NiTaC-13 that had a cellular band, and two tensile specimens were machined to have the band and the adjacent aligned fiber material within the gage section. Bar DB9 was made from NiTaC-13F, an alloy modification that was developed in a separate GE program to eliminate the sortout zone and is indicated to have properties equivalent to the parent alloy, NiTaC-13 (Section 2.4.5). This bar had a dendritic-cellular band in an otherwise aligned fiber microstructure, and two tensile specimens were machined in the same manner described for DB22.

The 1200°F tensile data and microstructural classifications at the fracture surface are given in Table 18. By inspection of the data in the table, it can be seen that the aligned carbide fiber material had the highest ultimate tensile strength and tensile ductility. With increasing degeneration of the fiber morphology to cellular and dendritic cellular, ultimate

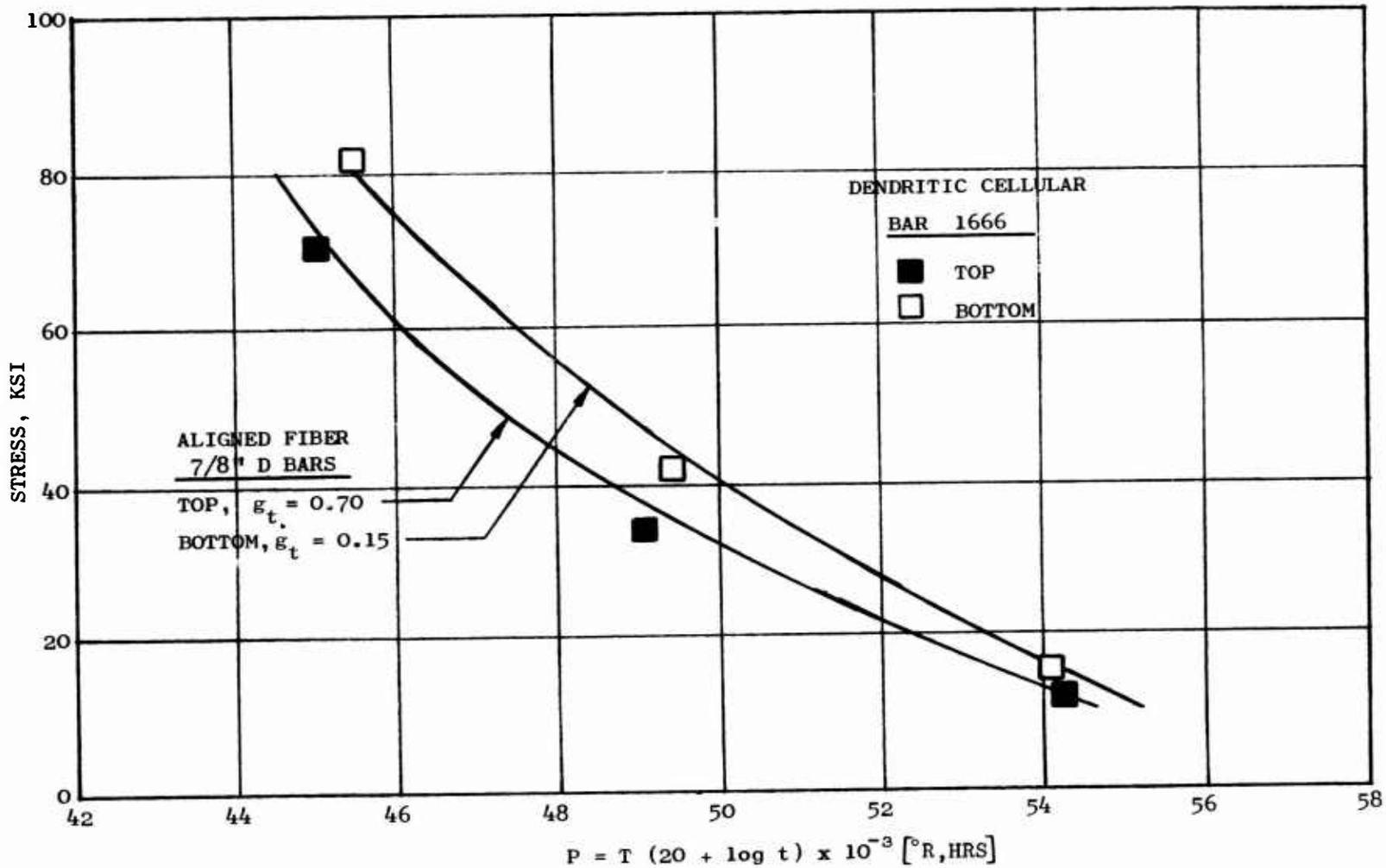

Figure 35. Comparison of Longitudinal Stress Rupture Data for Aligned Fiber and Dendritic Cellular NiTaC-13 from the Bottom and Top Sections of Bars. All Tests in Air

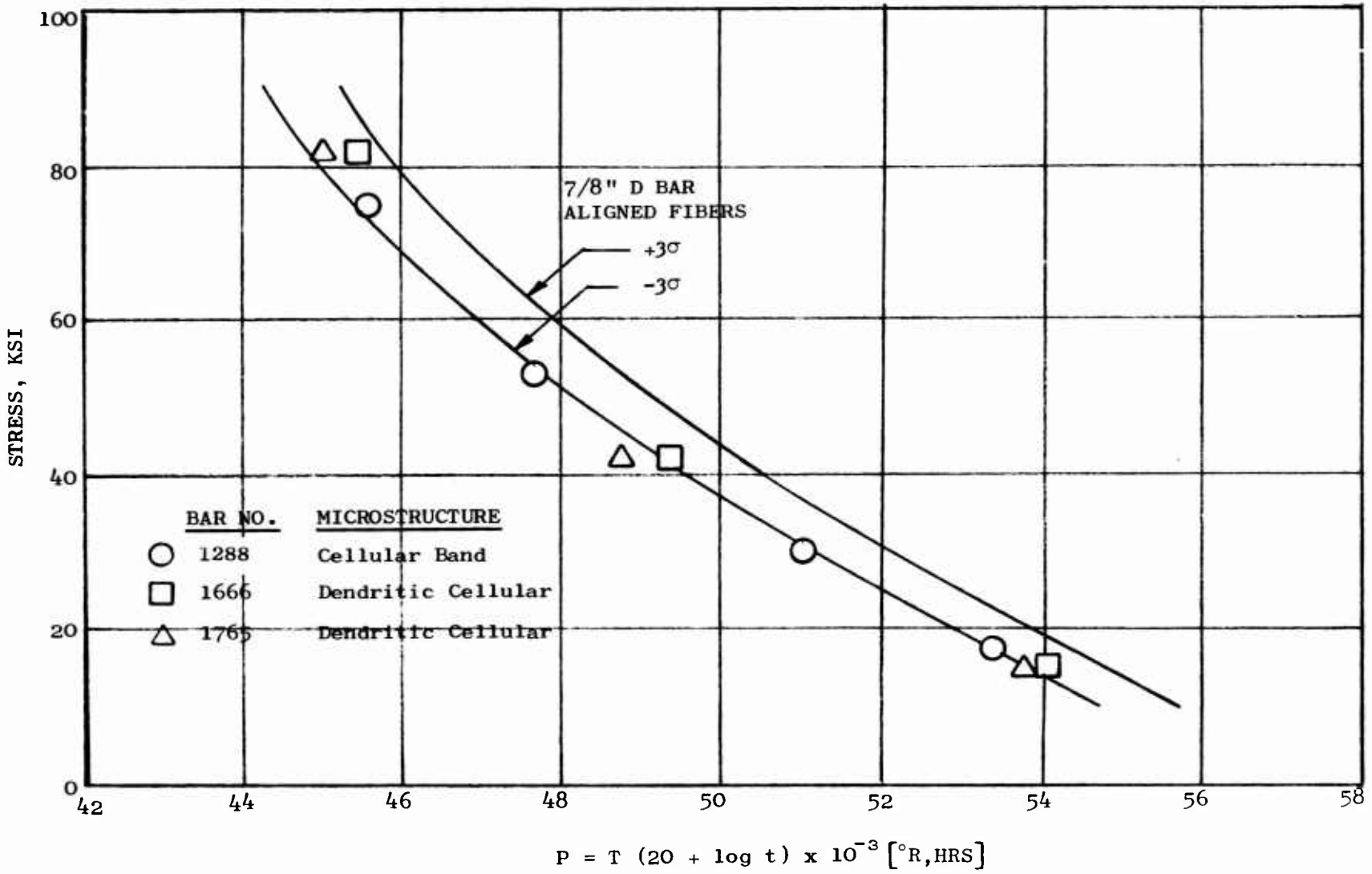

Figure 36. Longitudinal Stress-Rupture Strengths of Carbide Defect Structures Compared to Aligned Fiber NiTaC-13. All Material from Bottom Sections of Bars and All Tests in Air

TABLE 17

LONGITUDINAL STRESS-RUPTURE DATA FOR 1400°F TESTS IN AIR OF ALIGNED FIBER NiTaC-13 AND CARBIDE DEFECT STRUCTURES

Spec No.	Bar No.	Bar Diam., In.	R, In./Hr	*Micro-structure	Stress, Ksi	Hours To Rupture	% RA
1150	B70B	1-5/8	1/4	F	130	38	20
1151	B70T	1-5/8	1/4	F	130	35	23
1188	B70B	1-5/8	1/4	F	130	37	24
1189	B70B	1-5/8	1/4	F	120	189	21
1191	B72B	1-5/8	3/8	C/DC	120	345	19
1190	B72B	1-5/8	3/8	C/DC	108	801	15
1179	DS1782	7/8	1/2	DC	130	134	6
1178	DS1782	7/8	1/2	DC	120	442	14

* F = Aligned Fibers, C = Cells, D = Dendritic Cells

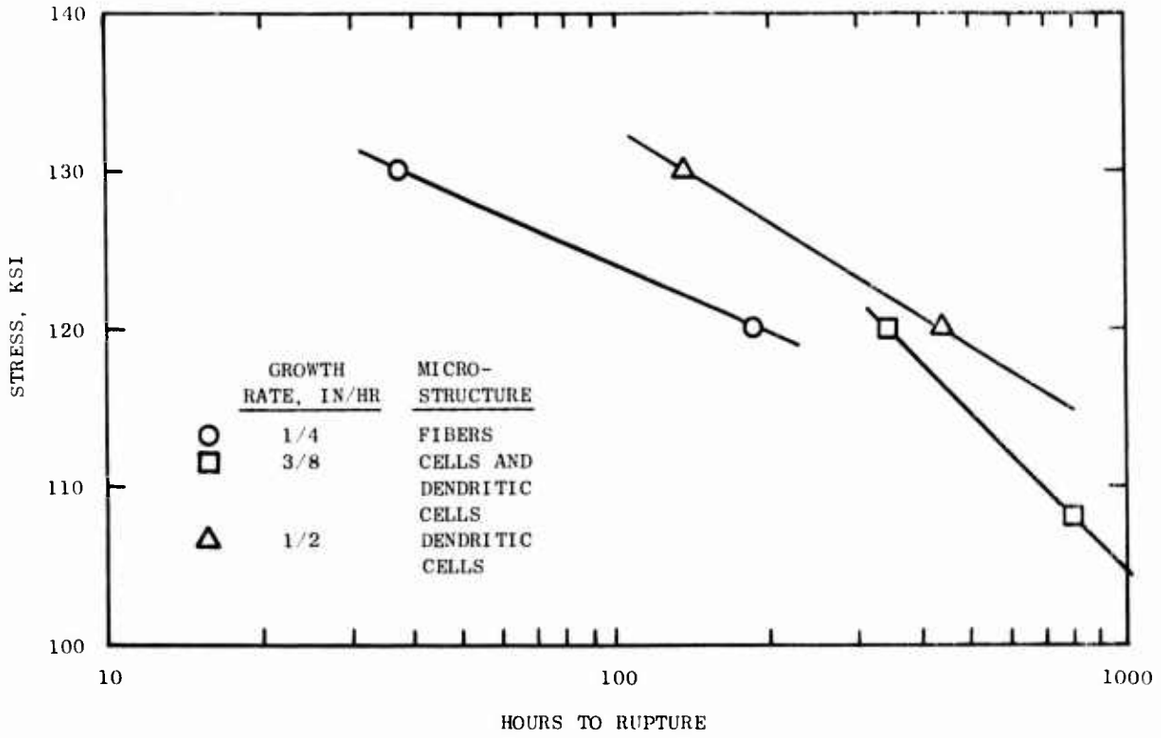

Figure 37. 1400°F Longitudinal Stress-Rupture Lives of Aligned and Misaligned Fiber NiTaC-13 Bar Bottoms (g_t~0.27) Tested in Air

TABLE 18

1200°F LONGITUDINAL TENSILE DATA FOR THREE DIFFERENT NiTaC-13 MICROSTRUCTURES

*Bar No.	R, In/Hr	+Micro-structure	Yield Stress, Ksi	0.2% Yield Stress, Ksi	U.T.S., Ksi	% Elong.	% R/A
70B	1/4	F	108	121	170	15.3	18.0**
71B	5/16	F	117	130	183	16.4	22.6**
70T	1/4	F	114	126	175	15.6	24.0**
71T	5/16	F	120	132	174	13.3	17.2**
77B	5/16	F-C	117	126	165	5.6	16.0
46B	3/8	C	119	129	160	4.8	9.3
65B	5/16	C	114	125	177	12.9	18.0**
72B	3/8	C	121	131	164	6.2	10.8
63T	5/16	D-C	121	129	149	3.6	11.6
65T	5/16	D-C	121	130	153	2.9	8.8
46T	3/8	D-C	125	133	152	3.3	8.5
72T	3/8	D-C	125	133	145	1.8	6.5
Banded Samples							
DB-22B	1/4	C	115	128	157	3.4	12.5
DB-22B	1/4	C	119	134	167	4.4	13.3
DB-9B	1/4	D-C	108	118	142	4.5	12.4
DB-9B	1/4	D-C	113	124	147	3.0	9.9

* B = bottom of bar; T = top of bar.

** Shear failure

\+ F = fibers; C = cells; D-C = Dendritic cells.

tensile strength and tensile ductility decreased. These effects are illustrated in Figure 38 which uses all data in Table 18 except results for DB-9B which was NiTaC-13F. The data in Figure 38 also indicate that yield strength increased with increasing fiber misalignment.

The results in Table 18 for the samples with bands are in reasonably good agreement with the bar results for equivalent microstructures. Microscopic analysis of longitudinal sections of the samples after test showed that the fracture path in each of the four banded samples was through the center of the band. The two transition zones in each sample were obviously stronger than the material within the band, and were therfore not indicated to be zones of weakness.

2.6.2.3 1200°F LCF - For this evaluation, a total of five rods were machined from three microstructural types of NiTaC-13 bars. Rene' 77 shoulders were then inertia welded to both ends of each rod and, finally, notched (K_t = 2.0) bars were machined. Load controlled, axial-axial LCF tests were conducted at 1200°F using an A ratio (alternating stress/mean stress) of 0.95 and a loading frequency of 20 cycles per minute. A description of the materials tested and the test data are summarized in Table 19. The data are also presented graphically in Figure 39 and indicate that LCF strength was degraded somewhat with increasing fiber misalignment.

2.6.2.4 1500°F HCF - For this evaluation, a total of five specimen blanks were machined from the same three sections of bars as were used for the LCF specimens. Rene' 77 shoulders were also inertia welded to both ends of the NiTaC-13 blanks, after which smooth LCF bars were machined. Three load controlled axial-axial tests were attempted at 1500°F at an A ratio of 0.95 and a loading frequency of 1800 cycles per minute. The three tests were unsuccessful because the specimens failed in the inertia welded joints. Therefore, the minimum diameters in the gage sections of the two remaining specimens were reduced, and two specimens were successfully tested by a step loading procedure to maximize information gained from so few specimens. The data presented in Figure 40 suggest that the cellular microstructure caused a slight reduction in 1500°F HCF strength.

2.6.2.5 1200°F HCF - To provide data for HCF life analysis of the blade shank region, discussed later in Section 5.2.3, it was necessary to obtain 1200°F HCF data for dendritic cellular NiTaC-13, representative of material present in all blade shanks. For this evaluation, three unnotched specimens were machined from a dendritic cellular bar, M-39, grown at 1/2 inch/hour using material from Heat V-423-C. These specimens were tested at 1200°F in a bending mode at an A ratio of ∞ with the following results:

Alternating Stress, ksi	N_f, Cycles to Failure
120	7,000
105	16,000
85	86,000

Comparison with corresponding data for aligned fiber material, presented in Section 3.2.6, indicates that dendritic cellular NiTaC-13 has substantially lower HCF strength under the test conditions used. (Figure 41).

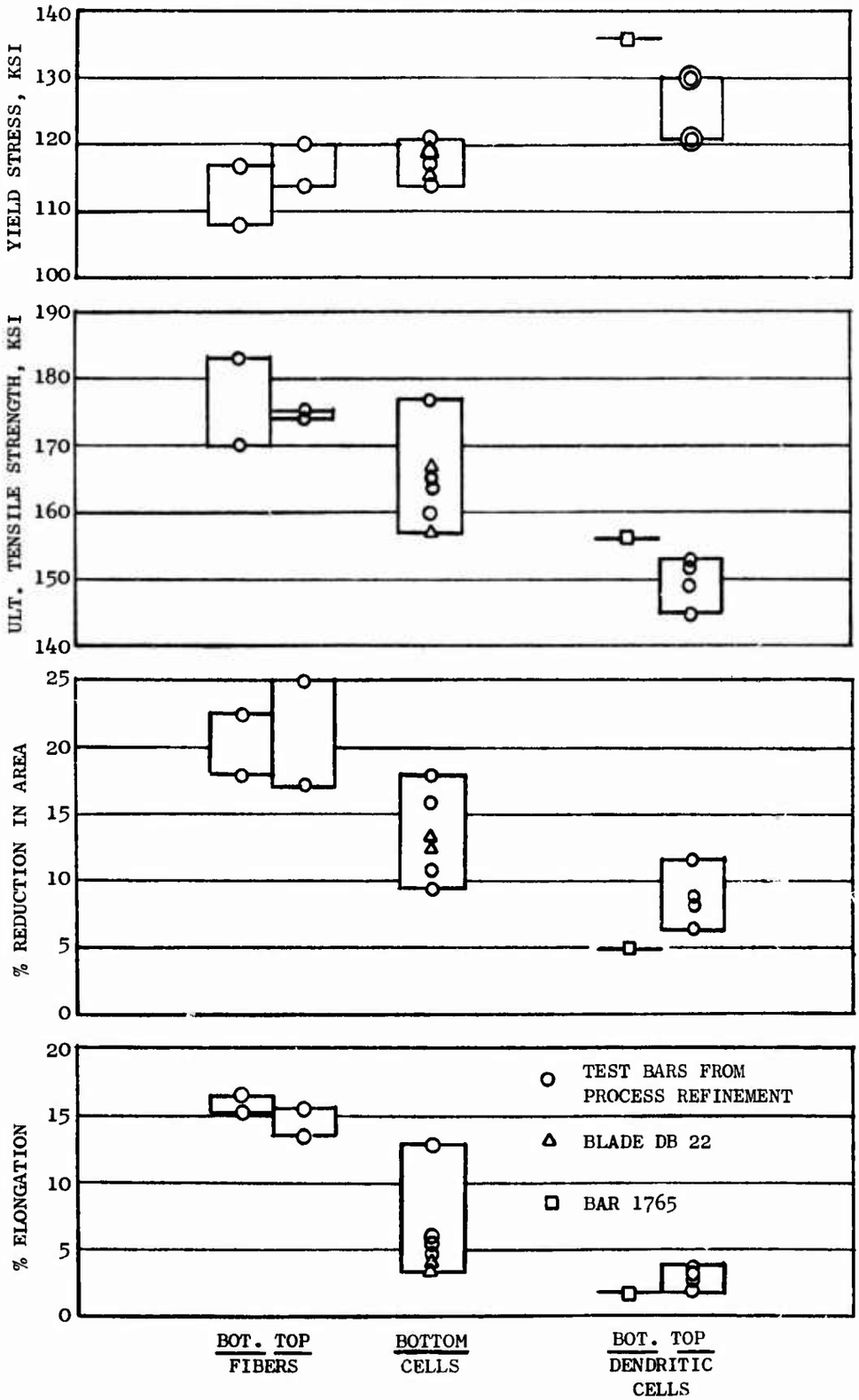

Figure 38. Effects of Carbide Defect Structures on 1200°F Longitudinal Tensile Properties

TABLE 19

AXIAL-AXIAL LCF DATA FOR LONGITUDINAL SPECIMENS OF THREE MICROSTRUCTURAL TYPES OF NiTaC-13

(Tests at 1200°F/K_t = 2.0/A = 0.95/20 cpm)

Bar No.	*Micro-structure	+Approx. g_t	Alt. Net Section Stress, Ksi	°Est. Alt. Pseudo Stress, Ksi	N_f, Cycles to Failure
63B	F	0.19	70	140	1,289
63B	F	0.19	50	100	107,000 (Run Out)
69B	C	0.18	60	120	7,882
69B	C	0.18	65	130	1,463
69T	D-C	0.53	60	120	1,738

* F = Aligned Fibers, C = Cells, D-C = Dendritic Cells

+ g_t= Volume fraction solidified at center of gauge (Based on metal volume above sort-out zone)

° Est. Alt. Pseudo Stress = K_t x Alt. Net Section Stress

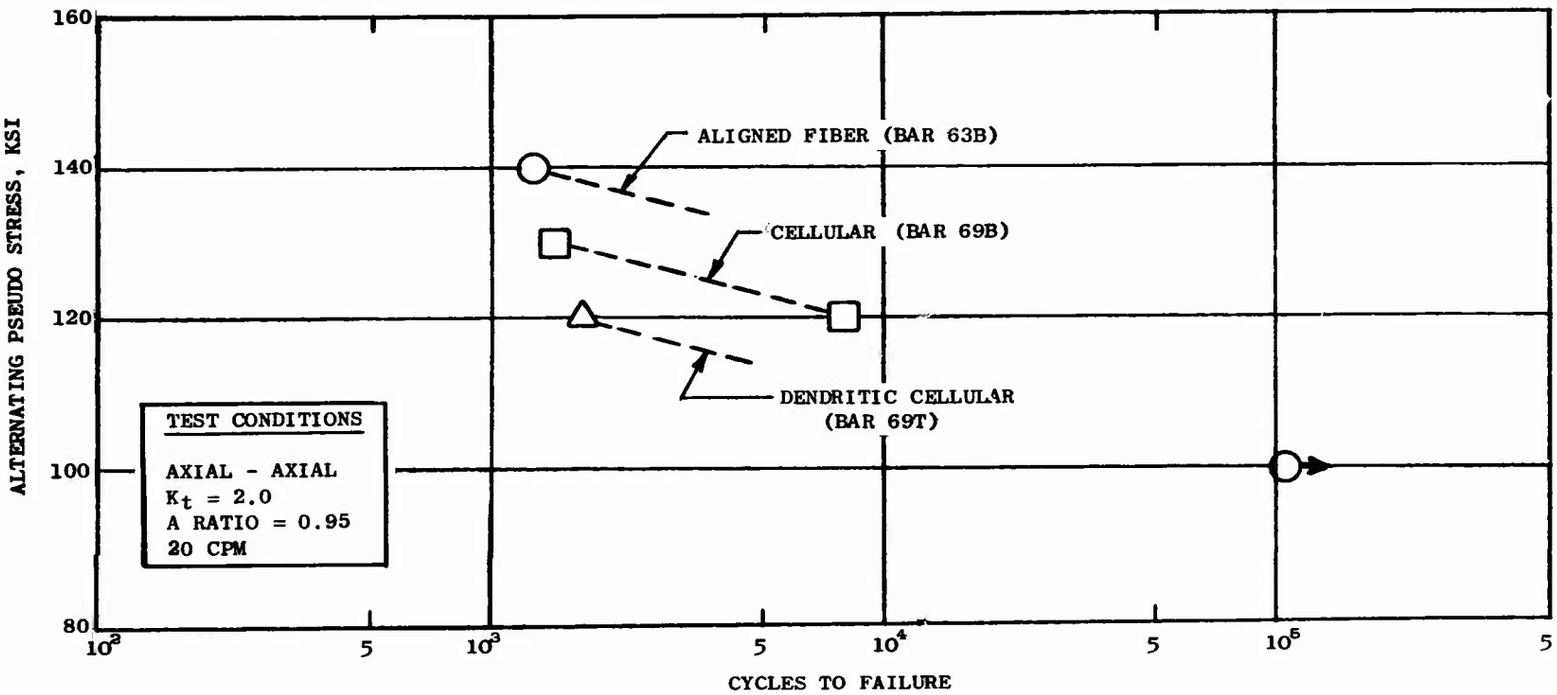

Figure 39. Effects of Carbide Defect Structures on 1200°F Longitudinal LCF Strength

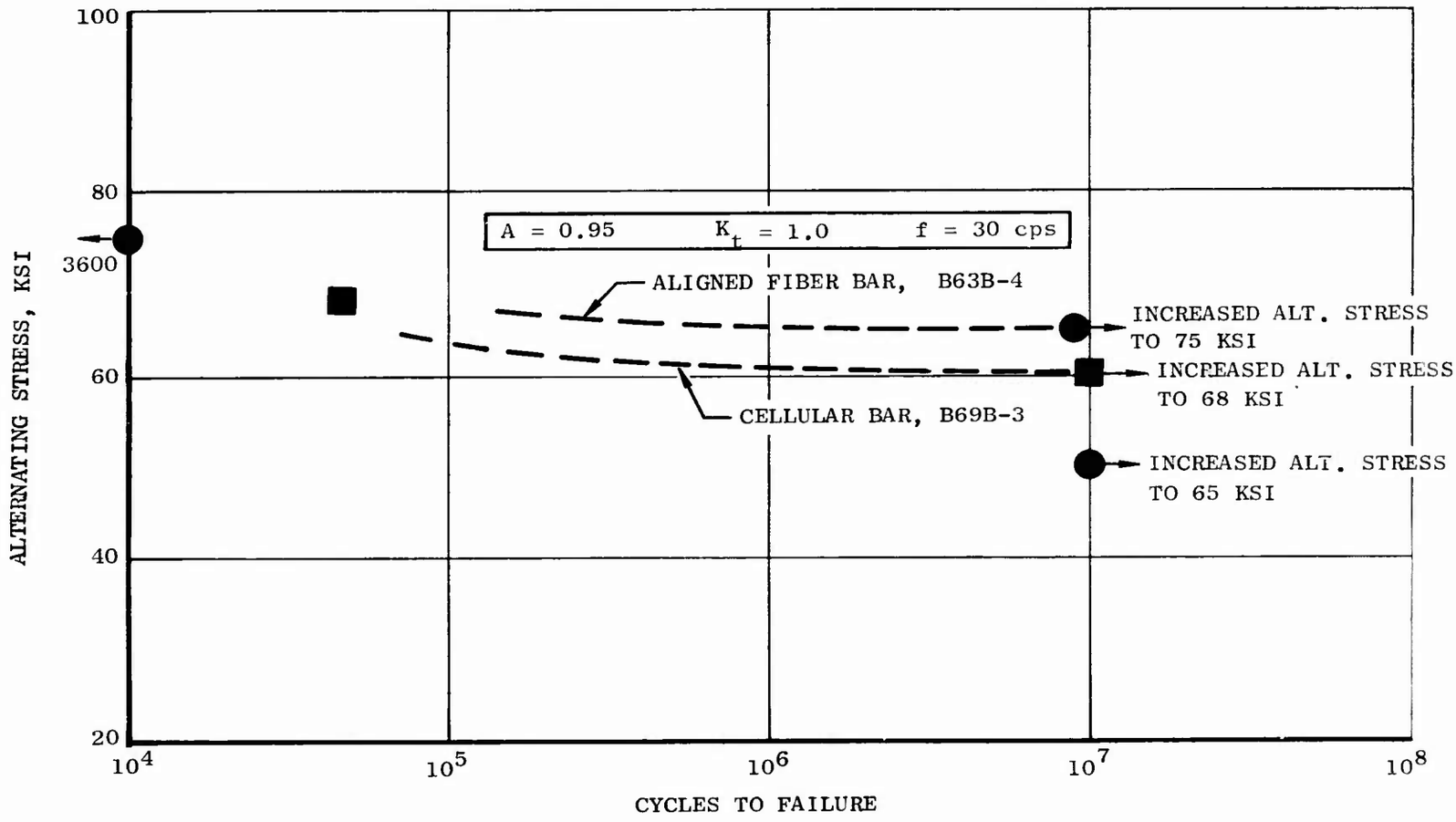

Figure 40. Effects of Carbide Defect Structure on 1500°F Longitudinal HCF Strength

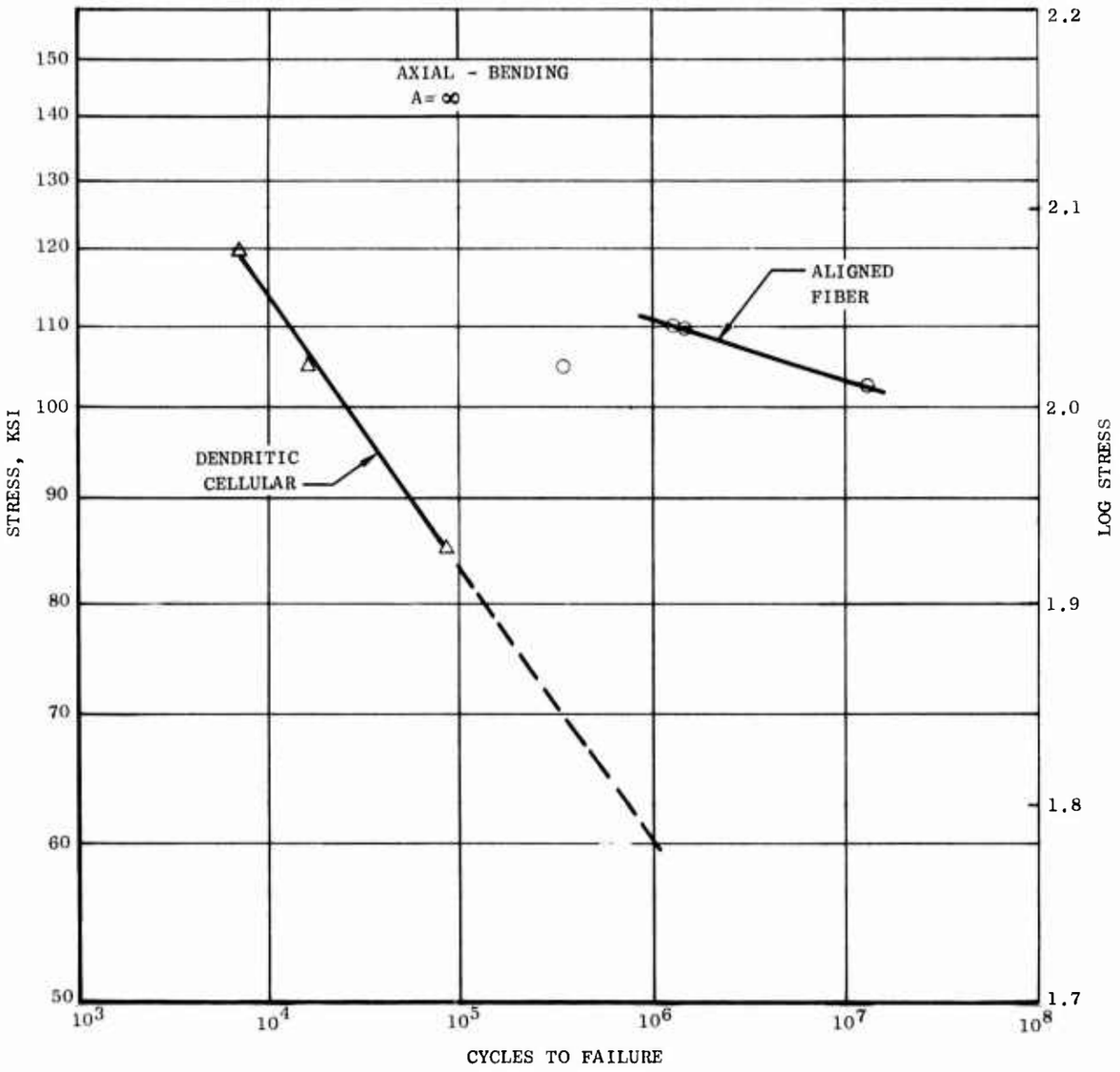

Figure 41. Effects of Carbide Defect Structure on 1200°F Longitudinal HCF Strength

6.2.6 Summary of Effects of Carbide Defect Structures on Longitudinal Properties

e NiTaC-13 property data in the foregoing sections indicated that Type II carbide defect crostructures, cells and dendritic cells, generally resulted in small decreases in strength low aligned fiber material. Exceptions included 0.2% yield strength at 1200°F and stress pture strength at 1400°F, where material with carbide defect structures were stronger. ıe latter may be due to a relatively small contribution of fibers to the total composite :ength in this temperature range.

:ess rupture and tension tests showed that transition regions, where carbide morphology anges from one form to another, are not regions of unusual weakness because banded ecimens were never observed to fail in transition regions.

ı the basis of these results, it was concluded that an inability to develop a fully aligned ıde casting would not seriously reduce the probability of meeting the overall program als and objectives. It was further concluded that a long range goal for NiTaC eutectics ould be to develop a process for producing blade castings having fully aligned airfoils d dovetails: possibly the carbide defect microstructures could be tolerated in the atform region.

7 BLADE CASTING DEVELOPMENT

he objective of this work was to develop a process, similar to the test bar process, for ısting J101 LPT blades having an aligned fiber microstructure throughout and as close to nal dimensions as practicable. This work was performed by CRD and included studies of egregation and carbide defect structures discussed in other sections, and the development PFS equipment and process parameters for blade casting.

.7.1 Blade Casting Facilities

'wo large Bridgman-type facilities were used in blade casting work: the first, designated .B, was used for early process development and; the second, designated DB, was a ıodification of LB that was built by General Electric and used exclusively for J101 LPT lade casting.

The LB facility consisted of two connected environmental chambers. The upper metal :hamber housed the melt crucible where the charge was melted by direct inductive coupling vhich promoted stirring and homogenization of the molten alloy. Power to the induction :oil was supplied by a 15 KW motor-generator set. The lower chamber consisted of a 9 .nch diameter silica tube which contained a 2-1/2 inch inner diameter graphite susceptor :hermally insulated from the silica tube by alumina beads. The susceptor was supported oy an alumina ring which rested on six alumina rods. Below the susceptor was a movable water cooled copper chill plate to which the mold and the screw type withdrawal mechanism were attached. The susceptor was heated inductively by means of a 25 KW RF oscillator (455 KHz) and a 9 inch diameter coil wound on the outside of the silica tube.

The LB design was considered inadequate for process development work of this program because: it was difficult to evacuate, making purging times very long (12 hours); the lack of ports made instrumentation difficult, and; the RF coil was located far from the susceptor making it both inefficient and difficult to focus the RF energy.

Therefore, the new DB facility was designed to incorporate the desired improvement. The upper melting chamber was the same as in the LB. The lower unit, illustrated in Figure 42, was a stainless steel tank with four access ports for observation, instrumentation, atmosphere and power feed through. Inside of the tank, a graphite susceptor was supported on an alumina stand. Surrounding the susceptor was an alumina tube and the space between the two was filled with bubbled alumina. The RF coil was positioned around the alumina tube and within the thank. Both chambers could be rapidly evacuated to a pressure of 20 microns and back filled with high purity argon.

During initial trails of the DB facility, arcing occurred at two locations causing premature termination of runs: at the RF coil feed through, and between the RF coil and the alumina sleeve which served as the outer wall of the furnace. To solve the problem of arcing at the lead through, a new entrance port was constructed which had a Re-X® ceramic insulator for the hot lead, as illustrated in Figure 43.

The cause of arcing between the RF coil and the alumina sleeve was assigned to the high electrical conductivity of alumina at elevated temperatures. During early tests, the alumina sleeve reached temperatures in the range of 1500° to 1800°F, and arcing occurred in this range. This problem was solved by a new furnace design and improved thermal insulation, illustrated in Figure 44.

With this design the outer surface temperature of the furnace reached only about 400°F, and the power requirements for casting were reduced by about 40 percent.

2.7.2 Preliminary Blade Casting Experiments

There were three questions concerning blade casting that needed initial attention:

- Blade casting oversize requirements
- Temperature capability of the GE mold
- Microstructural quality of prototype blade castings

Experiments described in the sections that follow were performed to answer these questions.

®Registered trade mark of the General Electric Co.

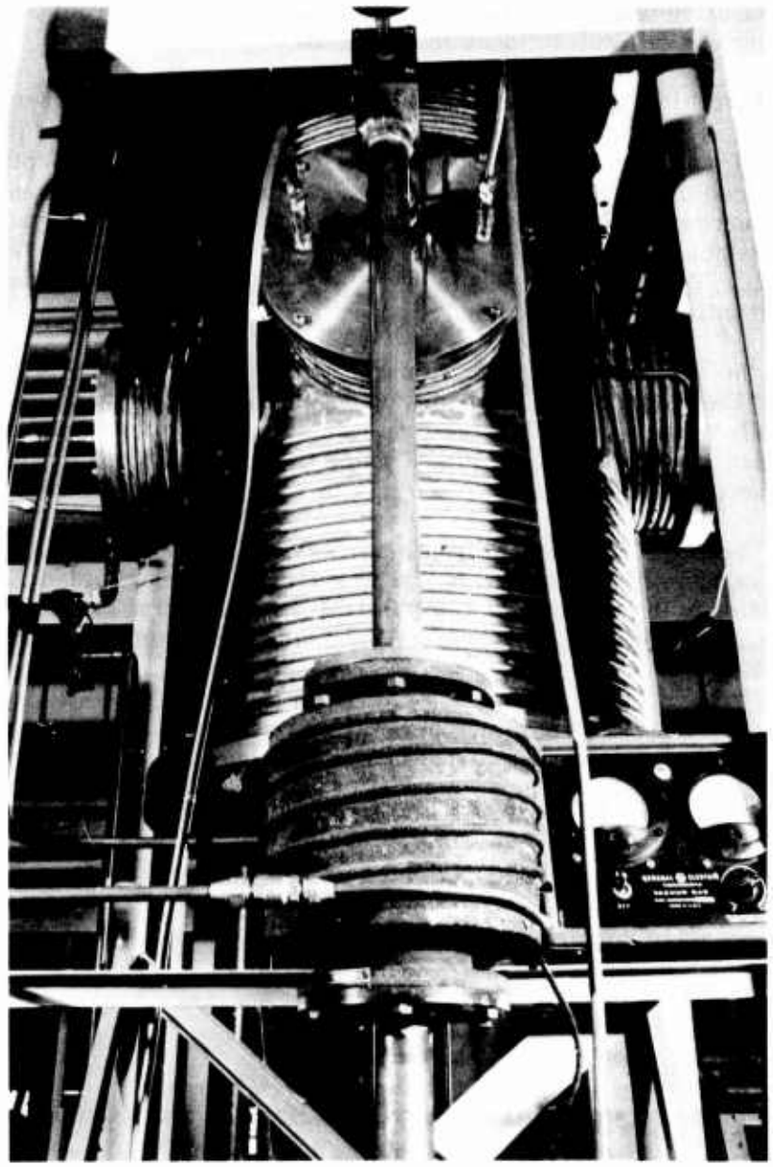

Figure 42. View of Lower Tank Containing Induction Heated Furnace in DB Facility

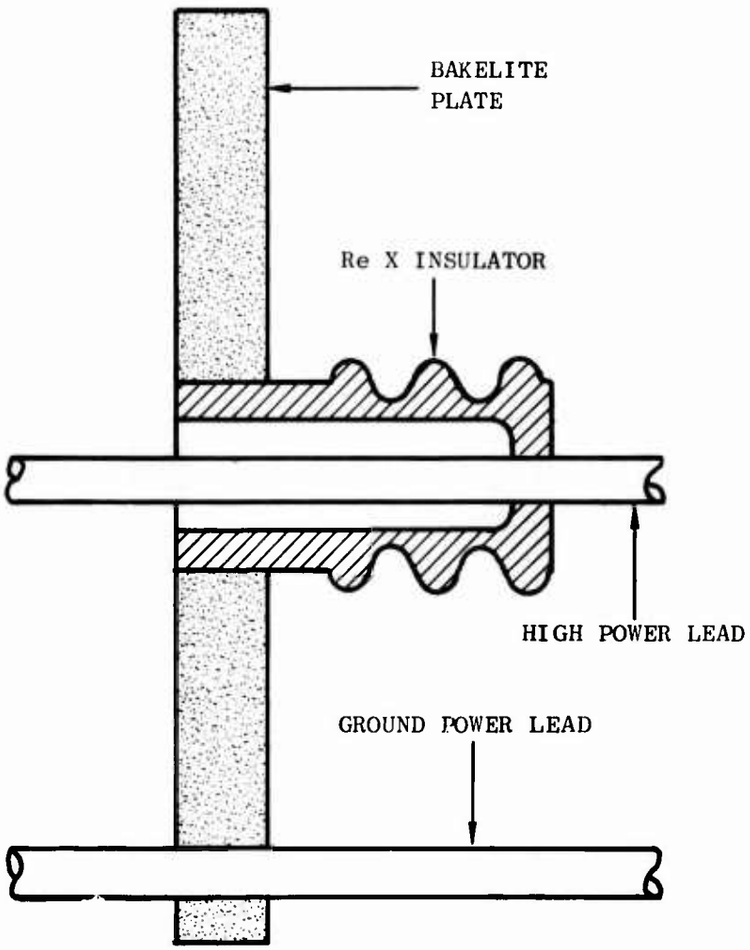

Figure 43. Schematic View of RF Power Feedthrough

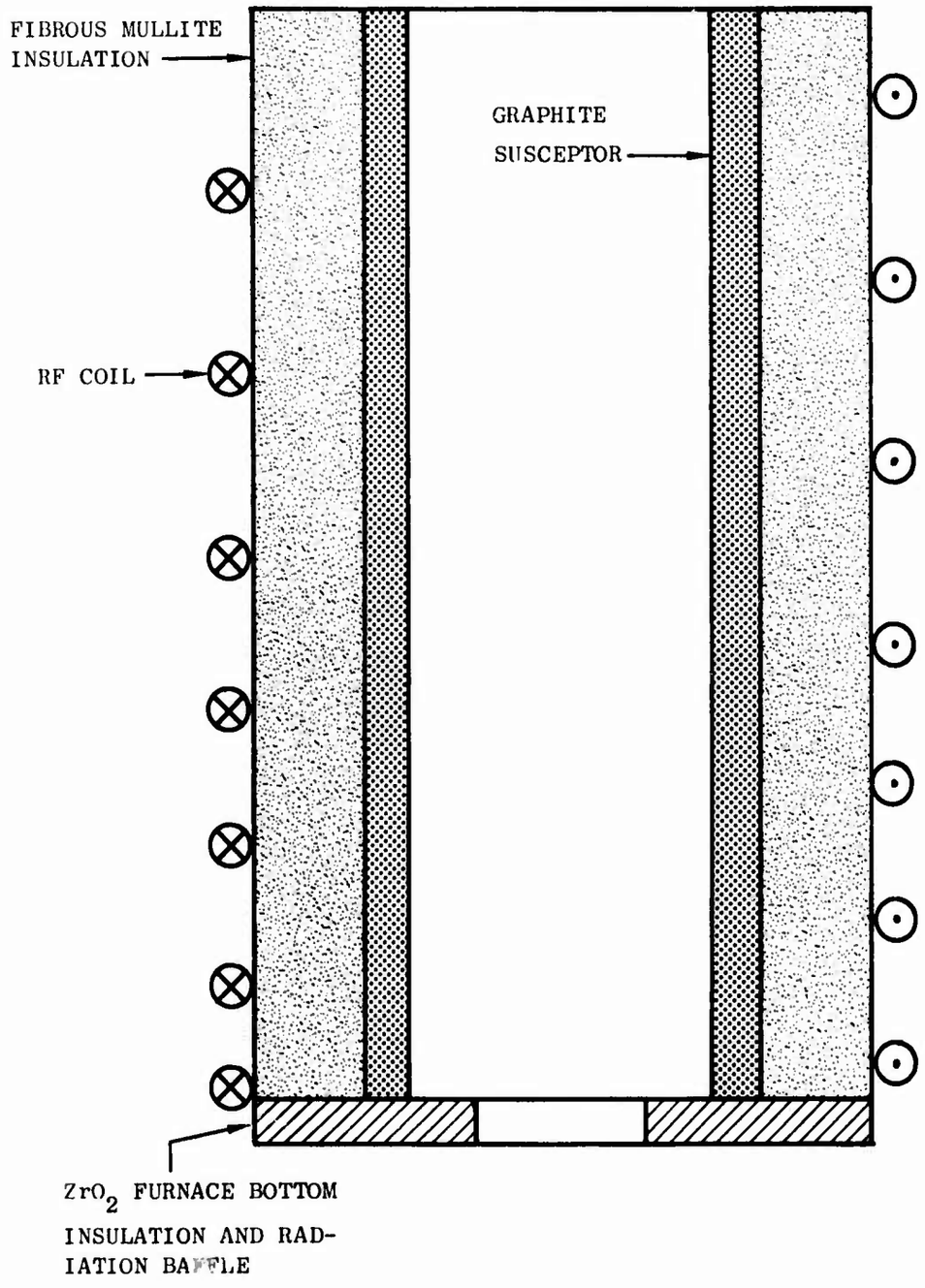

Figure 44. Schematic View of Induction Heated PFS Furnace Configuration

2.7.2.1 NiTaC-13 J101 LPT Blade Casting Design - To establish the oversize requirements, two blade casting designs were used to evaluate microstructural and dimensional factors. The first design included the final size J101 LPT airfoil and a rectangular parallelepiped for the platform/dovetail section. The second design also included the final size J101 LPT airfoil, but had a close-to-size dovetail/platform section. Both designs used dovetail and airfoil extensions to provide starter blocks for the sort-out zone, extra molten metal for maintenance of G_L, and reservoirs to reduce segregation. Wax patterns for the first design were made in relatively crude silicone rubber molds, and those for the second design were standard superalloy J101 LPT blade waxes to which were welded the wax extensions.

Shell molds of silica bonded alumina developed prior to this program by General Electric[7] were made to have thin cross sections with minimal changes in cross sectional area. The advantages of these extended blade and mold designs were:

1) Thin mold cross sections promote high thermal gradients,

2) Minimal changes in cross sectional area reduce the problem of providing an effective radiation baffle at the furnace bottom,

3) The relatively low volume fraction solidified when the blade is cast reduces segregation, and

4) The airfoil extension provides the means to maintain a high gradient through PFS of the blade casting.

PFS NiTaC-13 castings of both designs are shown in Figure 45. Tip-up castings of the first design in Figure 45A had well aligned fibers throughout the airfoil and dovetail sections, with the exception of one dendritic cellular band that occurred in the dovetail section just below the platform. Microstructures of selected areas of this casting are shown in Figure 46.

Tip-up castings of the second blade design, Figure 45B, also had well aligned fibers throughout the airfoil but bands were observed just below the platform as in the first design, and in the regions of the dovetail tangs.

Blade castings were examined to determine the depth of surface layer flaws which is important to the establishment of blade casting oversize requirements. The most common type of flaw observed was a coarse dendritic carbide that appeared to be surface nucleated. These penetrated to depths of about 0.02 inches in the dovetail section, and about 0.01 inch in the lower section of the airfoil. Hence, from the standpoint of surface layer flaws, an envelope of 20 mils around the blade was indicated to be adequate.

Other considerations important to establishment of the blade casting oversize requirements were mold distortion during PFS, and thermal expansions of both NiTaC-13 and the mold material. Although these factors would not have a large unpredictable effect on the dimensions of a given blade cross section, they could have a large effect on the spatial location of sections and intensify problems in final machining to meet dimensional specifications.

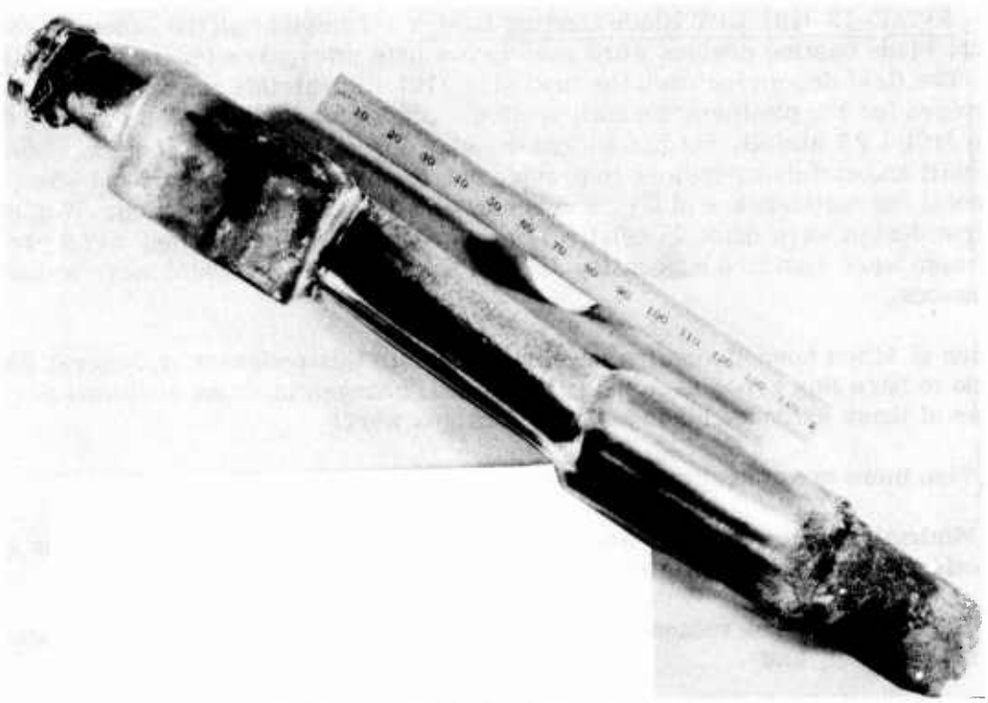

A. PARALLELEPIPED DOVETAIL SECTION

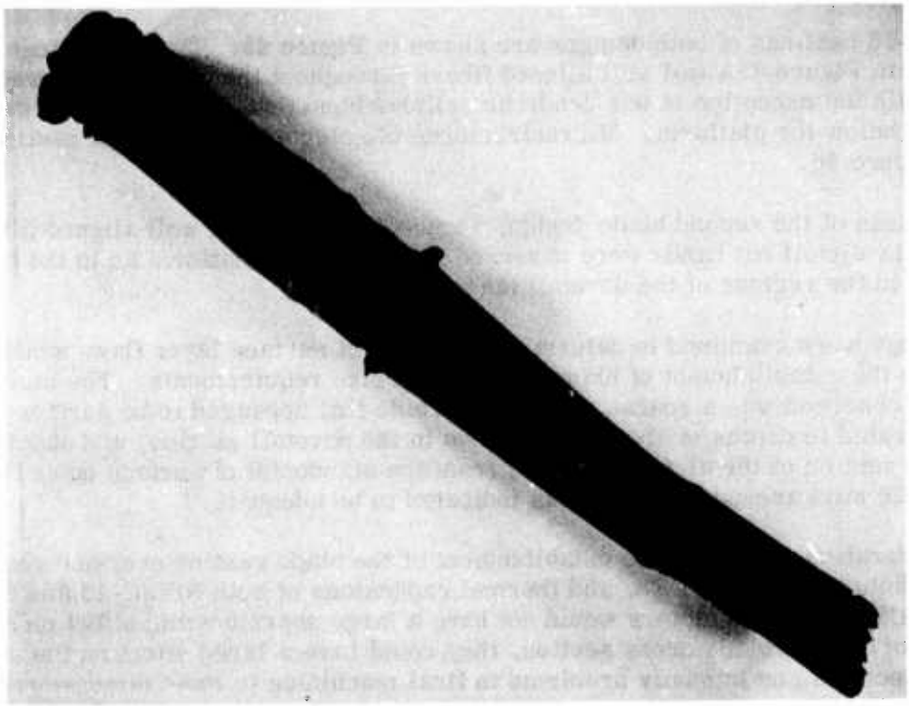

B. CLOSE-TO-SIZE DOVETAIL SECTION

Figure 45. Extended Blade Casting Designs

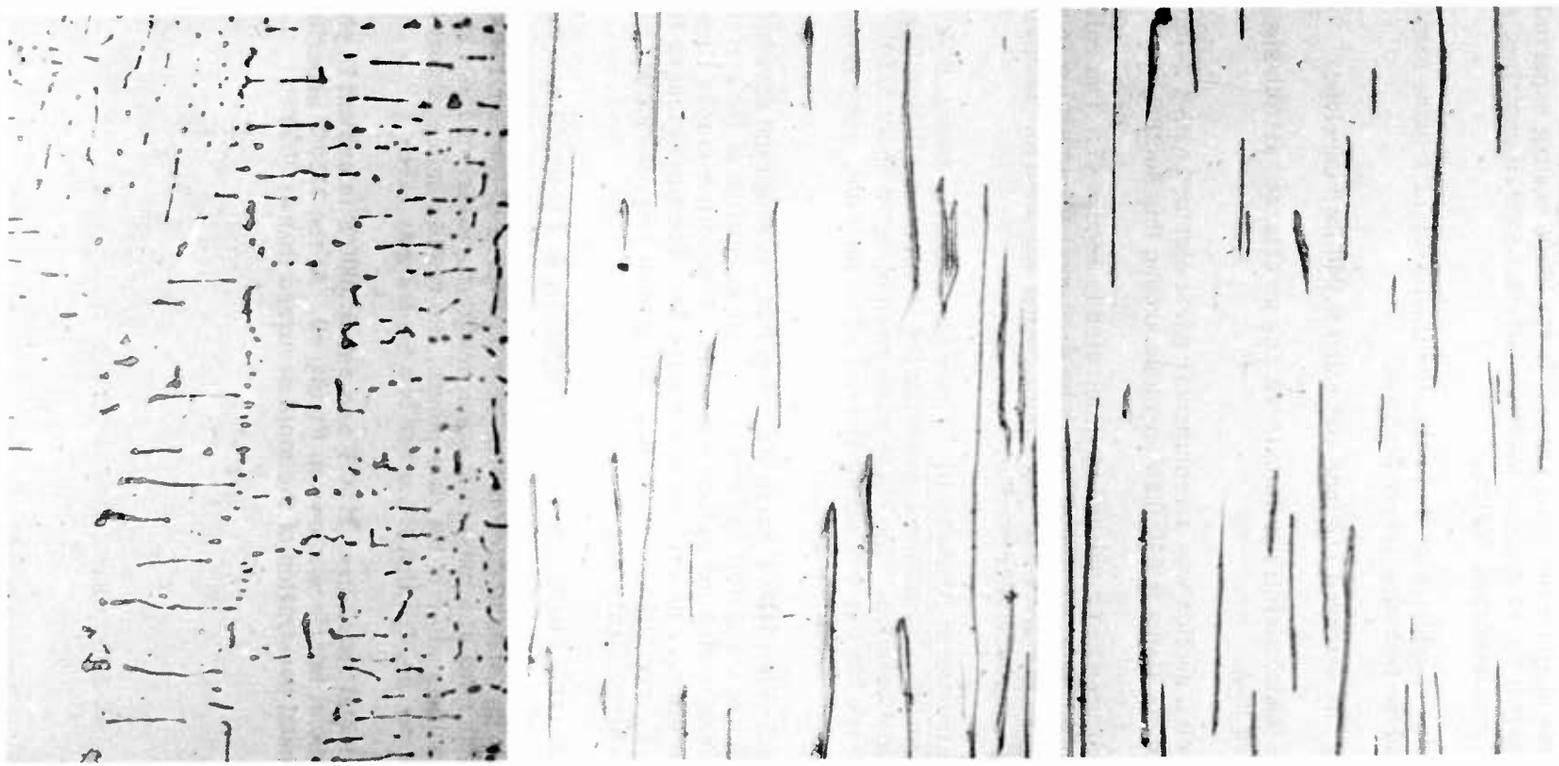

A. BAND AT DOVETAIL-AIRFOIL TRANSITION REGION

B. AIRFOIL NEAR DOVETAIL

C. AIRFOIL TIP

Figure 46. Photomicrographs of Longitudinal Sections from NiTaC-13 Blade Casting

A final consideration was the platform/dovetail shape. In the blade casting experiments just described, it was found that the cast close-to-size platform/dovetail contained more bands than the rectangular parallelepiped design.

After evaluating the foregoing consideration and data, the final J101 LPT blade casting design was selected and had the following major features:

1) The airfoil section was extended 1/2 inch and had a 0.040 inch envelope.

2) At the tip of the extended airfoil section, there was an enlarged airfoil-shape extension, 3 inches long.

3) The platform/dovetail section was a rectangular parallelepiped with a 2-inch extension. There was also a 0.040 inch envelope around this section.

Wax pattern tooling was procured and a pattern is illustrated in Figure 47. The volume of this wax pattern was measured as a function of length by progressive immersion in water, and the results are also shown in Figure 47. This information was used for modifying the casting configuration to minimize segregation.

2.7.2.2 Temperature Limitations of Blade Mold - Three blade casting runs (LB76, LB80 and LB81) were made to provide information concerning the temperature limitations of the GE silica bonded alumina mold system. One blade was grown tip up at about 3180°F superheat temperature and two blades, one tip up and the other tip down, were grown at about 3000°F.

Microstructural examination of the 3180°F blade indicated that, although the dovetail/platform and bottom one inch of the airfoil had fibers, the upper portion of the airfoil contained areas without fibers, indicating carbon depletion. Photomicrographs illustrating the differences between the two regions are given in Figure 48. The fibers among the denuded areas in Figure 48B were aligned, indicating that growth was not cellular but that it was PFS growth from a carbon poor melt.

Carbon analysis data for the three blades are shown graphically in Figure 49 as a function of g_b, the volume fraction solidified. Also shown in Figure 49 are the locations of the three blades with respect to g_b, and the carbon profile from Figure 10 for Bar 1340 that was PFS in recrystallized alumina at a maximum superheat temperature of about 2930°F. Although there was appreciable scatter of the data points, the results indicated that blade LB81 (3000°F) did not lose carbon, but that the other two blades may have.

Further evidence of mold-metal reaction of 3180°F and not at 3000°F is evident in photomicrographs of the mold-metal interface shown in Figure 50. At the 3180°F superheat temperature much more metal penetration of the mold occurred than at 3000°F.

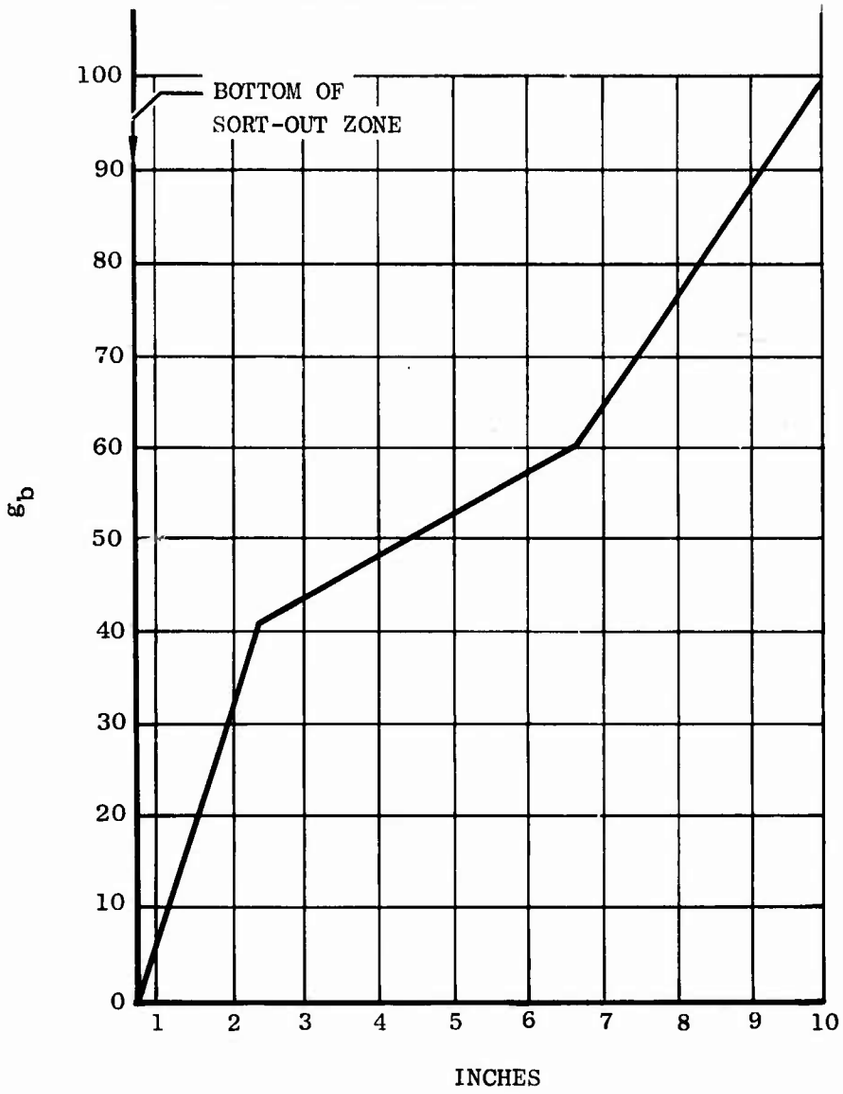

Figure 47. Eutectic J101 LPT Blade Wax Pattern and g_b as a Function of Distance from Bottom of Dovetail for Tip Up Casting

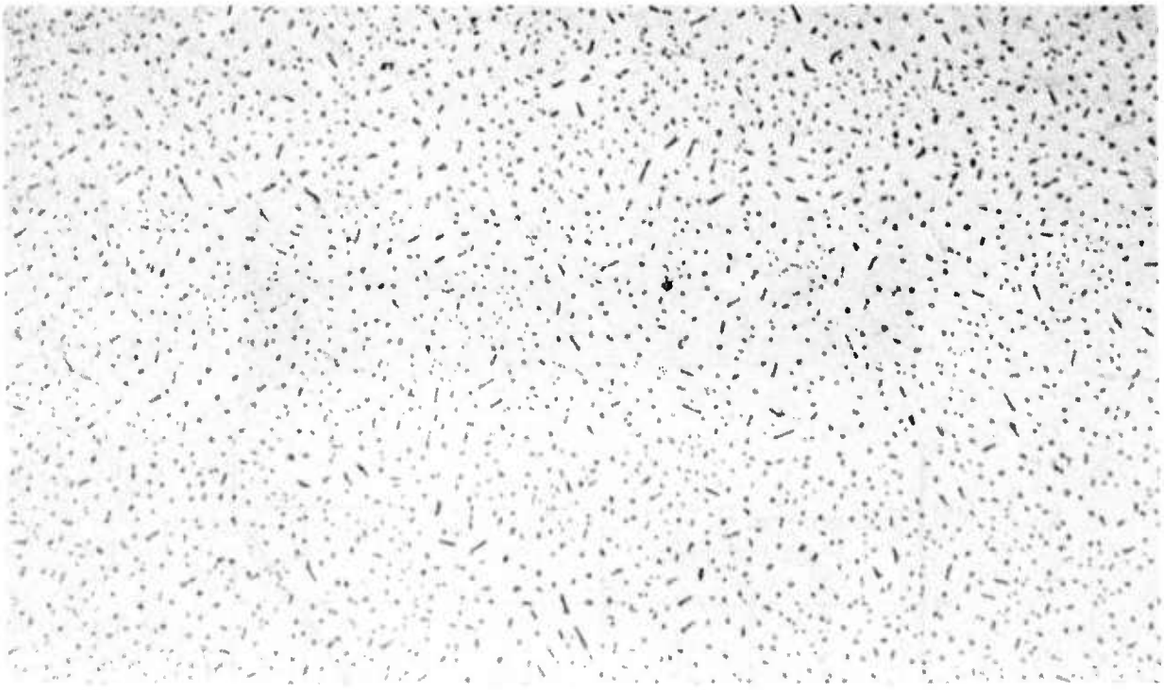

A. DOVETAIL SECTION

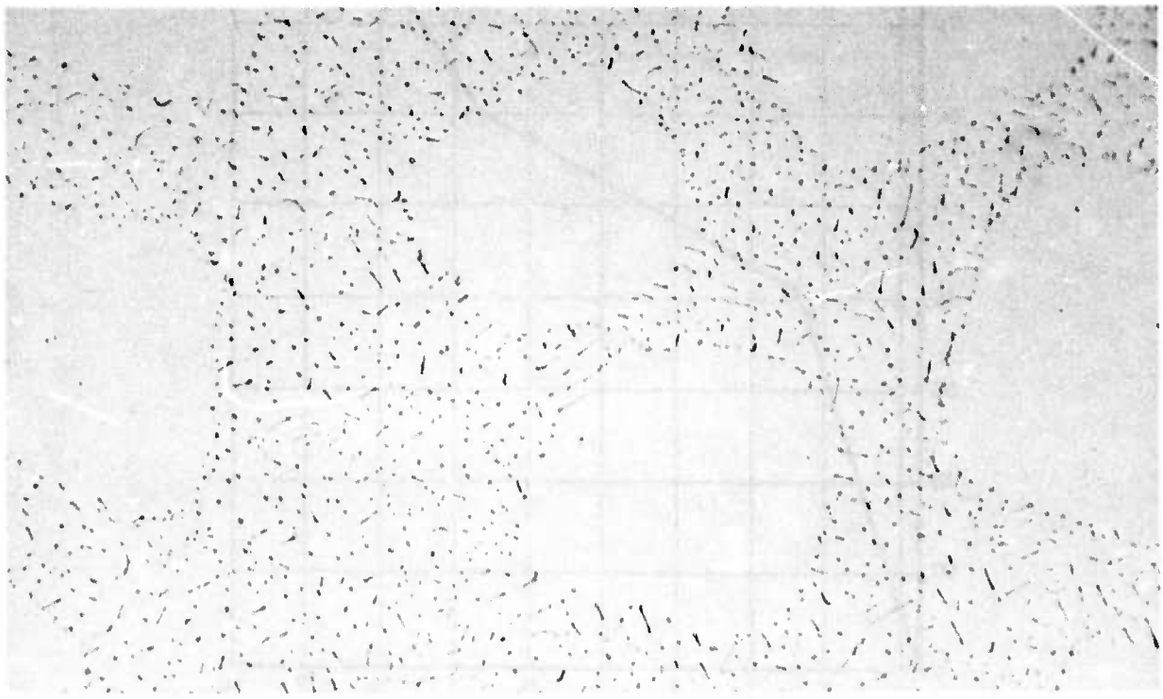

B. AIRFOIL, 1" ABOVE PLATFORM

Figure 48. Photomicrographs of Transverse Sections from NiTaC-13 Blade Cast Tip up with T_{MAX} of 3180°F

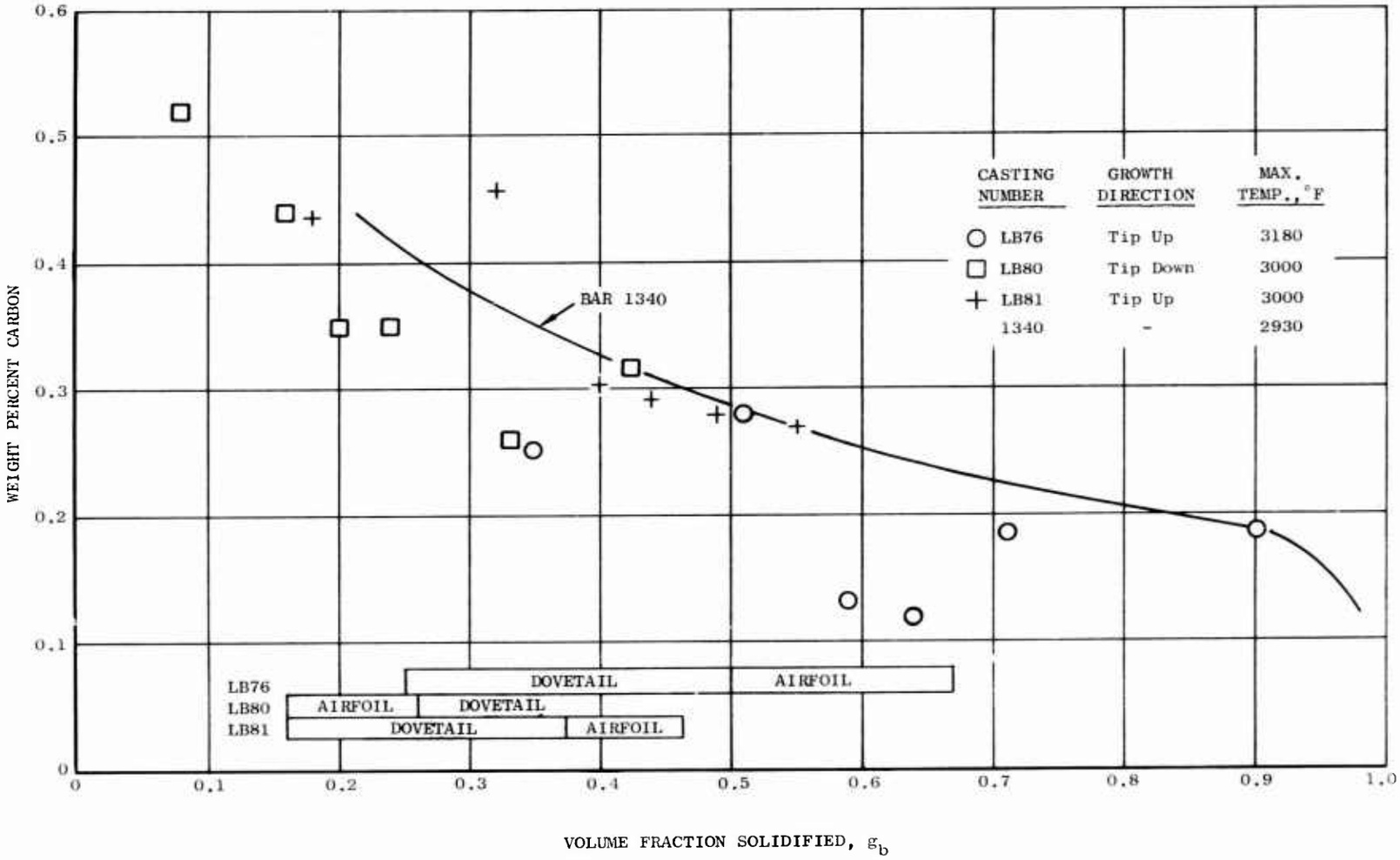

Figure 49. Carbon Gradients in PFS NiTaC-13 Blades Cast in Silica Bonded Alumina Molds and Bar 1340 PFS in a Recrystallized Alumina Crucible

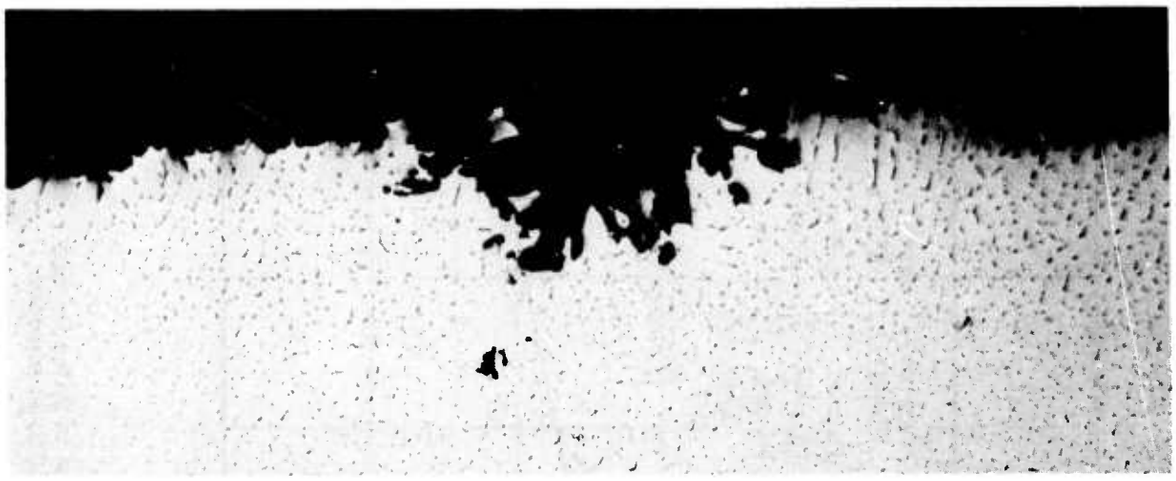

A. TRANSVERSE SECTION, T_{max} = 3180°F, 160X

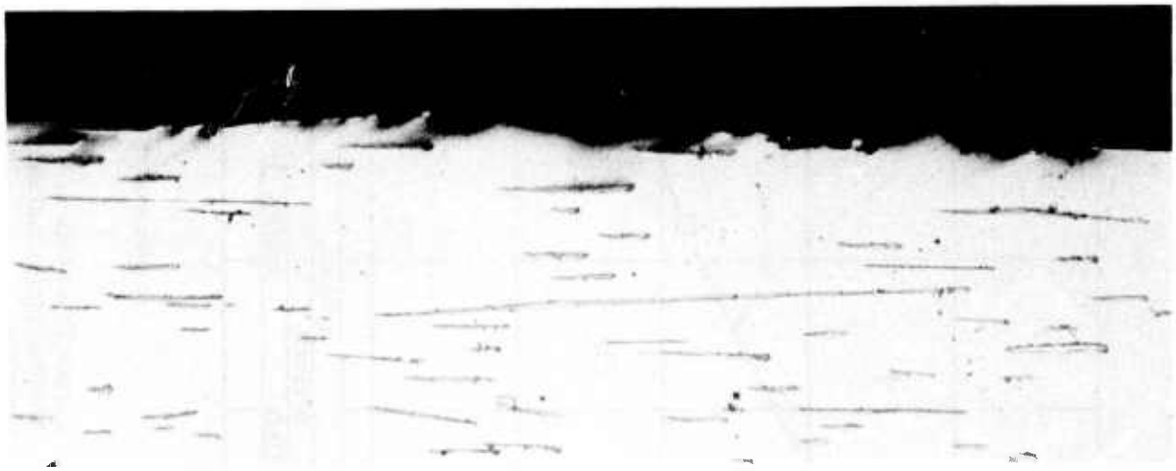

B. LONGITUDINAL SECTION, T_{max} = 3000°F, 315X

Figure 50. The Effect of T_{MAX} on the Appearance of the Mold/Metal Interface

On the basis of these results, it was concluded that the upper temperature limitation of the mold system was between 3000° and 3180°F.

2.7.2.3 Formation of Dendritic Cellular Band in Blade Dovetail - Blades cast in the GE silica bonded alumina molds had a rough surface, some surface layer pits penetrating up to 0.012 inches, and a band in the dovetail section just below the platform. It was anticipated that the oversize blade casting design described in Section 2.7.2.1 would provide sufficient stock for removal of the surface flaws. The band, however, was undesirable.

In order to study the mechanism of formation of the band, a PFS run was made using an oversize airfoil design (similar to Figure 45A) to permit measurement of the liquid/solid interface position during mold withdrawal at 1/4 inch/hour. The measurements were made by probing the melt with a thin rod of high purity alumina and measuring the position of the interface. These data were then used to calculate solidification rates and the results are given in Figure 51. The following interpretation of the measured variations in solidification rate provides a reasonable explanation of why the band was formed:

1) The initial solidification rate was less than 1/4 inch/hour because, as mold withdrawal began, the furnace bottom insulation was heated by radiation from the mold. This tended to lower the liquid/solid interface position with respect to the furnace bottom.

2) As the solid-liquid interface approached the airfoil section, the smaller airfoil area could not provide a sufficiently high heat flux to maintain a high gradient at the larger area of the dovetail section. Therefore, the gradient decreased and the solid/liquid interface moved up relative to the furnace bottom, thus increasing the solidification rate. This in turn reduced G_L/R below the minimum required for fiber growth and formed a dendritic cellular band.

3) After the interface was in the airfoil region, sufficient heat was supplied to maintain an adequate gradient and the interface again moved down with respect to the furnace bottom. This decreased the solidification rate and, as the insulation temperature reached steady state, the solidification rate approached the withdrawal rate. During this period, G_L/R increased and fiber growth resumed.

On the basis of this study, the plan formulated for producing a fully aligned blade casting included:

1) Refining the furnace configuration and PFS parameters to maximize G_L

2) Modifying the blade casting design and mold configuration

2.7.3 Blade Furnace Configuration Refinement

Initial work was aimed at establishing a furnace configuration and operating parameters that would yield a G_L of at least 300°F/inch which was slightly above the minimum value for PFS of NiTaC-13 bars at 1/4 inch/hour. Higher values of G_L were being sought as a means to eliminate the dendritic cellular band in the platform/dovetail section of blade castings. A major operating parameter investigated was T_{max}.

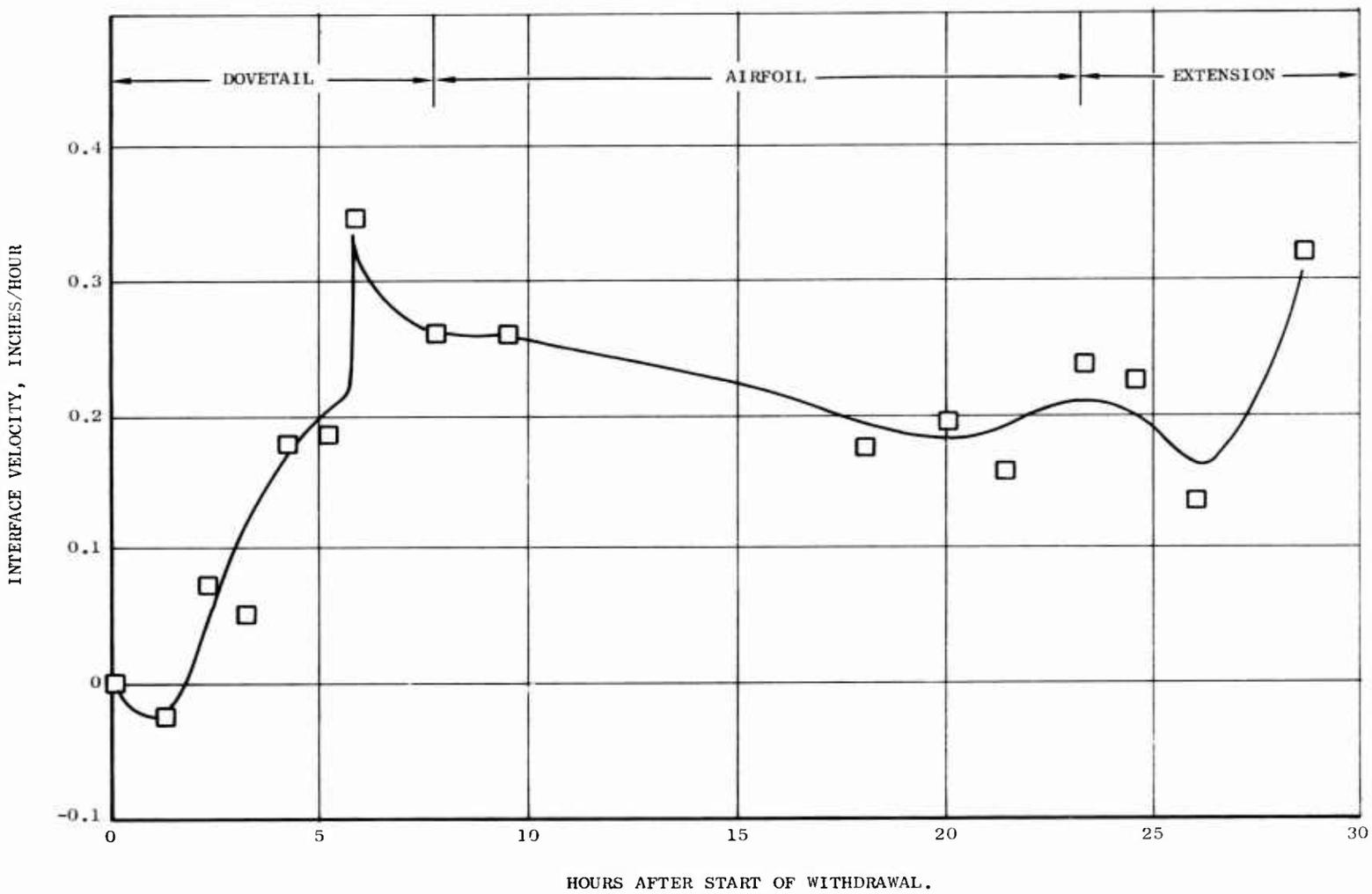

Figure 51. Variations in Solidification Rate During Withdrawal at 1/4-Inch/Hour of NiTaC-13 Blade LB 87

The principal variables in furnace configurations evaluated were the designs of the RF coil, the susceptor, and the furnace bottom insulation which also served as a radiation baffle. Variations tried were as follows:

1) RF Coil Designs

   - 7 inch diameter, 7 turns
   - 9 inch diameter, 7 turns

2) Graphite Susceptor Designs - All susceptors were 2-1/2 inches ID x 3-1/2 inches OD x 12 inches long. These were slotted to concentrate heat in the unslotted regions. Slot configurations used were:

   - Slotted from top to 4, 3 or 2 inches above bottom
   - Slotted in middle leaving 2 inches unslotted at bottom and 1 inch unslotted at top

3) Hybrid Susceptor Designs - In these a center section of the susceptor was alumina and the two end sections were graphite. Lengths of each section were varied as follows:

	Section Length, Inches		
Susceptor Design	Graphite Bottom	Alumina Center	Graphite Top
1	3	8	1
2	4	4	4

4) Furnace Bottom Insulation/Radiation Shield - Many thickness ranging from 1/2 to 1-1/2 inches of several insulating materials, including Al_2O_3, ZrO_2 and Fiberfrax, were used singly or in combination.

A total of 34 runs were initiated to evaluate the cited variables. Runs included 1-1/2 and 1-5/8 inch diameter bars using recrystallized alumina tubes (no bottoms) and J101 LPT blades (tip up) using silica bonded alumina shell molds. Both tubes and molds were attached to the bottom chill plate. The first 11 runs were bars and the NiTaC-13 charge was in-situ melted. Thereafter, all tubes and blade molds were heated empty and then filled with molten metal. Power to the plate of the RF oscillator tube was used to regulate temperature prior to the start of a run. After a minimum time of 15 minutes for temperature equilibration, the liquid metal temperature profile was measured to determine G_L. This was done through use of a probe consisting of a Pt/Pt-Rh or W/W-Re thermocouple with the bead recessed into a double hole alumina insulation tube and protected by a plasma sprayed alumina coating. For the measurements, the probe was lowered into the melt until it touched the solid/liquid interface. Temperature was measured at the interface and in 0.1 inch steps above it for the first inch and in 1 inch steps thereafter.

2.7.3.1 Temperature Gradient Prior to Start of Withdrawal - Details of the 17 completed runs with all-graphite susceptors are presented in Table 20. G_L and T_{max} data for bars and blades are compared in Figures 52 and 53, respectively, with the average curve obtained previously for bar runs in the resistance heated facility, Figure 22. There was more scatter in the induction furnace data than in the resistance furnace data, and the trend of increasing G_L with increasing T_{max} was not as strong in the former, particularly for the blade data. On the basis of a study of all data in Figures 52 and 53, the cause of data scatter could not be assigned to any of the furnace configuration factors that were evaluated. It is possible that variations in other unmeasured heat transfer factors were major contributors to scatter, such as mold dimensions, RF coil location, or degree of coupling of the casting to the bottom chill plate.

2.7.3.2 Effect of Withdrawal Distance on Temperature Gradient - During blade Runs DB33 and 34, temperature profiles and solid/liquid interface positions were measured at increasing mold withdrawal distances. Results for tip up Run DB34, given in Figure 54, were typical of both runs and show G_L and T_{max} at various positions of the liquid/solid interface in the blade during solidification. As shown, G_L was about 310°F/inch when the interface was below the platform in the dovetail section. Then, as withdrawal continued and the interface moved into the airfoil section, there was a large increase in G_L to a maximum of about 560°F/inch. This was accompanied by a significant increase in T_{max} from about 2980° to about 3035°F. Thereafter, both G_L and T_{max} decreased continuously to values of about 340°F/inch and 2825°F, respectively, in the airfoil top. Throughout this run the position of the interface with respect to the furnace bottom remained relatively constant, indicating that the solidification rate equaled with withdrawal rate.

The data in Figure 54 indicate that G_L in the dovetail/platform region was sufficiently high to achieve aligned fibers at a withdrawal rate of 1/4 inch/hour. The fact that a cellular band was almost always observed here in blade castings indicated the possibility that the band was caused by solute dumping. The latter could be due to local rejection of solute ahead of the liquid/solid interface because of the changes in blade area in this transition region. Solute dumping, then could cause an increase in the critical G_L ratio to a value above the actual.

The decrease in G_L and T_{max} in the airfoil section, Figure 54, indicated that the power control method used in the DB facility may not have been adequate and that direct control of furnace temperature may be required.

2.7.3.3 Hybrid RF Susceptor Design - Susceptor design 1 described in Section 2.7.3 was used in conjunction with a 7 inch diameter RF coil, having 3 turns around the bottom graphite section and one turn around the top graphite section. With this design there was insufficient heat to reach the required maximum melt temperature.

Two tip up blade runs were successfully made with susceptor design 2 and a 7 inch diameter RF coil, having 4 turns around the bottom graphite section and 2 turns around the top graphite section. In both runs, DB38 and DB39, the power required to reach a maximum metal temperature range of 2900° to 3000°F was about 15 percent greater than that for all-graphite susceptors. During each run, G_L was measured at different mold withdrawal

TABLE 20

EXPERIMENTS TO REFINE FURNACE CONFIGURATION FOR BLADE CASTING

DB Run No.	*Mold Type	R-F Coil, Diam/Turns	Unslotted Susceptor Length, Inches	Furnace Bottom Insulation Thickness, In.	R-F Oscillator Plate Current Amps	T_{max} °F	Initial G_L* °F/In.
3	1-1/2" Bar	9"/7	4	1-1/2	1.00	2950	345
6	1-1/2" Bar	9"/7	4	1	1.00	3075	270
9	1-5/8" Bar	9"/7	4	1	1.10	3000	315
10	1-5/8" Bar	9"/7	3	1	1.10	3040	455
15	1-5/8" Bar	7"/7	3	1	1.45	3195	510
18	Blade	7"/7	3	11/16	1.20	2945	365
20	Blade	7"/7	3	1	1.40	3075	630**
21	Blade	7"/7	3	1	1.35	3075	220
22	1-5/8" Bar	9"/7	2	1	1.20	3180	465
23	Blade	9"/7	4	1-1/2	1.12	3025	345
25	Blade	9"/7	4	1-1/2	1.12	3155	240
26	1-5/8" Bar	9"/7	2 (Bottom) 1 (Top)	1	1.10	3130	280
29	Blade	7"/7	3	1-1/2	1.28	2915	230
31	Blade	7"/7	3	11/16	1.20	2915	245
32	Blade	7"/7	3	1/2	1.20	2915	230
33	Blade	7"/7	3	1/2	1.25	2945	395
34	Blade	7"/7	3	1/2	1.30	2980	305

* All Blades Grown Tip-Up
** Measured in Airfoil

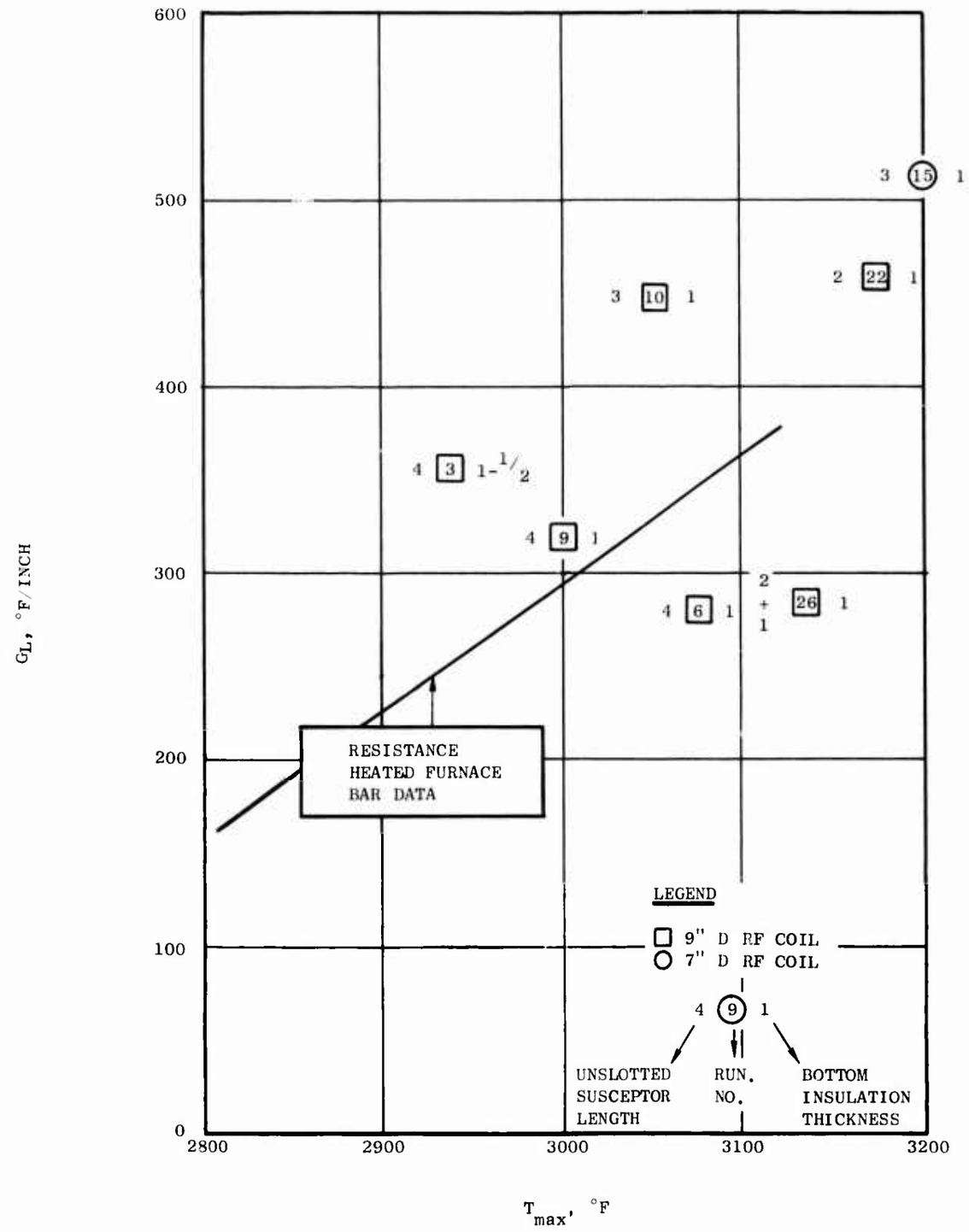

Figure 52. Comparison of T_{MAX} Versus G_L Bar Data from Induction and Resistance Heated Furnaces

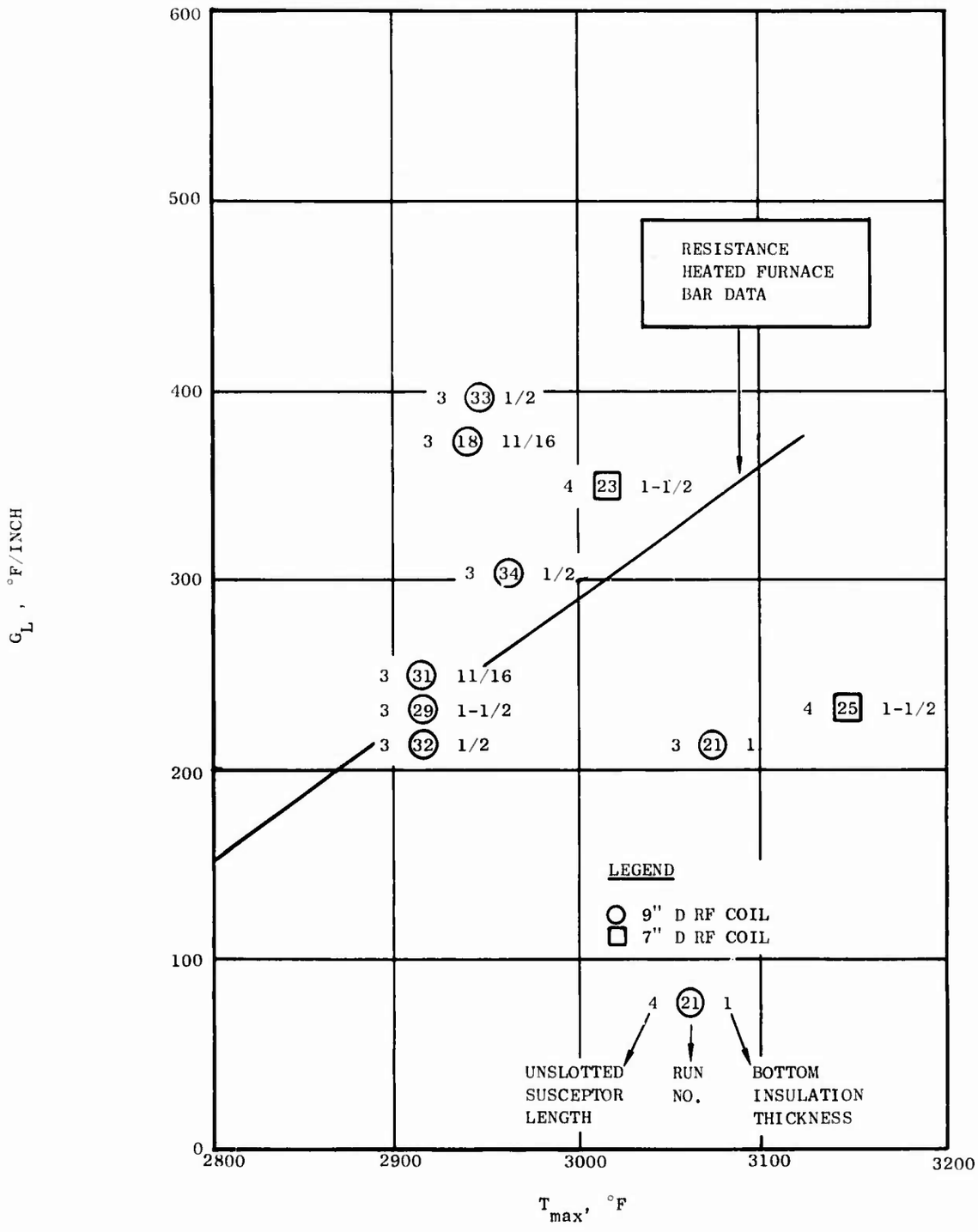

Figure 53. Comparison of T_{MAX} Versus G_L Blade Data from Induction Furnace with Bar Data from Resistance Furnace

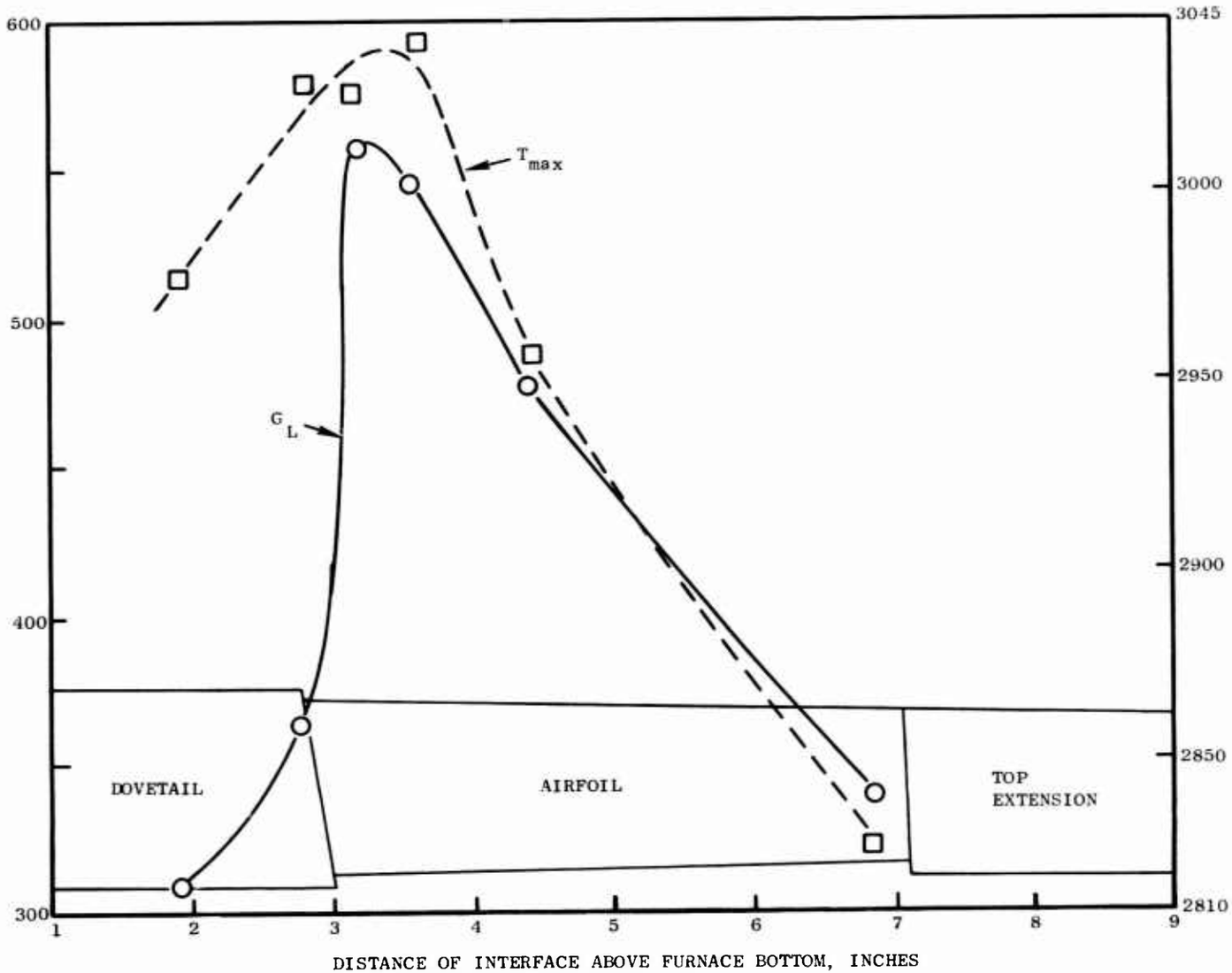

Figure 54. Effect of Liquid/Solid Interface Position on G_L and T_{MAX} in Tip-Up Blade Run 34

positions. The data for DB39 are shown in Figure 55 and compared with data for blade run, DB34, made with an all-graphite susceptor. Although the G_L levels in run DB39 were equivalent or higher than in run DB34 from the root to the airfoil midspan, thereafter G_L in DB39 fell to unacceptably low levels; hence, the all-graphite susceptor was selected for future work.

2.7.3.4 RF Coil Location - To maximize G_L and approach an idealized temperature profile illustrated in Figure 56, it was essential to maximize the RF energy transferred to the base of the susceptor. To determine the optimum coil location, the RF flux within a 7-turn, 7 inch diameter coil was measured as a function of axial position using an RF probe. The data given schematically in Figure 57 show that the maximum RF field intensity was located between turns 2 and 3 of the coil design evaluated. Therefore, maximum heat input to the bottom of the susceptor should occur with the susceptor bottom located between turns 2 and 3 of the RF coil.

2.7.3.5 Selection of Best Blade Furnace Configuration - The furnace configuration selected for additional process development work was as follows:

RF Coil - 7 inch diameter with 7 turns positioned to have the bottom of the susceptor between turns 2 and 3.

Susceptor - All graphite slotted from the top to 3 inches above the bottom

Furnace Bottom Insulation - 1/16 inch thick layer of alumina-silica fiber on top of 1/8 inch thick layer of ZrO_2 board.

Through the use of the selected configuration and T_{max} of about 3100°F, initial G_L values in excess of 300°F/inch were anticipated. However, all blade castings produced previously under a wide variety of conditions had a dovetail band, indicating that elimination of the band would require modifications to the casting design and/or mold configuration, because a sufficiently high G_L had not been achieved.

2.7.4 Blade Casting Configuration Studies

Measurements of G_L as a function of interface position in tip up and tip down configurations showed that the gradients achieved in both were sufficient to produce well aligned fiber airfoils at a withdrawal rate of 1/4 inch/hour, but were insufficient to produce aligned fiber dovetails. Gradient profiles for the two configurations are shown schematically in Figures 58 and 59. The low gradients measured in the root section were not due to an inability to achieve high gradients in large cross sections. Instead they were due to the perturbations in heat balance caused by the change in cross sectional areas at the airfoil-dovetail transition. Referring to Figure 58 for tip up casting runs, the gradient dropped at the dovetail-airfoil transition because the airfoil could not supply all the heat needed in the dovetail for uniform interface velocity. Hence, the solid/liquid interface moved up into the furnace, thereby increasing the solidification rate. This, in turn, reduced G_L/R below the critical value and produced a misaligned fiber microstructure in the dovetail. At the airfoil-extension transition, Figure 58, the opposite effect took place. The extension provided heat at a higher rate than could be removed by the smaller cross-section airfoil. Therefore the gradient decreased and the liquid/solid interface moved toward the furnace bottom. However, this reduced the solidification rate, G_L/R did not drop below the critical value, and aligned fiber growth continued. A similar effect took place in the tip down

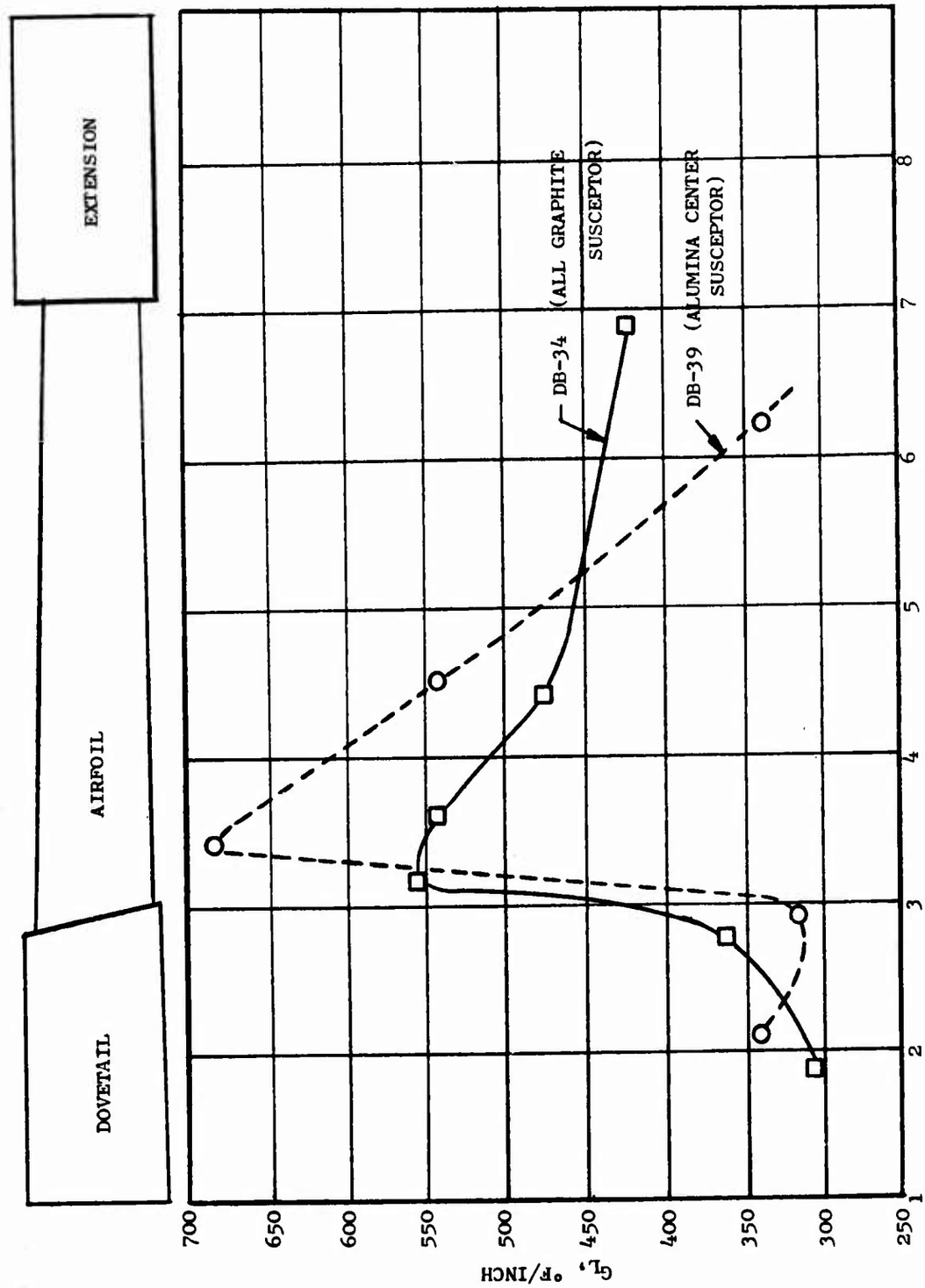

Figure 55. Comparison of G_L Profiles Achieved with Graphite-Alumina and All-Graphite Susceptors During Tip Up Blade Runs

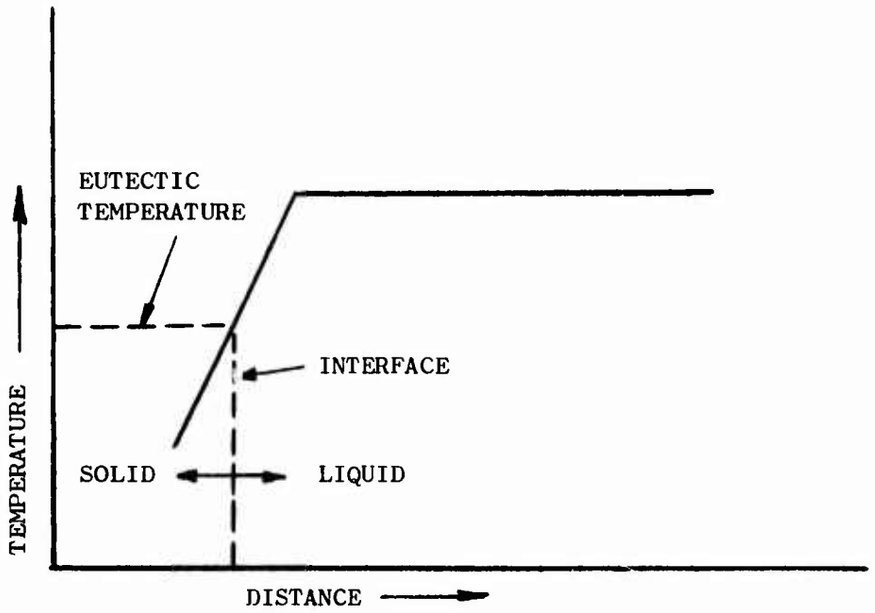

Figure 56. Idealized Temperature Profile for Planar Front Solidification

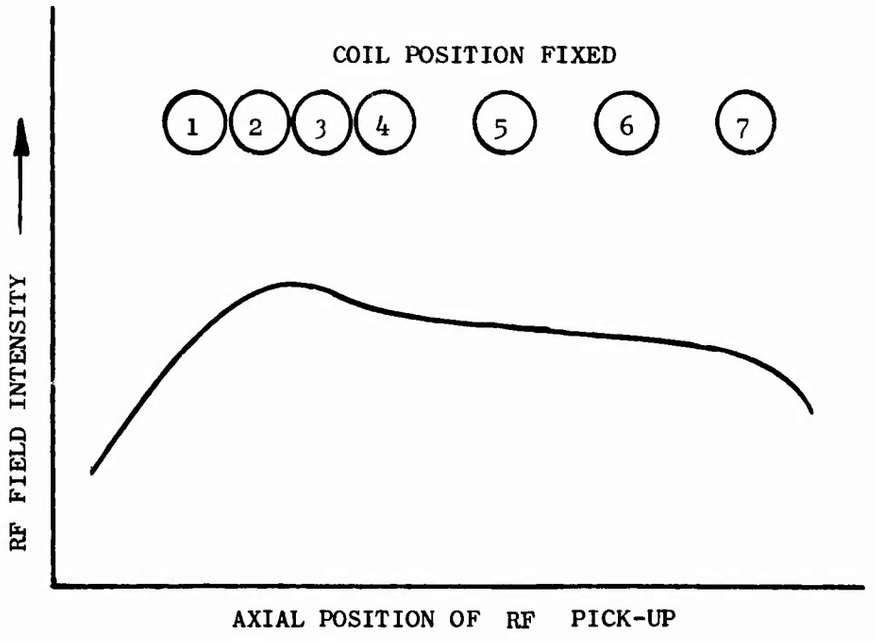

Figure 57. Schematic Illustration of RF Field Intensity Profile Determination

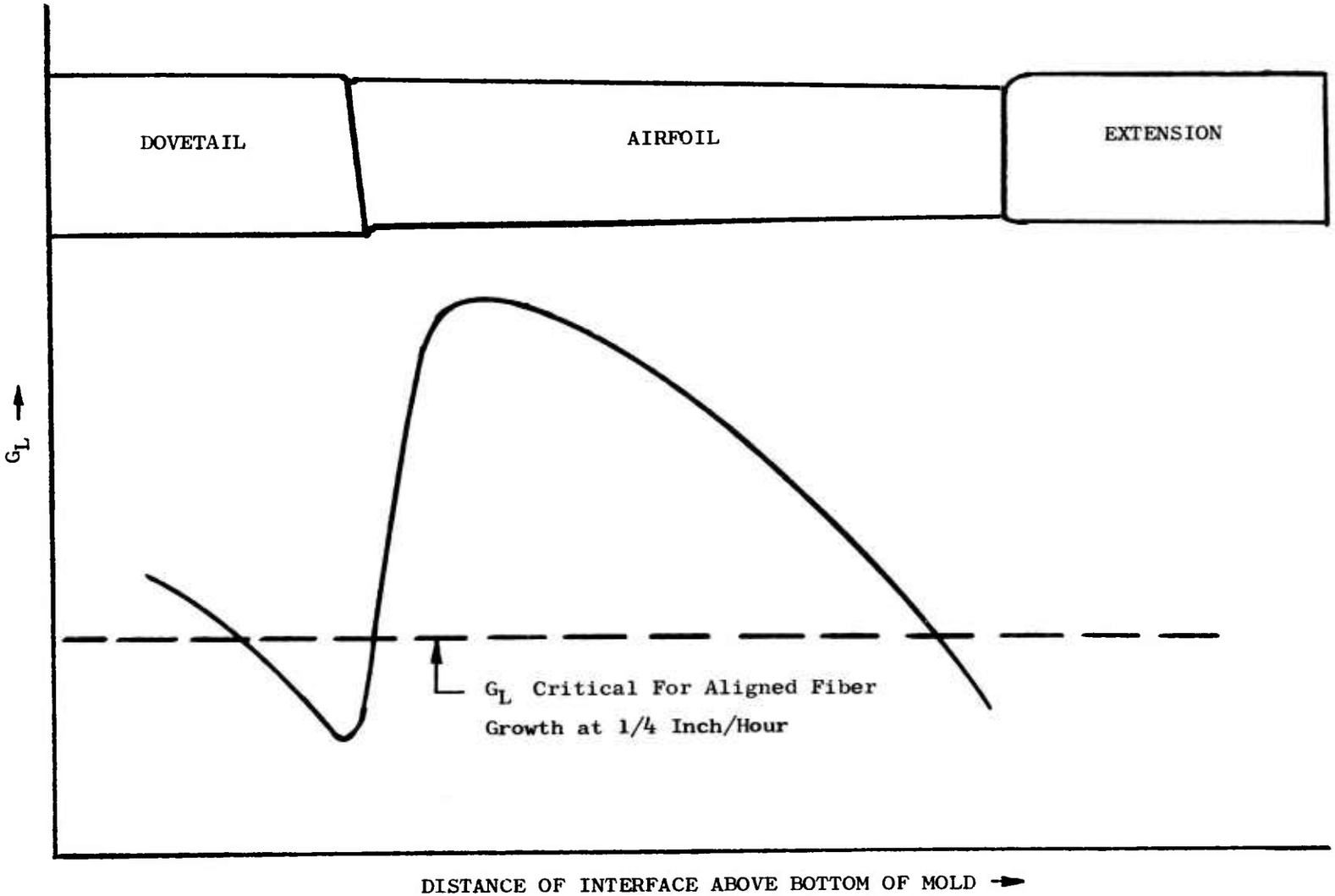

Figure 58. Schematic Illustration of G_L Profile During Tip Up Blade Casting Run

configuration, Figure 59. In this case, the gradient decreased as the solid/liquid interface moved through the airfoil and approached the dovetail section until G_L fell below the critical value required for aligned fiber growth at 1/4 inch/hour. Thereafter, when the interface was about one inch into the dovetail, G_L increased to a value above the critical. This reduction in gradient at the airfoil-root transition was due to a heat removal limitation of the airfoil section.

For the airfoil section in both casting configuration, the general trend was for G_L to decrease as the liquid/solid interface moved through the airfoil. This decrease was assigned to the lack of a tight fitting radiation baffle which permitted undesired radiative heating of the solidified portion of the casting.

In an attempt to correct the problem of radiative heating of the solidified casting, a tip up filled-in mold was tried in run DB40. The filled-in mold had straight sides and the same cross section as the dovetail section and, therefore, had a much thicker wall in the airfoil section. The gradient profile measured during withdrawal, presented in Figure 60, shows that G_L in the airfoil was higher than those shown previously in Figure 55, but that it was substantially lower in the dovetail section. This type of mold was therefore abandoned.

Four blade casting configurations, illustrated in Figure 61, were established for a final attempt to solve the heat balance problem and produce fully aligned fiber blades. As illustrated in Figure 61, the fins used in two configurations were planar extensions from the platforms that were parallel to the airfoil, and were added to improve the heat balance at the airfoil-dovetail transition in both configurations.

Special attention was paid to the length of the starter section and top reservoir section of each configuration in order to minimize g_b in the blade section of the casting. The four configurations and the estimated values of g_b were as follows:

	g_b At Several Blade Positions		
Configuration	Dovetail Base	Airfoil Root	Airfoil Tip
Tip Up	.26	.42	.58
Tip Up + fins	.24	.39	.62
Tip Down	.41	.28	.15
Tip Down + fins	.48	.38	.16

The above estimations indicated that the maximum g_b would also be small in all configurations. The tip down configurations were more desirable, however, because the maximum g_b was substantially lower than in the tip up configurations and the lowest g_b values were in the airfoil. As shown previously (Figure 17), rupture strength decreases with increasing g_b and it was highly desirable to maximize rupture strength of the airfoil.

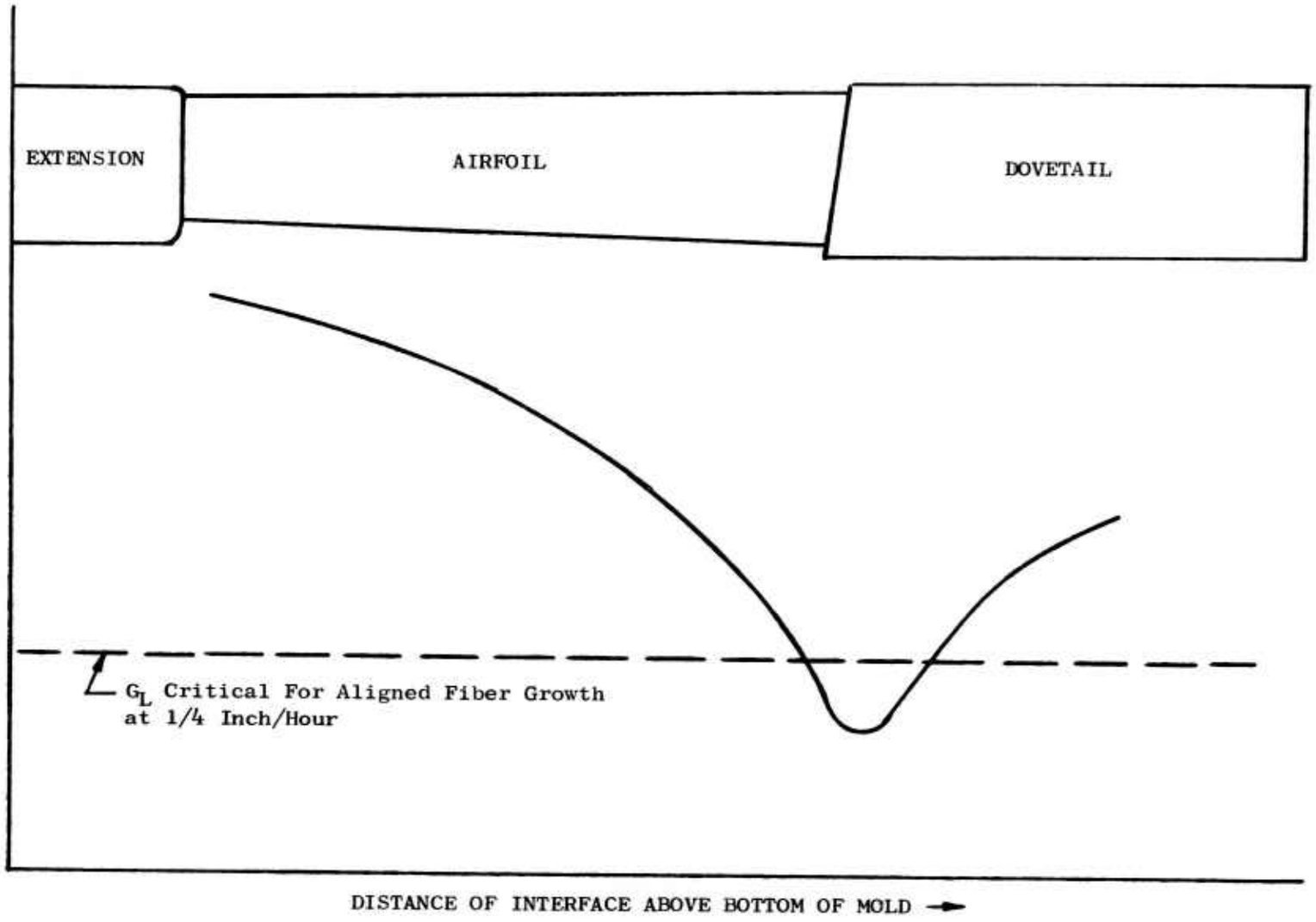

Figure 59. Schematic Illustration of G_L Profile During Tip Down Blade Casting Run

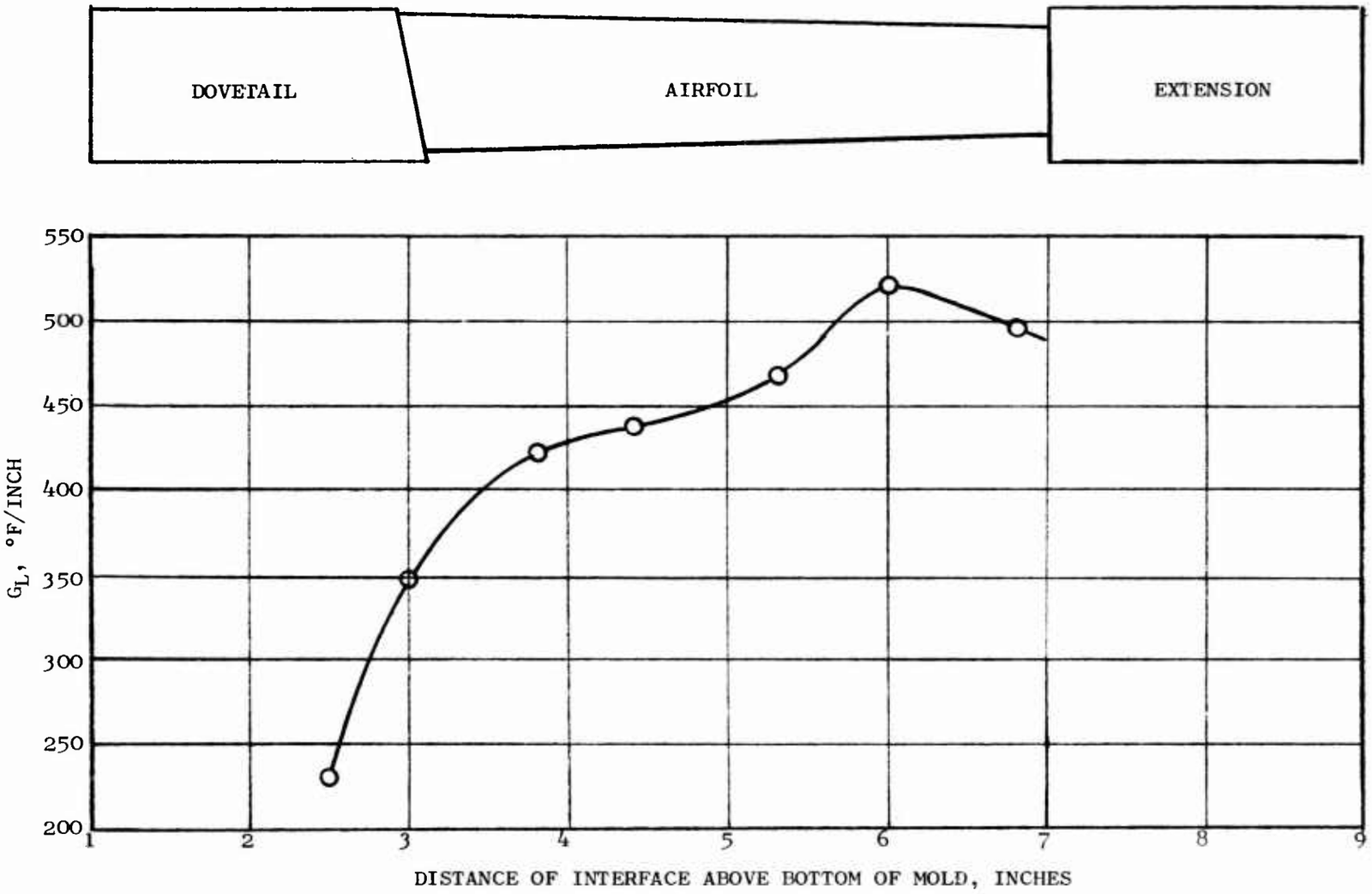

Figure 60. G_L Profile for Filled-In Mold, Tip Up Blade Run DB 40

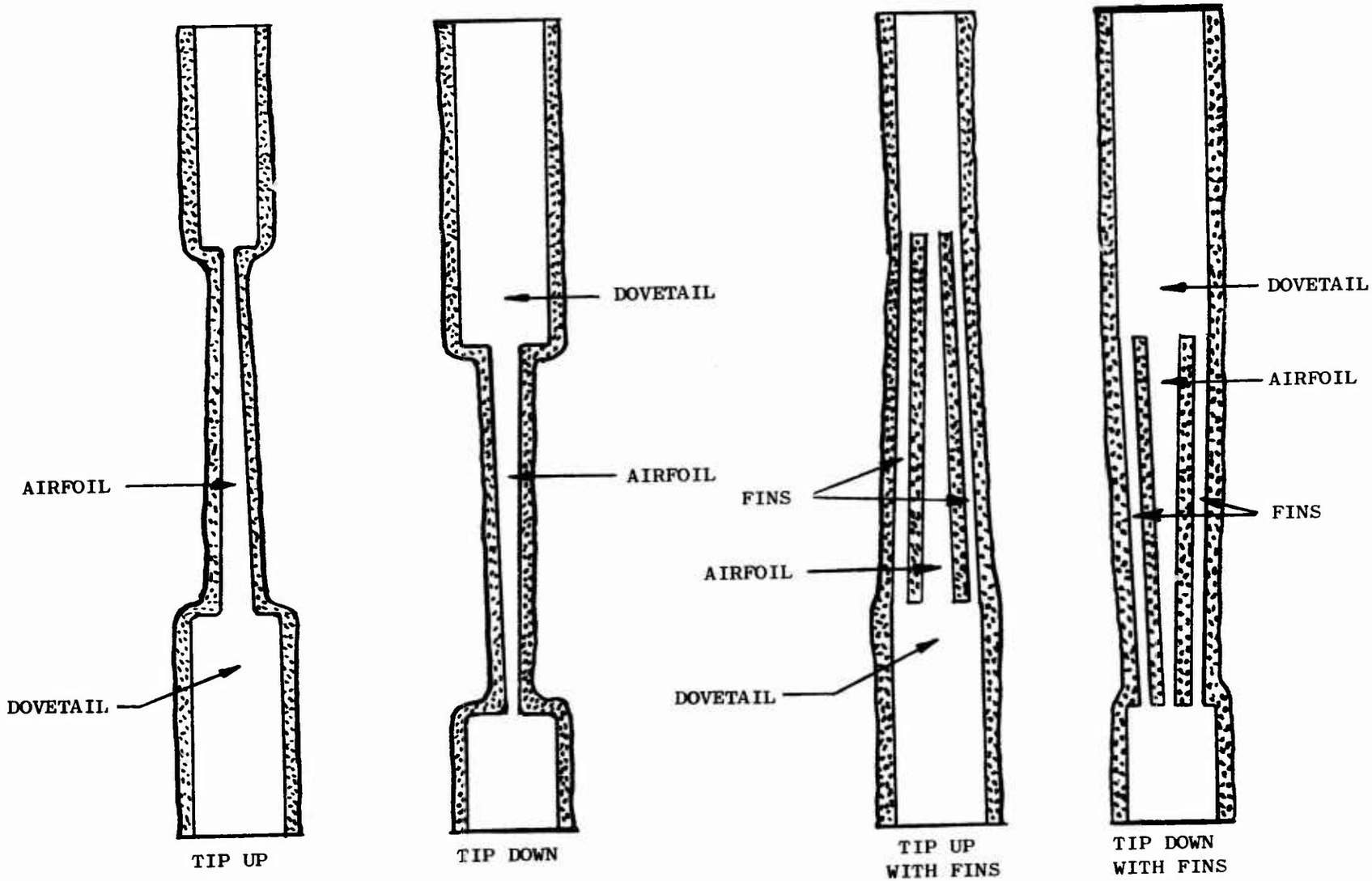

Figure 61. Final Four Blade Casting Configurations

For the casting trials, a water cooled side chill was added to the PFS furnace below the radiation baffle to improve lateral heat withdrawal from the solidified casting, and a stainless steel pull rod extension from the bottom chill plate was used to minimize heat removal by the bottom chill. These modifications are illustrated in Figure 62.

Five runs were made using the four configurations after which the castings were metallographically evaluated with the following results:

Run No.	Casting Configuration	Approx. Initial T_{max}, °F	Microstructure	
			Airfoil	Dovetail
DB54	Tip down	2930	Fibers	Cells
DB55	Tip up	2935	Fibers	Cells
DB56	Tip down	3020	Fibers	Fibers, Band at Transition
DB58	Tip down + fins	3020	Fibers, 1 Band	Cells
DB60	Tip up + fins	2985	Fibers, 2 Bands	Fibers, Band at Transition

The best results were obtained with the tip down configuration, Run DB56. Although the dovetail microstructure in the tip up with fins configuration of DB60 was essentially equivalent to DB56, the presence of misaligned fiber bands in the airfoil made this configuration much less desirable than the simple tip down.

At the conclusion of these studies, the casting results and available property data for carbide defect structures were reviewed with Design personnel. A decision was made that the simple tip down blade configuration was most desirable because the airfoil had lowest g_b material and would have the highest rupture strength of the four configurations tried. However, more property data were required of the banded dovetail material for a final decision of the acceptability of the tip down blade casting for the program. It was further decided to proceed with a trial run with the tip down blade to assess blade casting reproducibility and properties.

2.7.5 Blade Trail Casting Run and Evaluation

Four blades (DB62, 64, 65, and 66) were cast tip down under conditions that duplicated those used for blade DB56. All five of the blades were to be used in an evaluation of microstructure and stress-rupture properties to determine reproducibility of the blade process and equivalency of test bar and blade material. Because of the banded dovetail, it also became necessary to evaluate tensile, HCF and LCF properties of the blade casting to determine acceptability of the casting for the program.

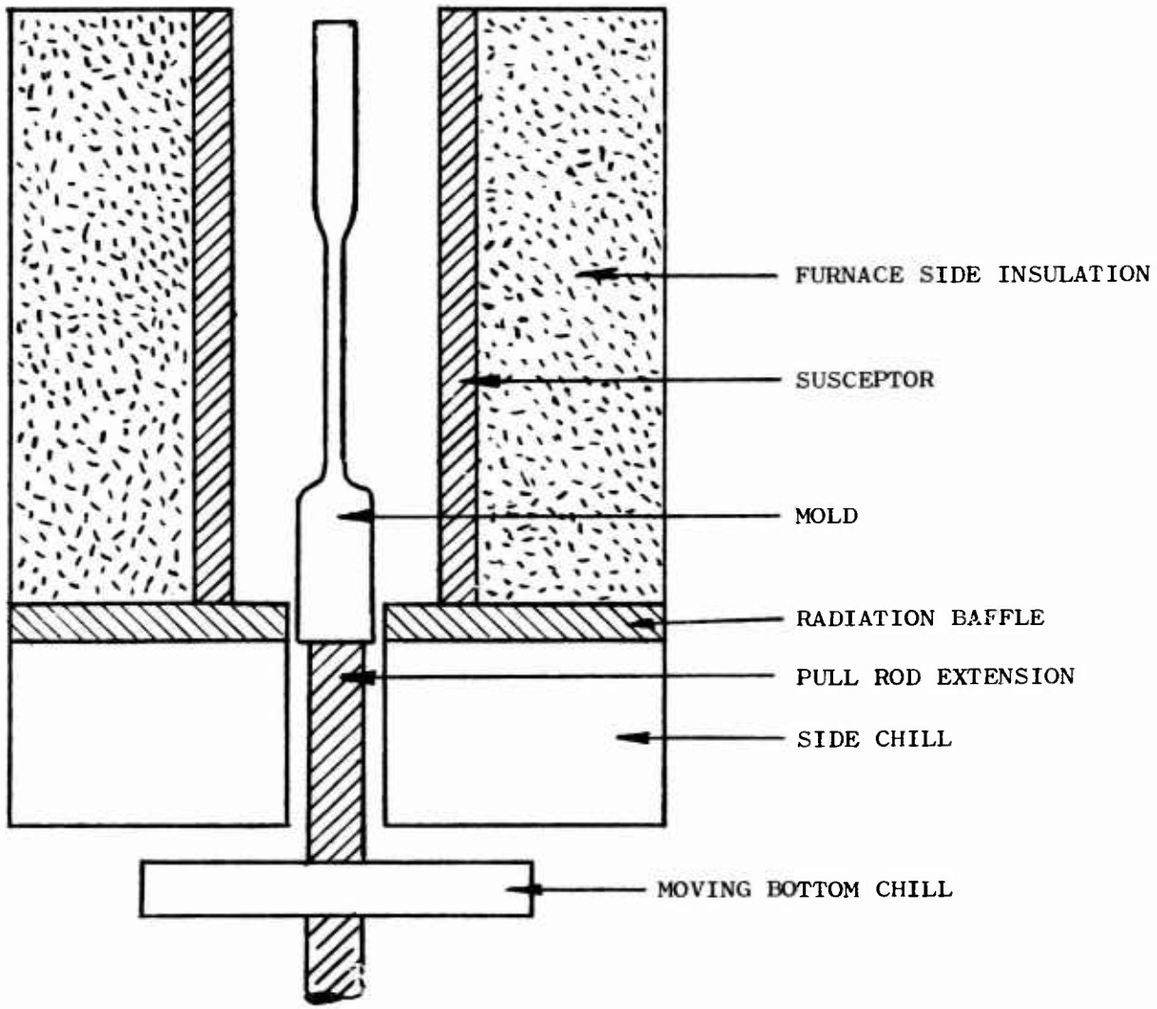

Figure 62. Modified PFS Furnace for Blades, Illustrating Addition of Side Chill and Pull Rod Extension

Prior to completion of this evaluation, it was decided to begin production of blade casting with the DB56 blade process because the maximum production rate was only 3 blades per week and an early start was necessary to maintain the program schedule.

2.7.5.1 Microstructure - Metallographic evaluation showed that airfoils of the five blades (including DB56) were completely aligned and band free. In contrast, all dovetails starting at the platform had an approximately 0.4 inch length containing numerous bands of cellular and dendritic cellular material. Typical blade microstructures are illustrated in Figure 63.

X-ray radiographs of airfoils generally showed indications of line defects, illustrated in Figure 64, that were originally interpreted as evidence of bands. However, microscopic examination of longitudinal cross-sections in the regions of X-ray indications almost always showed an absence of misaligned fiber bands. It was, therefore, considered possible that the X-ray indications were caused by minor changes in carbide fiber size and spacing or by chemistry variations due to solute dumping.

To study this problem further, microprobe traces were taken through an X-ray line indication region of blade DB62. Elements analyzed for included Ni, Co, Cr, Al, W, Re, V and Ta. The only observable difference was in the Ta analysis which showed a relative increase of 20 percent at the X-ray line indication over the adjacent material. This result indicated the possibility that the number and/or size of carbide fibers was somewhat higher in the region of the X-ray line indication.

Fiber population densities were measured in 12 transverse airfoil sections of blade casting DB62, and the mean value for the 12 sections was 22.4×10^3 fibers/mm^2. Fiber population densities had also been determined for bars and blades cast during process development, yielding the results shown in Table 21.

TABLE 21

FIBER POPULATION DENSITIES IN NiTaC-13 BARS AND BLADES GROWN AT 1/4 INCH PER HOUR

Ident. No.	Fibers/mm^2 x 10^{-3}		
	Bottom	Middle	Top
TEST BARS			
64	22.8	19.1	15.8
70	25.1	23.6	18.4
73	24.5	19.3	17.4
BLADES			
LB-82	Cells	17.3	18.1
LB-86	23.6	17.5	17.3

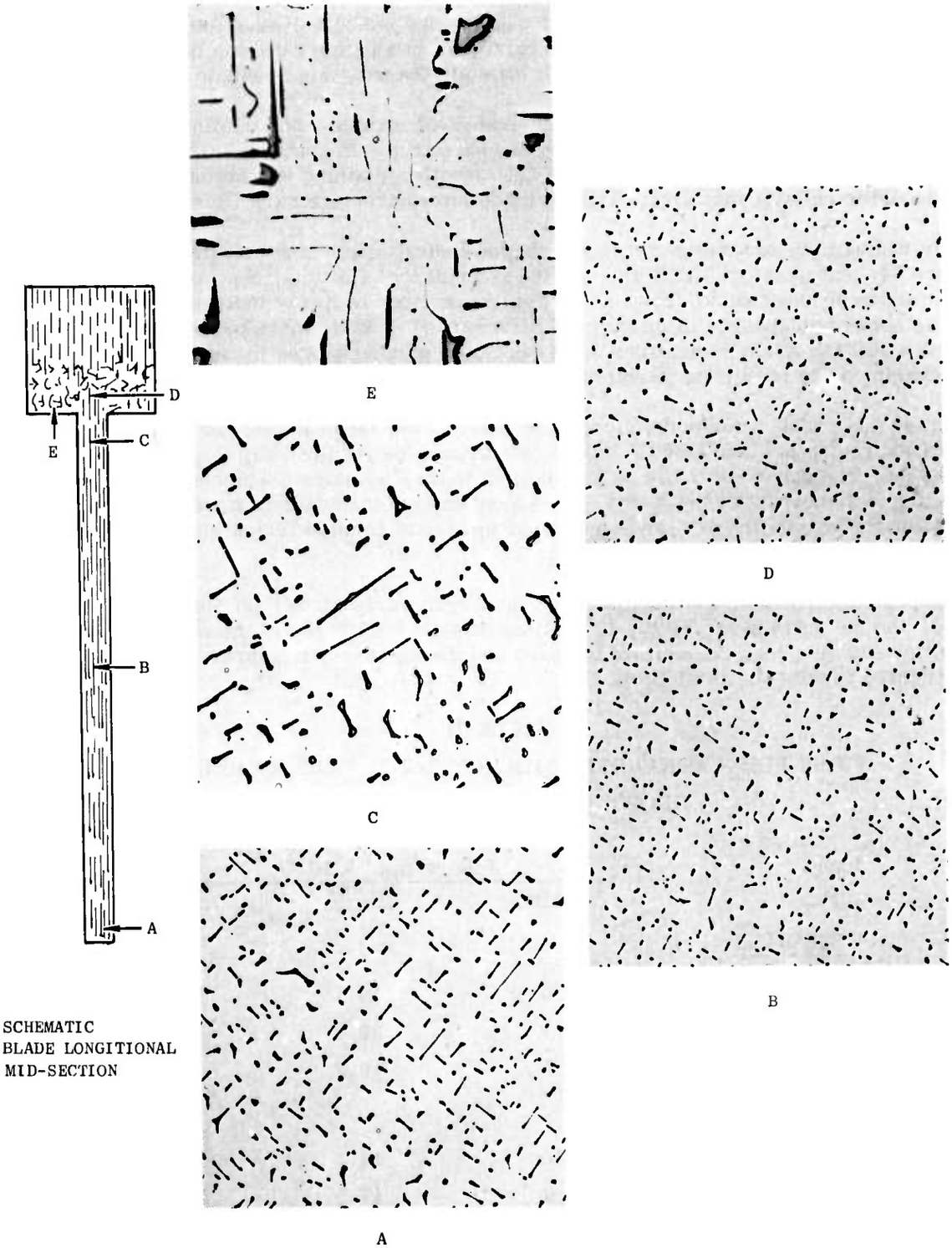

Figure 63. Transverse Microstructures of NiTaC-13 Blade Casting DB62 Grown Tip Down

Figure 64. Typical X Ray Radiographs of PFS NiTaC-13 Blade Castings

The earlier results in Table 21 indicated population densities slightly lower in blades than in bars. The result for the airfoil of DB62, when compared with equivalent g_b material from bars (bottom and middle), was in good agreement and it was concluded that blade airfoils and test bars were equivalent in this microstructural factor.

2.7.5.2 Longitudinal Properties - This evaluation included material from blades of the trial casting run and blades cast in earlier stages of the development.

Stress-Rupture - Material for test specimens were sectioned from airfoil, platform, and dovetail locations in five blade castings. Table 22 shows details of the specimens, stress-rupture test conditions, and results. Comparative data for bars at equal g_b values are also given.

From inspection of the Larson-Miller parameter numbers in Table 22, it can be seen that material from blades, including carbide defect structures, had stress-rupture strengths equivalent to aligned fiber test bar material. Figure 65 compares the aligned fiber results for material from blades with the average curve for bottom material (g_b = 0.27) from test bars to be discussed in Section 3.2.2. There was good agreement between the two sets of data with the exception of the 2000°F airfoil test results which was low by about one parameter number. This point, however, was in close agreement with the result of a test bar sample tested under similar conditions (specimen 3B54-B5 in Table A-2 of Appendix A).

By comparing the reduction in area data in Table 22, it can be seen that the rupture ductility of blades and bars were about equivalent.

On the basis of these test results it was concluded that stress rupture properties of blades and test bars were equivalent.

Tensile - Two specimens were machined from the dovetail of blade casting DB47, which had a completely dendritic cellular microstructure and was considered a worst case. Results of 1200°F tension tests in air for the two specimens are compared with average results for aligned fiber material as follows:

Bar No.	0.2% Yield Strength, ksi	Ult. Tensile Strength, ksi	% Elongation	% RA
DB47	142	165	2.4	6.3
DB47	145	164	2.4	5.7
Avg. Aligned Fiber Bar Results	120	175	17.5	16.5

TABLE 22

STRESS-RUPTURE DATA FOR TESTS IN AIR OF LONGITUDINAL NiTaC-13 SPECIMENS MACHINED FROM TIP DOWN BLADE CASTINGS COMPARED WITH TEST BAR RESULTS

Specimen No.	Blade Casting No.	Specimen Location[1]	Micro-Structure[2]	g_b Volume Fraction Solidified	Test Conditions Temp, °F	Stress, Ksi	Rupture Life, Hours	Larson-Miller Parameter × 10^{-3} Blade	Bar[3]	Rupture Ductility %RA Blade	Bar[3]
ALIGNED FIBER SPECIMENS											
1085	LB79	D	F	0.33	2000	13.5	132.9	54.4	54.5	44	45-60
1155	DB47	A	F	0.12	1800	40	156.0	50.2	50.1	44	25-30
1165	DB54	A	F	0.17	1800	40	215.1	50.5	50.0	36	25-30
1087	LB79	A	F	0.57	1800	35	156.3	50.2	50.3	32	25-30
1153	DB46	A	F	0.44	1800	35	186.1	50.3	50.5	46	25-30
1193	DB66	A	F	0.18	1600	80	115.5	45.4	45.5	9	10-15
1197	DB56	A	F	0.25	1600	80	99.2	45.3	45.4	19	10-15
1192	DB66	A	F	0.25	1400	124	77.2	40.7	--	24	-
1196	DB56	A	F	0.18	1400	124	314.4	41.8	--	23	-
MISALIGNED FIBER SPECIMENS											
1195	DB66	D	C	0.44	2000	13	195.3	54.8	54.3	44	45-60
1199	DB56	D	C	0.44	2000	13	106.0	54.2	54.3	67	45-60
1187	DB54	D	C	0.40	1800	40	82.0	49.5	49.8	31	25-30
1194	DB66	D	C	0.44	1800	40	148.5	50.1	49.7	24	25-30
1198	DB56	D	C	0.44	1800	40	73.8	49.4	49.7	31	25-30
1086	LB79	P	C/DC	0.50	1600	71	187.6	45.9	45.9	20	10-15
1152	DB46	P	C/DC	0.24	1600	75	170.9	45.8	45.8	13	10-15
1154	DB47	P	C/DC	0.31	1600	78	101.8	45.3	45.5	16	10-15
1166	DB54	D	C	0.40	1600	75	139.3	45.6	45.7	19	10-15
1167	DB54	D	C	0.40	1400	130	8.4	38.9	--	10	-
1185	DB54	D	C	0.40	1400	130	10.6	39.1	--	13	-
1200	DB66	D	C	0.44	1400	124	589.0	42.4	--	--	-
1201	DB56	D	C	0.44	1400	124	60.4	40.5	--	19	-
1186	DB54	D	C	0.40	1400	120	92.8	40.9	--	11	-

(1) A = Airfoil; D = Dovetail; P = Platform

(2) F = Fibrous; C = Cellular; DC = Dendritic Cellular

(3) Average aligned fiber bar data, estimated on basis of g_b value

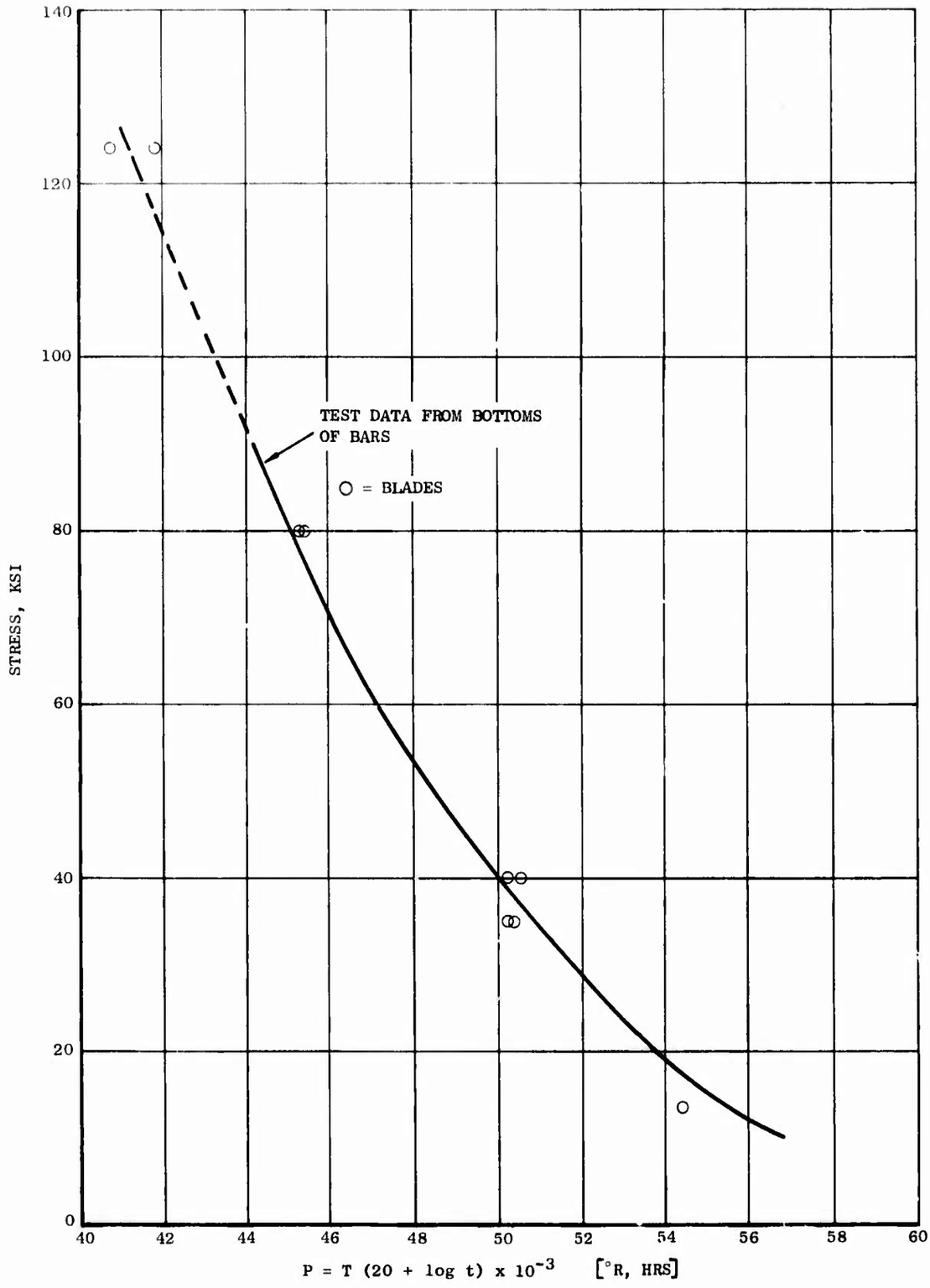

Figure 65. Longitudinal Stress-Rupture Strength of Aligned Fiber NiTaC-13 Specimens Machined from Blade and Test Bar Castings

This comparison showed the same trends, as was observed with test bar material, Table 18 of Section 2.6.2.2. The carbide defect structure had higher yield strength, but lower ultimate tensile strength and tensile ductility.

Fatigue - Two properties of importance to the dovetail are LCF and HCF. Tests were run using material from blade casting DB68 to evaluate the effect of the carbide defect structure in the dovetail on these properties, and also to determine if the microstructural transition zones (fibers to cells to fibers) were zones of unusual weakness.

Figure 66 shows the cut-up plan for blade DB68. Specimens 1, 3, 5 and 6 had aligned fiber gage sections. In contrast, the gage sections of specimens 2, 4, 7 and 8 contained aligned fibers, the transition zone, and dendritic cells.

Load amplitude controlled LCF tests of smooth bar specimens were performed in air at 1200°F and an A ratio (alternating stress/mean stress) of 0.95. After the completion of each test, longitudinal sections of the specimens were examined metallographically to determine the microstructure at the fracture surface. The test results are presented in Table 23 and in Figure 67. Also shown in the figure are:

- One half of the 1200°F ultimate tensile strength of aligned fiber NiTaC-13 which defines the upper limit of LCF strength, and
- The estimated LCF strength of the conventional superalloy for the J101 LPT blade.

The results in Figure 67 show that LCF strength of aligned fiber material is higher and that of dendritic cellular material is lower than the J101 superalloy. These results are discussed in more detail in Section 4.2.4, where it is shown that the dendritic cellular dovetail easily met the blade design acceptability criterion for LCF life.

Microscopic examination showed that both blade dovetail samples failed in the dendritic cellular material, about 1/4 inch from the fiber to dendritic cellular transition zone. Therefore, it was concluded that the transition region is stronger than dendritic cellular material and is not abnormally weak.

HCF tests of smooth bar specimens from blade DB68 were performed at 1500°F and an A ratio of 0.95. After test, longitudinal sections of the samples were examined metallographically to determine the microstructure at the fracture surface. The results are presented in Table 24 and also in Figure 68 where they are compared with test bar data from Section 2.6.2.4, Figure 40. Also included in Figure 68 is the estimated HCF strength of the J101 blade superalloy. The results in Figure 68 indicated that carbide defect structures tend to decrease 1500°HCF strength somewhat, but all microstructural types of NiTaC-13 evaluated (fibers, cells and dendritic cells) exceeded the HCF strength of the J101 superalloy. With the exception of one data point, the bar and blade data were in good agreement and showed a trend of decreasing HCF strength with increasing fiber misalignment. The result for the aligned fiber, blade airfoil sample No. 1 fell well below corresponding bar data. In addition, at equal stresses sample No. 1 had a much lower life than the blade dovetail specimen No. 7. Microstructural analysis of specimen No. 7 showed that both the aligned fiber region and the transition zone present in the gage section were stronger

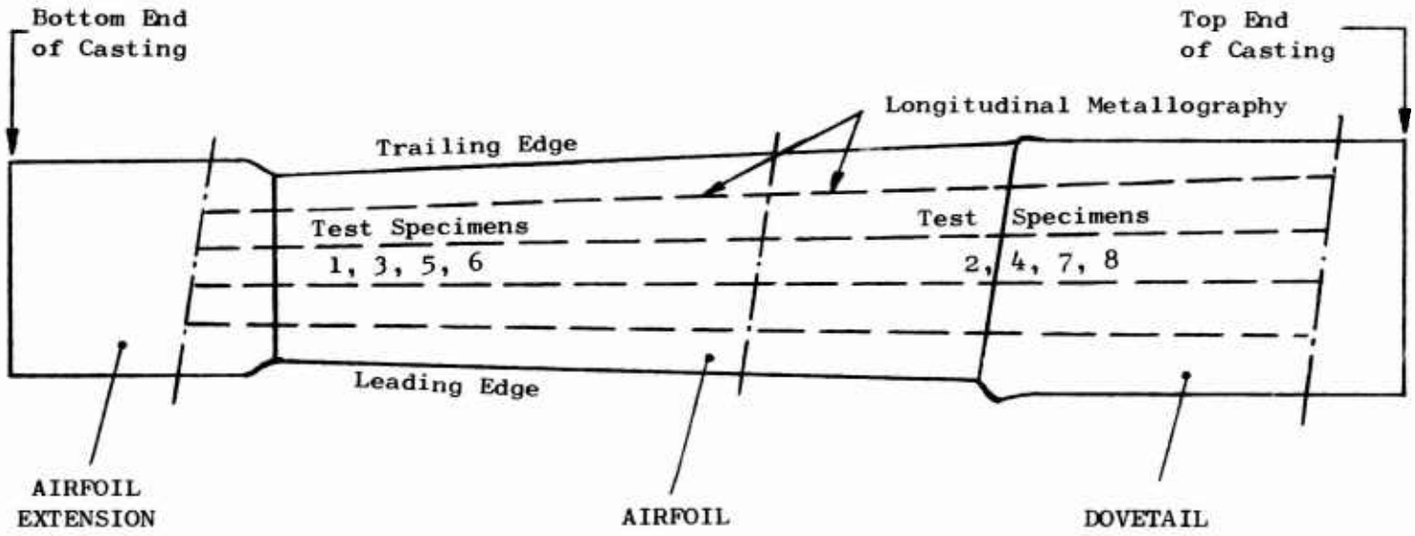

Figure 66. Cut Up Plan for NiTaC-13 Blade Casting, DB 68

TABLE 23

RESULTS OF LOAD AMPLITUDE CONTROLLED 1200°F LCF TESTS
OF LONGITUDINAL NiTaC-13 SPECIMENS MACHINED FROM BLADE DB 68

(A = 0.95 K_t = 1.0 F = 20 cpm)

Specimen No.	*Specimen Origin	Alternating Stress, ksi	Cycles To Failure x 10^{-3}	Microstructure At Fracture Surface
2	D/A	90 (Planned)	Failed on Loading to 157 ksi	Dendritic-cells
4	D/A	68	77.47	Dendritic-cells
5	A	80	64.69 (Test Stopped Before Failure)	Fibers Throughout Gage
6	A	75	85.39 (Loaded to 90 ksi)	-
		90	0.37	Fibers

* D/A = Dovetail-Airfoil Section of Blade
A = Airfoil Section of Blade

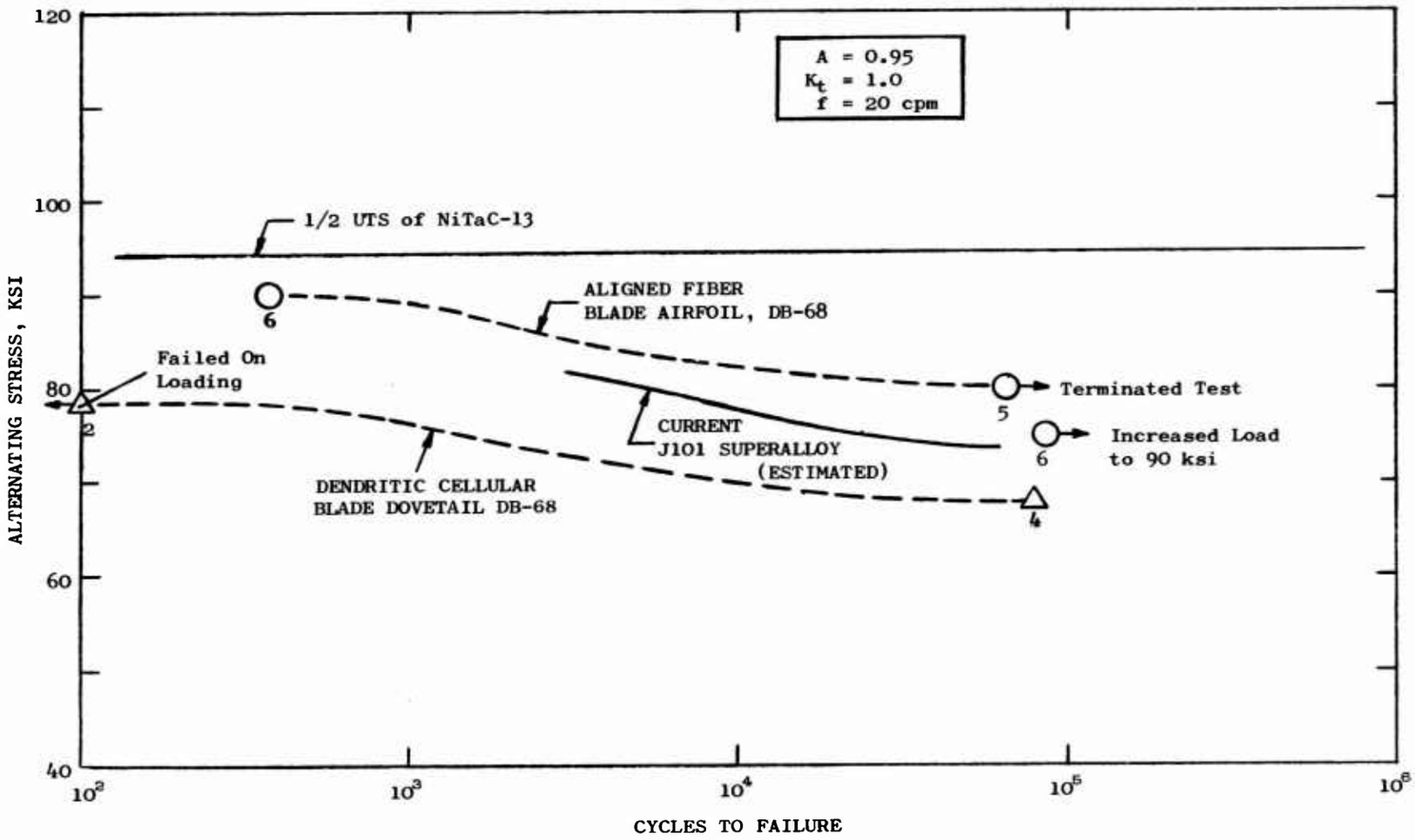

Figure 67. Longitudinal Smooth Bar 1200°F LCF Data for Aligned Fiber and Dendritic Cellular NiTaC-13 Specimens Machined from Blade DB68 Compared with J101 LPT Blade Superalloy

TABLE 24

RESULTS OF 1500°F HCF TESTS OF LONGITUDINAL NiTaC-13 SPECIMENS MACHINED FROM BARS AND BLADE DB-68
(A = 0.95 K_t = 1.0 f = 30 cps)

Specimen No.	*Specimen Origin	Alternating Stress, ksi	Cycles To Failure x 10^{-6}	Microstructure At Fracture Surface
63B-4	Bar 63B	50	10.0 (Loaded to 65 ksi)	-
		65	9.0 (Loaded to 75 ksi)	-
		75	0.0036	**Fiber
69B-3	Bar 69B	60	13.86 (Loaded to 68 ksi)	-
		68	0.044	**Cells
1	A	60	0.011	Fibers
7	D/A	60	0.112	Dendritic cells
8	D/A	55	0.168	Dendritic cells

*D/A = Dovetail-Airfoil Section of Blade
A = Airfoil Section of Blade

** Not determined at Fracture Surface: based on microstructure of other samples from bars.

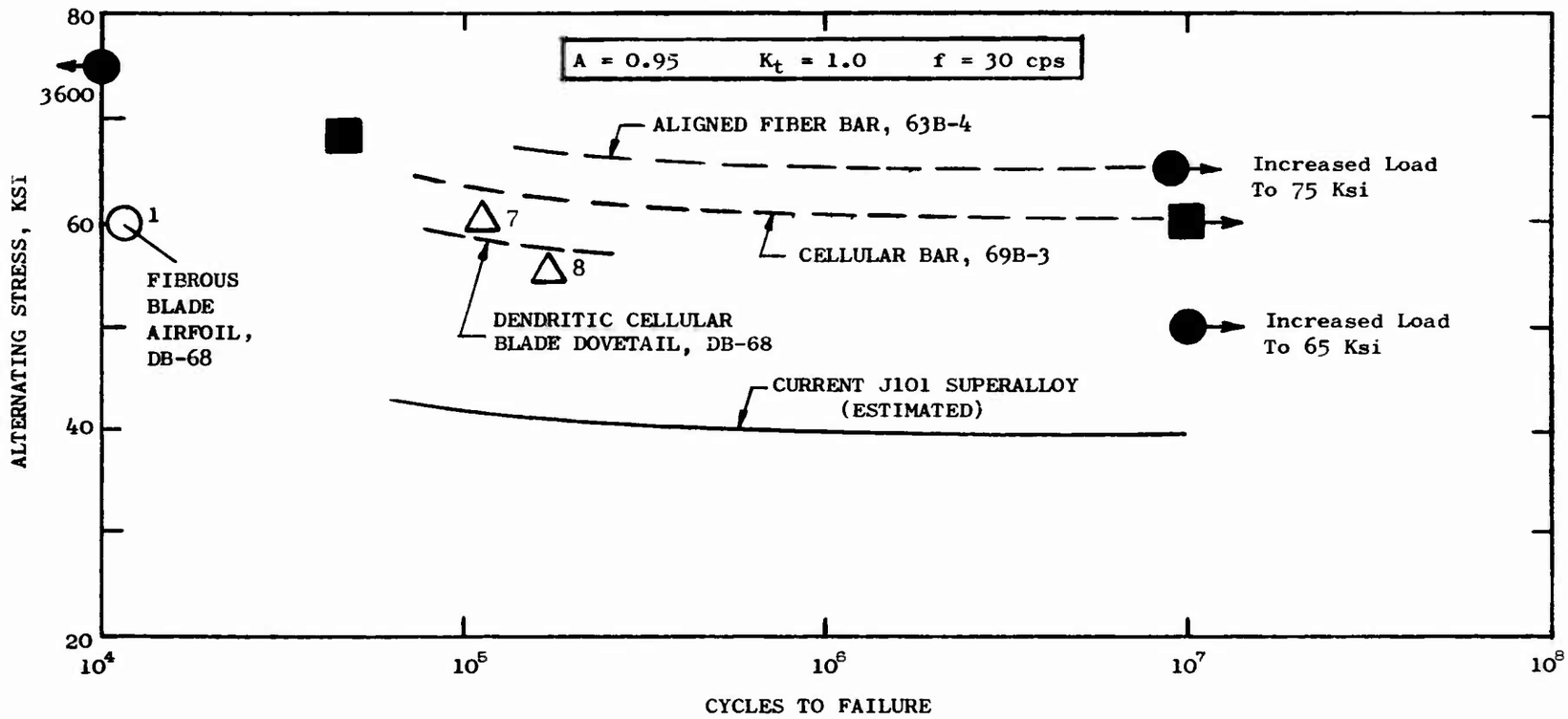

Figure 68. Longitudinal Smooth Bar 1500° F HCF Data for Three Microstructural Types of NiTaC-13 Compared to the J101 Superalloy

than the dendritic cellular material, also present in the gage section, because the fracture occurred in the dendritic cellular material at least 3/16 inch from the transition zone. Hence, the result for specimen No. 1 appeared anomalous, and no microstructural defects could be found to explain the low result. Because the HCF samples machined from blades had unusually long gage lengths and small diameters, it is possible that there was a misalignment problem in the test of specimen No. 1 that caused an unusually low test result.

2.7.5.3 Summary of Blade Casting Evaluation - Microstructural comparisons of aligned fiber material from blade airfoils and test bars showed that the two were equivalent. This equivalency was confirmed by results of stress-rupture tests of longitudinal specimens machined from bars and blade airfoils. It was concluded, therefore, that aligned fiber NiTaC-13 being made by the test bar process developed would be representative of aligned fiber blade material.

The carbide defect structure in the blade platform/dovetail properties (stress-rupture, tensile, LCF and HCF) using carbide defect structure material from bars and a blade dovetail showed the two sources to have equivalent properties and that the carbide defect structures reduced most of the measured properties to some extent. However, when compared to J101 LPT blade design operating conditions, it was concluded by Design and Materials program participants that the blade casting was acceptable and blade casting production, already in progress, was continued.

2.7.6 Selection of Final Blade Casting Process

The important features of the final blade casting process, established on the basis of the trial casting run, were as follows:

- Tip down casting configuration
- Water cooled side chill and pull rod extension
- Pre-heat mold in graphite susceptor slotted from top to 3 inches above base
- Pour molten NiTaC-13 into pre-heated mold
- Maximum liquid metal temperature of 3100°F
- Uniform withdrawal rate of 1/4 inch/hour

2.8 DEVELOPMENT OF INSPECTION PROCEDURES

The objectives of this work were to:

- Establish test bar and blade acceptability criteria
- Establish inspection procedures for test bars and blades

A significant feature of this work was to explore the effectiveness of many conventional and non-conventional NDE techniques in the evaluation of NiTaC-13 castings.

2.8.1 Inspection Objectives

Types of potential defects and microstructural features of importance to NiTaC-13 bars and blades produced for the program included:

Surface Defects	Internal Defects	Microstructure
Porosity	Porosity	Carbide Morphology
Cracks	Hot Tears	Misaligned Fiber Bands
Folds	Inclusions	Surface Nucleated Carbide Dendrites
		Segregation
		Grain Structure
		Arrest Lines

The surface and internal defects listed above are also concerns in conventionally cast superalloy blades and effective NDE procedures have been established. The microstructural factors, however, were unique to NiTaC-13 and presumably other eutectics. Therefore, NDE techniques required evaluation in order to establish inspection techniques for this program and to assess long range NDE development needs for eutectics. It was recognized that shallow surface defects were not a serious problem in this program, because gage sections of test specimens machined from bars would contain only material from well below the surface, and blade castings would have an approximately 0.04 inch envelope to be removed in finish machining. However, a longer range goal for eutectics is the precision casting of blades, and for this reason the evaluation of techniques for detecting surface defects was included in this work.

The objectives of this work, then, were to develop procedures for detecting defects listed previously, with particular emphasis on microstructural defects. The approach was to evaluate the effectiveness of various conventional and non-conventional NDE techniques.

2.8.2 Evaluation of NDE Techniques

The following evaluations were performed with test bars and blade castings:

NDE Techniques for Surface Defects

- Visual and Microscopic Inspection

  As-cast and Etched Surface

  Polished and Etched Surface

  Etch-Polished Surface

- Fluorescent Penetrant
  - Standard Sensitivity
  - High Sensitivity
- Laser Holographic Interferometry
- Eddy Current

NDE Techniques for Internal Defects

- X-ray Radiography
  - Low Energy
  - Medium Energy
  - High Energy
- Acoustic/Ultrasonic
  - Holography
  - Contact Pulse-Echo Scanning
  - Velocity

Details of procedures and results now follow.

2.8.2.1 Visual and Microscopic Examination - Prior to the inspection of bars, a flat surface was ground the full length and polished through 600 grit paper. For blade castings, the middle region of the convex side of the airfoil was polished full length and the leading edge side of the dovetail was also polished. After polishing, bars and blades were etched in a solution of 80 parts concentrated HCl to 20 parts H_2O_2 (30% solution) with intermittent scrubbing using steel wool.

Only surface connected pores and occasional folds were found and these were readily seen by visual inspection of the cast and etched surface. Grain structure was also readily seen on both cast and polished surfaces after etching. Determination of carbide morphology required microscopic examination at about 100X of either type surface although the polished surface was better for detection of bands and arrest lines illustrated previously in Figures 30 and 31. Relatively long misaligned fiber bands could be seen visually as striations on the cast and etched surface although this was not a positive indication because, in microscopic examination of surface striations, carbide defect structures were seldom found. Etch-polishing of the flat surface improved the microscopic delineation of carbides because it removed the γ-γ' phase outlines while accentuating the carbide/matrix interface, and was the preferred method for determining carbide morphology.

2.8.2.2 Fluorescent Penetrant - Bars were inspected using standard production sensitivity ZL22A with ZE-4A emulsifier and either ZE-4A dry developer or D499-C nonaqueous wet developer. They were also inspected with high sensitivity ZL-30A penetrant, ZP-4A emulsifier and D-499-C nonaqueous wet developer. On the cast and etched surfaces of bars, porosity indications were always present but the background fluorescence was not severe. No linear indications of cracks were found. On the polished and etched flat surface, linear transverse indications were observed between the unmelted zone and the sort-out zone. Also, linear indications running axially were observed in the transition region between the sort-out zone and the aligned (or misaligned) fiber section. Typical indications are illustrated in Figure 69. Although results with both penetrants were equivalent, the high sensitivity penetrant was preferred.

2.8.2.3 Laser Holographic Interferometry - This technique is normally used to detect weak areas that, under low stress levels, deform a different amount than surrfounding material. Holograms and interferograms were taken, in a General Electric laboratory set-up, of test bars as illustrated in Figure 70 for Bar B16. Thermal stress was applied through use of a heat gun. Analysis indicated no areas that deformed differently in any of the bars. This may have been due to the large mass of metal in the test bar, which would have overshadowed any small differences in deformation that may have occurred. It was concluded that this technique was not effective for the large test bars.

2.8.2.4 Eddy Current - Material for evaluation included test bars and blades having various microstructures including: aligned fibers, cells, dendritic cells, and cellular bands surrounded by aligned fibers. One piece of aligned fiber material was used as a standard during measurements. The equipment used was a Nortec Model NDT 11 and a Nortec flat probe. In measurements made along the length of each bar starting above the sort-out zone, there was a marked and continuous change in eddy current signal strength at all frequencies tested. A typical eddy current signal profile of a bar at a test frequency of 80 KHz, in Figure 71, showed a signal of -0.93 volts at the bottom of the bar which rose to +1.1 volts near the top. The arrow giving lift off direction in Figure 71 indicates the direction of error that variations in the gap between the probe and the specimen would produce; hence, there was negligible lift off error in the profile illustrated.

No significant difference in eddy current signal could be found among the three types of microstructure evaluated. Signal strengths were primarily dependent on position in the bars, as follows:

Measurement Position	Signal Range, Volts, For All Bars Tested
Top	+ 0.63 to + 0.97
Middle	+ 0.7 to + 0.43
Bottom	- 1.08 to - 0.88

Also no irregularities in signal were observed when traversing cellular bands known to be present in bars and blades on the basis of microstructural observations.

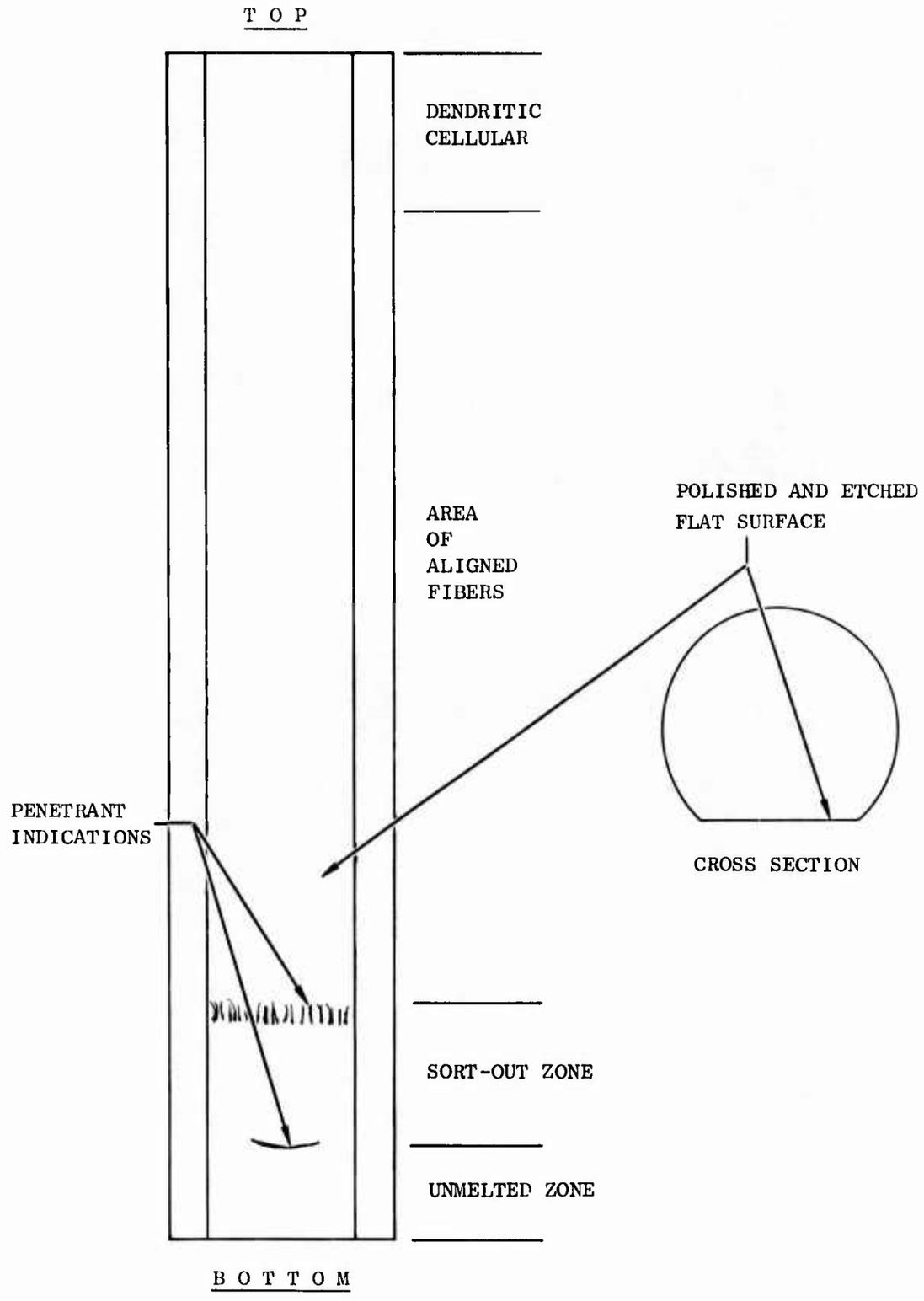

Figure 69. Locations of Linear Indications Detected with Fluorescent Dye Penetrants

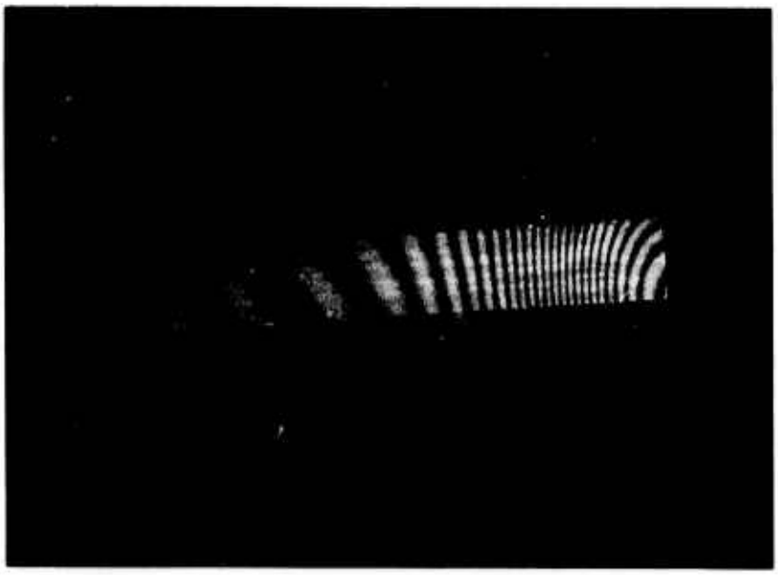

A. TOP OF BAR HEATED (RIGHT)

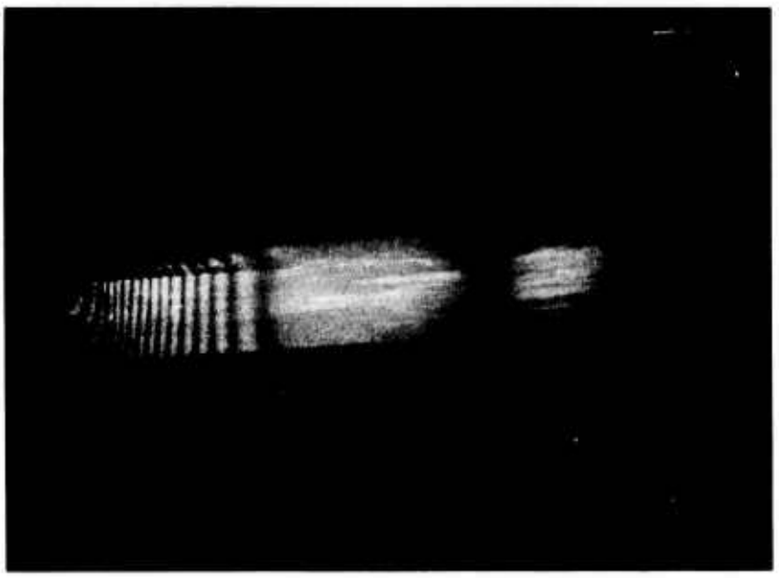

B. BOTTOM OF BAR HEATED (LEFT)

Figure 70. Laser Holographic Interferograms on Thermally Stressed Bar 16

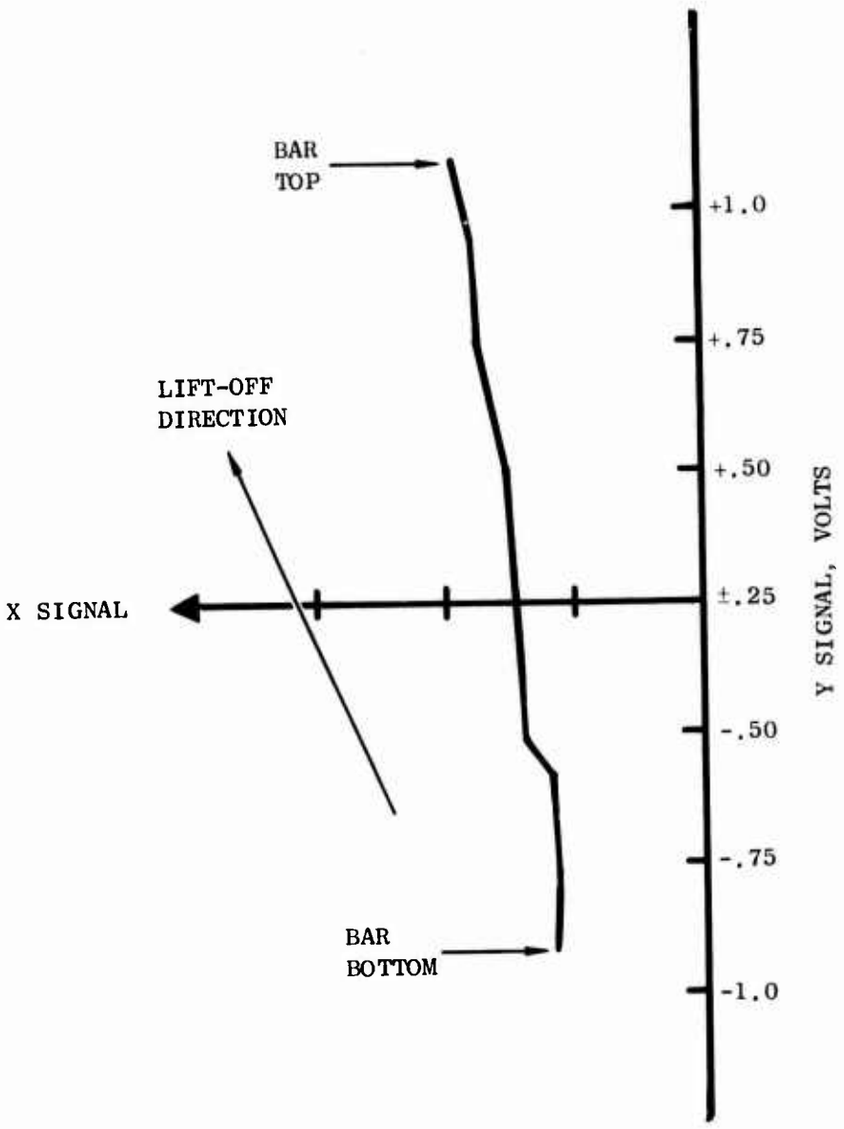

Figure 71. Eddy Current Signal Voltage Profile of Bar B17 at 80 KHz

The observed effect of bar position on eddy current signal was probably related to differences in chemical composition caused by segregation. Hence, it may be possible to develop this technique for determining average composition or g, the volume fraction solidified, if desired. However, the results indicated that it could not be used to distinguish aligned from misaligned fibers.

2.8.2.5 X-ray Radiography - Three levels of X-ray energy were evaluated for applicability to bars: low (up to 100 KV) with a Picker Hot Shot instrument; medium (100 to 320 KV) using Picker Gemini equipment, and; high (above 1 MEV), using a Van de Graaff accelerator. The low energy X rays did not penetrate the test bars. Initial results with medium energy X rays up to 320 KV were poor because of a large amount of scattering and low penetration of the test bars, but results were improved by imbedding the test bars in Rene' 95 powder. However, internal features of the test bars were best detected with high energy X rays (1.35 MEV). For example, with these high energy X rays the locations of the unmelted zone and the sort-out zone could be easily detected. Striations were also detected but, as in visual examination of cast and etched surfaces, microscopic examination of polished and etched surfaces showed that misaligned fiber bands were seldom present at X-ray striation location. The causes of the other striations were not identified.

X-ray radiography was also evaluated for blades, and it was found that medium energy X rays (250 KV) were sufficient for airfoil penetration, whereas high energy X rays (1 MEV) were required for the root. X-ray radiography was suitable for detecting striations or line indications illustrated previously in Figure 64, possibly indicating the presence of bands and arrest lines in blade castings. The detection of internal defects such as porosity and inclusions was made difficult because of surface defects, including small holes and protuberances, and no internal defects were detected. It was expected, however, that X-ray radiography of finish machined blades would be capable of detecting internal defects, if present.

2.8.2.6 Acoustic Holography - This work was performed at Batelle Memorial Institute of Columbus, Ohio. Attempts to penetrate test bars were not successful. In one bar, a section 3/8 inch thick by 2-1/2 inches long was removed to create a step. This step was not revealed by acoustic holography. In another trial, holes 1/16 and 1/8 inches in diameter were drilled halfway through a 1/4 inch thick plate. As shown in Figure 72, the holes could be detected from the undrilled side but they did not stand out strongly from the background. Hence, it was concluded that this technique was not applicable to the detection of internal flaws in either eutectic bars or blades.

2.8.2.7 Ultrasonic Contact Pulse-Echo Scanning - Scans made on two bars, B15 and B37, were recorded using the high resolution (0.015 index) gray scale "C" scan. Those for Bar B37 are illustrated in Figure 73. Although there was some correlation between misaligned fiber bands found by this technique and those found both by visual observation and radiography, poor resolution and excessive back scattered ultrasound hindered interpretation of the contact pulse-echo scans. It is possible that improved results could be obtained with other transducer designs and operating parameters; however, such development work was beyond the scope of this program. It was concluded that the standard technique evaluated was not of value for test bar inspection.

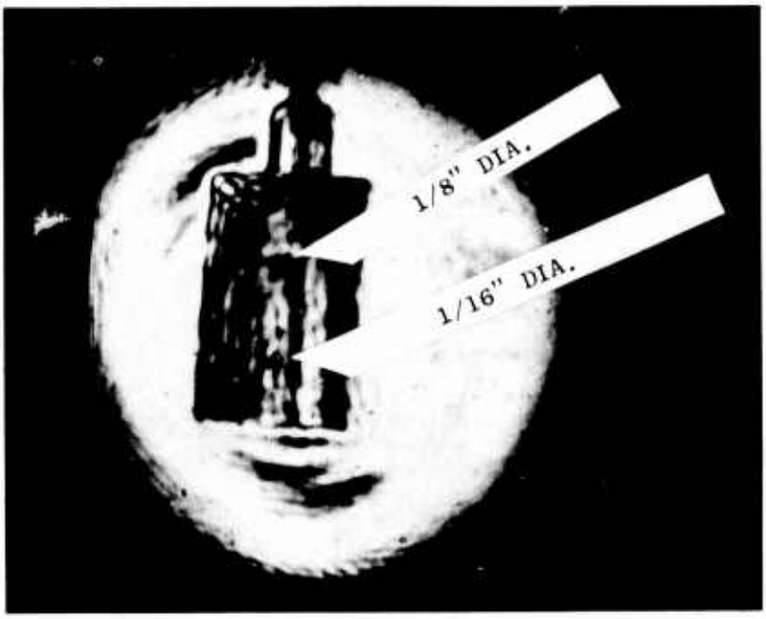

Figure 72. Acoustic Hologram of Undrilled Side of NiTaC-13 Plate Containing Two Holes Drilled to the Mid Plane

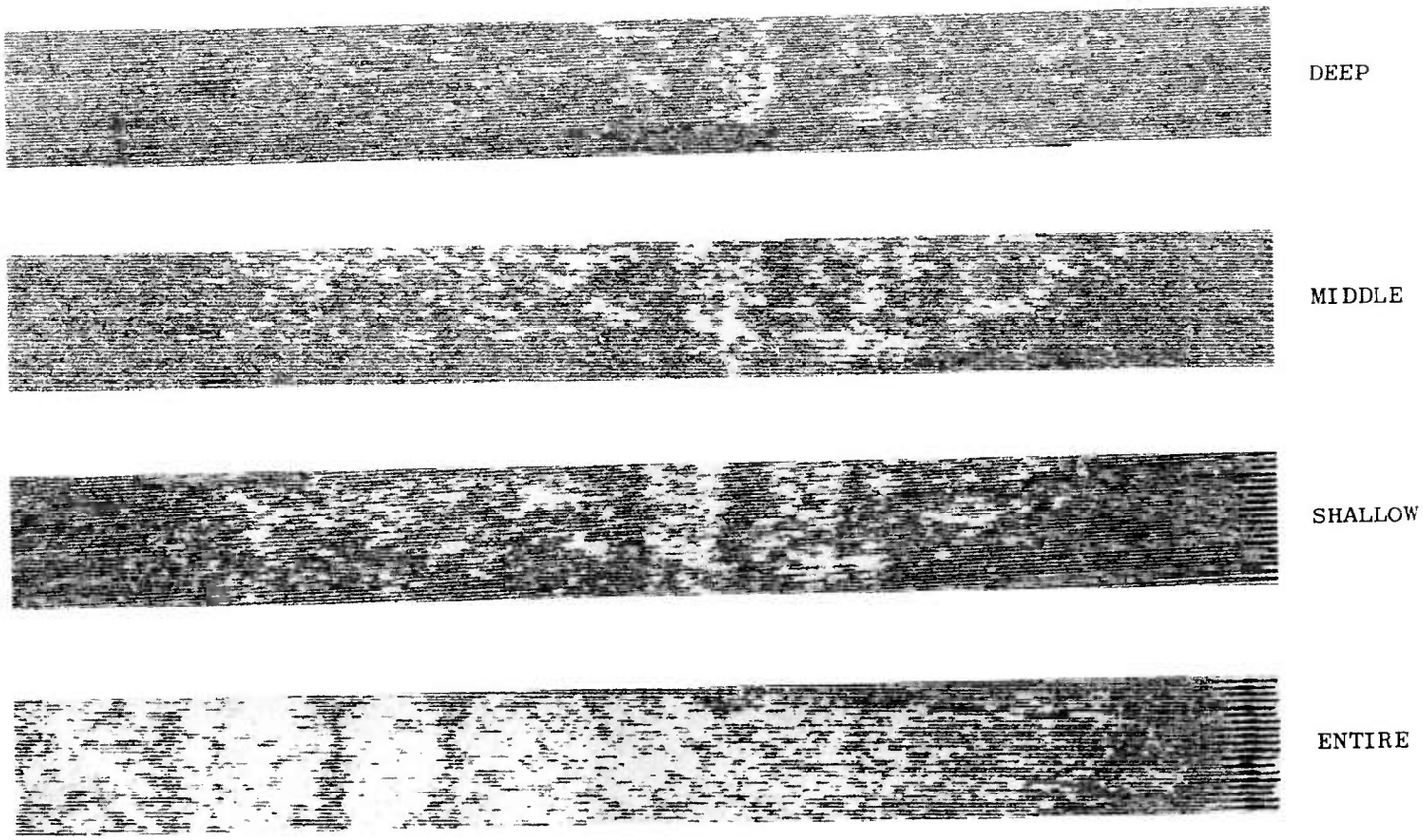

Figure 73. Contact Pulse-Echo Scans at Different Depths in Bar B37

2.8.2.8 Ultrasonic Velocity Measurements - Ultrasonic velocity is related to elastic modulus values of the material. Measurements were made on five bars in both the axial and transverse directions with the results shown in Table 25. Although differences were noted in the measured values for Bars B46, B65 and B66, these did not correlate well with rupture strength differences. Thus there was no evidence of indicate that this would be a beneficial NDE technique for this program.

2.8.2.9 Summary of Evaluation of NDE Techniques - Referring to the potential casting defects listed in Section 2.8.1, it was found that visual observation techniques were suitable for detecting surface defects and grain structure.

The detection of internal defects and surface nucleated carbides by methods evaluated was made difficult by the relatively poor surfaces of the bar and blade castings, and none were detected; however, it was considered reasonable to assume the X-ray radiography could be successfully used for this purpose with finish machined blades.

It was disappointing that none of the many NDE techniques evaluated was capable of distinguishing aligned from misaligned fiber material, even when the latter was present as a band in otherwise aligned material. X-ray radiography did reveal bands and arrest lines as striations, but positive identification was obscured by the presence of many other striations caused by unidentified material variations. The only reliable method established for microstructural classification was microscopic examination, preferrably of etch-polished surfaces. This is not considered a viable inspection procedure for full scale blade manufacture; hence, additional developmental work will be required.

2.8.3 Casting Acceptance Criteria and Inspection Procedures

2.8.3.1 Test Bars - The two criteria initially selected for determining acceptability of test bars to be produced for data acquisition and flame tunnel test specimens were:

- Aligned fiber length $\geq 4\text{-}1/2$ inches
- Band free (arrest lines were never observed in bars).

For the data acquisition work, the second criterion was relaxed to include bars containing bands, provided that test specimens could be machined to have band-free gage sections.

Inspection procedures selected for test bars, in order of decreasing importance included:

1. Microscopic examination at about 100X magnification of an etch-polished flat surface running the full length of the bar
2. Radiography with high energy X rays
3. Visual examination of the cast surface after etching

TABLE 25

ULTRASONIC VELOCITY MEASUREMENTS OF NiTaC-13 BARS

Bar No.	Avg. Axial Velocity In./Microsec.	Avg. Transverse Velocity, In./Microsec.
B17	.215 (1)	.229
B19	.216 (1)	.226
B46	.216 (2)	.227
B65	.217 (2)	.228
B66	.216 (2)	.230

(1) Taken through entire ingot before sectioning

(2) Taken through a 4-1/2" long section of ingot

2.8.3.2 Blade Castings - On the basis of work described in Sections 2.6.2.5 and 2.7.5.3, the acceptability criteria establsihed for blade castings to be produced for hardware evaluation included:

- Freedom from surface defects, such as pits and surface nucleated dendritic carbides, that penetrate the final blade envelope.
- Freedom from arrest lines within the final blade envelope.
- Freedom from cellular and/or dendritic cellular microstructures within the airfoil section.

As previously discussed, it was not possible within the program schedule to eliminate cellular and dendritic cellular bands in the dovetail section. On the basis of test results described in Sections 2.6.2.5 and 2.7.5.3 these carbide defect structures were somewhat deleterious to properties, but judged to be acceptable for this program. As part of the inspection, records were kept of the severity of bands in the root section.

Grain structure is of importance in DS superalloy castings and includes grain boundary intersection angles with leading and trailing edges, and dendrite orientations with respect to the blade longitudinal axis. For DS superalloy castings, angles more than about 10 degrees are generally cause for rejection. It was decided not to use this criterion for NiTaC-13 eutectic blades because the criticality of these factors on properties, such as thermal fatigue, had not been established for eutectic materials. However, it was decided to measure maximum grain boundary intersection angles as part of the inspection procedure.

Two inspections were to be performed on each blade casting: first, that by CRD as the blade producer and; second, that by M&PTL as the blade user.

The inspection procedures established for CRD included:

- Visual examination of as-cast surface
- Visual examination of etched surface
- Radiography - medium energy X rays for the airfoil and high energy X rays for the root
- Microscopic examination of polished convex surface of airfoil
- Microscopic examination of polished trailing edge of root section.

Figure 74 illustrates a blade in various stages of preparation for inspection, and Figure 75 illustrates several blades after etching to reveal grain structure.

The blade inspection procedures established for M&PTL included:

- Visual examination of blade castings received from CRD
- Examination of contact prints of CRD X-ray radiographs

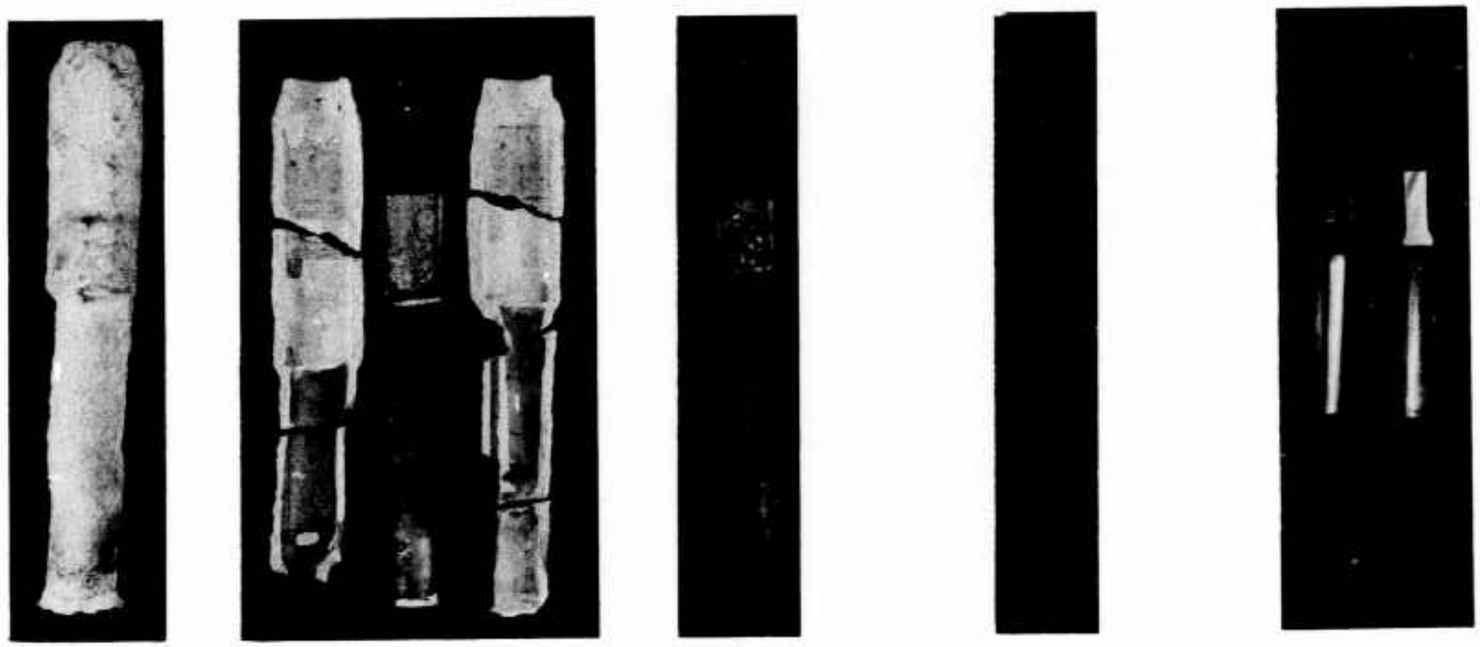

A. CASTING IN MOLD

B. MOLD REMOVED

C. BLADE EXTENSIONS CUT OFF

D. ETCHED

E. POLISHED AIRFOIL AND ROOT

Figure 74. **Preparation of Blade Castings for Inspection**

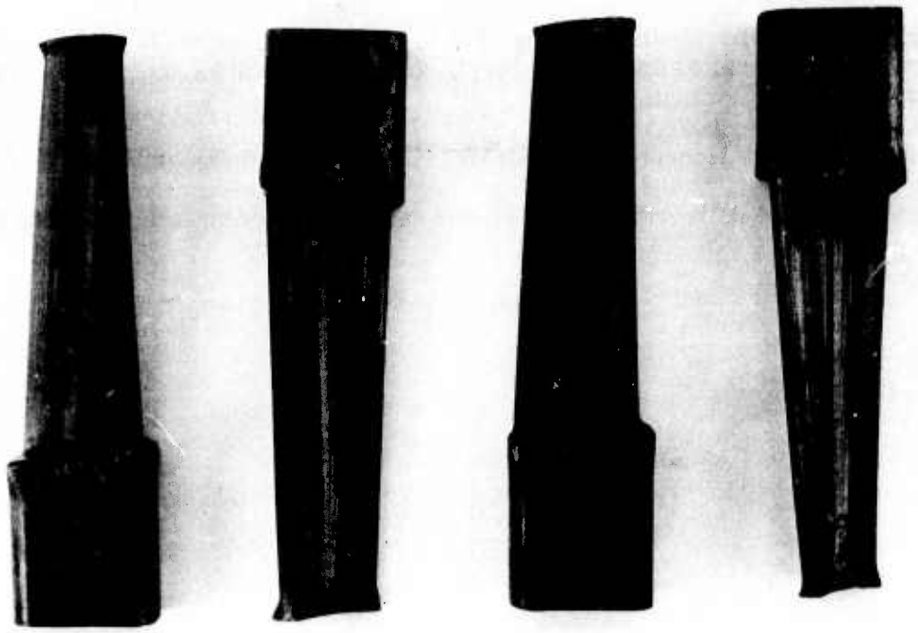

Figure 75. Blades After Etching with $HCl-H_2O_2$ to Show Grain Structure

- Microscopic examination of airfoil and root surfaces of blade castings as polished by CRD

- Measurement of maximum grain boundary intersection angles with leading and trailing edges

It was also planned to perform High Sensitivity fluorescent penetrant examination of all blades but this was discontinued when it was found that, due to the rough surface (much rougher than the bars), the background of indication was too heavy to detect surface flaws.

2.8.3.3 Finish Machined Blades - Final machining was performed by MAL Tool and Engineering of Manchester, Connecticut. Their inspections were the same as those used for developmental superalloy blades, including:

- Dimension at locations specified on blade drawing

- Radiography with medium energy (145 to 300 KV, inclusive) X rays (performed by Parker Industrial X-Ray Laboratory). Inspect for cracks, cold shuts, shrinkage, gas holes, and inclusions

- High sensitivity fluorescent penetrant. Inspect for cracks and nicks.

All blade records were delivered to M&PTL for review and acceptance decisions for discrepant parts.

3.0 NiTaC-13 PROPERTY EVALUATION

Turbine blade design and life analysis requires detailed information concerning many critical material properties and characteristics. These material requirements, with emphasis on eutectics for use in hollow high pressure turbine (HPT) blades, have been reviewed in detail by Jahnke and Bruch[8] and are summarized in Table 26.

Emphasis in the program was placed on the acquisition of mechanical and physical property data required for turbine blade design and life analysis. In addition, machinability of NiTaC-13 was evaluated both to establish procedures for finish machining of J101 LPT blades and to explore the applicability of a variety of machining techniques to this alloy class. Finally, the effectiveness of a Ni-20Cr-10Al-1Y coating for protection from oxidation and hot corrosion was evaluated. This was supplemented with tests to determine the effects of the coating on mechanical properties.

The amount of data required for a new material increases as it is transitioned from a feasibility demonstration to use in production engines. To meet the objectives of this program, the data acquired for NiTaC-13 and described in the sections that follow were at a level necessary for a General Electric developmental engine test.

3.1 TEST BAR PRODUCTION

To provide the NiTaC-13 required for the program, a total of thirty 1-5/8 inch diameter bars were produced using the PFS process described in Section 2.5.4 and inspected using procedures described in Section 2.8.3.1. Twenty-four of the bars were used for property data acquisition and six were used for flame tunnel tests.

Some details of the 30 bars are given in Table 27 where it can be seen that bars made in the two single station facilities generally had greater freedom from misaligned fiber bands than the three-station facility. Some test bars containing bands were accepted and used because cut up plans showed that the gage sections of test specimens would not contain bands.

TABLE 26

MATERIAL PROPERTIES AND CHARACTERISTICS IMPORTANT TO JET ENGINE TURBINE BLADE APPLICATIONS

MECHANICAL & PHYSICAL PROPERTIES

Property	Significance to Design
Creep & Rupture	Limit allowable airfoil metal temperature and stress.
High Cycle Fatigue	Vibration stresses at all locations on the blade must be less than the endurance limit of the material, as determined in smooth and notched bar tests.
Low Cycle Fatigue	Determines design, life: smooth bar data important to airfoil leading and trailing edges; notched bar data important to dovetail and bleed holes in air cooled blades.
Tensile	Limits dovetail/shank design.
Combined Steady State & Vibratory	Vibratory stress endurance limit is reduced by presence of steady state stresses.
Shear & Torsion	Adequate in conventional superalloys, but could be limiting in anisotropic materials, particularly in the dovetail.
Density	Affects blade and disk stresses.
Thermal Expansion	Affects blade expansion, important to gas leakage and tip rub.
Incipient Melting	Affects over-temperature capability of airfoil in the event of hot spots.
Elastic Constants	Affect blade material frequencies, and thermal stresses.

ENVIRONMENTAL RESISTANCE CHARACTERISTICS

Impact	Resistance to foreign object damage and loss of all blades in the event one blade fractures from other causes.
Surface Stability	Includes oxidation, hot corrosion and erosion resistance. Limits blade life, if uncoated, and capability to withstand loss of coating between inspections.
Coatings	Used for blade life extension, but generally affects microstructure and properties.
Microstructural Stability	Changes in microstructure and properties under engine operating conditions must be predictable.

BLADE FABRICATION CHARACTERISTICS

Castability	Affects cost effective production of precision complex shapes such as hollow air cooled blades free from cracks.
Machinability	Some machining is always required, including dovetails and surface holes in air cooled blades.

TABLE 27

SUMMARY OF 1-5/8 INCH DIAMETER TEST BARS PFS

AT 1/4 INCH/HOUR WITH G_L OF ABOUT 375°F INCH

Bar No.	Charge Material *Heat No.	Ingot	No. of Bands	Comments
Single Station Facility, B				
B88	V-371-C	3	0	
B90	V-371-C	4	0	
B91	V-371-C	4	0	
B92	V-371-C	3,4	0	
B93	V-371-C	3,4	1	
+B102	V-400-C	2,5	0	3B46 Re-run
+B114	V-416-C	1	0	Added 0.1%C
Single Station Facility, M				
M3	V-400-C	1,6	0	
M4	V-400-C	1,6	0	
+M43	V-416-C	6	0	B113 Re-run
+M52	V-435-B	1	0	
+M61	V-435-B	1	3	M55 Re-run
Three Station Facility, 3B				
3B24	V-371-C	3,4	0	
3B27	V-371-C	3	1	3B19 Re-run
3B33	V-371-C	3,4	0	
3B38	V-400-C	3	1	
3B39	V-400-C	3	2	
3B40	V-400-C	3	2	
3B41	V-400-C	2,5	1	
3B43	V-400-C	2,5	1	
3B47	V-371-C	3,4	1	3B34 Re-run
3B48	V-400-C	1,6	0	
3B49	V-400-C	1,5,6	1	
3B51	V-400-C	2,5	4	3B45 Re-run
3B52	V-400-C	1,6	2	B101 Re-run
3B53	V-400-C	1,6	2	B100 Re-run
3B54	V-371-C	3,4	1	
3B58	V-401-C	1	1	
+3B59	V-400-C	4	0	Bar 103 & 3B37 Two Re-runs
3B60	V-400-C	4	4	

* Ingots from Heat V-371-C were 2" diameter and required vacuum remelting and chill casting to 1-1/2" diameter ingots prior to PFS.

\+ Used for flame tunnel tests.

As shown in Table 27, all remelt ingots from heat V-371-C were 2 inches in diameter and had to be melted and chill cast in 1-1/2 inch diameter copper molds in order to fit 1-5/8 inch diameter alumina crucibles used for PFS. Also, nine of the bars were re-runs of previously rejected PFS bars. Finally, bar B114 was made from heat V-416-C which had been rejected because carbon was below specification. To correct for this, 0.1 weight percent carbon was added in a separate melting step prior to PFS of B114. Summarizing, 18 of the 30 bars were made from NiTaC-13 ingot material that had been melted and solidified either by chill casting or by PFS at least once prior to the final PFS. Nothing unusual was noted in the microstructures of these 18 PFS bars. Furthermore, stress-rupture tests of 1/2 inch diameter NiTaC-13 bars did not reveal any deleterious effects of repeat melting or PFS, so this was considered to be an acceptable practice.

3.2 MECHANICAL AND PHYSICAL PROPERTIES

The overall data acquisition plan for NiTaC-13 is summarized in Table 28. Because NiTaC-13 is anisotropic, property data were obtained with test specimens oriented parallel (longitudinal) and perpendicular (transverse) to the solidification direction. In addition, the effects of a Ni-20Cr-10Al-1Y coating on some properties were determined. All properties to be discussed were determined in tests performed in air.

In an effort to evaluate segregation effects on some properties, test bar cut up plans, illustrated in Figure 76, were designed to center the gage sections of test specimens at the following three levels of volume fraction solidified, g_b:

Location of Specimen in Test Bar	$^*g_b$
Top	0.66 ± 0.05
Middle	0.47 ± 0.05
Bottom	0.27 ± 0.05

$^*g_b$ calculated on basis of volume of liquid metal above the bottom of the sort-out zone

This division of test specimens into three g_b categories substantially reduced the number of data points obtained for each g_b level. Despite this, the data in Table 28 and other supplementary data generated during the program have identified effects of segregation on several properties.

The property data are summarized graphically or pictorially in the sections that follow, and in data tables presented in Appendix A.

TABLE 28

DATA ACQUISITION PLAN FOR ALIGNED FIBER NiTaC-13

*Property	**Number of Tests & Type Specimen							
	RT	1000°F	1200°F	1400°F	1600°F	1800°F	2000°F	2100°F
Tensile: 0.2 YS, UTS, %El, %RA	2,2T	2	2,2T	2	2	2,2T	2	
Stress Rupture: 100 Hr				1,1T	1	1,1C,1T,1TC	1,1C	1,1C
500 Hr				1,1T	1	1,1C,1T,1TC	1,1C	
1000 Hr				1,1T	1	1,1C,1T,1TC	1,1C	
Plastic Creep, 1%: 100 Hr				1	1	1C	1C	
500 Hr				1	1	1C	1C	
1000 Hr				1	1	1C	1C	
LCF (Strain Control): A = ∞			4		4	4		
A = 1			4		4	4		
A = 0.5			4		4	4		
LCF(Load Control), K_t = 1.6			4					
LCF (SPLCF), K_t = 1.6			≤ 5					
CSF: A = ∞			4	4,4T	4	4	4	
A = 1			4	4,4T,4C	4	4,4T,4C	4,4C	
A = 0.5			4	4,4T	4	4	4	
SETS: 5000 Cycles		—	—	2,2C	—	—	—	
Ballistic Impact	3			3	3	3	3	
Thermal Expansion		—	—	1,1T	—	—	—	
Modulus of Elasticity		—	—	1,1T	—	—	—	
Thermal Conductivity		—	—	1,1T	—	—	—	
Poisson's Ratio /Shear Modulus		—	—	1,1T	—	—	—	
Specific Heat		—	—	1	—	—	—	

*A = ratio of alternating to mean stress
SPLCF = Low cycle fatigue with hold time at peak load
CSF = Combined steady state mean load and high frequency alternating load
SETS = Simulated Engine Thermal Shock

**All longitudinal specimens except T = Transverse
C = Coated.

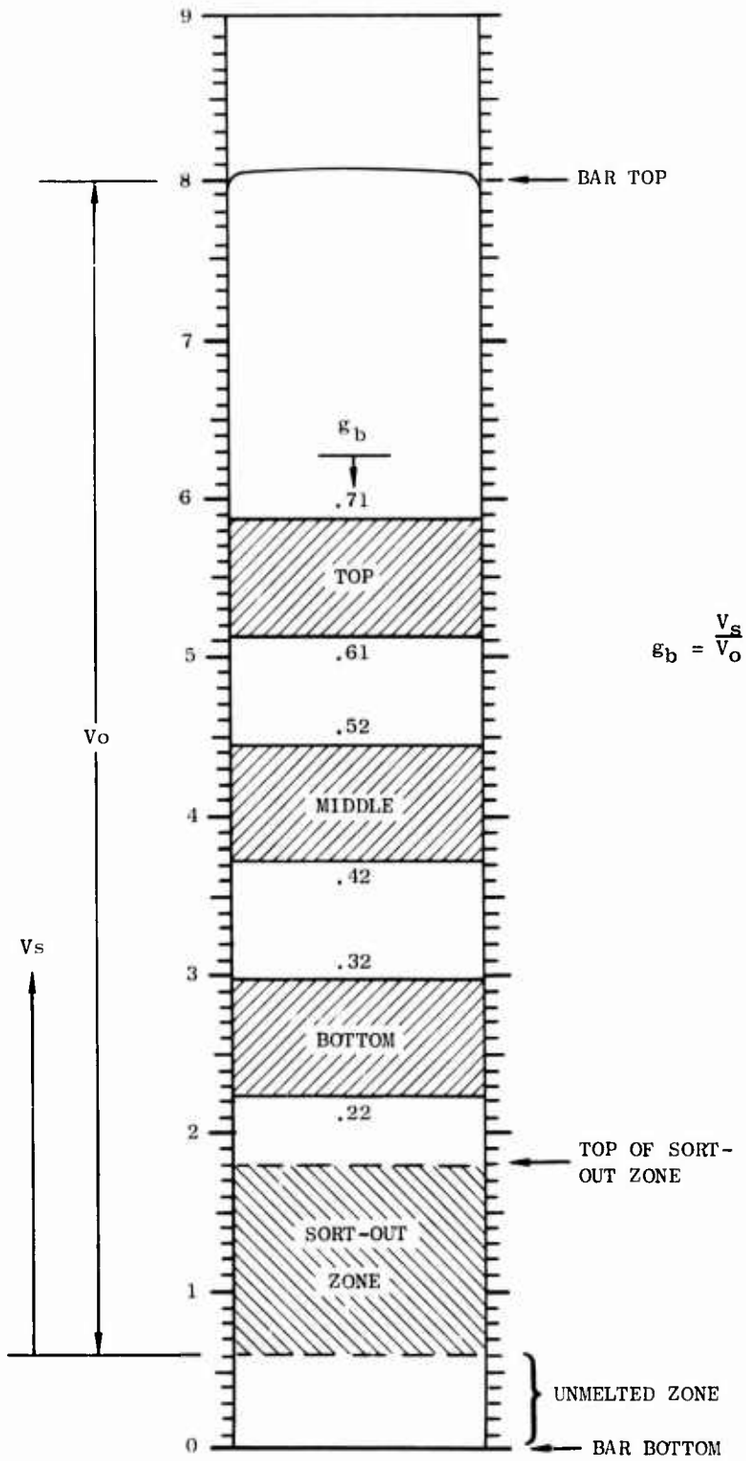

Figure 76. Position of Specimen Gage Sections in Typical Test Bar and Ranges in g_b for Top, Middle and Bottom Specimens

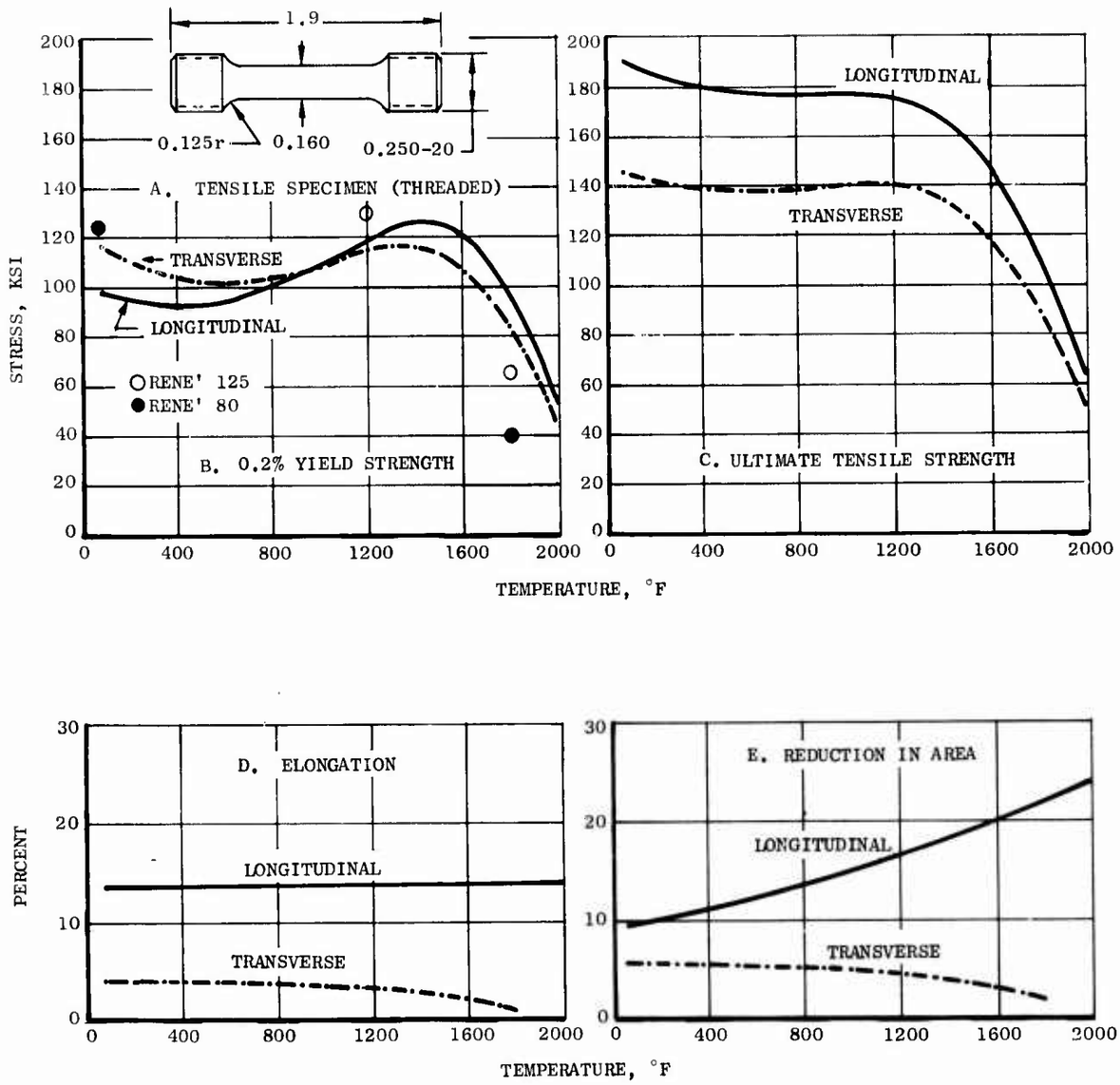

Figure 77. Tensile Properties of Aligned Fiber NiTaC-13

3.2.1 Tensile

Tensile properties from 75° to 2000° F were determined for the longitudinal and transverse directions of uncoated NiTaC-13.

Procedures - The test specimen is illustrated in Figure 77A. Elevated temperature tests were conducted in air using a resistance heated furnace and a 60,000 pound capacity Baldwin hydraulic testing machine. For all tests, the strain rate was initially set at 0.005 min^{-1} and an extensometer was used for elongation measurements until the 0.2 percent yield strength was exceeded slightly. At this point, the extensometer was removed and the test was continued to fracture, using the same loading rate as was used in the elastic region of the test. While the extensometer was in use, load-elongation curves were recorded, and used to determine yield strength and modulus of elasticity.

Results - The data are given in Table A-1 of Appendix A and average curves of temperature versus 0.2 percent yield strength, ultimate tensile strength, elongation, and reduction in area, as determined by regression analysis, are shown in Figure 77. Data analysis indicated that, within the range evaluated, there was no effect of g_b on tensile properties. As can be seen in Figure 77, longitudinal properties were generally superior to transverse. An exception was the 0.2 percent yield strength which was higher for the transverse direction at temperatures up to about 900°F where the curves cross. Several reasons for this behavior may be: first, carbide fibers in the as-cast material are in compression due to thermal expansion mismatches which reduces the longitudinal stress required up to the 0.2 percent yield point, or; second, the columnar grains have an <100> orientation in the longitudinal direction, whereas they have more random orientations in the transverse direction and strength is, therefore, higher in the latter direction.

Tensile ductility in the longitudinal direction increased with increasing temperature, whereas the opposite was true in the transverse direction.

Comparative data for 0.2 percent yield strength of two conventional superalloys, Rene' 80 and Rene' 125, shown in Figure 77B, indicate that NiTaC-13 is weaker up to about 1300°F, but stronger at higher temperatures.

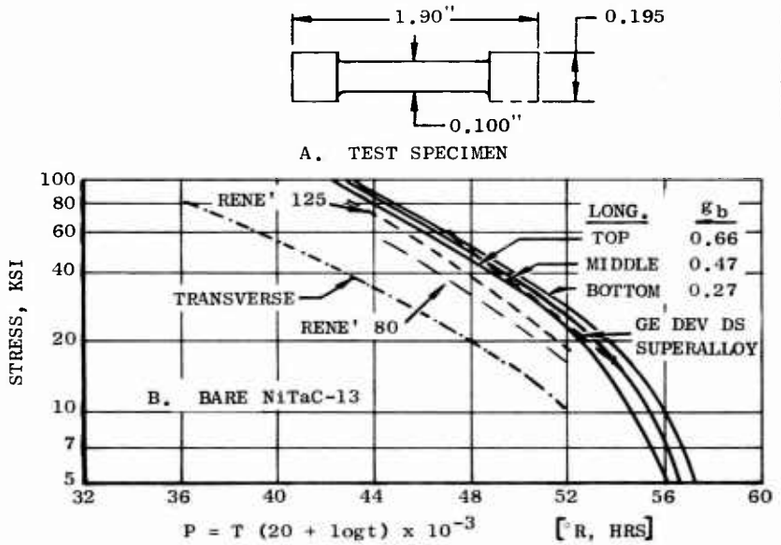

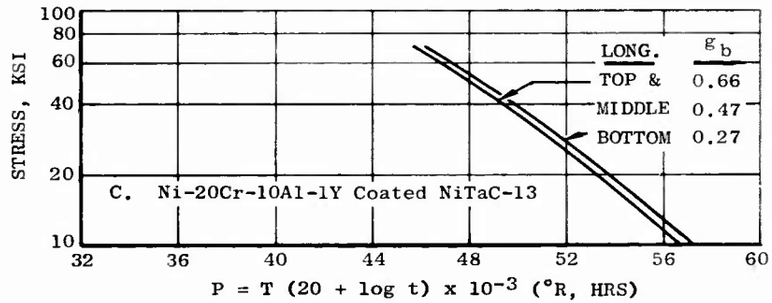

D. RUPTURE DUCTILITY

TEST	SPEC.	AVERAGE RUPTURE ELONGATION, PERCENT					
		BOTTOM		MIDDLE		TOP	
TEMP. °F	ORIENT.	BARE	COATED	BARE	COATED	BARE	COATED
1400	LONG.	—	—	—	—	7.7	—
1600	LONG.	7.5	10.3	8.0	—	—	—
1800	LONG.	9.9	19.5	8.1	10.9	7.9	—
2000	LONG.	—	—	9.8	9.0	7.4	—
2100	LONG.	14.8	24.9	—	—	—	6.0
1400	TRANS.	0.7	—	1.1	—	—	1.3
1800	TRANS.	—	1.0	0.6	1.0	—	—

Figure 78. Stress-Rupture Properties of Aligned Fiber NiTaC-13

3.2.2 Stress-Rupture

Rupture properties from 1400° to 2100°F were determined in air tests of bare and Ni-20Cr-10Al-1Y coated NiTaC-13 longitudinal and transverse specimens.

Procedures - The type specimen used for most of the tests is illustrated in Figure 78A. A similar test specimen with threaded ends was used for eight tests, and a much larger threaded-end specimen, having a gage section 0.25 inches in diameter and 1.15 inches in length, was used for three tests. Dead weight loading of the specimens, accurate to within one percent, was used either directly or through a lever system. Temperature was continuously recorded and controlled to within ± 5°F by means of thermocouples having beads in close proximity to the specimen surface at the center of the gage section.

Results - The data are listed in Tables A-2, 3, and 4 of Appendix A, and average curves of stress versus Larson-Miller Parameter, determined by regression analysis, are presented in Figures 78B and C. A strong effect of g_b was found for longitudinal bare NiTaC-13, as illustrated in Figure 78B. A similar effect is shown for longitudinal coated material in Figure 78C, but it was smaller, possibly due to the fewer number of tests. Analysis of the longitudinal coated and bare data showed that the Ni-20Cr-10Al-1Y coating had very little effect on stress-rupture strength at the lower test temperatures, but that it became increasingly beneficial with increasing temperature above 1900°F.

No effects of g_b or coating on rupture strength were found for the transverse direction. Transverse rupture strengths were about 40 percent of the longitudinal values.

Rupture ductility is best evaluated on the basis of elongation, because oxidation of the uncoated specimens results in erroneously high values for reduction in area. Comparison of rupture elongation data, Figure 78D, indicates the following trends:

- Longitudinal ductility of bottom material increased with increasing temperature. Middle and top material were little affected by temperature.

- Longitudinal ductility of bottom material was substantially increased by the coating, whereas the effect was small or absent for middle and top material.

- Transverse ductility was much lower than longitudinal and there were little, if any effects of temperature or coating. Work by Duhl and Sullivan[9] and by Kear et al[10] with DS MAR-M200 (without hafnium) showed that low transverse ductility in tension and stress rupture was not a problem with solid turbine blades, whereas hollow turbine blades sometimes exhibited grain boundary cracking during casting or during biaxial stress tests. These results, if applicable to NiTaC-13, indicate there should be no transverse ductility related problems with the solid J101 LPT blades of this program during casting or component testing. However, there may be a future problem with hollow NiTaC blades and alloy development work should endeavor to increase transverse ductility.

For comparative purposes, stress-rupture data for two conventional superalloys (Rene' 80 and Rene' 125) and one GE developmental DS superalloy (Ni76XB), all uncoated, are presented in Figure 78B. It can be seen that NiTaC-13 bottom material is substantially stronger than the two conventional superalloys, and significantly stronger than Ni76XB at stresses below 60 ksi.

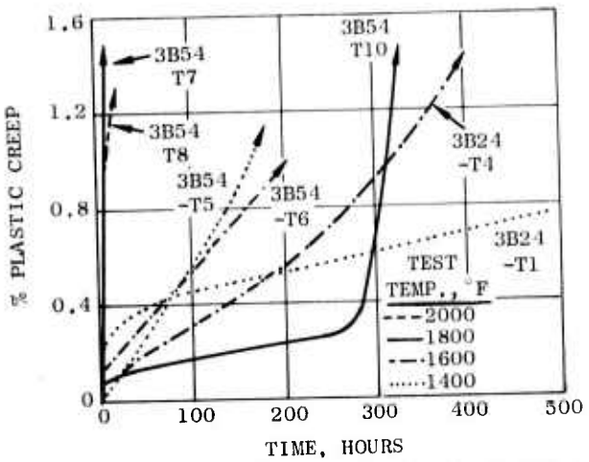

A. CREEP CURVES FOR NiTaC-13 FROM TOPS OF BARS

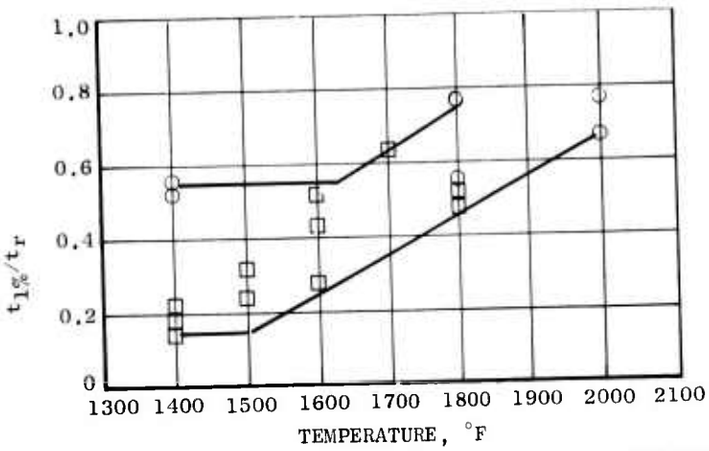

B. RATIO OF 1% PLASTIC CREEP LIFE TO RUPTURE LIFE FOR CONVENTIONAL TURBINE BLADE SUPERALLOYS

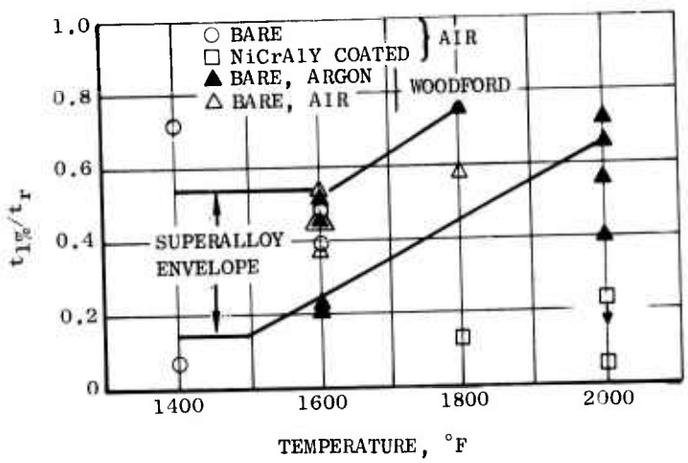

C. RATIO OF 1% PLASTIC CREEP LIFE TO RUPTURE LIFE FOR NiTaC-13 COMPARED TO CONVENTIONAL TURBINE BLADE SUPERALLOYS

Figure 79. Creep-Rupture Properties of Aligned Fiber NiTaC-13 in the Longitudinal Direction Compared to Conventional Turbine Blade Superalloys

3.2.3 Plastic Creep

Longitudinal creep strength for one percent plastic deformation was measured for bare material at 1400° and 1600°F and for coated material at 1800° and 2000°F.

Procedures - Twelve tests were performed using material from bars 3B24 and 3B54. The test specimen was the same as used for tension tests, Figure 77A. Most tests were performed by General Electric, but Joliet Metallurgical Lab., Inc., and Vulcan Testing Lab. each performed two tests. The general procedure used by GE involved attaching a thermocouple and extensometer to the sample, heating the sample to temperature, holding until temperature stabilized, and loading the sample while measuring extension to determine if plastic deformation occurred on loading. During the test, specimen elongation with time was continuously recorded by means of the linear voltage differential transformer of the extensometer. After termination of the test, reduction in area and total elongation of the specimen were measured.

In some cases, specimens were reloaded without extensometers and tested to rupture at the same temperature and stress as was used originally in the creep test. Stresses for coated specimens were calculated on the basis of bare cross sectional area.

Results - The data in Table A-5 of Appendix A show that seven tests were completed with bar top material ($g_b = 0.66$) whereas only two tests each were performed with middle ($g_b = 0.47$) and bottom ($g_b = 0.27$) material. Creep curves for top specimens in Figure 79A show that some specimens displayed classical three stages of creep on loading. The behavior was dependent on the stress-temperature combination used.

An analysis of the creep data indicated that the NiCrAlY coating may have reduced the creep strength of NiTaC-13. For the analysis, the ratio of one percent plastic creep life/to rupture life ($t_{1\%}/t_r$) was used. Figure 79B shows the effect of temperature on $t_{1\%}/t_r$ for two General Electric turbine blade superalloys. Data for several stresses at each temperature produced the scatter in points. As suggested by the envelope drawn, the general trend is for $t_{1\%}/t_r$ to increase with increasing temperature.

Figure 79C compares the envelope drawn for the superalloys with the following data for NiTaC-13: first, data from Table A-5 of Appendix A; and, second, data of Woodford[11] for bare specimens from bar bottoms tested in air and argon. In Woodford's tests, creep specimens were tested to rupture without ever unloading. It can be seen in Figure 79C that the coated specimens had unusually low $t_{1\%}/t_r$ ratios suggesting a deleterious effect of the coating which, if real, is not understood. There was also the possibility that the creep data for coated specimens were erroneous. Pursuit of this possibility, however, would have required an additional creep test program which was considered beyond the program scope.

The data in Figure 79C indicate that the creep-rupture behavior of NiTaC-13 is similar to that of conventional superalloys.

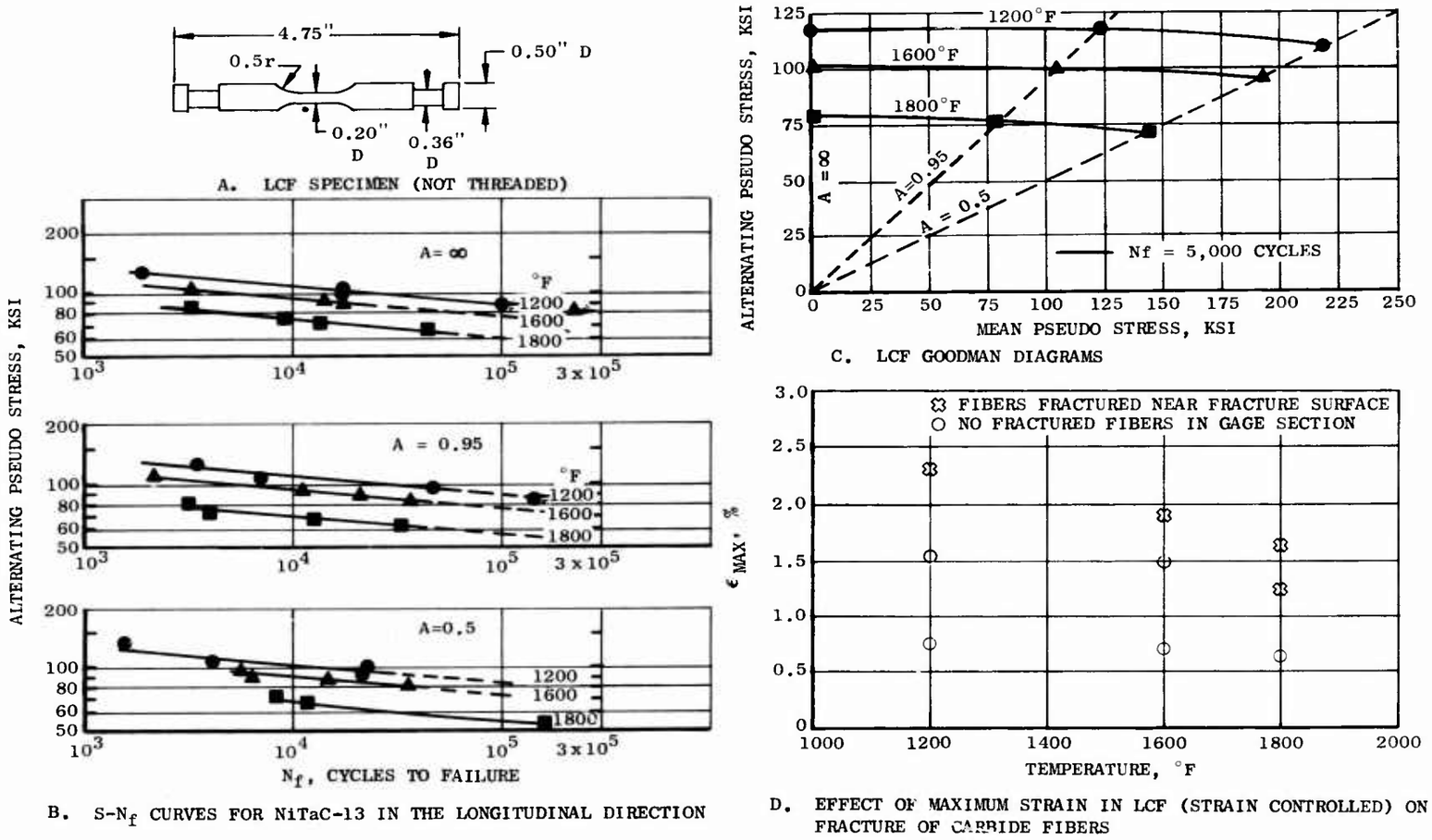

Figure 80. LCF (Strain Controlled) Strength of Aligned Fiber NiTaC-13 in the Longitudinal Direction

3.2.4 LCF - Strain Controlled

Smooth bar LCF properties were determined for bare longitudinal NiTaC-13 specimens from the middle sections of bars. Tests were performed in air at 1200°, 1600°, and 1800°F and at three A ratios (alternating strain/mean strain) including ∞, 0.95 and 0.5.

Procedures - All tests were performed by Metcut Research Association, Inc. The test specimen, illustrated in Figure 80A, was inductively heated in air to the selected test temperature. An extensometer was used to measure and control strain over a 0.75 inch gage length and cycling was conducted in the axial-axial mode at 20 cycles/minute. Load cycling was continuously recorded as a function of test time and used to detect crack initiation. Periodically during the test, a recording was made of one load-elongation cycle to check for drift and to determine the plastic strain contribution, if present, to the total strain. From the load-elongation recordings, Young's Modulus was computed, and the average value for all specimens at each temperature was used to calculate the alternating pseudo stress (Young's Modulus multiplied by alternating strain) for each specimen.

Results - A total of 36 tests were performed, and the results are summarized in Table A-6 of Appendix A. The data are also presented in Figure 80B as average curves of alternating pseudo stress versus cycles to failure (N_f). Straight lines of constant slope were force fitted through the data points. The curves of Figure 80B show that LCF strength decreased with increasing temperature, which is typical of superalloys.

Using the data in Figure 80B, partial Goodman diagrams at N_f equal to 5,000 cycles were constructed for the three test temperatures and are presented in Figure 80C. As shown, LCF strength decreased only slightly with increasing mean stress. This is also typical of superalloys, but the interesting point for NiTaC-13 is that maximum strains (ϵ_{max} in Appendix A, Table A-6) in the tests at each temperature increased with decreasing A ratio to values possibly exceeding fiber fracture strains. To investigate this possibility, longitudinal sections including the fracture surfaces of nine specimens (highest ϵ_{max} for each A ratio and temperature) were evaluated metallographically. The results in Table A-6 of Appendix A, are presented graphically in Figure 80D and show that no fractured fibers were observed in the gage sections of five samples. In the four samples containing fractured fibers, there is the possibility that the fibers fractured early in the test but did not cause a significant reduction in LCF strength. The 1600° and 1800°F data in Figure 80D also suggest that the strain to fracture carbide fibers decreases with increasing temperature.

The following comparative strain amplitude controlled axial-axial LCF test data for bare alloys show that NiTaC-13 is more than twice as strong as two conventional superalloys at 1800°F:

Alloy	Alternating Pseudo Stress (Ksi) for Failure in 10^4 Cycles at A = ∞
NiTaC-13	75
Rene' 125	34
Rene' 80	32

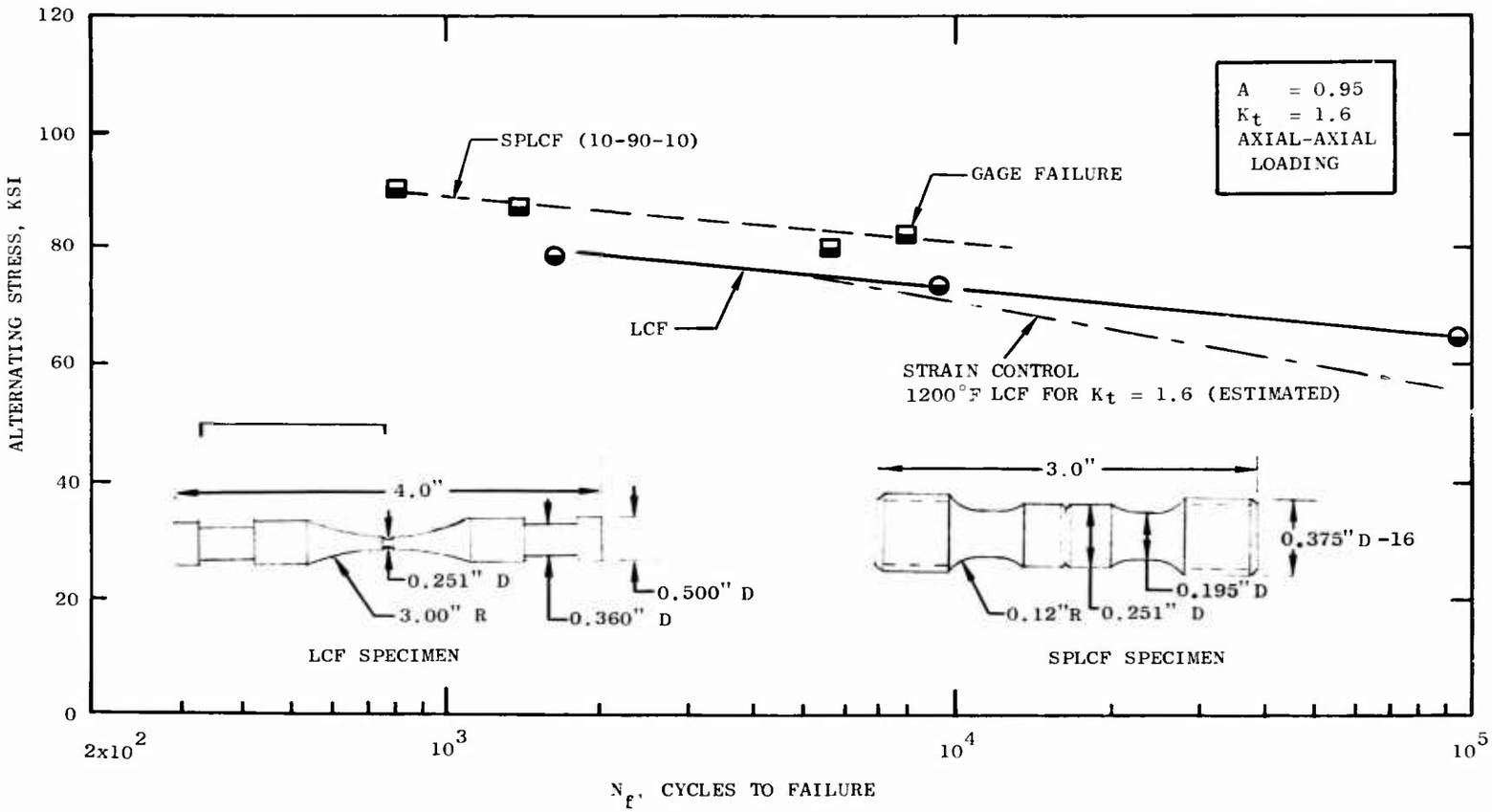

Figure 81. 1200°F Constant Load Amplitude LCF and SPLCF Data and Estimated 1200° F Constant Strain Amplitude LCF Curve. All Tests Performed with Bare Longitudinal Specimens from Middle of NiTaC-13 Bars

The superior LCF performance of NiTaC-13 is largely due to the absence of grain boundaries perpendicular to the stress axis and a Young's Modulus lower than conventional polycrystalline superalloys. Transverse grain boundaries present in superalloys are crack initiation sites, and the higher values of Young's Modulus in superalloys over NiTaC-13 result in a higher stress at a given strain.

3.2.5 LCF - Load Controlled

Notched bar LCF properties at 1200°F were determined for bare longitudinal NiTaC-13 specimens from the middle sections of bars, g_b equal to 0.47. In one type of test, the load was continuously cycled whereas in a second type of test, sustained peak low cycle fatigue (SPLCF), the specimen was held at the maximum load during each cycle to combine creep and cycling effects.

Procedures - The two types of test specimens used, illustrated in Figure 81, had notches machined to $K_t = 1.6$. Specimens were inductively heated to 1200°F ; and, using constant load amplitude, axial-axial cycling and an A ratio (alternating load/mean load) of 0.95, LCF tests were performed under continuous cycling at 20 cpm and under the following SPLCF conditions: 10 seconds to peak load, 90 seconds hold at peak load, and 10 seconds to minimum load. Stress was calculated on the basis of the area at the base of the notch.

Results - The data are listed in Table A-7 of Appendix A, and average curves are presented in Figure 81, where it is shown that the strength of NiTaC-13 was higher in the SPLCF test than in the continuous load cycling LCF test. Turbine blade superalloys usually show SPLCF strength equal or lower than LCF strength. Therefore, this is an unusual and favorable result for NiTaC-13, and may be due to matrix strain hardening. Also shown in Figure 81 is an estimated 1200°F LCF curve for $K_t = 1.6$ and $A = 0.95$ which was derived from strain control LCF data in Figure 80 by dividing the alternating pseudo stress by 1.6, assuming local strain conditions prevail. As shown in Figure 81, there is good agreement between the two LCF curves. This is significant because it indicates that fiber fracture was not a problem under the 1200°F test conditions evaluated and confirms the observation that there were no fractured fibers in the strain controlled LCF tests used for this comparison.

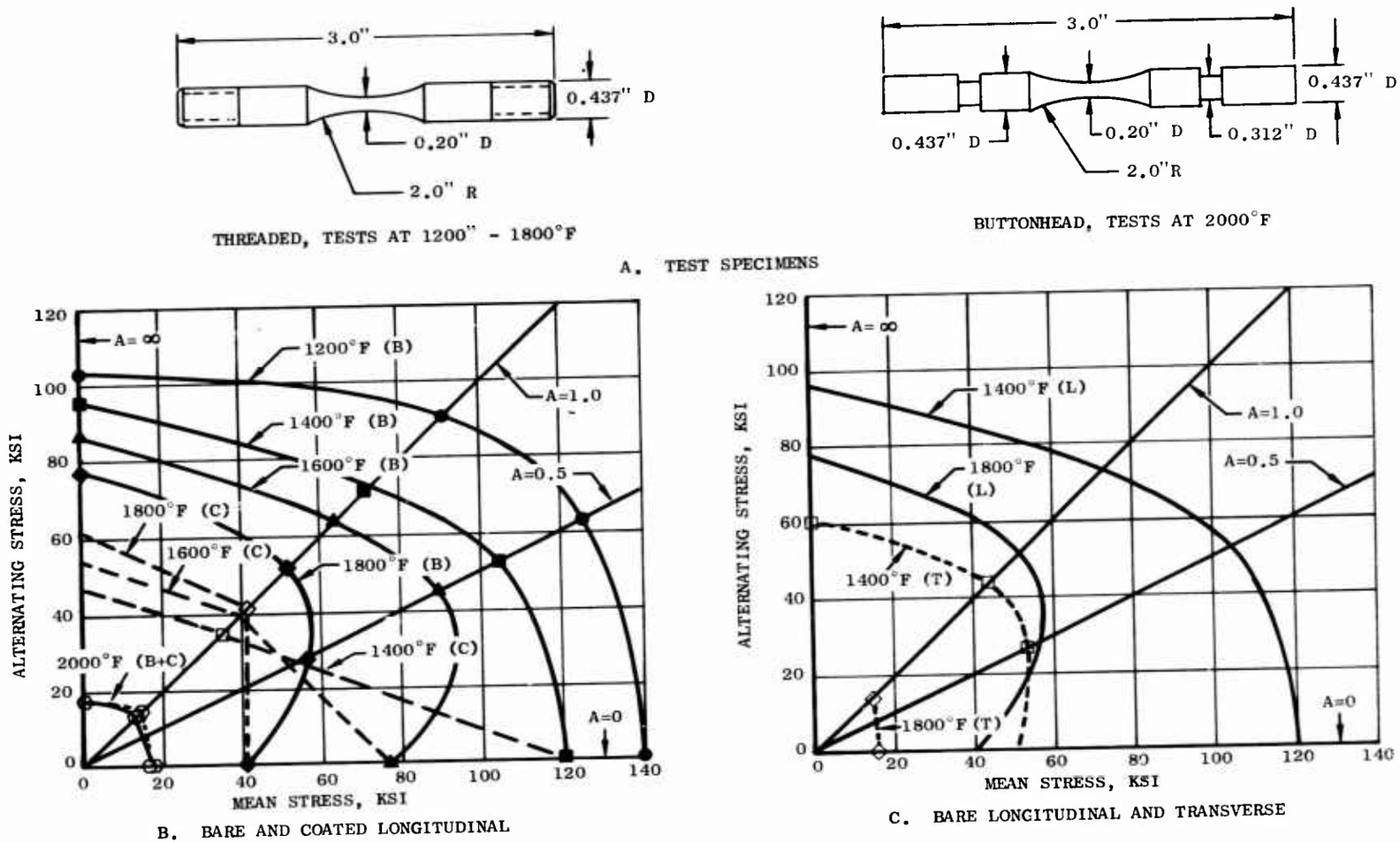

Figure 82. Average 100-Hour Goodman Diagrams for Bare (B) and NiCrAlY Coated (C) NiTaC-13

3.2.6 Combined Stress Fatigue

CSF properties from 1200° to 2000°F were determined for bare NiTaC-13 samples from the longitudinal and transverse directions of bottom, middle, and top sections of bars, g_b equal to 0.27, 0.46, and 0.66, respectively. Ni-20Cr-10Al-1Y coated longitudinal samples were also tested.

Procedures - The two types of test specimens used are illustrated in Figure 82A. Sonntag fatigue machines with provisions for applying an axial mean stress and a cyclic bending stress at 30 Hz were used to obtain A ratios (alternating stress/mean stress) of ∞, 0.95, and 0.5. Specimens tested at 1200° to 1800°F were heated in resistance furnaces, and those tested at 2000°F were inductively heated. In all cases, thermocouples were positioned close to the specimen gage sections for temperature control. The test objective was to determine the fatigue strength at 10^7 cycles. Specimens that reached 10^7 cycles without failure were step loaded to higher stresses to maximize information obtained with the limited number of specimens.

Results - A total of 87 tests were performed and the results are listed in Appendix A, Tables A-8 to A-11, inclusive. About 12 percent of the test results had to be discarded because of thread failures, excessive initial loads, and faulty microstructure. The first step in data analysis involved the construction of graphs of log stress versus log cycles to failure. Best fit straight lines were then drawn through each set of data points to determine the stress to failure in 10^7 cycles, which is approximately equal to 100 hours of cycling time. No effect of g_b was found. Using the derived fatigue strengths for 10^7 cycles and stress-rupture data (A = 0) from Figure 78 for middle sections of bars (g_b = 0.47), 100-hour Goodman diagrams were constructed.

Figure 82B presents Goodman diagrams for the longitudinal direction of bare and coated NiTaC-13, and shows all 10^7 cycle (100-hour) points derived from the basic data. Because of the limited number of points for coated material, the bare/coated alternating stress ratio at A = 1 was used to calculate the alternating stress at A = ∞, and straight lines were then drawn through points at A = ∞, 1, and 0. From inspection of the curves in Figure 82B, it can be seen that the coating reduced fatigue strength at 1400° and 1800°F but had negligible effect at 2000°F. The reduction in fatigue strength due to the coating was much greater at 1400° than at 1800°F. Therefore, to construct a 1600°F curve needed subsequently for coated material, it was estimated on the basis of 1400° and 1800°F data that the HCF strength of coated material would be 36 percent less than that of bare material at A = 1. The curve was then constructed as outlined above.

The deleterious effect of the coating is presumed to be due to the decrease in ductility of NiCrAlY coating alloys that occurs with decreasing temperature, but the mechanism of this effect has not been determined.

Figure 82C compares the longitudinal and transverse 100-hour Goodman diagrams for uncoated NiTaC-13 at 1400° and 1800°F. Analysis of these curves shows that the 1400°F vibratory stress capability of NiTaC-13 in the transverse direction is 50 to 60 percent of that in the longitudinal direction, but only about 35 percent at 1800°F, presumably due to grain boundary effects.

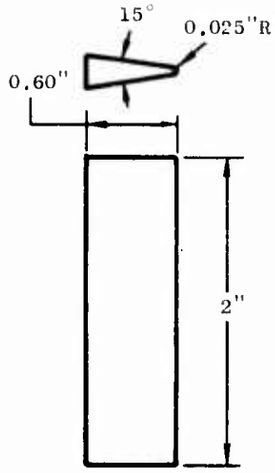

A. TEST SPECIMEN

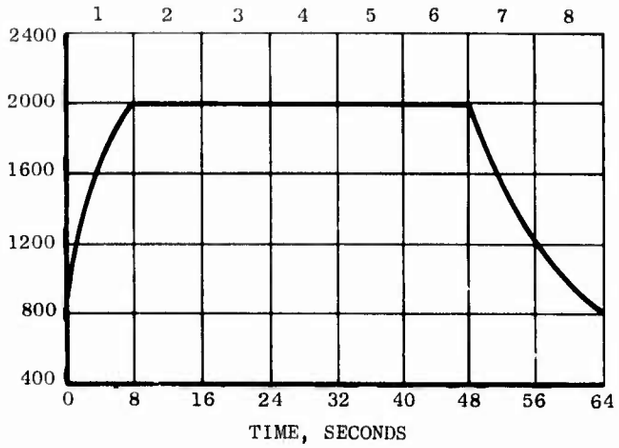

B. THERMAL CYCLE

C. INSPECTION - RATING *

No. of	BARE		COATED	
CYCLES	B91-T3	B91-T4	B91-T1	B91-T2
250	1	1	0	0
500	1	1	0	0
1000	1	1	0	0
1500	1	1	0	0
2500	1+	1+	0	0
5000	1+	1+	0	1

*0 = NO CRACKING OR SURFACE DETERIORATION
1 = PITS AT LEADING EDGE - NOT DISCERNIBLE AS CRACKS
2 = 1 TO 3 CRACKS WHICH DO NOT TRAVERSE LEADING EDGE ARC.

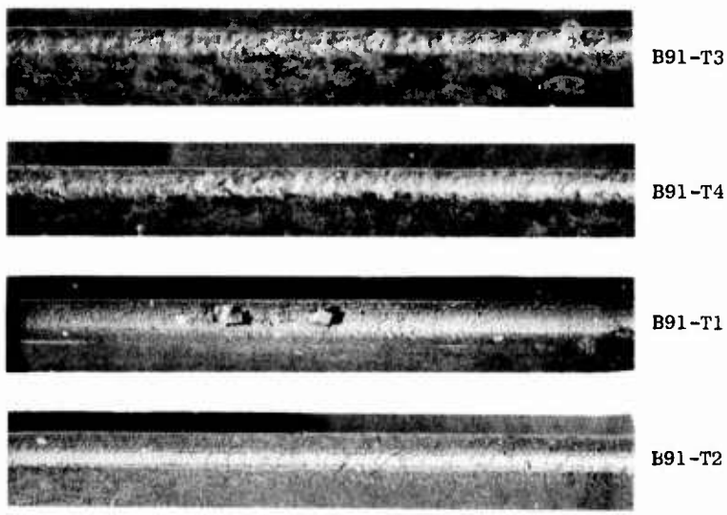

D. LEADING EDGES OF SPECIMENS AFTER 5000 CYCLES. 10X MAG.

Figure 83. SETS Test Results for Base and NiCrAlY Coated Longitudinal NiTaC-13 Specimens

The following comparative bending-axial HCF test data for bare alloys show that NiTaC-13 is more than twice as strong as two conventional superalloys at 1800°F:

Alloy	Alternating Stress (Ksi) for Failure in 10^7 Cycles at $A = \infty$
NiTaC-13	77
Rene' 125	32
Rene' 80	28

The superior HCF performance of NiTaC-13 is attributed to the absence of grain boundaries perpendicular to the stress axis, and the lower severity of other crack initiation sites, including coarse carbides and pores.

3.2.7 Thermal Fatigue

Simulated engine thermal severity (SETS) tests were conducted with two bare and two Ni-20Cr-10Al-1Y coated longitudinal samples all from the top section of Bar B91.

Procedures - The test specimen is illustrated in Figure 83A. In the test facility, there are eight stations for samples, which remain stationary. There are also eight jets that are either gas burners for heating or air jets for cooling. These jets rotate in discrete steps and heat each sample quickly to the selected upper test temperature, hold at temperature, and then cool quickly to the lower test temperature. Through variations in the flame temperatures, the distribution of heating and cooling gas jets, and the dwell time at each station, a wide variety of temperature profiles can be achieved. In the tests of NiTaC-13, the peak temperature was 2000°F, the minimum temperature was 800°F, and the dwell time at each station was eight seconds for a total cycle time of 64 seconds. The temperature profile illustrated in Figure 83B was more severe than is generally used for turbine alloys. Periodically, the test was interrupted and the specimens were removed and inspected for cracks using a stereo microscope at about 22X magnification.

Results - The four NiTaC-13 samples were given a total of 5,000 cycles. Inspection results in Figure 83C show that none of the specimens exhibited fatigue cracking in the test. However, the two coated samples quickly developed fine and apparently superficial cracks in the coating which remained unchanged throughout the test. Only at the final inspection was any coating loss observed. This was near the end of the leading edge of one sample and was not representative of the overall condition of that specimen. Oxidation of the two uncoated samples was substantial. Photographs of the four test specimens are shown in Figure 83D.

Under less severe thermal cycling, conventional polycrystalline superalloys exhibit substantial cracking in 1,000 to 2,000 cycles of SETS testing; hence, it was concluded that NiTaC-13 demonstrated excellent thermal fatigue resistance in the SETS test.

TABLE 29

BALLISTIC IMPACT TEST RESULTS FOR ALIGNED FIBER NiTaC-13

Specimen Origin, Bar No.	*Surface Finish	Test Temp., ^{o}F	Impact Energy, Ft. Lbs.	g_b	Failure Code Number
91-B1	32AA	72	4.7	-	3
91-B1	32AA	72	5.3	-	3
91-B1	32AA		5.8	-	3
91-B1	32AA		4.2	-	1
91-B2	400G	72	4.8	-	3
91-B2	400G	72	4.1	-	2
91-B2	400G	72	4.0	-	2
91-B2	400G	72	3.8	-	1
91-B5	32AA	1400	4.2	.35	3
91-B5	32AA	1400	2.4	.31	2
91-B5	32AA	1400	2.0	.29	2
91-B4	400G	1400	2.5	-	1
91-B4	400G	1400	3.0	-	1
91-B4	400G	1400	3.2	-	1
91-B4	400G	1400	3.6	-	2
91-B7	32AA	1600	1.9	.34	1
91-B7	32AA	1600	2.5	.32	2
91-B6	400G	1600	2.6	.20	1
91-B6	400G	1600	3.2	.24	3
91-B9	32AA	1800	2.5	.36	3
91-B9	32AA	1800	1.9	.33	1
91-B8	400G	1800	2.6	.20	1
91-B8	400G	1800	3.3	.25	1
91-B8	400G	1800	3.5	.30	3
92-B1	400G	2000	2.0	.14	1
92-B1	400G	2000	2.6	.16	1
92-B1	400G	2000	3.2	.20	1
92-B1	400G	2000	3.8	.23	3
91-B10	400G	2000	3.0	.20	1
91-B10	400G	2000	3.5	.25	1

** AA = Arithemitic Average; 400G = 400 grit polish

3.2.8 Ballistic Impact

Tests were conducted from room temperature to 2000°F using bare NiTaC-13 specimens from bottom sections of test bars, g_b ranging from about 0.15 to 0.35. This g_b range was representative of airfoil material from the NiTaC-13 J101 LPT blades, where ballistic impact resistance is most important.

Procedures - Specimens were 2 inches long x 3/4 inches wide x 0.1 inches thick and were ground to a 32AA surface finish. The grinding scratches were parallel to the specimen length (also the solidification direction). For the tests, the specimens were heated to the test temperature and were struck with 0.175 inch diameter steel projectiles fired from an air rifle. Projectile velocity was measured by an elapsed time counter for use in the calculation of projectile energy. The tensile (convex) sides of the indentations were inspected for cracks at 30X magnification, and a failure code number was assigned to each test result as follows:

Failure Code No.	Indentation Appearance
1	No visible crack
2	Very slight crack
3	Large crack(s)

Because the grinding scratches were relatively deep, it was difficult to detect very slight cracks (Failure Code 1). Also, the cracks were generally parallel to the scratches, raising the possibility that they contributed to cracking. Therefore, samples were polished with 400 grit silicon carbide paper, and additional tests were performed.

Results - All results are presented in Table 29. No effect of g_b, over the small range evaluated, was found. By emphasizing results for the polished samples, it can be seen that the maximum projectile energy absorbed without crack initiation (Failure Code No. 1) was nearly independent of test temperature, as follows:

Test Temp., °F	72	1400	1600	1800	2000
Max. Impact Energy Without Cracking, Ft. Lbs.	3.8	3.2	2.6	3.3	3.5

There was no observed minimum in tensile ductility (Figure 77) with temperature to support the possibility that the low 1600°F ballistic impact result represents a true minimum in the curve.

The results for NiTaC-13 were equivalent to those for conventional turbine blade superalloys currently in use.

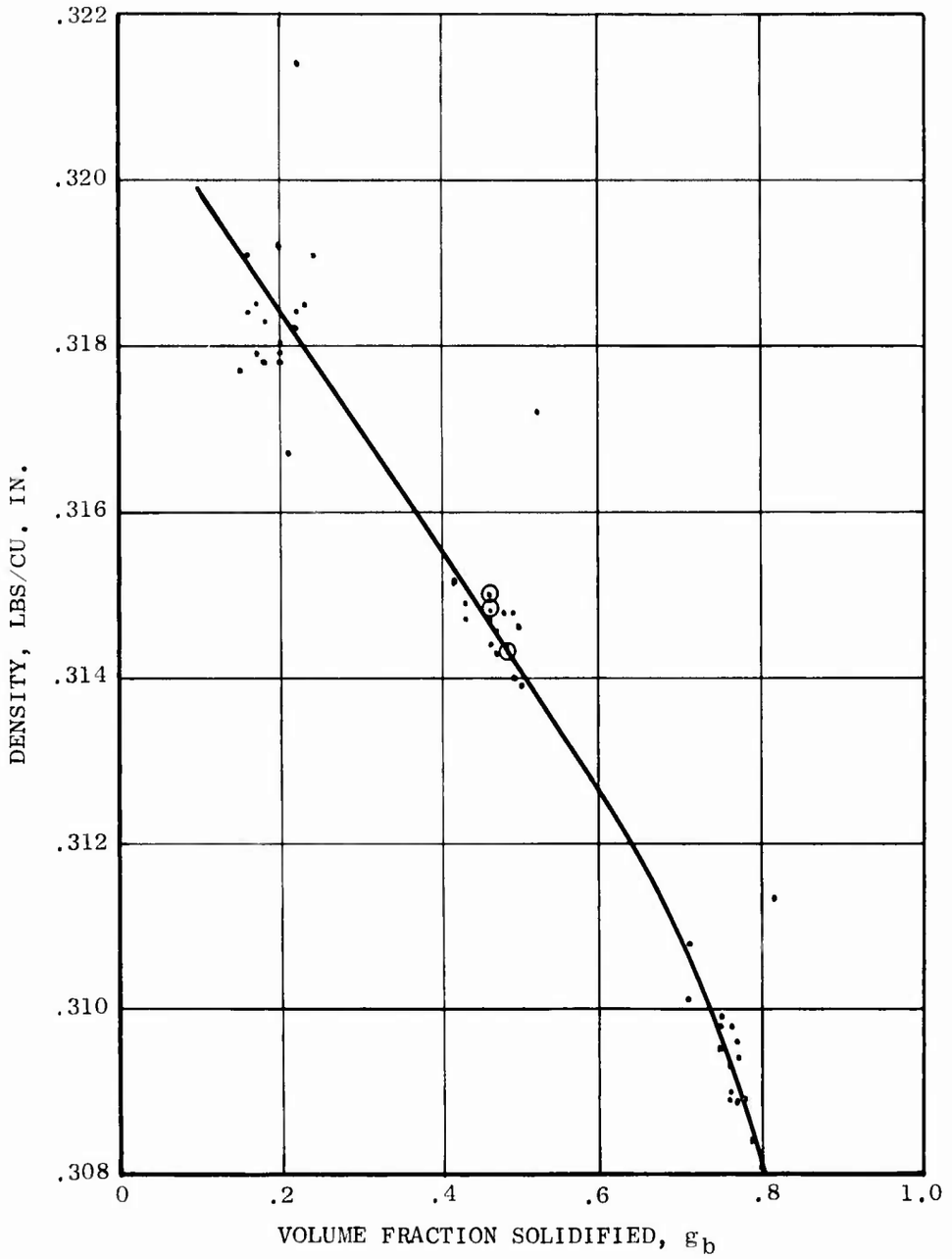

Figure 84. Room Temperature Density of NiTaC-13 as a Function of g_b

3.2.9 Density

Density measurements of NiTaC-13 were made at room temperature using samples from test bars produced in process development work, Section 2.5.3. Carbide morphologies in these bars included aligned fibers, cells, and dendritic cells. Samples for measurement were taken from the bottom, middle, and top of each bars.

Procedures - Measurements were made utilizing Archimedes principle, by which sample volume is calculated from the loss of weight in air during water immersion. Sample weights varied from 9.5 to 33.5 grams. Estimates of g_b for each sample were made on the basis of the sample location in each bar.

Results - The data are listed in Table A-12 of Appendix A, and presented graphically in Figure 84 as a curve of density versus g_b. The curve was drawn to favor results for aligned fiber material. With the exception of results for bar B84, the scatter of points around the curve drawn is within ± 0.5 percent. Reasons for the high results for bar B84 are not known. The results in Figure 84 show that there was a significant decrease in density from the bottom to the top of bars, which was due to segregation of alloying elements discussed in Section 2.4.

The density of NiTaC-13 bottom material is 3.4 percent higher than Rene' 125 and 7.9 percent higher than Rene' 80.

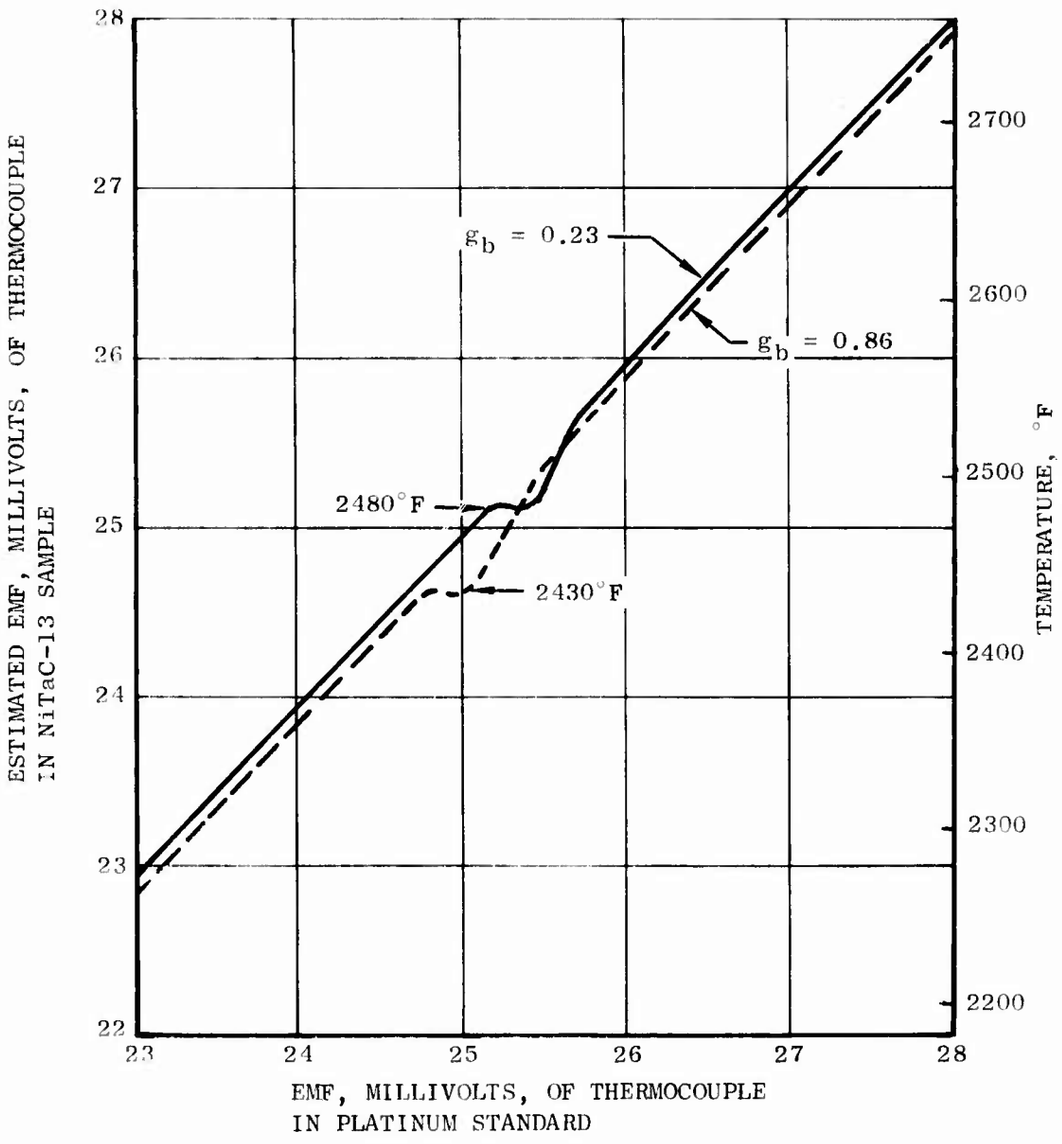

Figure 85. Heating Curves Derived From Differential Thermal Analysis Data to Show Thermal Arrests During Melting of Aligned Fiber NiTaC-13

3.2.10 Melting Temperature

Melting temperatures were determined for aligned fiber NiTaC-13 samples from the bottom and top of one bar at g_b levels of 0.23 and 0.86, respectively.

Procedures - Differential thermal analysis was performed by the University of Dayton School of Engineering. For each measurement, alumina insulated beads of a differential thermocouple made of W-3 Re/W-25 Re were inserted into the hollow NiTaC-13 sample and a hollow platinum standard which were contained in separate alumina crucibles within the furnace. Heating and cooling runs were made at constant rates ranging from 9 to 12.5°F/minute, while separately recording the EMF of the thermocouple in the Pt standard, and the differential EMF between the Pt standard and the NiTaC-13 sample. Subsequently, differential EMF values for the two heating runs were converted to estimated EMF values of the thermocouple in the NiTaC-13 sample.

Results - Figure 85 presents curves of the estimated EMF of each NiTaC-13 sample versus EMF of the platinum standard during heating. (The latter is equivalent to elapsed time.) As illustrated in Figure 85, there was one pronounced thermal arrest for each sample. The sample with g_b of 0.23 began melting at about 2480°F, and the one with g_b of 0.86 began melting at about 2430°F. The gradual return of the curves to the same slopes as existed prior to the thermal arrests suggest that each sample had a melting temperature range. Other results not illustrated show that, on cooling, the thermal arrest temperatures were reduced by about 17°F.

The substantial difference in melting temperatures of bottom and top material is another manifestation of segregation discussed in Section 2.4.

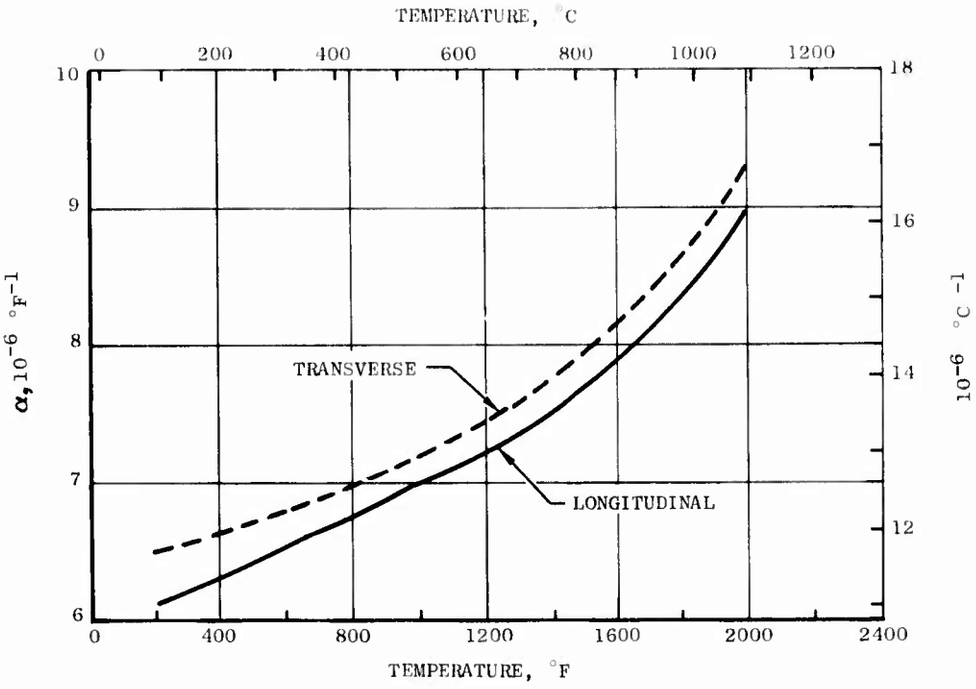

A. COEFFICIENT OF LINEAR THERMAL EXPANSION

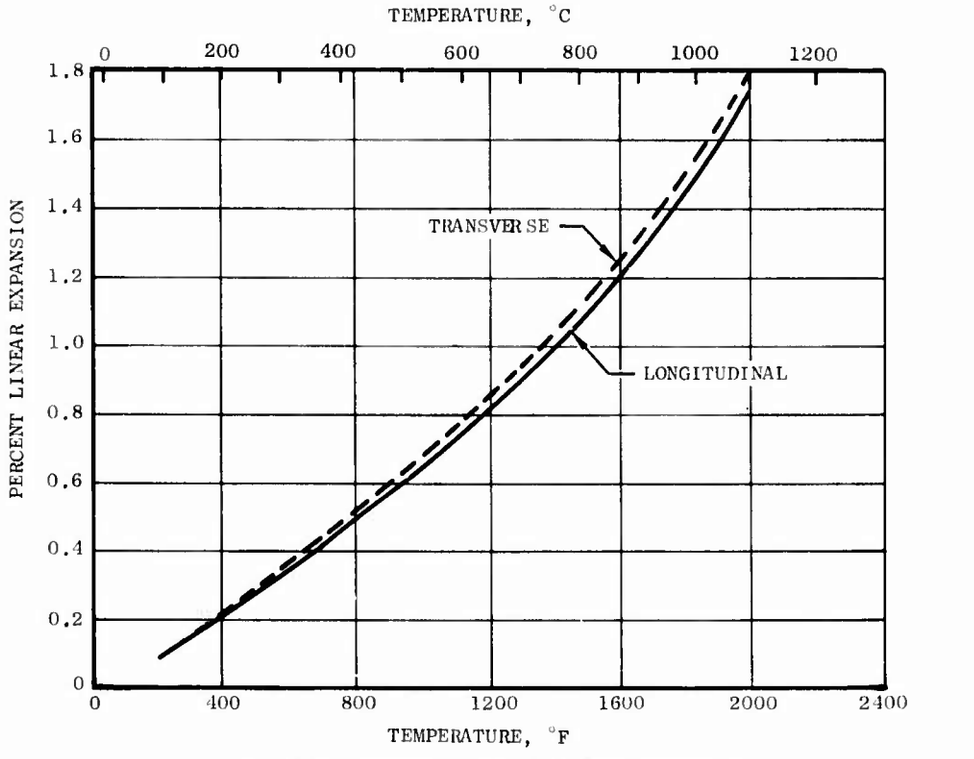

B. PERCENT TOTAL LINEAR THERMAL EXPANSION

Figure 86. Thermal Expansion of Aligned Fiber NiTaC-13 in the Longitudinal and Transverse Directions

3.2.11 Thermal Expansion

Thermal expansion from 77° to 2012°F was measured in both the longitudinal and transverse directions of NiTaC-13 using material from the middle section of bar B92.

Procedures - Specimens lengths were nominally 2.5 inches, requiring two sections for the transverse direction. Measurements of sample length as a function of temperature during heating and cooling in air were made and recorded, using a Chevenard Model 50 instrument.

Results - The data are presented in Table A-13 of Appendix A and in Figure 86, which shows the coefficient of linear expansion curves and total percent linear expansion curves as a function of temperature during heating. As can be seen in these graphs, NiTaC-13 thermal expansion is slightly higher in the transverse direction.

The thermal expansion coefficients of Rene' 80 and Rene' 125 at room temperature are both $7 \times 10^{-6} {}^{\circ}F^{-1}$, slightly higher than that of NiTaC-13.

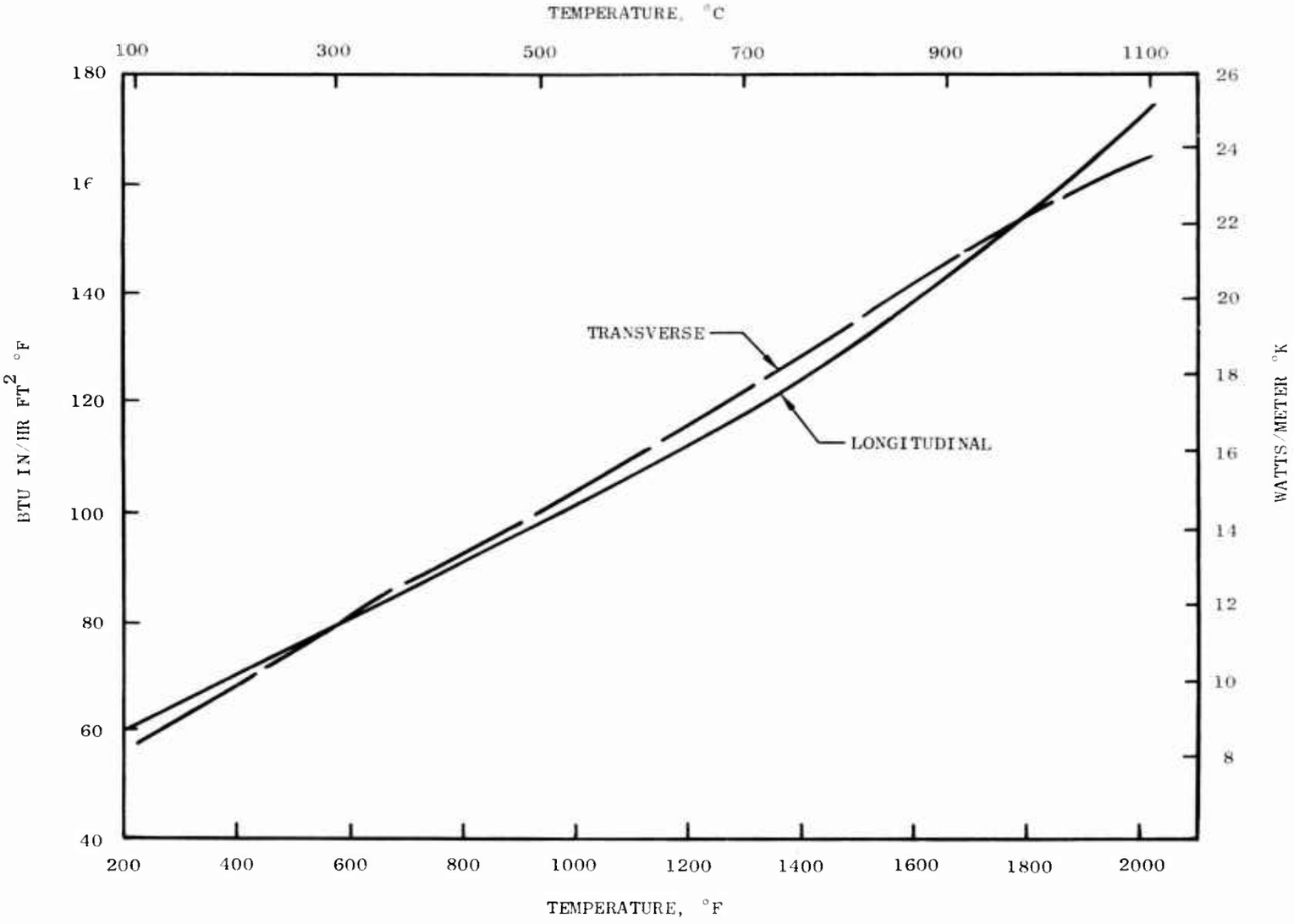

Figure 87. Thermal Conductivity of Aligned Fiber NiTaC-13 in the Longitudinal and Transverse Directions

3.2.12 Thermal Conductivity

These measurements of aligned fiber NiTaC-13 were performed over the temperature range from -103° to 2012°F, using a longitudinal specimen from the top of bar B88 and a transverse specimen from the middle of bar B91.

Procedures - The measurements were made by Dynatech R/D Company using a comparative cut-bar technique. Each cylindrical NiTaC-13 specimen, 25mm in diameter by 25 mm in length, was instrumented with an insulated thermocouple just below the two end surfaces and placed between Inconel 702 references standards having similar geometries and thermocouple instrumentation. The composite stack of three was placed between the plates of an upper heater and a lower heat sink. A reproducible load was applied to the top of the complete system. Surrounding this stack was a guard tube which could be heated or cooled in three regions to match the temperature gradient of the test stack, thereby minimizing radial heat loss. After temperature equilibrium was obtained at each measurement point, temperatures at all sample locations were recorded. Thermal conductivity was calculated from the average energy flow in the two reference samples, the temperature difference across the NiTaC-13 sample, and the sample dimensions.

Results - The data are listed in Table A-14 of Appendix A, and shown graphically in Figure 87. The differences between the two curves are slight, less than five percent, indicating very little, if any, anisotropy in the thermal conductivity of aligned fiber NiTaC-13.

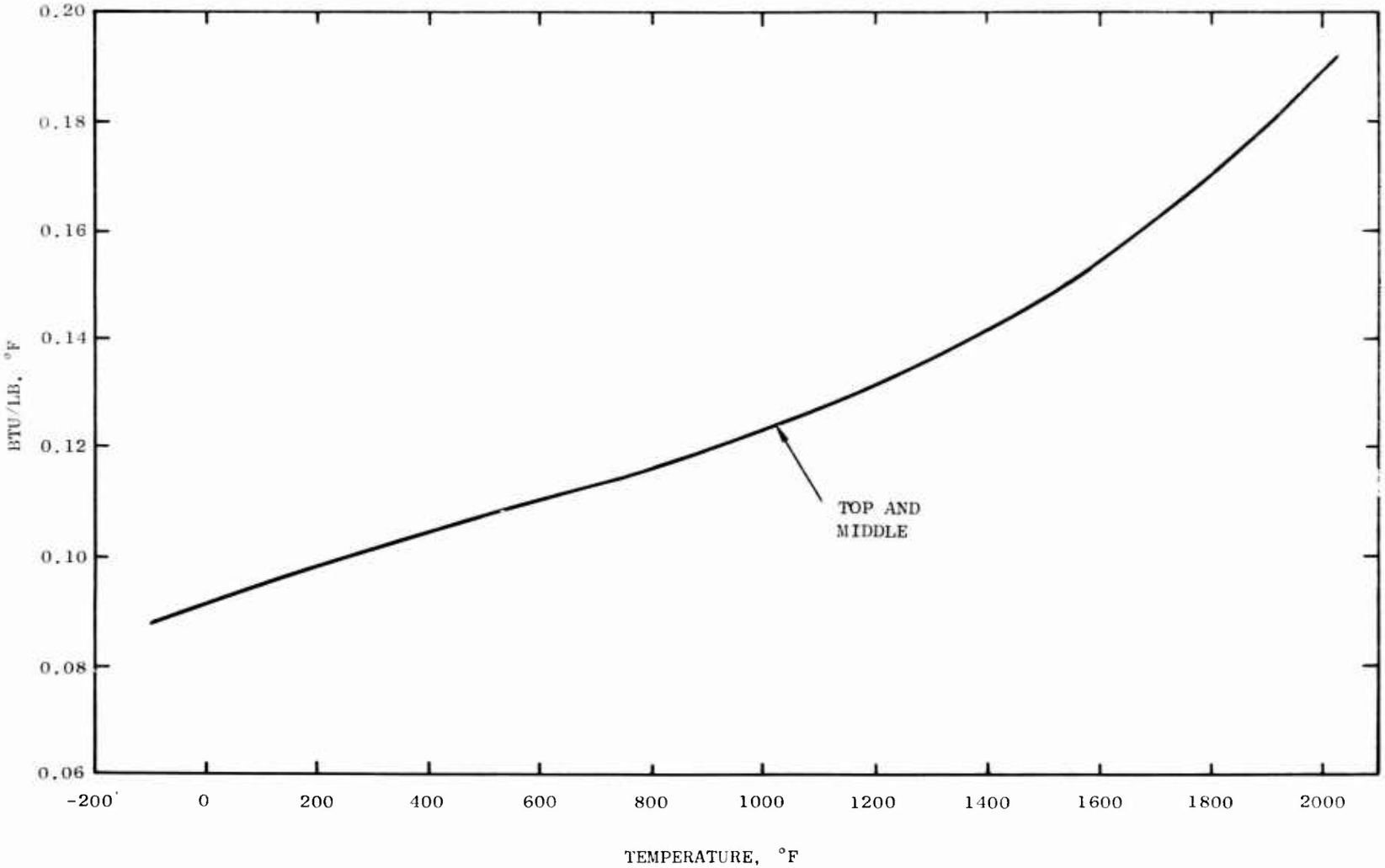

Figure 88. Specific Heat of Aligned Fiber NiTaC-13 from Top and Middle Sections of Bars

3.2.13 Specific Heat

Specific heat over the temperature range of -100° to 2000°F was measured using the same samples that were used for thermal conductivity measurements, Section 3.2.12.

Procedures - These measurements were made by Dynatech R/D Company using a standard drop calorimeter technique. For each measurement, the sample was first held at the desired temperature for one to two hours until an equilibrium temperature was attained. The sample was then dropped into a calibrated copper receiver, and temperature of the receiver was measured over a period of two hours after the drop. From these data, specific heats were calculated. Two measurements were performed at each temperature with each sample.

Results - The data are listed in Table A-15 of Appendix A, and are shown graphically in Figure 88. No difference was found in the specific heat of material from the top and middle of bars, g_b equal to 0.66 and 0.47, respectively. The specific heat of NiTaC-13 is typical of current turbine blade superalloys.

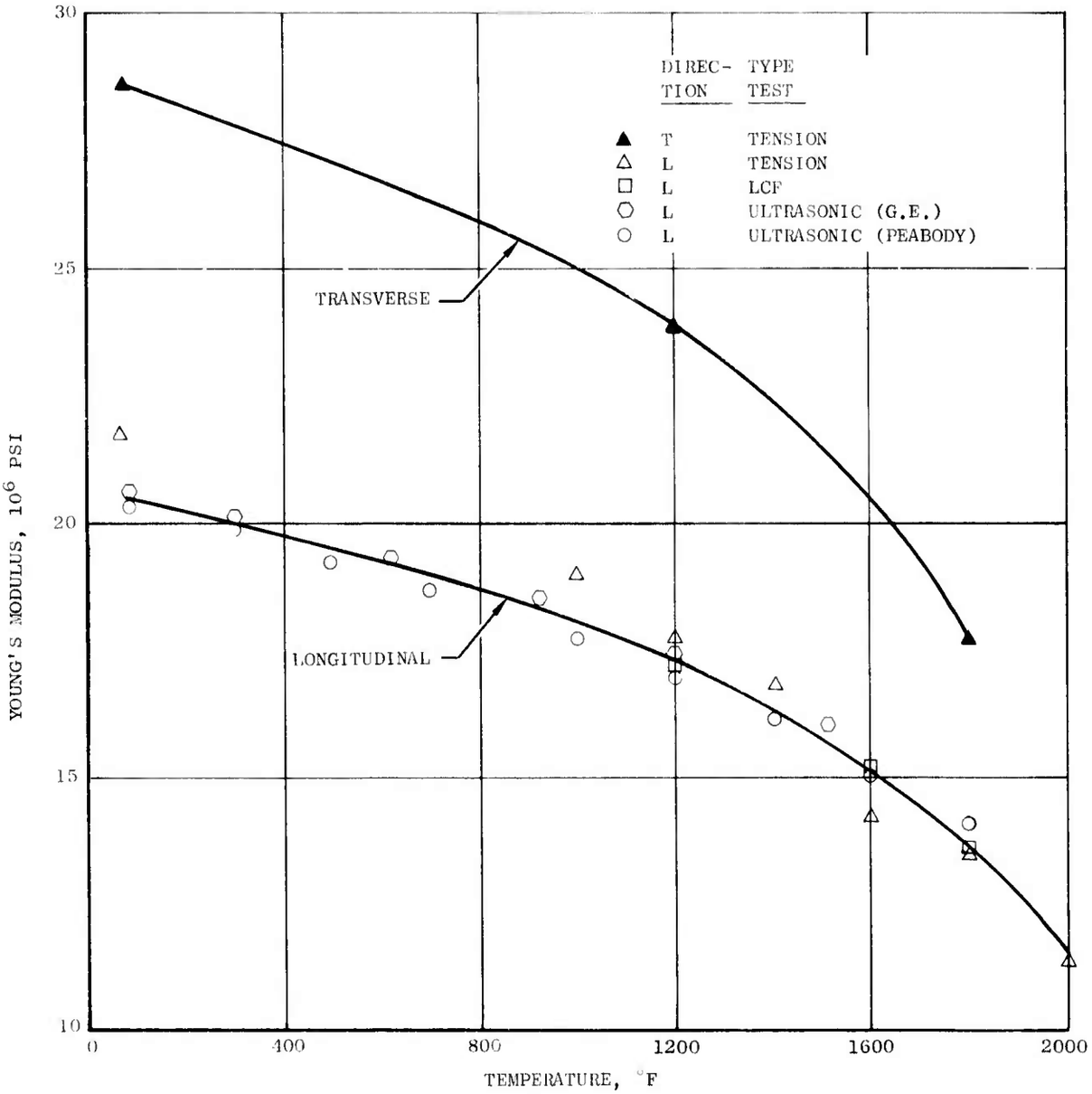

Figure 89. Young's Modulus (E) of NiTaC-13 in the Longitudinal and Transverse Directions

3.2.14 Elastic Constants

The objective was to determine, by ultrasonic methods, Young's Modulus (E), shear modulus (G), and Poisson's ratio (μ) of NiTaC-13 in the longitudinal and transverse directions from room temperature to 2000°F. Success was achieved with measurements of longitudinal E, but values obtained for longitudinal G and μ are considered unreliable because of multiple resonance frequencies.

Procedures - Cylindrical samples, 4.5 inches long by 0.360 inches in diameter, were used for ultrasonic measurements of transverse (bending), torsional, and longitudinal resonance frequencies which are used to calculate the three elastic constants above. Of the two aligned fiber samples initially provided to Peabody Testing, one was from the longitudinal direction (B90-M20). The other was from the transverse direction; but, to obtain the required total length, two transverse pieces were butt welded together. The weld interfered with the signals, and the test was therefore invalid. A second longitudinal sample (M39-M1) was purposely provided from a misaligned fiber bar grown at 1/2 inch/hour to learn if there was an effect of fiber morphology on elastic properties. Initial values of the longitudinal elastic constants measured by Peabody Testing-Magnaflux of Los Angeles, California, with B90-M20 were considered to be in error. Hence, a more comprehensive search for a consistent set of resonance frequencies with longitudinal specimen M39-M1 was conducted. As will be discussed below, this appears to have been partially successful for longitudinal E.

No other testing laboratory could be found to perform the measurements of the other elastic properties required, particularly in the transverse direction. Therefore, to reinforce the results by Peabody Testing, ultrasonic measurements of longitudinal E were made by GE/M&PTL, and use was also made of values for E determined in both tension tests and strain-controlled LCF tests.

Results - The data obtained by ultrasonic techniques are summarized in Table A-16 of Appendix A. In addition, E values determined in tension and load controlled LCF tests are given in Tables A-1 and A-6 of Appendix A, respectively. All results for E are also presented in Figure 89 where it can be seen that, for the longitudinal direction of NiTaC-13, there is good agreement among the values determined by the different methods. Most points are within five percent of the average curve drawn. These results also indicate that misaligned fibers (open circles) do not affect longitudinal E significantly, if at all.

For the transverse direction, only values of E determined in the tension test were available and the curve in Figure 89 has been drawn through the three points. Lower values of E in the longitudinal direction are expected because all grains have the [100] orientation, which has the lowest E. In contrast, the grains in the transverse specimens are randomly oriented about the <100> growth direction, resulting in a higher average E.

Young's modulus at room temperature is much lower in the longitudinal direction of NiTaC-13 than the values of 30.6×10^6 and 29.5×10^6 psi for Rene' 80 and Rene' 125, respectively.

3.3 MACHINABILITY EVALUATION

The primary purpose of this work was to provide information necessary for machining of NiTaC-13 J101 LPT blades for the program. In evaluating the relative machinability of NiTaC-13, the general procedure was to apply machining techniques used for superalloys, evaluate the results, and modify parameters slightly where necessary. All of the following machinability tests were performed on surfaces parallel to the solidification direction: electrochemical machining (ECM), shaped tube electrochemical machining (STEM), electric discharge machining (EDM), hand grinding or polishing, surface grinding, drilling, and milling. In addition, some of the tests were performed normal to the solidification direction, depending on the applicability of the test to blade machining.

The test results revealed that NiTaC-13 can be machined by all processes tested except STEM. Highlights of the tests and results are covered in the sections that follow.

3.3.1 Test Material

NiTaC-13 from the top and bottom sections of three PFS bars, B19, B39, and B49, described in Tables 8 and 9, were used for this work. Hardness tests provided the following data:

Sample No.	Avg. Rockwell "C" Hardness	
	Normal	Parallel
19T	38	39
19B	40	39
39T	37	38
39B	40	40
49T	35	39
49B	37	38

All machinability tests were performed with the as-cast material.

3.3.2 Non-Conventional Machining

ECM - Details of the tests and some of the results are summarized in Table 30A. Metallographic examination of samples after test showed that undesirable preferential metal attack occurred under the electrode and was greater at a current density of 200 than at 600 amps/sq. in., as illustrated in Figure 90. Furthermore, preferential metal attack was even greater in regions away from the electrode where current density was lower than under the electrode, as illustrated in Figure 91.

The results indicate that ECM should probably be used only for semi-finish machining and prior to finish machining of other surfaces, due to the high susceptability of NiTaC-13 to stray current attack in areas remote from the cutting zone.

TABLE 30

NON-CONVENTIONAL MACHINING TESTS OF NiTaC-13

A. ECM WITH 5/8-INCH DIAMETER ELECTRODE AND REVERSE FLOW OF NaCl (1 LB/GAL) ELECTROLYTE AT 100°F

Test No.	Bar No.	*Surface Machined	Test Parameters		Surface Finish, AA		Hole Depth, In.
			Volts	Feed, In/Min	Side	Bottom	
1	39T	P	15	0.06	35	145	0.28
2	39T	P	7.5	0.02	45	40	0.30
3	39T	P	17	0.06	60	75	0.30
4	39T	P	20	0.06	85	65	0.30
5	39T	N	20	0.06	30	45	0.30
6	39T	N	7.5	0.02	30	55	0.30

B. STEM DRILLING WITH 0.05-INCH DIAMETER TUBE AND 0.05 IN/MIN FEED

Test No.	Bar No.	*Surface Machined	Test Parameters		Remarks
			Electrolyte	Volts	
1	19B	P	10% H_2SO_4	10-15	Could not obtain any appreciable dissolution
2	19B	P	10% HCl	12	Carbide fibers appear not to dissolve. Poor hole shape and size.

C. EDM OF SQUARE HOLE WITH NEGATIVE TOOL AND TEXACO NO. 499 OIL DIELETRIC

Test No.	Bar No.	*Surface Machined	Test Parameters				Surface Finish, AA		Time to Penetrate 1/4-In., Min	Electrode Wear, In.
			Volts	Freq, KHz	Capacitance, Mfd	Amps	Side	Bottom		
1	19B	N	80	64	14	5	110	145	19	0.020
2	19B	N	70	8	38	30	140	240	4	0.028
3	19B	P	70	8	38	30	150	240	4	0.028
4	19B	P	80	64	14	5	115	140	19	0.020

*P = Parallel to solidification direction; N = Normal to solidification direction

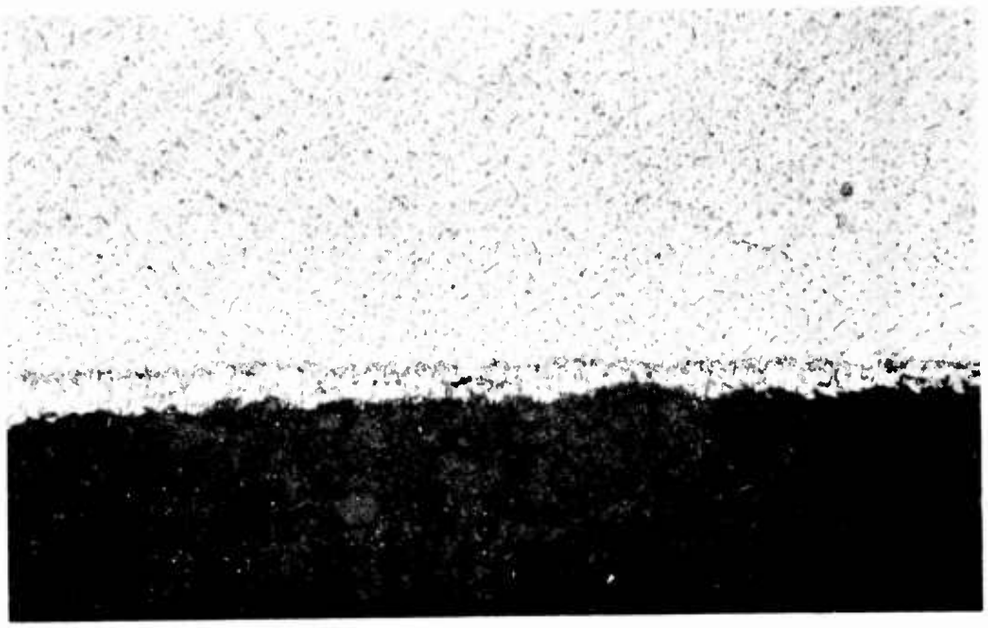

A. ECM TEST NO. 5 OF PARALLEL SURFACE AT 20 VOLTS, 600 AMPS./SQ. IN.

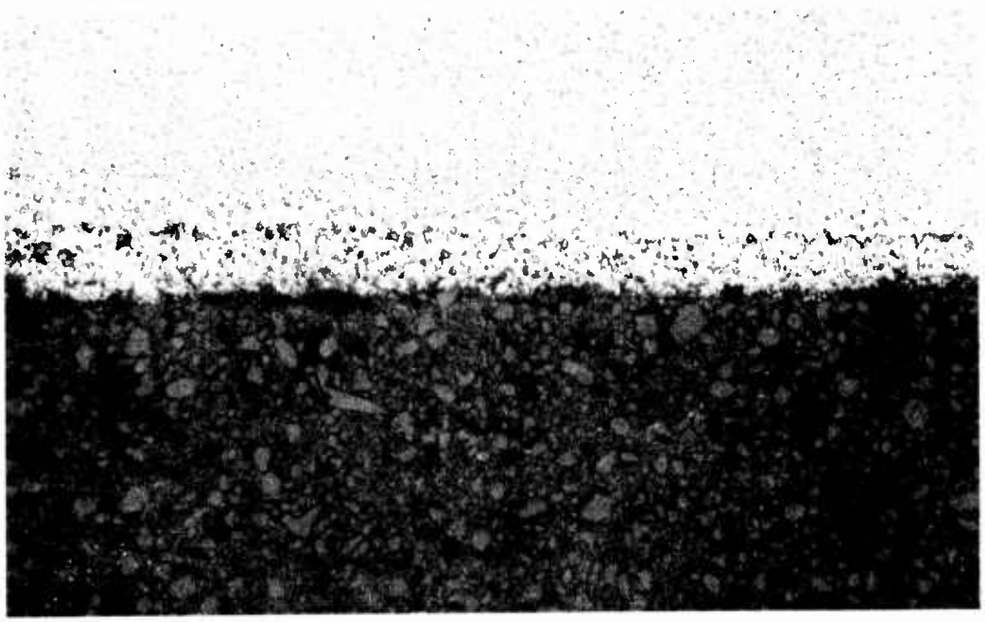

B. ECM TEST NO. 6 OF PARALLEL SURFACE AT 7.5 VOLTS, 200 AMPS./SQ. IN.

Figure 90. Photomicrographs Illustrating Greater Preferential Metal Attack Under Cutting Electrode with Decreasing ECM Current Density

A. SURFACE UNDER ELECTRODE

B. SURFACE AWAY FROM ELECTRODE - AT LOWER CURRENT DENSITY THAN A ABOVE

Figure 91. Photomicrographs Illustrating Metal Attack Due to Stray Currents

STEM - Details of two STEM drilling tests are given in Table 30B. It was found that some constituents of NiTaC-13 do not dissolve in the standard H_2SO_4 or HCl electrolytes, and machining was difficult. STEM penetration with HCl was possible, but results were erratic and the holes had poor geometry and surface finish.

It is concluded that STEM drilling under the conditions evaluated is not suitable for NiTaC-13. However, it is possible that suitable electrolytes and process parameters could be developed to make this process applicable to NiTaC alloys.

EDM - Test conditions evaluated and results obtained are summarized in Table 30C. The maximum recast layer thickness was 0.002 inches, even under roughing conditions, and the average recast layer thickness was 0.0005 inches which is normal for superalloys. Although surface finishes under 150 AA were obtained, experience indicates that 150 AA is a practical lower limit. Figure 92 shows the microstructures of samples that were EDM under "gentle" and "rough" conditions to illustrate surface finishes and the recast layer. It appears that the fibers tended to be dissolved in the molten layer created during the EDM process.

It is concluded that EDM with standard procedures is suitable for NiTaC-13.

3.3.3 Conventional Machining

Hand Grinding and Polishing - Parallel and normal tests with 240 grit Al_2O_3 abrasive belts resulted in excellent surface finishes in the range of 5 to 6 AA.

Surface Grinding - Test conditions are given in Table 31. Surface grinding ratios, G (volume of work removed/volume of wheel worn), were found to be 9.7, which is equivalent to Astroloy at 9.0, M252 at 10.0, and Udimet 500 at 8.0. Surface finishes were in the range of 5 to 15 AA.

Drilling - Parallel tests were made with carbide and cobalt H.S.S. drills under conditions listed in Table 31. Seven 0.18 inch diameter holes were successfully drilled to a depth of 0.08 inch using an 883 grade carbide master drill. An attempt to drill similar holes with the cobalt H.S.S. drills met with failure due to corner chipping of the drill on the first hole. The surface finishes of carbide drilled holes was 67 AA.

Milling - Tests included end milling and face milling using conditions given in Table 31. Carbide ball end milling was performed successfully when using very light cuts, 15 minutes average time in the cut, and a 9 inch length of cut. In contrast, face milling with both carbide and cobalt H.S.S. inserts met with rapid tool wear. Surface finishes were 32 AA under gentle conditions (new tool and 0.005 in./pass.) and rough under abusive conditions (worn tool and 0.001 in./pass.).

Recommended Procedures - Metallographic evaluations of specimens indicated no distressed material zones as a result of the grinding, polishing, milling, and drilling tests in parallel and normal machining. Recommended conditions for these four conventional machining operations are summarized in Table 32.

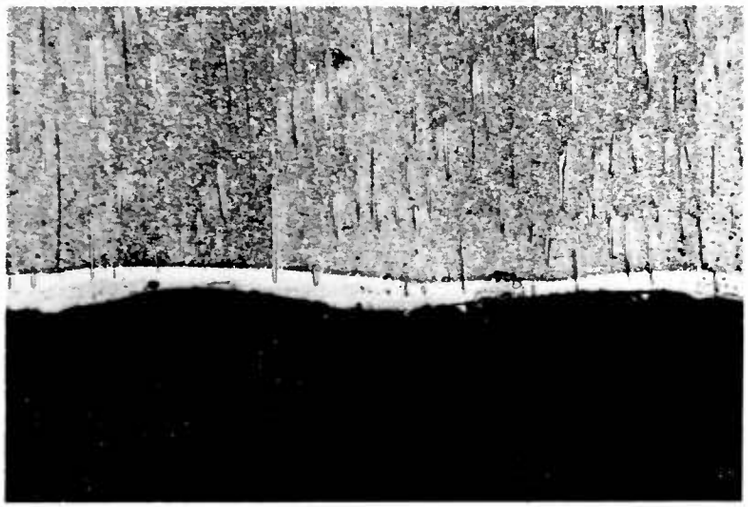

A. TEST NO. 1 - NORMAL CUT
UNDER GENTLE CONDITIONS

B. TEST NO. 2 - NORMAL CUT
UNDER ROUGH CONDITIONS

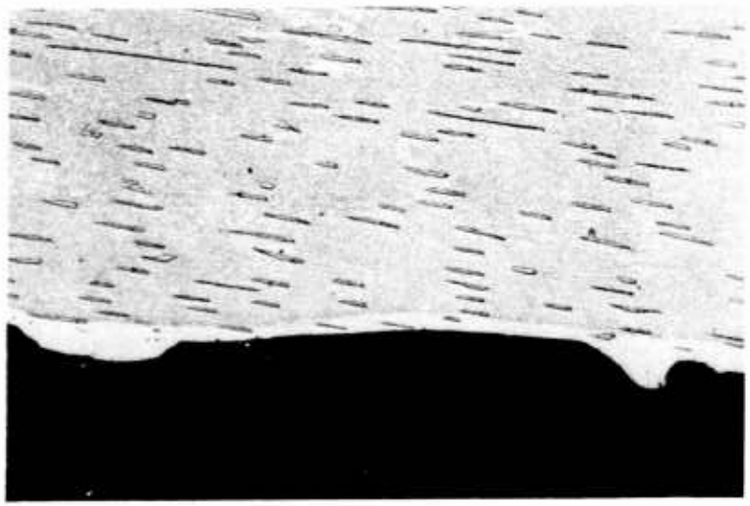

C. TEST NO. 4 - PARALLEL CUT
UNDER GENTLE CONDITIONS

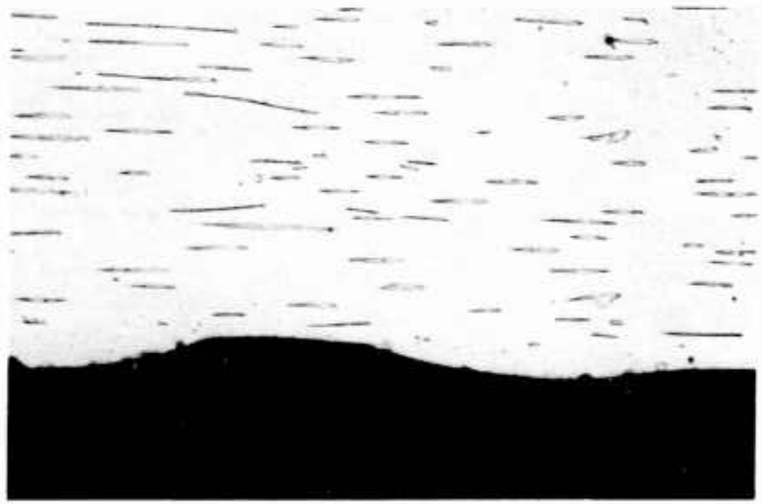

D. TEST NO. 3 - PARALLEL CUT
UNDER ROUGH CONDITIONS

Figure 92. Photomicrographs Illustrating Recast Layer and Surface Finish After EDM Under Gentle and Rough Conditions

TABLE 31

CONVENTIONAL MACHINING TESTS OF NiTaC-13

Test No.	Bar No.	Type of Machining	Speed, SFM	Feed	Depth, In.	Width, In.	Tool Geometry	Tool Wear	Tool Life	Surface Finish, AA	Tool Material	Surface Machined	Remarks
			-	-	-	-	240 Grit Al_2O_3 Belt	-	-	5-6	-	P&N	
7	19T	Belt Polish											
8	39B	Surface Grind*	2500/50	.0002 D/F	-	.050 C/F		-	"G" Ratio 9.7	5/15	-	P&N	
3	19T	Drilling (Carbide)	30	.0015 IPR	.080 Deep	-	Straight Flute Master Drill	.0015	7 Holes	63	883	P&N	Drills Satisfactory
4	19T	Drilling (HSS)	30	.003 IPR	.080 Deep	-	NAS 907 Type J	Fail.	4 Holes	Rough Turn	M42	P	Corners Chipped
5	49T	Ball End Mill (Carbide)	30	.0005 C/T	.015	Slot	3/8" Dia. 4 Flute S/E Fed. Mog. - Cat. 155	.012	14.4 Min.	32	883	P	
5b	49T	Ball End Mill (Carbide)	30	.001 C/T	.030	Slot	Continued Same Tool	Add. .006	Add. 10.4	Rough Surface	11	P	
6	49T	Ball End Mill (Carbide)	30	.0005 C/T	.015	Slot	3/8" Dia. 4 flute S/E Fed. Mog. Cat. 155	.013	17.6	32	883	N	
6b	49T	Ball End Mill (Carbide)	30	.001 C/T	.030	Slot	Continued Same Tool	Add. .007	Add. 3.3	Rough Surface	883	N	
1	39B	Face Milling (HSS)	75	.0035 C/T	.060	2.0	3.0" Dia. Futurmill 45° SCEA - 3/4" Sq. Insert	Fail.	1.0 Min.	-	M-33	P	Rapid Wear
2	39B	Face Milling (Carbide)	75	.0010 C/T	.030	2.0	SPG-432	Fail.	2.6	30	883	P	Tool Chipped

*SFM = Surface Feet/Minute
IPR = Inches/Revolution
P = Parallel to Solidification Direction
N = Normal to Solidification Direction
**Wheel Speed = 2500 SFM; Table Speed = 50 SFM

D/F = Inches Down Feed/Pass
C/F = Inches Cross Feed/Pass
G = Vol. Material Removed/Vol. of Wheel Worn

TABLE 32

RECOMMENDED CONVENTIONAL MACHINING CONDITIONS

Surface Grinding (Low Stress)

Wheel Speed	2500 SFM
Table Speed	50 SFM
Cross Feed	.050"/Pass
Down Feed	.0002"/Pass
Fluid	S & C1 Oil (Tu99)
Wheel Grade	A60I 10 V

Belt Polishing

Type Grain	Al_2O_3 (Tested)
Grit Size	240

Ball End Milling (Carbide - Slotting)

Cutting Speed	30 SFM
Feed	.0005 Chip/Tooth
Depth	.015 (Tested)
Fluid	Water Base (Trim Sol)
Tool Grade	883 Carbide
Tool Geometry	4 Flute Single End
	Feedrate Mogul
	Catalog # 155 (Tested)

Drilling (Carbide)

Cutting Speed	30 SFM
Feed	.0015 1PR
Fluid	Water Base (Trim Sol)
Tool Grade	883 Carbide
Tool Geometry	Straight Flute
	Master Drill
	Metal Removal Co. (Tested)

3.4 Ni-20Cr-10Al-1Y COATING EVALUATION

Early tests indicated that the oxidation resistance of NiTaC-13 was inferior to that of current turbine blade superalloys. Therefore, exploratory tests of several coatings for NiTaC-13 were performed in 1972 leading to a selection of the Ni-20Cr-10Al-1Y coating for use and more extensive evaluation in this program.

Preliminary oxidation tests of bare and coated NiTaC-13 were first conducted at 1950°F for 275 hours, and the results closely repeated 1972 results, confirming both the coating and the coating process. Following this, more extensive oxidation and hot corrosion tests were conducted according to the following plan:

	Upper Test Temperature, °F			
	1600	1700	1800	2000
Dynamic Cyclic Oxidation				
Mach 0.05 for 100, 500, 1000 hours	X	-	X	X
High Velocity Cyclic Oxidation				
Mach 1 for 100 hours	-	-	-	X
Hot Corrosion				
500 hrs/1 ppm NaCl	X	-	-	-
500 hrs/5 ppm NaCl	-	X	-	-

Results of these tests are covered in the sections that follow.

3.4.1 Test Material and Specimens

The 4-1/2 inch long sections from three bars (B64, B67, and B68, described in Table 12) were selected for test material. The sections from bars B64 and B67 contained fully aligned fibers, whereas bar B68 had a dendritic cellular fiber microstructure near the top, although most of the length of this bar had fully aligned fibers. Some dendritic cellular material was included for test to learn if any unusual oxidation/hot corrosion problems would be encountered.

Five specimens, 1/4 inch in diameter by 4 inches long with one fully rounded end, were machined from Bar B67 for the high velocity oxidation tests. A total of 54 specimens, 1/8 inch in diameter by 1-1/2 inches long with fully rounded ends, were machined from bars B64 and B68 for use in all other tests. Half of the specimens were taken from the top sections of the bars, and half from the bottoms. The axis of all specimens was parallel to the solidification direction.

3.4.2 Coating Procedures

The coating was applied by the physical vapor deposition (PVD) process. During coating, the samples were heated to about 1850°F while in the coating alloy vapor produced by electron beam melting of Ni-20Cr-10Al-1Y master alloy. Deposition time was one hour, producing a coating 0.002 to 0.006 inches thick. Next, the coated samples were heat

treated in vacuum for two hours at 2000°F to promote a good bond between coating and substrate. Finally, the samples were shot peened with 100 mesh glass beads and heat treated again in vacuum for two hours at 2000°F. The purposes of the last step are to heal the characteristic fissures formed during the PVD process and to recrystallize the coating.

The microstructures after coating and after final heat treatment are illustrated in Figure 93. Effects of the coating process steps on the substrate are illustrated in Figure 94. As can be seen, the depth of carbide fiber denudation increased after each heat treatment. After the final step, the denuded layer was about 0.0012 inches thick.

A few stress rupture tests were conducted to evaluate effects of the two post-coating treatments, using specimens from the bottom section of bar B79. The results in Table 33 indicate that most benefit of the coating and post-coating treatment occurs at very high temperatures.

3.4.3 Preliminary Oxidation Test

This test consisted of 275 hours exposure at 1950°F in Mach 0.05 flowing air. Six times each hour the samples were quickly cooled to 800°F in order to induce thermal stresses in the coating and accentuate any propensity of the coating to spall. Samples of bare NiTaC-13 and Rene' 80 were included for comparative purposes.

Details of the test and the test results are shown in Table 34 where they are compared with the 1972 results. Important observations from the data include:

1) Previous and new results for NiCrAlY coated NiTaC-13 are about equal, and show good oxidation protection by the coating.

2) The new test results for bare NiTaC-13 and bare Rene' 80 indicate that test conditions may have been more severe because weight losses were greater than in 1972 tests. Increased test severity could have occurred due to differences in maximum temperature or the temperature differential of the thermal cycle. It is also possible that, in the new tests, the cooling to room temperature for weight measurements may have aggravated cracking and spallation of the oxide which, in turn, may have increased the overall oxidation rate when testing was resumed.

3) The new tests showed Rene' 80 to be slightly more oxidation resistant than NiTaC-13. This result is opposite to that found in the 1972 tests, and may be due to differences in test severity.

Further microscopic analysis of samples showed the presence of an acicular phase in both bare and coated NiTaC-13. As illustrated in Figure 95, this phase was present in about equal amounts in both bare and coated samples that were exposed for 500 hours in the low velocity dynamic oxidation test at 2000°F.

Other work with coatings for NiTaC-13 by Jackson et al[8] under NASA contracts also showed the development of an acicular phase during cyclic oxidation testing of both bare and NiCrAlY coated NiTaC-13. They also conducted stress-rupture tests in air and

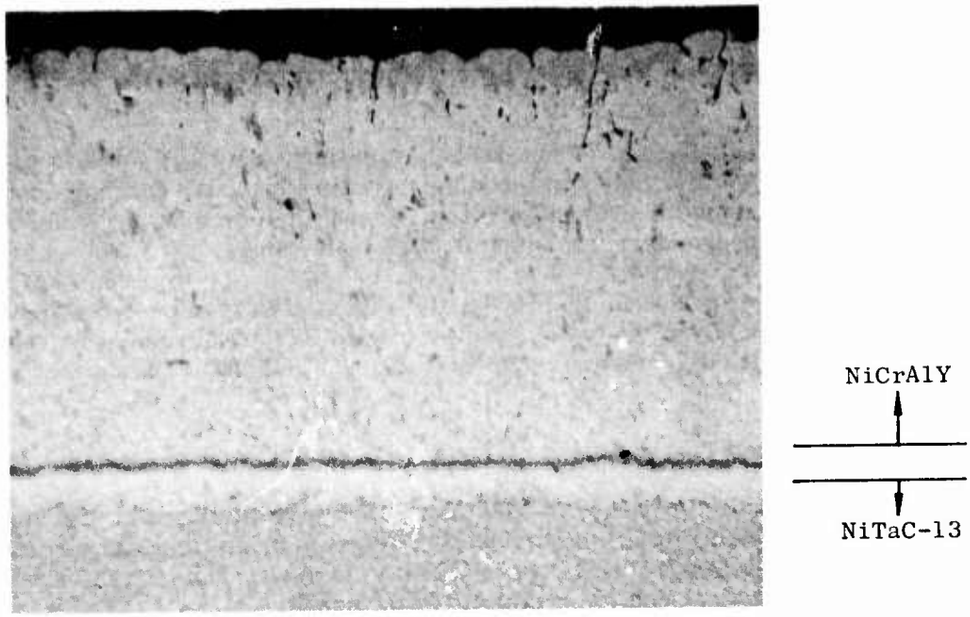

A. AS-DEPOSITED PVD NiCrAlY COATING ON NiTaC-13. COATING HAS FISSURES

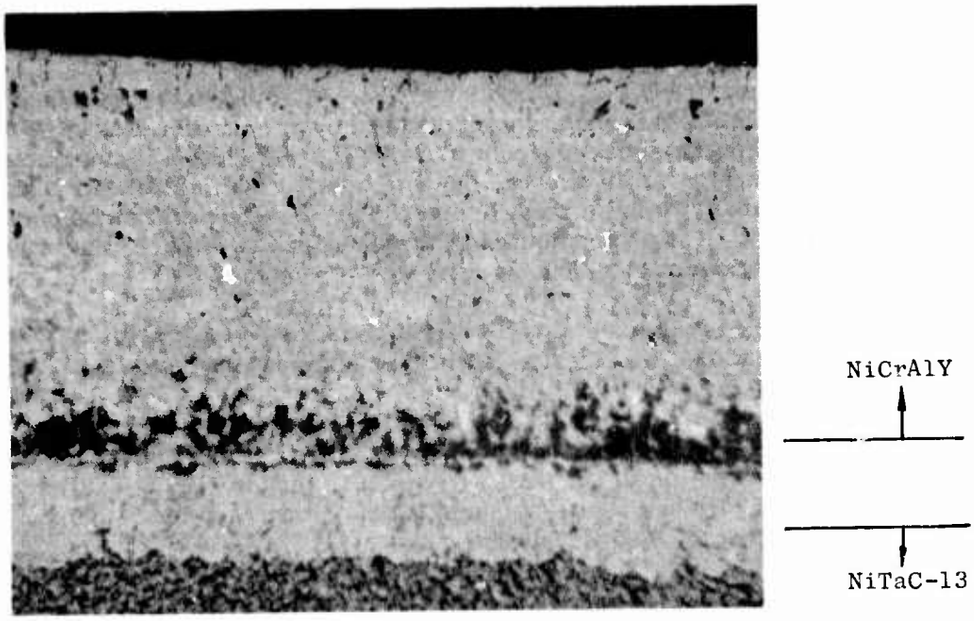

B. AFTER POST COATING HEAT TREATMENTS AND SHOT PEENING. COATING IS FREE OF FISSURES

Figure 93. Photomicrographs Illustrating as - Deposited and Fully Processed Coating. 500X Magnification

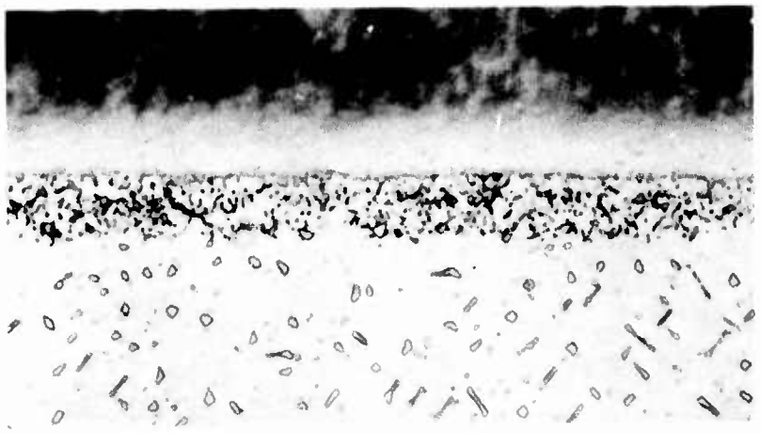

A. AS-DEPOSITED PVD NiCrAlY ON NiTaC-13

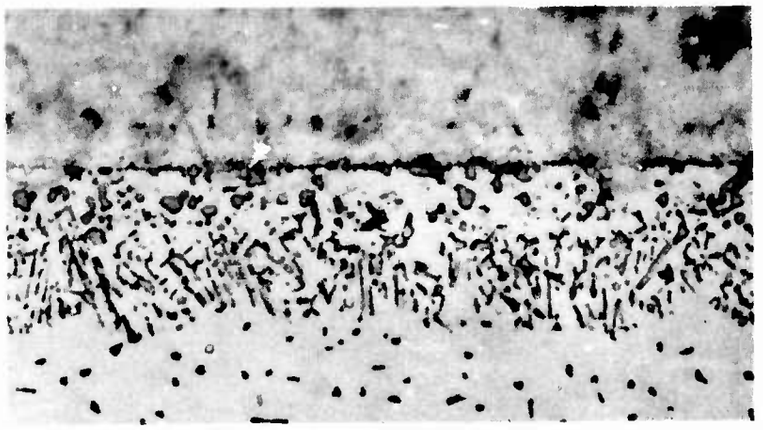

B. AFTER A + 2000°F/2 HOURS/VACUUM

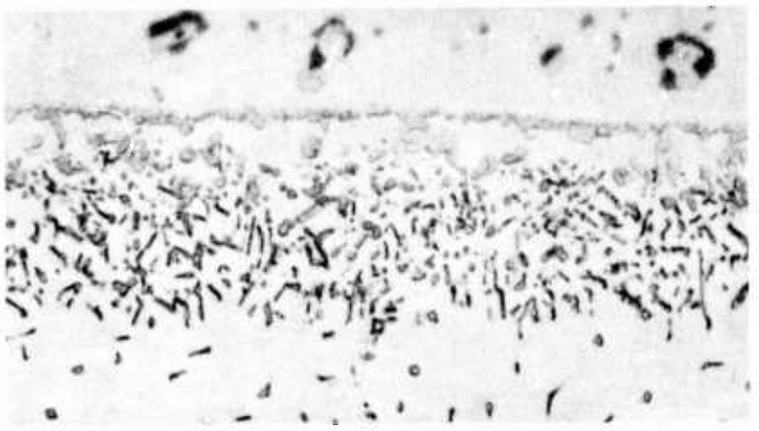

C. AFTER B + SHOT PEEN + 2000°F/2 HOURS/VACUUM

Figure 94. Photomicrographs Illustrating Coating/Substrate Interactions After Each Coating Process Step. 1000X Magnification

TABLE 33

THE EFFECTS OF COATING PROCESS STEPS ON STRESS-RUPTURE LIFE

Test Conditions		Hours to Rupture in Air Tests			
		Bare			
Temp., °F	Stress Ksi	*Avg.	B79	Coated +H.T.	Coated + H.T. + Shot Peen + H.T.
1600	70	216	-	263.4	231.0
1800	44	66	76.9	-	72.1
1900	35	196	108.8	-	142.3
2100	10	76	-	125.9	218.0

*Avg. data for bottoms of bars, Section 3.2.2

TABLE 34

RESULTS OF PRELIMINARY OXIDATION TESTS OF NiTaC-13
COATED WITH Ni-20Cr-10Al-Y

Alloy	Bar No.	Coating Type	Coating Thickness, Inches x 10^3	Weight Change, mg/cm^2 100 Hrs.	200 Hrs.	275 Hrs.	275-Hr. Max Depth of Attack, In. x 10^3
1972 RESULTS							
NiTaC-13	-	None	-	-	-	-22.8	2.5
NiTaC-13	-	NiCrAlY	2.8	-	-	+ 0.8	-
*Rene' 80	-	None	-	-	-	-49.7	5.0
Rene' 80	-	Codep	3	-	-	+ 0.5	-
PROGRAM RESULTS							
NiTaC-13	64T	None	-	-19.2	-	-	-
NiTaC-13	64B	None	-	-24.4	-66.6	-99.1	6.0
NiTaC-13	68B	None	-	-24.6	-70.2	-109.8	6.0
NiTaC-13	64T	NiCrAlY	4	+ 0.8	+ 1.3	+ 1.5	0.1
NiTaC-13	64B	NiCrAlY	4	+ 0.8	+ 1.4	+ 1.4	0.1
NiTaC-13	68B	NiCrAlY	4	+ 0.6	+ 1.2	+ 1.3	0.1
Rene' 80	-	None	-	- 6.1	-43.9	-79.3	4.6

* Samples cycled from 800° to 1950°F six times per hour in Mach 0.05 flowing air.

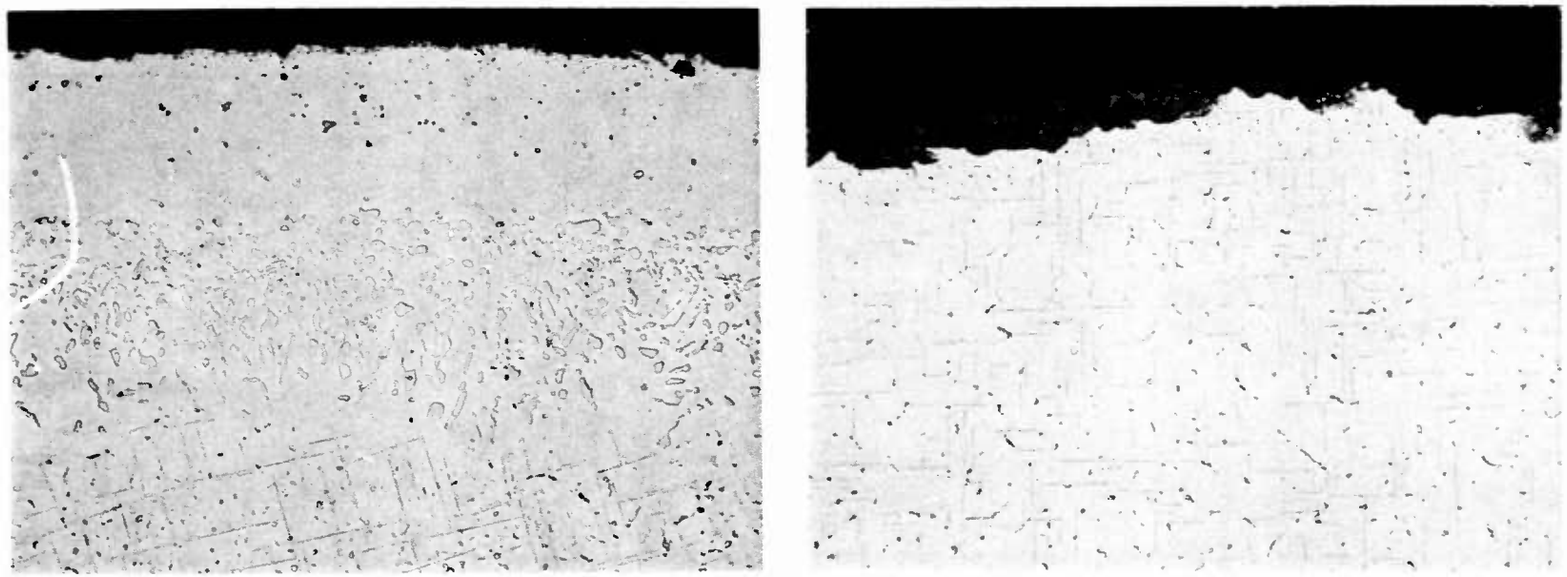

A. Ni-20Cr-10Al-1Y COATED

B. BARE

Figure 95. Acicular Phase Formed in NiTaC-13 During 500 Hour Exposure in Low Velocity (Mach 0.05) Dynamic Oxidation Test at 2000°F. 500X Magnification

argon, using bare and coated samples before and after thermal cycling. Using test results for as-cast bare material in argon as the reference, they found that a Ni-20Cr-15Al-1Y coating (and also a duplex coating) reduced 1600° and 2000°F stress-rupture properties of coated and heat treated NiTaC-13. Possible reasons for the strength degradation included: surface structure, faults or brittleness of the coating, or fiber denudation at the coating/substrate interface. Thermal cycling of coated samples from about 200° to 2000°F for 150 hours or more caused further stress-rupture strength degradation, about one Larson-Miller parameter number, which they attributed to microstructural changes unrelated to the presence of a coating.

On the basis of consultation with Jackson at the completion of the preliminary tests, it was concluded that the Ni-20Cr-10Al-1Y coating was among the best available for NiTaC-13, and it was selected for use in the program as originally planned.

3.4.4 Dynamic Cyclic Oxidation

Both bare and Ni-20Cr-10Al-1Y coated pin-type samples of NiTaC-13 were exposed in a Mach 0.05 gas stream for up to 1000 hours at 1600°, 1800°, and 2000°F. Samples of Rene' 80, both bare and coated with Type 1 Codep B, were exposed concurrently as standards. During exposure, temperature was cycled six times per hour from the test temperature to about 850°F. Periodically, the test specimens were cooled to room temperature for measurements, and some were removed from the test for microscopic analysis.

Measurements to determine oxidation resistance included the following:

1) Oxide penetration depth - measured on a polished and etched transverse section, either from the original sample surface (when identifiable) or determined from measurements of substrate diameter.

2) Alloy depletion layer - measured on the polished and etched transverse section prepared in Step 1, from the oxide/substrate interface to the position where there was no obvious alteration in microstructure of the substrate.

3) Total metal loss per side - the sum of 1 and 2.

4) Weight Change - the original weight minus the weight after exposure, divided by the surface area of the sample.

5) Base alloy depletion layer thickness - measured on a polished and etched transverse section from the original coating/substrate interface to the position where there was no obvious alteration in microstructure of the substrate.

The weight change data and alloy penetration data are summarized in Tables A-17 and A-18 of Appendix A, respectively. The penetration results are also shown in Figure 96. By inspection of the data in the two tables and Figure 96, it can be seen that in a low velocity gas stream, bare NiTaC-13 and Rene' 80 have equivalent oxidation resistance at 1600°F, but that Rene' 80 is superior at 1800° and 2000°F. The data show that oxidation of NiTaC-13 is severe.

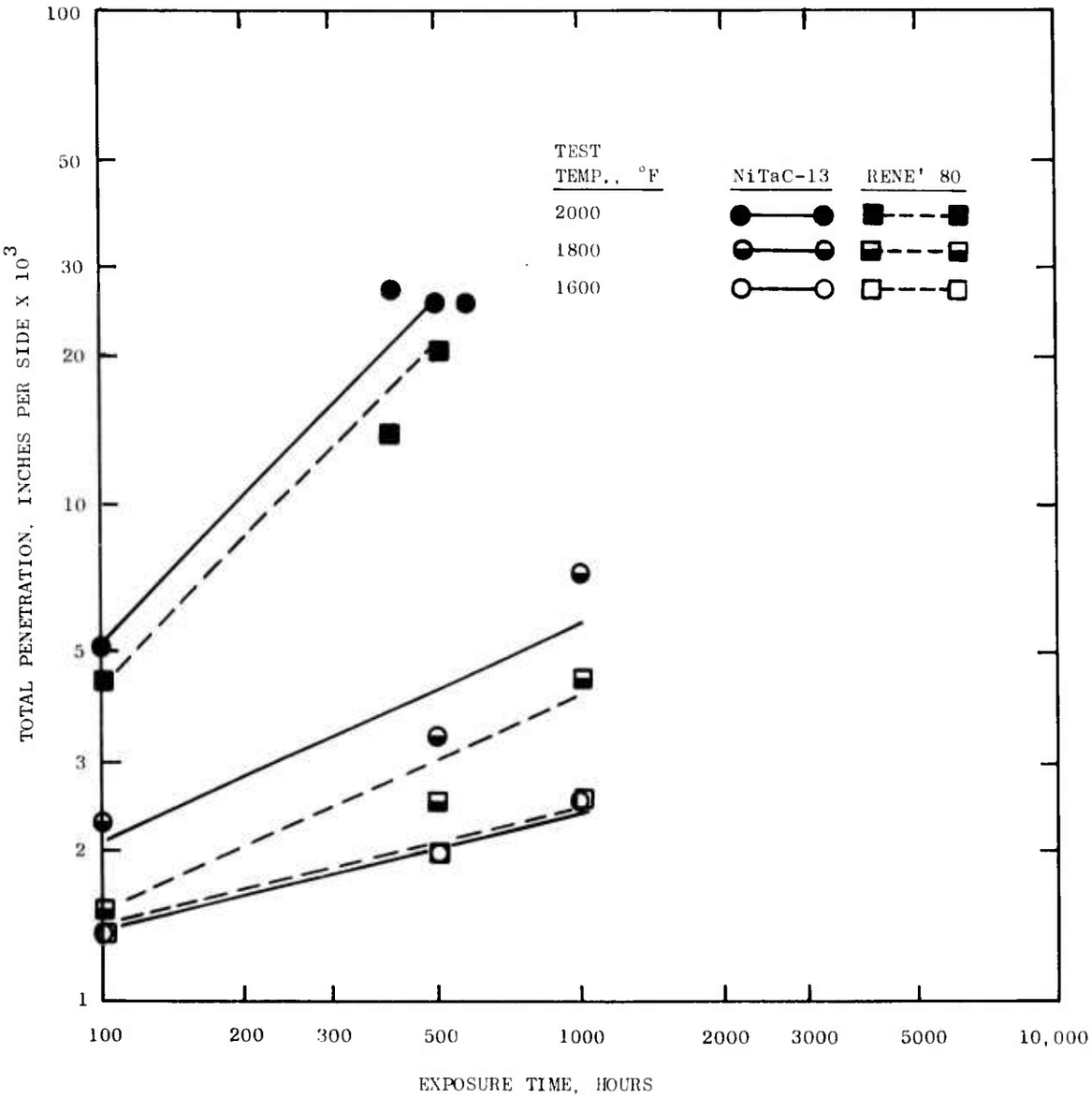

Figure 96. Low Velocity (Mach 0.05) Dynamic Oxidation of NiTaC-13 and Rene' 80, Bare

A typical longitudinal microstructure of bare NiTaC-13 after 100 hours at 2000°F, Figure 97, illustrates the oxide layer and the decarburization zone in which the carbide fibers are either absent or are much smaller than those at the interior. Samples of the oxide scale produced during oxidation tests were analyzed by Debye-Scherrer X-ray diffraction techniques and found to be primarily NiO. This oxide offers only limited protection and explains the higher oxidation rate of NiTaC-13 over Rene' 80. Current superalloys normally form spinels or alumina layers which are more protective than NiO.

The Ni-20Cr-10Al-1Y coating on NiTaC-13 performed very well in all oxidation tests, as indicated in Table A-17. Figure 98 illustrates the transverse microstructure of a sample tested for 1000 hours at 2000°F. The bright phase of the coating in Figure 98 is gamma prime (γ') and the dark phase is nickel solid solution (γ) formed because of the gradual loss of the γ' forming element, Al, to the oxide scale layer. There was no indication of coating penetration in the sample shown in Figure 98; hence, the coating was protective even after 1000 hours at 2000°F.

Also shown in Figure 98 are a globular phase at the coating/substrate interface, a carbon depleted zone, and an acicular phase in the substrate. The carbide denudation zone was about 0.003 inches thick compared to about 0.0012 inches after coating. Partial analysis by SEM/EDAX of the globular and acicular phase, illustrated at higher magnification by SEM in Figure 99, showed the globular precipitate to be rich in Re, Cr, and V, and the acicular phase (sigma) to be rich in Re, with some Cr and V.

To achieve satisfactory service lives, Rene' 80 blades require a coating; hence, it is obvious from the data that NiTaC-13 blades also would require a coating. The data for Ni-20Cr-10Al-1Y coated NiTaC-13 show that this coating provides excellent protection in low velocity oxidizing environments for exposures up to 1000 hours at 2000°F.

3.4.5 High Velocity Cyclic Oxidation

In this test, specimens were cycled between 2000° and 200°F once an hour while in a Mach 1 gas stream. Periodically, the specimens were cooled to room temperature for weight measurements and inspection of the coating for indications of coating failure. The total exposure time was 98 hours.

Two coated and one bare specimen were tested. The bare specimen was heavily attacked and had a 15.5 percent loss in weight (4.71 grams). In an equivalent test, bare Rene' 80 lost 3.08 grams. Each of the two coated NiTaC-13 samples gained only 0.009 grams, and the appearances of the samples after test were excellent; hence, it can be concluded that the Ni-20Cr-10Al-1Y coating offers excellent protection for NiTaC-13 from oxidation in this severe test environment.

Microscopic examination and measurements showed that the oxide penetration depth into the uncoated sample was 0.015 inches and that there was an alloy depletion layer about 0.001 inch thick. For the coated samples, the loss of coating thickness due to oxidation was less than 0.0001 inch, and the alloy depletion layer was 0.0025 inches thick, measured from the coating/substrate interface. Figure 100 illustrates the features just discussed and shows that γ phase was formed in the coating due to aluminum depletion, the same as observed in some low velocity dynamic oxidation tests.

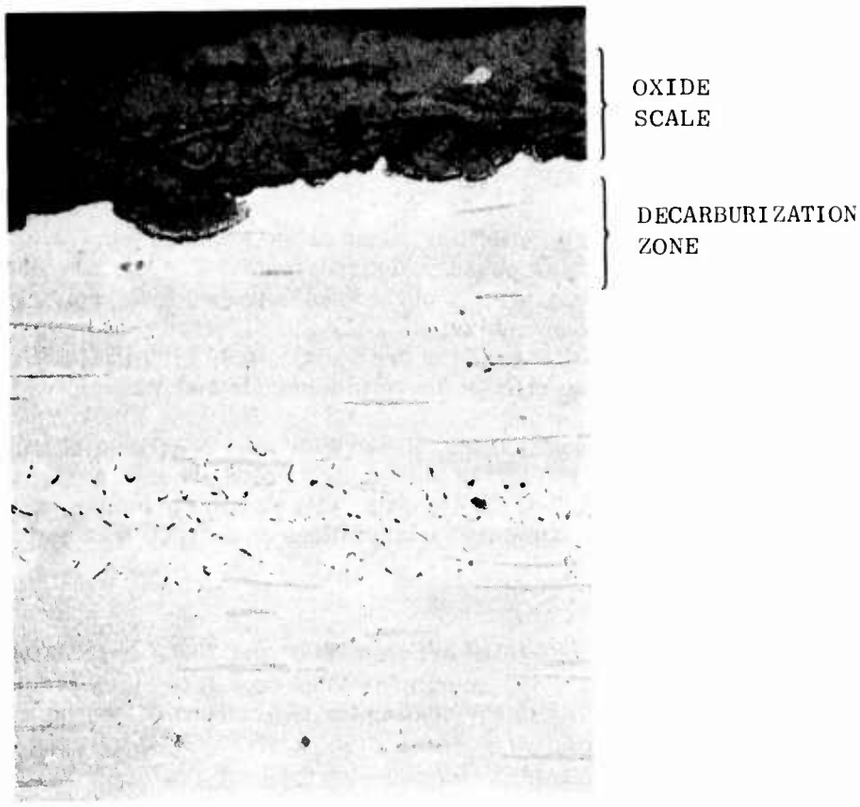

Figure 97. Longitudinal Microstructure of Bare NiTaC-13 after 100 Hours in Low Velocity (Mach 0.05) Dynamic Oxidation Test at 2000°F. 500X Magnification. Electrolytic Etch with 2% H_3PO_4.

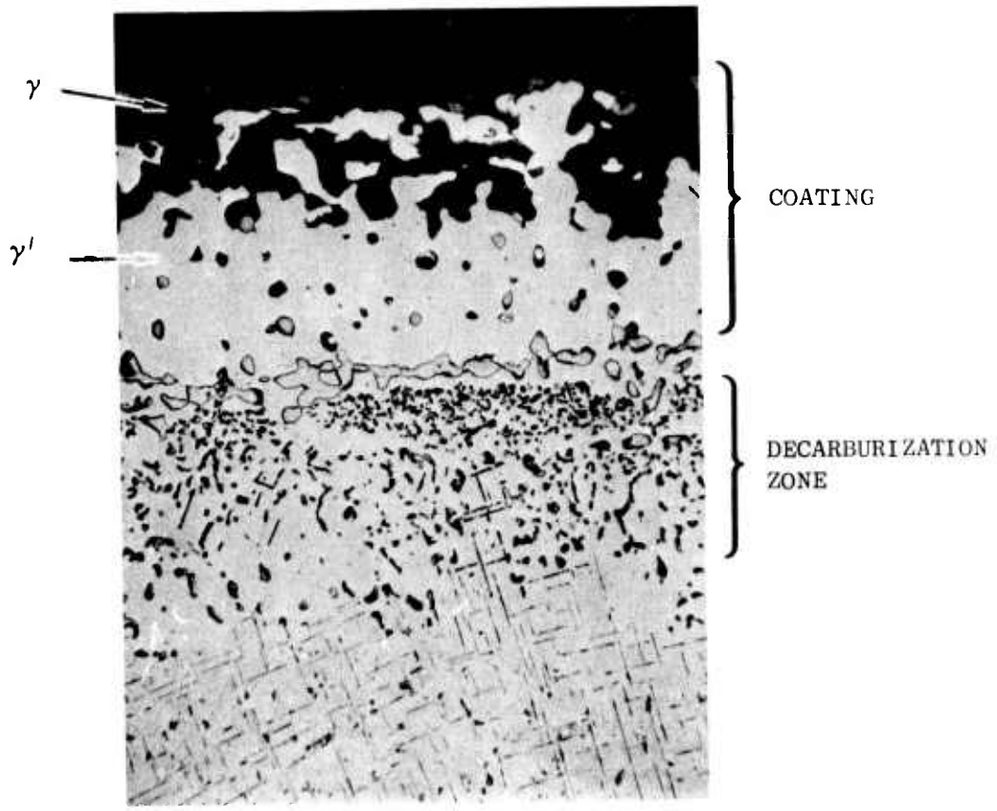

Figure 98. Transverse Microstructure of Ni-20Cr-10Al-1Y Coated NiTaC-13 after 1000 Hours in Low Velocity (Mach 0.05) Dynamic Oxidation Test at 2000°F. 500X Magnification. Electrolytic Etch with 2% H_3PO_4.

Figure 99. Globular and Acicular Phases Present in NiTaC-13 Substrate Near Ni-20Cr-10Al-1Y Coating Interface after 1000 Hours In Low Velocity (Mach 0.05) Dynamic Oxidation Test at 2000°F. 3150X Magnification

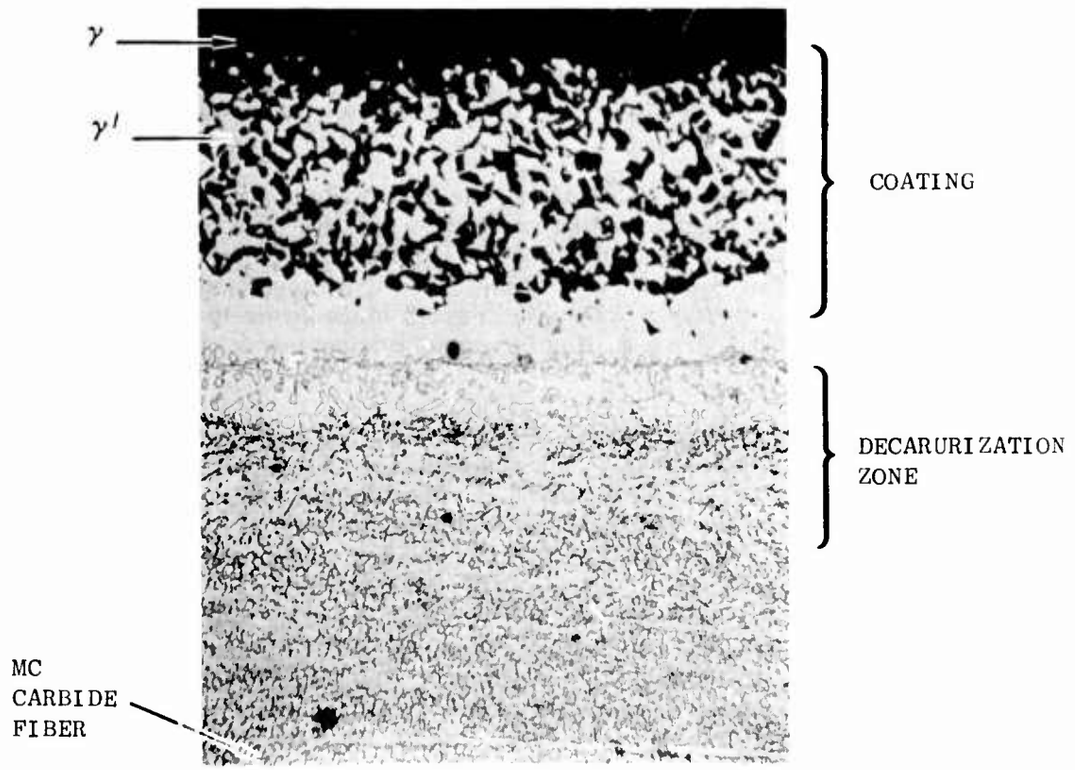

Figure 100. Longitudinal Microstructure of Ni-20Cr-10Al-1Y Coated NiTaC-13 after 100 Hours in High Velocity (Mach 1.0) Dynamic Oxidation Test at 2000°F. 500X Magnification. Electrolytic Etch with 2% H_3PO_4.

3.4.6 Hot Corrosion

Each of the following two BuShips burner rig tests were initiated with four bare and four coated NiTaC-13 specimens from bar B68 bottom and top:

1) Up to 506 hours exposure at 1600°F with 1 ppm synthetic sea salt added to JP5 regular fuel doped to 0.35 wt. % sulfur.

2) Up to 502.5 hours exposure at 1700°F with 5 ppm synthetic sea salt added to JP5 regular fuel doped to 0.35 wt. % sulfur.

Each working day, the specimens were cooled to room temperature for inspection; and, when appropriate, specimens were removed from test for metallographic examination. The latter included measurements of total penetration in bare NiTaC-13 and determination of coating failure.

The results are summarized in Table 35 and the penetration data for bare NiTaC-13 are also shown in Figure 101 together with comparative data for bare Rene' 80 obtained in other tests. In the less extreme test, 1600°F/1 ppm synthetic sea salt, NiTaC-13 is indicated to be equivalent to Rene' 80 up to 500 hours. However, in the 1700°F test with a higher salt addition to the fuel, NiTaC-13 is much more severely attacked than Rene' 80. NiTaC-13 blades would require a coating for protection against a severe hot corrosion environment.

In visual inspections of the bare NiTaC-13 samples during the two tests, it was observed that a glassy scale formed initially. This scale subsequently spalled as the tests were continued, probably aggravated by the one thermal cycle per day in the test. Analysis by Debye-Scherrer X-ray diffraction techniques showed the scale to be NiO, with a thin surface layer of Na_2SO_4. Additional analysis of the scale using SEM/EDAX confirmed that the scale was primarily NiO. This is illustrated in Figure 102 for a bare NiTaC-13 sample after exposure for 310 hours at 1600°F. Figure 102 is a SEM micrograph of a transverse section showing the oxide scale and the NiTaC-13 substrate. Figure 102B is the spectrum of the substrate showing the major NiTaC-13 alloying elements. Figures 102C and D show the spectra of two areas in the scale. Both are similar to each other and show that the primary element present is nickel with small amounts of aluminum and cobalt. The microstructures of uncoated and coated NiTaC-13 after 506 hours exposure at 1600°F, illustrated in Figures 103 and 104, show that there was negligible decarburization.

The Ni-20Cr-10Al-1Y coating gave excellent protection for NiTaC-13 during the 506 hours duration of the 1600°F/1 ppm test. However, under more severe conditions, 1700°F/5 ppm, the NiCrAlY coating failed after 368 hours. Because under these same conditions the NiCrAlY coating lasted 500 hours on an oxide dispersion strengthened nichrome substrate, it is possible that the early failure in the present tests was due either to localized defects in the coating or to reactions between the coating and NiTaC-13. Based on the test results, coatings with better hot corrosion resistance are needed for applications in such environments.

TABLE 35

ALLOY PENETRATION RESULTS FOR HOT CORROSION TESTS
OF NiTaC-13, BARE AND COATED WITH Ni-20Cr-10Al-1Y

Alloy Condition	Exposure Hours	Total Penetration, 10^{-3} Inches Per Side	Remarks
1600°F/1 ppm Synthetic Sea Salt			
Bare	310	2.5	
Bare	506	5.5	
Coated	506	2.0	No substrate metal attack
1700°F/5 ppm Synthetic Sea Salt			
Bare	89	14.5	
Bare	296	19.5	
Bare	503	21.0	
Coated	368	-	Coating failed

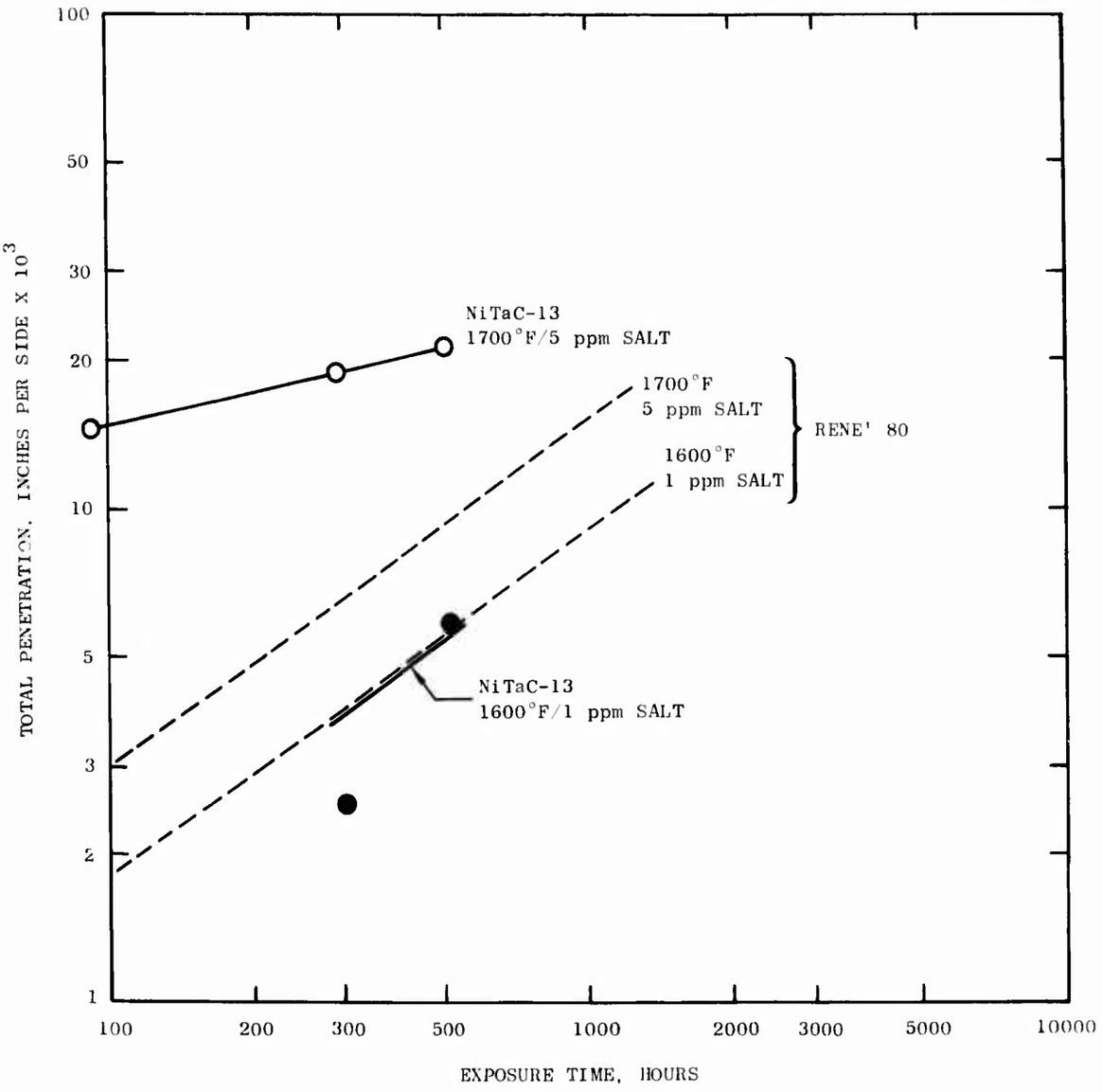

Figure 101. Hot Corrosion of NiTaC-13 and Rene' 80, Bare

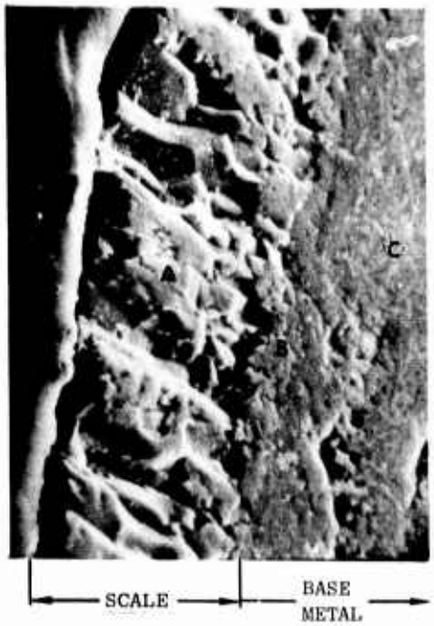

A. 1400X SEM

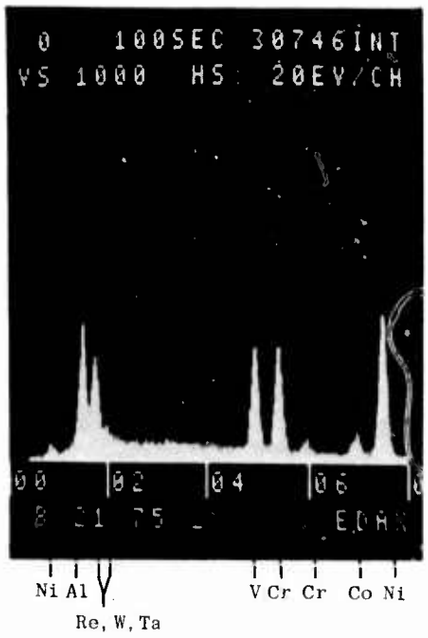

B. AREA C

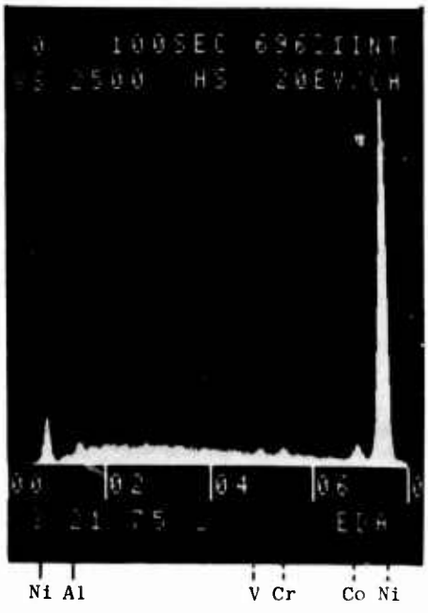

C. AREA B

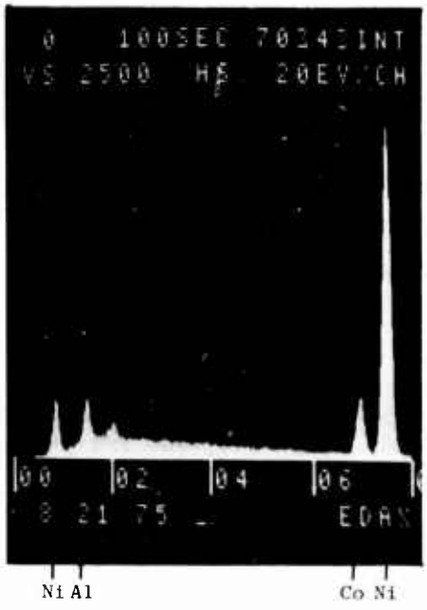

D. AREA A

Figure 102. SEM/EDAX Analysis of Scale and Base Metal After Exposure of Bare NiTaC-13 to 1600°F/1 ppm Sea Salt for 310 Hours

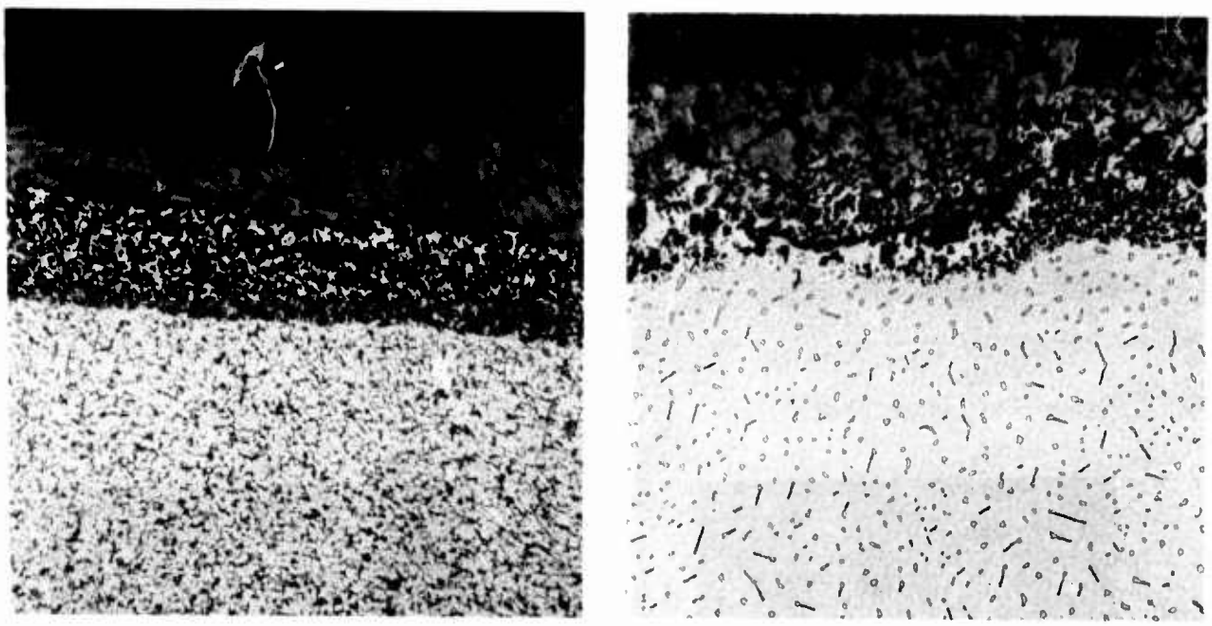

A. ELECTROLYTIC ETCH WITH 2% H_3PO_4

B. ETCH POLISHED

Figure 103. Transverse Microstructure of Bare NiTaC-13 after Exposure to 1600°F/1 ppm Sea Salt for 560 Hours. 500X Magnification

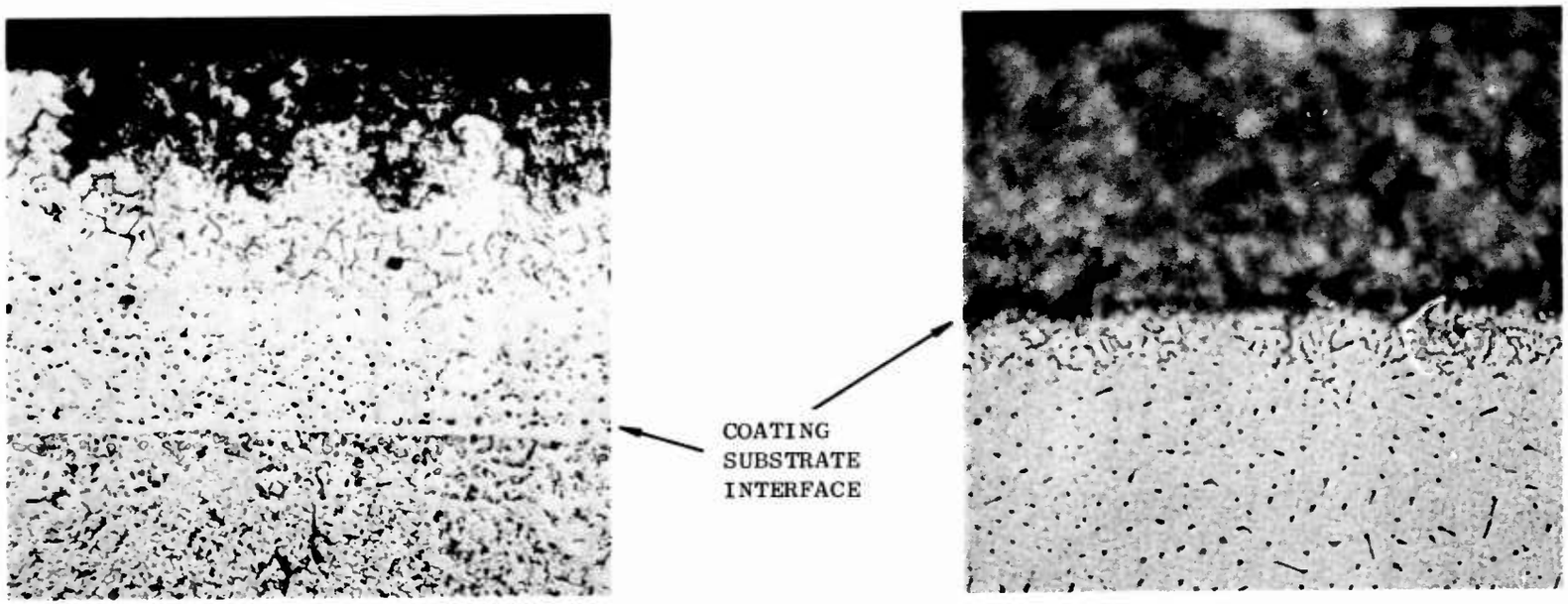

A. ELECTROLYTIC ETCH WITH 2% H_3PO_4

B. ETCH POLISHED

Figure 104. Transverse Microstructure of Ni-20Cr-10Al-1Y Coated NiTaC-13 after Exposure to 1600°F/1 ppm Sea Salt for 506 Hours. 500X Magnification

3.4.7 Summary of Coating Evaluation

Oxidation tests of bare NiTaC-13 in a low velocity (Mach 0.05) gas stream show that, in the temperature range of 1800° to 2000°F, metal loss is substantial and somewhat higher than occurs with Rene' 80. Other oxidation tests of bare NiTaC-13 in a high velocity (Mach 1) gas stream indicate that the rate of metal loss is about three times higher than in a low velocity gas stream (about 0.015 inches versus 0.005 inches in 100 hours at 2000°F). Hence, it is concluded that a coating for NiTaC-13 would be required for engine endurance testing or service.

In hot corrosion tests of bare NiTaC-13 under mild conditions, 1600°F with 1 ppm of synthetic sea salt and 0.35 wt. % sulfur added to the fuel, the loss of NiTaC-13 metal is indicated to be three times higher than under simple oxidizing conditions. Similar results are obtained for Rene' 80. Hot corrosion tests of bare NiTaC-13 under more severe conditions, 1700°F with 5 ppm of synthetic sea salt and 0.35 wt. % sulfur added to the fuel, indicate that the rate of metal loss is further increased to about five times that under simple oxidizing conditions and at least twice as great as hot corrosion rates for Rene' 80. Hence, a coating for NiTaC-13 is more urgently needed for use in hot corrosion environments.

In low velocity (Mach 0.05) oxidation tests, the Ni-20Cr-10Al-1Y coating for NiTaC-13 has been shown to provide excellent protection against oxidation for at least 1000 hours at temperatures up to 2000°F. In the more severe high velocity (Mach 1) oxidation tests, the NiCrAlY coating also provided excellent protection for 100 hours at 2000°F and microscopic examination of the coating after test indicates that it would be protective for a substantially longer period.

Although the data indicate the possibility of even longer periods of oxidation protection by the coating, observed interactions between the coating and substrate may limit service life. In these interactions, NiTaC-13 suffers carbide fiber denudation near the coating interface, both during the coating process and during subsequent high temperature exposure.

Hot corrosion tests of Ni-20Cr-10Al-1Y coated NiTaC-13 showed that, under mild conditions, this coating gave excellent protection for the 500 hours duration of the test. However, under more severe hot corrosion conditions, the coating failed prematurely and did not provide adequate protection. Hence, for the present program, test conditions that would cause severe hot corrosion must be avoided.

In conclusion, tests of the Ni-20Cr-10Al-1Y coating show it to provide satisfactory protection against oxidation and mild hot corrosion. However, several problems were encountered with the coating on NiTaC-13, including:

- premature failure under severe hot corrosion conditions,
- carbide fiber denudation during coating and subsequent high temperature exposure, and
- degradation of 1400° to 1800°F HCF properties, as discussed in Section 3.2.6.

In view of these problems, it is clear that an improved coating is required for general service of NiTaC type alloys in jet engine turbines.

With respect to the planned 30-hour engine test, the data show that no oxidation or hot corrosion problems would be expected for Ni-20Cr-10Al-1Y coated blades. Engine testing of bare blades has some risk because of metal loss due to oxidation and hot corrosion. Clearly, a severe hot corrosion environment must be avoided; and, if this is done, the data indicate that Rene' 80 and NiTaC-13 blades would be nearly equivalent. The risk could be reduced by periodic inspection of the NiTaC-13 blades during the test.

4.0 NiTaC-13 J101 LPT BLADE DESIGN AND ANALYSIS

The goal of this work was to establish an uncooled NiTaC-13 J101 LPT blade design that, as determined by blade mission life analysis, was predicted to have life equivalent to the existing air cooled superalloy blade design. The eutectic blade was also required to have the same external geometry as the existing blade so that there would be complete interchangeability to facilitate an engine test with existing hardware.

Blade design and life analysis was done in two stages. The first was preliminary analysis of two blade designs, solid and hollow tip, utilizing the limited amount of pre-program NiTaC-13 property data and simplified design analysis procedures. The preliminary work, indicating that the overall goal would be met with the solid design, was completed early in the program to provide the blade design for use in process development work.

The second analysis stage was final design and life analysis of the same two blades in the bare and coated conditions which utilized more extensive property data acquired for NiTaC-13 in the program and more detailed life analysis procedures. While this analysis was in progress, solid blades were being produced to meet the overall schedule. It had been decided that, if detailed analysis showed a need for a tip cavity to meet design acceptability criteria, the cavity would be formed by machining.

The second analysis stage was not fully completed until after all blades had been cast and 47 had been finish machined to the solid design. At this point, results of the design analysis predictions showed that even the hollow tip design did not fully meet design acceptability criteria, and that a redesign beyond the program scope would be required. However, an analysis of blade capabilities predicted that the bare solid blade would meet all requirements for a 30-hour engine test. It was, therefore, decided to proceed with bench tests of the solid blade design.

4.1 PRELIMINARY BLADE DESIGN

Drawings illustrating the superalloy J101 LPT blade and a typical airfoil section are presented in Figures 105 and 106. As shown in Figure 105, the superalloy blade had a tip cavity in the upper 20 percent of the airfoil and a small cavity on each of the two sides of the platform. These cavities were used to reduce airfoil and dovetail stresses. In addition, there were five internal longitudinal holes, not illustrated, for air cooling.

The approach taken to eutectic blade design was to evaluate two modifications of the superalloy blade design: a completely solid design and a hollow tip design. Neither modification had cooling holes or platform cavities. The solid blade design was preferred because it would have the following advantages:

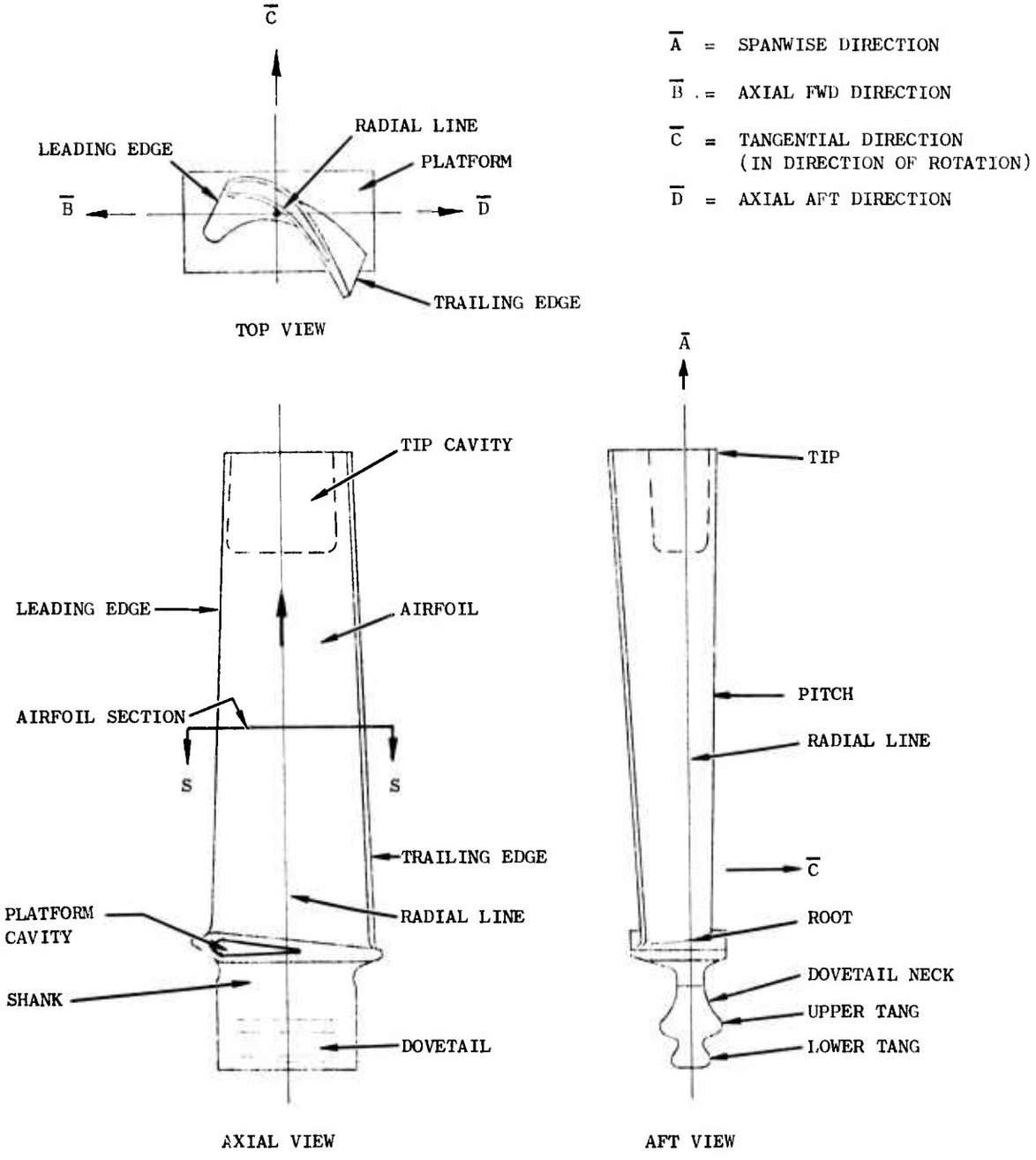

Figure 105. J101 LPT Blade and Nomenclature

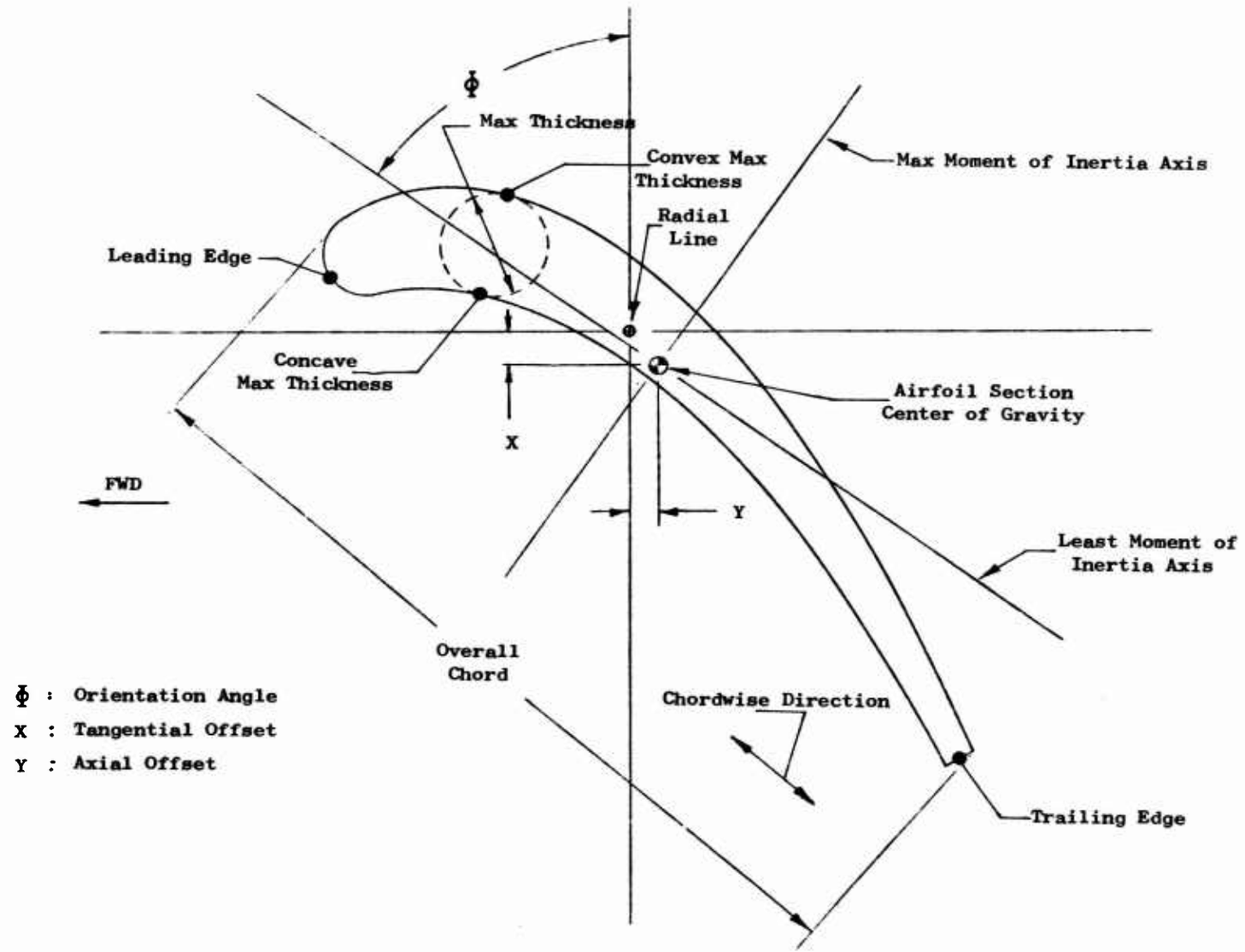

Figure 106. Typical J101 LPT Blade Airfoil Section and Nomenclature

- Increased performance - No cooling air required
- Blade geometry simplification - Solid blade, easier to cast
- J101 hardware compatibility - No change in external geometry

4.1.1 Design Acceptability Criteria

The preliminary criteria established for the NiTaC-13 blade and shown in Table 36 were based on the requirements of the superalloy blade for 1200 hours of operation under a specific J101 engine mission cycle involving many modes of operation including idle, take-off, and cruise. Because the analysis was preliminary, a complete mission study was not performed. Instead, it was assumed that the eutectic blade life would be limited at the pitch section and that is where the preliminary blade airfoil analysis was focused.

4.1.2 Procedures

The flowpath of the procedures used for preliminary analysis of the two eutectic blades designs is shown in Figure 107. As indicated, there were two General Electric computer programs used in the analysis, designated: ADAM MECHANICAL SECTION PROPERTIES, and ADAM TWISTED BLADE. Details of the general inputs, outputs, and the use of the outputs for these programs are given in Appendix B, Tables B-1 and B-2, respectively. Specific inputs and results are detailed in the following steps:

- Engineering drawings of seven airfoil and five dovetail/shank sections of the superalloy J101 LPT blade were modified for the two eutectic blade designs. The modified sections were digitized by selecting coordinates around the perimeter and entered into ADAM MECHANICAL SECTION PROPERTIES.

- Required outputs from the previous step were fed into ADAM TWISTED BLADE which computes deflections, spanwise stresses, loads, and vibratory frequencies of the blade. The program assumes isotropic material properties.

- The engine operating conditions required for ADAM TWISTED BLADE were supplied by the J101 Project for an engine rotor speed of 13, 533 rpm and included steady state axial and tangential gas loads, and the gas temperature (T_{TB}) profile presented in Figure 108.

  NiTaC-13 properties required for ADAM TWISTED BLADE included density, dynamic modulus of elasticity (E) and shear modulus (G), all as a function of temperature. A density of 0.306 lb/cu. in. was used and assumed to be temperature independent. To establish the temperatures at each section being analyzed, blade metal temperatures were based on data in Figure 108 for the J101 for conditions of peak temperature. General Electric experience had shown that the bulk metal temperature for a solid blade is about 30°F lower than T_{TB}; hence, the bulk metal temperature estimated for the pitch sections of the two NiTaC-13 blade designs was 1790°F. Preliminary longitudinal data for E of NiTa-13 are shown in Figure 109. Shear modulus was calculated from the equation:

$$G = E/2\,(1 + \mu)$$

  where Poisson's ratio, μ, was assumed to be 0.3 and temperature independent.

TABLE 36

PRELIMINARY ACCEPTABILITY CRITERIA FOR NiTaC-13 J101 LPT BLADE DESIGN

1. Rupture Life - Blade pitchline must exhibit equal or greater life than the superalloy J101 LPT blade.

2. High Cycle Fatigue Life - Blade pitchline must exhibit 100 hour Goodman diagram capability.

3. Low Cycle Fatigue Life - Maximum dovetail stress must meet 1200-hour mission cyclic life requirement.

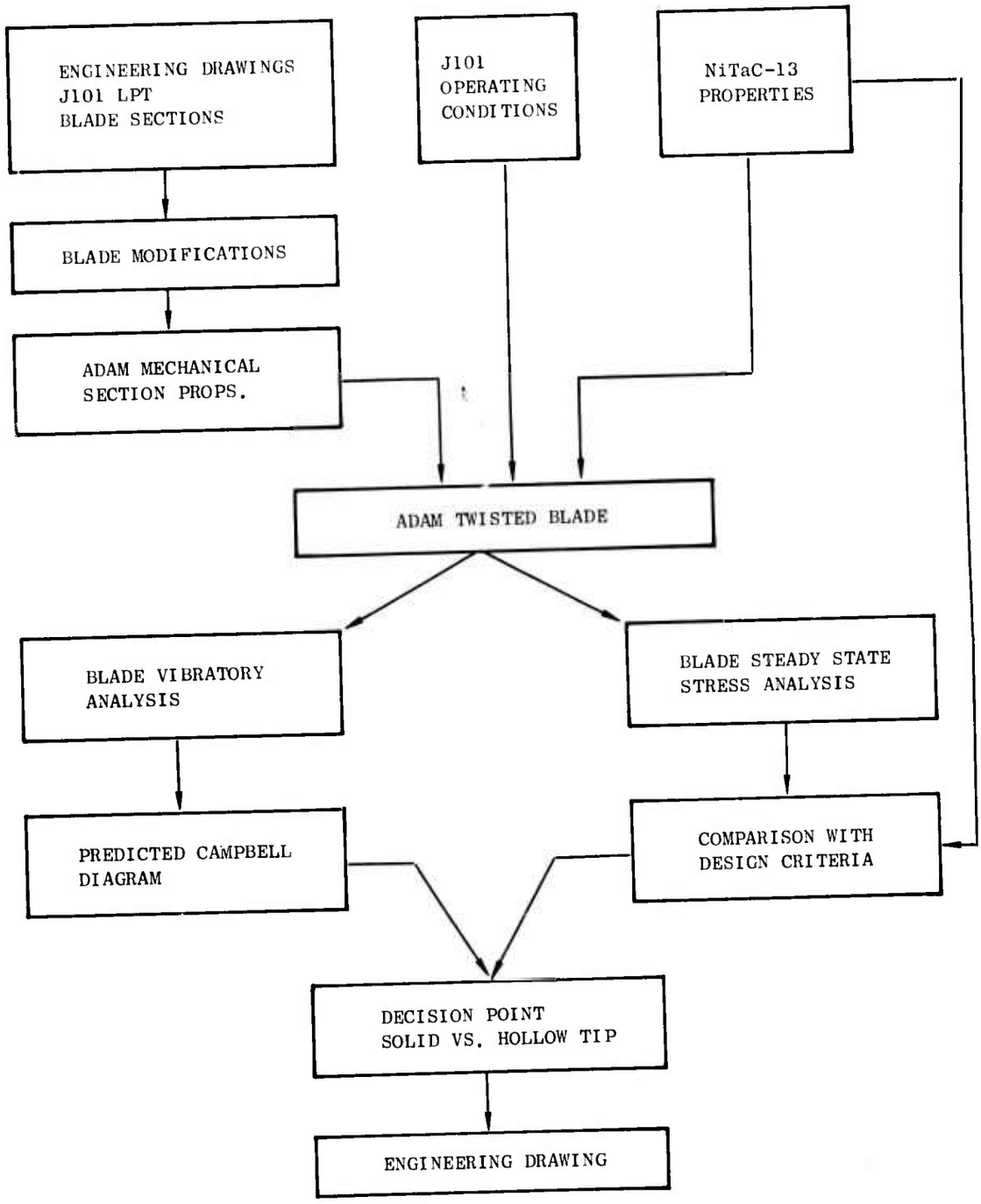

Figure 107. Flowpath of Preliminary NiTaC-13 J101 LPT Blade Pitch Section Life Analysis

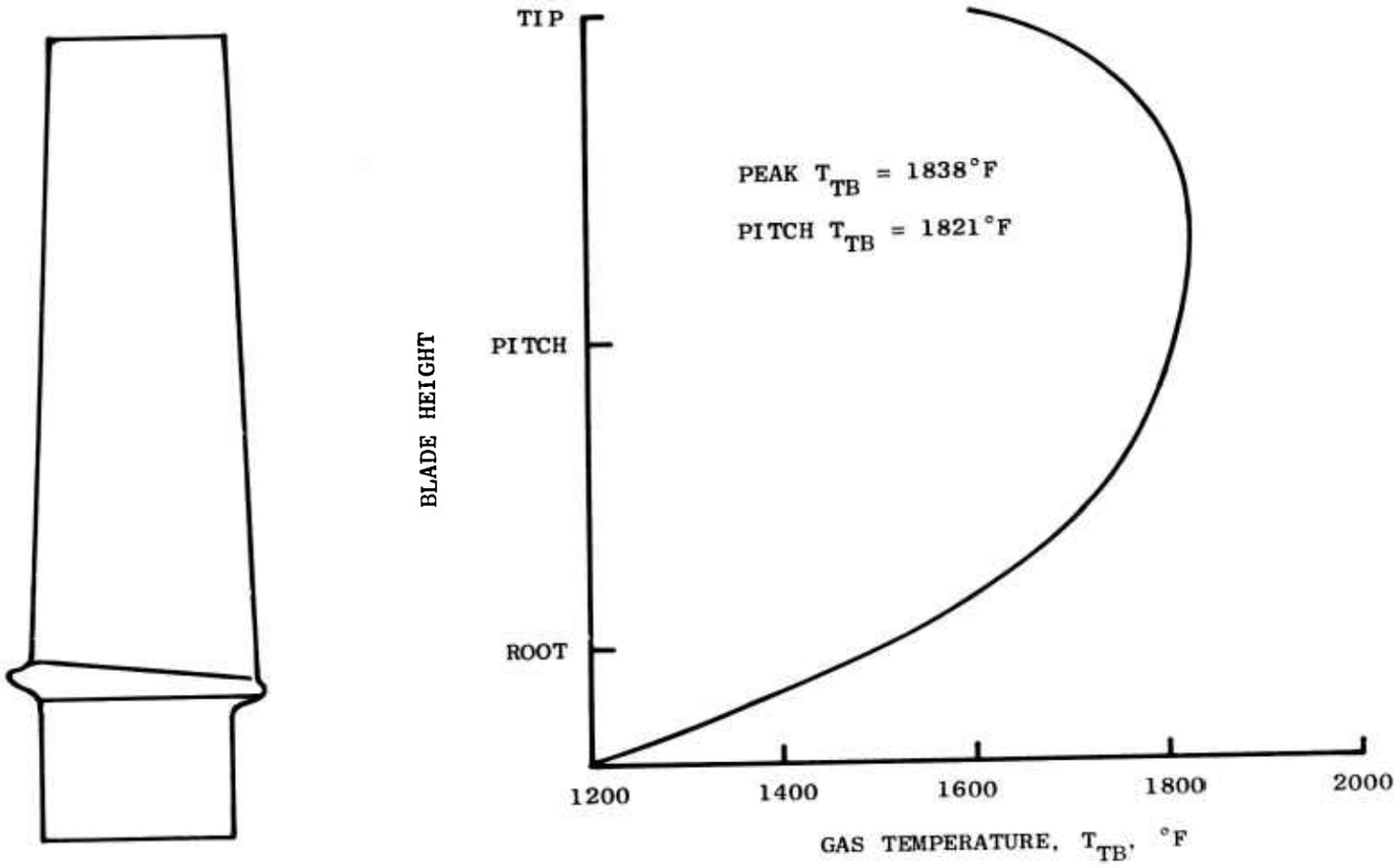

Figure 108. Preliminary Gas Temperature Profile for J101 LPT at Peak Temperature Operating Conditions

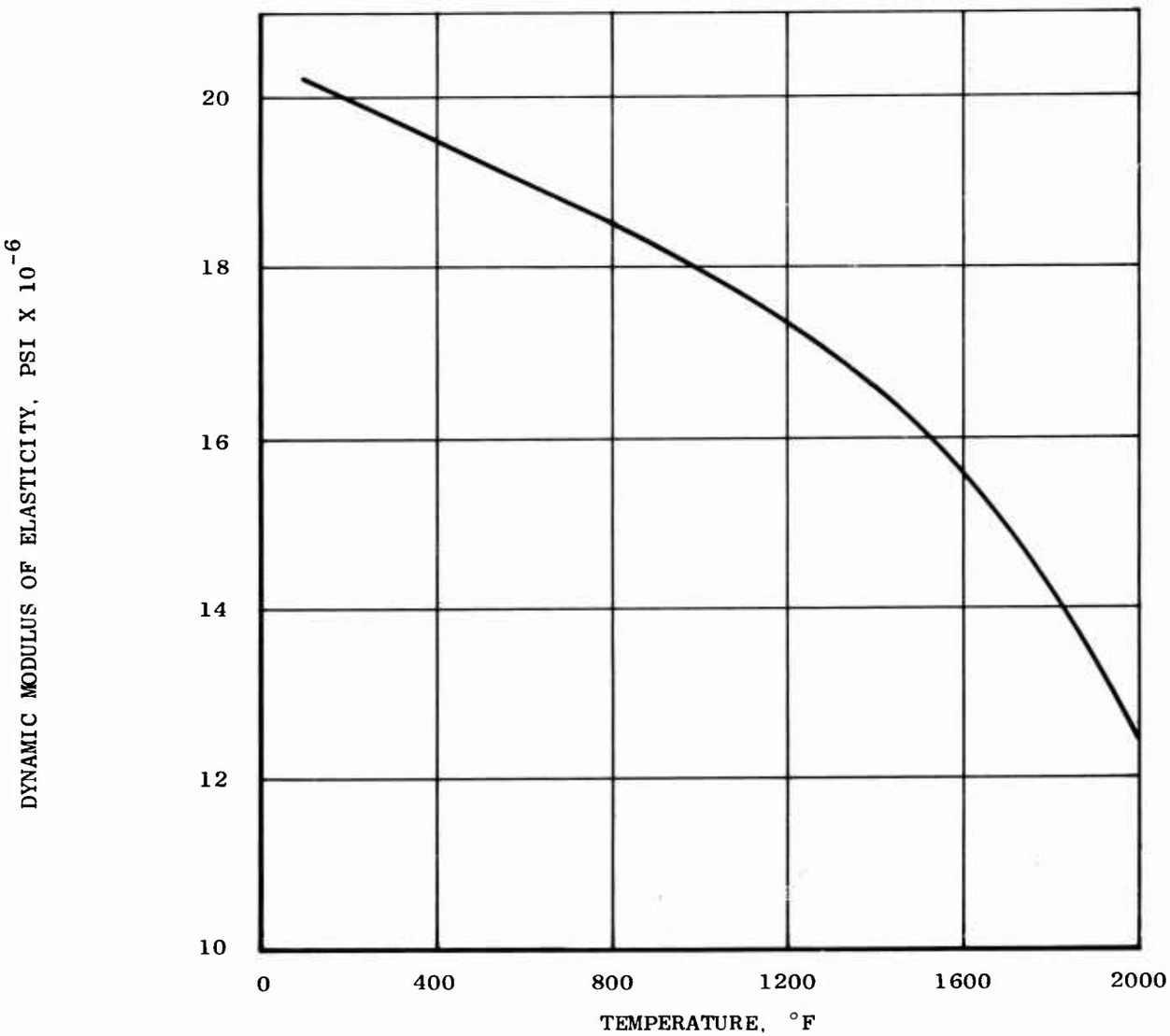

Figure 109. Preliminary Dynamic Modulus of Elasticity for NiTaC-13 in the Longitudinal Direction

Blade resonance frequencies computed by ADAM TWISTED BLADE are summarized in Table 37. These results showed that the differences in resonance frequencies for the two blade designs were small, ranging from about 12 percent at the lower frequencies to 5 percent at the higher frequencies.

Campbell diagrams constructed for the two blade designs, presented in Figures 110 and 111, are similar. The solid blade was slightly better because the resonance frequencies occurred at lower rotational speeds; however, both designs were considered acceptable because, with one exception for each blade design, no resonance problems were indicated at idle or 100 percent speed. The potential resonance problems for each blade design occurred at idle and relatively high frequencies where excitation stimuli are generally weak.

Vibratory modes of blades are sensitive to boundary conditions. For the foregoing analysis it had been assumed that the blade was rigidly clamped at the pressure face of the upper dovetail tang. A prior study of the superalloy J101 blade had shown that, if adjacent blades come in contact at the platforms, blade frequencies can be increased by up to 20 percent. Therefore, the frequencies shown in Figures 110 and 111 were considered to be the lower limits of blade frequency response that could be encountered in an engine.

The most important steady state centrifugal and resultant stresses from ADAM TWISTED BLADE are summarized in Table 38. Resultant stresses included gas bending, blade untwisting, and centrifugal stresses. The most significant difference between the two eutectic blade designs was a 4.2 ksi greater centrifugal stress at the pitch section of the solid blade.

Dovetail stresses for the two eutectic blades were estimated on the basis of an analysis performed by the J101 project for the cooled superalloy blade. The superalloy blade stresses were increased by 10 percent for the solid eutectic blade and five percent for the hollow tip eutectic blade on the basis of the higher weights estimated for the two uncooled blade designs. The results are presented in Figure 112.

The foregoing analytical results were required for preliminary blade life predictions which are described in the next section.

4.1.3 Acceptability of Preliminary Blade Designs

Maximum power conditions of the mission were used for this comparison because here material temperatures are the highest and material life is consumed most rapidly. At maximum power, engine speed was 12,523 rpm compared to 13,533 rpm used in preceding calculations. Therefore, stresses previously computed for the two blades were adjusted down (by the rpm ratio squared) to correct for the lower engine speed.

An additional correction to previous calculations was also required because new measurements showed that the average density of NiTaC-13 was about 0.315 instead of the 0.306 lbs./cu. in. used previously. This correction increased stresses previously given by three percent and reduced vibrational frequencies by 1.5 percent.

TABLE 37

PRELIMINARY RESONANCIES FREQUENCIES FOR NiTaC-13 J101 LPT

BLADE DESIGNS COMPUTED BY ADAM TWISTED BLADE

Vibration Mode	Resonance Frequency, Hz			
	Solid Blade		Hollow Blade	
	Cold	Hot	Cold	Hot
1st Flex	526	635	587	683
1st Axial	1,728	1,620	1,942	1,800
2nd Flex	2,355	2,050	2,519	2,190
1st Torsion	3,455	3,123	3,716	3,330
2nd Axial	5,814	5,063	6,138	5,338
2nd Torsion	7,091	6,230	7,439	6,526

Cold: 0 RPM, Room Temperature

Hot: 13,533 RPM, Max Metal Temperature

Density = 0.306 lb.in.^{3}

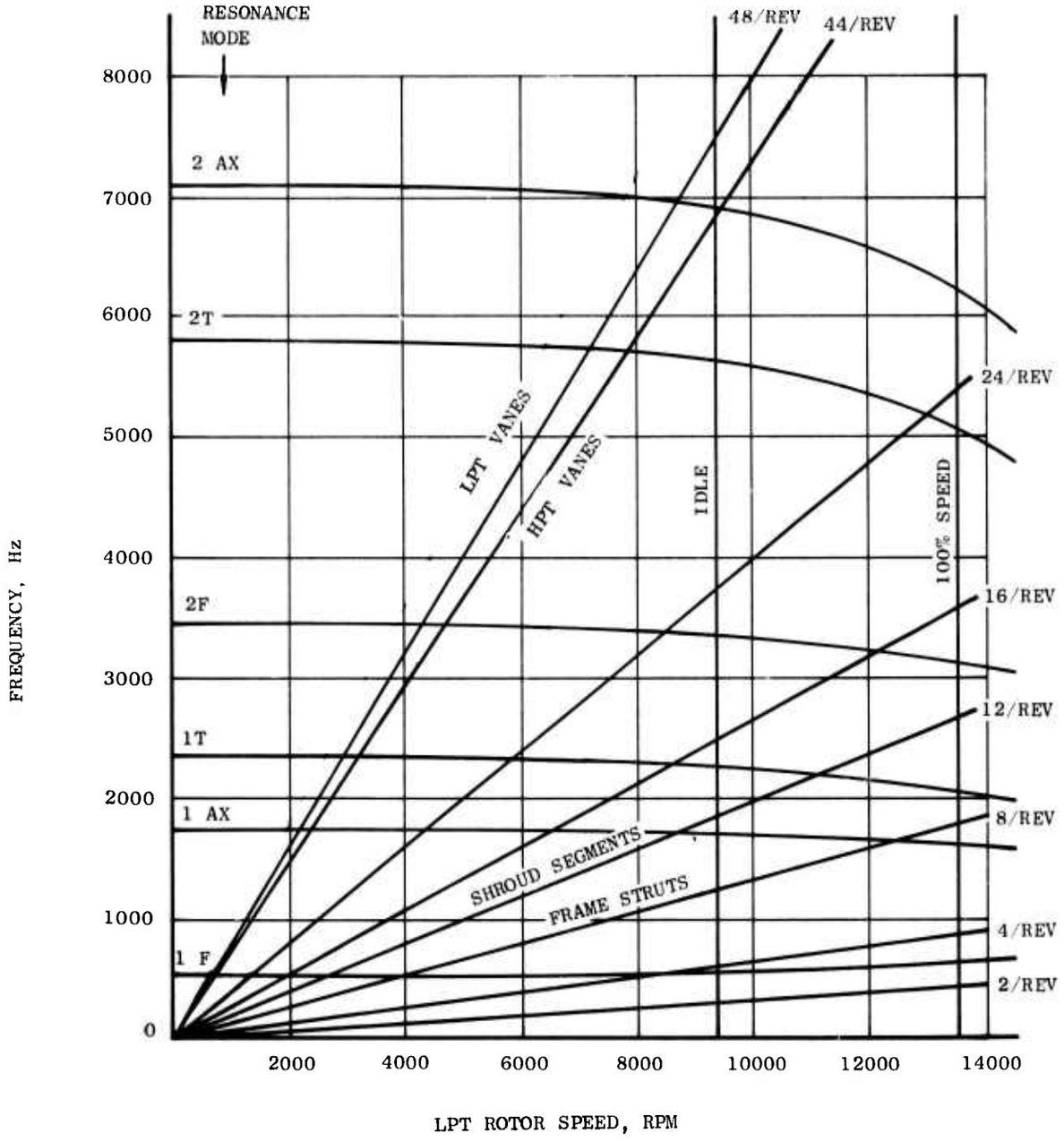

Figure 110. Preliminary Campbell Diagram for Solid NiTaC-13 J101 LPT Blade

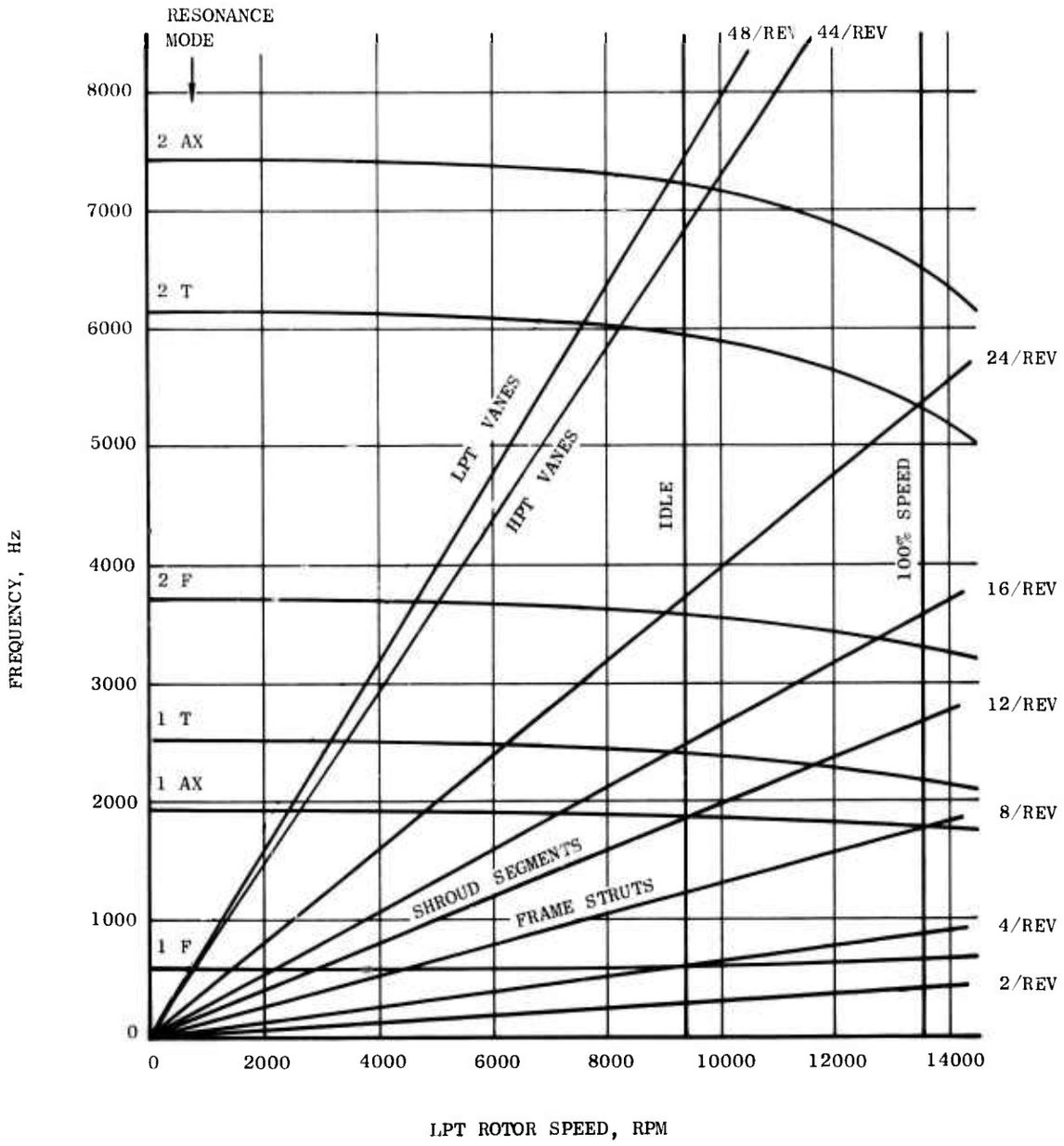

Figure 111. Preliminary Campbell Diagram for Hollow Tip NiTaC-13 J101 LPT Blade

TABLE 38

PRELIMINARY STEADY STATE AIRFOIL STRESSES FOR NiTaC-13

J101 LPT BLADE DESIGNS COMPUTED

	Solid	Hollow Tip
Resultant Centrifugal Stress (KSI)		
Pitch	27.4	23.2
Root	47.8	44.2
Resultant Spanwise Stress (KSI)		
Root Leading Edge	36.2	35.6
Root Trailing Edge	31.0	35.0
Root Convex	58.4	51.1
Root Concave	45.6	42.7

RPM = 13,533 Density = 0.306 lb./in.^{3}

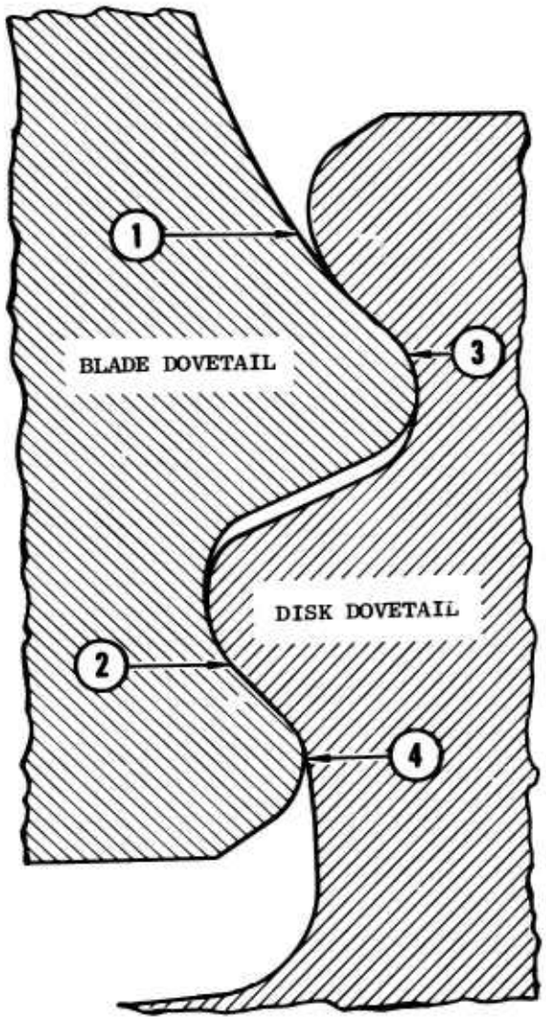

	MAXIMUM STRESS, KSI			
COOLED SUPERALLOY	1	2	3	4
NECK CENTRIFUGAL	58.6	33.3	39.3	41.7
TANG BEND	29.7	37.7	48.4	46.6
COMBINED	99.0	107.1	135.1	122.1
UNCOOLED SOLID NiTaC-13				
NECK CENTRIFUGAL	61.4	36.5	42.5	45.0
TANG BEND	31.2	41.4	52.3	50.3
COMBINED	108.6	117.5	146.0	132.0
UNCOOLED HOLLOW TIP NiTaC-13				
NECK CENTRIFUGAL	59.2	35.2	41.1	43.7
TANG BEND	30.9	39.8	50.7	48.8
COMBINED	104.6	113.2	141.5	127.8

RPM = 13,533

ρ = .306 lb/in^3

Figure 112. Preliminary J101 LPT Dovetail Stresses in Blade and Disk

4.1.3.1 Rupture Life Prediction - This analysis was performed for the solid eutectic blade on the basis of the following maximum temperature and the centrifugal stress at the pitch section:

- 1790°F bulk metal temperature
- 24.4 ksi resultant centrifugal stress, after correcting result in Table 38 for decreased engine rotor speed and increased density of NiTaC-13.

Using the above conditions, the rupture half life was predicted on the basis of the preliminary stress rupture data for NiTaC-13 in Figure 113. The estimated thin wall -3 σ curve of Figure 113 was used, resulting in a predicted half life of 750 hours. The thin wall derate was applied because conventionally cast superalloys are observed to have significantly lower rupture strengths with decreasing casting wall thickness, and this effect was assumed to be applicable to NiTaC-13. (This derate was not used later in detailed design analysis.) The use of half life is an additional safety factor applied by General Electric. The corresponding half life prediction for the superalloy blade was also 750 hours. These lives were lower than would be predicted for a mission mix analysis, because the former were based on continuous operation at peak engine operating conditions.

Thus, the predicted rupture life of the solid NiTaC-13 blade met the first preliminary design criterion by equaling the predicted life of the superalloy blade.

4.1.3.2 High Cycle Fatigue Life - For this comparison, average and -3σ (thin wall) Goodman fatigue diagrams for 1800°F/100 hours, presented in Figure 114, were estimated from preliminary 50 hour 2000°F HCF data for NiTaC-13, and the stress-rupture curves in Figure 113. Curves for the J101 LPT blade superalloy at 1600°F/100 hours are also shown in Figure 114. The maximum centrifugal spanwise stress of 24.4 ksi estimated for the pitch section of the solid NiTaC-13 blade fell within the 1800°F/100 hour Goodman diagram and indicated an allowable alternating stress of 11 ksi. This value was lower than the allowable 35 ksi alternating stress estimated for the superalloy blade, but is adequate for engine test.

Hence, the solid eutectic blade met the second preliminary design acceptability criterion of Table 36.

4.1.3.3 Low Cycle Fatigue Life - Dovetail stresses for the two eutectic blade designs shown previously in Figure 112 included neck centrifugal, tang bending, and combined stresses. The latter includes the resolved centrifugal and tang bending stresses, and stress concentration factors for tang curvatures. The eutectic blade stresses of Figure 112 were increased by three percent to correct for the higher density (0.306 to 0.315 lbs/cu. in.) of NiTaC-13.

Preliminary data for 1200°F LCF strength of NiTaC-13 are compared in Figure 115 with corresponding data for the J101 LPT blade superalloy. The data were obtained from load controlled sustained peak low cycle fatigue (SPLCF) tests in which specimens of both materials were held at maximum load for 90 seconds to combine potential creep effects with LCF such as occurs in engine hardware. Notched specimens were also included to

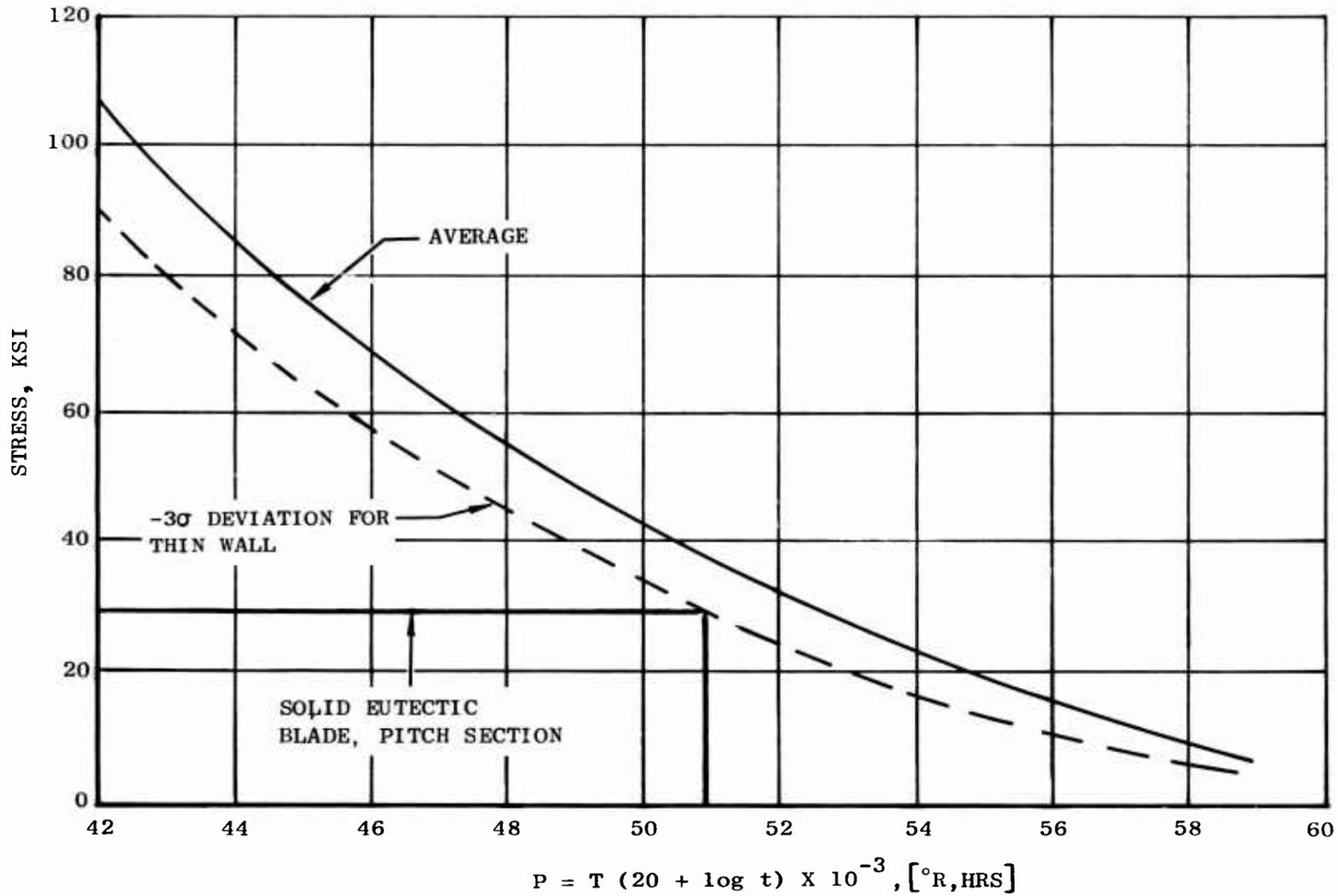

Figure 113. Preliminary Longitudinal Rupture Data for NiTaC-13

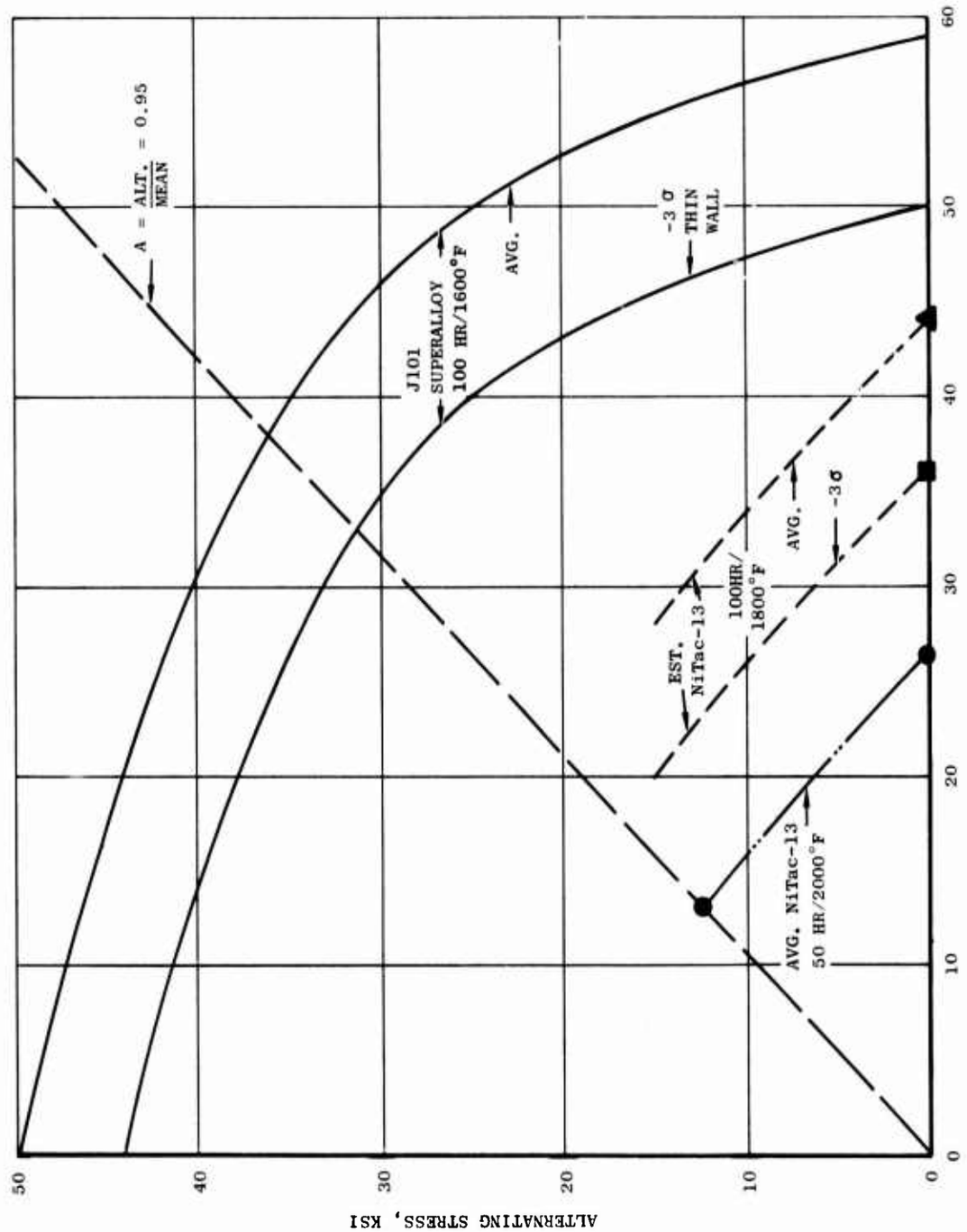

Figure 114. Goodman Diagrams for NiTaC-13 (Preliminary Estimate) and J101 LPT Blade Superalloy

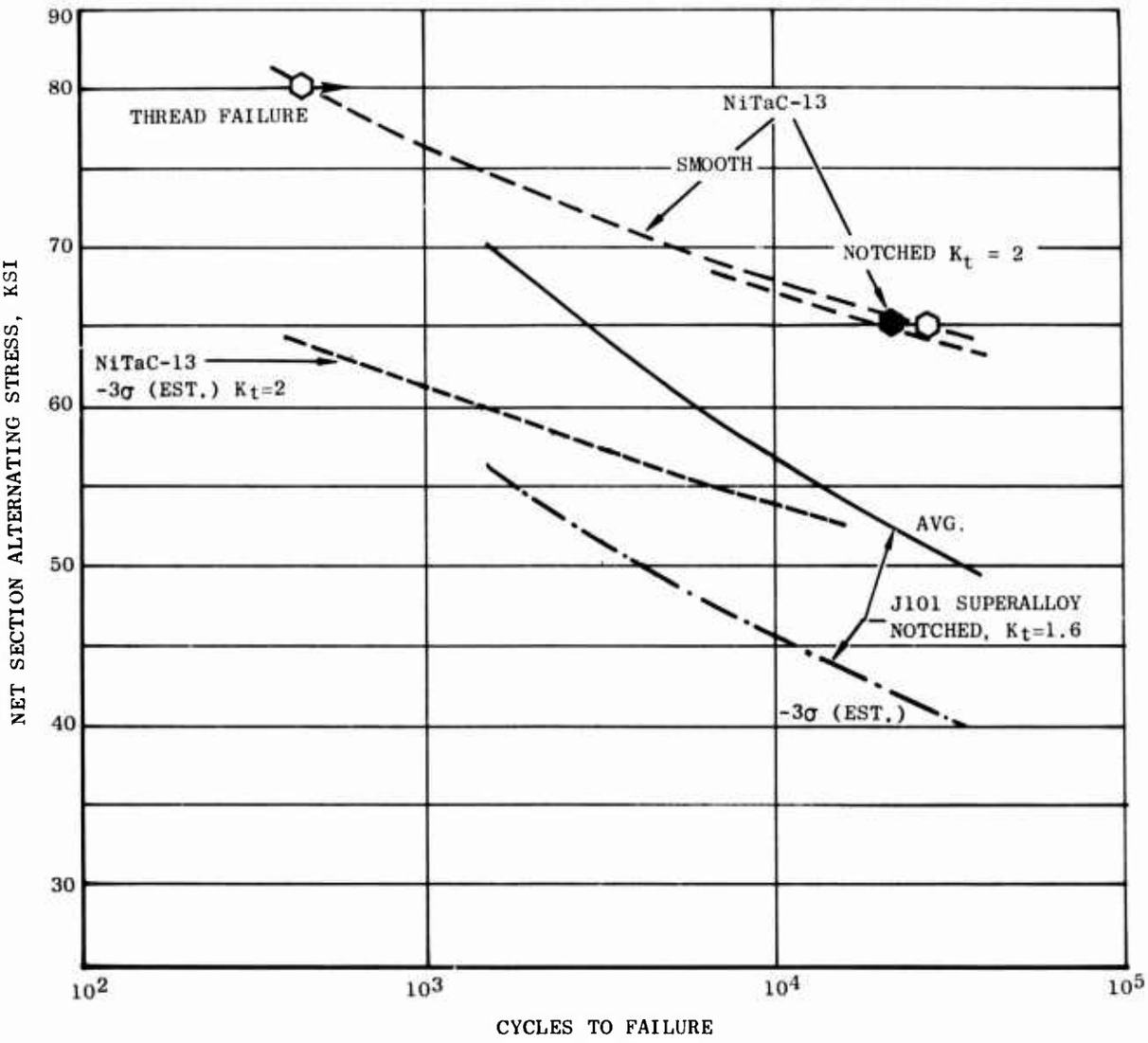

Figure 115. Preliminary Load Controlled 1200°F Sustained Peak Low Cycle Fatigue Data (10-90-10 Second Cycle) For NiTaC-13 Compared to J101 LPT Blade Superalloy. A Ratio = 0.95.

simulate dovetail stress concentrations, and net section stresses were based on the cross sectional area at the base of the notch. The -3σ curves in Figure 115 were estimated as 80 percent of the average curves.

Because the SPLCF data were obtained with notched bars, the most appropriate data from Figure 112 for use in LCF life predictions are the sums of neck centrifugal and tang bending stresses. The SPLCF data in Figure 115, then, include the approximate stress concentration factor for the dovetail tangs. Maximum stress sums and cyclic lives estimated from the -3σ curves of Figure 115 are as follows:

Blade	Neck Centrifugal + Tang Bending Stress, ksi	Cycles to Failure
Cooled Superalloy	88.3	1.2×10^4
Uncooled Solid NiTaC-13	95.4	$>10^5$
Uncooled Hollow Tip NiTaC-13	92.8	$>10^5$

On the basis of the above data, the solid blade was predicted to have a cyclic life which substantially exceeded that predicted for the superalloy blade and exceeded the number of cycles to be encountered in 1200 mission hours of the J101.

Thus, the solid eutectic blade met the third preliminary acceptability criterion in Table 36.

4.1.4 Selection of Preliminary Blade Design

The results of blade life analysis for the solid NiTaC-13 blade are summarized in Table 39 and compared with corresponding life analysis for the superalloy blade. As shown in Table 39, the preferred solid eutectic blade design was predicted to meet the three preliminary design acceptability criteria in Table 36. Furthermore, the Campbell diagram presented in Figure 110 indicated that the solid eutectic blade would not have resonance problems in the engine operating range and was acceptable. Therefore, the preliminary design for the NiTaC-13 J101 LPT blade was selected as the solid blade, and the detail drawing given in Figure 116 was released for blade process development work.

The selection of the solid instead of the hollow-tip blade simplified blade casting process development because it eliminated the need to cast a tip cavity as was required for the superalloy blade. It was expected that if the subsequent detailed blade analysis revealed a need to reduce blade stresses, a tip cavity could be formed by machining.

4.2 DETAILED DESIGN ANALYSIS

Analysis work was initiated in mid-1973 using preliminary NiTaC-13 data in order to establish methods for orthotropic stress analysis. The analysis was revised several times as new NiTaC-13 data were acquired, but only the final analysis will be presented here.

TABLE 39

PRELIMINARY LIFE ANALYSIS AT MAXIMUM ENGINE POWER OF BARE SOLID NiTaC-13 J101 LPT BLADE COMPARED TO COOLED SUPERALLOY BLADE

	Solid NiTaC-13	Hollow Superalloy
Alloy Density, lb/in.^{3}	0.315	0.306
Blade Weight, lb.	0.262	0.231
Pitch Stress, ksi	24.4	20.6
Bulk Metal Temperature at Pitch, ^{o}F	1790	1634
Rupture Half Life at Pitch, hrs	750	750
Allowable Alternating Stress, ksi, for 100 hour HCF Life	~ 11	~ 35
Maximum Dovetail Alternating Stress, ksi	47.7	44.2
Low Cycle Fatigue Life, Cycles	$> 10^5$	1.2×10^4

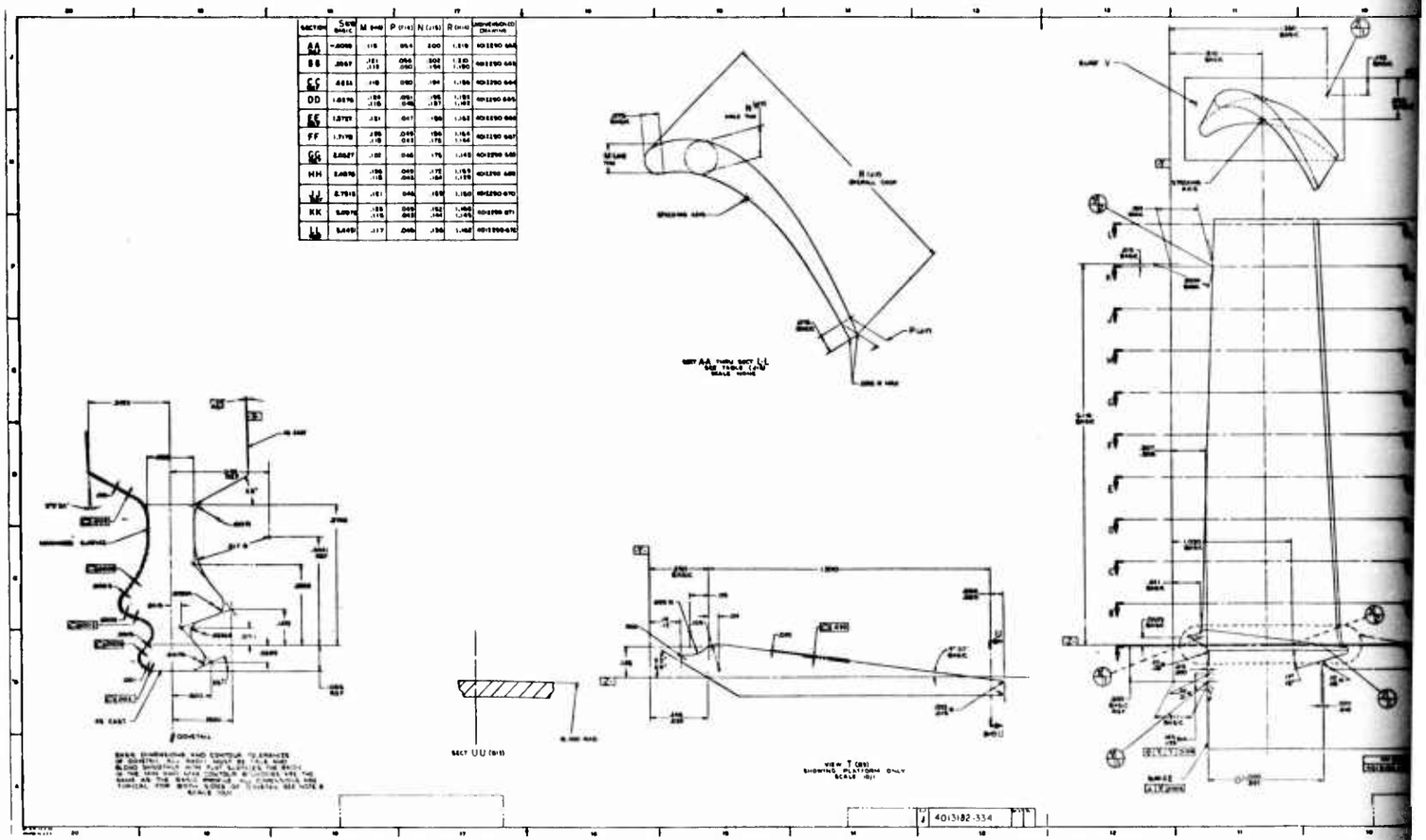
SECT AA THRU SECT LL
SEE TABLE (2/3)
SCALE NONE
SECT UU (6/1)
VIEW T (6/1)
SHOWING PLATFORM ONLY
SCALE 10/1
401382-334

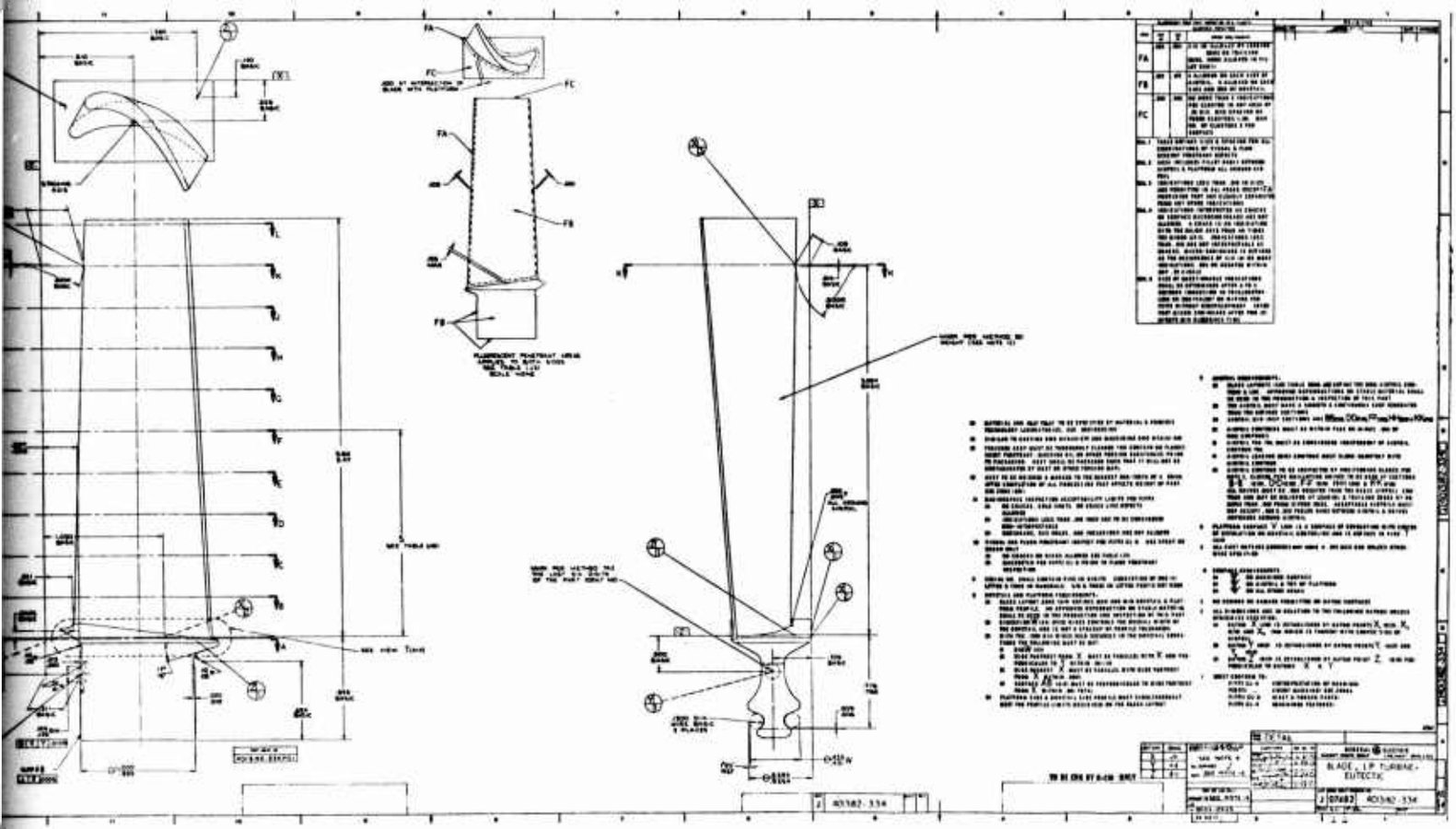

Figure 116. Preliminary Solid Eutectic J101 LPT Blade Design

Four blade configurations were subjected to analysis: solid and hollow tip, each bare and NiCrAlY coated. Although coated blades were preferred for life extension, bare blades were included because data discussed previously in Section 3.2.6 indicated that the coating substantially reduced the 1400°F HCF strength of NiTaC-13. This could be a problem in spin and engine tests and would favor selection of bare blades for both tests.

The design acceptability criteria, shown in Table 40, were revised slightly from Table 36 to reflect the fact that the entire airfoil was to be subjected to analysis, and not just the pitch section.

4.2.1 General Procedure

The flowpath used for detailed blade analysis is presented in Figure 117. Six General Electric computer programs were used as follows:

ADAM MECHANICAL SECTION PROPERTIES

TRANSIENT HEAT TRANSFER

ADAM TWISTED BLADE

BUCKET CREEP III

MISSION

MASS (TAMP) - Isotropic and Orthotropic

Details of the inputs and outputs of these programs are given in Appendix B; and, where appropriate, more specific details will be given in the sections that follow.

4.2.1.1 Heat Transfer Analysis

Steady state bulk metal temperatures for the two uncoated eutectic blade designs and the superalloy blade, computed by TRANSIENT HEAT TRANSFER, are shown graphically in Figure 118 as a function of blade height. These temperatures were subsequently used in rupture life analysis, Section 4.2.2, because temperature gradients were small within all of the blade sections analyzed and did not contribute significant thermal stresses. For example, the steady state temperature distribution in the pitch section is presented in Figure 119 where it can be seen that the maximum temperature differential throughout the section was only 24°F. Figure 119 also illustrates the finite element model used for airfoil cross sections.

4.2.1.2 Steady State Stress Analysis

Centrifugal and resultant spanwise steady stresses were calculated for the four blade configurations at 100 percent engine speed (13,533 RPM) using ADAM TWISTED BLADE. The computed centrifugal airfoil stresses as a function of blade height are presented in Figure 120. These stresses were used subsequently in rupture life analysis, Section 4.2.2.

TABLE 40

FINAL DESIGN ANALYSIS ACCEPTABILITY CRITERIA
FOR NiTaC-13 J101 BLADE DESIGN

1. Rupture Life - Limiting blade section must exhibit equal or greater life than the superalloy blade.

2. High Cycle Fatigue Life - Limiting blade section must exhibit 100 hour Goodman diagram capability.

3. Low Cycle Fatigue Life - Limiting blade airfoil and dovetail section must exhibit 5,000 cycle capability.

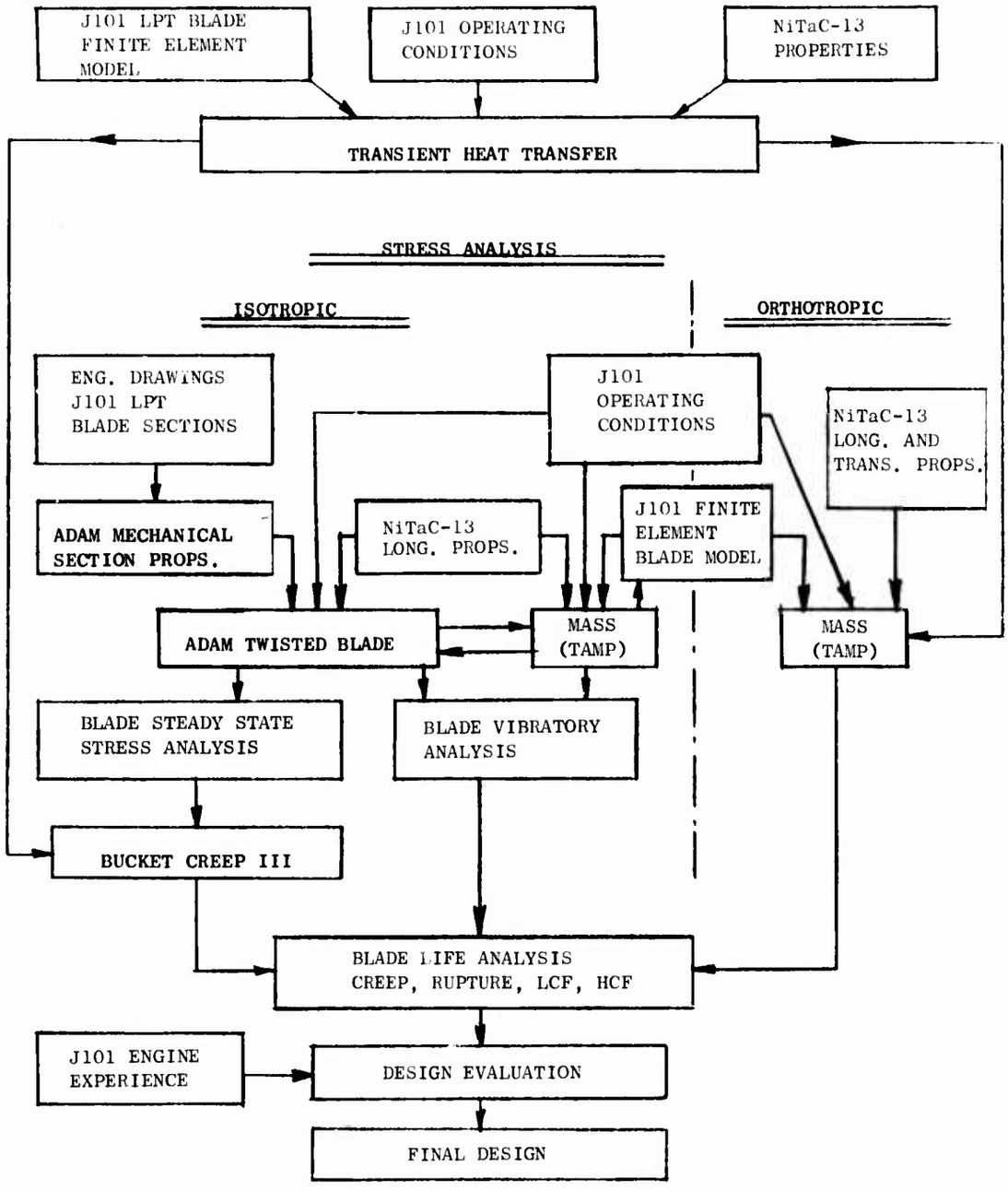

Figure 117. Flowpath for Detailed Blade Analysis

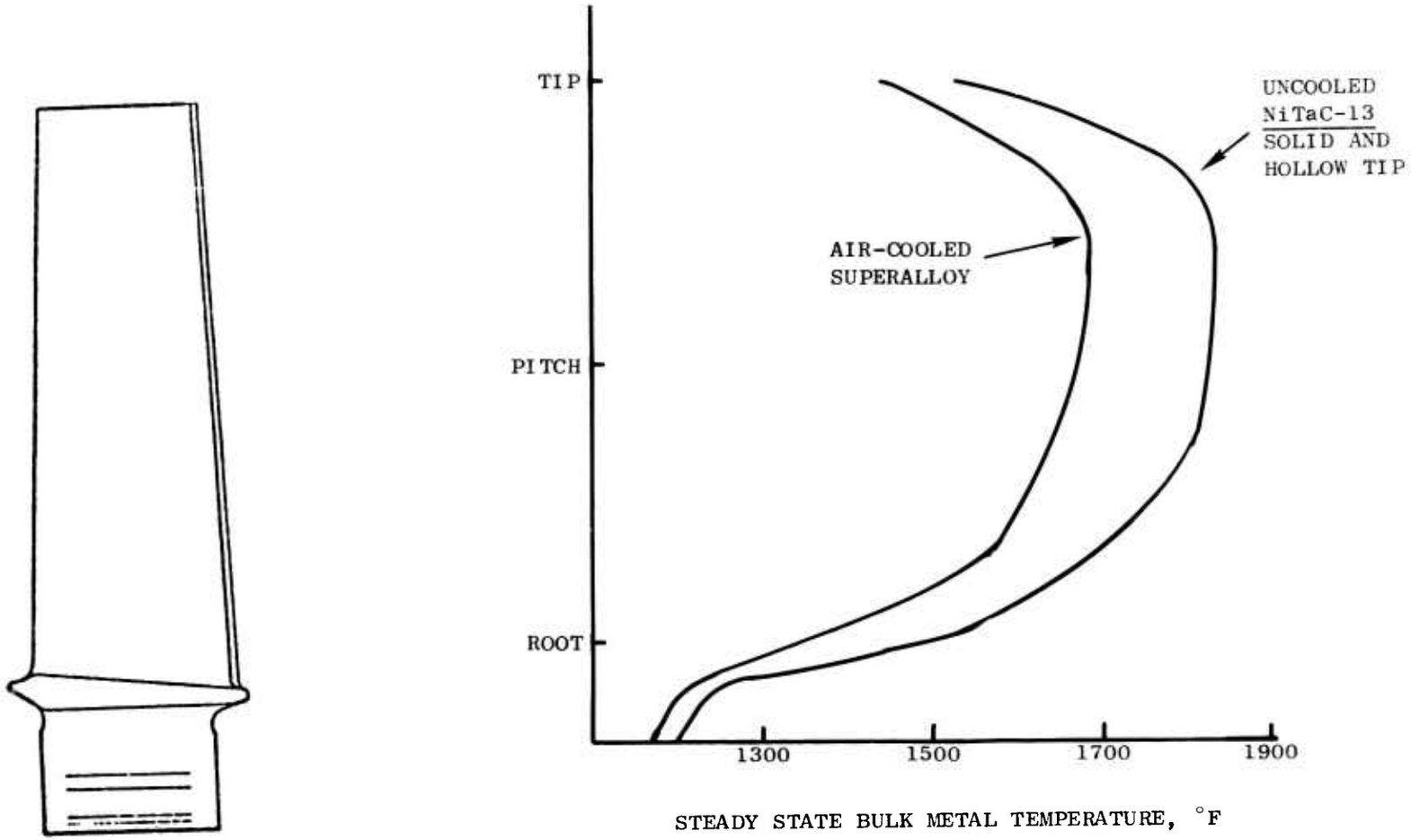

Figure 118. Steady State Bulk Metal Temperatures of Bare J101 LPT Blade Designs Computed by TRANSIENT HEAT TRANSFER

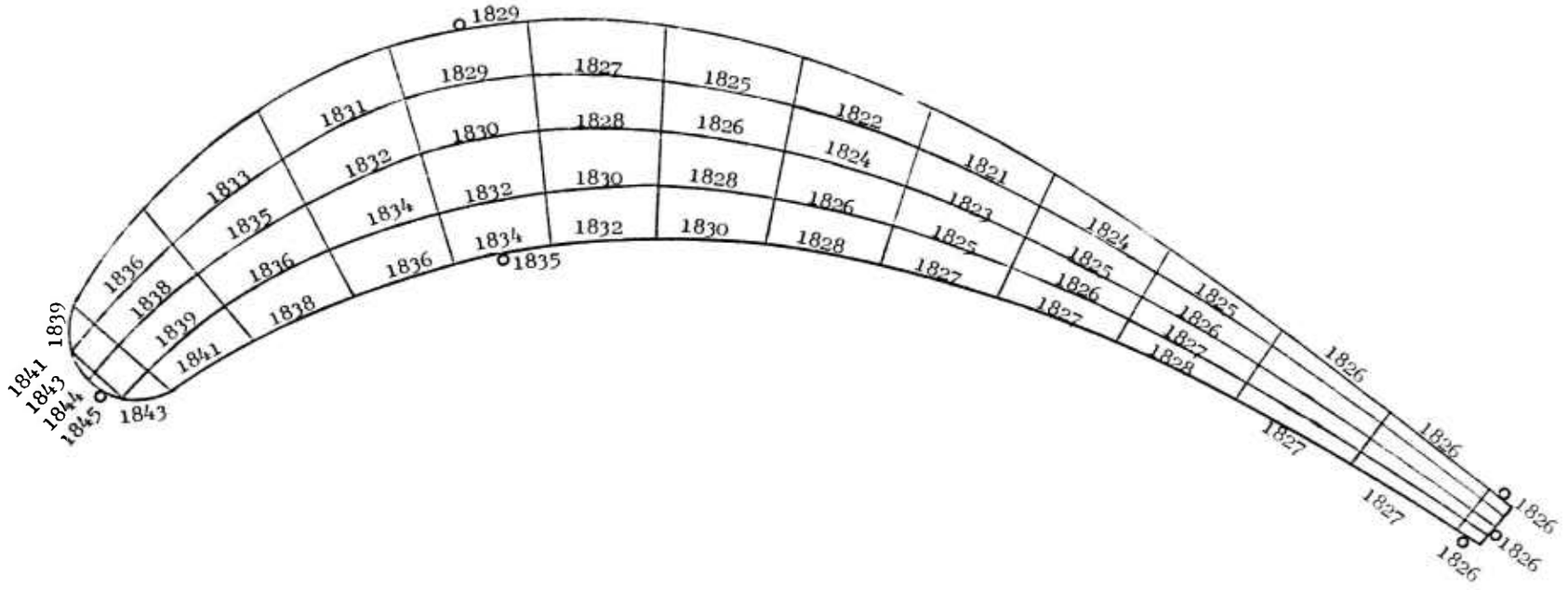

Figure 119. Solid Bare NiTaC-13 J101 LPT Blade Pitch Section Temperatures (°F) Computed by TRANSIENT HEAT TRANSFER

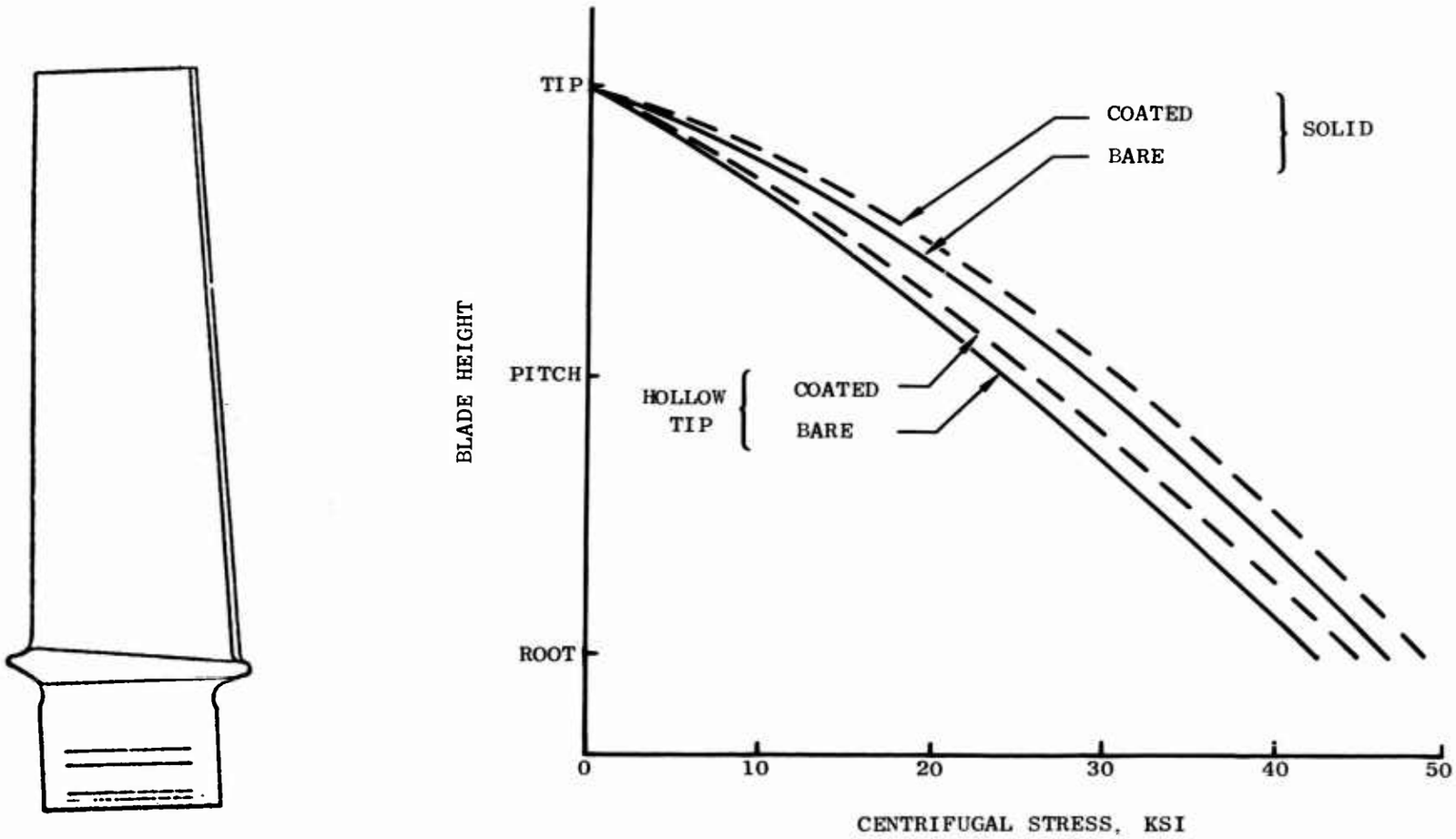

Figure 120. Centrifugal Stresses at 100 Percent Engine Speed in NiTaC-13 J101 LPT Blades Computed by ADAM TWISTED BLADE

The resultant spanwise stresses as a function of blade height at 100 percent engine speed, also computed by ADAM TWISTED BLADE, are illustrated in Figure 121 for the bare solid blade design. In addition to the centrifugal stress, the resultant stress includes gas load and airfoil untwisting effects. Although not used for rupture life analysis, the resultant stresses were used to establish the mean stress level at various blade locations for subsequent HCF life analysis in Section 4.2.3.

4.2.1.3 Resonance Frequencies Analysis

Blade resonance frequencies can be computed by either ADAM TWISTED BLADE or MASS (TAMP), but only the latter program can treat orthotropic materials such as NiTaC-13. Initially MASS was run isotropically to verify the validity of the selected finite element model through comparison with ADAM TWISTED BLADE results. After a second iteration of the model, there was satisfactory agreement between the results of the two computer programs. MASS (TAMP) was then run in the orthotropic mode to predict more accurately the room temperature blade resonance frequencies for later comparison with bench tests results. The results from the two computer programs are presented in Table 41, where it can be seen that the largest discrepancies occurred in the 3rd and 4th vibration modes. These results will be compared with bench test results later in Section 5.2.3.

4.2.2 Rupture Life Analysis

This analysis was performed for the 1200-hour mission mix provided by the J101 project and shown in Table 42. Prior to this program, analysis by a time share computer technique predicted that the cooled J101 superalloy blade satisfied the 1200 hour mission mix requirements of Table 42. For analysis work here, a new computer program, MISSION, was written to duplicate the logic (and result) of the original J101 blade rupture life calculation and was used for comparative rupture life calculations.

Inputs to MISSION for the four NiTaC-13 blade configurations included:

- Centrifugal stresses, Figure 120,
- Temperature, Figure 118,
- Longitudinal stress-rupture strength for bottom material from Figure 78 minus one Larson-Miller parameter number which was the estimated -3 sigma. A thin-wall derate of -0.5 Larson-Miller parameter numbers was not used because new data indicated it was not applicable to DS superalloys, and
- J101 mission mix, Table 42.

In addition to the calculations for the NiTaC-13 blade designs, the cooled superalloy blade life was also recalculated using the most recent minimum (-3σ) stress-rupture data for the alloy and the additional thin-wall derate of 0.5 Larson-Miller parameter numbers, which is a standard General Electric procedure for conventionally cast superalloys.

The predicted lives for the superalloy and four NiTaC-13 blade configurations are presented in Table 43, which also lists the airfoil section (expressed as percent of span) where calculated life was lowest and, therefore, limiting. As derived from the table, the

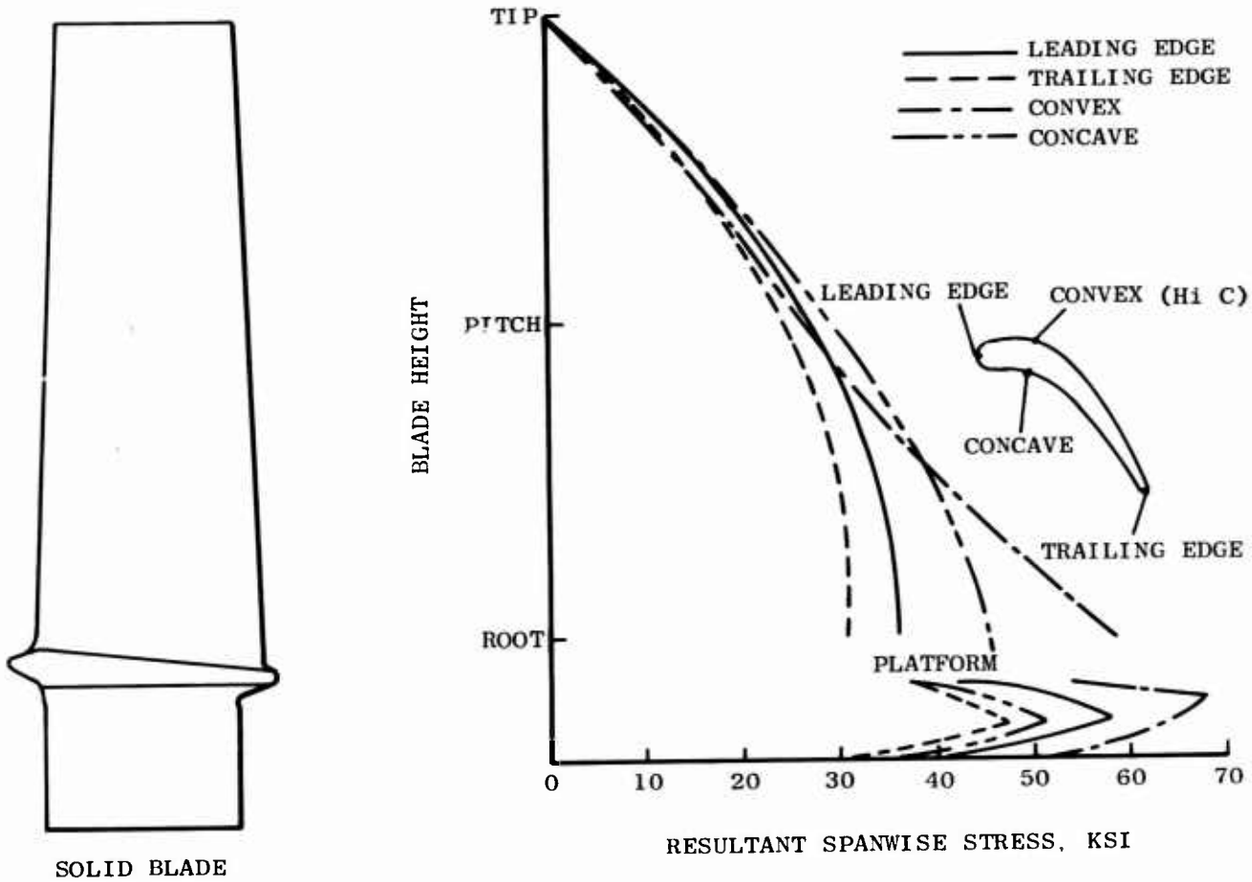

Figure 121. Resultant Spanwise Stresses at 100 Percent Engine Speed in Bare Solid NiTaC-13 J101 LPT Blade Computed by ADAM TWISTED BLADE

TABLE 41

RESONANCE FREQUENCIES FOR THE BARE SOLID NiTaC-13 J101 LPT BLADE PREDICTED BY ADAM TWISTED BLADE AND ISOTROPIC MASS (TAMP) COMPUTER PROGRAMS

Resonance Mode		Computed Resonance Frequency, Hz			
		TWISTED BLADE		Orthotropic MASS (TAMP)	
No.	Type	Cold	Hot	Cold	Hot
1	1st Flex	527	623	524	651
2	1st Axial	1,732	1,547	1,549	1,358
3	2nd Flex	2,270	1,835	3,171	2,696
4	1st Torsion	3,458	2,940	2,195	1,782
5	2nd Axial	5,546	4,561	5,084	4,151
6	2nd Torsion	6,970	5,779	7,143	5,775
7	--	7,962		8,794	
8	--	10,504		9,908	

Cold: Zero RPM, Room Temp.

Hot: 13533 RPM

Density: 0.3182 lbs./cu.in.

TABLE 42

J101 MISSION DEFINITION

Mission Point	LPT Exit Gas Temp., °F	LPT Rotor Speed, RPM	Time at Mission Point, Hours
1	1565	14,200	14.1
2	1590	14,200	14.1
3	1620	14,200	14.1
4	1645	14,200	14.1
5	1671	13,950	14.1
6	1697	13,950	14.1
7	1704	13,730	14.1
8	1704	13,520	16.8
9	1704	13,500	42.0
10	1704	13,490	16.8
11	1704	13,480	16.8
12	1704	13,460	14.1
13	1704	13,450	4.8
14	1704	13,420	4.8
15	1704	13,400	19.8
16	1705	13,300	0.6
17	1706	13,220	0.6
18	1706	13,130	0.6
19	1706	13,050	0.6
20	1706	12,970	25.8
21	1706	12,570	3.0
22	1444	12,960	225.0
23	~ 1350	10,720	225.0
24	~ 1000	8,710	454.3
			1200

TABLE 43

J101 MISSION RUPTURE LIVES OF VARIOUS BLADES PREDICTED BY MISSION COMPUTER PROGRAM

Blade Material	Blade Configuration	Life Limiting Section, % Span	Mission Life, Hours	% of Design Criteria
Bare Superalloy	Hollow Tip, Cooled	40	903	(base)
Bare NiTaC-13	Hollow Tip, Uncooled	30	515	57
Bare NiTaC-13	Solid, Uncooled	30	229	25
Coated NiTaC-13	Hollow Tip, Uncooled	30	270	30
Coated NiTaC-13	Solid, Uncooled	30	135	15

new predicted superalloy blade life was about 75 percent of the earlier value of 1200 hours (Section 4.2.2). None of the NiTaC-13 blade configurations met the rupture life acceptability criterion in Table 40. The closest approach was the bare hollow tip uncooled blade, predicted to have 57 percent of the cooled superalloy blade life. The bare solid NiTaC-13 blade was predicted to have only 25 percent of the superalloy blade life, whereas in the preliminary analysis equal lives were predicted. The two coated blade configurations also had relatively low predicted rupture lives. This was due to stresses added by the weight of the non-load bearing coating, and a slightly lower stress-rupture strength of coated material in the stress-temperature regime involved.

Between preliminary design and detailed blade analysis, many factors contributed to the decrease in predicted rupture life of the solid eutectic blade (equivalent to a loss of about 1.3 Larson-Miller parameter numbers), as follows:

1) Longitudinal stress rupture data for bare NiTaC-13 in Figure 122 fell below the preliminary data by about 0.6 Larson-Miller parameter numbers in the critical stress range of 30 to 40 ksi, and the NiCrAlY coating did not enhance rupture strength in the operating temperature range.

2) The preliminary analysis of the eutectic blade involved only the pitch section (50% span), which was assumed to be life limiting. The detailed analysis showed the 30 percent span to be the worst case, having a life about 70 percent less than the pitch section, which is equivalent to a loss of about 1.2 Larson-Miller parameter numbers.

3) A thin wall derate of -0.5 Larson-Miller parameter numbers used in preliminary design was not used in the final analysis of eutectic blades.

These combined factors indicate a loss of 1.3 parameter numbers in agreement with that derived above on the basis of results given in Table 43.

Despite the fact that none of the NiTaC-13 blade configurations met the rupture life criterion, all four were indicated to have adequate life for an engine test planned as an extension of this program.

4.2.3 HCF Life Analysis

Based on the detailed rupture life analysis, the 30 percent span represents the most severe combination of stress and temperature for the bare solid NiTaC-13 blade. In particular, the convex airfoil surface at 30 percent span is the most limiting local region and has a temperature of 1790°F (Figure 118) and a resultant spanwise (mean) stress of 40 ksi (Figure 121) for the bare solid blade. In the 1800°F/100 hour Goodman diagram shown in Figure 123 for bare bar data taken from Figure 82, it can be seen that the bare solid blade falls just within the average property HCF capabilities, but exceeds the -3σ curve used as the design criterion and, therefore, does not have 100 hour Goodman diagram capability. The mean stress point for the longest rupture life blade configuration, the bare hollow tip, is also shown in Figure 123. This blade falls just short, about 1 ksi, of having 100 hour Goodman diagram capability.

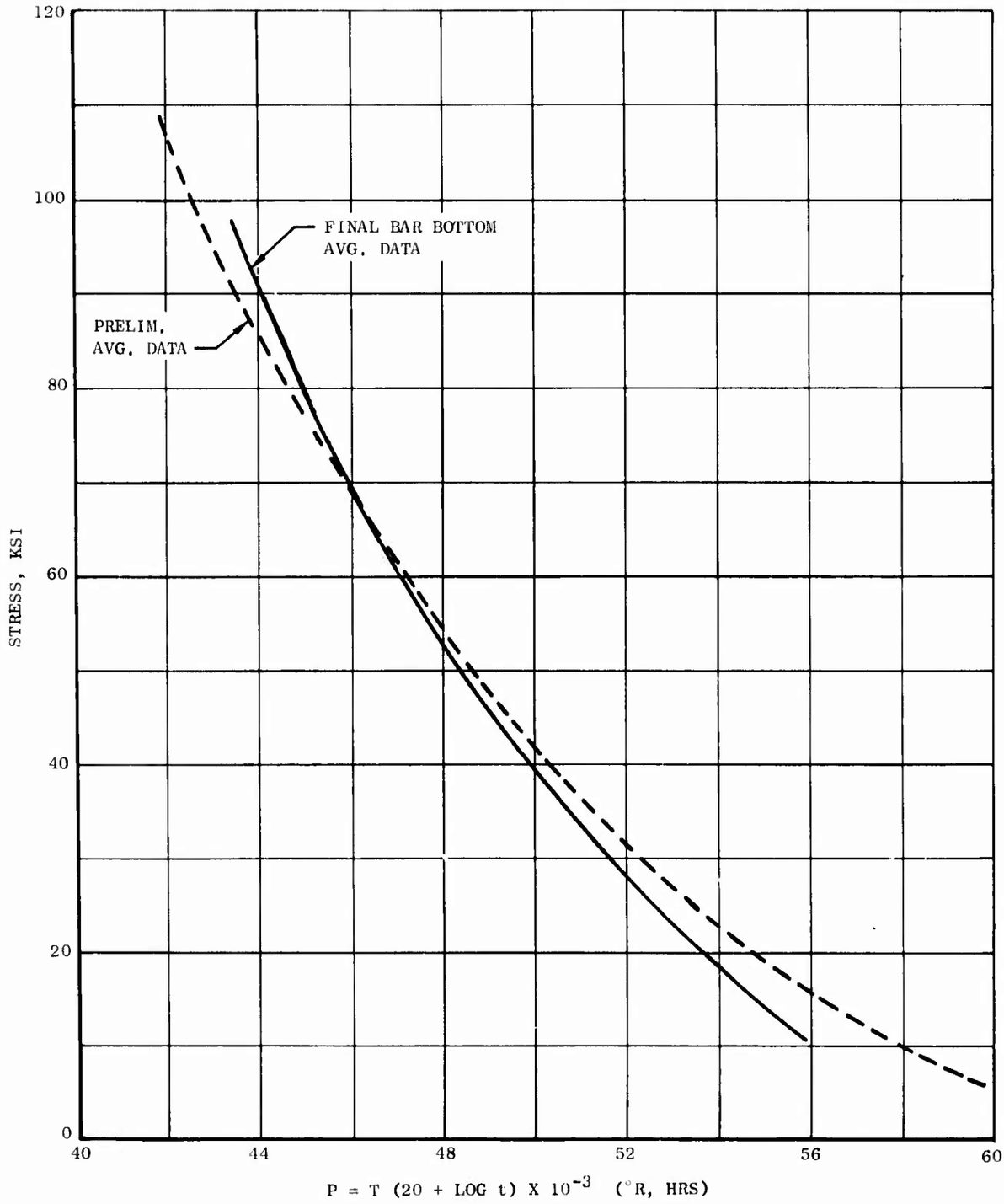

Figure 122. Comparison of Preliminary and Final Stress-Rupture Curves for NiTaC-13

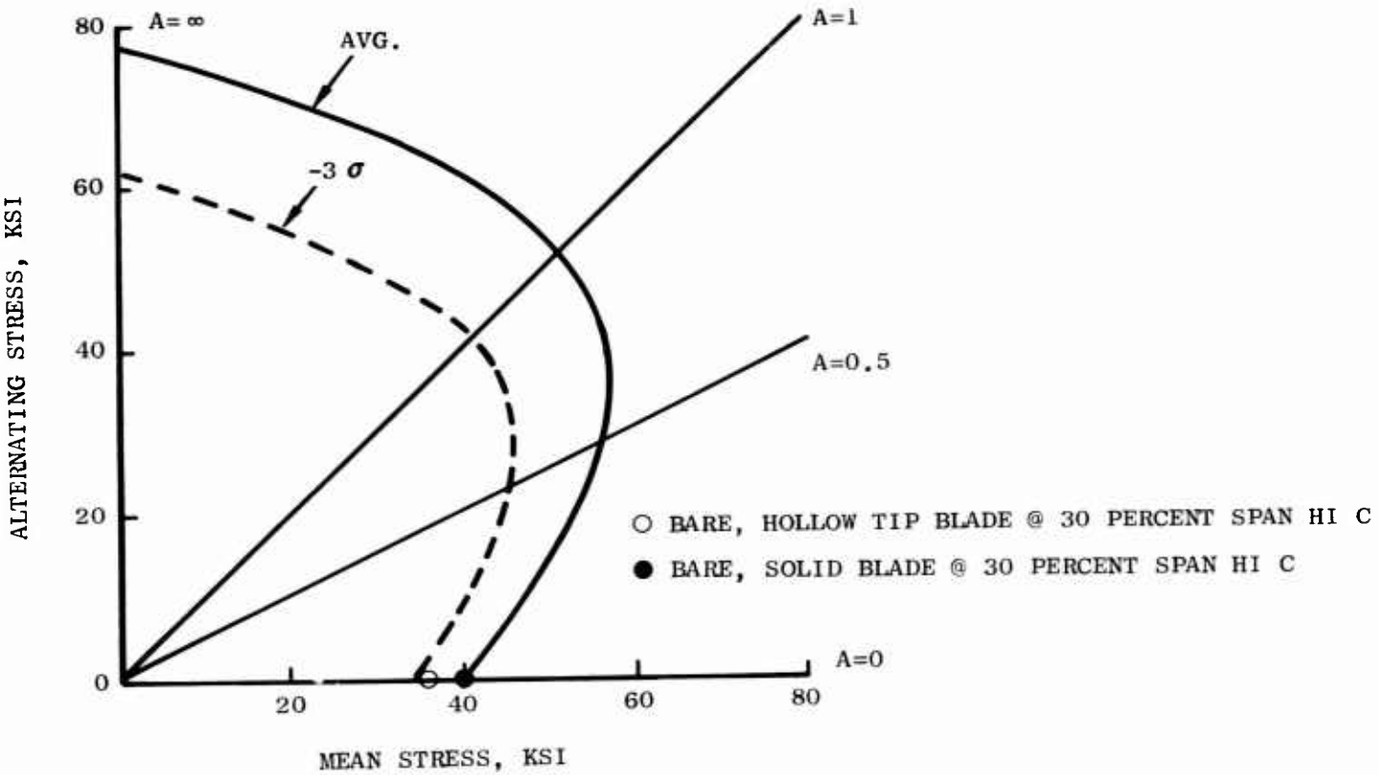

Figure 123. 1800°F/100 Hour Goodman Diagram Based on Bar Bottom Data

Thus, the HCF design criterion in Table 40 was narrowly missed by the bare hollow tip NiTaC-13 blade. However, this does not mean that these blade designs are unacceptable for engine evaluation. The HCF acceptability criterion in Table 40 was based on the requirement of 1200 mission hours for production J101 engines. For a demonstration engine test of 30 hours, proportionally less Goodman diagram capability is required. Based on the bar data in Figures 123 and 78, the bare solid blade has approximately a 40 hour Goodman diagram capability, while the bare hollow tip blade shows 80 hours HCF life. These are more than adequate lives for demonstrator engine testing, particularly when blade vibratory stresses are monitored by strain gage instrumentation to avoid blade resonances with resultant high vibratory stresses.

4.2.4 LCF Life Analysis

Turbine blades are subjected to severe thermal and stress transients, such as occur during take-off, throttle bursts, and thrust reversal during landing. These transients produce LCF conditions that are a major mode of crack initiation leading eventually to blade failure. LCF life of both the airfoil and dovetail are important considerations that are treated separately.

4.2.4.1 Airfoil - Hollow high pressure turbine (HPT) blade airfoils can be LCF limited through a combination of high thermal stresses generated by air cooling and local stress concentrations due to cooling holes or internal pin fins. General Electric experience with solid, uncooled superalloy LPT blades has shown that airfoil LCF life of such blades is not of major concern; hence, this analysis was not performed for the NiTaC-13 blade airfoil. However, consideration was given to data showing that NiTaC-13 LCF properties are superior to present superalloys while having a lower longitudinal modulus of elasticity (due to the <001> grain orientation) than conventional polycrystalline superalloys, thereby reducing stress for a given thermal strain. As a result, NiTaC-13 blade airfoils are expected to be far superior to the polycrystalline superalloy blade, and this was demonstrated both in thermal fatigue tests described in Section 3.2.8 and in a flame tunnel test to be described in Section 5.3.3.

4.2.4.2 Dovetail - This analysis was based on the detailed dovetail analysis performed for the superalloy J101 LPT blade and discussed in Section 4.1.2.2 of the preliminary analysis. Because the NiTaC-13 blade designs have the same dovetail geometry as the superalloy blade, the primary factor affecting dovetail stresses is the increased centrifugal loads of the heavier NiTaC-13 blades. Stresses in the two bare NiTaC-13 blade designs were estimated simply by multiplying all superalloy dovetail stresses, given previously in Figure 112, by the ratio of eutectic blade weight to superalloy blade weight. The results are presented in Figure 124.

LCF properties of dendritic cellular material representative of that present in NiTaC-13 blade dovetails is required to predict LCF life. The limited amount of such data, given in Figures 41 and 67, indicates that LCF strength of dendritic cellular material is about 85 percent that of aligned fiber material. This microstructural derate was applied to the SPLCF average data for aligned fiber NiTaC-13 given previously in Figure 81, and is shown in Figure 125, together with the -3σ curve for dendritic cellular material estimated as 80 percent of the average curve for dendritic cellular material. Also shown are the average and -3σ curves for the J101 LPT blade superalloy taken from Figure 115.

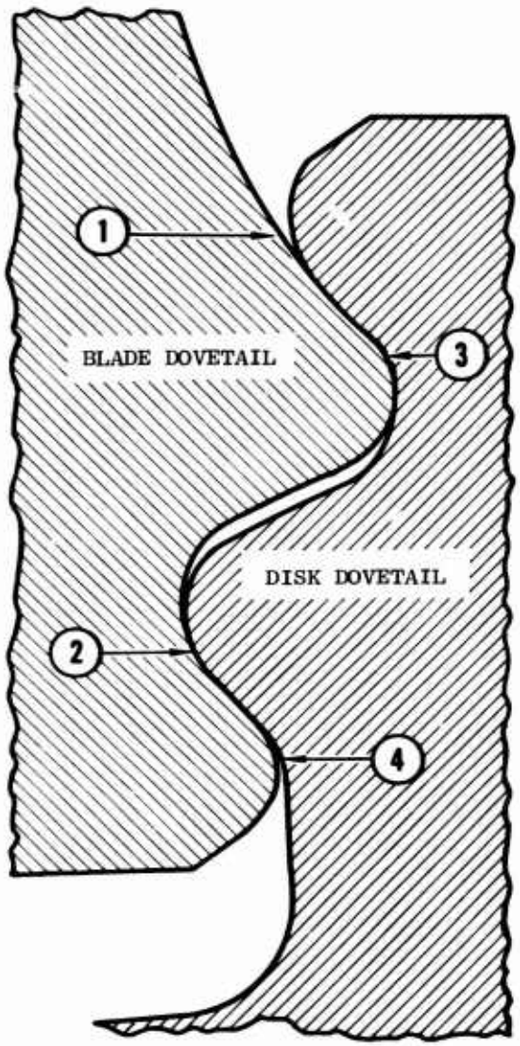

	MAXIMUM STRESS, KSI			
	1	2	3	4
COOLED SUPERALLOY: WEIGHT = 105 g				
NECK CENTRIFUGAL	58.6	33.3	39.3	41.7
TANG BEND	29.7	37.7	48.4	46.6
COMBINED	99.0	107.1	135.1	122.2
PREDICTED LCF LIFE	1.2×10^4	$\sim 10^5$	$>10^5$	$>10^5$
UNCOOLED, BARE, SOLID NiTaC-13: WEIGHT = 128 g				
NECK CENTRIFUGAL	71.4	40.6	47.9	50.8
TANG BEND	36.2	46.0	59.0	56.8
COMBINED	121.0	130.3	164.2	148.2
PREDICTED LCF LIFE	1.5×10^4	$>10^5$	$>10^5$	$>10^5$
UNCOOLED, BARE, HOLLOW TIP NiTaC-13: WEIGHT = 123 g				
NECK CENTRIFUGAL	68.6	39.0	46.0	48.8
TANG BEND	34.8	33.3	56.7	54.6
COMBINED	116.3	125.2	157.8	142.4
PREDICTED LCF LIFE	4.3×10^4	$>10^5$	$>10^5$	$>10^5$

RPM = 13,533
LCF LIFE = CYCLES TO FAILURE

Figure 124. J101 LPT Dovetail Stresses in Blade and Disk from Detailed Design Analysis

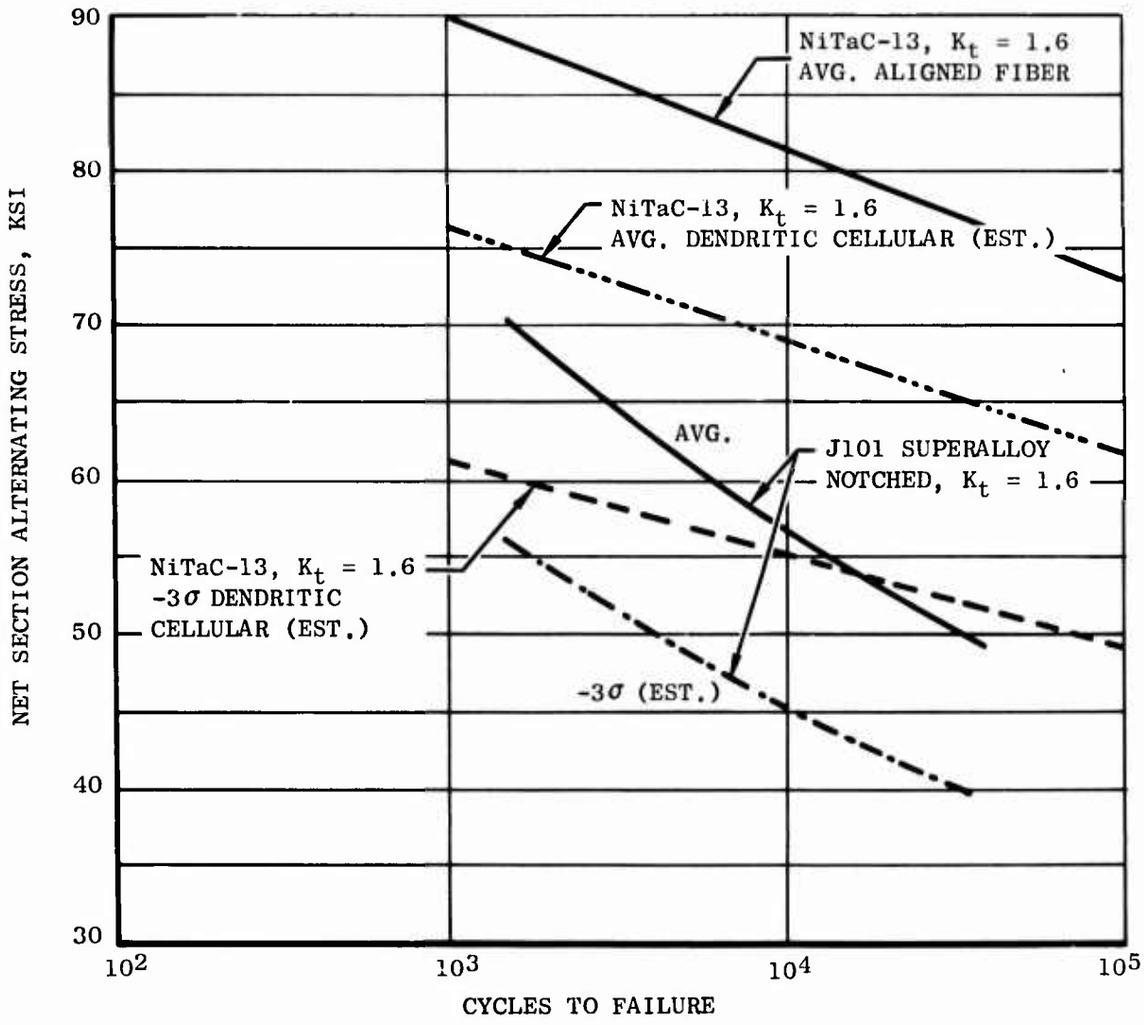

Figure 125. Final Load Controlled 1200°F Sustained Peak Low Cycle Fatigue Data (10-90-10 Second Cycle) For NiTaC-13 Compared to J101 LPT Blade Superalloy. A Ratio = 0.95.

The sums of neck centrifugal and tang bending stresses were used as the basis for LCF life prediction by the same procedures as were used in preliminary blade analysis and described in Section 4.1.3.3. The predicted LCF lives of the two bare eutectic blades, also presented in Figure 124, easily surpass the 5000 cycle criterion in Table 40, and also exceed the predicted J101 LPT blade superalloy capability.

4.3 FINAL BLADE DESIGN

On the basis of the detailed design analysis, the solid NiTaC-13 blade design selected in preliminary design analysis did not meet the final design acceptability criteria. The hollow-tip design had higher rupture life but still fell short of the goal. Coatings further reduced properties of both blade designs, primarily due to the added weight of non-load bearing material.

At this point in the program, all blades had been cast, 47 blades had been finish machined to the solid design, and 20 of the 50 blades had been coated. Further, HCF test results for blades indicated that the coating derate was substantial and that uncoated blades should be used for spin and engine tests.

It was clear that, to meet the program goals fully, it would be necessary to redesign the blade by introducing additional cavities, such as blind longitudinal holes, to reduce stresses below those in the hollow tip design. Redesign of the blade was beyond the program scope at this point, but machining of the tip cavity was a possibility; however, a vendor stated that while machining of a tip cavity was possible, it involved manufacturing complexities and the resulting risk of low blade yields.

Design and Materials personnel reviewed the data and the planned blade hardware test program, including the 30-hour engine demonstration test under consideration at that time. It was concluded that only marginal benefits would be derived by machining the blade tip cavity and that the program could be satisfactorily completed with the solid blade. Therefore, the solid blade was selected as the final design. Although both bare and coated blades were to be used in the bench test program, only bare blades would be used in the spin and engine tests.

5.0 BLADE HARDWARE EVALUATION

In the development of new turbine blade materials/designs, General Electric pursues a progression of design analysis and tests of increasing severity prior to committing to an engine test. Blade hardware evaluation is used to verify design analysis and is the last test procedure prior to engine test.

The evaluation of NiTaC-13 blade hardware included a series of six bench tests and a spin test. Two types of components tested included bare and Ni-20Cr-10Al-1Y coated solid NiTaC-13 J101 LPT blades, and Ni-20Cr-10Al-1Y coated flame tunnel specimens that simulated the blade airfoil.

The results verified the conclusion reached in design analysis that the bare solid NiTaC-13 blade had adequate properties to merit the planned 30-hour engine test. Although the blade met the LCF life goal, it fell somewhat short of the stress-rupture and HCF life goals established for the program on the basis of a 1200 hour J101 mission. The deficiencies were due to:

- Stress-rupture strength of process scale-up NiTaC-13 was somewhat lower than preliminary data;
- Blade stresses were substantially higher in the eutectic blade than in the cooled superalloy blade because of high NiTaC-13 density and insufficient weight reducing cavities;
- The Ni-20Cr-10Al-1Y coating increased blade stresses but did not produce any benefit in stress-rupture strength over the operating temperature range, and the coating reduced HCF strength substantially.

Because one NiTaC-13 blade design closely approached or met all goals, it is concluded that there is high potential for this eutectic alloy system.

Details of blade hardware evaluation are discussed in the sections that follow.

5.1 BLADE PRODUCTION

For hardware evaluation, a total of 60 acceptable blade castings were produced by the process described in Section 2.8.3.2. All blades had fully aligned fiber airfoils free of bands, and were free of arrest lines throughout. Fifty-nine blade castings were delivered to Mal Tool and Engineering of Manchester, Connecticut, for finish machining. One blade casting was used to determine dovetail properties as described in Section 2.7.5.2.

Finish machining was accomplished by hand belt grinding of the airfoil and low stress grinding of the dovetail. The finished blades were inspected by procedures described in Section 2.8.3.3. A total of three blades were dimensionally unacceptable and were not delivered to General Electric. Several of the remaining 56 blades had dimensional discrepancies or X-ray indications of carbide dendrite flaws in the tips. One blade had a small pore on the leading edge.

All deficient blades were reviewed with respect to the criticality of dimensional discrepancies and flaws to the bench, spin, and engine tests. Material flaws were not the responsibility of the machining vendor. On the basis of the review, it was decided to accept all 56 blades and to use discrepant blades in bench tests where the particular discrepancies were inconsequential.

After the blade test plan had been established, a total of 20 blades were coated by the process described in Section 4.4.2. It was initially planned to engine test six of these coated blades. Although it had been planned originally to coat at least 18 more blades, deleterious effects of the coating on HCF strength were uncovered which resulted in a decision to perform spin and engine tests with uncoated blades. Hence, no additional blades were coated.

The results of blade inspections and blade dispositions for component test are summarized in Table 44. As can be deduced from the table, the best blades were reserved for the engine test.

5.1.1 Casting Yield

Blade production began with run DB 67. After analysis of the first 20 runs, it was found that there was a high rejection rate for runs begun on Monday through Thursday, while weekend runs had a low rejection rate. Monitoring of the power input to the RF oscillator showed large voltage fluctuations at the beginning and ending of normal work days. These power fluctuations caused abrupt changes in furnace temperature and resulted in the formation of arrest lines and/or bands. Therefore, a proportional controller was designed and constructed. It was installed after the 25th run, DB 101, and thereafter no blades were rejected because of carbide defect structures.

Blade yields have been computed on the basis of both the number of runs initiated and on the number of runs completed, as follows:

	Runs Before Proportional Controller Used	Runs After Proportional Controller Used	All Runs
No. Runs Initiated	25	54	79
No. Castings Accepted	14	46	60
% Yield Based on Runs Initiated	56	85	76
No. Castings Produced	22	47	69
No. Castings Accepted	14	46	60
% Yield Based on Castings Produced	64	98	87

TABLE 44

BLADE INSPECTION RESULTS AND ALLOCATION FOR COMPONENT TESTS

Blade Numbers S/N	Blade Numbers DB	Inspection Results: Casting: Dovetail Micro	Casting: Max. Grain Intersection Angle LE	Casting: Max. Grain Intersection Angle TE	Machined: Dimensions	Machined: Blade Tip X Ray	Surface Finish
NODAL PATTERNS							
33	138	D+	0	8	A+	0	C
NODAL PATTERNS & STRAIN DISTRIBUTION							
46	140	B	0	7	A+	0	C
47	129	B	0	12	A+	0	C
TEMP. CALIBRATION FOR HCF TESTS							
13	106	A+	0	0	D	0	B
HCF - ROOM TEMP.							
3	75	C	0	10	C	0	B
9	89	D	5	0	C	0	B
11	100	C	0	0	B	0	B
HCF - ELEVATED TEMP.							
2	74	B	-	-	B	0	C
14	107	A+	0	0	C	0	C
23	116	B	-	-	C	0	C
24	123	A	-	-	B	0	C
27	142	B	0	8	A+	0	C
39	132	B	0	0	A+	0	C
41	133	B-	0	8	A+	0	C
43	125	B-	0	12	A+	0	C
44	136	D+	0	5	A+	0	C
45	147	D	0	0	A+	0	C
1	71	D+	-	-	A	S	B
4	78	C	-	-	A	S	B
5	80	D	2	0	A+	S	B
16	109	A+	0	0	A+	P	B
50	151	D+	0	5	A+	0	B
58	159	B-	0	0	A+	0	B
STEADY STATE PULL							
10	96	B+	-	-	B	S	B
26	134	C+	0	5	A+	0	C
CYCLIC PULL							
21	114	A+	0	0	B	P	B
22	115	A	0	0	C	0	B
30	130	D+	0	4	A+	0	B

Blade Numbers S/N	Blade Numbers DB	Inspection Results: Casting: Dovetail Micro	Casting: Max. Grain Intersection Angle LE	Casting: Max. Grain Intersection Angle TE	Machined: Dimensions	Machined: Blade Tip X Ray	Surface Finish
SPIN TEST							
6	83	A	0	0	D	0	B
7	85	A	0	0	A+	P	B
12	105	A+	0	5	A+	S	B
17	110	A+	0	0	C	0	B
25	124	B	0	5	A+	0	B
32	146	B-	0	0	A+	0	B
35	128	C	0	5	A+	0	B
36	126	C	0	7	A+	0	B
38	144	C-	0	0	A+	0	B
51	152	B-	0	10	A+	0	B
54	155	A-	3	5	A+	0	B
57	158	A-	0	0	A+	0	B
ENGINE TEST							
29	143	A	0	5	A+	0	B
31	135	A+	0	7	A+	0	B
34	148	A-	0	5	A+	0	B
37	141	A+	0	10	A+	0	B
52	153	A+	0	5	A+	0	B
53	154	A	0	10	A+	0	B
*15	108	A+	0	0	A	0	C
*18	111	A-	0	0	A	0	C
*19	112	A+	0	6	A+	0	C
*28	131	A-	0	0	A+	0	C
*40	149	A-	0	7	A+	0	C
*42	145	A-	0	0	A+	0	C
SPARES							
8	86	D	0	0	A+	P	B
20	113	A+	-	-	D	-	B
55	156	D	0	7	A+	P	B
56	157	D	0	0	A+	P	B

* Not to be engine tested

RATING SYSTEMS:

Dovetail Microstructure
- A - 0.4" Dendritic Cellular + Cellular
- B - 0.6" Dendritic Cellular + Cellular
- C - Same as A + 0.6" Banded
- D - 1" Dendritic Cellular + Cellular

Blade, Tip X-Ray
- O - No Carbide Dendrites
- S - Slight Dendrite
- P - Pronounced Dendrite

Dimensions
- A No Discrepancies
- B <3
- C 3-9
- D >10 or a major discrepancy

Surface Finish
- B - Bare
- C - NiCrAlY Coated

These yields were exceptionally high, due to the fact that microstructure was the primary acceptance criterion: other common reasons for rejection of DS blades, such as dimensions, surface flaws, and grain orientations did not come into play because the blades were generously oversize. From the data in Table 44, it can be seen that grain intersection angles with leading and trailing edges were generally small, and only about two blade castings may have been rejected if a 10° limit had been imposed. Final inspection of finish machined blades, however, would probably have resulted in rejection for engine use of at least six and possibly 11 blades that had carbide dendrites in the tip, thereby lowering the casting yield considerably. The carbide dendrites were not detected in the initial reviews of the X-ray radiographs of the castings; however, a re-evaluation of these radiographs confirmed the X-ray inspection results for the finished blades. The presence of carbide dendrites in blade tips was most likely due to variations in the volume of the starter block, which was a hand made wax pattern that was attached to the blade wax pattern. The carbide sort-out zone of NiTaC-13 occupies 18 percent of the initial volume of liquid metal; hence, a small reduction in the volume of the starter block would cause the sort-out zone to end in the airfoil tip. It is anticipated that the chemistry optimization of future NiTaC eutectics to eliminate the sort-out zone will greatly alleviate the carbide dendrite problem.

5.2 BLADE BENCH TESTS

Bench tests are conducted by General Electric to verify blade design analysis and to establish actual design margins. These bench tests have in the past been able to prove out new designs before actual engine operation. To prove out the solid NiTaC-13 blade, the following series of six separate bench tests were conducted:

- Blade frequency and nodal patterns - Blade resonance frequencies were determined by scanning through the frequency spectrum from 0 to about 10,000 Hz, and results were compared with analysis. Nodal patterns were determined for each resonance mode.

- Blade strain distributions - Blades were extensively covered with strain gages to determine relative strain distributions at each resonance frequency. Locations of maximum vibratory stress points for each resonance mode were combined with steady state stresses from analysis, and allowable vibratory stresses were established.

- Blade HCF tests - Blades were tested at room temperature and at engine operating temperature levels to determine the HCF capabilities. Stress concentrations due to geometry effects were established by comparison of blade test results with smooth test bar data. The results were used to adjust Goodman vibratory stress diagrams and refine blade stress limits during engine testing.

- Blade steady state dovetail pull tests - Blades were pulled in tension at room temperature, using dovetail fixtures that duplicated the disk dovetail slot, to determine the ultimate tensile strength of the blade dovetail.

- Blade cyclic dovetail pull test - Blade dovetails were tested in LCF at the engine operating temperature by using the disk dovetail fixture and cycling between the loads calculated for idle and top engine speed.

- Flame tunnel tests - Blade airfoils were evaluated for stress rupture and LCF lives under simulated engine conditions and compared with analysis predictions.

Details of the bench test program are given in the sections that follow.

5.2.1 Frequency and Nodal Patterns

Blade resonance nodal patterns were determined at room temperature for three coated blades while clamped at the dovetail. For the measurements, a small metal tab was attached to each blade tip, and the blade was then vibrated at each of its natural resonance frequencies by means of a magnetic driver. While at resonance in each of eight vibration modes, a crystal pickup was manually traced over the airfoil to find nodal lines where no vibrational movement was present. Results were very similar for all three blades. Figure 126 illustrates the nodal patterns for eight different resonance modes observed with one blade. These nodal patterns facilitated measurements of resonance frequencies of the remaining 51 blades.

Frequency tests at zero LPT rotor speed and room temperature were completed for 54 blades, and the results are presented in the Campbell diagram of Figure 127. Also shown for each resonance frequency are the measured ranges in frequencies for the 54 blades. No effect of the coating on blade resonance frequencies was observed. In Figure 127, the results have been projected to 100 percent LPT rotor speed using slopes determined in the orthotropic MASS computer program. A comparison of measured blade frequencies with those calculated using both the TWISTED BLADE and the orthotropic MASS computer programs is shown in Table 45. It should be recalled that only estimated values of longitudinal and transverse elastic properties (G, and μ) were available for the computations. Orthotropic MASS was expected to provide more accurate results than TWISTED BLADE because it is a more complete analysis. As shown in Table 45, there was excellent agreement between measured resonance frequencies and those computed by orthotropic MASS for the first three vibrational modes: first flex, first axial, and second flex. However, the fourth vibrational mode, first torsion, showed a large discrepancy of 35 percent which indicated that the longitudinal shear modulus estimated for NiTaC-13 was too low. For the last four vibrational modes, the agreement between measured and calculated frequencies was good.

In view of the consistency of the test data for all 54 blades, it was concluded that the experimentally based Campbell diagram in Figure 127 presents the best available vibration evaluation of the NiTaC-13 J101 LPT blade. No resonance problems at 100 percent LPT rotor speed are indicated; however, an engine test is required to verify this under hot engine environmental conditions.

5.2.2 Strain Distribution

Two coated blades were used for these measurements, S/N 46 and 47. Each had 84 strain gages attached to the airfoil and dovetail shank surfaces at critical locations illustrated in Figure 128. Strain measurements were made with each blade clamped at the platform

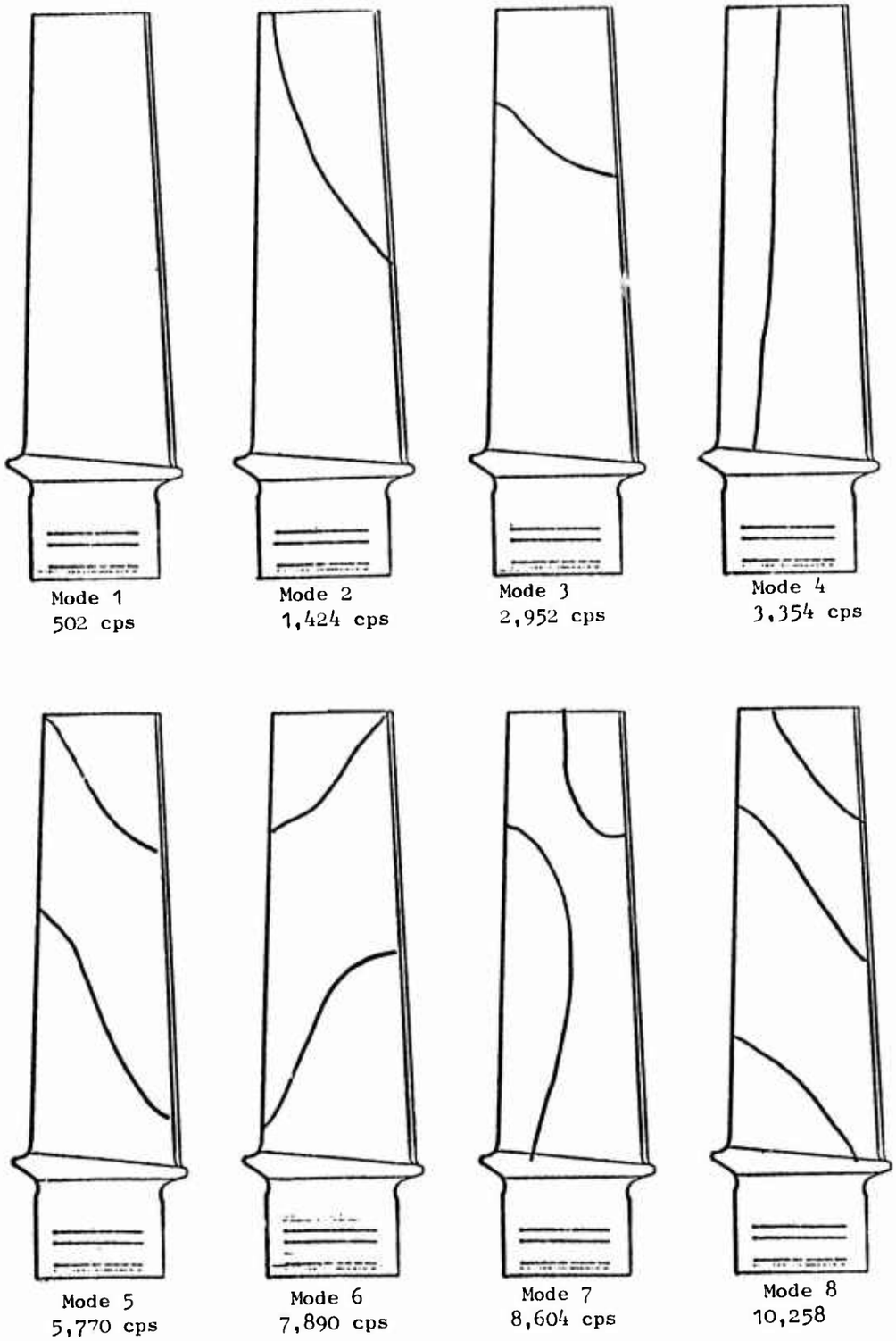

Figure 126. Nodal Patterns for Eight Resonance Frequencies of Ni-20CR-10Al-1Y Coated Solid NiTaC-13 J101 LPT Blades, Clamped at Dovetail

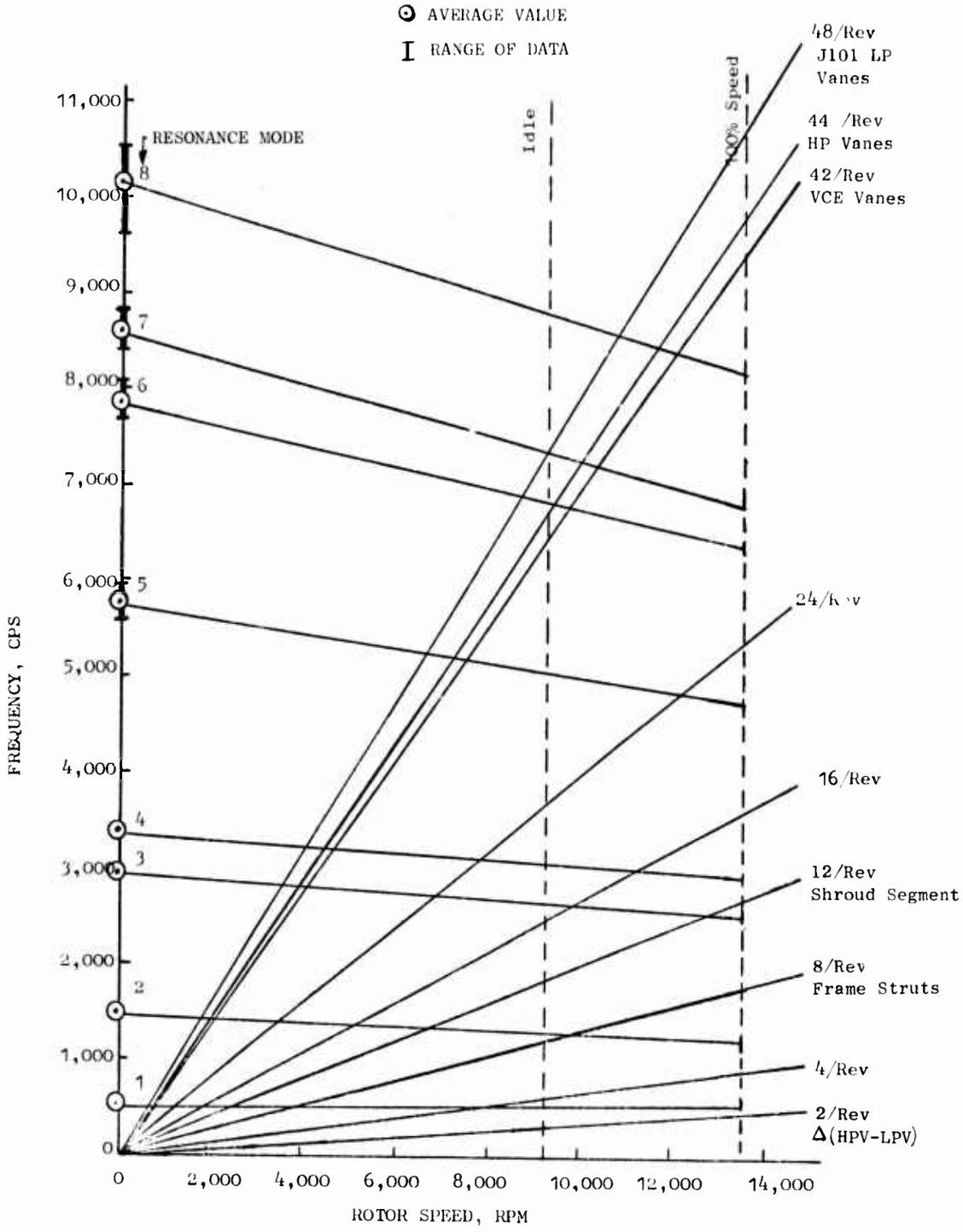

Figure 127. Blade Resonance Frequency Test Results at Zero Rotor Speed and Room Temperature for A Total of 54 Bare and Coated Solid NiTaC-13 J101 LPT Blades, and Estimated Campbell Diagram

TABLE 45

MEASURED AND CALCULATED ROOM TEMPERATURE RESONANCE FREQUENCIES FOR 45 NiTaC-13 J101 LPT BLADES, COATED AND UNCOATED

Vibration Mode		Resonance Frequencies, cps				% Deviation of MASS From Measured Frequencies
		Calculated*		Measured		
No.	Type	TWISTED BLADE	Orthotropic MASS	Avg.	Range	
1	First Flex	527	524	502	493/518	+4
2	First Axial	1,732	1,549	1,443	1,404/1,504	+7
3	Second Flex	2,270	3,171	2,958	2,862/3,040	+7
4	First Torsion	3,458	2,195	3,370	3,312/3,488	-35
5	-------	5,546	5,084	5,740	5,606/5,948	-12
6	-------	6,970	7,143	7,840	7,702/8,086	-9
7	-------	7,962	8,794	8,594	8,402/8,812	+2
8	-------	10,504	9,908	10,200	9,600/10,500	+3

* Using the following physical properties:

	Long.	Trans.
Elastic Modulus x 10^{-6} psi	21.6	31.8
Shear Modulus x 10^{-6} psi (Est)	7.77	13.9
Poisson's Ratio (Est)	0.14	0.39

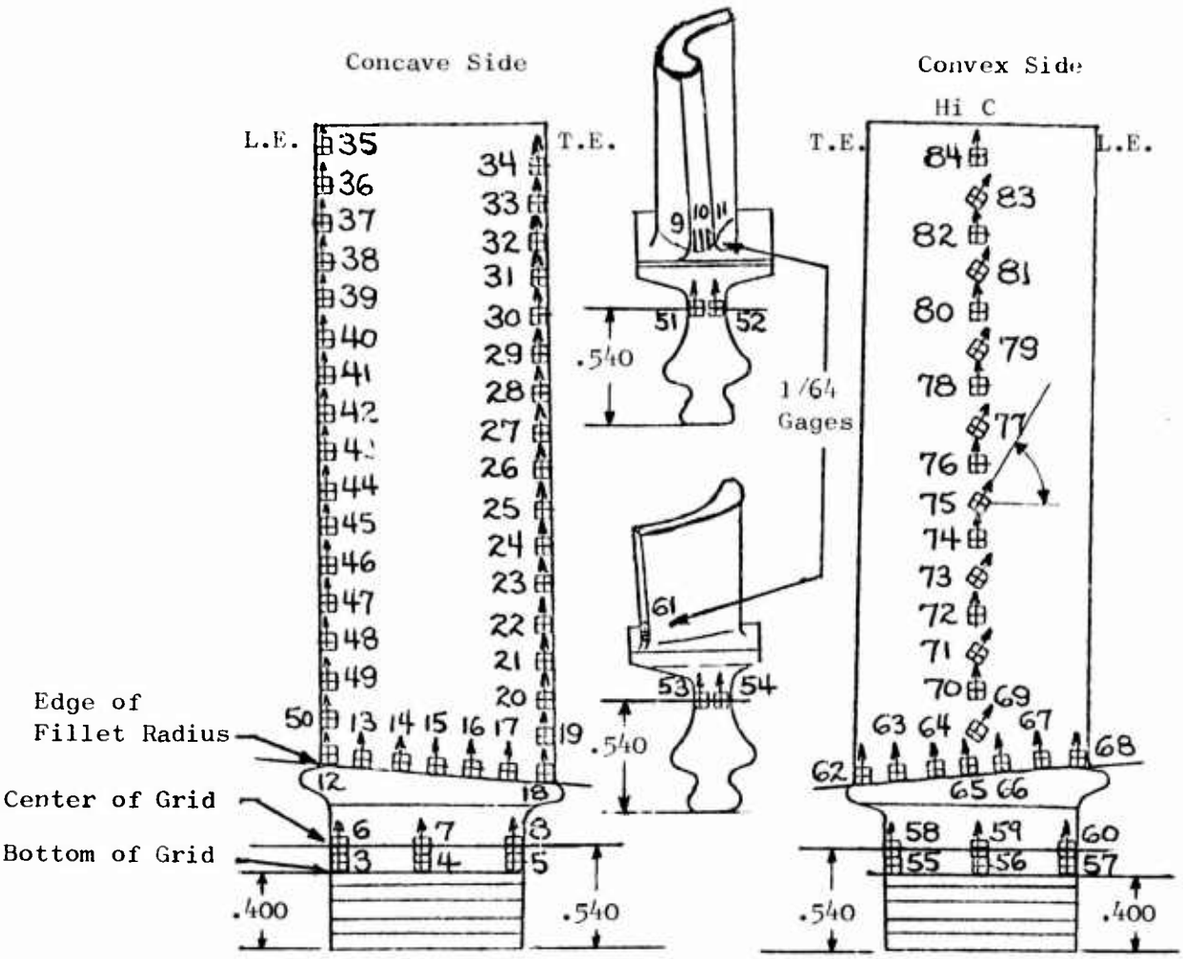

NOTES: 1. Gages are .050" except where noted.

2. Leads are 36 gage teflon, 5 ft. long with copper splice.

3. Gages are equally spaced at root and .2" at L.E., T.E., and Hi C.

Figure 128. Strain Gage Positions for Measurement of Blade Strain Distributions

and then at the dovetail. By means of an air siren, the blades were excited at room temperature to each of the eight resonance frequencies previously observed. Amplitudes were kept sufficiently low to avoid failure by HCF, and strains were measured in all 84 locations. The results were used subsequently to set stress levels in HCF tests of blades.

Strain measurements for the two blades, clamped at the platform and resonated in the first flex mode, were normalized to the maximum observed strain, and the results are presented in Table 46. Similar data were obtained for the seven other resonance frequencies. By comparing results for the two blades in Table 46, it can be seen that there was appreciable scatter which may have been due to small differences in strain gage locations and/or blade dimensions and material. The maximum alternating strain (100%) observed was at gage 50 (leading edge) for blade S/N 46, and at gage 19 (trailing edge) for blade S/N 47. Evaluation of average results for the two blades shows that there were four regions of high strain, as shown in Table 47. These were all potential failure sites while in Mode 1 resonance.

5.2.3 High Cycle Fatigue Tests

A total of 13 HCF tests were initially planned, including three bare blades at room temperature and 10 coated blades at elevated temperature. When the 10 coated blade test results were found to be uncomfortably low, additional high temperature tests of six bare blades were performed.

For elevated temperature tests, in which the specimens were heated inductively, it was first necessary to establish the RF power requirements to achieve the desired temperature. This was accomplished with a calibration blade, instrumented with 14 thermocouples at positions illustrated in Figure 129. This figure also shows the results of temperature measurements under conditions used for the two test temperatures, 1400° and 1600°F. As indicated in Figure 129, the blade test region just above the platform (thermocouples 4, 5, and 13) had nearly uniform temperatures from leading to trailing edges at both test temperatures. There were, however, substantial spanwise temperature gradients.

All test blades were instrumented with a strain gage at position 65 (Figure 128) and blades for elevated temperature tests were also instrumented with a thermocouple at position 14 (Figure 129). To prevent test failures in the blade shank region where elevated temperatures were not attainable, each blade was clamped at both the dovetail and the platform. In the strain calibration, each blade was driven in the first flex resonance frequency (Mode 1) at room temperature by means of a shake table. During excitation, tip deflection was measured using a proximity probe, and a calibration of tip deflection versus alternating strain at gage position 65 was established. Alternating stresses were computed by multiplying the alternating strain by the value of Young's modulus at the test temperature. In all tests, the A ratio (alternating stress/mean stress) was ∞. The proximity probe was then used in all tests to measure and automatically control blade tip deflection, hence stress, through feedback to the power supply for the shake table. Each blade was tested in the first resonance mode at pre-selected stress levels until crack initiation occurred as indicated by a sudden shift in blade frequency that shut off the equipment, or until it completed 10^7 cycles without crack initiation.

TABLE 46

STRAIN DISTRUBITION MEASUREMENTS AT FIRST-FLEX RESONANCE FREQUENCY FOR TWO COATED SOLID NiTaC-13 J101 LPT BLADES CLAMPED AT PLATFORM

Gage Position No.	*Relative Strain, % Blade S/N 46	Blade S/N 47	Gage Position No.	*Relative Strain, % Blade S/N 46	Blade S/N 47	Gage Position No.	*Relative Strain, % Blade S/N 46	Blade S/N 47
3	12	11	30	14	15	57	27	- 1
4	0	0	31	8	6	58	-44	-10
5	3	-13	32	4	4	59	-36	-28
6	46	33	33	0	0	60	- 3	-12
7	28	9	34	0	0	61	19	47
8	30	9	35	0	0	62	25	13
9	47	51	36	2	1	63	- 3	- 4
10	57	68	37	5	4	64	-47	-52
11	81	69	38	9	9	65	-75	-77
12	93	72	39	15	14	66	-79	-63
13	65	50	40	21	20	67	-47	-26
14	49	40	41	28	20	68	23	30
15	44	31	42	30	33	69	-53	-49
16	48	43	43	41	37	70	-76	-70
17	48	58	44	47	43	71	-47	-39
18	43	69	45	54	41	72	-62	-47
19	93	100	46	43	58	73	-34	-24
20	94	88	47	72	67	74	-48	-49
21	72	72	48	77	71	75	-28	-27
22	77	73	49	93	79	76	-34	-37
23	62	72	50	100	88	77	-19	-22
24	60	59	51	7	- 3	78	-23	-25
25	50	52	52	36	27	79	- 7	-12
26	38	43	53	13	6	80	-12	-13
27	33	34	54	-28	- 7	81	- 2	- 5
28	27	28	55	-30	0	82	- 3	- 5
29	22	22	56	-10	- 8	83	0	0
						84	0	0

Resonance Frequency: S/N 46 = 651 Hz, S/N 47 = 683 Hz

* Negative numbers show locations of compression when locations with positive numbers are in tension

TABLE 47

REGIONS OF HIGHEST STRAIN IN COATED SOLID NiTaC-13 BLADES
WHILE IN MODE 1 RESONANCE AND CLAMPED AT PLATFORM

Blade Location	Gage No.	Percent Relative Strain		
		Blade S/N 46	Blade S/N 47	Avg.
Trailing Edge	19	93	100	96.5
	20	94	88	91
	21	72	72	72
	22	72	73	75
Leading Edge	50	100	88	94
	49	93	79	86
	48	77	71	74
Leading Edge & Airfoil Root	12	93	72	82.5
	11	81	69	75
Hi C and Airfoil Root	65	75	77	76
	66	79	63	71

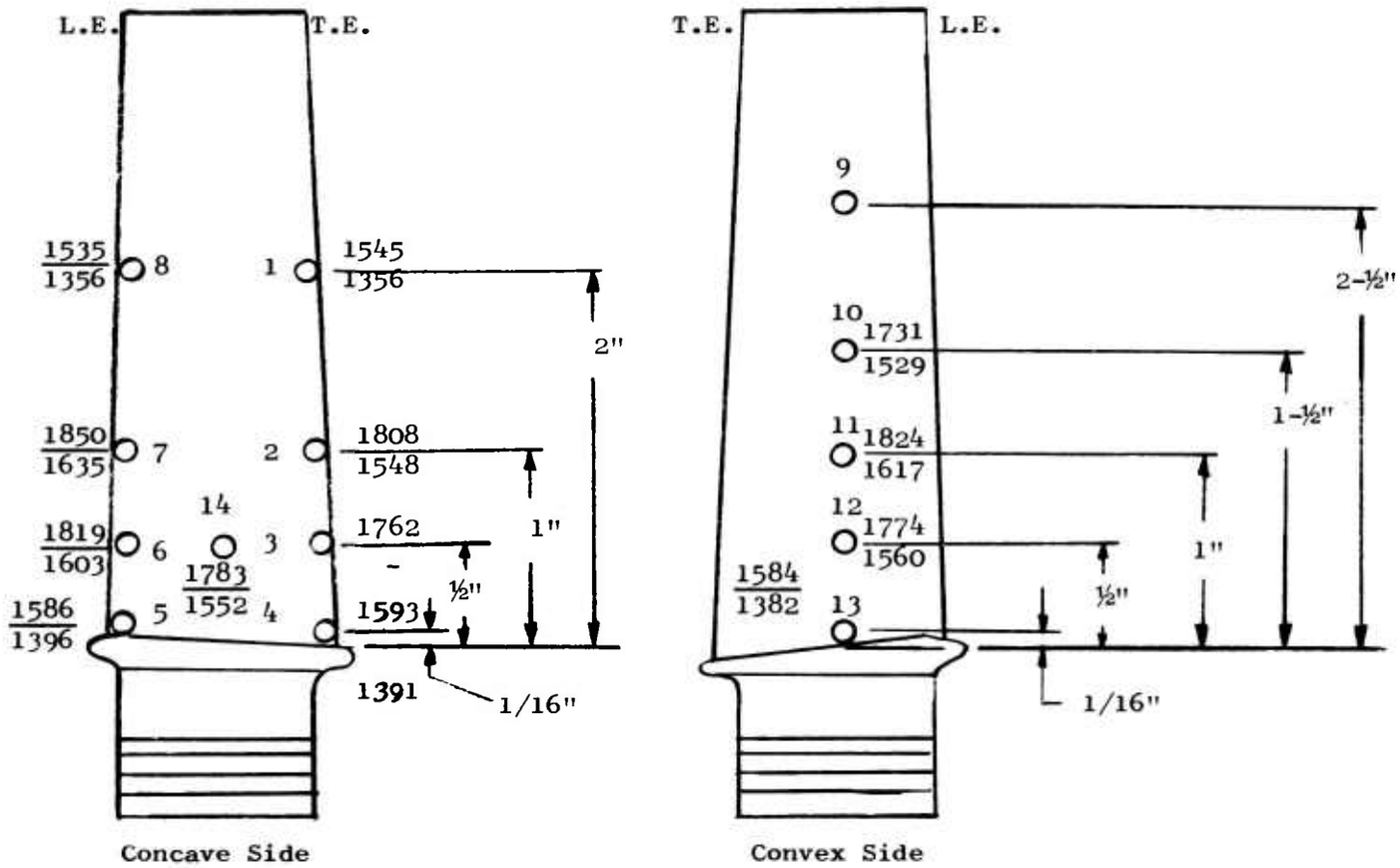

Figure 129. Thermocouple Positions and Results of Temperature Measurements in 1600°F (Numerator) and 1400°F (Denominator) Test Set Ups

All test results are summarized in Table 48 and the locations of the fractures in all failed blades are shown in Figure 130. As illustrated in the figure, all cracks initiated in the four regions of high strain (and stress) shown in Table 47. Generally, there was only one major crack in the blades tested to crack initiation.

A cursory inspection of the data in Table 48 shows that the coated blades had much lower 10^7 cycle fatigue strengths than bare blades. To evaluate blade capabilities in more detail, 100-hour Goodman diagrams were estimated on the basis of blade HCF test results and test bar data given previously in Figure 82. The estimated 1400° and 1600°F Goodman diagrams are shown in Figures 131 and 132, respectively. Minus three standard deviation (-3σ) curves for blades were constructed through points calculated for A ratios of ∞, 1, and 0.5 on the assumption that the -3σ alternating stresses were 80 percent of the average values at the corresponding A ratios.

It can be seen in Figures 131 and 132 that blade test results were considerably lower than would be predicted from test bar data, and that coated blades had substantially lower HCF strengths than bare blades. These points are illustrated more clearly by the data for $A = \infty$ presented in Table 49. Here it is shown that the coating reduced the 10^7 cycle fatigue strength of bare NiTaC-13 bars and blades by about 50 percent at 1400°F and about 36 percent at 1600°F. It is also shown that both bare and coated blades had 30 percent lower 10^7 cycle fatigue strengths at both 1400° and 1600°F than corresponding bar material. The reasons why blade HCF strengths are lower than test bars are presumed due to one or more of the following factors:

1) Peak blade stresses in HCF tests could be higher than measured because strain gages may not have been at optimum positions for strain distribution measurements and because the gages average strain over a finite area;

2) Machining and material defects may be more severe in blades than in bars;

3) Unmeasured notch effects may be operative: many blades failed at the Hi C root fillet radius.

4) The frequency in the blade tests was substantially higher than that used in bar tests, approximately 500 versus 30 Hz, respectively. HCF fatigue strength of nickel-base superalloys is known to decrease with increasing frequency.[13] Because the bench test simulates the blade resonance frequency in an engine, the bar test data tends to overestimate component HCF strength.

In an effort to explain partially the discrepancy between NiTaC-13 blade and bar data, an additional test was run on blade S/N 8 to determine if a significant steady state stress was imposed in the most common blade failure region, the Hi C fillet, due to the dovetail and platform clamping method. This blade was instrumented with one strain gage at the Hi C fillet tangency point. The measured mean stress was less than 3 ksi, too low to affect HCF results. It was, therefore, concluded that factors such as those discussed previously were responsible for the blade and bar discrepancies.

A more detailed analysis of the bare solid NiTaC-13 blade allowable vibratory stresses for engine test, based on blade HCF test results, was performed by the following steps:

TABLE 48

HCF TEST RESULTS FOR BARE AND Ni-20Cr-10Al-1Y COATED SOLID NiTaC-13 J101 LPT BLADES CLAMPED AT DOVETAIL AND PLATFORM, AND TESTED IN FIRST RESONANCE MODE

Blade S/N No.	*Estimated Max. Alt. Stress, Ksi	Cycles To Crack Initiation X 10^{-6}	Failure Location
Room Temperature, Bare			
3	166	Failed on Loading	T.E.
9	116	0.034	Hi C Fillet & L.E.
11	87	0.119	L.E.
1600°F, Coated			
2	38.4	> 10.	-
2	43.0	0.211	Hi C Fillet
24	38.4	> 10.	-
23	43.0	0.372	Hi C Fillet
41	38.4	> 10.	-
43	43.0	0.994	Hi C Fillet
1400°F, Coated			
39	37.7	> 10.	-
39	42.4	> 1.	-
39	47.2	0.629	T.E.
14	42.4	0.450	T.E.
27	37.7	0.878	Hi C Fillet
44	32.9	> 10.	-
45	37.7	> 10.	-
1600°F, Bare			
1	78.7	~ 0.001	Hi C Fillet
4	54.9	> 10.	-
4	61.8	5.7	Hi C Fillet
50	58.3	> 10.	-
50	65.2	0.19	Hi C Fillet
1400°F, Bare			
5	50.2	> 10	-
5	56.7	> 10	-
5	63.2	9.9	T.E.
16	63.2	> 10	-
16	69.7	0.71	Hi C Fillet
58	63.2	> 10	-
58	69.7	1.6	Hi C Fillet

* A ratio (alternating stress/mean stress) = ∞

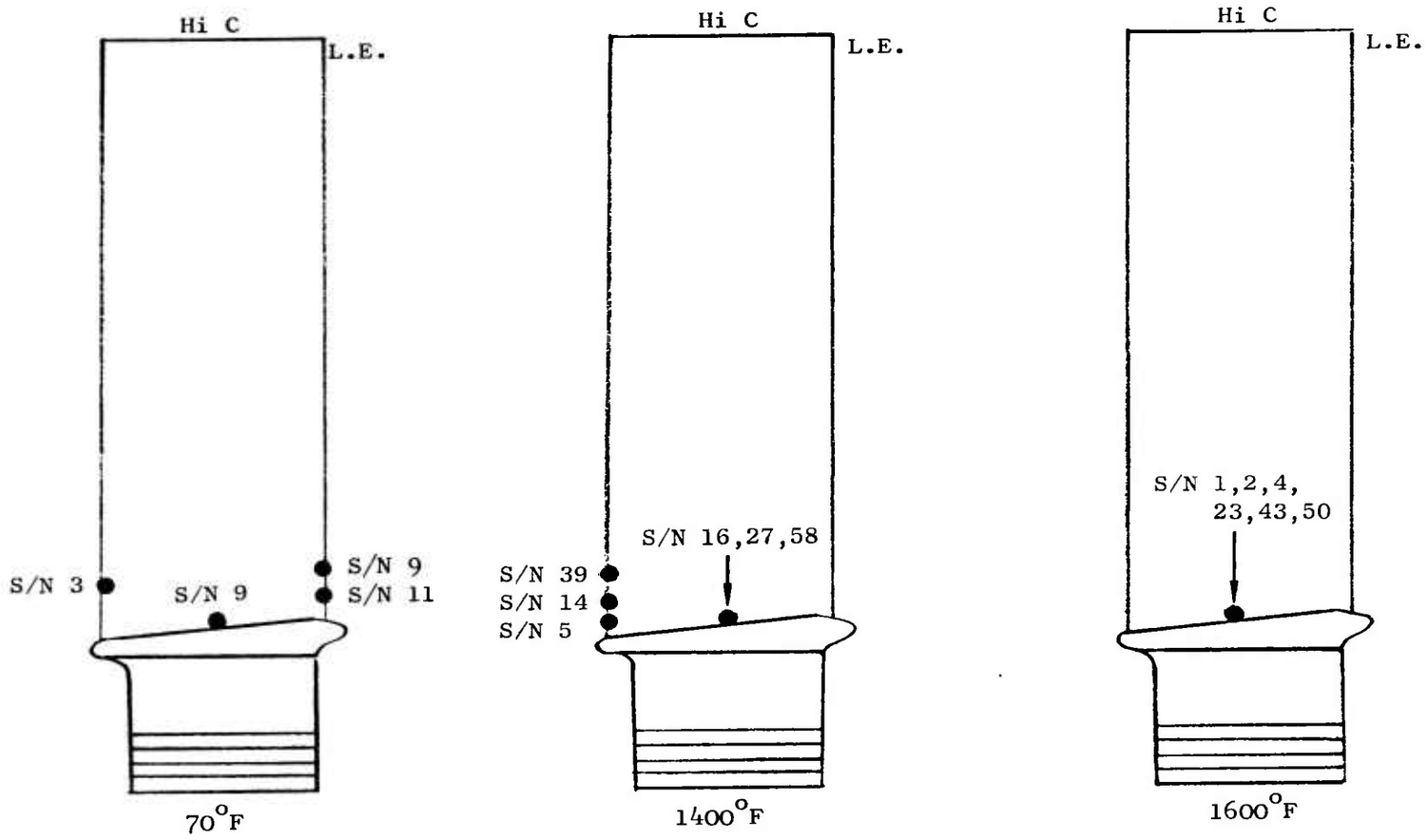

Figure 130. HCF Test Failure Locations in Bare and Coated Solid NiTaC-13 J101 LPT Blades

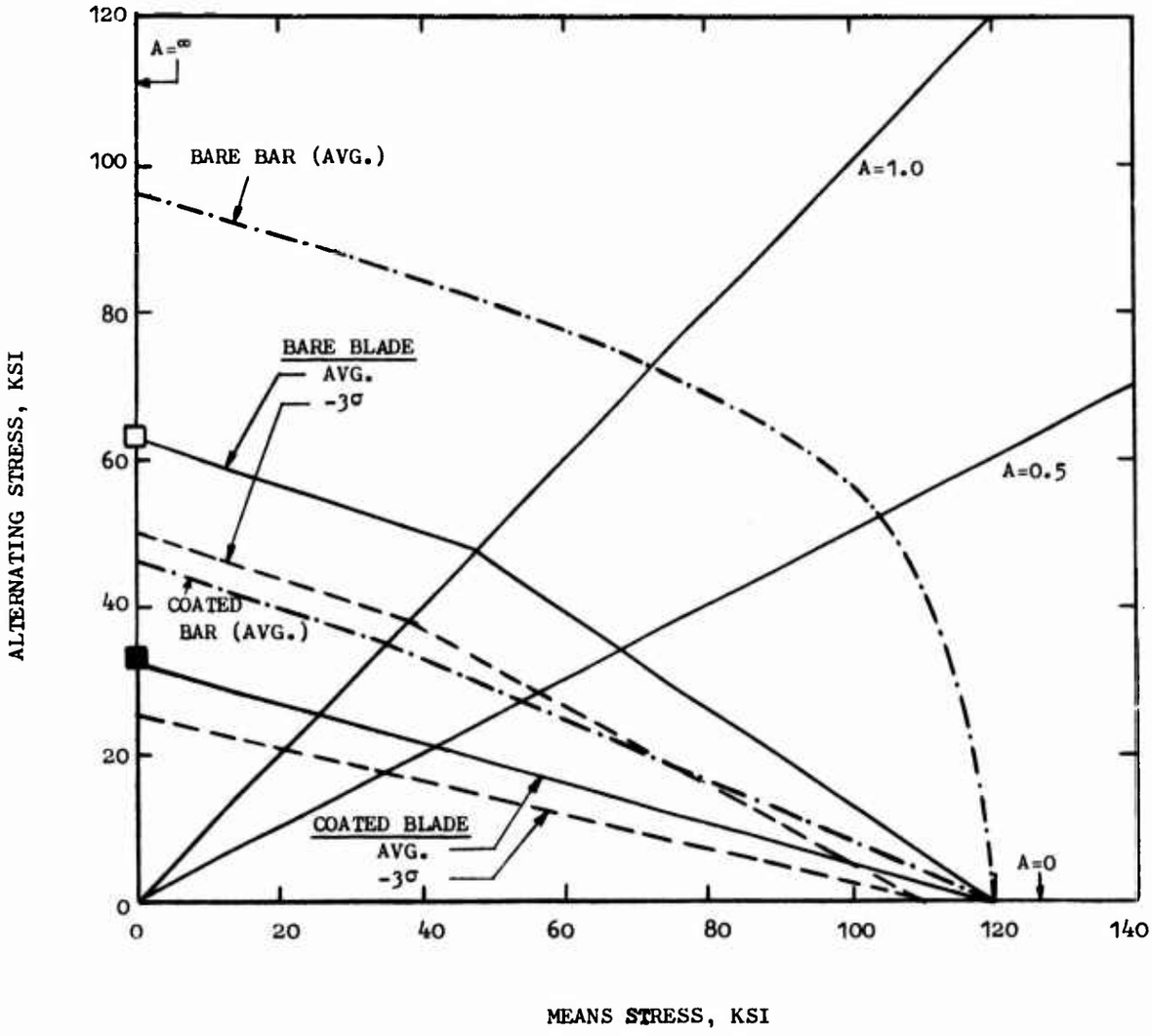

Figure 131. 1400°F/100-Hour Goodman Diagrams for Longitudinal NiTaC-13 Bars and Blades, Bare and Coated

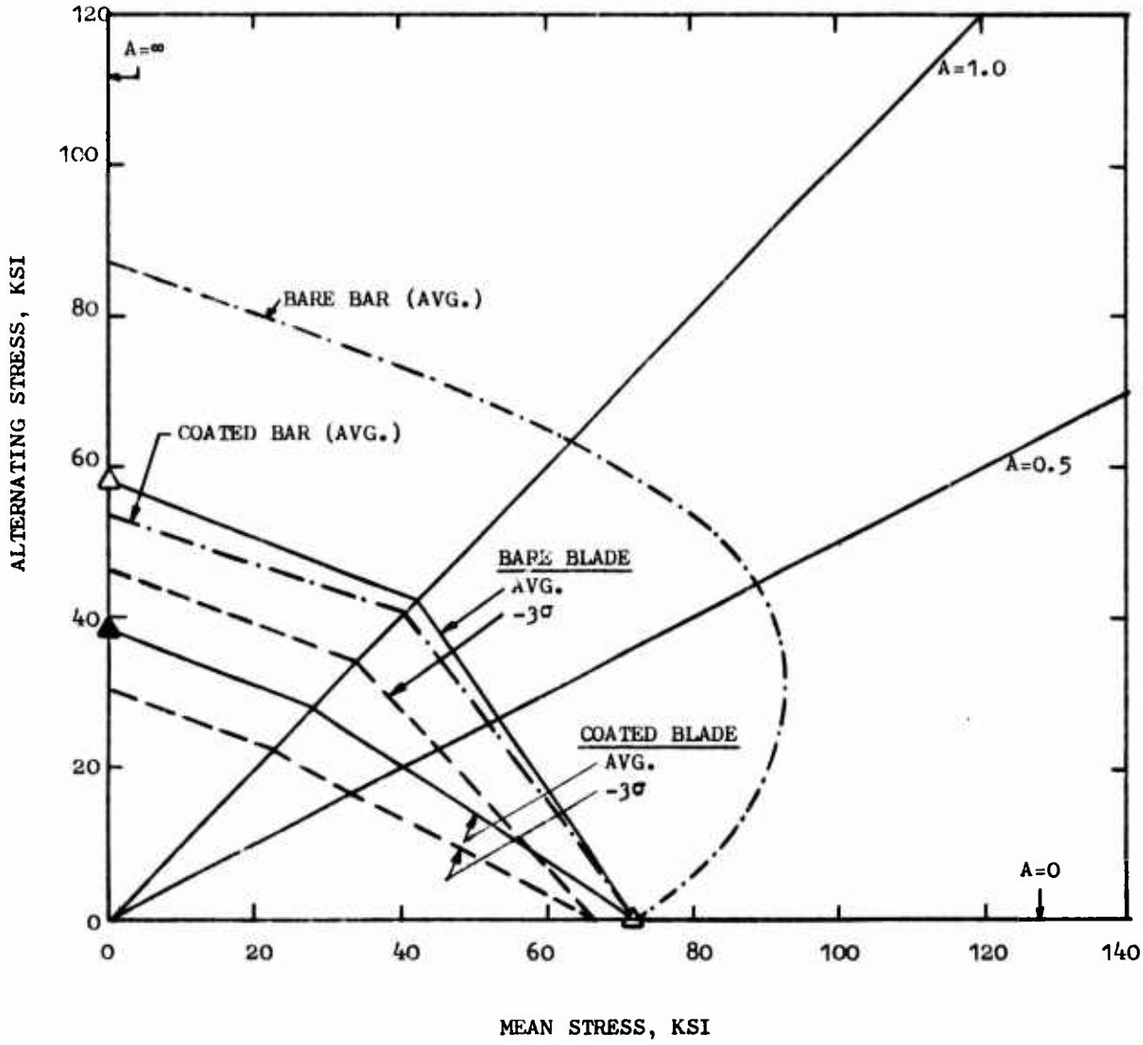

Figure 132. 1600°F/100-Hour Goodman Diagrams for Longitudinal NiTaC-13 Bars and Blades, Bare and Coated

TABLE 49

COMPARISON OF HCF TEST RESULTS FOR BARE AND COATED NiTaC-13 BLADES AND BARS

	10^7 Cycle HCF Strength, Alternating Stress in Ksi		Blade Geometry Derate, %
	Test Bar	Blade	
1400°F Results			
Uncoated	96	63.2	-34
Coated	46	32.9	-28
Coating Derate, %	-52	-48	-
1600°F Results			
Uncoated	86	58.3	-32
Coated	54	38.4	-29
Coating Derate, %	-37	-34	-

* A ratio (alternating stress/mean stress) = ∞

+ Average properties

1) For each of the resonance modes and the two clamping positions, tables were made up to show the following calculation results for each of the 84 strain gage positions.

   - resultant spanwise stress (mean stress) from Figure 121
   - steady state bulk metal temperatures from TRANSIENT HEAT TRANSFER

2) Average property 100-hour Goodman diagrams for the bare solid blade over the temperature range (in 100°F intervals) covered by step 1 above, were estimated by applying the 30 percent derate for blades to the bare bar data of Figure 82 at $A = \infty$ and 1.0. For A = 0, the mean (stress rupture) strengths of bars and blades were assumed equal on the basis of the excellent flame tunnel rupture test results to be described in Section 5.3.2. At lower temperatures such as 1200° and 1400°F, it was necessary to use ultimate tensile strength for estimating stress-rupture strength. The -3σ curves were constructed as 80 percent of the average blade curve for $A = \infty$ and 1.0, and equal to the -3σ bar strength at A = 0.

3) Using the -3σ 100-hour Goodman diagrams of step two, and the mean stress and bulk metal temperature from step one, the allowable vibratory stress was estimated for each gage position described in step one.

4) To establish the most probable blade failure location for each resonance frequency and clamping method, the ratio of relative strain distribution to allowable alternating stress was determined for each gage position. The highest ratio is the most probable failure site.

5) The estimation of the maximum allowable alternating stress was refined by constructing 100-hour Goodman diagrams for the exact temperature of each limiting gage position.

As a result of this analysis, it was found that the bare solid blade did not have 100-hour Goodman diagram capability, confirming the result of design analysis. The most limiting gage position was number 72 where the mean stress was 44 ksi and the bulk metal temperature was 1760°F. By inspection of the data given previously in Figure 82, it can be seen that the bare solid blade does not have 100-hour Goodman diagram capability.

The primary reason for failing to meet 100-hour Goodman diagram capability, which preliminary blade design had predicted could be met, is that the blade stress determined for the life limiting section was calculated to be much higher in detailed blade analysis than that used in preliminary analysis.

For the planned 30 hour engine demonstration test of the NiTaC-13 J101 LPT blade, a 10-hour Goodman diagram capability is more than adequate. Prediction of this capability would be based on 10 hours at the most extreme conditions of temperature and stress; but in the engine test, the time at these peak conditions will be substantially less than 10 hours.

Therefore, to determine the 10-hour Goodman diagram capabilities of the bare solid blade, the analysis described previously was repeated using estimated 10-hour Goodman diagrams. In this analysis, however, it was essential to incorporate 1200°F stress-rupture

and HCF strength data for dendritic cellular material, typical of material present in the shank section of all blades cast in the program. Stress-rupture properties at 1200°F for use in construction of a 10-hour Goodman diagram were estimated from data in Figures 36, 37, and 38. HCF data from Section 2.6.2.5 are presented in Figure 133 and are compared with data for aligned fiber NiTaC-13 from Table A-6 of Appendix A. As shown in Figure 133, the 1200°F HCF strength of dendritic cellular material is substantially below that of aligned fiber material. A straight line extrapolation was used to estimate the alternating stress for 10^6 cycles to failure, which is equivalent to 10 hours of life. The results for all resonance modes and two dovetail clamping positions, presented in Table 50, show: the life limiting gage position; the accompanying bulk metal temperature and mean stress, and; the maximum allowable alternating (vibratory) stress determined from the 10-hour Goodman diagram. As shown in Table 50, allowable vibratory stresses are sufficiently high to conclude that the bare blade is adequate for the planned engine test.

5.2.4 Steady State Dovetail Pull Test

These tests were performed to test the strength of the shank and dovetail region of the blade. To facilitate the test, a large portion of the airfoil was brazed into a machined split block that was used to load this end of the blade. Prior to brazing, a 3/8 inch diameter hole was machined through the block and airfoil, and an alignment pin was inserted. A special dovetail block was machined from Rene' 95 and used to load this end of the blade. Load was applied through the airfoil and dovetail blocks. Initially, 10 strain gages were attached to the dovetail shank section and used to align the blade with the load axis, thereby minimizing bending stresses in the dovetail region.

Two blades, S/N 10 and S/N 26, were pulled to failure at room temperature. Blade S/N 10 fractured at a load of 22,000 pounds in the blade airfoil region containing the hole for the fixture alignment pin, as illustrated in Figure 134A. This was unexpected and caused by poor braze coverage of the airfoil, which was not detectable by visual examination before test. Blade S/N 26 failed in the dovetail shank, illustrated in Figure 134B, at a load of 25,500 pounds. For both test blades, the calculated maximum stresses at the airfoil root and dovetail shank sections at failure are given in Table 51 where they are also expressed as a percentage of the room temperature ultimate tensile strength of aligned fiber NiTaC-13. Other data shown in Table 51 include the temperatures and stresses in blade sections for J101 design point conditions, and the estimated blade section strengths at the design point temperatures. The latter were calculated on the basis of the ultimate tensile strength of aligned fiber NiTaC-13 at the indicated temperatures multiplied by the percent of UTS obtained in the room temperature tests. Finally, the table shows the estimated percentages by which the various section ultimate tensile strengths exceeded the design point stresses. As shown in Table 51, the estimated strength of the dovetail shank section exceeded the design point stress by at least 62 percent, which is a very satisfactory margin.

It is to be noted in Table 51 that failure occurred in the shank section of blade S/N 26 at a stress lower than that in the airfoil. This was presumed to be due to the dendritic cellular microstructure of the shank versus the aligned fiber microstructure of the airfoil. As discussed in Section 2.6.2.2, the 1200°F ultimate tensile strength of dendritic cellular material from bars was about 15 percent less than that of aligned fiber material. However, the failure stress in the shank of blade S/N was about 25 percent less than the

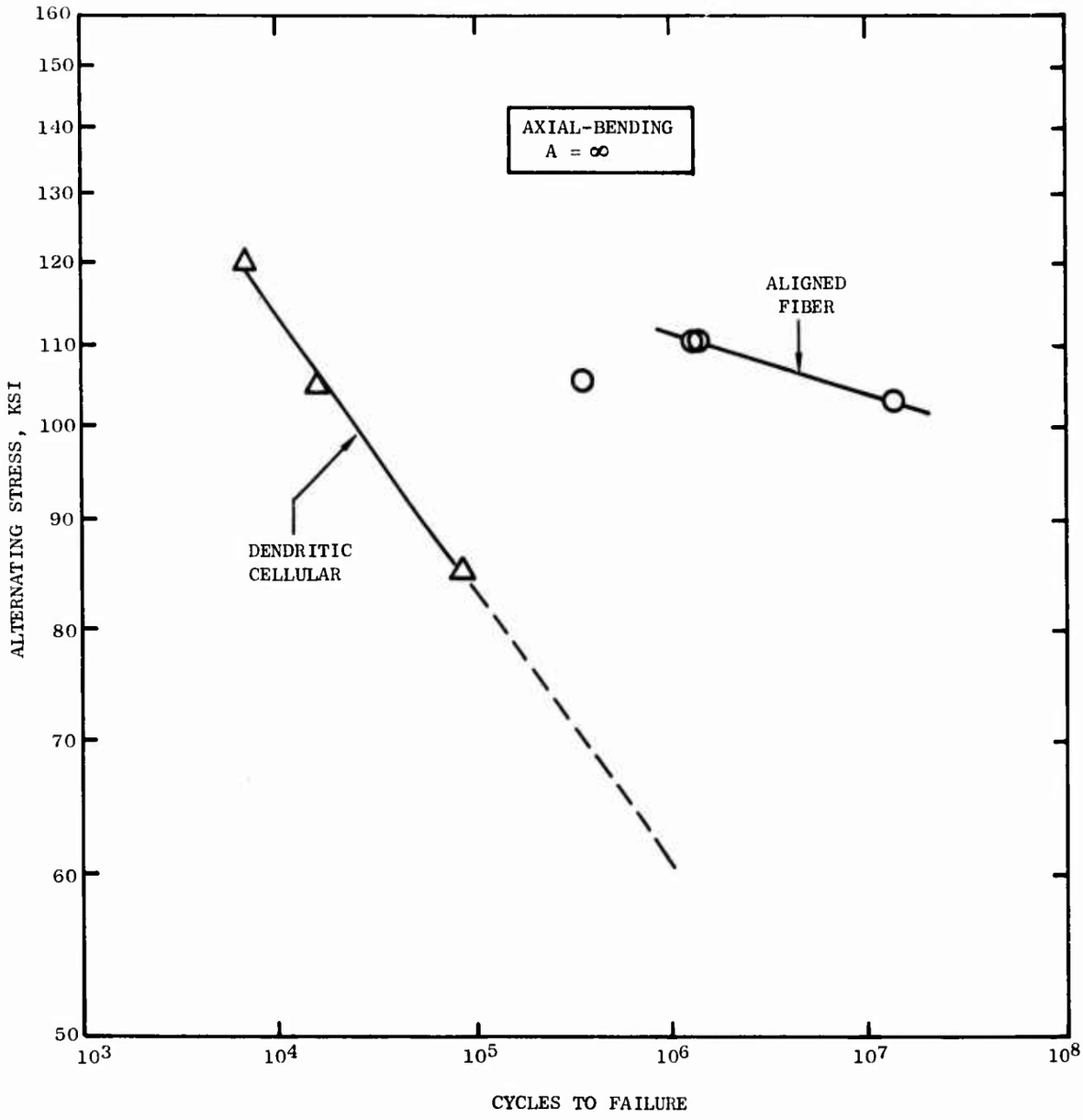

Figure 133. Effect of Carbide Defect Structure on 1200° F Longitudinal HCF Strength of NiTaC-13

TABLE 50

MAXIMUM ALLOWABLE ALTERNATING STRESSES DURING ENGINE DEMONSTRATION TEST OF THE BARE SOLID NiTaC-13 J101 LPT BLADE

Resonance Mode	Life Limiting Conditions: Location, Strain Gage No.	Section, % Span	Temp., °F	Mean Stress, ksi	Allowable Alt. Stress for 10-Hr. Life, ksi
BLADE CLAMPED AT DOVETAIL					
1	6	Shank	1200	71.4	18.3
2	8	Shank	1200	71.4	18.3
3	6	Shank	1200	71.4	18.3
4	71	19	1725	49.0	11.0
5	70	13	1667	54.0	14.0
6	55	Shank	1200	71.4	18.3
7	5	Shank	1200	71.4	18.3
8	55	Shank	1200	71.4	18.3
9	24	34	1805	30.0	24.0
BLADE CLAMPED AT PLATFORM AND DOVETAIL					
1	70	13	1667	54.0	14.0
2	8	Shank	1200	71.4	18.3
3	74	36	1810	37.4	13.0
4	43	50	1852	30.0	18.5
5	72	25	1772	44.0	11.5
6	29	63	1840	21.0	29.0
7	70	13	1667	54.0	14.0

TABLE 51

ROOM TEMPERATURE STEADY STATE DOVETAIL PULL TEST RESULTS

FOR BARE SOLID NiTaC-13 BLADES

Blade S/N No.	Load at Failure, Lbs.	Test Results				Under J101 Design Point Conditions			
		Blade Section	Section Area, In^2	Max. Stress @ RT Ksi	Max. Stress @ RT % of UTS*	Temp., ^oF	Stress, Ksi	Section Strength at Design Temp., % UTS	% Safety Margin**
10	22,000	Airfoil (B-B)	0.180	122	64	1630	49	35	84
10	22,000	Dovetail Shank	0.1936	114	60	1250	64	37	62
26	25,500	Airfoil (B-B)	0.180	142	75	1630	49	35	114
26	25,500	Dovetail Shank	0.1936	132	69	1250	64	37	86

* UTS of Aligned Fiber NiTaC-13

** % Safety Margin $= \left(\frac{\text{Test \% UTS}}{\text{Design Pt. \% UTS}} - 1 \right) \times 100$

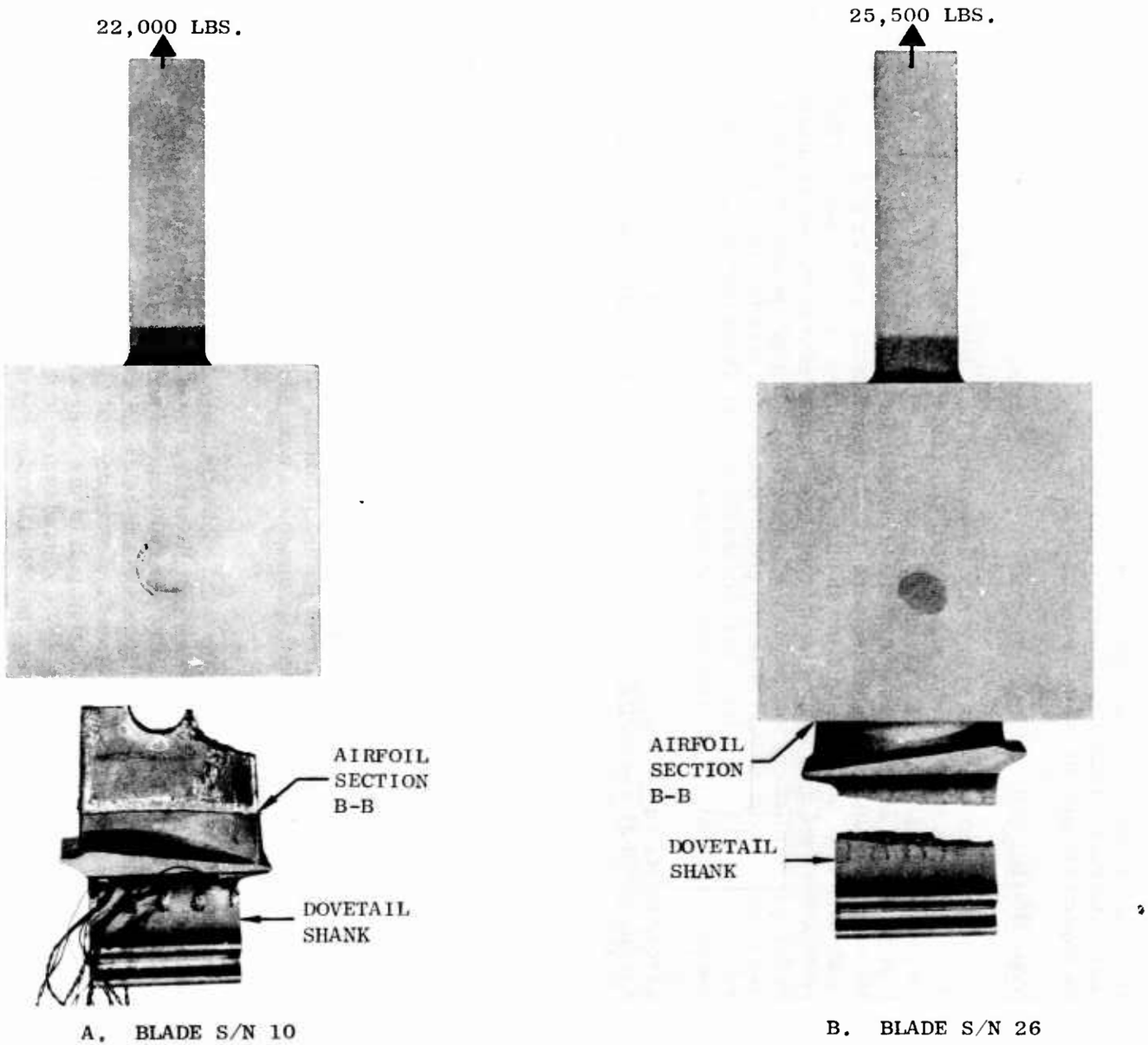

A. BLADE S/N 10

B. BLADE S/N 26

Figure 134. Photographs Illustrating Failure Locations in Steady State Dovetail Pull Tests of Blades

ultimate tensile strength of aligned fiber material. This difference is presumed to be due to a coarser and more severely misaligned fiber microstructure in the blade shank than in the dendritic cellular bar material previously evaluated.

Despite the reduced strength of the shank of the NiTaC-13 blade due to the dendritic cellular microstructure, it has a large margin over the J101 design stress, and no problems were expected in spin pit or engine tests.

5.2.5 Cyclic Dovetail Pull Test

The cyclic pull tests were performed to verify the dovetail LCF design requirement of 5000 cycles. The same type of airfoil and dovetail clamping fixtures were used for these tests as in the steady state pull tests described previously. Six strain gages attached to the shank were used for initial alignment of the blade with the loading axis to minimize bending stresses. To simulate engine temperature, an induction coil coupled to a metallic yoke around the dovetail and blade shank was used to heat these regions to 1200°F. Five thermocouples were used to monitor temperatures during testing: two on the blade, one on the dovetail pull fixture, and two on the heating yoke. During the test, the blades were cycled from a maximum load of 14,000 pounds down to 200 pounds, which was an A ratio of 0.97. The resulting stress range in the dovetail and shank region equaled the highest engine loading conditions, including gas bending effects.

A total of three blades were tested in this manner, but only the first test was successful. In this test, blade S/N 21 was cycled until it completed the design requirement of 5,000 cycles, at which time it was inspected using fluorescent penetrant. No indications of cracks were detected, and the testing was resumed until failure at 5,785 cycles. As shown in Figure 135, failure occurred in the airfoil at the junction with the brazed loading fixture where the stress field is unknown due to the abrupt fixture-blade transition. The calculated shank and dovetail stresses for these test conditions are given in Table 52, together with required, predicted, and actual LCF lives. The predicted life was above 10^5 cycles and was based on data for dendritic cellular NiTaC-13 in Figure 125.

Blade S/N 30 was then tested under identical conditions. After 221 cycles, the blade failed through the airfoil loading pin hole similar to the failure experienced on steady state pull specimen S/N 10 in Figure 134A. Again, the cause of failure was insufficient braze coverage. Two attempts were made to rebraze the remaining airfoil section back into the fixture block, but each time the rebrazed specimen was unable to sustain the full cyclic load at the elevated temperature.

The same test conditions were set for the third cyclic specimen, S/N 1. After 2,950 cycles in this test, one side of the dovetail pull fixture fractured as illustrated in Figure 136. The other side of the fixture was also severely cracked and close to failure. The cracks initiated at the edge of the loading bolt cutout below the lower tang, as illustrated in Figure 136. This cutout created a stress concentration that is not present in the actual disk dovetail and led to failure of the dovetail pull fixture after a cumulative total of about 9,000 LCF cycles. Inspection of blade S/N 1 showed cracks in the fillet between the upper and lower tangs. This result, in conjunction with the deformed shape of the fixture, indicates that as the fixture LCF cracks propagated, the fixture tangs deformed and the lower blade tang picked up most of the cyclic load, becoming highly overstressed. The blade failure thus was due to failure of the dovetail pull fixture.

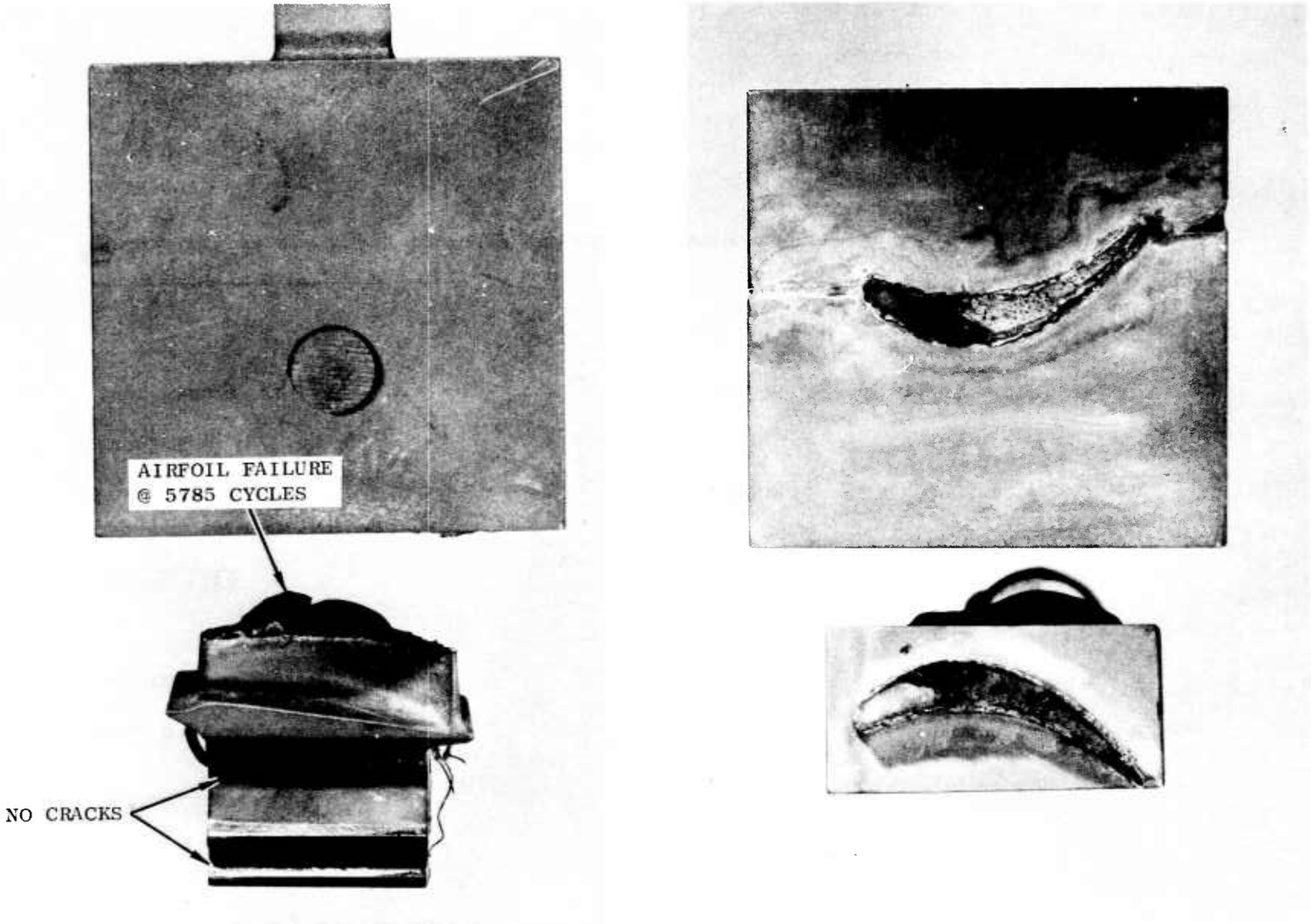

A. SIDE VIEW

B. END VIEWS OF FRACTURE SURFACE

Figure 135. Photographs Illustrating Failure Location in Cyclic Dovetail Pull Test of Blade S/N 21

TABLE 52

1200°F CYCLIC DOVETAIL PULL TEST RESULTS FOR BLADE S/N 21

TEST CONDITIONS	Blade Location	
	Shank	Dovetail
Peak Stress, Ksi	71.4	*130.3
Alternating Stress, Ksi	35.7	* 65.2
CYCLIC LIFE		
Required	5000	5000
Predicted	$> 10^5$	$> 10^5$
Test Result	>5785	>5785

* Combined stress which includes computed stress concentration factors

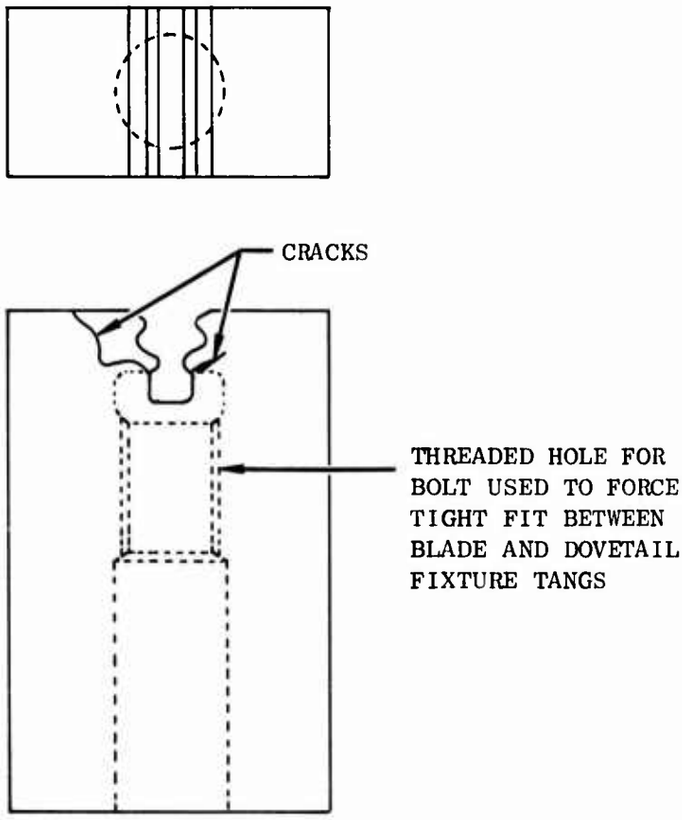

Figure 136. Schematic Illustration of Failure in Dovetail Pull Fixture

In spite of these testing difficulties, the excellent test result for blade S/N 21 verified that the NiTaC-13 blade meets the LCF acceptability criterion, in Table 40, as predicted by detailed design analysis in Section 4.2.4.2.

5.3 FLAME TUNNEL TESTS

Of the six flame tunnel tests specimens, one was used to calibrate specimen temperatures, four were tested in stress rupture, and one was tested in low cycle fatigue.

The specimen, illustrated in Figure 137, was an existing design that had a straight, uncambered airfoil gage section similar in dimensions to the J101 LPT blade airfoil. The specimen was about seven inches long, requiring use of almost the total length of a 1-5/8 inch NiTaC-13 bar remaining after the sort-out zone was cut off. Over the nominal 3-3/4 inch gage section of the specimen, g_b ranged from 0.28 to 0.78. Since the maximum g_b in airfoil of the NiTaC-13 blades was about 0.28, the results require interpretation with respect to this important factor.

5.3.1 Temperature Calibration

Calibrations were performed with flame tunnel Specimen M-61 which was initially instrumented with 11 thermocouples located around the perimeter of the central cross section (pitch), as illustrated in Figure 138. Concurrent with specimen temperature measurements, two thermocouple probes were used to determine horizontal and vertical flame temperature profiles slightly downstream from the specimen. Because two specimens tested in stress-rupture fractured at a section located about 0.68 inches from the pitch section, an additional calibration was required. For this purpose, Specimen B-61 was re-instrumented with seven thermocouples attached around the fracture section 0.68 inches from the central cross section, and four were left at the original positions for reference.

The results of three calibrations are presented in Figure 139, as curves of metal surface temperature versus position in the cross section from leading to trailing edge. In the two calibrations of the pitch section for bulk metal temperatures of 1828° and 1860°F in Figure 139, it can be seen that surface temperature deviated by ± 13°F from the bulk metal temperature. The calibration results for the fracture section showed temperatures to be only about 5°F higher than the pitch section.

In the subsequent flame tunnel tests, the two thermocouple probes were used to monitor and control the flame temperature, and no thermocouples were attached to the test specimens.

5.3.2 Stress-Rupture Tests

The first flame tunnel specimen, 3B59, was tested at 1828°F pitch section bulk metal temperature and 40 ksi. This test temperature was higher than the 1790°F bulk metal temperature predicted for the life limiting blade section (30 percent span) under J101 design point operating conditions. At 17.7 hours of testing, a limit switch in the cooling water supply line tripped causing an immediate shutdown of the facility. The resulting rapid thermal transient caused a failure of the grips in the loading mechanism and bent the test specimen. In subsequent visual inspection of the specimen, no cracks could be found. After resumption of the test, the specimen failed at 20.5 hours total test time.

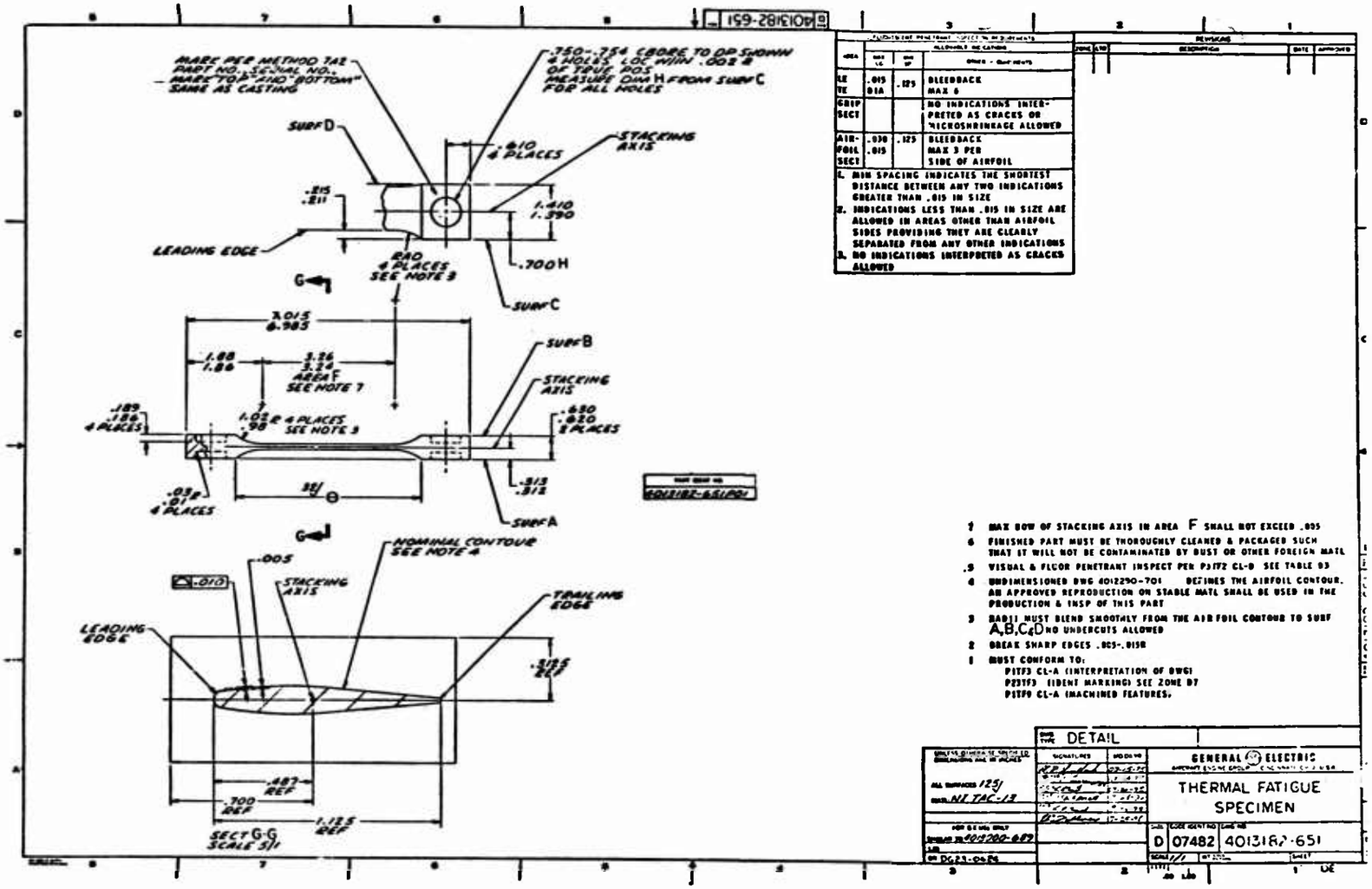

Figure 137. Flame Tunnel Test Specimen

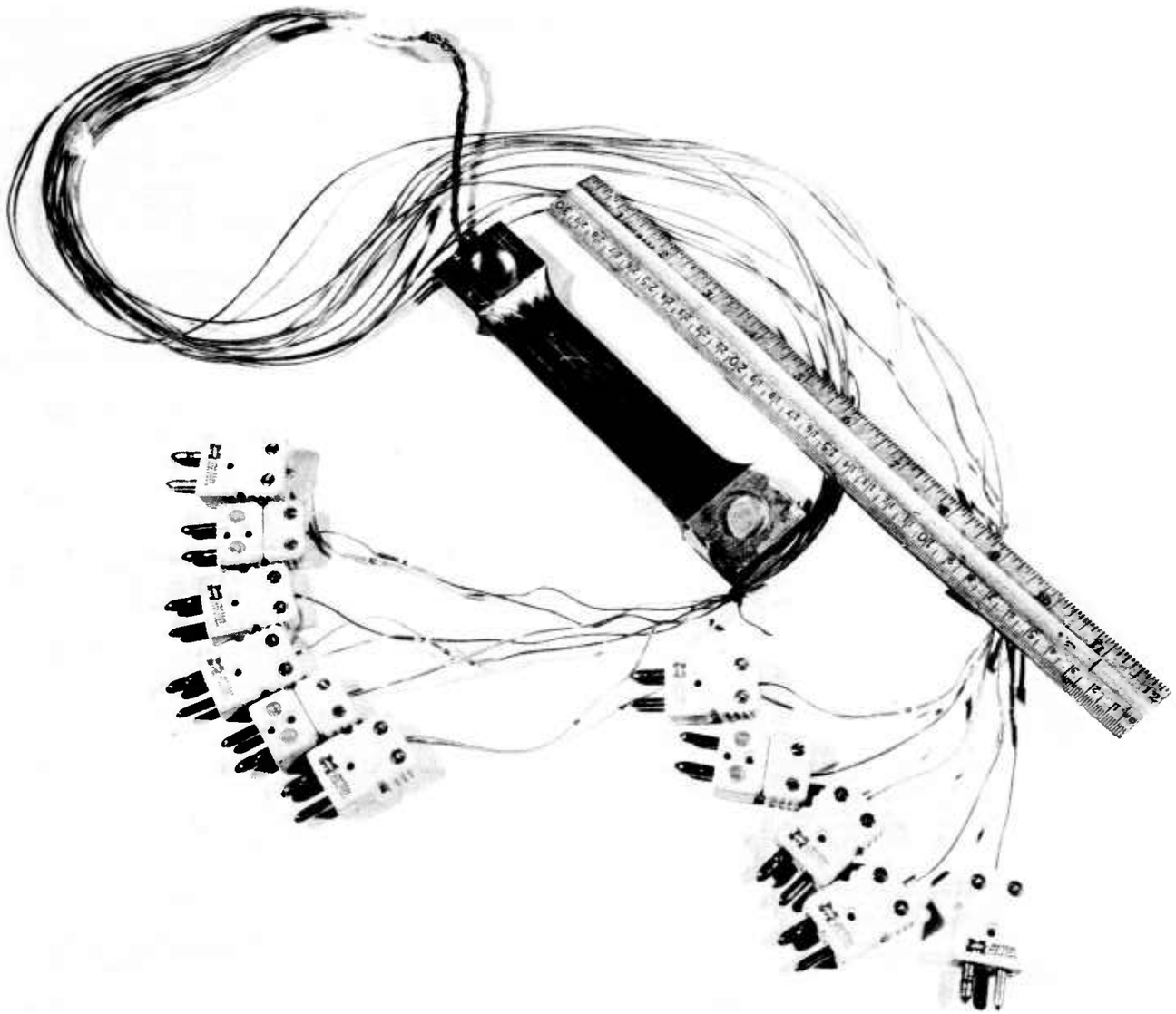

Figure 138. Flame Tunnel Specimen Instrumented for Temperature Calibration

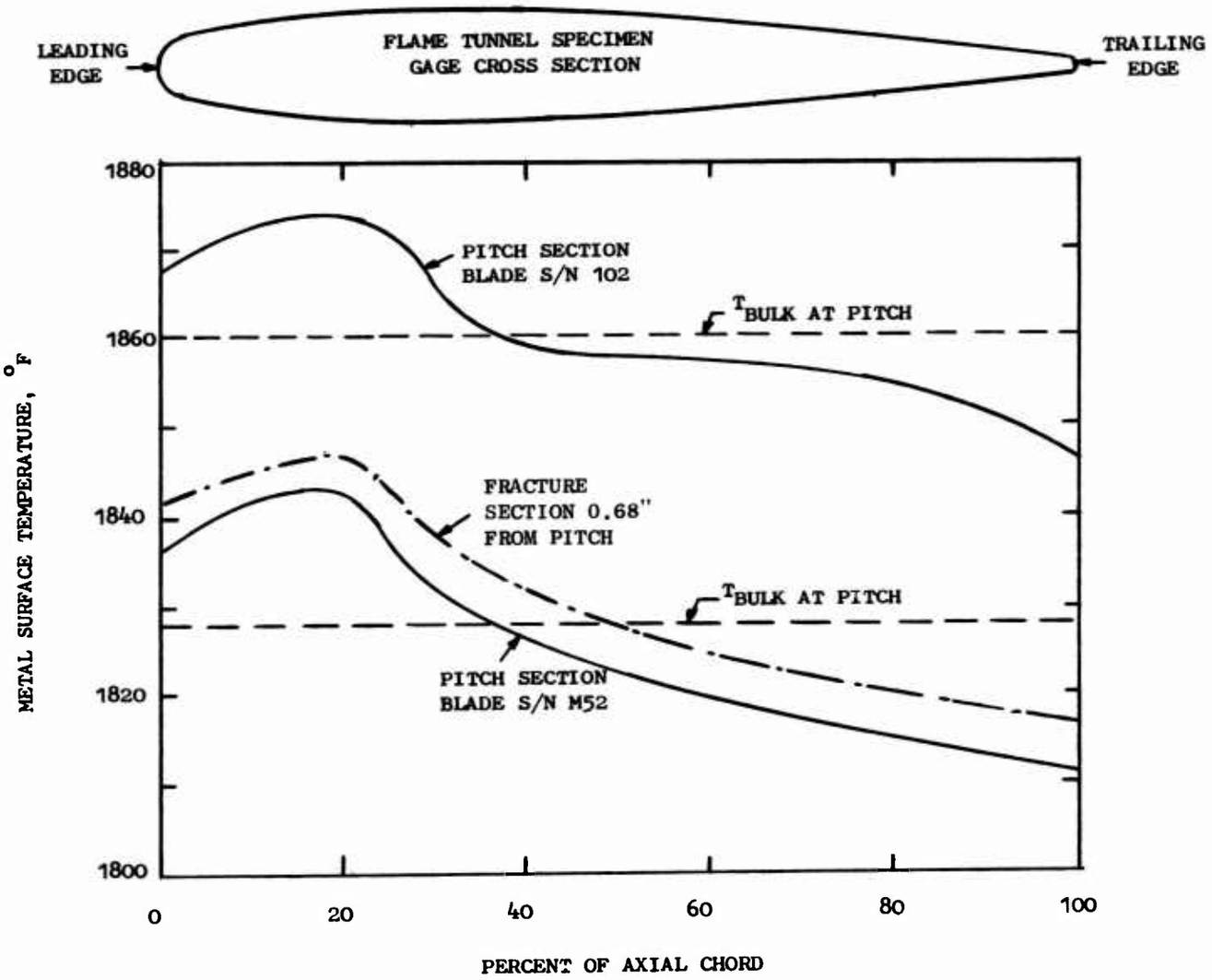

Figure 139. Temperature Profiles During 1828° and 1860°F Rupture Tests of Flame Tunnel Specimens

Photographs of the specimen before and after fracture are shown in Figure 140. Fracture occurred at a g_b value of about 0.52, which is approximately equivalent to the middle position in test bars. The fracture occurred in the region where the sample was bent during the grip failure, indicating that the sample was severely damaged by the bending. Previous tension tests of NiTaC-13 showed that fibers fracture when a critical strain is exceeded. At elevated temperatures such as 1800°F where the matrix does not work harden, the tensile specimen undergoes localized deformation and fracture in the cross-sectional region where fibers first fractured. Hence, it was concluded that final fracture of this specimen was premature.

This was confirmed by the test of a second specimen (M-52) which duplicated the conditions of the first test. In this case, the sample ruptured after 58.5 hours of test. The fracture occurred at a g_b value of about 0.66, which was equivalent to the top location of test bars.

A third specimen, B114, was tested in stress-rupture at 1828°F pitch section bulk metal temperature and 33 ksi, which represented the most severe operating conditions estimated to occur at the blade 40 percent span. On the basis of early (and invalid) average longitudinal stress-rupture curves for NiCrAlY coated NiTaC-13, predicted life was 58 hours. However, on the basis of final average data for coated material (Figure 78C) and the excellent test result for Bar M-52 obtained while the test of B114 was in progress, the predicted life was increased to 187 hours. Because of the longer estimated life, this test was discontinued after completing a total of 70 test hours which exceeded the minimum life predicted on the basis of average properties minus three standard deviations.

The fourth specimen, B102, was subjected to an applied stress of 40 ksi and a pitch section bulk metal temperature of 1860°F. These conditions were more severe than anticipated for an actual engine blade. Based on the final average coated longitudinal rupture data, failure was predicted at 29 hours. Actual failure occurred at 31 hours.

The test conditions and results for the four isothermal rupture tests are summarized in Table 53, where the actual rupture lives are compared with those predicted on the basis of final test bar data for coated material from bar tops previously given in Figure 78C. Test temperatures were revised 5°F upward in Table 53 on the basis of temperature calibration data for the fracture section (Figure 139). As can be seen in the table, all samples exceeded the predicted -3σ lives. In the two valid and completed tests, Bars B-52 and B102, rupture lives substantially exceeded lives predicted on the basis of average coated bar top properties representative of the fracture locations in the flame tunnel test specimens. In fact, rupture lives of both specimens exceeded those predicted on the basis of average coated bar bottom properties, which are significantly higher than bar top properties. The high performance of the flame tunnel specimens may have been due to a size effect, because they were much larger than stress-rupture test specimens used for property data acquisition.

Because the flame tunnel test specimens simulated the J101 LPT blade airfoils, these excellent test results indicated that no stress rupture problem would be encountered in the 30-hour engine test of blades and that blades may more closely approach the rupture life goal than predicted on the basis of test bar data.

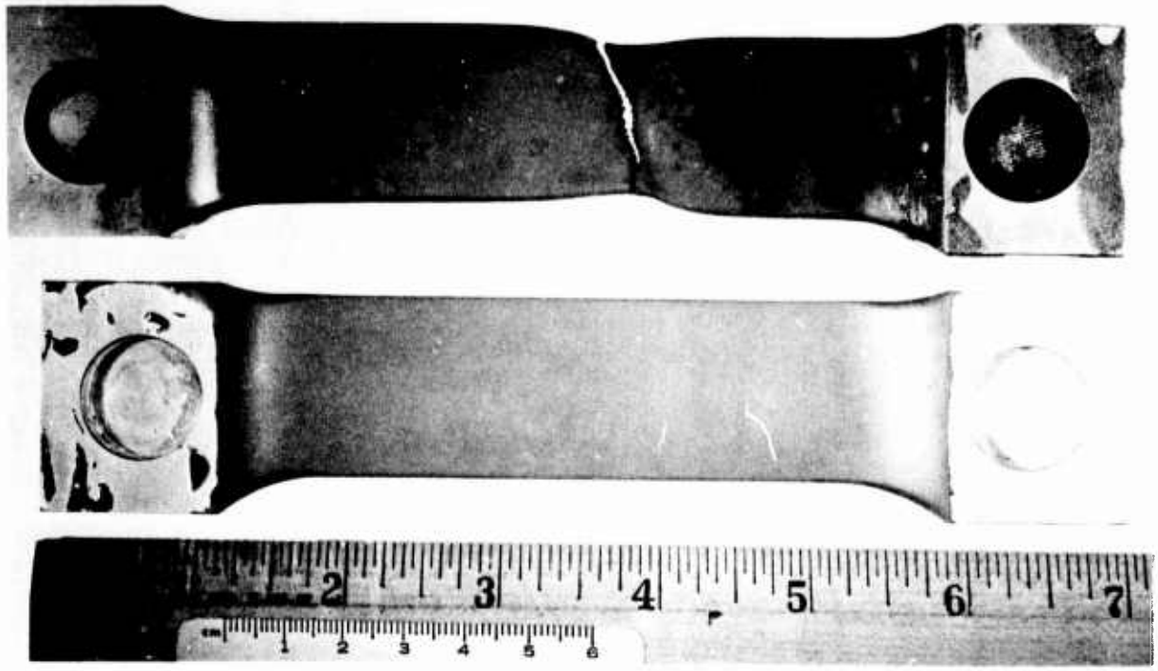

Figure 140. Flame Tunnel Test Specimen 3B59 Before Test and After Fracture

TABLE 53

SUMMARY OF ISOTHERMAL FLAME TUNNEL RUPTURE TESTS OF Ni-20Cr-10Al-1Y COATED NiTaC-13

Specimen Number	*T_{Bulk}, °F	Stress, Ksi	g_b at Failure Location	+ Predicted Life, Hrs.			Actual Life, Hrs.	Comments
				-3σ	Avg.	+3σ		
3B59	1833	40	.52	10.5	28.6	78.1	20.5	Specimen damage due to grip failure
M52	1833	40	.66	10.5	28.6	78.1	58.5	
B102	1833	40	.61	5.4	14.5	39.0	31.0	
B114	1833	33	-	35.0	95.5	260.6	>70	Test discontinued

* At specimen cross section where failures occurred in specimens M52 and 103, 0.67" from center of gage.

+ Based on stress rupture data for Ni-20Cr-10Al-1Y coated NiTaC-13 from top sections of test bars, $g_b \sim 0.67$.

5.3.3 Low Cycle Fatigue Test

LCF testing of the simulated airfoil was conducted with flame tunnel Specimen M-43. In the test, the temperature of the specimen leading edge was estimated to cycle between 900° and 1840°F, as illustrated in Figure 141. Specimen temperature estimations were based on the measured flame tunnel gas temperature cycle and corresponding metal temperatures computed by TRANSIENT HEAT TRANSFER.

Also, as shown in Figure 141, a 40 ksi tensile stress was applied at the start of cool-down. This stress nearly equaled the 44 ksi centrifugal stress computed by ADAM TWISTED BLADE for the coated solid blade at the rupture life limiting section, 30 percent span. During cool down, the leading and trailing edges were stressed in tension due to thermal strains, and the applied stress produced an additive strain.

After testing for 5,310 cycles, the specimen was examined visually before and after being subjected to a dye penetrant test. Inspection showed that there were no gross cracks, although there were some superficial cracks in the coating at the colder ends of the test sample.

Life predictions for these test conditions were made using TRANSIENT HEAT TRANSFER, BUCKET CREEP III, and LCF data for three alloys: Rene' 80, Rene' 125, and NiTaC-13. The results in Table 54 show that the life predicted for NiTaC-13 was far in excess of those predicted for the two superalloys, and also more than double the 5,310 test cycles completed.

One design acceptability criterion given previously in Table 40 is that the blade must meet the J101 LCF life requirement of 5,000 cycles. This requirement applies to both the blade airfoil and the dovetail. Previous results in Section 5.2.5 showed that the dovetail met the LCF goal. The results just described for flame tunnel test specimen M-53 demonstrated that the airfoil also met the LCF goal. Although Specimen M-53 was coated, stress-rupture data in Figure 78 show essentially no difference between bare and coated specimens in the applicable test range of stress and temperature. Hence, it was concluded that the solid NiTaC-13 eutectic blade completely meets the LCF design acceptability goal.

5.4 SPIN TEST

The primary purpose of the spin test was to verify blade dovetail capabilities in an actual rotor centrifugal field. As described in Sections 5.2.4 and 5.2.5, results of static bench tests that simulated engine steady state and cyclic conditions indicated that the dovetails were satisfactory for engine test.

The spin test facility consists of a reinforced concrete pit with a sealable hatch cover. The test rotor is placed in the pit and spun about a vertical axis by an air turbine attached to the hatch cover. A vacuum is drawn in the pit prior to testing to eliminate windage losses which would greatly increase the power required to drive the test rotor. A total of twelve solid, uncoated NiTaC-13 blades were spin tested in a standard J101 LPT rotor assembly, illustrated in Figure 142. To maintain uniform disk and disk dovetail post

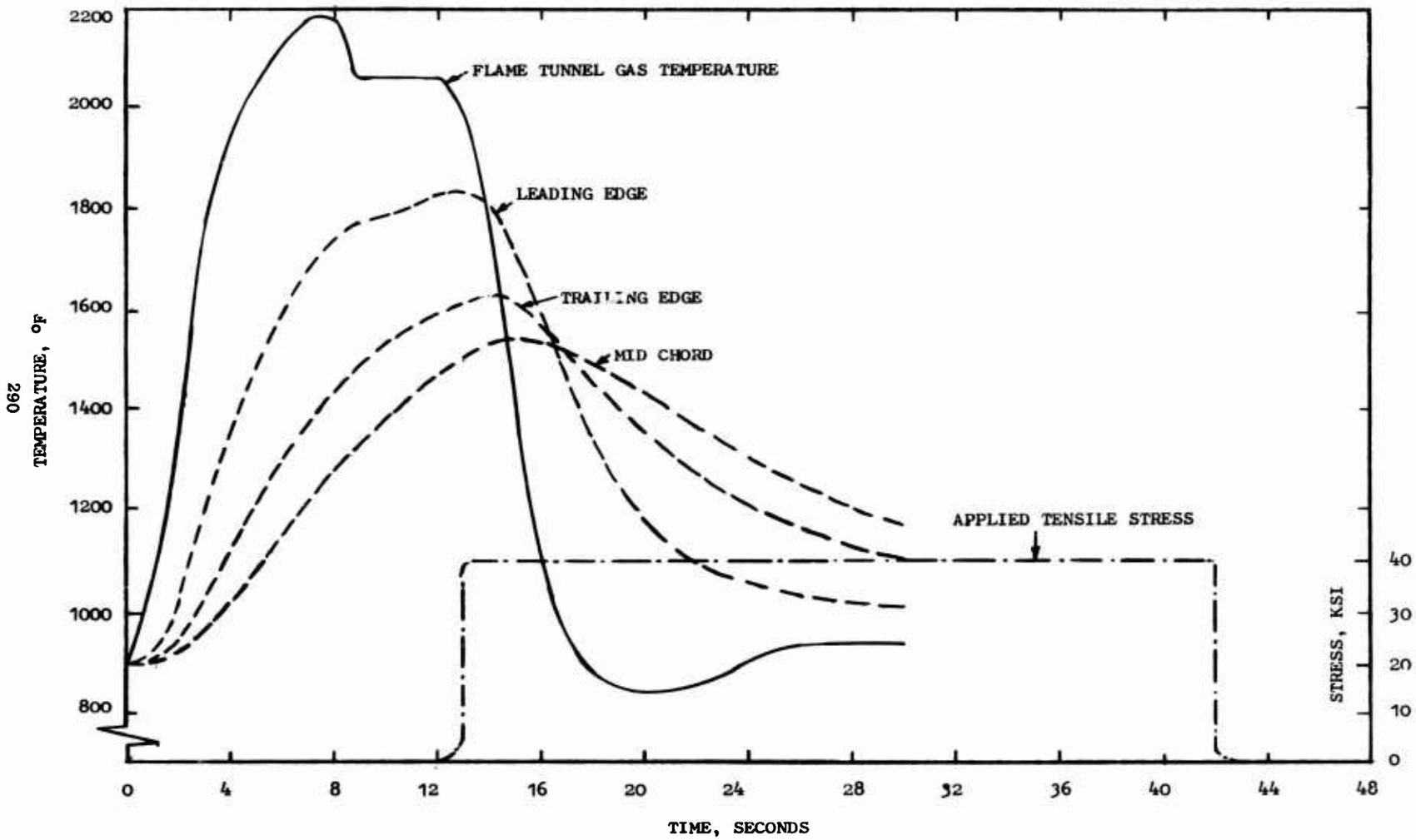

Figure 141. Temperature and Load Cycles for Flame Tunnel LCF Test of NiTaC-13 Airfoil. Specimen Temperature Calculated with TRANSIENT HEAT TRANSFER Computer Program

TABLE 54

FLAME TUNNEL LCF TEST RESULT* FOR Ni-20Cr-10Al-1Y COATED NiTaC-13 COMPARED WITH RESULTS PREDICTED FOR RENE' 80 AND RENE' 125

	Rene' 80	Rene' 125	NiTaC-13
Max Alternating Pseudo Stress, Ksi	79.6	76.5	56.1
Max Alternating Strain	-	-	0.0036
Cycles predicted for Average Properties	780	1600	$>10^5$
Cycles predicted for -3σ Properties	220	510	10^4
Test Result, Cycles to Crack Initiation	-	-	5310 (no cracks)

* A Ratio = 3.4

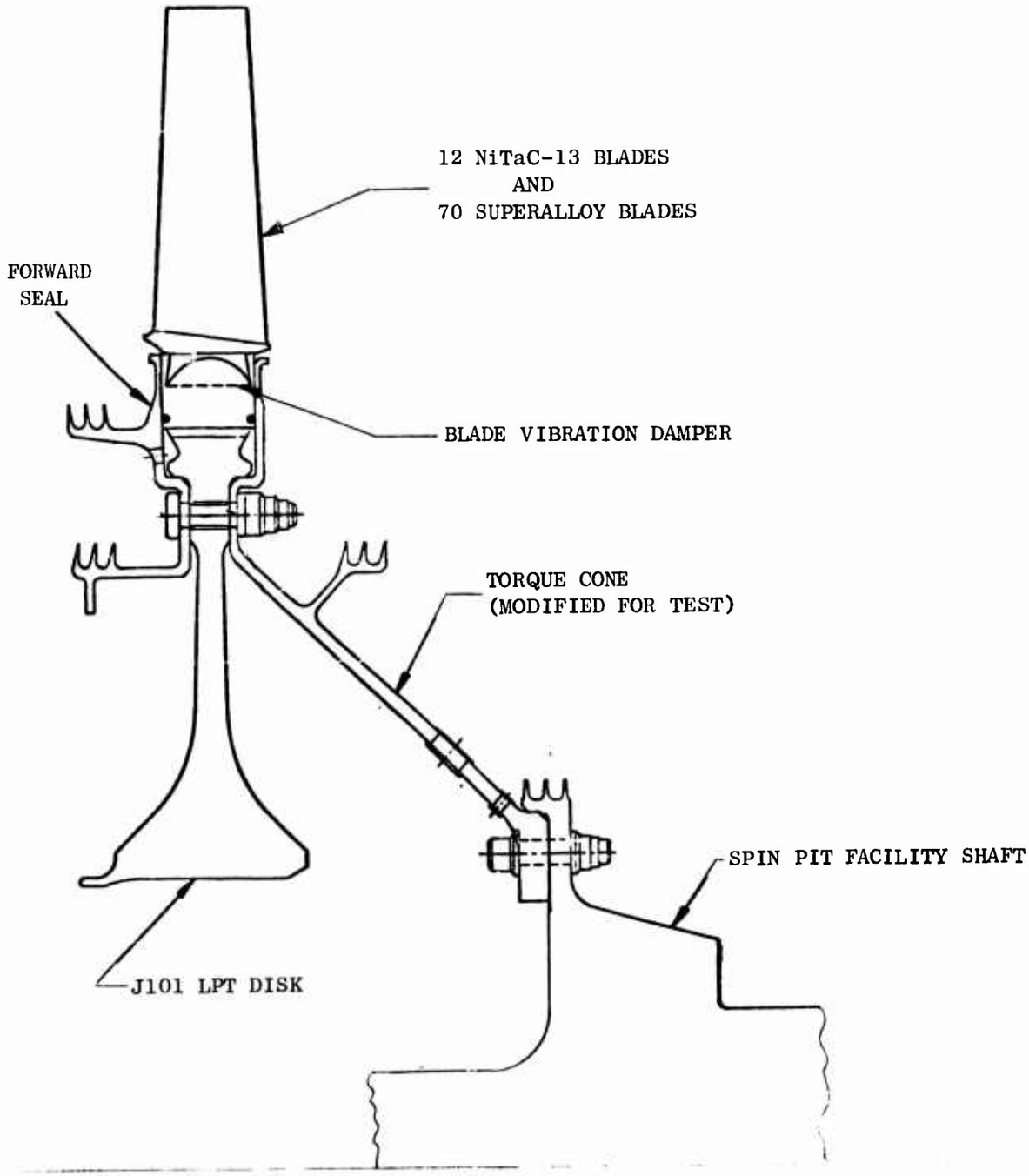

Figure 142. J101 Spin Test Hardware Assembly

loading, a full set of 82 blades were run in the test, including 70 standard superalloy J101 blades. The heavier NiTaC-13 blades were spaced circumferentially around the disk to facilitate balancing of the rotor assembly. A photograph of the assembled rotor prior to testing is presented in Figure 143. The NiTaC-13 blades can be identified by their solid tip configuration.

Spin testing was conducted in two phases. The first phase consisted of a stress distribution survey in which the blade shank stresses were monitored as a function of rotor speed. The second phase consisted of 5,000 LCF cycles to 100 percent rotor speed (13,533 RPM).

For the stress distribution survey, three of the NiTaC-13 blades (S/N 51, 54, and 57) were instrumented with six strain gages each, as illustrated in Figure 144. These locations correspond to those used for the steady state and cyclic bench pull tests in order to provide a basis for data correlation and interpretation. Of these 18 gages, apparently one was damaged during assembly and two became inoperative early in testing before reaching 100 percent speed. Stress readings were taken at rotor speeds corresponding to 0, 10, 20, 30, 40, 60, 80, and 100 percent of the design load. These readings showed linear stress-load relationships as anticipated. A non-linear relationship would have indicated undesirable point loadings or uneven dovetail face line contacts. A summary of the stresses versus axial shank locations for the three instrumented blades at 100 percent load (also 100 percent speed) is presented in Figure 145. The stress distributions for blades S/N 51 and 54 correlate extremely well. Blade S/N 57 also correlates well, except for one gage. Because of the excellent correlation of the other gages, the accuracy of this gage is quiestionable. The results in Figure 145 also show a wide spread in stress between the concave and convex trailing edge stresses at the aft shank gages. This is due to the fact that the trailing edge of the airfoil overhangs the shank on the concave side (Figure 144), thus unloading the aft convex shank at the expense of the concave shank region.

The spin test shark stress distribution results are compared with a composite of the steady state pull bench test readings in Figure 146. As shown, the convex and concave stresses for the pull test blades were identical since the blade pull axis was carefully aligned to minimize bending loads. Note that the stress distribution of the pull test blades went through a maximum at the center whereas stresses varied linearly with axial location in the spin test blades. Evidently, the manner of applying the bench test loads through a brazed block and pin through the airfoil did not allow the loads to distribute evenly before entering the shank region. However, the maximum stress observed in both the bench test and the spin test at 100 percent load were virtually identical.

The second phase of the spin test consisted of 5,000 LCF cycles from 4,000 RPM (10 percent load) to 13,533 RPM (100 percent load). These cycles were run without incident at an average rate of 0.57 cycles/minute. Following completion of testing, the rotor was disassembled and all blades and spool hardware were inspected visually and with fluorescent penetrant. No indications of cracks were found on any of the NiTaC-13 blades or the standard J101 parts. Some fretting of the blade dovetail tang faces did occur, however, as can be seen in Figure 147. Fretting of the disk dovetail tang faces also occurred, but was less severe. This behavior can be greatly reduced or eliminated through the use of wear coatings, as is done with many other GE blade designs.

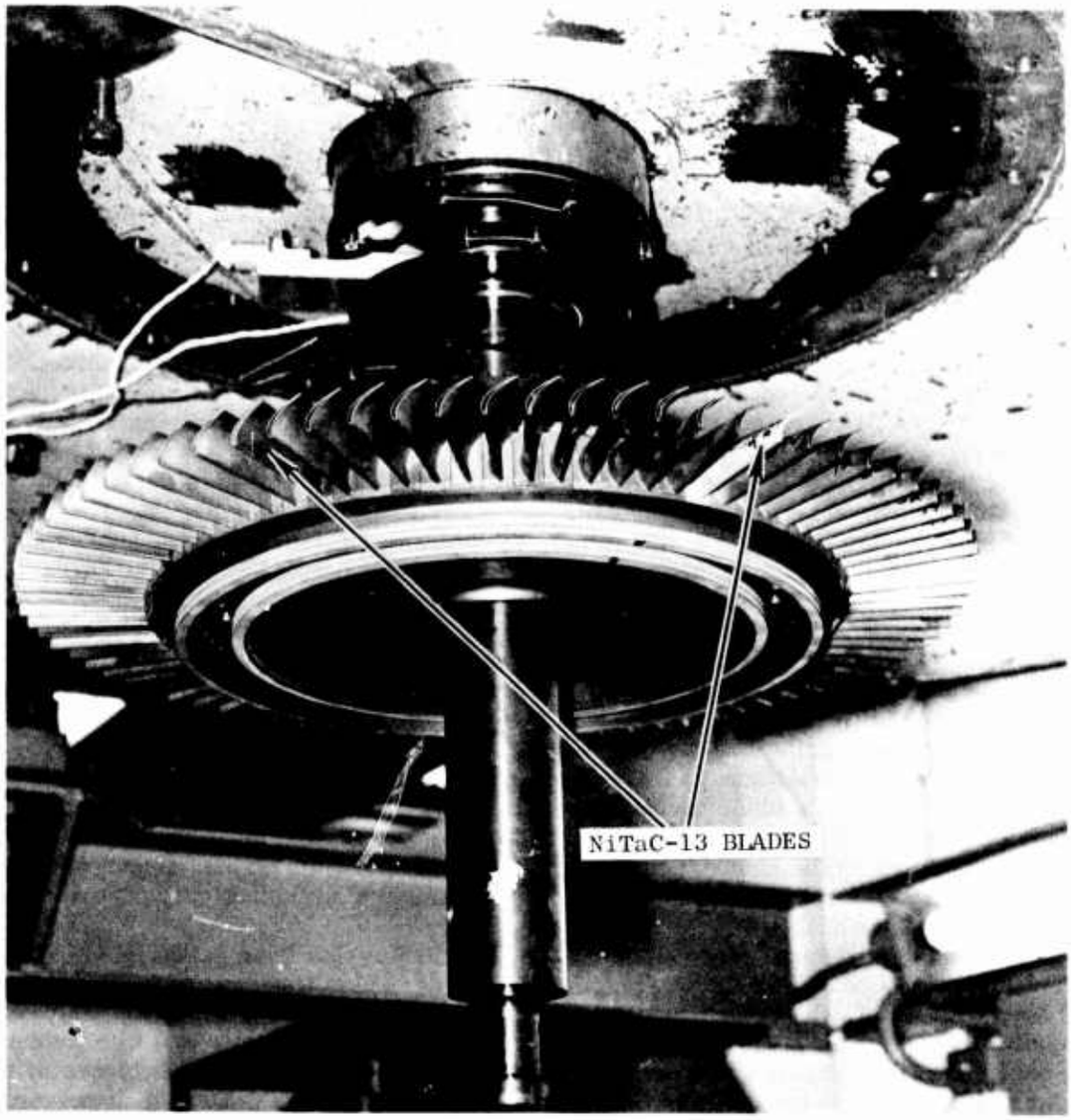

Figure 143. J101 LPT Rotor Assembly Prior to Spin Pit Test

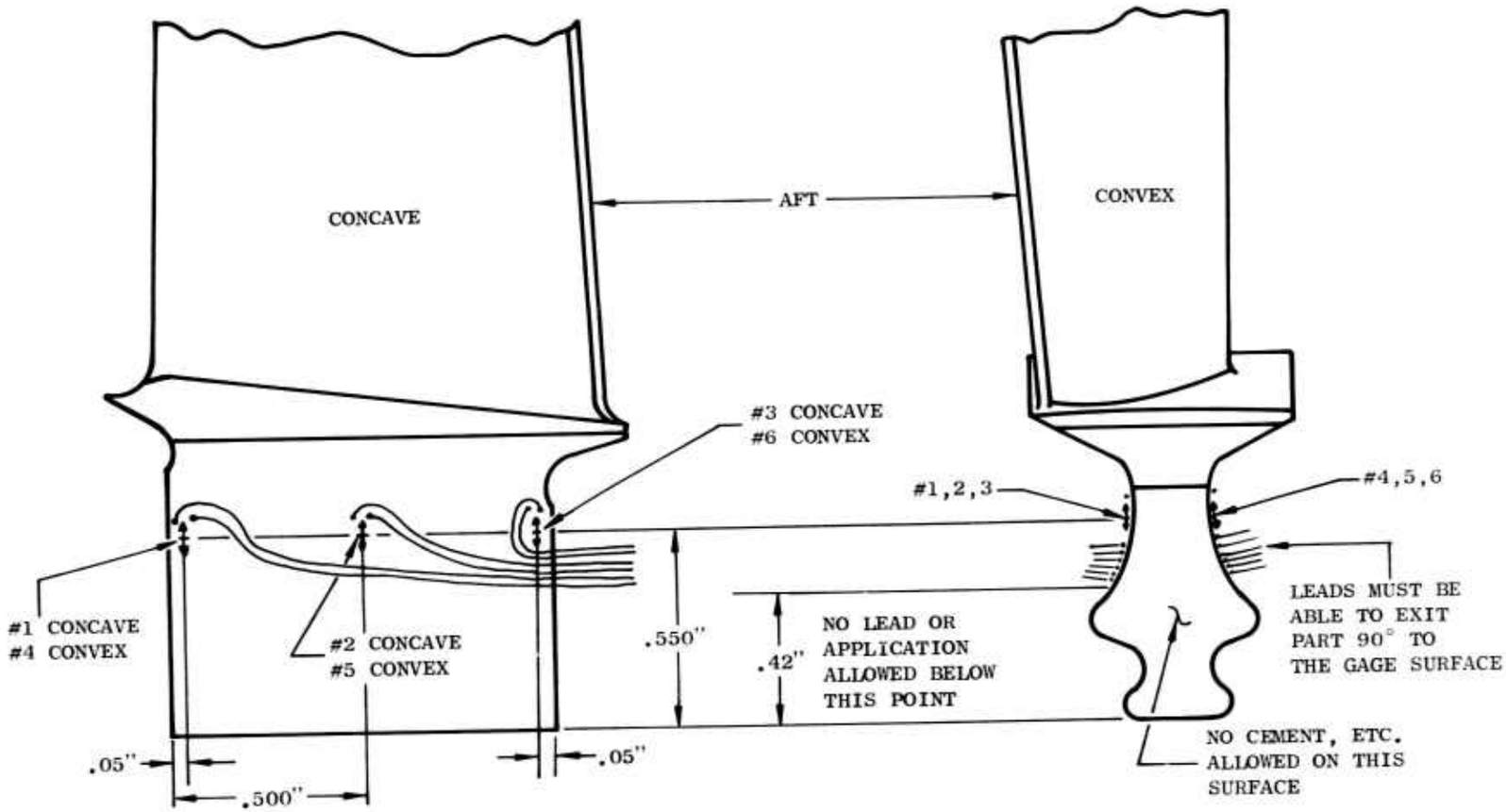

Figure 144. Spin Test Blade Instrumentation

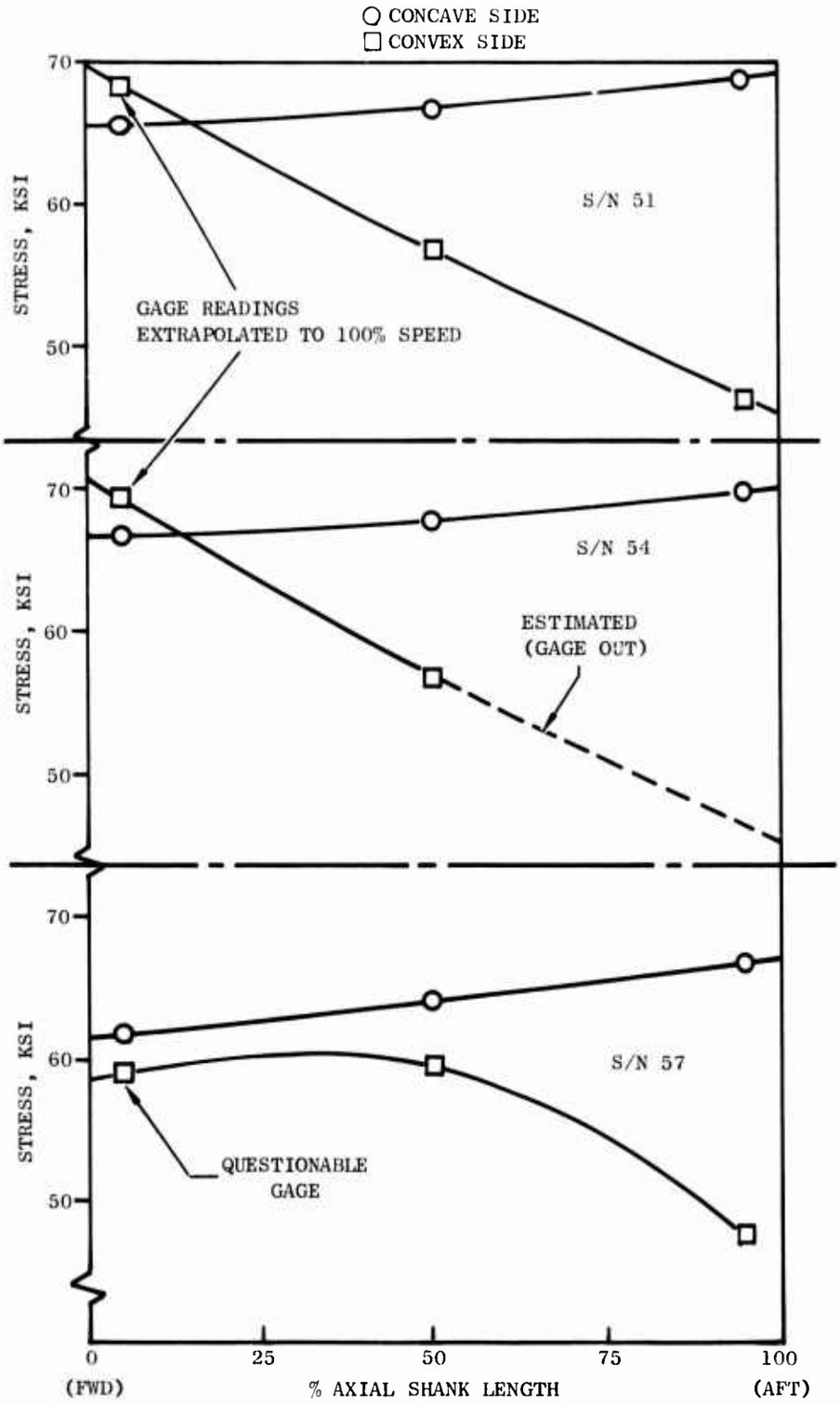

Figure 145. Spin Test Shank Stress Distribution @ 100% Speed (13,533 RPM)

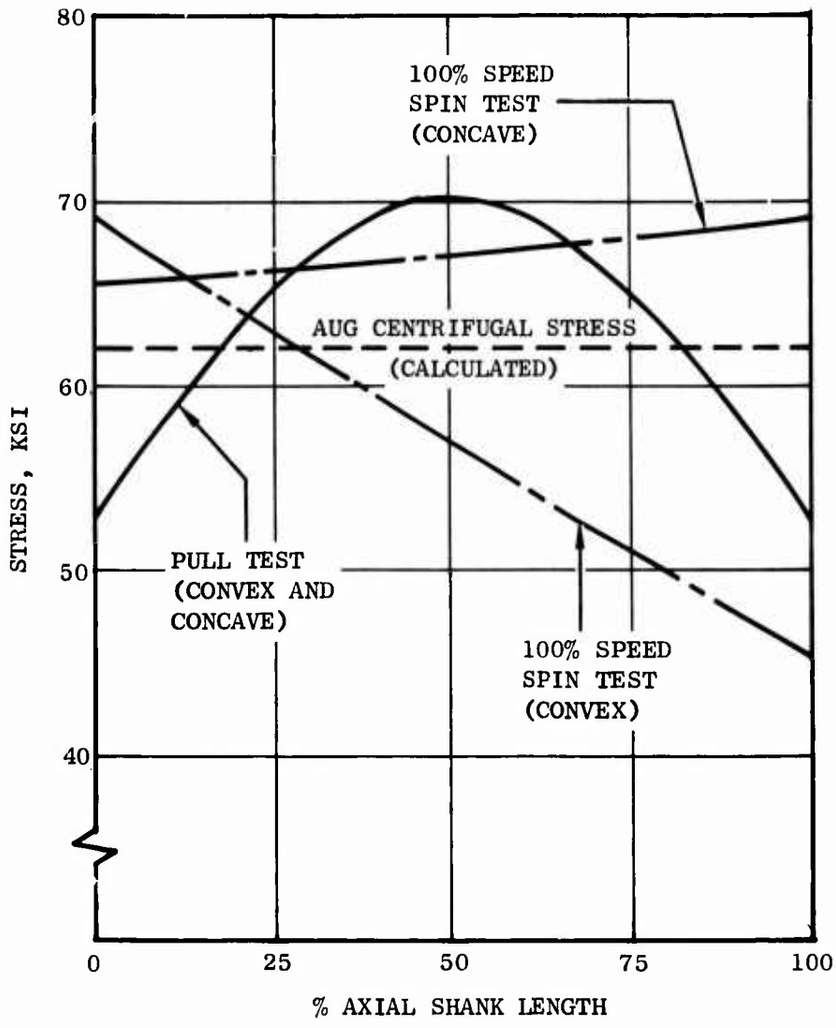

Figure 146. Comparison of Shank Stress Distributions From Spin Test at 100 Percent Rotor Speed and Bench Pull Tests

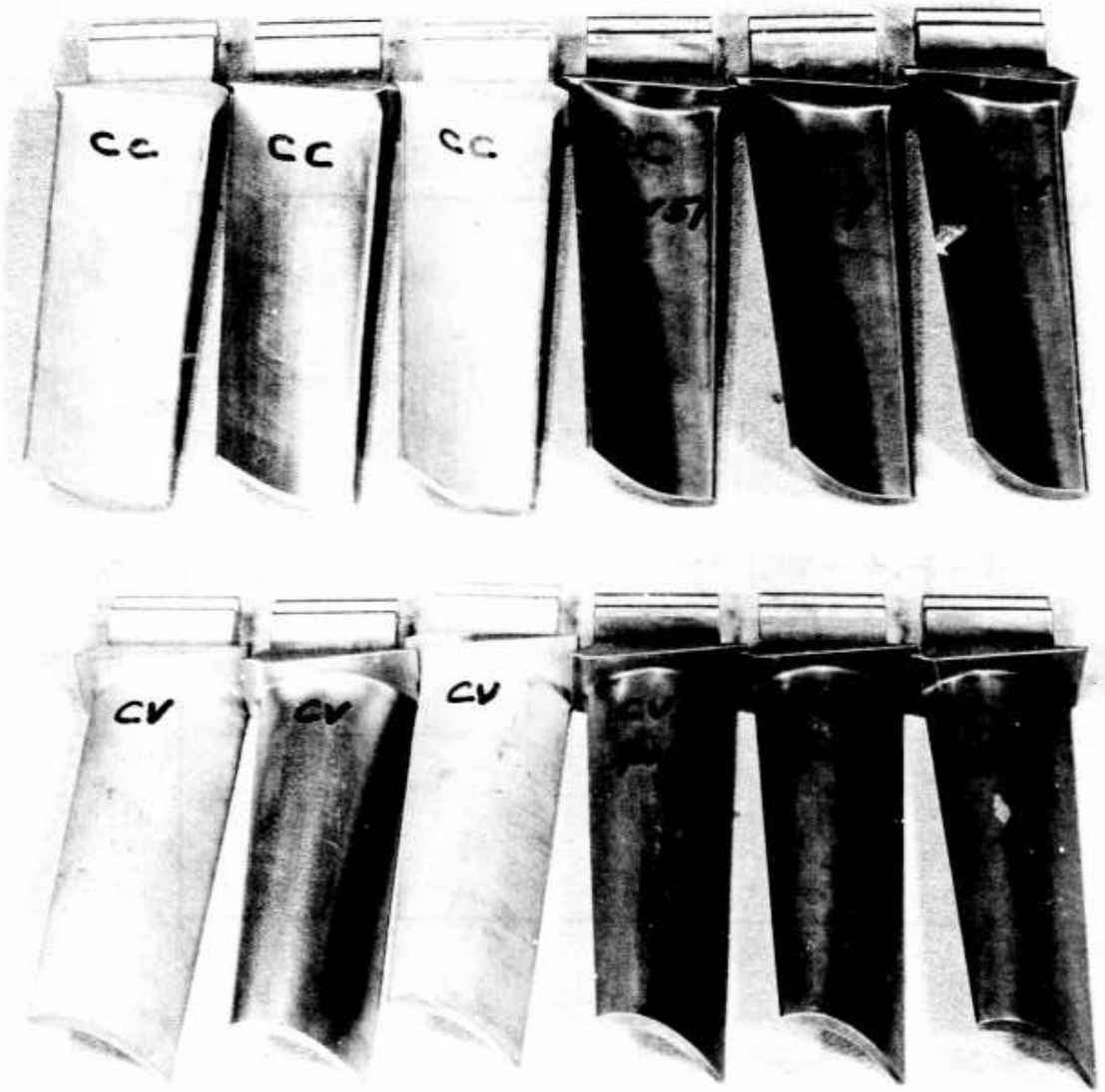

Figure 147. Photographs of Six of the Twelve Solid NiTaC-13 J101 LPT Blades, After Completion of 5000 - Cycle Spin Test

The dovetail fretting was not unique to the NiTaC-13 blades, however, but was also present on the superalloy blades. In these, the dovetail wear patterns indicated greater loading on the lower dovetail tang than the upper tang, whereas the NiTaC-13 blades had a very uniform load distribution. The relatively low longitudinal Young's Modulus of NiTaC-13 may have allowed non-uniform applied loadings, due to slight machining tolerance mismatches, to redistribute more evenly than was the case for the superalloy blades.

The spin testing has thus further verified the NiTaC-13 blade LCF capabilities previously established by detailed design analysis and bench cyclic pull tests. No LCF or significant fretting problems are anticipated in the planned 30 hours of engine testing. Because of the relatively short engine test, antifretting coatings will not be used on any of the blades.

6.0 CONCLUSIONS

1) Blade Life Analysis and Bench Tests

- The goal of producing an uncooled NiTaC-13 J101 LPT blade having a predicted life equal to that predicted for the cooled superalloy blade was closely approached by the bare, hollow-tip eutectic blade design.
- Hollow tip blade life analysis, based on test bar property data, predicted:
  - LCF life greatly exceeds goal of 5,000 cycles
  - HCF life is about 5 percent below goal of 100-hour Goodman diagram capability
  - Stress-rupture life is about 43 percent less than predicted life of cooled superalloy blade
- Bench tests confirmed LCF and HCF life predictions, but indicated blade life would meet the stress-rupture life goal. Extended engine testing would be required to confirm this result.
- The bare solid NiTaC-13 blade is predicted to have adequate life for testing in a J101 engine.

2) Planar Front Solidification (PFS) Casting Process

- The laboratory process for small bars is applicable to much larger bars and blades.
- The critical ratio of G_L/R (liquid metal temperature gradient to casting rate)$_2$ necessary for aligned fiber growth in NiTaC-13 is approximately 1170 ± 50°F.[2] For practical G_L values, therefore, the maximum casting rate is 1/4 inch/hour.
- An improved mold is required for casting blade airfoils to final dimensions. Surface defects with the present molds including pits and coarse dendritic carbides, are up to 0.02 inches deep.
- Segregation of alloying elements during PFS is unavoidable, but can be minimized by judicious design of the casting configuration.
- Perturbations to the PFS facility during casting, including power and mechanical disturbances, can produce bands of undesirable misaligned carbide fibers extending across the entire cross section of the casting.

- Large changes in cross sectional area of the casting can also produce misaligned fiber bands unless appropriate changes are made to the G_L/R ratio.

3) Properties

- NiTaC eutectic alloys have high potential for meeting turbine blade requirements for advanced engines.
- Nearly all measured longitudinal strength properties of aligned fiber NiTaC-13 are superior to the best available cast superalloys, including: ultimate tensile, creep-rupture, thermal fatigue, LCF and HCF strength.
- Carbide fiber misalignment degrades strength somewhat.
- Segregation during PFS decreases stress-rupture strength and density.

4) Machinability

- NiTaC-13 is readily machinable by many conventional and non-conventional techniques used for superalloys.
- Drilling of large holes by STEM (shaped tube electrochemical machining) produced unsatisfactory results.

5) NDE

- Detection of carbide fiber misalignment, such as in bands, will require development of a new NDE technique.

6) Surface Stability and Coatings

- NiTaC-13 requires a coating for protection against oxidation and hot corrosion.
- The Ni-20Cr-10Al-1Y evaluated in the program is inadequate. Although it provides excellent protection against oxidation and hot corrosion under mildly corrosive conditions, it is difficient under severe corrosive conditions. The coating also degrades HCF strength substantially.

7.0 RECOMMENDATIONS

The following course of action should be pursued to develop the total technology required to realize the full potential of NiTaC eutectics for turbine blade applications in aircraft engines:

1. Continue the development of blade design and life analysis techniques

   - Obtain required on and off-axis NiTaC properties
   - Extend procedures to 2D and 2D finite element analysis

2. Continue NiTaC alloy development

   - Increase strength and transverse ductility
   - Increase surface stability (oxidation, hot corrosion, erosion resistance)
   - Increase allowable casting rate
   - Decrease alloy cost

3. Continue casting process development

   - Improve furnace design to maximize temperature gradient attainable for a given metal superheat temperature
   - Improve furnace stability - resistance to mechanical and electrical peturbations that cause misaligned fiber bands
   - Optimize blade casting designs to obtain aligned fibers throughout airfoil, shank and dovetail. Misaligned fibers in platform may be acceptable

4. Continue non-siliceous core material development and initiate mold development

   - Achieve necessary chemical compatibility for precision casting of hollow blades
   - Increase temperature capability of molds and cores to allow increased casting rates

5. Continue development of external and internal coatings

   - Increase blade service temperature and life
   - Reduce or eliminate degradation of NiTaC alloy properties due to coating material/process

6. Initiate development of blade finishing processes

   - Establish surface and internal hole drilling techniques
   - Establish joining procedures, such as may be required for tip caps

7. Extend the development of turbine blade technology to hollow, air cooled high pressure turbine blades where payoffs are the highest. This work should incorporate results of the other necessary developing technologies listed above, and be similar to scope of the program covered by this report

8. Following HPT blade development, initiate program to increase cost effectiveness of NiTaC alloys

   - Decrease NiTaC alloy costs through reductions in amount of expensive alloying elements, use of lower cost charge materials, and scrap reversion
   - Decrease casting costs through decreases in mold/core material and process costs, increased casting rates, and process automation
   - Decrease blade finish machining costs through precision casting of airfoils, development of low cost machining and hole drilling processes, and development of low cost joining alloys/processes
   - Decrease coating material/process costs

APPENDIX A

TABULATED NiTaC-13 PROPERTY DATA

TABLE A-1

TENSILE DATA FOR ALIGNED FIBER NiTaC-13 SPECIMENS

MACHINED FROM BARS AND TESTED IN AIR

Specimen No.	Heat No.	g_b, Volume Fraction Solidified	Test Temp., °F	0.02% Yield Strength, Ksi	0.2% Yield Strength, Ksi	UTS, Ksi	%RA	%Elong.	Young's Modulus, 10^6 Psi
LONGITUDINAL									
3B 54-T1	V-371-C	0.62	75	97.5	100.5	182.5	10.0	14.5	21.4
3B 54-T2	V-371-C	0.62	75	95.5	100.0	189.7	10.6	15.2	22.0
3B 24-M9	V-371-C	0.40	1000	97.8	112.4	181.8	10.9	10.1	19.5
3B 38-B1	V-400-C	0.25	1000	90.5	108.3	169.3	18.1	15.8	18.4
3B 24-T2	V-371-C	0.63	1200	107.8	122.4	181.2	13.6	12.5	15.7
3B 38-B2	V-400-C	0.25	1200	101.8	116.1	180.7	17.1	13.6	19.7
3B 24-M6	V-371-C	0.40	1400	104.0	120.4	168.3	18.1	15.9	17.1
3B 38-B3	V-400-C	0.25	1400	107.8	121.4	167.3	19.1	16.2	16.4
3B 24-T3	V-371-C	0.63	1600	112.0	129.5	140.8	24.0	17.5	13.5
3B 38-B4	V-400-C	0.25	1600	99.5	126.6	139.4	21.1	11.8	14.8
3B 24-M7	V-371-C	0.40	1800	54.0	81.2	106.3	20.6	10.7	-
3B 38-B5	V-400-C	0.25	1800	72.6	98.5	111.1	21.1	10.9	13.4
3B 54-T3	V-371-C	0.62	2000	37.7	52.3	57.8	24.6	-	11.1
3B 54-T4	V-371-C	0.62	2000	46.2	56.5	60.6	26.6	16.8	11.6
TRANSVERSE									
3B 24-B1	V-371-C	0.22	75	103.5	124.3	158.8	5.5	4.0	28.6
3B 38-M2	V-400-C	0.55	75	95.5	108.0	137.2	5.0	4.3	-
3B 24-B2	V-371-C	0.17	1200	99.0	114.3	138.9	5.0	2.9	26.1
3B 38-T2	V-400-C	0.66	1200	99.5	112.8	133.7	5.0	2.9	21.6
B 92-B13	V-371-C	0.35	1800	53.0	72.9	80.2	2.5	0.9	15.7
3B 38-M1	V-400-C	0.60	1800	69.1	87.7	99.2	1.5	1.6	19.7

TABLE A- 2

STRESS-RUPTURE DATA FOR BARE AND COATED LONGITUDINAL NiTaC-13

SPECIMENS MACHINED FROM BARS AND TESTED IN AIR

Specimen No.	Heat No.	g_b, Volume Fraction Solidified	Test Conditions Temp., °F	Test Conditions Stress, Ksi	Rupture Life, Hours	Larson-Miller Parameter x 10^{-3}, C=20	%RA	%Elong.	Remarks
LONGITUDINAL - UNCOATED									
B92-B2	V-371-C	0.27	1400	120	5.3	38.6	3.9	3.4	Radius Failure
B92-M2	V-371-C	0.50	1400	98	1696.0+	43.2+	-	-	Test Discontinued
B91-T5	V-371-C	0.69	1400	108	441.3	42.1	16.0	7.7	
B92-M3	V-371-C	0.50	1600	75	67.5	45.0	10.4	6.6	
B92-B3	V-371-C	0.27	1600	62	451.9	46.7	2.9	7.7	
3B38-M7	V-400-C	0.50	1600	60	306.8	46.3	1.1	9.5	
3B54-B4*	V-371-C	0.26	1600	60	654.7	47.0	11.6	7.3	
3B54-B3*	V-371-C	0.26	1800	34	43.4+	49.0+	-	-	Threads Damaged-Test Discontinued
B92-B4	V-371-C	0.27	1800	43	88.9	49.6	27.2	9.9	
B91-T7	V-371-C	0.69	1800	34	98.0	49.7	25.8	7.9	
3B38-M10	V-400-C	0.50	1800	23	564.9	51.4	47.6	9.8	
B92-M4	V-371-C	0.50	1800	30	257.8	50.7	26.7	6.4	
3B38-M6	V-400-C	0.50	2000	25	10.9	51.8	69.2	10.1	
B92-M5	V-371-C	0.50	2000	15	105.6	54.1	69.1	9.4	
B91-T8	V-371-C	0.69	2000	10	206.9	54.9	55.9	5.9	
3B54-B5*	V-371-C	0.26	2000	15	145.6	54.4	71.7	-	
3B24-T6	V-371-C	0.69	2000	6	524.6	55.9	73.5	8.9	
3B24-T5	V-371-C	0.69	2000	6	634.0	56.1	64.7	-	
3B38-B8	V-400-C	0.25	2100	10	68.9	55.9	81.1	14.8	
B92-B5	V-371-C	0.27	2100	6	184.8+	57.0+	-	-	Badly Oxidized-Test Discontinued
LONGITUDINAL - COATED**									
3B24-M2	V-371-C	0.40	1800	26.1	525.0	51.3	34.5	10.9	
3B38-B7	V-400-C	0.25	1800	56.9	2.2	46.0	41.7	15.2	Specimens Damaged by grips. Test Invalid
3B24-T8	V-371-C	0.63	1800	36.1	46.1	49.0	12.4	4.4	
3B24-M3	V-371-C	0.40	2000	17.4	91.5	54.1	51.3	9.0	
3B24-M4	V-371-C	0.40	2000	10.1	1.7+	49.8+	-	-	Grip Failure, Specimen Bent, Test Discontinued
3B24-T7	V-371-C	0.63	2100	9.7	173.0	57.0	59.2	6.0	

* 0.25" Diameter gage section. All other specimens had 0.1" diameter gage sections

** Stress based on bare cross section

TABLE A-3

STRESS-RUPTURE DATA FOR BARE AND COATED TRANSVERSE NiTaC-13 SPECIMENS MACHINED FROM BARS AND TESTED IN AIR

Specimen No.	Heat No.	g_b, Volume Fraction Solidified	Test Conditions: Temp., °F	Test Conditions: Stress, Ksi	Rupture Life, Hours	Larson-Miller Parameter x 10^{-3}, C=20	% RA	% Elong.	Remarks
TRANSVERSE - UNCOATED									
92-B9	V-371-C	0.18	1400	80	0.5	36.6	3.2	0.7	
38-T1	V-400-C	0.66	1400	60	72.4	40.6	11.5	1.3	
38-M5	V-400-C	0.41	1400	45	191.9	41.4	3.9	1.1	Failed close to fillet
92-B10	V-371-C	0.22	1800	6	1287.4	52.2	50.5	-	Weights Bumped - Fracture
92-M10	V-371-C	0.45	1800	15	133.1	50.0	9.6	0.6	
38-M4	V-300-C	0.47	1800	4	1171.0+	52.1	-	-	Test discontinued
TRANSVERSE - COATED									
92-M9	V-371-C	0.40	1800	11.2	104.7	49.7	1.0	0.8	
92-B12	V-371-C	0.31	1800	16.5	59.0	49.1	1.5	1.0	
38-M3	V-300-C	0.51	1800	10.5	173.6	51.6	1.1	1.3	

TABLE A-4

RESULTS OF SUPPLEMENTARY TESTS TO DETERMINE EFFECTS OF THE Ni-20Cr-10Al-1Y COATING/PROCESS ON LONGITUDINAL STRESS-RUPTURE PROPERTIES OF NiTaC-13

**Type Coating	Temp., °F	Stress Ksi	Rupture Life, Hours	Larson-Miller Parameter, X 10^{-3}, C = 20	% RA	% Elong
A	1600	70	263.4	46.18	10.8	7.5
B	1600	70	231.0	46.06	7.6	10.3
None	1800	44	76.9	49.46	38.2	-
B	1800	44	72.1	49.39	42.0	19.5
None	1900	25	108.8	52.00	68.8	-
B	1900	25	142.3	52.27	92.7	-
A	2100	10	125.9	56.57	43.7	18.0
B	2100	10	218.0	57.18	80.7	24.9

*All specimens from bottom section of bar B79 ($g_b \sim 0.27$)
**A = Ni-20Cr-10Al-1Y COATED + HEAT TREATED AT 2000°F FOR 2 HOURS IN VACUUM
B = A + SHOT PEENED + HEAT TREATED AGAIN AT 2000°F FOR 2 HOURS IN VACUUM

TABLE A-5

CREEP-RUPTURE DATA FOR BARE AND COATED LONGUTIDINAL NiTaC-13 SPECIMENS MACHINED FROM BARS AND TESTED IN AIR

Spec. No.	g_b	(1) Where Tested	Test Conditions: Temp., °F	(2) Stress, Ksi	Time, Hours: 1% Plastic Creep	Rupture
UNCOATED						
3B24-M8	.47	GE	1400	108.0	50.0	747.6(3)
3B54-T5	.66	GE	1400	104.0	166.0	235.4
3B24-T1	.66	GE	1400	98.0	810.0	-
3B24-M5	.47	GE	1600	58.0	364.0	745.3
3B24-T4	.66	GE	1600	52.0	323.0	830.5(3)
3B54-T6	.66	GE	1600	49.0	204.0	-
COATED WITH Ni-20Cr-10Al-1Y						
3B54-T7	.66	GE	1800	38.1	5.9	45.6(3)
3B54-B2	.27	J	1800	30.9	18.2	-
3B54-T10	.66	GE	1800	29.0	309.0	-
3B54-T8	.66	V	2000	13.2	11.4	213.1(3)
3B54-B1	.27	V	2000	7.7	135.0	> 597
3B54-T9	.66	J	2000	6.6	Extensometer Failed	

(1) J = Joilet Metallurgical Labs Inc., Joliet, Ill.
V = Vulcan Testing Lab., Birmingham, Ala.

(2) Stress for coated samples based on uncoated area

(3) Re-loaded to original stress of creep test

TABLE A-6

LCF DATA FOR STRAIN CONTROLLED TESTS IN AIR OF BARE LONGITUDINAL NiTaC-13 SPECIMENS

Specimen Number	(1) A_ϵ Ratio	Longitudinal Strain Range x 10^{-6} Cycle of Measurement	ϵ_e	ϵ_p	ϵ_t	ϵ_{max} %	(2) Engineering Stress Range, Ksi 1st Cycle	Nf/2	(3) Calculated E at $N_f/2$ 10^6 Psi	(4) Alt. Pseudo Stress at $N_f/2$, Ksi	Cycles to N_i	Cycles to N_f	(5) Post Test Micro-structure
TESTS AT 1200°F													
3B43-M1	∞	560	1.51	0	1.51	0.76	246.0	258.6	17.1	129.2	1,893	1,960	N
3B41-M2	∞	3,190	1.25	0	1.25	0.62	210.2	216.6	17.3	106.9	17,059	17,449	-
3B43-M2	∞	3,175	1.20	0	1.20	0.60	202.9	210.5	17.5	102.6	16,942	17,134	-
3B43-M3	∞	102,495	1.04	0	1.04	0.52	174.3	177.5	17.1	89.0	N.D.	102,500+	-
3B39-M2	0.95	580	1.50	0	1.50	1.54	242.8	248.5	16.6	128.3	3,439	3,492	N
3B33-M4	0.95	3,325	1.25	0	1.25	1.28	213.2	217.7	17.4	106.9	7,000	7,098	-
3B33-M2	0.95	12,960	1.16	0	1.16	1.19	201.0	200.3	17.3	99.2	46,006	46,270	-
3B39-M3	0.95	111,360	0.99	0	0.99	1.02	171.9	173.2	17.5	84.7	N.D.	145,776+	-
3B49-M2	0.5	1,040	1.53	0	1.53	2.30	252.4	261.8	17.1	130.9	1,500	1,531	F
3B39-M4	0.5	2,230	1.26	0	1.26	1.89	206.1	209.3	16.6	107.8	3,976	4,120	-
3B49-M1	0.5	4,830	1.20	0	1.20	1.80	198.4	202.2	16.8	102.6	22,312	22,642	-
3B49-M3	0.5	3,014	1.10	0	1.10	1.65	184.1	187.3	17.0	94.1	20,960	22,310	-
TESTS AT 1600°F													
3B48-M3	∞	1,725	1.42	.01	1.43	0.72	187.8	210.3	•	107.7	2,919	3,243	N
3B48-M2	∞	6,625	1.25	0	1.25	0.62	172.9	191.2	15.3	94.1	13,969	14,455	-
M3-M2	∞	2,815	1.17	0	1.17	0.58	161.1	175.2	15.0	88.1	16,682	17,090	-
3B48-M1	∞	224,503	1.10	0	1.10	0.55	155.9	165.8	15.1	82.8	N.D.	224,567+	-
3B41-M1	0.95	840	1.43	.03	1.46	1.50	196.2	208.3	•	109.9	2,057	2,159	N
3B58-M2	0.95	6,605	1.25	0	1.25	1.28	176.9	187.6	15.0	94.1	10,747	11,089	-
3B58-M1	0.95	3,876	1.20	0	1.20	1.23	172.2	179.8	15.0	90.4	20,684	20,984	-
3B41-M3	0.95	4,250	1.13	0	1.13	1.16	162.3	173.1	15.3	85.1	36,632	36,868	-
3B49-M4	0.5	3,245	1.30	0	1.30	1.95	189.2	191.1	14.7	97.9	5,596	5,692	F
M4-M2	0.5	2,905	1.20	0	1.20	1.80	177.1	180.3	15.0	90.4	6,137	6,239	-
M4-M3	0.5	4,161	1.15	0	1.15	1.72	173.7	171.2	14.9	86.6	13,948	14,344	-
M4-M1	0.5	21,020	1.10	0	1.10	1.65	162.4	168.8	15.3	82.8	35,359	35,575	-
TESTS AT 1800°F													
3B58-M3	∞	1,640	1.22	.07	1.29	0.64	152.9	164.3	•	86.7	2,855	3,275	N
3B58-M4	∞	4,820	1.07	.03	1.10	0.55	132.5	147.1	•	73.9	7,502	9,104	-
3B48-M4	∞	5,880	1.02	.02	1.04	0.52	126.1	141.7	•	69.9	12,522	13,962	-
3B39-M1	∞	3,260	.98	.02	1.00	0.50	124.5	139.8	•	67.2	41,260	43,689	-
3B33-M1	0.95	1,005	1.11	.09	1.20	1.23	143.9	158.5	•	80.6	2,735	3,137	F
M3-M3	0.95	1,940	1.03	.07	1.10	1.13	138.2	145.9	•	73.9	3,276	3,852	-
3B33-M3	0.95	5,735	.97	.03	1.00	1.03	129.9	138.2	•	67.2	11,936	12,710	-
M3-M1	0.95	25,035	.93	0	.93	0.95	119.9	126.2	13.5	62.5	32,844	33,288	-
3B41-M4	0.5	4,265	1.10	0	1.10	1.65	142.1	140.8	12.8	73.9	7,575	8,307	F
M3-M4	0.5	4,270	1.00	0	1.00	1.50	129.9	133.8	13.4	67.2	11,590	11,698	-
M4-M4	0.5	5,855	.90	0	.90	1.35	117.2	124.8	13.9	60.5	18,560	19,190	-
3B43-M4	0.5	81,460	.80	0	.80	1.20	108.5	109.1	13.6	53.8	160,169	161,165	-

(1) A_ϵ Ratio = Alternating ϵ_t Mean ϵ_t
(2) Engineering Stress Range Based on Original Area
(3) E = Engineering Stress Range at $N_f/2 \div \epsilon_t$
(4) Alternating Pseudo Stress = $\epsilon_t/2$ x E Avg.
(5) N = No Fractured Fibers in Gage Section
F = Fractured Fibers Adjacent to Fracture Surface

• E not calculated because of plastic strain
N.D. Not detected
+ Test discontinued

TABLE A-7

1200°F CONSTANT LOAD AMPLUTUDE LCF AND SPLCF DATA FOR BARE LONGITUDINAL SPECIMENS FROM MIDDLE OF NiTaC-13 BARS

(K_t=1.6, A=0.95, Axial-Axial Loading)

Specimen Number	Alt. Stress, Ksi	Mean Stress, Ksi	Cycles x 10^{-5} Ni, Crack Initiation	Nf, Failure
LCF at 20 CYCLES/MINUTE				
3B40-M4	75	78.9	Machine Malfunctioned	
3B40-M5	75	78.9	-	.016
3B40-M2	70	73.7	.077	.092
3B40-M3	65	68.4	.686	.944
SPLCF 10-90-10 SECONDS				
88-M8	90.7	94.7	-	.0079
90-M10	87.0	91.9	-	.0137
88-M9	82.7	86.7	-	.0786*
3B40-M1	80.3	84.3	-	.0554

* Specimen failed outside the notch

TABLE A-8

1200° AND 1600°F CSF TEST RESULTS

Specimen Ident.	g_b	A-Ratio	Alt. Stress, Ksi	N_f, Cycles x 10^6	Remarks
1200°F					
B93-B1	.27	∞	110.0	1.395	
3B51-T1	.66	∞	105.0	0.340	
3B51-T2	.66	∞	102.0	13.308	
B93-T5	.66	∞	110.0	1.297	Tested at 1100°F
3B51-T3	.66	1.0	100.0	0.055+	Thread Failure
3B51-T4	.66	1.0	100.0	0.096+	Thread Failure
B93-B3	.27	1.0	90.0	12.800+	Runout
B93-B2	.27	1.0	60.0	10.099+	Runout
3B52-B5	.27	0.5	80.0	0.039	
3B52-T1	.66	0.5	74.0	0.038	
3B27-T1	.66	0.5	66.7	10.224+	Runout
3B27-B5	.27	0.5	55.8	14.900+	Runout
1600°F					
3B27-T5	.66	∞	95.0	6.824	
3B52-T5	.66	∞	92.5	1.266	
3B27-T4	.66	∞	90.0	5.553	
3B53-T6	.66	∞	88.0	8.662	
3B53-B2	.27	1.0	85.0	5.226	
3B53-B3	.27	1.0	82.0	0.045+	Thread Failure
3B47-B3	.27	1.0	75.0	0.618	
3B47-B4	.27	1.0	65.0	12.768+	Runout
3B47-T1	.66	0.5	70.0	0.006	
3B47-T2	.66	0.5	47.0	2.929	
3B60-B1	.27	0.5	45.0	12.307+	Runout
3B53-B6	.27	0.5	44.0	11.095+	Runout

TABLE A-9

1400°F CSF TEST RESULTS

Specimen Ident.	g_b	A-Ratio	Alt. Stress, Ksi	N_f, Cycles x 10^{-6}	REMARKS
LONGITUDINAL - UNCOATED					
B93-B5	.27	∞	100.0	2.762	
3B51-T5	.66	∞	95.0	12.144+	Runout
3B52-T2	.66	∞	92.5	20.213+	Runout
B93-B4	.27	∞	90.0	10.300+	Runout
3B52-T4	.66	1.0	90.0	0.355+	Thread Failure
3B52-T3	.66	1.0	80.0	15.184+	Runout
3B27-T2	.66	1.0	70.0	6.924	
3B27-T3	.66	0.76	75.0	4.574	
3B53-T5	.66	0.5	75.0	-	Failed on Loading
3B47-B2	.27	0.5	65.0	12.242+	Runout
3B53-B1	.27	0.5	56.6	1.571	
3B47-B1	.27	0.5	50.0	5.955	Fixture Failed, Spec Reloaded
LONGITUDINAL - Ni-20Cr-10Al-1Y COATED					
B93-T6	.66	1.0	85.0	0.033	
B93-B6	.27	1.0	73.0	0.031	
3B52-B6	.27	1.0	65.0	0.034	
3B52-T6	.66	1.0	50.0	0.113	
TRANSVERSE - UNCOATED					
B88-M2	.61	∞	85.0	0.005	
B90-B7	.34	∞	72.0	0.101	
B90-T1	.76	∞	42.5	17.365+	Runout
B88-T1	.64	∞	38.9	15.920+	Runout
B88-B6	.30	-	Not Tested	-	Dendrites in Gage
B90-M4	.55	1.0	45.0	12.834+	Runout
B90-T2	.70	1.0	42.5	10.351+	Runout
B88-M3	.50	1.0	32.5	15.000+	Runout
B90-T3	.64	0.5	29.2	0.685	
B88-B7	.18	0.5	26.7	12.235+	Runout
B88-M4	.44	0.5	23.3	12.200+	Runout

TABLE A-10

1800°F CSF TEST RESULTS

Specimen Ident.	g_b	A - Ratio	Alt. Stress, Ksi	N_f, Cycles x 10^{-6}	Remarks
LONGITUDINAL - UNCOATED					
3B47-B5	.27	∞	90.2	0.256	
3B47-B6	.27	∞	80.0	5.539	
3B53-B4	.27	∞	78.0	5.834	
3B53-B5	.27	∞	74.0	1.532	
3B47-T3	.66	1.0	70.0	0.264	
3B47-T4	.66	1.0	65.0	0.509	
3B60-B2	.27	1.0	55.0	6.614	
3B60-B3	.27	1.0	52.0	3.899	
3B47-T6	.66	0.5	75.0	-	Failed on Loading
3B47-T5	.66	0.5	60.0	-	Failed on Loading
3B60-B4	.27	0.5	30.0	0.679+	Thread Failure
3B60-B5	.27	0.5	25.0	14.866+	Run Out
LONGITUDINAL - Ni-20Cr-10Al-1Y COATED					
3B27-T6	.66	1.0	70.0	0.031	
3B27-B6	.27	1.0	50.0	2.750	
3B51-T6	.66	1.0	40.0	3.949	
3B60-B6	.27	1.0	30.0	14.738+	Run Out
TRANSVERSE - UNCOATED					
B90-M5	.48	1.0	35.0	0.035	
B90-M6	.41	1.0	25.0	0.065	Dendrites in Gage
B92-T3	.64	1.0	15.0	4.138	
B90-B8	.26	1.0	12.5	10.238+	Run Out

TABLE A-11

2000°F CSF TEST RESULTS

Specimen Ident.	g_b	A-Ratio	Alt. Stress, Ksi	N_f, Cycles x 10^{-6}	Remarks
LONGITUDINAL - UNCOATED					
3B52-B2	.27	∞	25.0	1.938	
3B52-B1	.27	∞	22.0	2.437	
B93-T1	.66	∞	18.0	7.128	
B93-T2	.66	∞	17.0	9.281	
3B27-B1	.27	1.0	30.0	0.658	
3B53-T4	.66	1.0	20.0	3.724	
3B53-T2	.66	1.0	15.0	6.713	
3B27-B4	.27	1.0	13.0	5.521	
B93-T4	.66	0.5	20.0	0.024	
3B52-B3	.27	0.5	10.0	5.057	
B93-T3	.66	0.5	7.0	8.953	
3B52-B4	.27	0.5	7.0	11.848	
LONGITUDINAL - Ni-20Cr-10Al-1Y COATED					
3B27-B3	.27	1.0	20.0	0.227	
3B53-T3	.66	1.0	16.0	10.000+	Runout
3B53-T1	.66	1.0	15.0	5.204	
3B27-B2	.27	1.0	14.0	12.063+	Runout

TABLE A-12

*DENSITY OF NiTaC-13 VERSUS g_b

Bar No.	BOTTOM g_b (Est.)	BOTTOM ρ	MIDDLE g_b (Est.)	MIDDLE ρ	TOP g_b (Est.)	TOP ρ
B46	.15	.3177	.43	.3147	.73	.3101
B62	.18	.3178	.46	.3148	.76	.3089
B63	.22	.3182	.50	.3139	.80	.3080
B64	.18	.3183	.46	.3150	.74	.3100
B65	.16	.3184	.46	.3150	.77	.3089
B66	.21	.3167	.49	.3140	.77	.3096
B67	.16	-	.44	-	.75	-
B68	.17	.3179	.46	.3148	.76	.3093
B69	.20	.3179	.46	.3144	.75	.3095
B70	.16	.3191	.42	.3152	.71	.3108
B71	.22	.3184	.48	.3148	.76	.3098
B72	.20	.3178	.48	.3143	.75	.3098
B73	.17	.3185	.43	.3149	.71	.3101
B77	.23	.3185	.50	.3146	.77	.3094
B78	.20	.3180	.48	.3143	.75	.3099
B79	.24	.3191	.47	.3143	.76	.3090
B83	.20	.3192	.49	.3148	.79	.3084
B84	.22	.3214	.52	.3172	.81	.3113

* Density is in lbs./cu. in.

g_b is volume fraction solidified

TABLE A-13

THERMAL EXPANSION DATA FOR ALIGNED FIBER NiTaC-13 IN THE LONGITUDINAL AND TRANSVERSE DIRECTIONS

Temp. Range, ^{o}F	ΔT, ^{o}F	*Longitudinal		*Transverse	
		Total Expansion, Percent	Expansion Coefficient, $^{o}F^{-1} \times 10^{6}$	Total Expansion, Percent	Expansion Coefficient, $^{o}F^{-1} \times 10^{6}$
77-212	135	0.088	6.51	0.092	6.78
77-392	315	0.198	6.30	0.208	6.62
77-572	495	0.320	6.47	0.333	6.72
77-752	675	0.452	6.70	0.467	6.92
77-932	855	0.590	6.90	0.614	7.18
77-1112	1035	0.733	7.08	0.760	7.34
77-1292	1215	0.892	7.34	0.925	7.61
77-1472	1395	1.061	7.60	1.101	7.89
77-1652	1575	1.255	7.97	1.298	8.24
77-1832	1755	1.467	8.36	1.521	8.67
77-2012	1935	1.744	9.01	1.800	9.30

* Longitudinal Specimen B92-M1, Heat V-371-C

Transverse Specimen B92-M11 and M12, Heat V-371-C

TABLE A-14

THERMAL CONDUCTIVITY OF ALIGNED FIBER NiTaC-13 IN THE LONGITUDINAL AND TRANSVERSE DIRECTIONS

Temperature		*Longitudinal		*Transverse	
^{o}F	^{o}C	Btu · In / Hr. Ft.^{2} ^{o}F	Watts / M · ^{o}K	Btu · In / Hr. Ft.^{2} ^{o}F	Watts / M · ^{o}K
-103	-75	43.7	6.3	41.6	6.0
212	100	60.4	8.7	56.9	8.2
392	200	-	-	68.0	9.8
572	300	79.1	11.4	78.4	11.3
932	500	97.1	14.0	99.9	14.4
1112	600	-	-	111.0	16.0
1292	700	117.9	17.0	-	-
1472	800	-	-	133.2	19.2
1652	900	142.9	20.6	145.7	21.0
1832	1000	-	-	156.8	22.6
2012	1100	173.5	25.0	165.1	23.8

* Longitudinal Specimen B88-T21, Heat V-371-C

Transverse Specimen B91-M19, Heat V-371-C

TABLE A-15

SPECIFIC HEAT OF ALIGNED FIBER NiTaC-13 FROM TOP AND MIDDLE SECTIONS OF BARS

Temperature		Specific Heat		
		$J\ kg^{-1}\ deg\ K^{-1}$		$BTU/lb.\ ^{o}F$
^{o}C	^{o}F	*M19	*T21	Average
-73	-100	370	370	0.0884
260	500	450	450	0.1076
482	900	500	500	0.1195
704	1300	570	570	0.1362
816	1500	620	620	0.1482
1093	2000	800	800	0.1912

*Longitudinal Specimen B88-T21, Heat V-371-C
Transverse Specimen B91-M19, Heat V-371-C

TABLE A-16

ULTRASONIC MEASUREMENTS OF ELASTIC CONSTANTS E AND G

FOR NiTaC-13 IN THE LONGITUDINAL DIRECTION

Test Temp., °F	Long. Resonance Freq., Hz	Long. E, 10^6 Psi	Trans. (Bending) Resonance Freq., Hz	Long. E, 10^6 Psi	Torsional Resonance Freq., Hz	G, 10^6 Psi
TEST SAMPLE B90-M20, ALIGNED CARBIDE FIBERS (1)						
75	21,023	29.43	2746	25.59	13,076	11.38
	-	-	3107	32.76	-	-
310	20,789	28.71	2712	24.91	12,946	11.13
500	20,543	28.00	2688	24.43	12,775	10.82
	-	-	3058	31.62	-	-
700	17,181	19.55	2651	23.72	12,599	10.50
	20,239	27.13	3026	30.91	-	-
1000	19,770	25.82	2589	22.57	12,281	9.95
	-	-	2980	29.89	-	-
1200	19,392	24.80	2536	21.61	12,039	9.55
1395	18,925	23.59	2493	20.87	11,764	9.10
	-	-	2910	27.52	-	-
1600	18,348	22.12	-	-	11,407	8.55
1800	17,640	20.42	-	-	-	-
TEST SAMPLE M39-M1, MISALIGNED FIBERS (1)						
74	17,024	19.22	2455	20.33*	10,010	6.64
	17,198	20.33*	-	-	10,874	7.87
	20,555	28.01	-	-	-	-
300	16,795	18.66	2428	19.85*	9,873	6.44
	17,210	19.85*	-	-	-	-
	20,323	27.34	-	-	-	-
490	16,558	18.11	2396	19.30*	9,789	6.32
	16,992	19.07*	-	-	-	-
	20,055	26.57	-	-	-	-
700	16,329	17.59	2364	18.75*	9,628	6.11
	16,799	18.61*	2722	24.87*	9,791	6.32
	19,783	25.81	2789	26.10	-	-
1000	15,974	16.79	2304	17.77*	12,001	9.47
	16,398	17.69*	2672	23.90	-	
	19,304	24.52	2726	24.87	-	
1200	15,710	16.21	2256	17.01*	11,717	9.01
	16,007	16.83*	2687	24.13	-	-
	18,929	23.54	-	-	-	-
1400	15,381	15.52	2201	16.16*	11,467	8.62
	15,617	15.99*	2587	22.33	-	-
	18,465	22.16	2637	23.20	-	-
1600	15,085	14.90*	2125	15.04*	11,069	8.01
	17,836	20.82	-	-	-	-
1800	14,649	14.02*	-	-	10,685	7.46
	17,182	19.29	-	-	-	
TEST SAMPLE B90-M20, ALIGNED CARBIDE FIBERS (2)						
83	-	-	2513	20.6*	-	-
300	-	-	2480	20.1*	-	-
620	-	-	2431	19.3*	-	-
920	-	-	2377	18.5*	-	-
1200	-	-	2310	17.4*	-	-
1510	-	-	2215	16.0*	-	-

* Test result used in graphical analysis of E versus temperature

(1) Tests by Peabody Testing - Magnaflux, Los Angeles, Calif.

(2) Tests by G.E.

TABLE A-17

WEIGHT CHANGE RESULTS FOR LOW VELOCITY (MACH 0.05) DYNAMIC (1) (2) OXIDATION TESTS OF NiTaC-13 AND RENE' 80, BARE AND COATED

Alloy	Condition	Upper Test Temp., °F	Weight Change, Mg/cm^2, After Exposure, Hours					
			100	200	275	400	500	1000
NiTaC-13	U	1600	+ 1.3	-	-	-	+3.1	-4.0
Rene' 80	U	1600	- 0.1	-	-	-	-2.4	-2.0
NiTaC-13	C	1600	+ 0.4	-	-	-	+0.7	-0.8
Rene' 80	C	1600	+ 0.3	-	-	-	+0.7	-0.6
NiTaC-13	U	1800	+ 2.7	- 4.0	-	-48.6	-65.3	-146.9
Rene' 80	U	1800	+ 1.0	- 2.0	-	- 4.5	-8.7	-45.5
NiTaC-13	C	1800	+ 0.6	+ 0.8	-	+ 1.3	+1.4	+2.2
Rene' 80	C	1800	+ 0.5	+ 0.6	-	+ 0.7	+0.7	+1.1
NiTaC-13	U	1950	-22.7	-68.4	-104.4	-	-	-
Rene' 80	U	1950	- 6.1	-43.9	- 79.3	-	-	-
NiTaC-13	C	1950	+ 0.8	+ 1.3	+ 1.4	-	-	-
NiTaC-13	U	2000	-114.0	-	-	-359.6	-487.3	-
Rene' 80	U	2000	-44.0	-	-	-222.0	-340.0	-
NiTaC-13	C	2000	+ 1.1	-	-	-	-10.0(3)	-36.7(3)
Rene' 80	C	2000	+ 0.5	-	-	-	+1.4	+1.9

(1) Samples cycled 6 times per hour between 850°F and Upper Test Temperature
(2) NiTaC-13 coated with Ni-20Cr-10Al-1Y; Rene' 80 coated with Type I Codep B
(3) High weight loss not due to coating failure - due to lack of coating on base specimen.

TABLE A-18

ALLOY PENETRATION* RESULTS FOR LOW VELOCITY (MACH 0.05) DYNAMIC OXIDATION TESTS**
OF BARE NiTaC-13 AND RENE' 80

Alloy	Exposure Time, Hours	1600° F			1800° F			2000° F		
		O.P.	A.D.	T	O.P.	A.D.	T	O.P.	A.D.	T
NiTaC-13	100	1.0	0.4	1.4	2.0	0.3	2.3	5.0	0.2	5.2
Rene' 80	100	-	-	-	1.0	0.5	1.5	3.5	1.0	4.5
NiTaC-13	400	-	-	-	-	-	-	27.0	-	27.0
Rene' 80	400	-	-	-	-	-	-	12.5	1.0	13.5
NiTaC-13	500	1.5	0.5	2.0	2.5	1.0	3.5	25.0	-	25.0
Rene' 80	500	1.5	0.5	2.0	1.5	1.0	2.5	20.0	1.0	21.0
NiTaC-13	600	-	-	-	-	-	-	25.0	-	25.0
NiTaC-13	1000	2.0	0.5	2.5	7.0	0.5	7.5	-	-	-
Rene' 80	1000	2.0	0.5	2.5	3.5	1.0	4.5	-	-	-

*O.P. = oxide penetration depth, 10^{-3} inches per side
A.D. = alloy depletion layer thickness, 10^{-3} inches per side
T = total alloy loss per side, 10^{-3} inches per side

**Samples cycled 6 times per hour between 850° F and upper test temperatures of 1600°, 1800°, and 2000° F.

APPENDIX B

GENERAL PROCEDURES FOR USE OF GE COMPUTER PROGRAMS IN ANALYSIS OF NiTaC-13 J101 BLADE DESIGNS

TABLE B-1

ADAM MECHANICAL SECTION PROPERTIES

INPUTS

- Blade drawing and precision masters for airfoil and dovetail sections selected for analysis.

OUTPUTS

For each section: area, center of gravity, orientation angle, principal axis, chord length, maximum thickness, first moments, principal moments, third moments, polar moments, fourth moments, torsional stiffness, bending stress function, induced tensile stress functions, and end effect parameters.

WHERE USED

- Inputs to

  ADAM TWISTED BLADE,
  Isotropic MASS (TAMP), and
  Orthotropic MASS (TAMP) computer programs

TABLE B-2

ADAM TWISTED BLADE

INPUTS

- Steady state temperatures from TRANSIENT HEAT TRANSFER.
- Outputs from ADAM MECHANICAL SECTION PROPERTIES.
- Steady state axial and tangential gas loads.
- NiTaC-13 Longitudinal Properties: Young's modulus and shear modulus versus temperature, and; room temperature density (0.3182) and Poisson's ratio (0.39).

OUTPUTS

- Steady state deflections.
- Resultant spanwise (radial) stresses.
- Centrifugal stress, and combined gas bending and blade untwisting stresses.
- Predicted blade resonance frequencies.

WHERE USED

- Compared with isotropic MASS (TAMP) results to verify selected finite element blade model.
- Blade vibration analysis.
- Blade steady state stress analysis.

TABLE B-3

TRANSIENT HEAT TRANSFER

INPUTS

- o J101 LPT Blade Finite Element Model
  1) Airfoil: used 11 radial sections with 64 elements per section, illustrated in Figure B-1.
  2) Dovetail: used seven sections, variable number of elements per section.
- o J101 Operating Conditions
  1) Blade row inlet conditions including pressures, airflow, radial gas temperature distribution, and upstream radiation signature.
  2) Gas temperature distribution over the pressure and suction side airfoil surfaces as calculated using blade velocity profiles.
- o NiTaC-13 Properties
  1) Specific heat versus temperature.
  2) Thermal conductivity versus temperature.
  3) RT Density versus blade position.

OUTPUTS

- o Steady state nodal temperature, illustrated in Figure 119 of text.
- o Transient nodal temperatures.

WHERE OUTPUTS WERE USED

- o Inputs to

  MISSION,

  BUCKET CREEP III,

  Isotropic MASS, and

  Orthotropic MASS

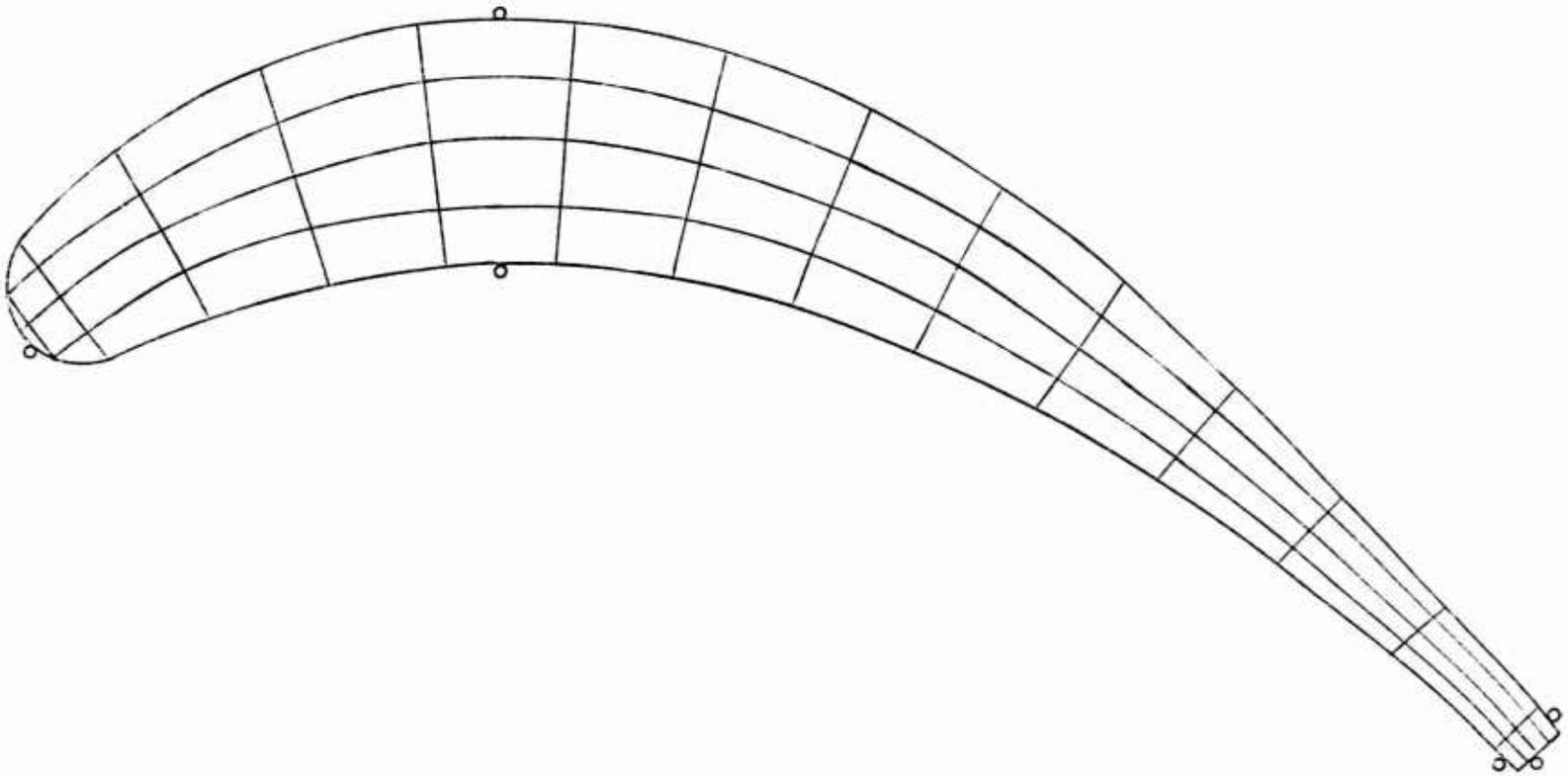

Figure B-1. TRANSIENT HEAT TRANSFER and BUCKET CREEP Finite Element Model for Eutectic J101 LPT Blade Pitch Section

TABLE B-4

BUCKET CREEP III

INPUTS

- Finite element model illustrated in Figure B-1 at three blade locations: 10%, 30% and 50% of airfoil span.
- Transient nodal temperature from TRANSIENT HEAT TRANSFER.
- Steady state stresses and bending loads versus span from ADAM TWISTED BLADE.
- J101 mission profile for time and temperature in Table 42 of text.
- Longitudinal NiTaC-13 properties as a function of temperature: density, Young's modulus, shear modulus, Poisson's ratio, tensile yield strength, average creep constants minus three standard deviations, and average rupture strength minus three standard deviations.

OUTPUTS

- Mechanical strain (pseudo stress = E x strain) for each mission point.

WHERE USED

- Blade rupture life analysis.

TABLE B-5

MISSION

INPUTS

- Steady state, bulk metal temperatures at J101 design point for blade sections analyzed from TRANSIENT HEAT TRANSFER.
- Centrifugal stresses at 100% speed, illustrated in Figure 120 of text. These are ratioed for RPM changes.
- J101 mission time-speed-temperature profile, illustrated in Table 42 of text.
- NiTaC-13 average longitudinal Larson-Miller parameter curve minus three standard deviations.

OUTPUT

- Blade mission mix rupture life at each section.

WHERE USED

- Blade rupture life analysis

TABLE B-6

ISOTROPIC AND ORTHOTROPIC MASS (TAMP)

INPUTS

- Outputs from ADAM MECHANICAL SECTION PROPERTIES.
- J101 LPT finite element blade model illustrated in Figures B-2 and B-3.
- Blade gas loads versus airfoil span position.
- NiTaC-13 properties: density as a function of blade position and properties tabulated below:

	Long.	Trans.
Young's Modulus X 10^{-6} psi	21.6	31.8
Shear Modulus X 10^{-6} psi	7.77	13.9
Poisson's Ratio	0.14	0.39

OUTPUT

- Resultant spanwise stresses, the sum of gas bending, centrifugal and thermal stresses.
- Predicted blade resonant frequencies.

WHERE USED

- Orthotropic MASS - blade HCF life analysis - Campbell diagram.
- Isotropic MASS - resonant frequencies compared with TWISTED BLADE results to verify finite element blade model.

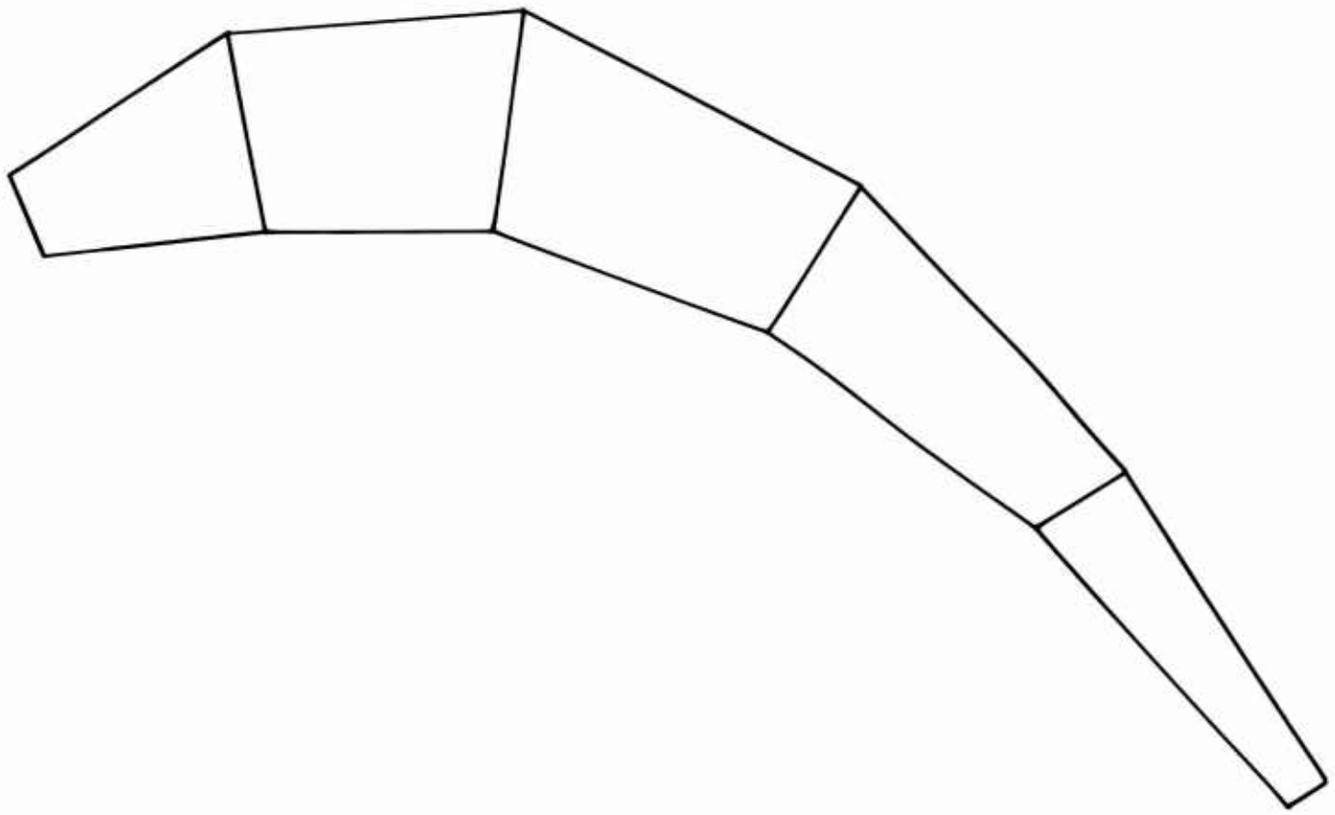

Figure B-2. MASS (TAMP) Finite Element Model for Eutectic J101 LPT Blade Pitch Section

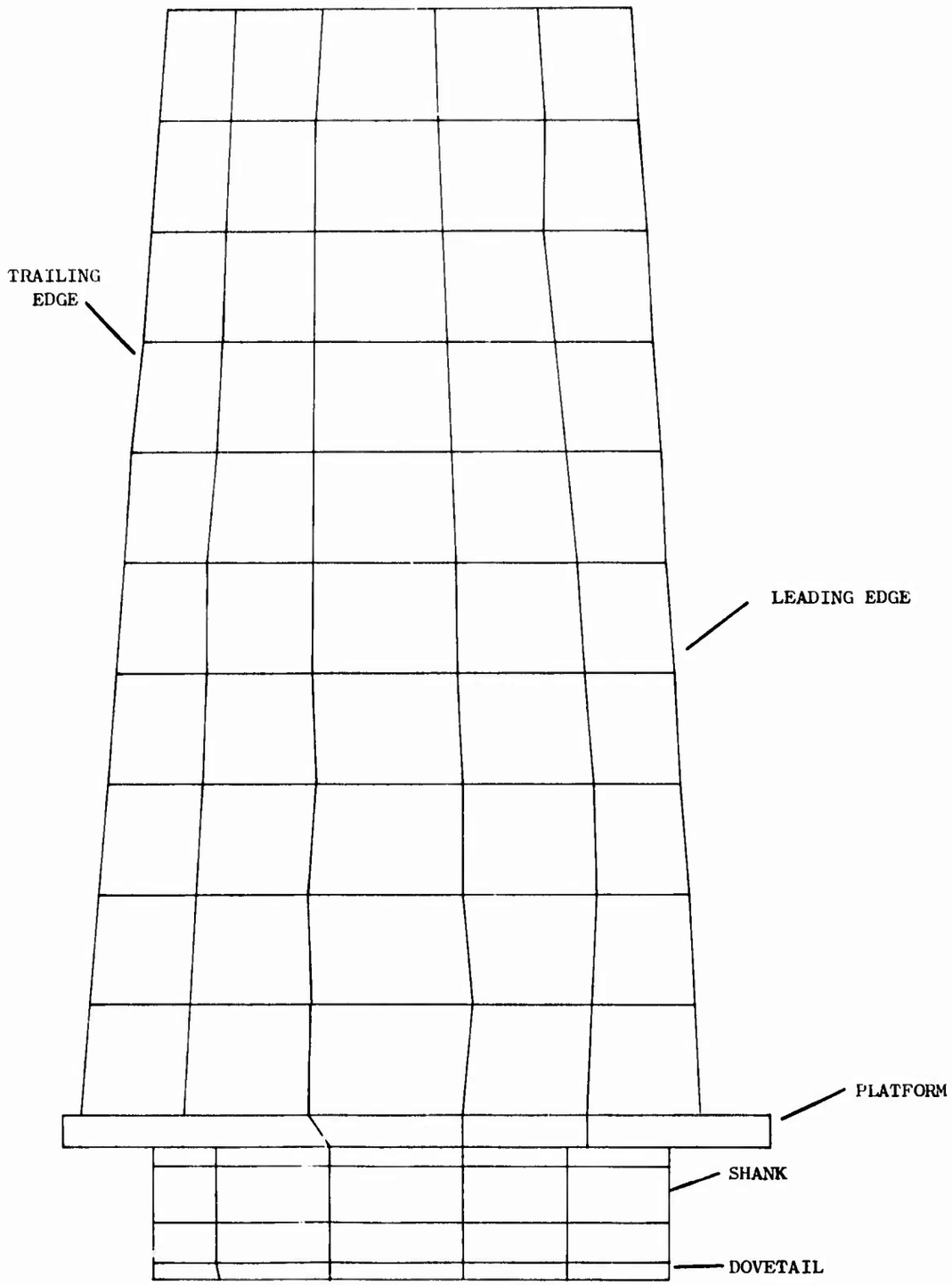

Figure B-3. MASS (TAMP) Finite Element Model (Convex Side) for Eutectic J101 LPT Blade

REFERENCES

1. CA Steinhagen, CL Stotler, and D. Edkins, "Eutectic Composite Turbine Blade Development - Phase V - Systems Analysis", Final Technical Report, AFML Contract F33615-73-C-5050, Report No. AFML-TR-74-119, July 1974, (Confidential Security Classification).

2. MG Benz, ER Buchanan, LV Hampton, MF Henry, MR Jackson, LA Johnson, JR Rairden, TF Sawyer, and JL Walter, "Exploratory Development for Synthesis and Evaluation of Directionally Solidified Composites for High-Temperature Application", Final Technical Report, AFML Contract F33615-72-C-1870, Report No. AFML-TR-73-213, September 1974.

3. MFX Gigliotti and MF Henry, "Segregation in a Plane Front Solidified γ/γ' - MC Alloy", Compsites - II, Bolton Landing, New York, Sept. 5-7, 1975.

4. WA Tiller, KA Jackson, JW Rutler, and B. Chalmers, "The Redistribution of Solute Atoms During the Solidification of Metals", Acta Met., Vol. 1, 1953, p. 428.

5. WG Pfann, "Principles of Zone Melting", J. Metals, Vol. 4, 1952, p. 747.

6. DJS Cooksey, MG Day and A Hellawell, Proc. International Conference on Crystal Growth, Boston, 1966, p. 151.

7. MFX Gigliotti and CD Greskovich, "Ceramic Molds Having a Metal Oxide Barrier for Casting and Directional Solidification of Superalloys", U.S. Patent No. 3,955,616, May 11, 1976.

8. LP Jahnke and CA Bruch, "Requirements for and Characteristics Demanded of High Temperature Gas Turbine Components", Specialists Meeting on Directionally Solidified In-Situ Composites, AGARD Conference Proceedings No. 156, August 1974, p. 3.

9. DN Duhl and CP Sullivan, "Some Effects of Hafnium Additions on the Mechanical Properties of a Columnar - Grained Nickel-Base Superalloy", J. Metals, July 1971, p. 38.

10. BH Kear, AF Giamei, and JE Doherty, "Transverse Grain Boundary Strengthening in a Directionally Solidified Nickel-Base Alloy", Proc. of the Third International Conference on the Strength of Metals and Alloys, Vol. I - Microstructure and Design of Alloys, Institute of Metals, Cambridge England, August, 1973, p. 134.

REFERENCES (Cont'd)

11. D.A. Woodford, "Creep and Rupture of an Advanced Fiber Strengthened Eutectic Composite Superalloy", Submitted to Metallurgical Transactions for publication consideration.

12. M.R. Jackson, J.R. Rairden, and L.V. Hampton, "Coatings for Directional Eutectics", Final Technical Report, NASA Contract NAS 3-16793, Report No. NASA CR-134665, January, 1974.

13. M. Gell and G.R. Leverant, "Mechanisms of High-Temperature Fatigue", ASTM STP 520, American Society for Testing and Materials, 1973, p. 63.

☆ U. S. GOVERNMENT PRINTING OFFICE: 1977 — 757-001/456

AD B020280

AUTHORITY:
AFWAL ltr,
21 Sep 82